

The University of Nottingham

UNITED KINGDOM · CHINA · MALAYSIA

Synthesis, Reactivity, and Electronic Structure of Molecular Uranium Nitrides

Peter A. Cleaves, MSci

Thesis submitted to the University of Nottingham for the degree of Doctor of Philosophy

2016

Declaration

The work presented in this thesis was carried out from October 2012 to August 2015 at The University of Nottingham, and from September 2015 to August 2016 at The University of Manchester, under the supervision of Prof. Stephen T. Liddle. Except where stated, all the work was conducted by Peter A. Cleaves and has not been previously submitted for any degree at this or any other university.

Peter A. Cleaves

Abstract

The study of metal-ligand multiple bonding offers insight into the electronic structure and bond of metal systems. Until recently, for uranium, such systems were limited to uranyl, and terminal chalcogenide, imide and carbene complexes. In 2012, this was extended to nitrides with the first preparation of a uranium–nitride (U≡N) species isolable under standard conditions, namely [U(Tren^{TIPS})(N)][Na(12C4)$_2$] (**52**), which is prepared by the two-electron reduction of sodium azide with a trivalent uranium(III) precursor [U(Tren^{TIPS})] (**15**), and the subsequent sequestration and encapsulation of the loosely bound sodium cations.

In order to then fully explore the bonding within this newly isolated fragment, alternative routes to prepare uranium–nitrides were investigated, in order to both expand the family of known uranium–nitrides, as well as remove the synthetic bottleneck that occurs due to issues in scale-up. The reduction of the pre-installed azide ligand of [U(Tren^{TIPS})(N$_3$)] (**13**) with one-electron external reductants, namely the alkali powders or metals (lithium and sodium, rubidium and caesium) and potassium graphite, affords the dinuclear uranium(V)–nitride species of the form [{U(Tren^{TIPS})(μ-N)(μ-M)}$_2$] (M = Li, Na, K, Rb, Cs; **51**, **106** – **109**). Analogously to the preparation of the first terminal uranium–nitride system, encapsulation of the cation affords separated ion pair species of the form [U(Tren^{TIPS})(N)][M(crown)$_2$] (M = Na, K, Rb, Cs; **52**, **114** – **117**), or if a slightly larger co-ligand is utilised, capped uranium–nitrides of the form [U(Tren^{TIPS}){(μ-N)(μ-M)(crown)}] (M = Li, Na, K, Rb, Cs; **53**, **111** – **113**, **118**, **119**). Oxidation of the separated ion pair nitrides affords the neutral uranium(VI)–nitride, [U(Tren^{TIPS})(N)] (**54**).

Attempts to prepare dinuclear uranium–nitrides by the reduction of **13** with benzyl potassium (KCH$_2$Ph) afforded instead the cyclometallated species [U{*C*H$_2$CH(Me)Si(^{i}Pr)$_2$*N*CH$_2$CH$_2$*N*(CH$_2$CH$_2$*N*Si^{i}Pr$_3$)$_2$}] (**110**). Unexpectedly, in an inversion of the anticipated reactivity trend, attempts to prepare a thorium congener of **110** did not initially form a cyclometallated species, with the reaction of [Th(Tren^{TIPS})(I)] (**123**) and KCH$_2$Ph affording [Th(Tren^{TIPS})(CH$_2$Ph)] (**124**); and cyclometallation was thermolytically induced. Computational calculations indicate

that this is due to the stabilisation of the σ-bond metathesis transition state in the uranium case.

A combination of experimental and computational studies allows for the determination of the electronic structure of the families of uranium(V)–nitrides, by considering all the spectroscopic data available for the dinuclear, terminal separated ion pair and capped species in conjunction with *ab initio* calculations. This approach then leads to a description of the ground and excited states of Tren–uranium(V) nitrides, where [{U(Tren^{TIPS})(μ-N)(μ-K)}$_2$] (**107**) and [U(Tren^{TIPS}){(μ-N)(μ-Na)(15C5)}] (**53**) exhibit a $j_z \approx \pm 5/2$ ground state doublet, with a $j_z \approx \pm 3/2$ first excited state doublet, in contrast to all other nitrides studied, where the reverse is the case. The excited states can be derived from spectroscopic data (EPR and UV-vis-NIR), which corroborate these findings.

A series of investigations into the small molecule activation chemistry of uranium–nitrides were instigated. The reaction of Tren–uranium(VI) or uranium(V)–nitrides (**54**, with carbon monoxide resulted in two-electron reductive carbonylation to afford the corresponding uranium(IV)– and uranium(III)–isocyanates, [U(Tren^{TIPS})(NCO)] (**135**), [U(Tren^{TIPS})(NCO)][K(Bn-15C5)$_2$] (**136**), [U(Tren^{TIPS}){(μ-NCO)(μ-K)(18C6)}] (**137**). Reduction of **135** with potassium graphite afforded complete nitrogen atom transfer to eliminate KOCN and generate **15**. In the presence of crown, the uranium–nitrogen bond is retained and **136** or **137** can be isolated. A synthetic cycle for the conversion of NaN_3 to NaOCN was investigated employing the U^{III}-U^{V} redox couple by the reaction of **15**, NaN_3 and CO in pyridine, where one turnover was observed. DFT calculations were used to model these reactions, and they provided evidence for nucleophilic behaviour and explained the difference in the rates of reaction.

The reaction of heteroallenes (CE_2, E = O, S) with Tren–uranium nitrides was also investigated. It was found that terminal uranium–nitrides react with CO_2 to afford uranium–oxo–isocyanates, with retention of uranium oxidation state. In the case of uranium(V), [U(Tren^{TIPS})(O)(NCO)][K(Bn-15C5)$_2$] (**138**) is stable, though for uranium(VI), [U(Tren^{TIPS})(O)(NCO)] (**139**), a cyanate radical is extruded, which decomposes *via* diisooxocyan to afford N_2 and CO, preparing [U(Tren^{TIPS})(O)]

(**122**). With CS_2, uranium(V)–nitrides undergo overall disproportionation to afford uranium(IV)–trithiocarbonates [U(Tren^{TIPS})(κ^2-CS_3)][K(Bn-15C5)$_2$] (**140**) and [{U(Tren^{TIPS})(μ-κ^2:κ^1-CS_3)(μ-K)(Bn$_2$-18C6)}$_2$(μ-C_6H_6)] (**141**), and uranium(VI)–nitride (**54**), alongside the formation of [K(crown)$_n$][SCN]. The reaction of **54**, which cannot engage in disproportionation chemistry, with CS_2 prepares a uranium(IV)–isothiocyanate, [U(Tren^{TIPS})(NCS)] (**142**), by the elimination of sulfur, which can be scavenged by triphenylphosphine. Calculations reproduced experimental outcomes, and show that while uranium(V)–nitrides (**115**) engage in outer-sphere type reactivity, uranium(VI)–nitrides (**54**) instead react *via* inner sphere mechanisms.

Publications arising from this work

The role of 5f-orbital participation in unexpected inversion of the σ-bond metathesis reactivity trend of triamidoamine thorium(IV) and uranium(IV) alkyls; B. M. Gardner, P. A. Cleaves, C. E. Kefalidis, J. Fang, L. Maron, W. Lewis, A. J. Blake and S. T. Liddle, *Chem. Sci.*, 2014, **5**, 2489.

Two-electron reductive carbonylation of terminal uranium(V) and uranium(VI) nitrides to cyanate by carbon monoxide; P. A. Cleaves, D. M. King, C. E. Kefalidis, L. Maron, F. Tuna, E. J. L. McInnes, J. McMaster, W. Lewis, A. J. Blake and S. T. Liddle, *Angew. Chem. Int. Ed.*, 2014, **53**, 10412.

Molecular and electronic Structure of terminal and alkali metal-capped uranium(V)-nitride complexes. D. M. King, P. A. Cleaves, A. J. Wooles, B. M. Gardner, N. F. Chilton, F. Tuna, W. Lewis, E. J. L. McInnes and S. T. Liddle, *Nat. Commun.*, 2016, Manuscript Accepted.

Acknowledgements

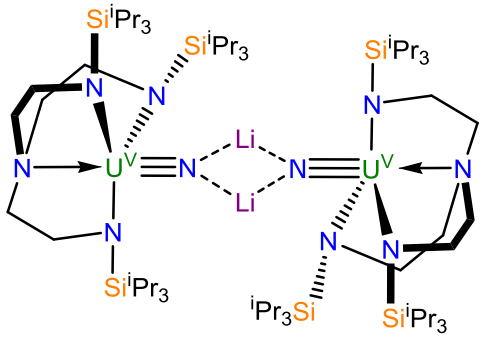
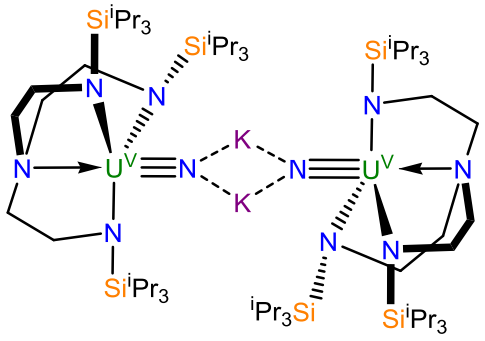
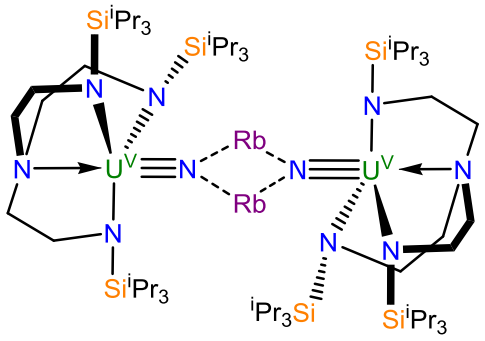
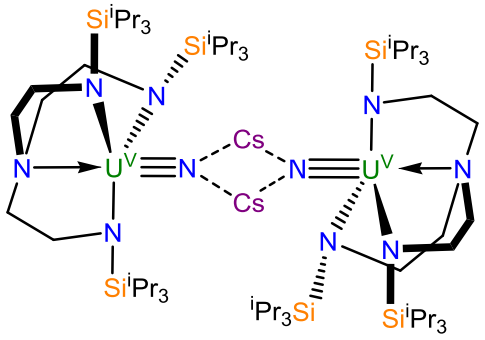
I would like to thank Prof. Stephen T. Liddle for his guidance and support throughout my PhD. I would also like to thank all the post-docs within the group, both past and present: Dr David Mills, Dr Dipti White (née Patel), Dr John Stewart, Dr Benedict Gardner, Dr Ashley Wooles, Dr Erli Lu, Dr David King, Dr Matthew Gregson, Dr Laurence Doyle, Dr Adi Nako and Dr Markus Zegke. Special thanks go to Dave K.: this thesis is the continuation of his work, and his thesis has been my own personal "Bible", of sorts; to Ash, who has borne the brunt of my many questions (some more rhetorical than others); to Matt, who has been a good neighbour both in the Lab and Office these last two years; and to Ben, with whom I collaborated for the work featured in Chapter 3. All four of these post-docs also put in a lot of effort towards the preparation of the assembled masses of uranium–nitride structures presented in Chapter 2.

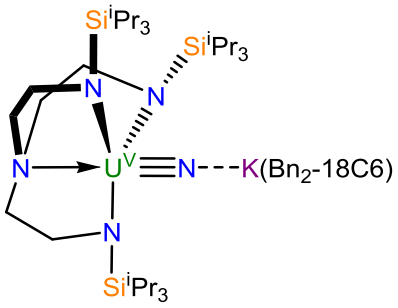
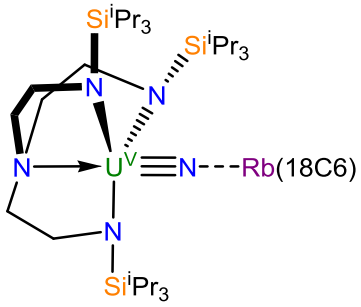
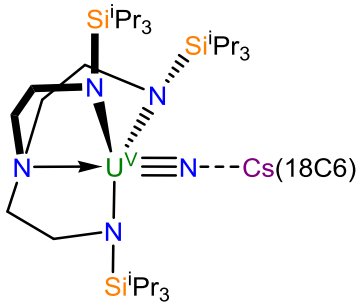
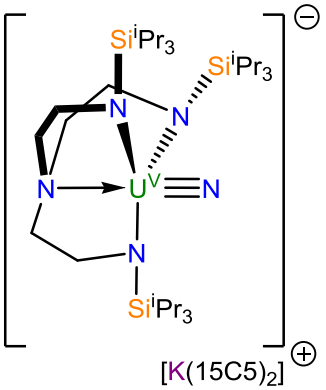
Thanks also go to the rest of the Liddle group, past and present, Dr Oliver Cooper, Dr Andrew Cornish, Dr Lyndsay Soutar, Alexander Ayres, Elizabeth Wildman, Mark Jackson, Thomas Rookes, Philip Cobb, Georgina Hatton, Joseph Ostrowski, John Seed, Rosie Magnall and Emanuele Zanda, as well as all 4th year undergraduate Master's and summer students. Special thanks go to Liz and Tom, who have managed to bear both living and working with me this last year in Manchester, and to Robert Bannister and James Hickson, who I supervised in their Master's projects. Thanks also go to the Liddle group's lab neighbours in Nottingham, the Stockman and Kays groups, for providing a friendly working atmosphere in the North Wing, and to the Schröder group, who have provided me with a source of carbon dioxide in Manchester.

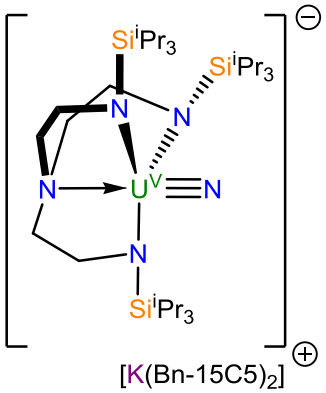
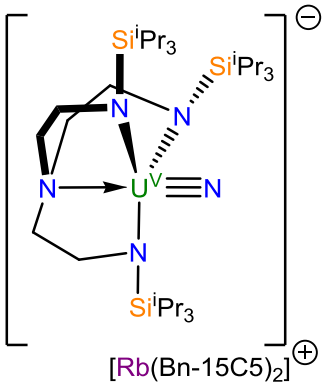
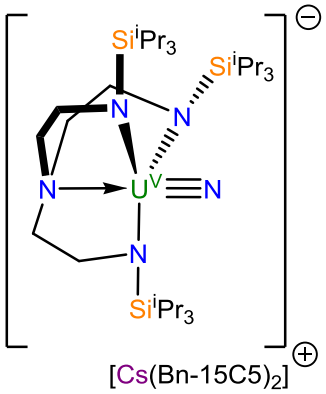
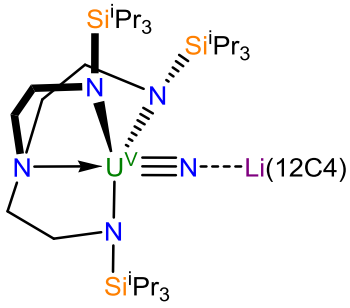
I would also like to thank the following researchers and technicians for their help during my studies: Dr Floriana Tuna, Prof. Eric McInnes and Dr Nicholas Chilton, for their work in SQUID magnetometry and EPR spectroscopy, as well as their uncovering of the electronic structure of Tren–uranium nitrides, as discussed in Chapter 4; to Prof. Alexander Blake and Dr William Lewis for teaching me about Crystallography; to Dr Tong Liu for elemental analysis; and to Dr Adrienne Davis, Kevin Butler and Shazad Aslam for NMR spectroscopy.

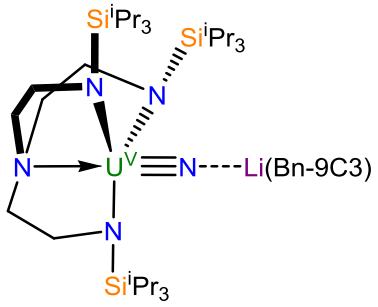
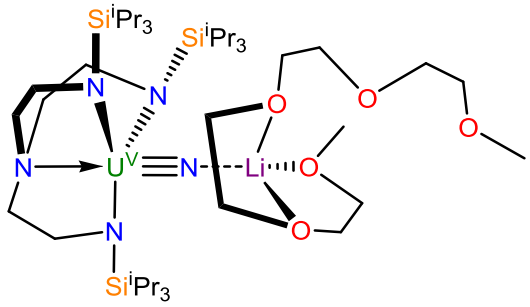
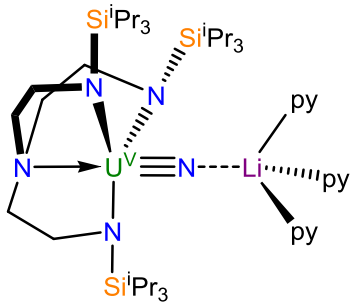
Finally, I would like to thank to following bodies for funding: the Engineering and Physical Sciences Research Council, the European Research Council, the National Nuclear Laboratory, the Royal Society of Chemistry, COST Action CM1006 and the European f-element Network (EUFEN), the University of Nottingham and the University of Manchester.

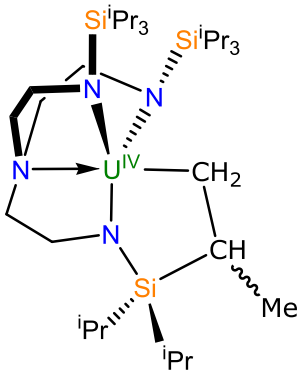
List of Novel Complexes

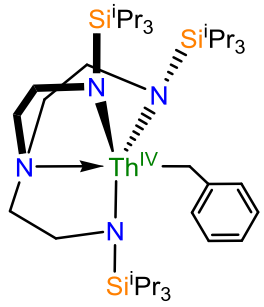
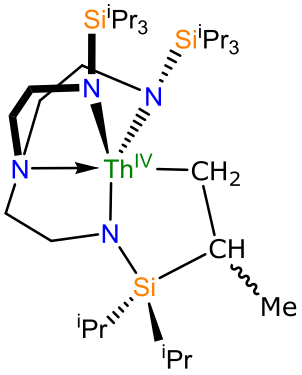
Chapter Two		
Complex	**Formula**	**Structure**
106	$[U(Tren^{TIPS})(\mu\text{-}N)(\mu\text{-}Li)\}_2]$	
107	$[U(Tren^{TIPS})(\mu\text{-}N)(\mu\text{-}K)\}_2]$	
108	$[U(Tren^{TIPS})(\mu\text{-}N)(\mu\text{-}Rb)\}_2]$	
109	$[U(Tren^{TIPS})(\mu\text{-}N)(\mu\text{-}Cs)\}_2]$	

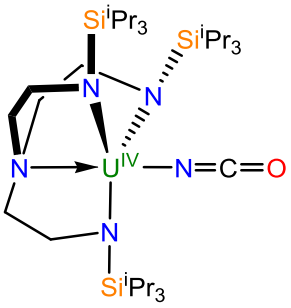
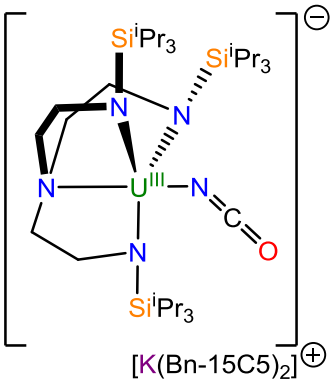
111	[U(Tren^{TIPS})(μ-N)(μ-K)(Bn$_2$-18C6)}]	
112	[U(Tren^{TIPS})(μ-N)(μ-Rb)(18C6)}]	
113	[U(Tren^{TIPS})(μ-N)(μ-Cs)(18C6)}]	
114	[U(Tren^{TIPS})(N)][K(15C5)$_2$]	

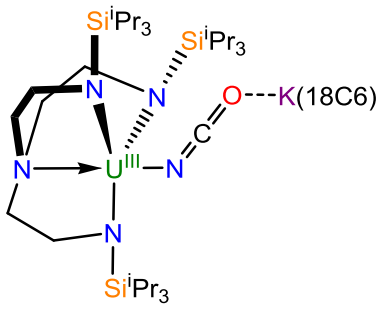
115	[U(Tren^{TIPS})(N)] [K(Bn-15C5)$_2$]	
116	[U(Tren^{TIPS})(N)] [Rb(Bn-15C5)$_2$]	
117	[U(Tren^{TIPS})(N)] [Cs(Bn-15C5)$_2$]	
118	[U(Tren^{TIPS})(μ-N)(μ-Li)(12C4)}]	

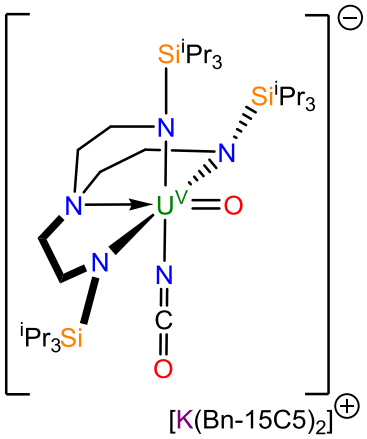
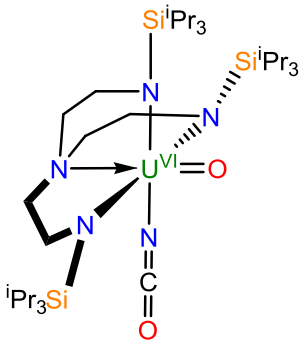
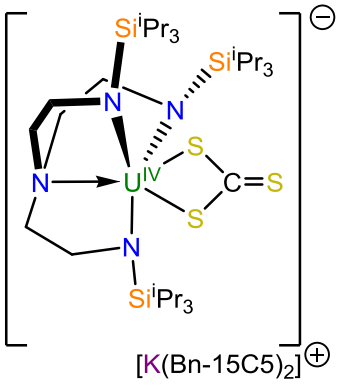
119	[U(Tren^{TIPS})(μ-N)(μ-Li)(Bn-9C3)}]	
120	[U(Tren^{TIPS})(μ-N)(μ-Li)(tetraglyme)}]	
121	[U(Tren^{TIPS})(μ-N)(μ-Li)(py)$_3$}]	

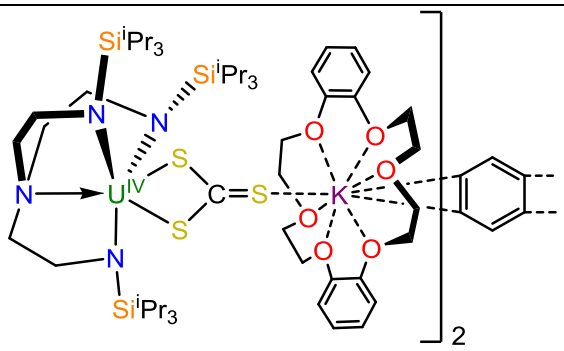
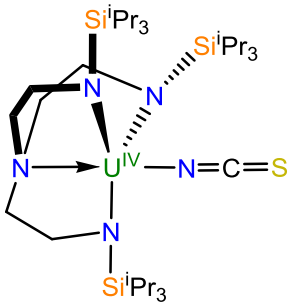
Chapter Three		
Complex	**Formula**	**Structure**
110	[U{$CH_2CH(Me)Si(^iPr)_2N$ $CH_2CH_2N(CH_2CH_2NSi^iPr_3)_2$]	

124	[Th(Tren^{TIPS})(CH_2Ph)]	
125	[Th{$CH_2CH(Me)Si(^iPr)_2N$ $CH_2CH_2N(CH_2CH_2NSi^iPr_3)_2$]	

Chapter Five		
Complex	**Formula**	**Structure**
135	[U(Tren^{TIPS})(NCO)]	
136	[U(Tren^{TIPS})(NCO)] [K(Bn-15C5)$_2$]	

137	[U(Tren^{TIPS})(μ-NCO)(μ-K)(18C6)}]	

Chapter Six		
Complex	**Formula**	**Structure**
138	[U(Tren^{TIPS})(O)(NCO)][K(Bn-15C5)$_2$]	
139	[U(Tren^{TIPS})(O)(NCO)]	
140	[U(Tren^{TIPS})(CS_3)][K(Bn-15C5)$_2$]	

141	[{U(Tren^{TIPS})(μ-κ^2:κ^1-CS_3)(μ-K[18C6])}$_2$(μ-η^2:η^2-C_6H_6)]	
142	[U(Tren^{TIPS})(NCS)]	

Abbreviations

Å	Ångström, 1 x 10^{-10} m
Ad	Adamantyl, $C_{10}H_{15}$
An	Actinide
Ar	Aryl
Ar_F	4-FC_6H_4
Ar_F'	2-F-5-MeC_6H_4
atm	Atmosphere
ATR	Attenuated total reflectance
$BIPMH^{TMS}$	*bis*-Iminophosphoranomethanide, $HC\{P(Ph)_2NSiMe_3\}_2$
Bn-9C3	Benzo-9-crown-3 ether
Bn-15C5	Benzo-15-crown-5 ether
Bn_2-18C6	Dibenzo-18-crown-6 ether
br	Broad
^nBu	n-Butyl, C_4H_9
^sBu	*sec*-Butyl, $CH(CH_3)(C_2H_5)$
^tBu	*tert*-Butyl, $C(CH_3)_3$
c	Speed of light
C	Celsius
ca.	Circa
CASSCF	Complete active space self-consistent field
CF	Crystal field
cm^{-1}	Wavenumber
COT	Cyclooctatetraene, η^8-C_8H_8
Cp	Cyclopentadienyl, C_5H_5

Cp*	C_5Me_5
Cp^{Me}	MeC_5H_4
crypt	2,2,2-Kryptofix, $N\{(CH_2CH_2O)_2CH_2CH_2\}_3N$
CT	Charge transfer
Cy	Cyclohexyl, C_6H_{11}
cyclam	$\{CH_2\mathit{N}R(CH_2)_2\mathit{N}R(CH_2)_3\}_2$
d	Doublet
D	Deuterium, ^2H
D	Axial zero-field splitting parameter
DAB	Diazabutadiene, HN=CH-CH=NH
dbabh	Dibenzo-7-azabicyclo[2.2.1]hepta-2,5-diene anion
DFT	Density Functional Theory
DMBS	Dimethyl-*tert*-butylsilyl, $SiMe_2{}^tBu$
DME	Dimethoxyethane, $MeOCH_2CH_2OMe$
dppe	$Ph_2PCH_2CH_2PPh_2$,
E	Energy
E_a	Energy of activation
EPR	Electron paramagnetic resonance
Et	Ethyl, C_2H_5
FTIR	Fourier transform infrared
GCMS	Gas chromatography mass spectrometry
H	Magnetic field
H_c	Coercive magnetic field
HIPT	Hexa-*iso*-propyl-terphenyl, $3,5\text{-}(2,4,6\text{-}{}^iPrC_6H_2)_2C_6H_3$
HMDSO	Hexamethyldisiloxane, $O(SiMe_3)_2$
HMPA	hexamethylphosphoramide, $OP(NMe_2)_3$

HOMO	Highest occupied molecular orbital
HTBT	Hexa-*tert*-propyl-terphenyl, 3,5-(2,4,6-^{t}BuC_6H_2)$_2C_6H_3$
Im	Imidazole, $C_3H_2N_2$
IR	Infrared
ITI	Inverse *trans* influence
j	Total electron angular momentum
J	Total atomic angular momentum
$^{n}J_{xy}$	Coupling constant
K	Kelvin
Kcal	Kilocalories
kJ mol^{-1}	Kilojoules per mole
L	Total orbital angular momentum
Ln	Lanthanide
LUMO	Lowest unoccupied molecular orbital
m	Medium
m	Multiplet
M	Molar, mol dm^{-3}
M	Metal
M	Magnetisation
m_e	Mass of an electron
Me	Methyl, CH_3
Mes	1,3,5-$Me_3C_6H_2$
Mes*	1,3,5-$^{t}Bu_3C_6H_2$
m_l	Individual orbital angular momenta
ml	Millilitre
mmol	Millimole

MO	Molecular orbital
m_s	Individual electronic spin angular momentum
N″	*bis*-Trimethylsilylamide, $N(SiMe_3)_2$
nacnac	$HC\{C(Me)N\text{-}2,6\text{-}^{i}Pr_2C_6H_3\}_2$
NBO	Natural bond order
NCA	Non-coordinating anion
NIR	Near infrared
nm	Nanometre (1×10^{-9} m)
NMR	Nuclear magnetic resonance
NNO	$1\text{-}(O)\text{-}2,4\text{-}(^{t}Bu)_2\text{-}6\text{-}\{NC(Me)_2\text{-}2\text{-}(C_5H_4N)\}\text{-}C_6H_2$
nP	Neopentyl, $CH_2C(CH_3)_3$
NPA	Natural population analysis
OTf	Triflate, OSO_2CF_3
Ph	Phenyl, C_6H_5
PMDETA	Pentamethyldiethylenetriamine, $MeN(CH_2CH_2NMe_2)_2$
PN	$1\text{-}N(2,4,6\text{-}Me_3C_6H_2)\text{-}2\text{-}P(^{i}Pr_2)\text{-}4\text{-}Me\text{-}C_6H_3$
PNP	$N(CH_2CH_2PR_2)_2$
PNP′	$N\{Si(Me)_2CH_2PR_2\}_2$
POP	$O\{Si(Me)_2CH_2PR_2\}_2$
ppm	Parts per million
^{i}Pr	*iso*-Propyl, $CH(CH_3)_2$
py	Pyridine, C_5H_5N
q	Quartet
QTAIM	Quantum theory of atoms in molecules
QTM	Quantum tunnelling of the magnetisation
RE	Rare earth metal

RECP	Relativistic effective core potential
RT	Room temperature
s	Singlet
s	Strong
S	Total electronic spin angular momentum
Salen	$\{CH_2NCHC_6H_4O\}_2$
SMM	Single molecule magnet
SOC	Spin orbit coupling
SQUID	Superconducting quantum interference device
t	Triplet
T	Temperature
T	Tesla
tacn	Triazacyclononane
T_B	Blocking temperature
TEMPO	(2,2,6,6-Tetramethylpiperidin-1-yl)oxyl
THF	Tetrahydrofuran, C_4H_8O
TIPS	Tri-*iso*-propylsilyl, Si^iPr_3
TM	Transition metal
TMEDA	Tetramethyleneethylenediamine, $Me_2NCH_2CH_2NMe_2$
TMS	Trimethylsilyl, $SiMe_3$
Tol	Tolyl, 4-MeC_6H_4
Tp*	$HB\{NC(Me)CHC(Me)N\}_3$
TPP	Tetraphenylporphyrin
tpy	2,2′,6′,2″-terpyridine
TPS	Triphenylsilyl, $SiPh_3$
Tren	$N(CH_2CH_2NH_2)_3$

TS	Transition state
vis	Visible
U_{eff}	Effective thermal energy barrier
UV	Ultraviolet
VT-NMR	Variable temperature NMR
w	Weak
W	Watt
X	Halide
Xy	Xylyl, 3,5-$Me_2C_6H_3$
XRD	X-ray diffraction
Z	Atomic number
ZFS	Zero-field splitting
$\Delta H^{\ddagger}$	Enthalpy of transition
$\Delta S^{\ddagger}$	Entropy of transition
δ	Chemical shift
ε	Absorption coefficient
λ	Spin orbit coupling constant
λ	Wavelength
μ	Crystal quantum number
μ_B	Bohr magneton
μ_{eff}	Effective magnetic moment
ν	Frequency
τ	Relaxation time
τ	Geometry index
χ_M	Molar magnetic susceptibility
χ_M'	In-phase magnetic susceptibility

χ_M''	Out-of-phase magnetic susceptibility
$\{^1H\}$	Proton decoupled
12C4	12-crown-4 ether
15C5	15-crown-5 ether
18C6	18-crown-6 ether

Table of Contents

1. Introduction 1

1.1. General uranium introduction 2

1.2. Introduction to Tren chemistry 10

1.2.1. Transition metal chemistry 10

1.2.2. Highlights from f-block chemistry 14

1.2.2.1. Uranium 14

1.2.2.2. Thorium 19

1.2.3. Triamidoamine cyclometallates 20

1.3. Introduction to transition metal nitrides 25

1.3.1. Background 25

1.3.2. N-atom transfer 27

1.3.3. Azide decomposition 29

1.3.4. Small molecule activation 32

1.3.5. N-E bond scission 34

1.4. Reactivity of transition metal nitrides 36

1.4.1. General outline of reactivity 36

1.4.2. Reactivity of transition metal nitrides towards CO 39

1.4.3. Reactivity of transition metal nitrides towards CE_2 (E = O, S) 42

1.5. Towards uranium nitrides 46

1.6. Reactivity of uranium species towards small molecules 58

1.6.1. Reactivity of uranium species towards CO 58

1.6.2. Reactivity of uranium species towards CO_2 65

1.6.3. Reactivity of uranium species towards CS_2 73

1.6.4. Reactivity of uranium nitrides 75

1.7. Aims of Project 77

1.8. References 78

2. The Synthesis of Uranium Nitrides 87

2.1. Introduction and Aims 88

2.2. Reactivity Studies of [U(Tren^{TIPS})(N_3)] Towards Reducing Agents 89

2.3. Reactivity Studies of [{U(Tren^{TIPS})(μ-N)(μ-M)}$_2$] (M = Li, Na, K, Rb, Cs) Towards Crown Ethers 99

2.3.1. Overview 99
2.3.2. Preparation of [U(Tren^{TIPS}){(μ-N)(μ-M)(crown)}] (M = Na, K, Rb, Cs) 100
2.3.3. Preparation of [U(Tren^{TIPS})(N)][M(crown)$_2$] (M = Na, K, Rb, Cs) 106
2.3.4. Reactivity studies of [{U(Tren^{TIPS}){(μ-N)(μ-Li)}$_2$] towards donor ligands 112
2.3.5. Solution phase electronic data for 52, 53, 111 – 121 118
2.4. Preparation of [U(Tren^{TIPS})(N)] (54) 124
2.5. Alternative Syntheses of [{U(Tren^{TIPS})(μ-N)(μ-K)}$_2$] (107) 124
2.5.1. Reactivity studies of [U(Tren^{TIPS})(N)] (54) towards reducing agents 124
2.5.2. Transmetallation reactions of [{U(Tren^{TIPS})(μ-N)(μ-Na)}$_2$] (51) 125
2.6. Summary and Conclusions 127
2.7. References 127

3. The Reactivity of Actinide Cyclometallates 129
3.1. Introduction and Aims 130
3.1.1. Bonding differences in uranium and thorium complexes 130
3.1.2. Aims 131
3.2. Actinide Cyclometallates 133
3.2.1. Uranium cyclometallates 133
3.2.2. Thorium cyclometallates 136
3.2.3. Computational investigations into actinide cyclometallates 140
3.3. Summary and Conclusions 146
3.4. References 147

4. The Electronic Structure of Uranium Nitrides 149
4.1. Introduction and Aims 150
4.1.1. An Introduction to Single Molecule Magnets (SMMs) 150
4.1.2. Highlights from the Literature 151
4.1.2.1. Transition Metal SMMs 151
4.1.2.2. Lanthanide SMMs 153
4.1.2.3. Actinide SMMs 156
4.1.3. Aims 158
4.2. Electronic Structure of Uranium(V)–Nitrides 159
4.2.1. Background 159

4.2.2. Ab initio modelling of $[U{\equiv}N]^{2+}$ 160
4.2.3. Ab initio modelling of $[U(NH_3)(NH_2)_3(N)]^-$ 164
4.2.4. Ab initio modelling of $[U(Tren^{TIPS})(N)]^-$ 169
4.3. Magnetic Structure of Uranium(V)–Nitrides 172
4.3.1. Magnetic measurements of uranium(V)–nitrides 172
4.3.2. EPR studies of uranium(V)–nitrides 178
4.3.3. Comparison of uranium(V)–nitrides with $[U(Tren^{TIPS})(O)]$, 122 183
4.3.4. Uranium(V)–nitrides as SMMs 185
4.4. Summary and Conclusions 188
4.5. References 190

5. The Reactivity of Uranium Nitrides Towards Carbon Monoxide 193
5.1. Introduction and Aims 194
5.2. Reactivity Studies of Uranium Nitride Complexes Towards CO 195
5.2.1. Tren–uranium(VI) nitride (**54**) 195
5.2.2. Tren–uranium(V) nitrides 199
5.2.3. Towards a synthetic cycle for the conversion of NaN_3 to NaOCN 207
5.2.4. Computational analysis 211
5.2.5. Reactivity of Tren–uranium nitrides towards phosphines 213
5.3. Summary and Conclusions 214
5.4. References 215

6. The Reactivity of Uranium Nitrides Towards Heteroallenes 217
6.1. Introduction and Aims 218
6.2. Reactivity Studies of Uranium Nitride Complexes Towards CE_2 219
6.2.1. CO_2 219
6.2.1.1. Tren–uranium(V) nitrides 219
6.2.1.2. Tren–uranium(VI) nitride (54) 227
6.2.2. CS_2 233
6.2.2.1. Tren–uranium(V) nitrides 233
6.2.2.2. Tren–uranium(VI) nitride (54) 242
6.2.3. Computational Analysis 247
6.2.3.1. $[U(Tren^{TIPS})(N)][K(Bn\text{-}15C5)_2]$ (115) + CO_2 247

6.2.3.2. ***[U(Tren^{TIPS})(N)] (54) + CO_2*** 248
6.2.3.3. ***[U(Tren^{TIPS})(N)][K(Bn-15C5)$_2$] (115) + CS_2*** 249
6.2.3.4. ***[U(Tren^{TIPS})(N)] (54) + CS_2*** 241
6.2.4. ***Discussion of mechanistic insights*** 252
6.3. Summary and Conclusions 256
6.4. References 258

7. Supporting Information 261
7.1. General Experimental Details 264
7.2. Experimental Details 269
7.2.1. ***Chapter 2*** 269
7.2.2. ***Chapter 3*** 280
7.2.3. ***Chapter 5*** 283
7.2.4. ***Chapter 6*** 286
7.3. X-ray Crystallographic Data 295
7.4. Magnetometric Measurements 304
7.4.1. ***Chapter 4*** 304
7.4.2. ***Chapter 5*** 314
7.4.3. ***Chapter 6*** 315
7.5. DFT and *ab initio* Calculations 316
7.5.1. ***Chapter 3*** 316
7.5.2. ***Chapter 4*** 319
7.5.3. ***Chapter 5*** 326
7.5.4. ***Chapter 6*** 327
7.6. References 328

Chapter One

Introduction

Table of Contents

1.1. General uranium introduction 2

1.2. Introduction to Tren chemistry 10

1.2.1. Transition metal chemistry 10

1.2.2. Highlights from f-block chemistry 14

1.2.2.1. Uranium 14

1.2.2.2. Thorium 19

1.2.3. Triamidoamine cyclometallates 20

1.3. Introduction to transition metal nitrides 25

1.3.1. Background 25

1.3.2. N-atom transfer 27

1.3.3. Azide decomposition 29

1.3.4. Small molecule activation 32

1.3.5. N-E bond scission 344

1.4. Reactivity of transition metal nitrides 36

1.4.1. General outline of reactivity 36

1.4.2. Reactivity of transition metal nitrides towards CO 39

1.4.3. Reactivity of transition metal nitrides towards CE_2 (E = O, S) 42

1.5. Towards uranium nitrides 46

1.6. Reactivity of uranium species towards small molecules 58

1.6.1. Reactivity of uranium species towards CO 58

1.6.2. Reactivity of uranium species towards CO_2 65

1.6.3. Reactivity of uranium species towards CS_2 73

1.6.4. Reactivity of uranium nitrides 75

1.7. Aims of Project 77

1.8. References 78

1.1. General uranium introduction

Our understanding of the chemistry of the f-block elements is often considered to be significantly behind that of the d-, p- and, to some degree, s-block elements, and so it is desirable to gain fundamental knowledge, and therefore understanding, of the chemistry of the lanthanides and actinides. The actinides consist of the elements between thorium and lawrencium, which have valence electrons in 5f orbitals. Only uranium and thorium occur naturally in substantial quantities (2.8 and ~6 ppm respectively),[1,2] the remaining actinides are either rare (protactinium) or synthesised using neutron bombardment techniques (the transuranic elements: neptunium – lawrencium).

Uranium, the heaviest naturally occurring element on Earth, was first discovered in 1789 by M. H. Klaproth in Berlin.[3] The most abundant uranium ore is uraninite (pitchblende), $[U_3(O)_8]$. Other ores include carnotite $[K_2(UO_2)_2(VO_4)_2.3H_2O]$ and coffinite $[U(SiO_4)_{1-x}\{(OH)_4\}_x]$ (the degree of substitution of siloxide by hydroxides varies sample to sample).[4] The largest deposits of pitchblende can be found in Katanga Province (Dem. Rep. Congo), near the Great Bear Lake (Canada) and at Jáchymov (formerly Joachimsthal, Czech Republic),[4] although the most significant mining countries are Australia, Kazakhstan and Russia, who together comprised 50% of the global uranium production in 2014.[1]

Isolation of uranium from these ores is possible *via* leaching with H_2SO_4 in the presence of an oxidising agent to give uranyl, $[U(O)_2]^{2+}$. Neutralisation with ammonia affords "yellow cake", which can be converted to $[U(O)_3]$ by subsequent heating to 300 °C. $[U(O)_2]$ is produced by the reduction of $[U(O)_3]$ with hydrogen gas at 700 °C. Reaction of $[U(O)_2]$ with HF gives $[U(F)_4]$, before reduction with magnesium yields uranium metal. All uranium isotopes are radioactive (^{234}U, ^{235}U, ^{236}U and ^{238}U), with ^{238}U, the most stable and abundant isotope, having a half-life of 4.47×10^9 years and a natural abundance of 99.27%.

Whilst the chemistry of the uranyl fragment is the dominant area of uranium research, there is a burgeoning interest in the non-aqueous chemistry of uranium,[5]

towards which this thesis contributes. The starting uranium reagent for our chemistry is $[U(Cl)_4]$, which is prepared by the reaction of $[U(O)_3]$ with hexachloropropene.[6]

The lanthanide and actinide elements possess valence electrons in f-orbitals, of which there are seven degenerate orbitals, which can be represented in two ways. For cubic geometries, with symmetry related x, y and z axes, the cubic set is used, with the abbreviated Cartesian functions: f_{x^3}, f_{y^3}, f_{z^3}, f_{xyz}, $f_{z(x^2-y^2)}$, $f_{y(z^2-x^2)}$ and $f_{x(z^2-y^2)}$. If non-cubic geometries are present, then the general set is used instead: f_{z^3}, f_{xz^2}, f_{yz^2}, f_{xyz}, $f_{z(x^2-y^2)}$, $f_{x(x^2-3y^2)}$ and $f_{y(3x^2-y^2)}$. Three of the orbitals are common to both representations: f_{z^3}, f_{xyz} and $f_{z(x^2-y^2)}$.[7,8]

The lanthanides and actinides, whilst often grouped together, have different electronic properties that affect their reactivity. The 4f orbitals are highly contracted with a limited radial extension (they are "core-like") and consequently are rarely involved in bonding. This means that the chemistry of the lanthanides is broadly similar across the period, irrespective of the $4f^n$ count. In contrast, the 5f orbitals have a much greater orbital extension (due to the additional node and the indirect relativistic effect, *vide infra*), and therefore these orbitals become chemically available (valence orbitals). Furthermore, the radial extension is comparable to that of the 6d orbitals, and therefore mixing can occur between 5f and 6d orbitals (see figure **1.1.**).

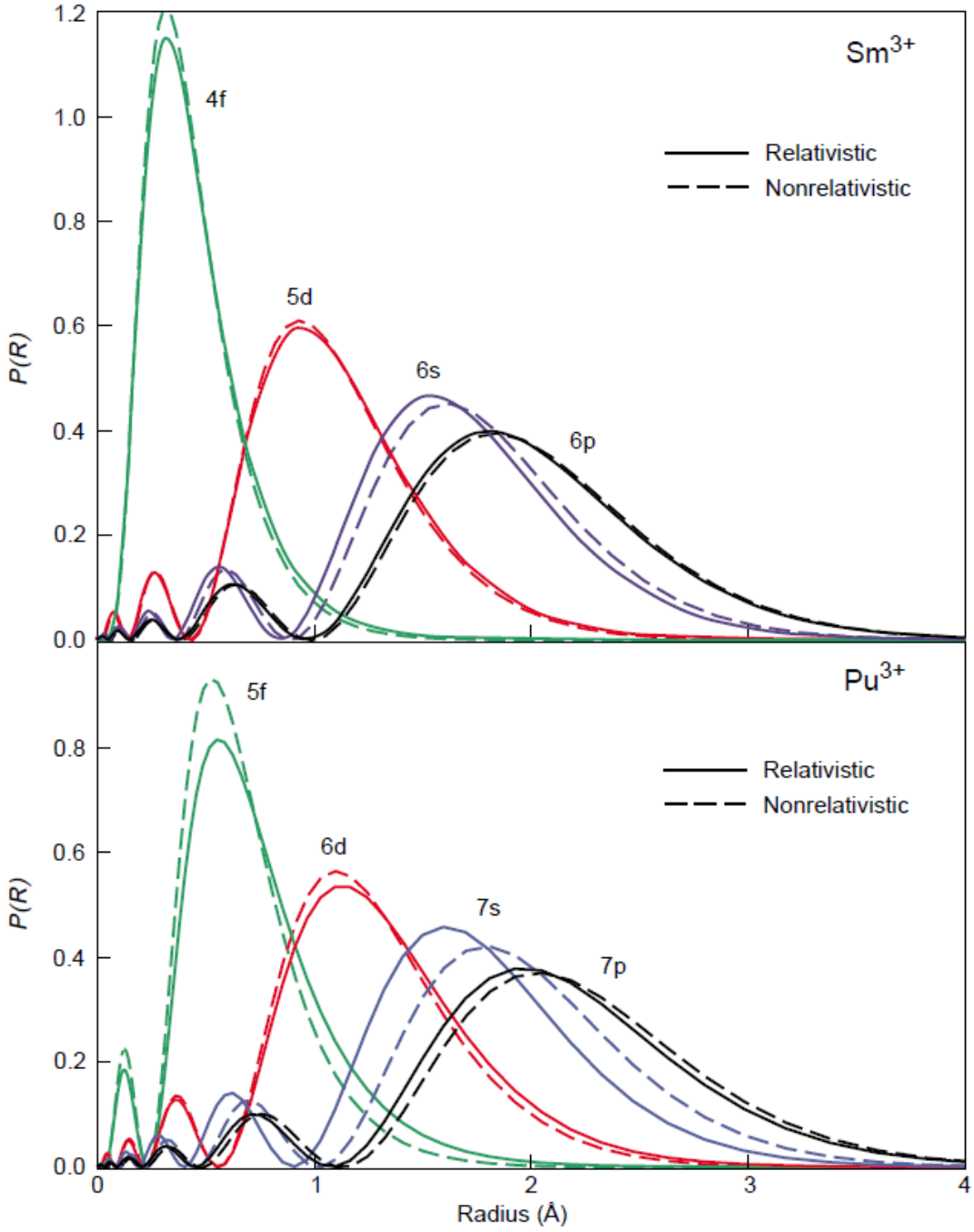


*Figure **1.1.** Relativistic radial distribution plots for Sm^{3+} and Pu^{3+}. Adapted from Clark.[9] The Pu^{3+} 6s and 6p orbitals are represented by dashed lines to indicate that these are normally considered as part of the [Rn] core.*

The degree to which 5f-6d mixing can occur was described by Bursten *et al.*[10] As can be seen by the plot of orbital energy calculations shown in figure **1.2.**, for Th^{3+}, there is a large 6d-5f separation. As the group is traversed, the relative energy of the

5f orbitals decreases and the 6d orbitals increases. This results in a cross-over at uranium, which therefore results in the most optimal mixing conditions being present for uranium system. Another implication of this is that uranium systems will be more covalent than corresponding thorium complexes, which can often be described as ionic.

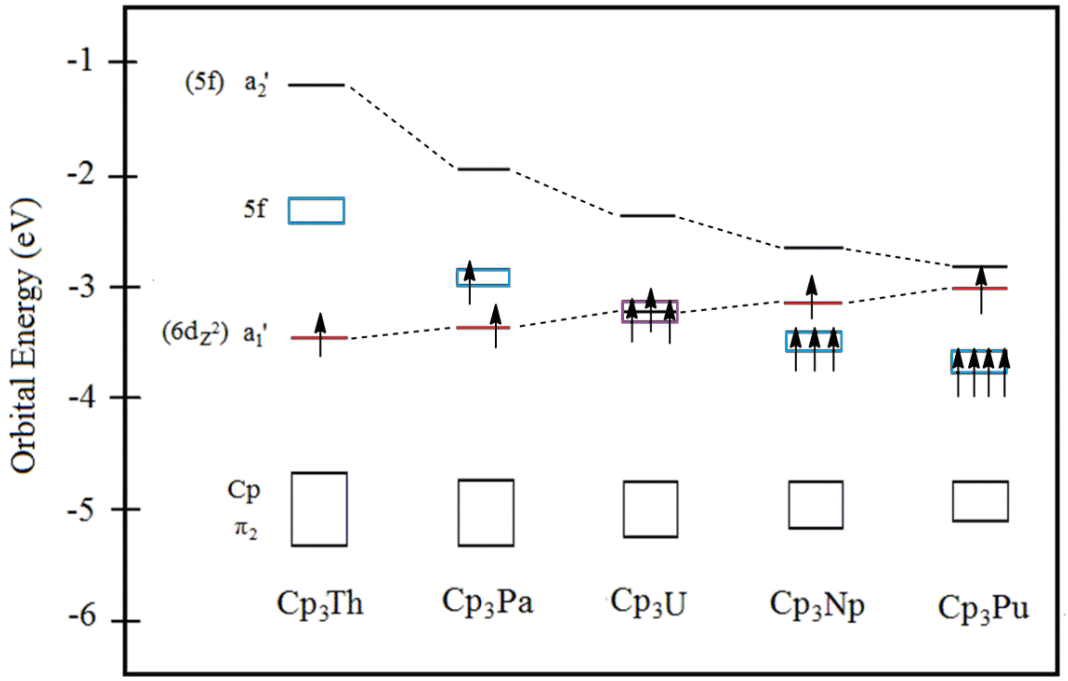


*Figure **1.2.** Metal-based orbital energies for the $5f^{n-1}6d^{1}$ electron configurations of planar $AnCp_3$ complexes (An = Th, Pa, U, Np, Pu). Adapted from Bursten et al.*[10]

For heavy elements, such as the actinides, relativistic effects become increasingly relevant. Einstein's special theory of relativity, wherein the mass of a particle tends to infinity as its velocity tends towards the speed of light (c), impacts on electrons; an electron in motion will have more mass that if it were stationary. This is the relativistic mass effect, and whilst negligible for lighter elements, it becomes considerable for larger elements, as the average radial velocity of the 1s electrons is proportional to Z (where Z is the atomic number). For uranium (Z = 92), this means that the velocity of the 1s electron in uranium is ~0.67c, and the mass of that electron is ~1.35 m_e.[11] The mass increase due to relativistic effects causes a marked contraction of the 1s orbital, which affords an energetic stabilisation. The other s-orbitals, and to a lesser degree the p-orbitals, also experience a contraction, as they

are orthogonal to the 1s orbital. This is the direct relativistic orbital contraction. The outer core s- and p-orbitals then provide increased nuclear shielding to d- and f-orbitals of a similar radial distribution, which causes the d- and f-orbitals to expand and become destabilised in comparison to non-relativistic analogues. This is the indirect relativistic orbital expansion. The destabilisation reduces the binding energy of the 5f electrons, where the 5f orbitals of a hypothetical non-relativistic uranium atom have a binding energy of 1665 kJ mol^{-1}, in contrast to the corresponding orbitals of a relativistic uranium atom which calculated by the same approach have a binding energy of 869 kJ mol^{-1}.[11] The destabilisation provides support for the greater range of oxidation states available to actinides, as they are more susceptible to electron removal.

The common range of oxidation states of uranium ions is +3 to +6 (electronic configurations of $5f^3$ to $5f^0$), and these have been investigated extensively. The +2 oxidation state ($5f^4$) has recently been isolated by the Evans and Meyer groups, as the complexes $[U(\eta^5\text{-}C_5H_4SiMe_3)_3][K(2,2,2\text{-crypt})]$[12] and $[U\{(^{AdMe}ArO)_3Mes\}][K(2,2,2\text{-crypt})]$[13] [2,2,2-crypt = 2,2,2-Kryptofix = $N\{(CH_2CH_2O)_2CH_2CH_2)\}_3N$, $\{(^{AdMe}ArO)_3Mes\}$ = 1,3,5-(1-O-2-Ad-4-Me-C_6H_2-2-CH_2-)$_3$-2,4,6-Me_3C_6, Ad = adamantyl, $C_{10}H_{15}$] respectively. In nature, the +6 oxidation state dominates due to the stability of the uranyl ion, $[U(O)_2]^{2+}$. In non-aqueous solvents, the +4 and +6 oxidation states are most prevalent, though the +3 and +5 oxidation states are gaining greater interest from chemists. The +3 oxidation state especially is being utilised as it undergoes a wealth of small molecule activation chemistry (see Section 6).[14,15]

The Schrödinger equation, as it does not treat time and space equally, is not compatible with the special theory of relativity. An alternative form of the Schrödinger equation was proposed by Dirac which involved electron spin (an extra in non-relativistic quantum mechanics). When an electron is part of an atom, its spin angular momentum and orbital angular momentum couple.

In the d-block, this spin-orbit coupling is small (< 200 cm^{-1}) and crystal field effects dominate the electronic environment (Δ_o ~ 15000 – 25000 cm^{-1}). For the lanthanides, the reverse is the case (small crystal field < 100 cm^{-1}, spin-orbit coupling can be

large > 1000 cm^{-1}). By contrast, for the actinides, the magnitudes of these effects are considerably more similar (~1000 cm^{-1} for crystal field effects, and ~2000 cm^{-1} for spin orbit coupling), and therefore both must be considered, i.e. there is an interaction between the spin angular momentum (*S*) and orbital angular momentum (*L*).

There are two limiting approaches to describing the electronic states of atoms: Russell-Saunders (*LS*) coupling, and *j-j* coupling. *LS* coupling is most appropriate when spin-orbit coupling is weak when compared to inter-electronic repulsions (i.e. for d-block metals), whilst *j-j* coupling is more appropriate for the reverse case (spin-orbit coupling is strong compared to inter-electronic interactions).

In Russell-Saunders coupling, the total atomic orbital angular momentum (*L*, the sum of individual orbital angular momenta, m_l) and the total spin angular momentum (*S*, the sum of the individual electronic spin angular momenta, m_s) couple to give a third quantum number, *J*. The combination of *L* (described with spectroscopic notation, i.e. 0 = S, 1 = P, 2 = D, 3 = F, 4 = G, etc.), with the spin multiplicity (2*S*+1), and *J* (which ranges from *L*+*S*, *L*+*S*-1… |*L*-*S*|) gives a term symbol of the form $^{(2S+1)}\boldsymbol{L}_J$. Using Hund's rules, the ground state can be determined (the ground state is the one with the largest values for *L* and *S*, and if the subshell is less than half-full, the lowest value of *J* is lowest in energy). The electronic configuration and ground states for the common uranium ions are U^{III} ($5f^3$, $^4I_{9/2}$), U^{IV} ($5f^2$, $^3H_4$), U^{V} ($5f^1$, $^2F_{5/2}$) and U^{VI} ($5f^0$, $^1S_0$).

For *j-j* coupling, first *L* and *S* combine to give a total angular momentum for each electron, which is denoted *j*. The coupling of these *j* then produces the total atomic angular momentum, *J*. As a result of the different ordering of the coupling of *L* and *S*, the total *J* can be different to that derived *via LS* coupling. A simple example which illustrates the contrasting answers the two scheme give is if we consider the first excited state of helium (i.e. $1s^1\ 2p^1$), then under *LS* coupling, we arrive at states $^1P_1$, $^3P_0$, $^3P_1$ and $^3P_2$, *via* $S = |s_1 + s_2| \ldots |s_1 - s_2|$ ($S = 0, 1$), $L = |l_1 + l_2| \ldots |l_1 - l_2|$ (L = 1 = P), and $J = |L + S| \ldots |L - S|$. Under *j-j* coupling, $j_n = |l_n + s_n| \ldots |l_n - s_n|$ ($j_1 = 1/2$, $j_2 = 1/2, 3/2$), which couple as $J = |j_1 + j_2| \ldots |j_1 - j_2|$ to give J = 0 or 1, and 1 or 2.

Therefore, where *LS* coupling afforded a singlet and a triplet state, *j-j* coupling affords two doublets. This is visualised in figure **1.3.**

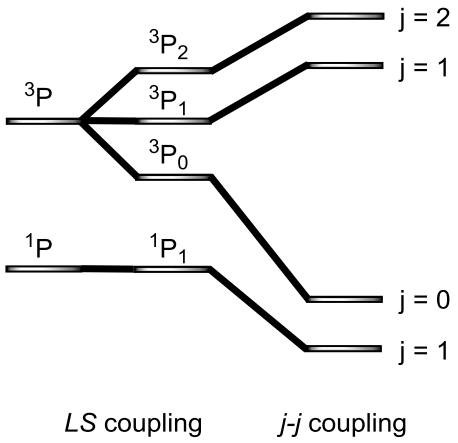


*Figure **1.3.** Descriptions of the electronic structure of the first excited state of helium.*

For the actinides, where inter-electronic repulsions and spin-orbit coupling are similar in energy, and neither dominates, neither approach to describing the states is truly accurate, though both are still useful to begin to describe their electronic states, and *LS* coupling is used to designate the ground term.[11] Final limitations of the use of Russell Saunders terms for actinides arise due to the high density of excited states, as well as that the ground state is not well isolated. Therefore, the *LS* term can only be used as a starting point for spectroscopic understanding.

For the d-block, magnetic behaviour is governed by the ground state, and theoretical magnetic moment (μ_{eff}) can be predicted by $\mu_{eff} = \{4S(S+1) + L(L+1)\}^{1/2}$. For f-block elements, as *L* and *S* couple (see above) we must consider *J* states. From the Russell-Saunders ground state electronic term, we can calculate a theoretical magnetic moment using the Landé equation: $\mu_{eff} = g_J\{J(J+1)\}^{1/2}$, where $g_J = 3/2 + \{S(S+1) - L(L+1)\}/\{2J(J+1)\}$.

The Landé equation predicts room temperature magnetic moments of 3.62 μ_B for U^{III}, 3.58 μ_B for U^{IV} and 2.54 μ_B for U^{V}, though experimentally derived values are wide ranging and overlapping.[16] Perhaps more diagnostic magnetic data for uranium species are the variable temperature magnetic moment traces. For uranium(III), ($5f^3$),

which has a spin multiplicity of a quartet at room temperature ($^4I_{9/2}$), at low temperatures two electrons spin pair, to give a spin multiplicity of a doublet at 1.8 K. The variable temperature SQUID (super-conducting quantum interference device) plot therefore tends to 2 μ_B at 1.8 K. For uranium(IV), ($5f^2$), at room temperature it has a triplet multiplicity ($^3H_4$) which spin pairs to a singlet at low temperatures, tending to 0 μ_B. Values can be larger than this (*ca*. 0.3 – 0.5 μB at low temperatures) due to temperature independent paramagnetism arising from the crystal field.[17] Finally, the single unpaired electron of uranium(V) ($5f^1$, $^2F_{5/2}$) is a doublet at all temperatures, usually exhibiting Curie-Weiss behaviour, which tends to 1 μ_B at low temperatures. The effective magnetic moments diminish with decreasing temperature as a result of the depopulation of low lying excited states. The difference between the low temperature magnetic moments for the doublet states of uranium(III) and uranium(V) arises due to the degree of separation between the ground state and the low lying excited states. Uranium(V) exhibits a greater degree of separation of these states, and hence a lower low temperature magnetic moment, whilst there is more mixing between the low-lying states of uranium(III), which increases its low temperature magnetic moment.

A consequence of *J* not being a good quantum number (due to 5f orbital interaction with the ligand environment and an increase in spin-orbit coupling) is that electronic absorption spectra are more difficult to interpret, as spectra vary due to oxidation state and ligand environment (the 5f orbitals are not core-like). Despite this, some general observations can be made for actinide spectra. Though the electron dipole and Laporte selection rules forbid f-f and d-d transitions, due to vibronic coupling (resulting from more covalent interactions between 5f orbitals and ligand environments), these transitions are stronger in actinide complexes than in lanthanides. The proximity of the energy levels of the 5f and 6d orbitals means that f-d transitions occur in the UV region for actinide complexes. Ligand to metal charge transfer transitions are fully allowed, with band maxima often in the UV region tailing into the visible region, accounting for the intense colours of some actinide complexes.

Uranium(III) complexes are often strongly absorbing in the UV region, as a result of multiple transitions arising due to excitation into a $5f^2\ 6d^1$ configuration, which begins at approximately 23000 cm^{-1}. For uranium(IV), which has a ground state of $^3H_4$, the electronic absorption spectrum is split by spin-orbit coupling. However, the $5f^2$ electronic configuration yields multiple f-f transitions which are of low intensity and difficult to interpret. This is in contrast to uranium(V), where there is only one electron ($5f^1$), and therefore f-f transitions are sharp, though weak ($\varepsilon < 50\ dm^3\ mol^{-1}\ cm^{-1}$). The transitions can be predicted based on a treatment first by splitting due to spin-orbit coupling, to give two *J* multiplets, with a ground state of $^2F_{5/2}$. These are then split again by the ligand crystal field into (2*J*+1)/2 doubly degenerate levels, resulting in four f-f transitions. These are described with double-group theory labels (*Γ*) to consolidate the combination of half integer spin (*S* = ½) and integer orbital (*L* = F = 3) contributions. As the splitting into (2*J*+1)/2 levels is crystal field dependent, the coordination geometry at uranium dictates the electronic absorption spectrum. This splitting is further explored for C_{3v} and O_h symmetries in Chapters 2 and 6 respectively, alongside an *ab initio* calculation of the energy levels for uranium(V) systems in Chapter 4. The use of double group theory to identify the expected absorptions (as will be seen in Chapters 2 and 6) contrasts to the *ab initio* calculation of m_j terms, (as will be seen in Chapter 4), and the use of m_j terms allows for a more tuneable understanding of the spectra produced. Uranium(VI) complexes have a closed shell ($5f^0$) configurations, and so therefore cannot exhibit f-f transitions, and their UV-vis-NIR spectra are typically dominated by charge transfer bands.

1.2.Introduction to Tren chemistry

1.2.1. Transition metal chemistry

The *tris*(2-amidoethyl)amine ["$Tren^R$", $\{N(CH_2HC_2NR)_3\}^{3-}$, R = H, alkyl, aryl, silyl etc] ligand has been widely studied over the last 25 years, and has found utility across the Periodic Table. Verkade, in a review of 1993,[18] describes a raft of "azatrane" (Tren) complexes of the p-block (including complexes of B, Al, Si, Ge, Sn and P), alongside "atrane" complexes ($\{N(CH_2CH_2O)_3\}^{3-}$, of Ti, Si, Ge, and P),

and this marks the beginning of the exploration of the chemistry of these ligand systems. Prior to the research of Verkade *et al.*,[18] the only examples of crystallographically characterised complexes of this type were the "atrane" complexes $[Pt(Cl)(PNMe_2Ph)_2\{Si(OCH_2CH_2)_3N\}]$[19] and $[\{Si(CH_2CH_2CH_2)_3N\}_2(\mu\text{-}O)]$.[20]

The first d-block metal Tren complexes were reported by Schrock *et al.* in 1992.[21] They reported the crystallographically characterised complex $[V(Tren^{TMS})(Cl)]$ (figure **1.4.**) alongside the titanium analogue $[Ti(Tren^{TMS})(Cl)]$. Both complexes were prepared in a facile manner *via* a salt elimination methodology, by the reaction of $[MCl_4L_2]$ (M = Ti, L = THF; M = V, L_2 = DME) with $Tren^{TMS}Li_3$, $[N\{CH_2CH_2N(SiMe_3)Li\}_3]$.[21,22] The complexes $[M(Tren^{TMS})(Cl)]$ (M = Ti, V) were assumed to be isostructural on the basis of their identical IR spectra.

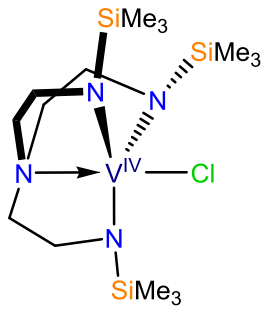
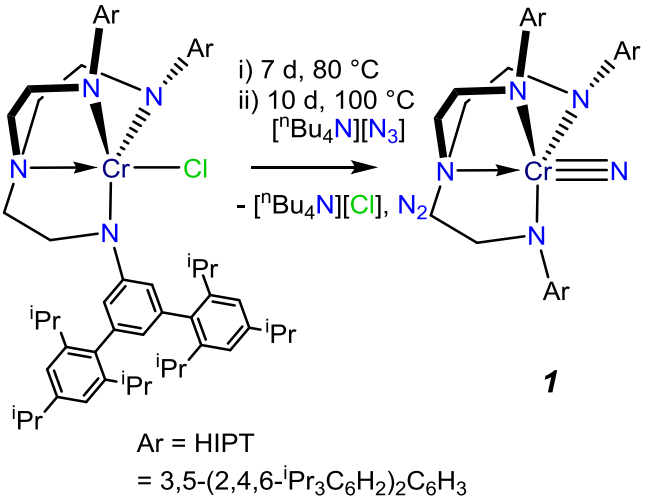


*Figure **1.4.** Complex $[V(Tren^{TMS})(Cl)]$*

Since this first report of d-block complexes of Tren, there has been a great deal of research into complexes of this type, which have been reviewed thoroughly by other authors.[23] Perhaps the most relevant species to discuss here are the examples of Tren-transition metal nitrides. These have all been prepared utilising aryl substituents on the amide nitrogens.

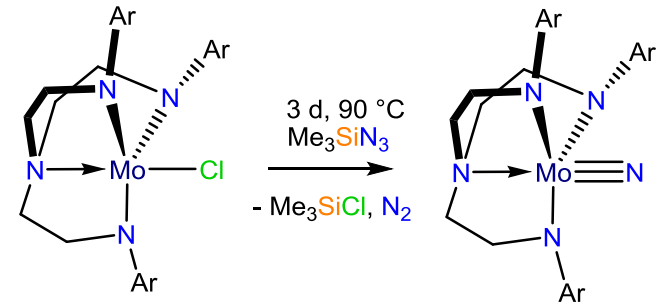
The chromium(VI)–nitride $[Cr(Tren^{HIPT})(N)]$ [**1**, HIPT, hexa-*iso*-propylterphenyl = 3,5-(2,4,6-$^{i}Pr_3C_6H_2)_2C_6H_3$] was prepared in 69% yield by a two stage reaction of $[Cr(Tren^{HIPT})(Cl)]$ with $[^{n}Bu_4N][N_3]$.[24] Heating a mixture of $[Cr(Tren^{HIPT})(Cl)]$ and $[^{n}Bu_4N][N_3]$ in benzene at 80 °C for 1 week, followed by the removal of $[^{n}Bu_4N][Cl]$ and excess $[^{n}Bu_4N][N_3]$ and heating the resultant mixture in toluene at 110 °C for 10 days affords **1** (scheme **1.1.**). Crystallisation of the reaction mixture after the initial

heating period (80 °C, 3 days, benzene) afforded a mixture of [Cr(Tren^{HIPT})(Cl)] and [Cr(Tren^{HIPT})(N_3)] (65:35), while heating at 100 °C for 5 days in benzene afforded a mixture of [Cr(Tren^{HIPT})(N_3)] and **1** (50:50). The two stage synthetic procedure optimises the ligand exchange and denitrification steps.



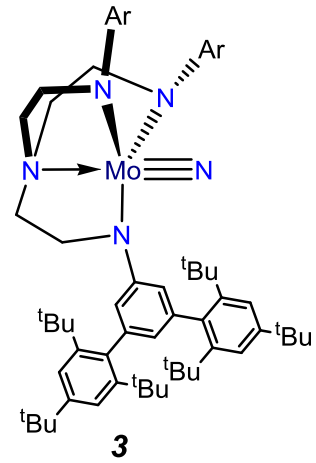
*Scheme **1.1.** Synthesis of **1**.*

Contrastingly, the reaction of [Mo(Tren^{HIPT})(Cl)] with two equivalents of Me_3SiN_3 at 90 °C afforded the nitride complex [Mo(Tren^{HIPT})(N)] (**2**) quantitatively over the course of 3 days (77% yield, scheme **1.2.**).[25] A moderate yield of nitride product could also be prepared by reaction of [Mo(Tren^{HIPT})(Cl)] with NaN_3 upon stirring for two days in THF at room temperature. An identical method was later utilised for the preparation of the {Tren^{HTBT}} analogue [Mo(Tren^{HTBT})(N)] [**3**, HTBT, hexa-*tert*-butylterphenyl = 3,5-(2,4,6-$^tBu_3C_6H_2)_2C_6H_3$, figure **1.5.**].[26]



Ar = HIPT
= 3,5-(2,4,6-$^{i}Pr_3C_6H_2)_2C_6H_3$ ***2***

*Scheme **1.2.** Synthesis of **2***

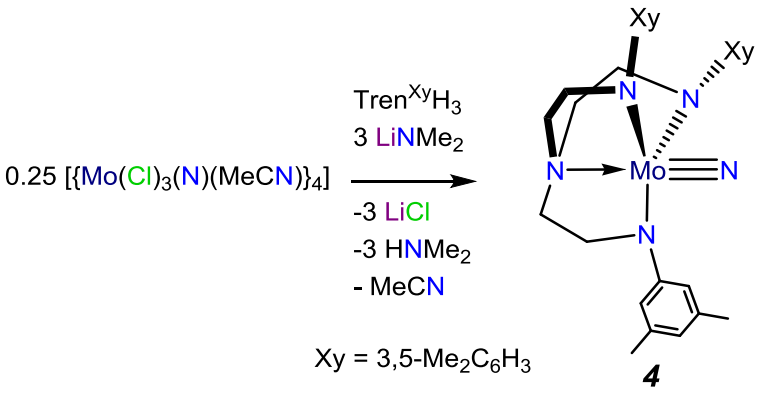


3

Ar = HTBT
= 3,5-(2,4,6-$^{t}Bu_3C_6H_2)_2C_6H_3$

*Figure **1.5.** Complex **3**.*

Finally, [Mo(Tren^{Xy})(N)] [**4**, Tren^{Xy} = (3,5-$Me_2C_6H_3$*N*$CH_2CH_2)_3$*N*] can be prepared either *via* an analogous method to that described above for **1**, **2** and **3** (chloride substitution of [Mo(Tren^{Xy})(Cl)] with Me_3SiN_3, then thermolytic N_2 elimination), or more conveniently by ligand exchange by addition of Tren$^{Xy}H_3$ to [{$Mo(Cl)_3$(N)(MeCN)}$_4$], utilising [$LiNMe_2$] to induce ligand deprotonation and salt elimination of lithium chloride to afford **4** in good yield (scheme **1.3.**).[27]



*Scheme **1.3.** Synthesis of **4**.*

A comparison of the preparations of **1**, **2**, **3** and **4**, and other methods towards transition metal nitride species are discussed in more detail in Section 3.

1.2.2. Highlights from f-block chemistry

1.2.2.1.Uranium

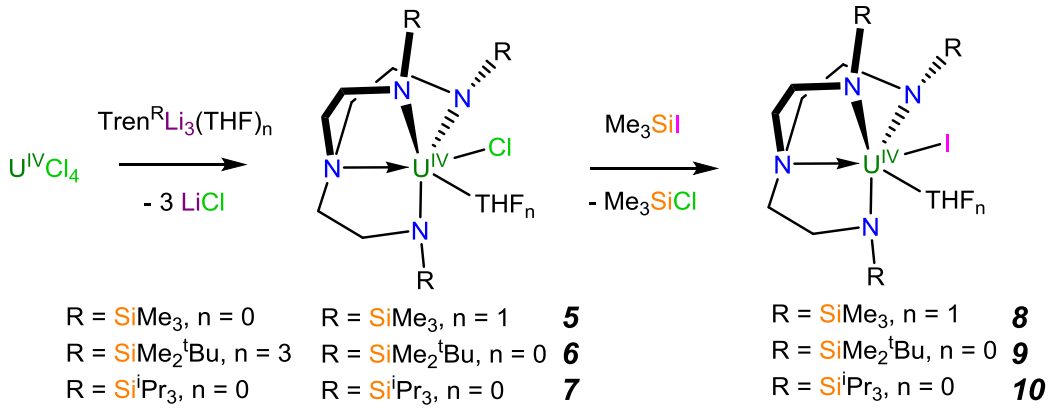
This section aims to outline the chemistry of Tren derived uranium complexes, to give the reader a feel for the chemistry in the area that this body of work is based upon. The reader will be notified of work that occurred concurrently to this research, and work which has derived in part from work which is presented herein, to inform the reader of the chronology of this chemistry.

Unlike d-block systems featuring the Tren framework, which utilise a wide array of substituents at the amide nitrogens, including alkyl, aryl and silyl substituents (though this generalisation does not do justice to the breadth and variety of systems prepared), uranium systems reported in the literature use only silyl substituents. Specifically, uranium is supported by $\{Tren^{TMS}\}^{3-}$, $\{Tren^{DMBS}\}^{3-}$ and $\{Tren^{TIPS}\}^{3-}$ [$N(CH_2CH_2NR)_3^{3-}$, R = $SiMe_3$, $SiMe_2{}^tBu$ and Si^iPr_3, respectively, ^{i}Pr = *iso*-propyl]. More recently, $\{Tren^{TPS}\}^{3-}$ (TPS = $SiPh_3$) has also been utilised for complexes of uranium.[28]

In the overwhelming majority of cases, the Tren framework is installed at uranium by means of salt elimination chemistry. The reaction of lithiated pro-ligand

[(Tren^{R})Li$_3$] with [U(Cl)$_4$] in THF affords [U(Tren^{R})(Cl)(THF)$_n$] (n = 1: R = TMS, **5**; n = 0: R = DMBS, **6**, TIPS, **7**, scheme **1.4.**).[29-31] A solvent free formulation for the Tren^{TMS} congener can be prepared by the sublimation of **5**, which affords the dinuclear complex [{U(Tren^{TMS})}$_2$(μ-Cl)$_2$].[32]

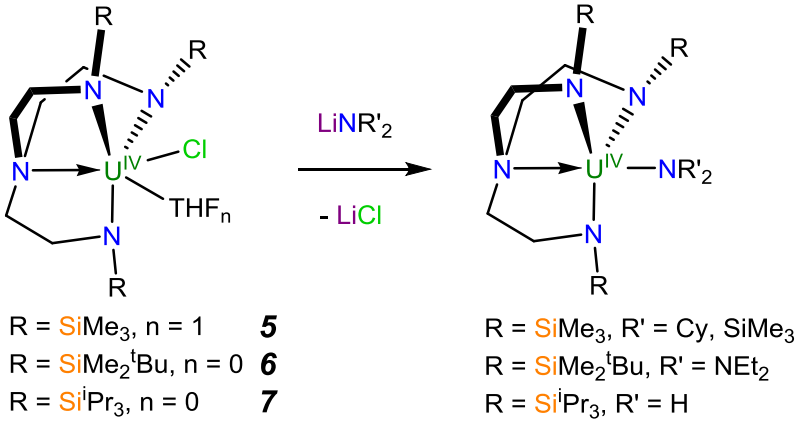
Halogen exchange reactions can be enacted utilising Me$_3$SiX (X = Br: R = DMBS; X = I: R = TMS, DMBS, TIPS) to afford [U(Tren^{R})(X)(THF)$_n$] (X = Br, R = DMBS, n = 0. X = I, n = 1: R = TMS **8**; n = 0: R = DMBS, **9**, TIPS, **10**, scheme **1.4.**).[30,33,34] Again, sublimation of **8** affords the solvent free dinuclear species [{U(Tren^{TMS})}$_2$(μ-I)$_2$].[35] The complexes were identified by NMR spectroscopy, elemental analysis, and single crystal X-ray diffraction studies, with the exception of the Tren^{TIPS} congener, **10**, for which X-ray diffraction studies were not able to be performed.



*Scheme **1.4.** Syntheses of uranium(IV)–halides [U(Tren^{R})(X)(THF)$_n$], **5** – **10**.*

Substitution of the chloride ligand in **6** by reaction with [LiNEt$_2$] afforded [U(Tren^{DMBS})(NEt$_2$)] (scheme **1.5.**).[30] This tetraamide is also the product of the amine elimination route towards the installation of Tren at uranium, as prepared by the reaction of half an equivalent of [{U(NEt$_2$)$_4$}$_2$] with protonated pro-ligand {Tren^{DMBS}H$_3$}.[30]

Several other Tren derived uranium(IV)–amides have been reported, as prepared *via* a salt elimination strategies. These include [U(Tren^{TMS})(NR′$_2$)], (R′ = Cy, SiMe$_3$),[35] and the primary amide [U(Tren^{TIPS})(NH$_2$)], see scheme **1.5.**[34,36]



*Scheme **1.5.** Syntheses of uranium(IV)–amides, [U(Tren^{R})(NR'$_2$)]*

Analogously to the preparation of uranium amide species, other U-N linkages can be prepared by salt elimination methodologies. The azide ligand (N_3^-) was installed at uranium to afford [U(Tren^{R})(N_3)]$_n$ (R = TMS, n = ∞, R = DMBS, n = 4, R = TIPS, n = 1, figure **1.6.**).[34,37] For Tren^{TMS} substituted uranium azides, this product is a polymeric chain [U(Tren^{TMS})(N_3)]$_\infty$ (**11**), wherein the azide ligands are bridging two uranium centres in a {μ-η^1*(N)*:η^1*(N″)*-N=N′=N″} fashion, and consequently each uranium features two mutually *cis* azide functionalities. Similarly, the Tren^{DMBS} analogue does not possess enough steric hindrance to prevent the coordination of two azide ligands to each uranium, however here, the resultant product is a tetramer, [{U(Tren^{DMBS})(N_3)}$_4$], **12**, with a similar bridging motif. In the case of Tren^{TIPS}, the steric bulk is large enough to prevent bridging connectivity, and consequently the monomeric species [U(Tren^{TIPS})(N_3)], **13**, is formed.[34] Azide groups are known precursors towards transition metal nitrides (*vide infra*, Section 3), often *via* photolysis or thermolysis routes, and this makes these species candidates for preparation of uranium nitrides. This will be discussed in due course (*vide infra*, Section 4).

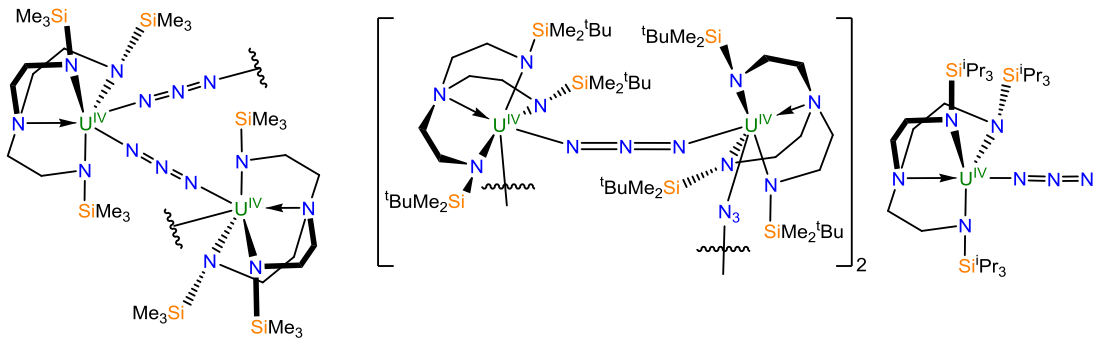
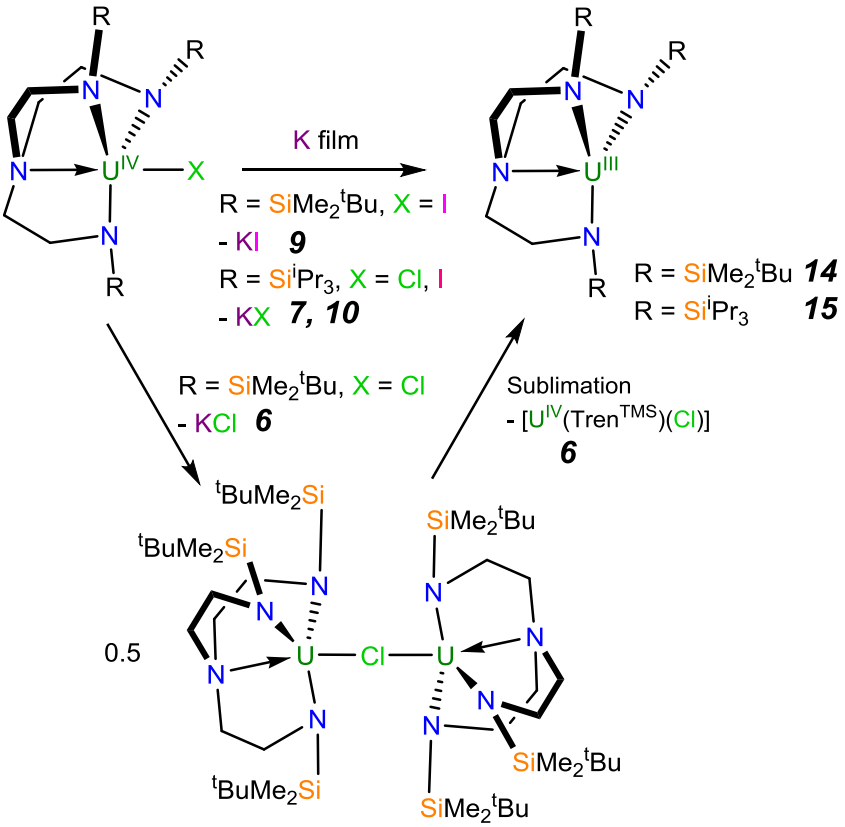


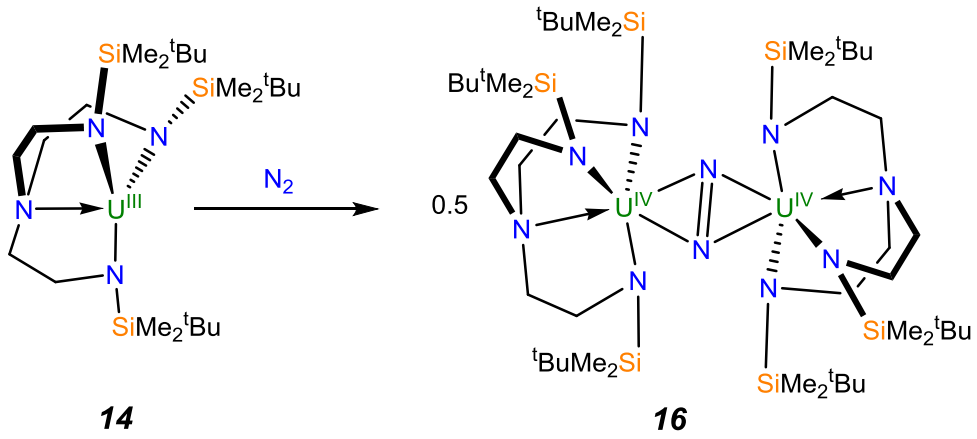
Figure ***1.6.*** *Solid state structures of [U(Tren^{R})(N$_3$)] (**11**, **12**, **13**).*

Reduction of the chlorides [U(Tren^{R})(Cl)] to the corresponding trivalent species [U(Tren^{R})] is possible for R = DMBS (**6**) (under an argon atmosphere, see below) and R = TIPS (**7**), though not without considerable effort on the part of the synthetic chemist. In the case of Tren^{TIPS},[31] stirring **7** over a potassium film for several days affords a slow colour change from green to dark purple. This is commensurate with the proposed trivalent species, [U(Tren^{TIPS})], **15**, and indeed crystallographic characterisation amongst other data are in agreement with this formulation. The same procedure is initially followed for the preparation of the DMBS congener. However, reduction of **6** over a potassium mirror does not effect the complete conversion to the trivalent species. Instead, the mixed valent uranium(III/IV) chloride bridged species, [{U(Tren^{DMBS})}$_2$(μ-Cl)] is formed.[38] Sublimation of this species affords the regeneration of the uranium(IV)–chloride precursor **6** and the desired trivalent product [U(Tren^{DMBS})], **14**.[38] If **9** is used instead of **6**, then **14** prepared by reduction over a mirror directly, without the need for fractional sublimation (see scheme **1.6.**).[39]



*Scheme **1.6.** Syntheses of [U(Tren^{R})], (**14**, **15**).*

Interestingly, upon exposure of samples of **14** to atmospheres of dinitrogen the bridged species [{U(Tren^{DMBS})}$_2$(μ^2-η^2:η^2-N$_2$)] (**16**) is formed (scheme **1.7.**).[40,41] Complex **14** is stable under an argon atmosphere, however contact with polar solvents must be rigorously avoided. No such activation of dinitrogen is observed for **15**, which is attributed to the larger steric bulk of the silyl substituents compared to **14**, which prevents side-on access for dinitrogen to the metal centre. In scheme **1.7.**, complex **16** is drawn featuring bonds to the nitrogen atoms. This accounts for change balancing in complex **16**. The authors do note, however, that the N-N bond distance in the dinitrogen fragment in **16** is 1.109(7) Å, virtually unchanged from that of the equivalent distance in dinitrogen gas (1.0975 Å), and hence they propose that the bonding is dative, with the uranium centres acting as extremely potent Lewis acids.



14 **16**

*Scheme **1.7.** Synthesis of **16**.*

From this point, Tren–uranium chemistry has expanded into areas such as uranium–metal bonds,[33,42,43] small molecule activation[44] and supporting multiple bond interactions with p-block elements.[31,36,45-47] The most consequential of these (with regard to this thesis) is the preparation of the first terminal uranium nitride species isolable at room temperature, and this will be discussed in Section 4.[31] For a more comprehensive review of Tren–uranium chemistry, the reader is directed towards a review written by Liddle and Gardner.[48]

1.2.2.2.Thorium

In contrast to uranium, the triamidoamine chemistry of thorium is relatively unexplored. The first reports of Tren-thorium chemistry came from Scott in 1994, alongside the report of $[\{U(Tren^{TMS})\}_2(\mu\text{-}Cl)_2]$. The thorium congener was identified by NMR spectroscopy and mass spectrometry, though its crystal structure was not determined.[32]

In a similar fashion, thorium analogues of $[U(Tren^{TMS})(C_5R_5)]$ (R = H, Me), $[U(Tren^{TMS})(H_3BH)(THF)]$, $[\{U(Tren^{TMS})(H_3BH)\}_2]$ and $[\{U(Tren^{TMS})(\mu\text{-}O^tBu)\}_2]$ are reported, as identified by NMR spectroscopy, though again crystal structures are only reported for the uranium congeners.[49]

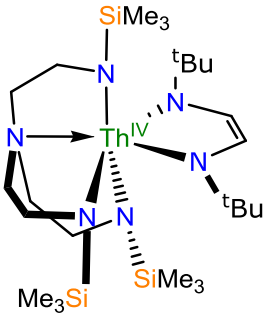


*Figure **1.7.** Solid state structure of [Th(Tren^{TMS})(^{t}Bu$_2$DAB)].*

The first (and so far only) crystal structure for a Tren^{TMS}-thorium complex was reported in 1995, and is the diazabutadiene complex [Th(Tren^{TMS})(^{t}Bu$_2$DAB)] (^{t}Bu$_2$DAB = ^{t}BuNCHCHN^{t}Bu, figure **1.7.**).[50] The bond lengths within the diazabutadiene fragment are consistent with the singly reduced radical anion formulation [i.e. ^{t}Bu$_2$DAB$^{\bullet-}$], commensurate with the assignment of a thorium(IV) centre.

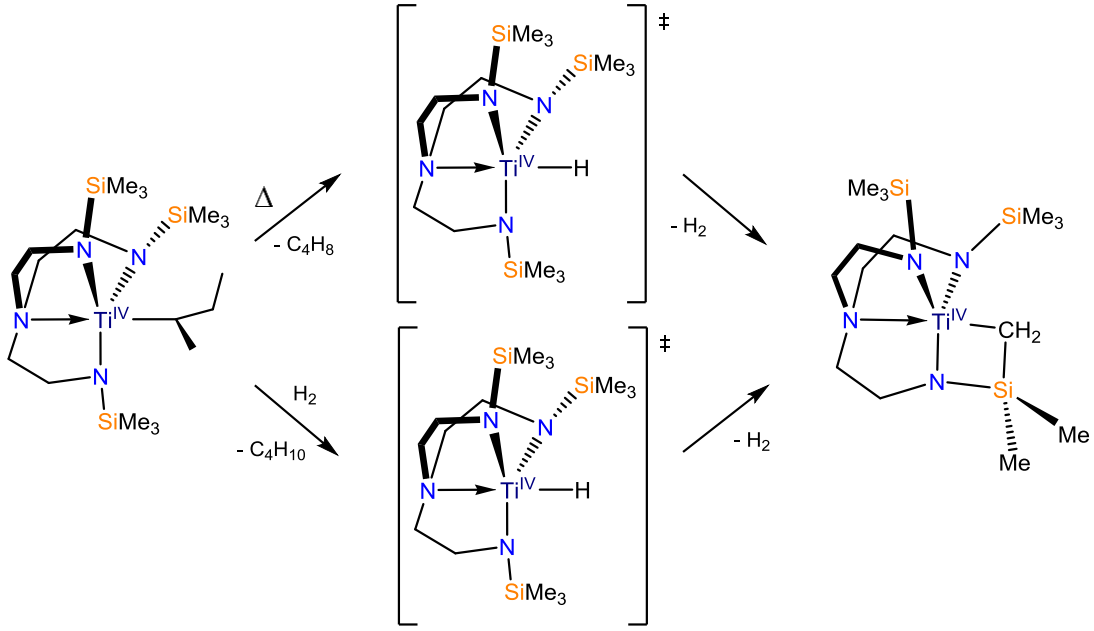
The Tren^{DMBS} complexes [Th(Tren^{DMBS})(Cl)], [Th(Tren^{DMBS})(Br)], [Th(Tren^{DMBS})(I)] (**17**) and [Th(Tren^{DMBS})(NEt$_2$)] were first reported alongside their uranium analogues, as identified by NMR spectroscopy.[30] The crystals structures for [Th(Tren^{DMBS})(Cl)(THF)], [Th(Tren^{DMBS})(I)] (**17**) and [Th(Tren^{DMBS})(NEt$_2$)] were later reported by Liddle *et al*.[51]

Prior to this work there were no examples of thorium Tren^{TIPS} complexes, which are presented in Chapter 3.

1.2.3. Triamidoamine cyclometallates

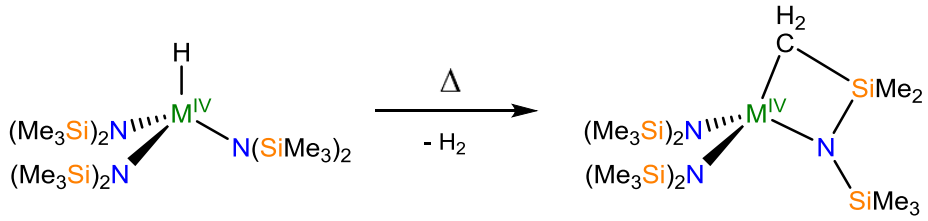
There are several examples of Tren-derived cyclometallate complexes of both transition metals and actinides. [Ti(Tren^{TMS})(^{s}Bu)] cleanly converts to the cyclometallated complex [Ti{*C*H$_2$Si(Me)$_2$*N*CH$_2$CH$_2$*N*(CH$_2$CH$_2$*N*SiMe$_3$)$_2$}] upon heating or the addition of H$_2$ (scheme **1.8.**).[52] The mechanism for the former invokes *β*-hydride elimination, with the loss of butenes and H$_2$, whilst the latter adds H$_2$ across the Ti-C bond *via* σ-bond metathesis, with the elimination of butane. Schrock *et al.* reported a resonance at δ = 8.29 ppm during the reaction promoted by

dihydrogen, which they tentatively assigned to the monohydride in [Ti(Tren^{TMS})(H)] prepared by hydrogenolysis.



*Scheme **1.8.** Synthesis of [Ti{$CH_2Si(Me)_2NCH_2CH_2N(CH_2CH_2NSiMe_3)_2$}]*

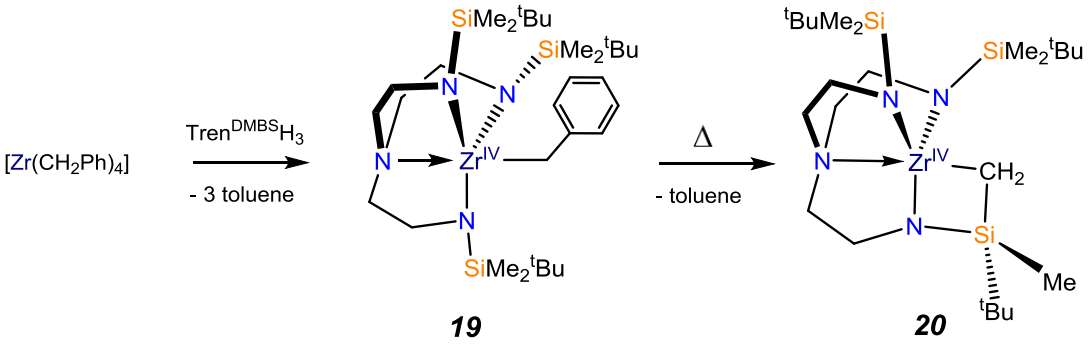
The observation of a hydride intermediate was shown in a related system [M{$N(SiMe_3)_2$}$_3$(H)] (M = Th, U) which lost H_2 upon cyclisation to yield [M{$CH_2Si(Me)_2NSiMe_3$}{$N(SiMe_3)_2$}$_2$] (scheme **1.9.**).[53]



*Scheme **1.9.** Preparation of [M{$CH_2Si(Me)_2NSiMe_3$}{$N(SiMe_3)_2$}$_2$] (M = Th, U).*

Waterman *et al.* have prepared the Tren^{TMS} cyclometallated zirconium species, namely [Zr{$CH_2Si(Me)_2NCH_2CH_2N(CH_2CH_2NSiMe_3)_2$}], (**18**) from the reaction [$Zr(CH_2Ph)_4$] with Tren$^{TMS}H_3$, and it was noted that this reaction is facile, and unlike for [Ti(Tren^{TMS})(^{s}Bu)], forcing conditions were not required to prepare the cyclometallated complex.[54]

In [Zr(CH$_2$Ph)$_4$], the benzyl groups act as bases and therefore deprotonate the pro-ligand. This protonolysis chemistry is utilised in the installation of Tren^{TMS} at zirconium. There is however a fourth deprotonation, of a methyl substituent (in a trimethylsilyl ligand arm) as opposed to an amine functionality, which results in the formation of **18**. Contrastingly, the benzyl complex [Zr(Tren^{DMBS})(CH$_2$Ph)], **19**, can be prepared for the Tren^{DMBS} system (scheme **1.10.**).[55] Complex **19** is the only example thus far of a benzyl substituent on a silyl Tren complex, where the silyl groups are thought to facilitate cyclometallation.[56] Heating **19** under vacuum afforded the cyclometallated complex [Zr{*C*H$_2$Si(Me)(^{t}Bu)*N*CH$_2$CH$_2$*N*(CH$_2$CH$_2$*N*SiMe$_2$^{t}Bu)$_2$}], **20**, *via* elimination of toluene.[55] Complex **20** could also be prepared by the reaction of **19** with H$_2$, analogously to [Ti(Tren^{TMS})(^{s}Bu)].[52]

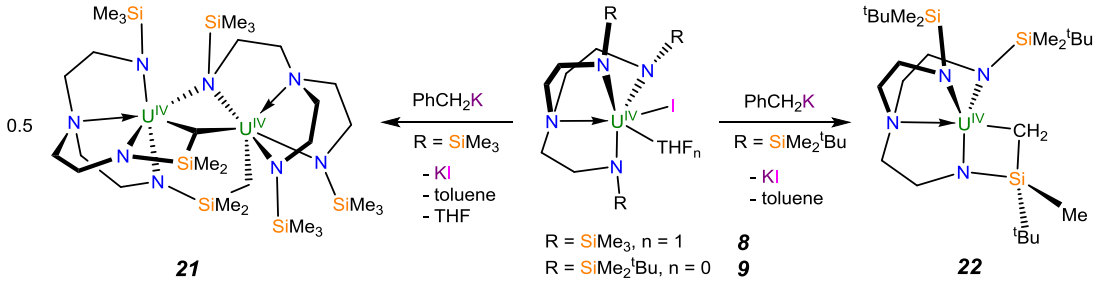


*Scheme **1.10.** Synthesis of **19** and **20**.*

The isolable molybdenum hydride complex [Mo(Tren^{TMS})(H)] evolves dihydrogen when heated to 100 °C to form the cyclometallated complex [Mo{*C*H$_2$Si(Me)$_2$*N*CH$_2$CH$_2$-*N*(CH$_2$CH$_2$*N*SiMe$_3$)$_2$}],[57] in parallel to the isolation of [Ti(Tren^{TMS})(^{s}Bu)]. This loss of H$_2$ from [Mo(Tren^{TMS})(H)] was shown to be reversible and the addition of D$_2$ to [Mo{*C*H$_2$Si(Me)$_2$*N*CH$_2$CH$_2$*N*(CH$_2$CH$_2$*N*SiMe$_3$)$_2$}], yielded [Mo(Tren^{TMS})(D)], with the second deuterium located on a TMS group.

Similarly, reaction of Tren–uranium halides with benzyl potassium (PhCH$_2$K) affords cyclometallated uranium–alkyl species. The form of these species is dependent upon the silyl ligand employed. For Tren^{TMS}, reaction of **8** with benzyl potassium affords, by the loss of KI, PhCH$_3$ and the coordinated THF, half an

equivalent of the dinuclear cyclometallated tuck-in tuck-over tuck-over dialkyl complex [U{$Me_3SiNCH_2CH_2N(CH_2CH_2NSi(Me)_2$-$\mu$-$CH_2)(CH_2CH_2NSi(Me)_2$-$\mu^2$-$CH_2)$}U{$(Me_3Si)$-$\mu$-$NCH_2CH_2N(CH_2CH_2NSiMe_3)_2$}] (**21**, where tuck-in refers to a chelating coordination of the alkyl, whereas tuck-over is a bridging coordination to a second metal centre scheme **1.11.**, left).[56] For Tren^{DMBS}, treatment of **9** with benzyl potassium in pentane eliminated toluene to afford [U{$CH_2Si(Me)(^tBu)NCH_2CH_2N(CH_2CH_2NSiMe_3)_2$}] (**22**, by the same nomenclature, a tuck-in alkyl, scheme **1.11.**, right).[58,59] There had been no reports on the reaction of systems of {U(Tren^{TIPS})} with benzyl potassium prior to this work, and these reactions shall be discussed in further detail in Chapter 3.



*Scheme **1.11.** Syntheses of Tren–uranium(IV) cyclometallates (**21**, **22**).*

Complex **22** features a remarkably long U-C σ-bond distance of 2.752(11) Å, this is likely due to its inclusion within a four membered [U-N-Si-C] ring. By contrast, complex **21** contains two four membered rings [U-N-Si-C] and [U-N-U-C], where the tuck-in bite angle {N-U(1)-C} is 67.13(13)° and the tuck-over bite angle {N-U(2)-C} is 81.89(12)°. The tuck-in U(1)-C bond distance is 2.667(5) Å, with the tuck-over U(2)-C bond distance a comparable 2.669(4) Å. This contrasts to the other tuck-over interaction, the bridging coordination of a second TMS methylene group from the Tren at U(1) to U(2), which is 2.493(5) Å, and broadly comparable to related metallocyclic uranium(IV) alkyls.[58,59]

Quantitative conversion of **9** to **22** was observed within minutes at room temperature. The reaction was found to be extremely facile and the proposed benzyl intermediate, [U(Tren^{DMBS})(CH_2Ph)] was not observed by variable temperature ^1H NMR studies. Deuterium exchange studies with D_2 were performed on **22**, which

found that all α-Si hydrogens were replaced, to afford [U{*C*D_2Si(CD_3)(^{t}Bu)*N*CH_2CH_2*N*(CH_2CH_2*N*Si[CD_3]$_2$^{t}Bu)$_2$}].[59] Similar deuterium exchange studies by Andersen *et al.* observed the replacement of α-Si hydrogens of [M{N($SiMe_3$)$_2$}$_3$(H)] to afford [M{N(Si[CD_3]$_2$}$_3$(D)] (M = U, Th).[53]

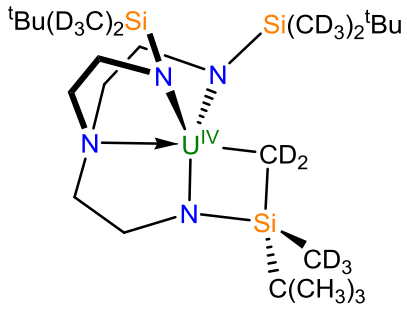
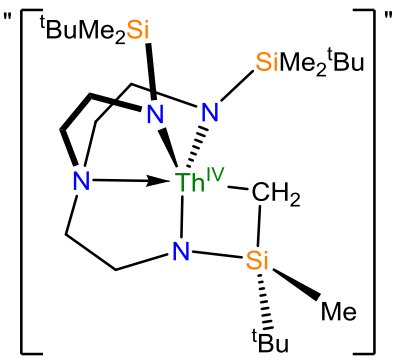
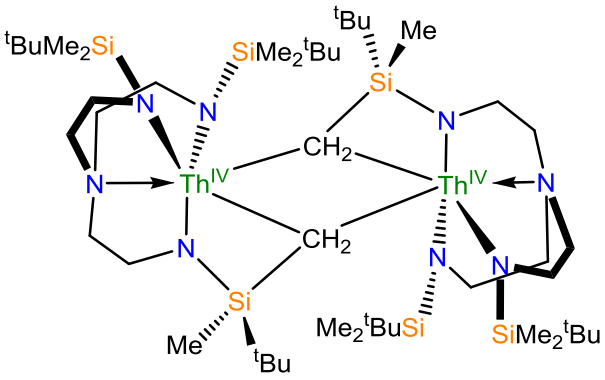


Figure ***1.8.****, Solid state structure of [U{CD_2Si(CD_3)(^{t}Bu)NCH_2CH_2N(CH_2CH_2NSi[CD_3]$_2$^{t}Bu)$_2$}].*

The uranium(III) analogue of **22** can be prepared from either **9** or **22** by the addition of potassium metal in toluene to afford the uranium(III)–cyclometallate [U{*C*H_2Si(Me)(^{t}Bu)*N*CH_2CH_2*N*(CH_2CH_2*N*$SiMe_2$^{t}Bu)$_2$}][K(tol)], **23**.[59] Oxidation of **23** to the uranium(IV)–cyclometallate **22** could be effected by the addition of $PhCH_2Cl$, with the elimination of toluene and KCl.



22-Th



24

Figure ***1.9.*** *The postulated structure of the {Th(Tren^{DMBS})} cyclometallate (**22-Th**), and the crystallographically characterised structure of the same, **24**.*

The thorium Tren^{DMBS} cyclometallate was first described by Scott *et al* in 1999,[59] but was not structurally characterised until some 15 years later by Liddle *et al*.[51] The

reaction of [Th(Tren^{DMBS})(I)] (**17**) with KCH_2Ph was postulated to form a complex with the same connectivity as the uranium analogue, **22**,[58] i.e. [Th{*C*H_2Si(Me)(^{t}Bu)*N*CH_2CH_2*N*(CH_2CH_2*N*$SiMe_3$)$_2$] (**22-Th**, figure **1.9.**, left). However, the crystal structure was later identified by Liddle *et al.*, and found to adopt the dinuclear structure [{Th(μ-*C*H_2Si[Me][^{t}Bu]*N*CH_2CH_2*N*[CH_2CH_2*N*$SiMe_2{}^t$Bu]$_2$)}$_2$], **24**, which exhibits two thorium centres and two metallated alkyls in a tuck-in, tuck-over formulation (figure **1.9.**, right). Complex **24** features the longest known thorium alkyl bond, at 2.875(9) Å, for the tuck-in interaction. This was reported to be longer than the sum of the covalent radii [2.50 (Pyykkö) or 2.82 Å (Alvarez) for an sp^3 hybridised carbon].[60,61]

1.3. Introduction to transition metal nitrides

1.3.1. Background

In this section, the general synthetic procedures towards the preparation of transition metal nitrides will be outlined. Due to the vast scope of this area of research, not all examples can be discussed, but all approaches will be covered. A number of reviews cover this topic in extensive detail, and the reader is directed there for further insights.[62-66]

It is instructive to visualise the bonding in transition metal nitrides, in order that the synthesis and reactivity of this class of compounds from across the d-block can be understood. A simplified representation of the bonding of transition metal nitrides places these compounds into two classes: one for nucleophilic and one for electrophilic nitrides (cases A and B respectively in figure **1.10.**, below). These behaviours can be explained by the corresponding electrophilic or nucleophilic metal, which are likely to be an early d-block metal or in a high oxidation state, or contrastingly a late d-block metal or in a low oxidation state. Consequently, the behaviour of the nitride is dependent upon the bringing together of these factors, which results in antibonding orbitals which are either metal or ligand based, and it is this character which infers the extent to which the nitride acts in an electrophilic or

nucleophilic manner. The simplified molecular orbital diagrams, along with the associated parameters, are illustrated in figure **1.10.** (adapted from [64]).

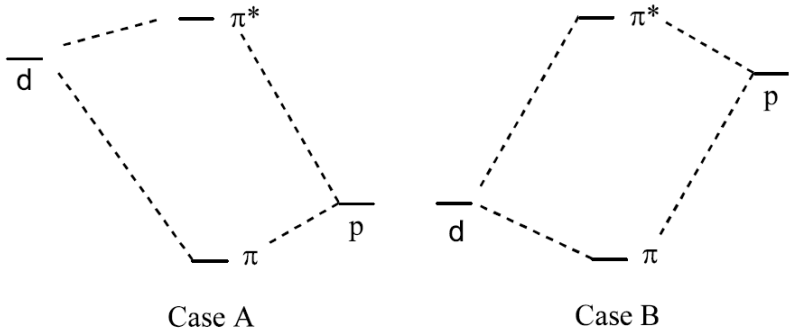


*Figure **1.10.** Simplified molecular orbital diagrams for transition metal nitrides.[64] Case A represents nucleophilic nitrides (electrophilic metals – early d-block/ high oxidation state) and Case B represents electrophilic nitrides (nucleophilic metals – late d-block/ low oxidation states.*

This bonding picture does not encapsulate all the factors that determine the reactivity of a transition metal nitride, and ancillary ligands can impart a considerable impact. Within the d-block, the strong donor properties of the nitride ligand cause a *trans*-influence, which destabilises the M-L bonds for ligands binding in the *trans* position. When two ligands are located *trans* to each other, they compete for the same metal valence orbitals. If one ligand has a larger overlap with these orbitals (such as a strongly bound nitride ligand) then there is a lessening of the overlap between the metal orbitals and the orbitals on the *trans* ligand.[67] The *trans* influence acts to stabilise low coordination numbers and results in many complexes adopting a square based pyramidal geometry. The effect that the nitride ligand has on the ligand field cannot be understated either, with some cases better described as weakly perturbed pseudo-linear complexes rather than strongly perturbed octahedral complexes (for example, $[Cr{\equiv}N]^{2+}$)[68].

The nitride is not always dominant within the ligand field, and supporting ligand orbital mixing can reduce the effect of the nitride, such as in $[M(N)(OR)_3]$ complexes (M = Cr, Mo, W; R = ^{t}Bu, ^{i}Pr). Here, the extent of orbital mixing is dependent upon the metal.[69] A combination of the 1π and 2σ molecular orbitals (MOs) of the M≡N fragment with the MOs of the $(RO)_3$ set (a_1, e_{perpen}, $e_{parallel}$, a_2)

affords mixing (see figure **1.11.**), such that the molecular orbitals of the nitride fragment are not isolated. The order of these orbitals is dependent upon the metal, such that for Mo and W, a $2a_1$ MO is highest in energy (figure **1.11.**, right), which derives mostly from the non-bonding 2σ orbital of the M≡N fragment. Hence donation of electrons results does not significantly destabilise the molecule. In contrast, for Cr, the highest energy orbital is the a_2 orbital (from the $(RO)_3$ set; figure **1.11.**, left), and so the nitride is less nucleophilic. Furthermore, substitution of the alkoxide ligands for thiolates in the Mo case, i.e. $[Mo(N)(SR)_3]$ changes the ordering of the MOs, such that the a_2 orbital is highest in energy (as was the case for the chromium alkoxide).[70] It is therefore important to investigate transition metal nitrides in order to understand how these factors come together and affect the reactivity of the nitride fragment.

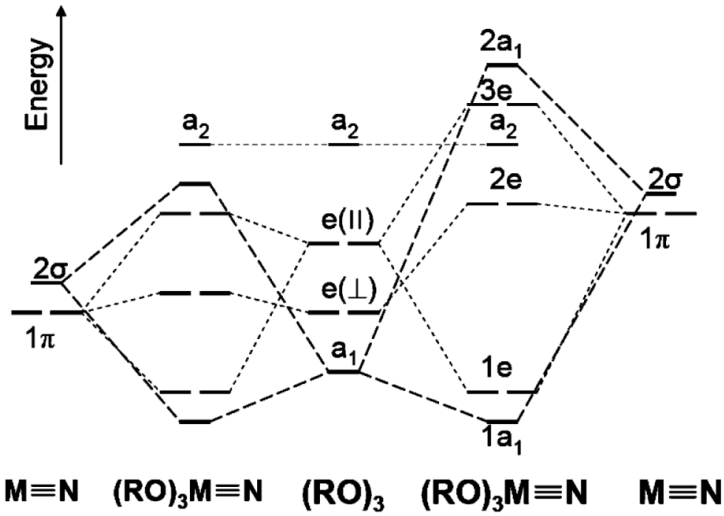


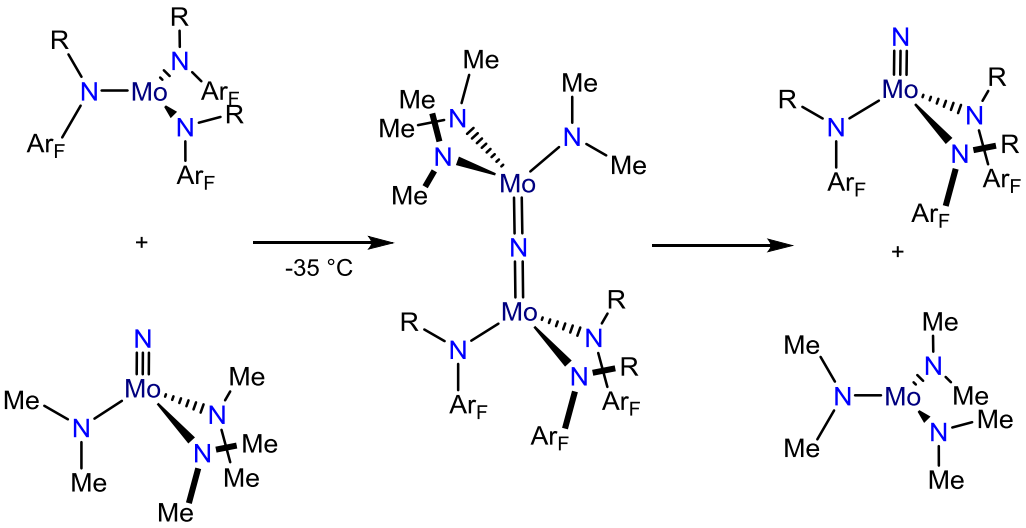
*Figure **1.11.** Qualitative diagram showing orbital mixing between M≡N and $(RO)_3$ fragments in $[M(N)(OR)_3]$ complexes, M = Cr (left), Mo and W (right). Symmetry labels are for the C_{3v} point group. Adapted from [69].*

1.3.2. N-atom transfer

Nitrogen atom transfer has been a proven route towards the synthesis of novel nitride complexes. [Mn(salen)(N)] (salen = $\{CH_2NCHC_6H_4O\}_2^{2-}$) is often utilised as the

nitrogen source for nitride transfer reactions. A thorough account of this type of synthesis was made by Woo in 1993.[71]

Salen-manganese(V) nitrides themselves are prepared by the oxidation of ammonia using ammonium hydroxide as a nitrogen source and bleach as the oxidant in aqueous conditions. The benefit of this is that this reaction occurs readily using cheap reagents, and is an easy route to high oxidation state nitrides. Such a route is not transferable to the synthesis of a uranium nitride (see Section 5) due to the hydrophilic nature of uranium centres.

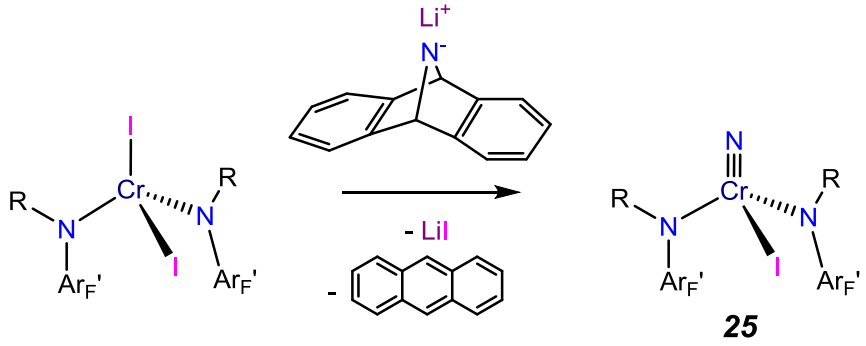


*Scheme **1.12.** Preparation of [Mo(N){N(R)(Ar$_F$)}$_3$], R = C(CD$_3$)$_2$Me, Ar$_F$ = 4-FC$_6$H$_4$.*

Mechanistically, the nitrogen transfer occurs *via* a bridged nitride intermediate {M(μ-N)M′}. Such an intermediate was first isolated by Cummins *et al.*, who were able to trap [{(Me$_2$N)$_3$Mo}(μ-N){Mo(N[R][Ar^F])$_3$}] [R = C(CD$_3$)$_2$Me, Ar$_F$ = 4-FC$_6$H$_4$], which was implicated in the nitride transfer from [Mo(N)(NMe$_2$)$_3$] to [Mo(N){N(R)(Ar$_F$)}$_3$].[72] The bridged intermediate was able to be isolated at low temperatures, and subsequently decomposed to [Mo(N){N(R)(Ar$_F$)}$_3$] upon warming (see scheme **1.12.**).

An organic reagent for N-atom transfer is the dibenzo-7-azabicyclo[2.2.1]hepta-2,5-diene anion (dbabh$^-$). Transfer of the N-atom to afford a nitride eliminates anthracene, as in the preparation of

[Cr(N)(I){N(R)(Ar$_F$′)}$_2$] by the reaction of [Li(dbabh)] with [Cr(I)$_2${N(R)(Ar$_F$′)}$_2$] [**25**, R = C(CD$_3$)$_2$Me, Ar$_F$′ = 2-F-5-MeC$_6$H$_4$, scheme **1.13.**].[73]



Scheme ***1.13.*** *Synthesis of [Cr(N)(I){N(R)(Ar$_F$′)}$_2$], R = C(CD$_3$)$_2$Me, Ar$_F$′ = 2-F-5-MeC$_6$H$_4$.*

In addition to N-atom transfer, ligand exchange reactions are widely used for more stable M≡N fragments to prepare complexes with more sterically demanding ligand environments. As previously discussed, [Mo(Tren^{Xy})(N)] (**4**) can be prepared by ligand exchange with [{Mo(Cl)$_3$(N)(MeCN)}$_4$].[27] This synthetic strategy is common for technetium and rhenium nitrides, which are prepared from starting materials such as [M(Cl)$_2$(PPh$_3$)$_2$(N)] (M = Tc, Re),[74-76] or ruthenium and osmium nitrides from [M(Cl)$_4$(N)] (M = Ru, Os).[77]

1.3.3. Azide decomposition

Azide decomposition is a common route to the preparation of transition metal nitride complexes. Most often this decomposition occurs *via* a thermolytic or photolytic route. There is little mechanistic understanding of the thermolytic route, despite it being a very important method for the preparation of nitride fragments.[78] A combined experimental and theoretical study of the thermolytic conversion of [Mo(Cp*)(N$_3$)$_2$] to [Mo(Cp*)(N$_3$)(N)] was conducted, and the authors propose that the dinitrogen dissociation occurs from the *endo* azide ligand, as there is a weaker overlap between the azide orbitals and the b$_1$ orbital of the metallocene fragment than the corresponding overlap between the b$_1$ orbital and the *exo* ligand (figure

1.12.). Subsequently, the remaining *exo* azide ligand rotates into an *endo* position. Here, they describe the *endo*-azide as directed towards the C_2 axis of the [Mo(Cp*)$_2$] fragment and the *exo*-azide as directed away.

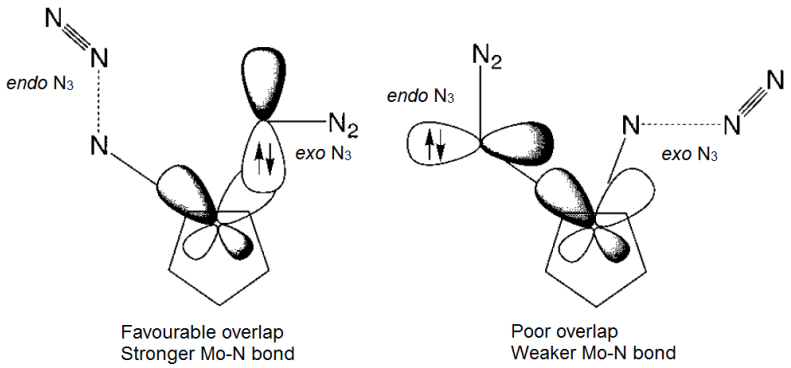
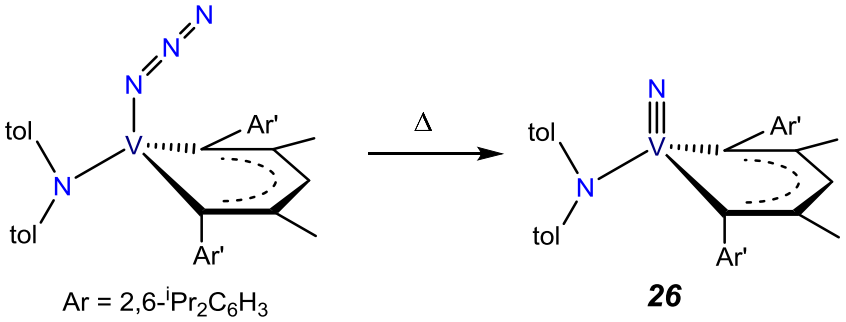


Figure ***1.12.*** *Enhanced π interactions stabilise the exo azide ligand in [Mo(Cp*)(N$_3$)$_2$]. Thermolysis results in N$_2$ dissociation from the endo azide ligand.*

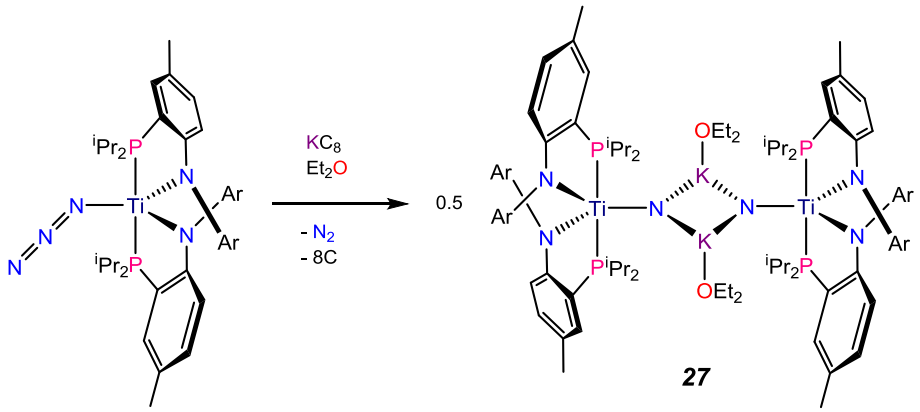
Contrastingly, the thermolytic preparation of [V(N)(nacnac){N(Ar)(tol)}] (**26**, nacnac = HC{C(Me)N-2,6-^{i}Pr$_2$C$_6$H$_3$}$_2$; Ar = tol, Mes; tol = 4-MeC$_6$H$_4$; Mes = 2,4,6-Me$_3$C$_6$H$_2$, scheme **1.14.**)[79] from an azide precursor is proposed to occur *via* Lewis acid assisted azide ligand activation (e.g. B(C$_6$F$_5$)$_3$ or [Sm(OTf)$_3$]).[80] The nitride species with Mes substituents is prepared directly from the [V(Cl)(nacnac){N(Mes)(tol)}] precursor by the addition of NaN$_3$ and thermolysis; the intermediate azide species could not be isolated.



Scheme ***1.14.*** *Synthesis of* ***26****.*

As discussed above, transition metal nitrides of Tren complexes, namely [Cr(Tren^{HIPT})(N)] (**1**) and [Mo(Tren^{Ar})(N)] (**2**, **3** and **4**) can also be prepared by thermolytic routes (see Section 2.1.).[24-27]

Under photolytic conditions, there are two possible reaction routes that can be followed. In the case of photolytic preparation of nitrides, this is a photooxidation reaction, and results from the cleavage of an N-N bond, ejecting N_2. Alternatively, there is the potential for a photoreduction product by the cleavage of the M-N bond to eliminate N_3. These competing pathways are discussed in the preparation of iron macrocyclic nitrides. Photooxidation of the low spin Fe^{III} azide precursor is proposed as favourable as the reorganisation energy associated with Fe^{V} nitride formation is low.[81] For related high spin Fe^{III} complexes, the reorganisation energy is larger, and therefore photoreduction is favoured instead.[82]



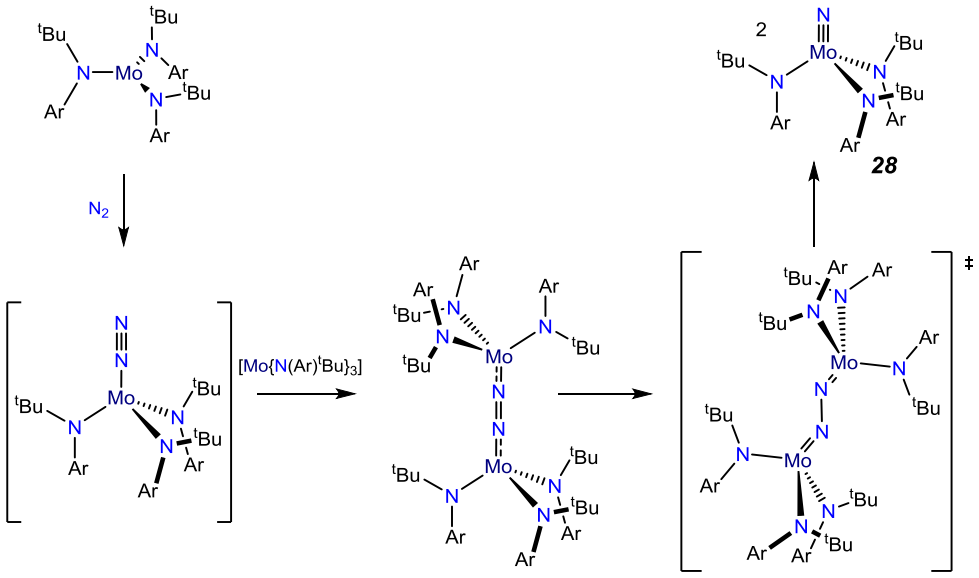
*Scheme **1.15.** Synthesis of **27**.*

A third route for azide decomposition utilises external reductants. Very recently, Mindiola *et al.* have prepared a terminal titanium nitride complex, [Ti(N)(PN)$_2$][K(2,2,2-crypt)], [PN$^-$ = 1-*N*(2,4,6-$Me_3C_6H_2$)-2-*P*(^{i}Pr$_2$)-4-Me-C_6H_3].[83] This report expands the range of groups for which transition metal nitrides are known to now include group 4. The terminal nitride complex [Ti(N)(PN)$_2$][K(2,2,2-crypt)] was prepared by the reaction of two equivalents of [LiPN] ligands with [Ti(Cl)$_3$(THF)$_3$] to afford [Ti(Cl)(PN)$_2$] by salt elimination, followed by salt elimination reaction of the remaining chloride with NaN_3 to give the azide species [Ti(N_3)(PN)$_2$]. Reduction of [Ti(N_3)(PN)$_2$] with KC_8 in diethyl ether afforded the bridged nitride species [{Ti(PN)$_2$(μ-N)$_2$(μ-K[OEt$_2$])$_2$}$_2$] (**27**, scheme **1.15.**). Encapsulation of the bridging potassium cations in **27** can be accomplished utilising 2,2,2-crypt, which gave the separated ion pair, terminal titanium–nitride species, [Ti(N)(PN)$_2$][K(2,2,2-crypt)]. Alternatively, the monomeric capped species,

[Ti(PN)$_2${(μ-N)(μ-K)(18C6)}], could be prepared utilising one equivalent of 18-crown-6 ether (18C6) per titanium, wherein the potassium cation is not removed from the nitride ligand.

1.3.4. Small molecule activation

The reductive cleavage of dinitrogen to afford a nitride species is a notable feat, as dinitrogen is not readily reduced. [Mo{N(Ar)^{t}Bu}$_3$] (Ar = 3,5-Me$_2$C$_6$H$_3$) cleaves dinitrogen to afford [Mo{N(Ar)^{t}Bu}$_3$(N)] (**28**, scheme **1.16.**).[84,85] The proposed mechanism is the coordination of dinitrogen to a molybdenum(III) centre, followed by the coordination of a second molybdenum centre to this adduct. N-N bond cleavage proceeds through a zigzag transition state.

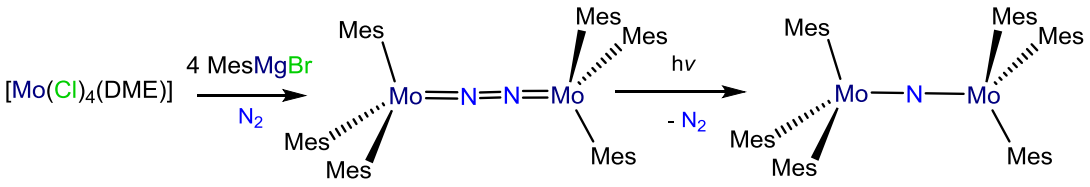


*Scheme **1.16.** Synthesis of **28**.*

The reduction of the pincer complex [Mo(^{t}BuPOCOP)(I)$_2$] [^{t}BuPOCOP = 1,3-(^{t}Bu$_2$*P*O)$_2$C$_6$H$_3$] under dinitrogen affords the molybdenum(V)–nitride [Mo(^{t}BuPOCOP)(I)(N)]. The N-N cleavage step is postulated to occur *via* a {Mo^{II}(μ-N$_2$)Mo^{II}} dinuclear intermediate.[86]

Unusually, [Mo(Mes)$_3$] (Mes = 2,4,6-Me$_3$C$_6$H$_2$) only cleaves dinitrogen under photolytic conditions (λ = 365.0 nm) to afford a bridged nitride species

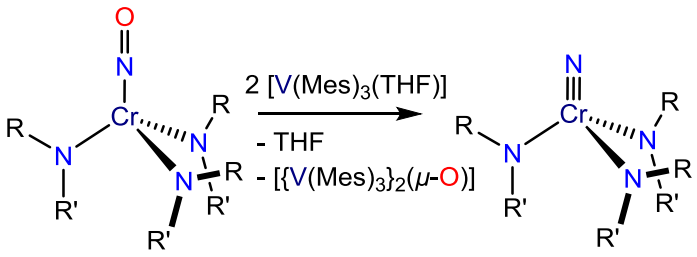
[{Mo(Mes)$_3$}$_2$(μ-N)] (scheme **1.17.**),[87] in contrast to [Mo{N(Ar)^{t}Bu}$_3$] which does not require external stimuli to activate dinitrogen. This is believed to be a consequence of the lowered basicity of molybdenum when coordinated by aryl ligands, as opposed to the σ and π donor properties of the amide ligands in [Mo{N(Ar)^{t}Bu}$_3$], which induce spontaneous thermal cleavage of the N-N bond.



*Scheme **1.17.** Synthesis of [{Mo(Mes)$_3$}$_2$(μ-N)].*

N_2O has also been shown to be a nitride source for a series of molybdenum(III) *tris*(anilido) complexes, [Mo{N(R)(Ar)}$_3$] [R = ^{t}Bu, C(CD$_3$)$_2$Me; Ar = 3,5-Me$_2$C$_6$H$_3$). The reaction of the molybdenum(III) precursor with N_2O affords [Mo{N(R)(Ar)}$_3$(N)] (**28**) and [Mo{N(R)(Ar)}$_3$(NO)], which was shown to be under N-N bond cleavage kinetic control.[88]

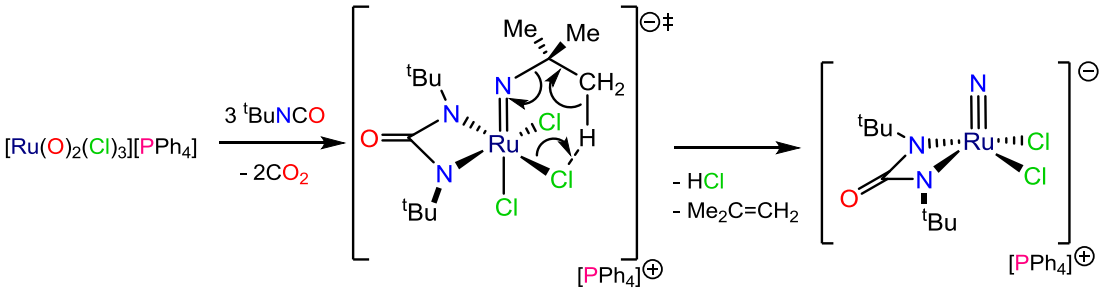
Deoxygenation of a nitrosyl ligand has also been reported to afford nitrides for low valent group 6 complexes. If the chromium complexes [Cr{N(R)(R′)}$_3$(NO)] [R = R′ = ^{i}Pr; R = C(CD$_3$)$_2$Me, R′ = 2-F-5-MeC$_6$H$_3$; R = C(CD$_3$)$_2$Me, R′ = 3,5-Me$_2$C$_6$H$_3$] are thermolysed in the presence of [V(Mes)$_3$(THF)], the corresponding chromium(VI)–nitride and [{V(Mes)$_3$}$_2$(μ-O)] are prepared (scheme **1.18.**).[89]



*Scheme **1.18.** Synthesis of [Cr{N(R)(R')}$_3$(N)].*

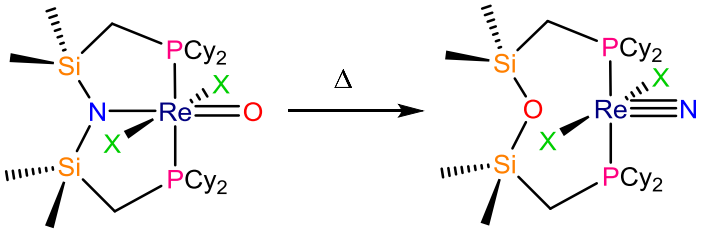
1.3.5. N-E bond scission

Transition metal nitride species can also be afforded by the scission of N-E bonds, including E = C, Si, N and P. The cleavage of N-C bonds is an unusual route towards nitrides, and these examples often originate from the cleavage of N-C bonds of imide species. The reaction of $[Ru(O)_2(Cl)_3][PPh_4]$ with excess ^tBuNCO affords the imide ureato species $[Ru(Cl)_3(N^tBu)\{^tBuNC(O)N^tBu\}][PPh_4]$ by the loss of two CO_2 molecules, then cycloelimination of HCl and $Me_2C{=}CH_2$ affords the nitride $[Ru(N)(Cl)_2\{^tBuNC(O)N^tBu\}][PPh_4]$ (scheme **1.19.**).[90]



*Scheme **1.19.** Synthesis of $[Ru(N)(Cl)_2\{^tBuNC(O)N^tBu\}][PPh_4]$.*

The cleavage of N-Si bonds is considerably more common than the cleavage of N-C bonds. Indeed the use of $N(SiMe_3)_3$ to prepare transition metal nitrides has been covered in a review.[91] The typical usage here is for a high valent metal complex with multiple chloride ligands, usually heavier mid d-block metals, where treatment with $N(SiMe_3)_3$ affords a nitride with the elimination of three equivalents of Me_3SiCl, where the formation of these strong M≡N and Si-Cl bonds is the likely driving force. An unusual example of intramolecular N-Si bond cleavage has also been described for the pincer complex $[Re(PNP^{Cy})(O)(X)_2]$ [X = Cl, Br; PNP'^{Cy} = $N\{Si(Me)_2CH_2P(Cy)_2\}_2$, Cy = cyclohexyl, where heating to 90 °C affords the double silicon atom migration to oxygen to afford $[Re(POP^{Cy})(N)(X)_2]$ [POP^{Cy} = $O\{Si(Me)_2CH_2P(Cy)_2\}_2$] (see scheme **1.20.**). Rearrangement of ligands around the rhenium centre affords *cis*-halides and *cis*-phosphines, which is a slow equilibrium process at room temperature.

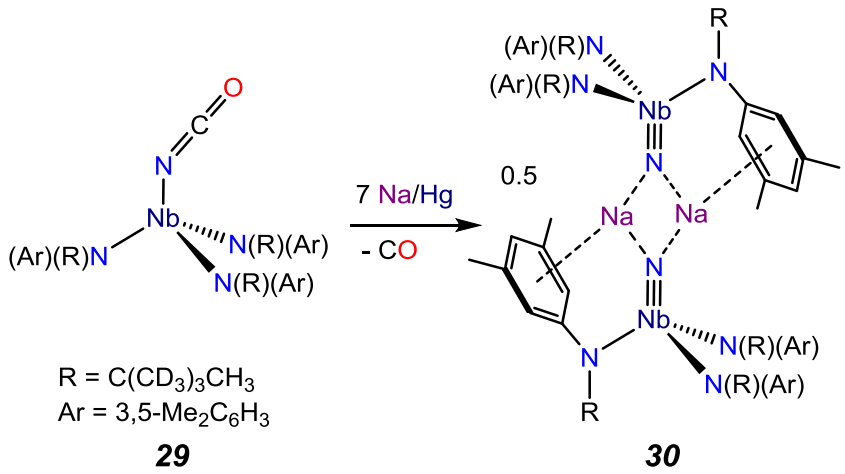


*Scheme **1.20.** Synthesis of [Re(POP^{Cy})(N)(X)$_2$], X = Cl, Br.*

Cleavage of the N-N bonds in hydrazido complexes can also afford nitride complexes. As for N-Si bond breaking for nitride formation, this transformation is more common for heavier mid-transition elements, in high oxidation states [e.g. +4 Mo, W; +5 Tc, Re; +6 Mo, Ru, Os; +7 Tc, Re]. This is due to the strong metal–nitride bonds which are formed. The N-N bond breaking was investigated mechanistically for the compound [W(dppe)$_2$(NNC$_5$H$_{10}$)] (dppe = Ph$_2$PCH$_2$CH$_2$PPh$_2$, NNC$_5$H$_{10}$ is the nitride-piperidine adduct), wherein the addition of acid in the presence of acetonitrile forms the nitride species [W(N)(dppe)$_2$(MeCN)] and piperidine (HNC$_5$H$_{10}$). The authors propose that the initial protonation of the hydrazido fragment permits solvent coordination which facilitates N-N bond cleavage.[92]

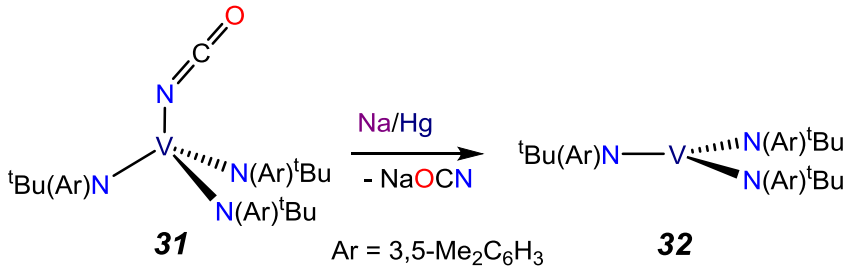
The reaction of [Tc(O)(Cl)$_4$][NBu$_4$] with Me$_3$SiNPPh$_3$ in DCM affords N-P bond cleavage to prepare [Tc(N)(Cl)$_2$(NHPPh$_3$)$_2$].[93] The formation of a nitride species from a phosphinimide is unusual as the reverse reaction (the preparation of phosphinimides by the reaction of nitrides with phosphines) is widely known (see Section 4.1.).

The reduction of the isocyanate fragment in [Nb{N(R)(Ar)}$_3$(NCO)] [**29**, R = C(CD$_3$)$_2$Me, Ar = 3,5-Me$_2$C$_6$H$_3$] with sodium mercury amalgam affords the bridged nitride species [{Nb(N[R][Ar])$_3$(μ-N)(μ-Na)}$_2$] (**30**) by a decarbonylation pathway (scheme **1.21.**).[94] The authors suggest that a substantial fraction of the carbon monoxide is evolved as free CO. This synthetic route, though highly unusual, is reminiscent of the denitrification of azide species to afford nitrides, many of which have been previously described.



*Scheme **1.21.** Preparation of **30**.*

It is worth noting here that the vanadium based analogue of **29**, [V{N(Ar)^{t}Bu}$_3$(NCO)] (**31**, Ar = 3,5-Me$_2$C$_6$H$_3$), does not undergo decarbonylation under the same conditions. Instead, sodium cyanate is eliminated to prepare the homoleptic *tris*(amide) compound [V{N(Ar)^{t}Bu}$_3$] (**32**, scheme **1.22.**).[95]



*Scheme **1.22.** Preparation of **32**.*

1.4. Reactivity of transition metal nitrides

1.4.1. General outline of reactivity

As discussed above, the nature of transition metal nitride behaviour can be ascribed to the molecular frontier orbitals and the ratio of *p*-orbital to *d*-orbital character in these MOs, i.e. the perceived electrophilic or nucleophilic character. This is not only the position of the transition metal within the d-block, but also the nature of the ancillary ligands and their number. Further to this, some nitrides can behave in an ambiphilic manner, which complicates the matter somewhat.

As transition metals generally have a large number of accessible oxidation states, changes in oxidation state of 0 to ±3 during reactions are common. In line with the broader reactivity observed at transition metals (oxidative addition, reductive elimination, salt elimination, protonolysis, migratory insertion, bond metathesis, etc.), the most common oxidation state changes during reactions are zero and two.

What follows will be a brief overview of transition metal nitride reactivity, with special attention being paid to reactions towards CO (Section 4.2.), and CE_2 (E = O or S, Section 4.3.).

The characteristic three electron reaction is intermetallic nitrogen atom transfer. This is primarily used for the preparation of novel nitride complexes, which cannot be prepared by other routes. The classic example is the use of [Mn(salen)(N)] as such a nitride transfer reagent. As this is a preparative technique, more details can be found in Section 3, or alternatively, in a review of 1993 by Woo.[71]

Nitrogen atom transfer is also known as a two electron process, often involving the exchange of a nitride ligand for a halide ligand. Here, again, [Mn(salen)(N)], is a key reagent in the preparation of nitrides (*vide supra*) and alongside the analogous porphyrin and corrole (tetrapyrrole) complexes, can be used to model the nitrogen atom transfer. These studies reveal that the transfer is governed by the ability of the supporting ligand to stabilise higher oxidation states.

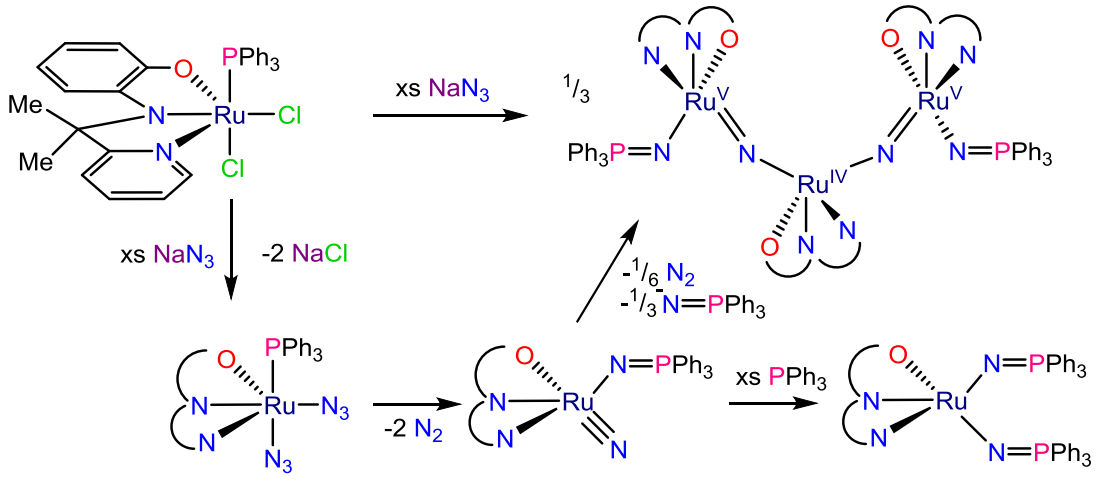


Scheme ***1.23.*** *Electrophilic nitrides react with phosphines to prepare phosphinimides.*

The reactivity of nitrides with phosphines to afford phosphinimides ($^{-}N=PR_3$) is often used as a model to describe all electrophilic reactivity. This is exemplified by the observation of this reactivity across the d-block, as illustrated by the reactivity of the early, middle and late transition metal nitride complexes $[V(N)(Cl)_2(PMe_2Ph)_2]$, [Mo(N)(TPP)], $[Fe\{(^{tBu}Im)_3BPh\}(N)]$ and $[Os(N)(Cl)_2(tpy)]$ [TPP = tetraphenylporphyrin; $(^{tBu}Im)_3BPh$ = $(^{t}BuNC_3H_2N)_3BPh$; tpy = 2,2′,6′,2″-terpyridine]

which all afford phosphinimides on reaction with phosphines (PMe_2Ph, PBu_3 and PPh_3 respectively).[96-99]

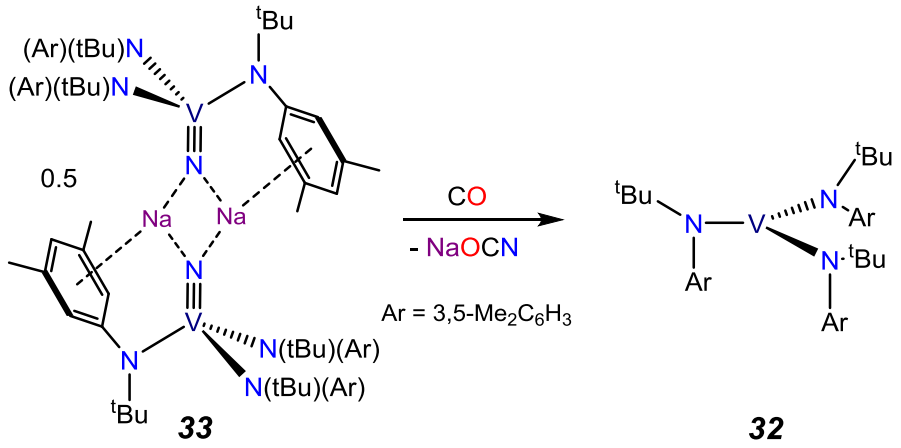
A further example of transition metal nitrides preparing phosphinimides comes from the reaction of $[Ru(NNO)(PPh_3)(Cl)_2]$ with excess NaN_3 in THF [NNO = pyridine aminophenol, 1-(*O*)-2,4-(^{t}Bu)$_2$-6-{*N*C(Me)$_2$-2-(C_5H_4N)}-C_6H_2, scheme **1.24.**].[100] The bridged nitride species $[Ru(NNO)\{(\mu\text{-}N)Ru(NNO)(NPPh_3)\}_2]$ is prepared on stirring the reaction mixture for 48 hours under argon, and the bonding description is best described as Ru=N–Ru–N=Ru, as determined by crystallographic data. This bridged species is postulated to form *via* first the di-substitution of the chloride ligands for azide ligands, then the loss of dinitrogen to afford $[Ru(NNO)(N)(NPPh_3)]$. Coupling of three of these intermediates affords the final product with the concomitant loss of 1/6 of an equivalent of dinitrogen and 1/3 of an equivalent of phosphinimide, or alternatively, this species can be trapped in the presence of excess PPh_3 to yield the *bis*(phosphinimide), $[Ru(NNO)(NPPh_3)_2]$, (scheme **1.24.**, lower right). Therefore, electrophilic reactivity of ruthenium nitrides to afford phosphinimides is here observed in both an intra- and inter-molecular fashion.



Scheme ***1.24.*** *Preparation of* $[Ru(NNO)\{(\mu\text{-}N)Ru(NNO)(NPPh_3)\}_2]$ *and* $[Ru(NNO)(NPPh_3)_2]$.

1.4.2. Reactivity of transition metal nitrides towards CO

Considering the utility of carbon monoxide as an ambiphilic reagent, and therefore able to probe the electrophilic or nucleophilic properties of a novel nitride system, there is a surprising lack of examples of transition metal nitride reactivity towards CO, and that which has been reported is relatively recent.

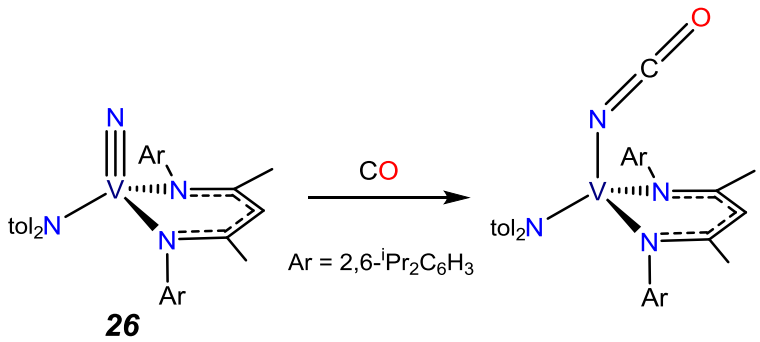


*Scheme **1.25.** Synthesis of **32**.*

The first instance featured the reaction of the vanadium nitride [{V(N[Ar]^{t}Bu)$_3$(μ-N)(μ-Na)}$_2$] (**33**, Ar = 3,5-Me$_2$C$_6$H$_3$) with carbon monoxide.[95] Stirring a THF solution of **33** in an atmosphere of CO at room temperature for 24 h afforded the conversion to the trivalent species [V{N(Ar)^{t}Bu}$_3$] (**32**) by the extrusion of NaOCN (scheme **1.25.**). Mechanistically, this proceeds firstly *via* the two electron reductive carbonylation of the nitride to afford an isocyanate linkage, before the oxidative extrusion of the cyanate salt from the anionic vanadium fragment to afford the neutral species (**32**). Since the isocyanate functionality can also be installed at vanadium by the reaction of **32** with AgOCN, (eliminating Ag^0), the subsequent reduction of the resultant isocyanate [V{N(Ar)^{t}Bu}$_3$(NCO)] (**31**) with sodium/mercury amalgam to eliminate NaOCN and prepare **32** experimentally verifies this mechanism. This reactivity is the opposite of that observed for the niobium analogue [{Nb(N[Ar]^{t}Bu)$_3$(μ-N)(μ-Na)}$_2$] (**30**), which was prepared by the decarbonylation of a niobium cyanate (**29**, see Section 3).[94] Therefore, the metal centre has a key role here in determining whether reduction of

[M{N(Ar)^{t}Bu)}$_3$(NCO)] effects the loss of cyanate (M = V, **31**) or carbon monoxide (M = Nb, **29**).

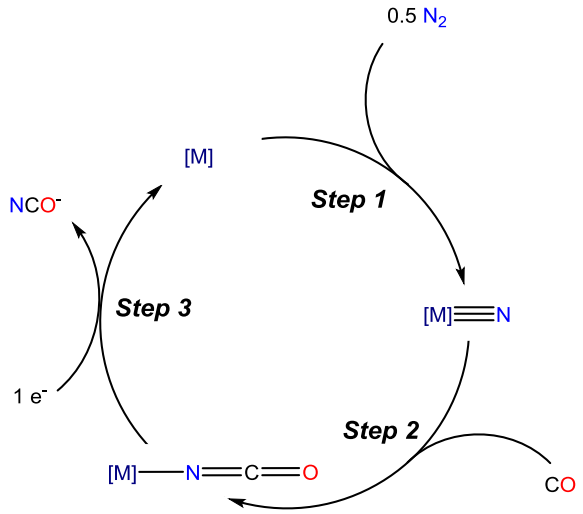
Mindiola *et al.* later reported the preparation and reaction of another vanadium nitride.[79] The reaction of [V(Cl)(nacnac){N(Ar)tol}] (nacnac = HC{C(Me)N-2,6-^{i}Pr-C$_6$H$_3$}$_2$; Ar = tol, Mes; tol = 4-MeC$_6$H$_4$; Mes = 2,4,6-Me$_3$C$_6$H$_2$) with NaN_3 and subsequent heating afforded first the installation of an azide ligand at vanadium (though this was only isolable for Ar = tol), then the loss of dinitrogen to afford the nitride species [V(N)(nacnac){N(Ar)tol}], **26**. Reaction of [V(N)(nacnac){N(tol)$_2$}] (i.e. Ar = tol) with CO was reported to form the isocyanate species [V(NCO)(nacnac){N(tol)$_2$}], (scheme **1.26.**). This reactivity parallels the initial steps proposed for the preparation of **32**, however in this instance there is no salt elimination driving force to induce the extrusion of the cyanate functionality, and so the cyanate fragment stays bound to the vanadium atom.



*Scheme **1.26.** Reductive carbonylation of **26**.*

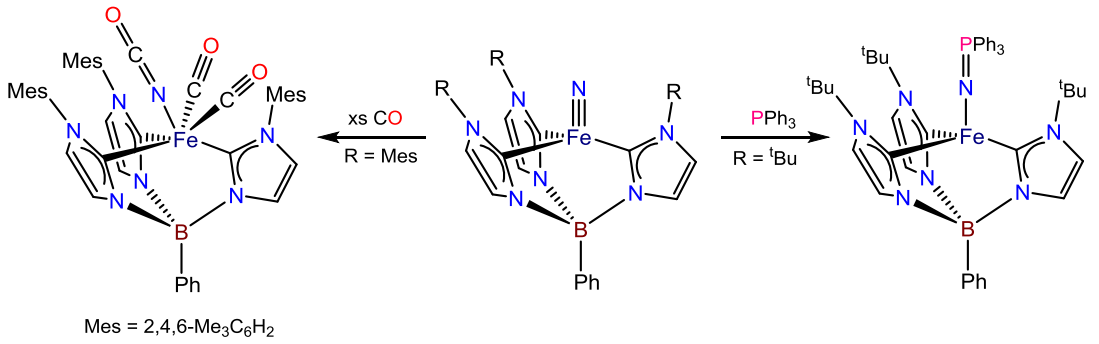
Cummins *et al*. proposed a three step synthetic cycle using vanadium or molybdenum species for (i) the installation of a nitride at the metal centre, followed by (ii) reductive carbonylation to afford isocyanates, then (iii) reduction to eliminate the cyanate fragment and regenerate the starting material (see scheme **1.27.**).[101] They intended to use nitrides prepared by the reaction of a trivalent species (e.g. [Mo{N(Ar)^{t}Bu}$_3$], Ar = 3,5-MeC$_6$H$_3$, *cf.* **32**) with dinitrogen as part of such a synthetic cycle (step 1). However they did not observe cyanate formation by the reaction of CO with nitrides [Mo{N(Ar)^{t}Bu}$_3$(N)] (**28**), [{Mo(N[Ar]^{t}Bu)$_3$}$_2$(μ-N)] or [Mo{N(Ar″)^{t}Bu}$_2$(N$_3$)(N)] (Ar″ = 2-N(Me)$_2$-5-MeC$_6$H$_3$), as required for step 2. Examples of cyanate installed by other means, such as in [Mo{N(Ar)^{t}Bu}$_3$(NCO)]

by the reaction of the trivalent precursor with AgOCN, did undergo reductive elimination of the cyanate on reaction with KC_8, an example of step 3.

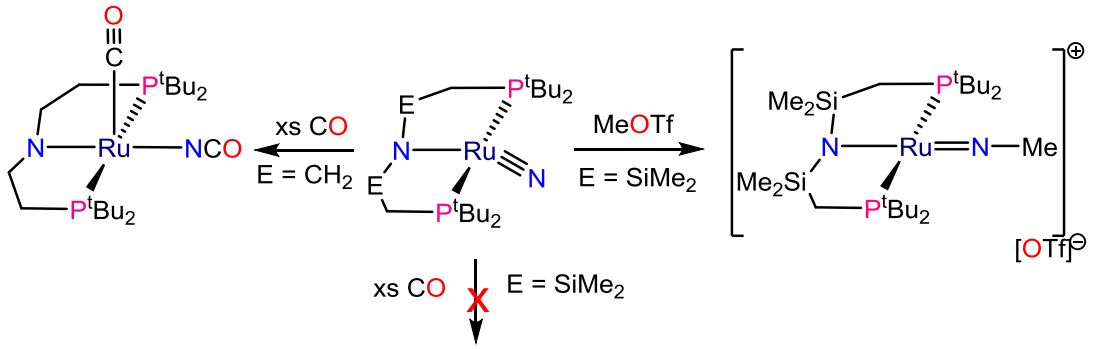


*Scheme **1.27.** A proposed three step synthetic cycle for the functionalisation of N_2 and CO.*

The typical reactivity observed therefore for transition metal nitrides with carbon monoxide is the formation of a cyanate functionality, which then either remains bound to the metal centre or is eliminated. Complexes which are not sufficiently sterically encumbered can also accommodate CO coordination as neutral ligands, such as in $[Fe\{(^{Mes}Im)_3BPh\}(NCO)(CO)_2]$[102] and $[Ru(PNP)(NCO)(CO)]$[103] [$(^{Mes}Im)_3BPh$ = (2,4,6-$Me_3C_6H_2$)-$NC_3H_2N\}_3BPh$, PNP = $N(CH_2CH_2P^tBu_2)_2$]. The synthesis of these cyanate compounds (which imply nucleophilic nitride centres) is in contrast to the previously discussed $[Fe\{(^{tBu}Im)_3BPh\}(N)]$,[98] which reacts with phosphines to prepare a phosphinimide (see scheme **1.28.**, right), and $[Ru(PNP')(N)]$[104] [PNP′ = $N(SiMe_2CH_2P^tBu_2)_2$] which does not react with CO (scheme **1.29.**, lower), and instead only reacts with strong electrophiles such as MeOTf (scheme **1.29.**, right). These compounds are therefore examples of differing reactivities of the nitride fragment based on small modifications of the ancillary ligands. Given these examples, and in light of the differing reactivities afforded on the reduction of group 5 cyanates (preparing variously **30** or **32**, see above, Schemes **1.21.** and **1.22.**) it is therefore necessary to test the reactivity of prepared nitride species, and not assume the reactivity of a system to be inherently deducible.



*Scheme **1.28.** Reactivity of [Fe{(^{R}Im)$_3$BPh}(N)] (R = Mes, ^{t}Bu).*

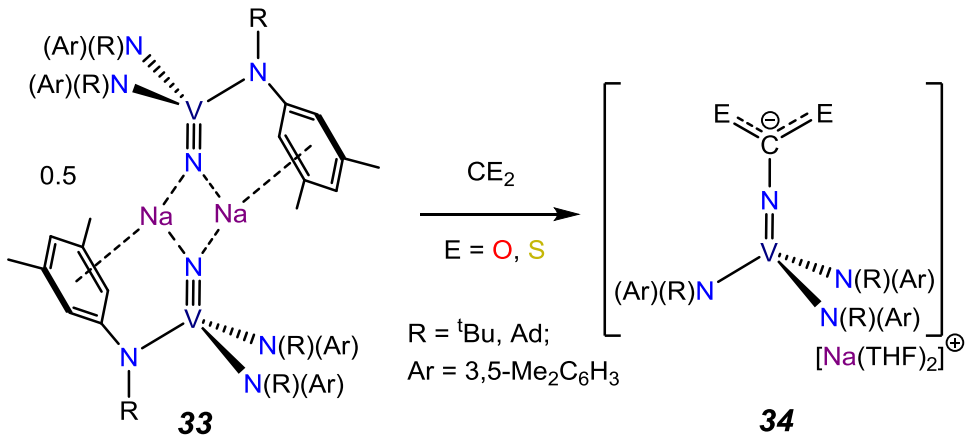


*Scheme **1.29.** Reactivity of [Ru{N(ECH$_2$P^{t}Bu$_2$)$_2$}(N)] (E = CH$_2$, SiMe$_2$).*

1.4.3. Reactivity of transition metal nitrides towards CE$_2$ (E = O, S)

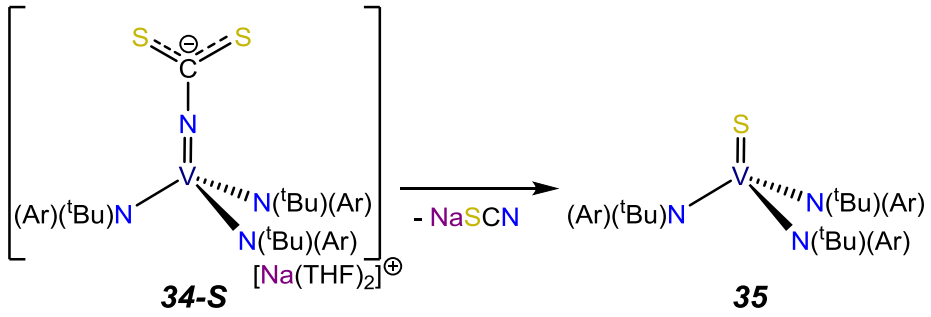
The chemistry of transition metal nitrides towards the heteroallenes (CE$_2$, E = O, S) has been investigated by many research groups. Reactivity of transition metal nitrides is dominated by the insertion chemistry of CE$_2$ into ancillary ligands, and ultimately only two examples of reactivity of heteroallenes at nitride centres have been reported.

Cummins *et al.* reported in 2002 the functionalisation of a vanadium nitride, [{V(N[Ar]R)$_3$(μ-N)(μ-Na)}$_2$], [Ar = 3,5-Me$_2$C$_6$H$_3$, R = ^{t}Bu (**33**), Ad] utilising both CO$_2$ and CS$_2$ to form the analogous pair of complexes [V{N(Ar)R}$_3$(NCE$_2$)][Na(THF)$_2$] (**34**, E = O, R = ^{t}Bu; E = S, R = ^{t}Bu, Ad, scheme **1.30.**).[105] The nucleophilic nitride reacts with the electrophilic heteroallene to afford the carbamate (**34-O**) or dithiocarbamate (**34-S**) species.



*Scheme **1.30.** Preparation of **34**.*

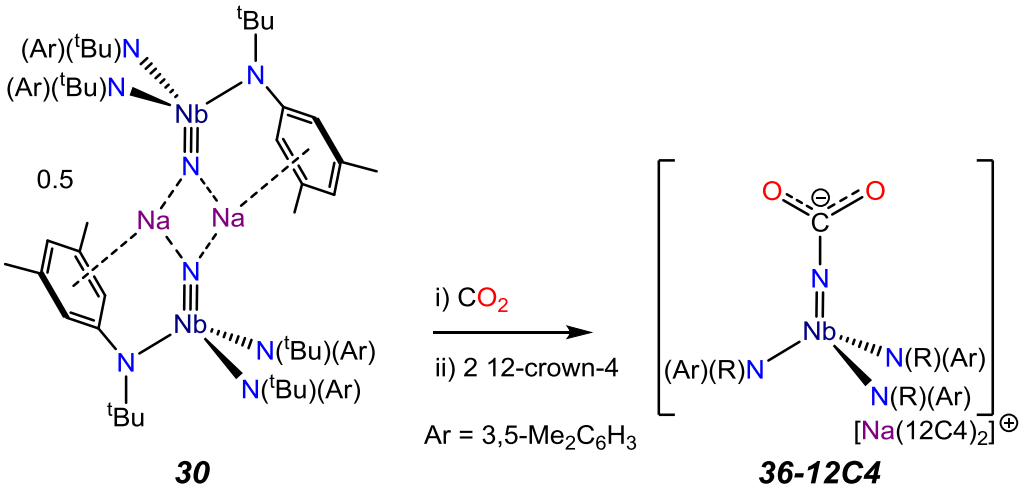
Storage of [V{N(Ar)^{t}Bu}$_3$(NCS$_2$)][Na(THF)$_2$] (**34-S**) at room temperature for 24 h resulted in the complete conversion to the sulfide complex [V{N(Ar)^{t}Bu}$_3$(S)] (**35**) *via* the extrusion of NaSCN (scheme **1.31.**). By comparison, the adamantyl analogue, [V(N[Ar]Ad)$_3$(NCS$_2$)][Na(THF)$_2$] (**34-S,Ad**), was stable in solution for several days, and only trace amounts of the corresponding sulfide [V{N(Ar)Ad}$_3$(S)] (**35-Ad**) could be observed by ^{1}H and ^{51}V NMR spectroscopies, even after refluxing for several hours. The authors note that an independently synthesised sample of **35-Ad** was stable under these conditions.[106] The stability of the carbamate complex [V{N(Ar)^{t}Bu}$_3$(NCO$_2$)][Na(THF)$_2$] (**34-O**) was also observed. An independently synthesised sample of the oxide species [V{N(Ar)^{t}Bu}$_3$(O)] (**35-O**) was prepared by reaction of **32** with pyridine N-oxide, to assess its accessibility, as it was not prepared by the decomposition of **34-O** (unlike the sulfide analogue).[105]



*Scheme **1.31.** Preparation of **35**.*

DFT studies of a model system of $[V(NMe_2)_3(N)]^-$, CO_2 and CS_2 were used to understand the difference in observed reactivity and stability of **34-O** and **34-S**. As such, the chemical components in the model system were consistent, and either CO_2 or CS_2 were formally added as necessary, to give end products of $[V(NMe_2)_3(O)]$ + NCO^- + CS_2, for example. The consumption of CS_2 was found to be 23.4 kcal mol^{-1} more exothermic than the corresponding CO_2 consumption. The lack of cyanate extrusion was proposed to be kinetic in origin, as treatment of the oxide $[V\{N(Ar)Ad\}_3(O)]$ with NaOCN resulted in no reaction.[105]

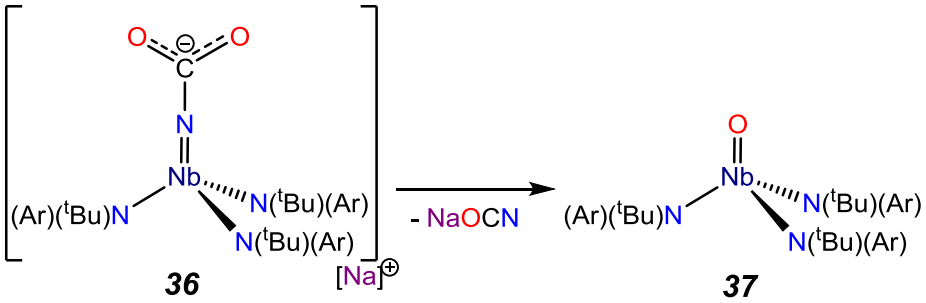
Similarly, Silvia and Cummins reported in 2010 the reactivity of a niobium–nitride with CO_2.[107] Analogously to the vanadium nitrides described above (**33**), the niobium–nitride **30** reacted with one equivalent of CO_2 at 0 °C to afford the carbamate complex $[Nb\{N(Ar)^tBu\}_3(NCO_2)][Na]$ (**36**). The reaction of **36** with two equivalents of 12-crown-4 ether (12C4) afforded the encapsulation of the sodium cation to give the crystallographically characterised complex $[Nb\{N(Ar)^tBu\}_3(NCO_2)][Na(12C4)_2]$ (**36-12C4**, scheme **1.32.**). This revealed that the carbamate functionality might be better described as an imido ligand bearing a CO_2 group, related to the acylimido functional group.



*Scheme **1.32.** Synthesis of **36**.*

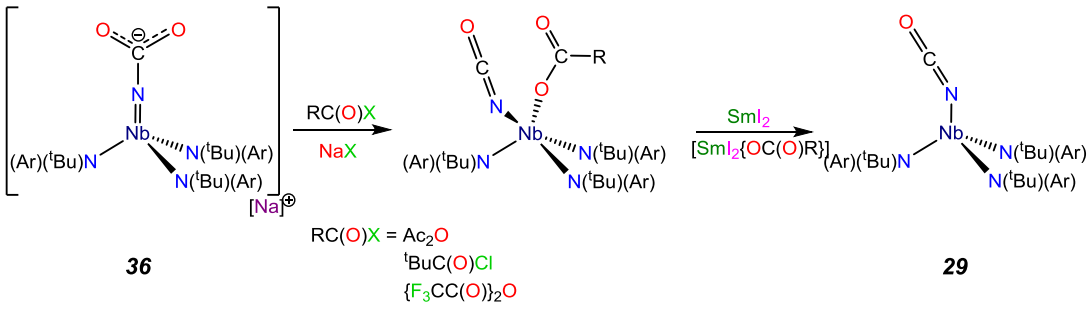
Whilst no cyanate extrusion was observed from $[V\{N(Ar)^tBu\}_3(NCO_2)][Na(THF)_2]$ (**34-O**), upon heating **36** to 70 °C for 80 h the formation of the oxo species $[Nb\{N(Ar)^tBu\}_3(O)]$ (**37**), was observed, with NaOCN eliminated as the by-product

(scheme **1.33.**). This parallels the formation of the vanadium–sulfide **35**, and again demonstrates the difference that a metal centre can impart on reactivity (*cf.* decomposition of the vanadium analogue **34-O** to the oxo species **35-O**, which was not observed, see above).



*Scheme **1.33.** Synthesis of **37**.*

Functionalisation of the carbamate in **36** utilising electrophiles of the form RC(O)X, [R(CO)X = Ac_2O, $^tBuC(O)Cl$ or $\{F_3CC(O)\}_2O$] afforded the isocyanate-acetate species $[Nb(N[Ar]^tBu)_3(NCO)\{OC(O)R\}]$ by loss of NaX (scheme **1.34.**, left). Reduction of $[Nb(N[Ar]^tBu)_3(NCO)\{OC(O)R\}]$ with sodium mercury amalgam gave the nitride precursor **30** by the elimination of [NaOC(O)R] and CO. These transformations represent a ligand based mediation of CO_2 to CO, and the regeneration of **30** closes the synthetic cycle for this process. Alternatively, reduction of $[Nb(N[Ar]^tBu)_3(NCO)\{OC(O)R\}]$ with samarium diiodide affords the loss of the acetate group, preparing **29** (scheme **1.34.**, right), which can also be reduced to prepare **30** (see above, Section 3.5.).[94]



*Scheme **1.34.** Preparation of **29**.*

1.5. Towards uranium nitrides

As can be seen from the transition metal examples discussed, a great deal can be learnt about the electronic structure of a metal by a consideration of metal-ligand multiple bonding interactions. For uranium, multiple bond interactions are dominated by examples containing the uranyl fragment, $[U(O)_2]^{2+}$ (> 2100 crystallographically characterised examples).[108] In addition to this, there are a growing number of examples of uranium–ligand multiple bonds to other main group elements, including carbene ($U{=}CR_2$),[109-115] imide ($U{=}NR$)[38,116-120] and mono-oxo ($U{=}O$)[45,119,121-125] for which there are approximately 30, 100 and 30 crystallographically characterised examples of each respectively.[108] There is only one crystallographically characterised example each of terminal uranium (U=E) sulfide (E = S), selenido (E = Se) and tellurido (E = Te), species[126] though there are a growing number of complexes which feature interactions with these elements.[127] Recently, and related to work in this thesis, are examples of parent uranium pnictide complexes: imide,[36] phosphide[46] and arsenide[47] species.

There was, however, a conspicuous lack of uranium nitride species. The first report of a uranium nitride was the binary [U≡N] in 1976, which was observed at temperatures less than 5 K using matrix isolation and isotopic labelling techniques.[128] Similar complexes were prepared in the following years, including [NUN],[129] [NUO],[130] [NUF_3],[131] [NUNH],[132] and $[NUO]^+$,[133] (see figure **1.13.**) which also employed mass spectrometric techniques alongside matrix isolation in their identification. Whilst there is a certain elegance to the preparation of these uranium nitrides, they remain challenging to work with as a result of the conditions required for their synthesis, and therefore the study of their properties is problematic. As a result, chemists attempted to synthesise a molecular uranium nitride that might be stable at ambient temperatures.

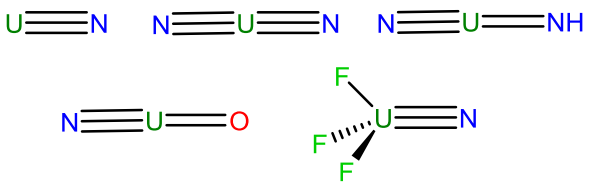
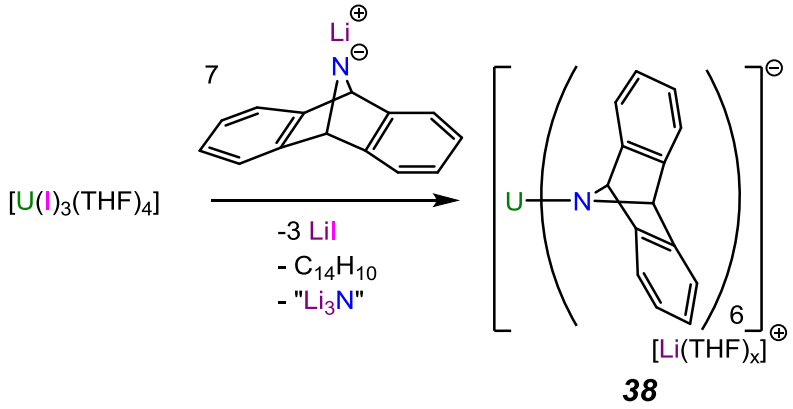


*Figure **1.13.** U≡N species prepared by matrix isolation.*

The first attempt to synthesise a uranium–nitride was reported by Cummins *et al*. in 2000.[134] Their attempted methodology employed [Li(dbabh)] (Hdbabh = 2,3:5,6-dibenzo-7-azabicyclo[2.2.1]hepta-2,5-diene), a nitride transfer reagent, to try and enact analogous chemistry to that reported for chromium, wherein addition of [Li(dbabh)] to a chromium iodide complex yielded the corresponding nitride species **25** with concomitant elimination of KI and anthracene (see above).[73] However, addition of [Li(dbabh)] to $[U(I)_3(THF)_4]$ instead resulted in the uranium(V)–*hexakis*(amide) product, $[Li(THF)_x][U(dbabh)_6]$, **38** (scheme **1.34.**).

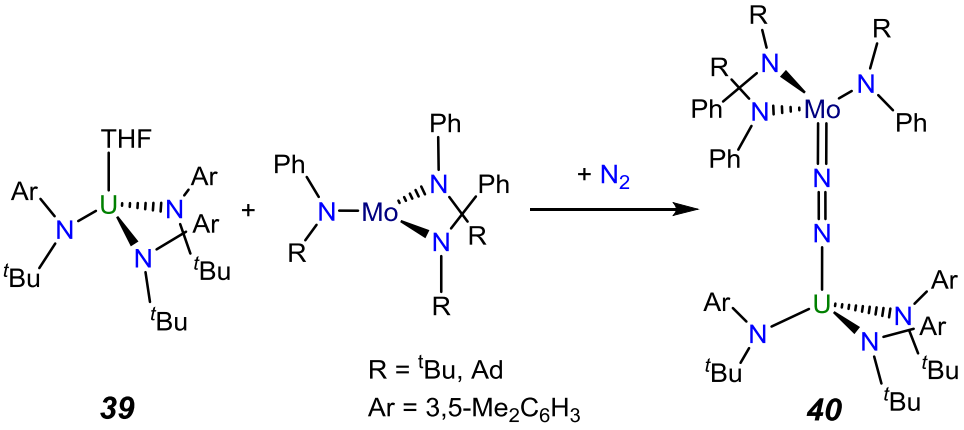


38

*Scheme **1.34.** Synthesis of **38**.*

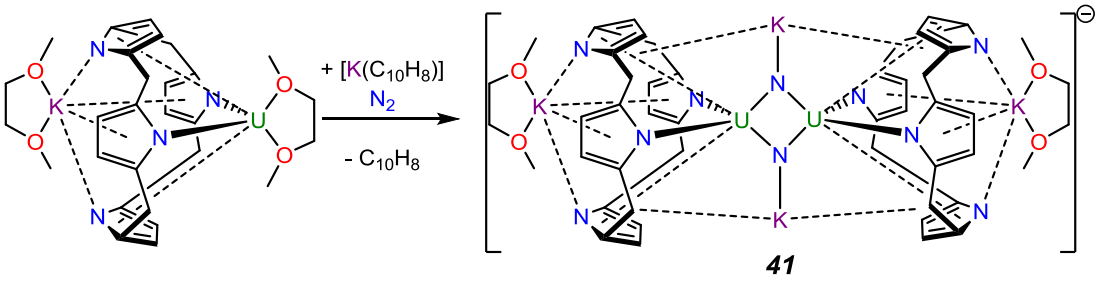
Subsequently, Cummins *et al*. attempted to form a terminal nitride species by cleaving the N≡N bond of dinitrogen, analogously to the reactivity reported for molybdenum complexes (see Section 3.4.).[84] However, in contrast to the anticipated cleavage of N_2, they instead reported the trapping of dinitrogen with the U^{III} and Mo^{III} precursors $[U\{N(Ar)^tBu\}_3(THF)]$ (**39**, Ar = 3,5-$Me_2C_6H_3$) and $[Mo\{N(R)(Ph)\}_3]$ (R = ^{t}Bu, Ad, *cf*. **28**) resulting in the synthesis of $[U\{N(^tBu)(Ar)\}_3(\mu\text{-}\eta^1\text{:}\eta^1\text{-}N_2)Mo\{N(R)(Ph)\}_3]$, **40** (see scheme **1.35.**).[135] Complex **40** demonstrates end-on binding of dinitrogen, as opposed to side-on binding, for which there is a precedence in uranium chemistry in the Tren complex $[\{U(Tren^{DMBS})\}_2(\mu\text{-}\eta^2\text{:}\eta^2\text{-}N_2)]$ (**16**, see Section 2.2.1.).[40] The N-N bond length in **40** is longer than in free N_2 [1.232(11) *vs* free N_2, 1.0975 Å],[38] suggesting that the

formation of this bridging complex is accompanied by reduction to an $(N_2)^{2-}$ unit.



*Scheme **1.35.** Synthesis of **40**.*

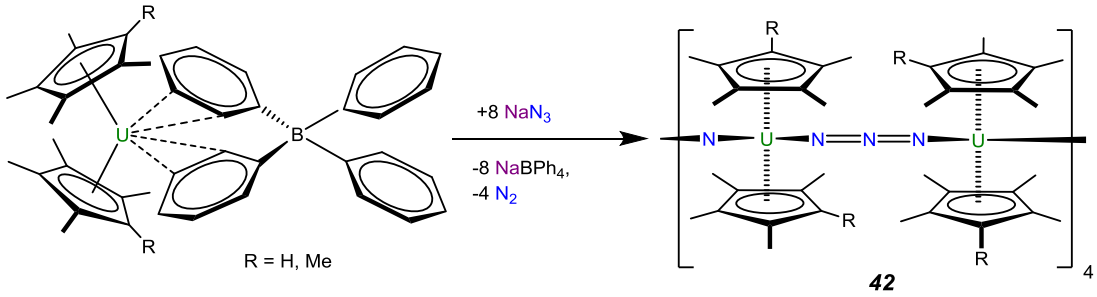
Gambarotta *et al*. reported the first example of a nitride species synthesised by the reduction of N_2 by a U^{III} species.[136] The reaction of [{K(DME)(Et_8-calix[4]tetrapyrrole)}U(DME)] (Et_8-calix[4]tetrapyrrole = {$(C_4H_2N)CEt_2\}_4$) with potassium naphthalenide [$K(C_{10}H_8)$] under a nitrogen atmosphere prepares [{K(DME)(Et_8-calix[4]tetrapyrrole)U}$_2$(μ-NK)$_2$][K(DME)$_4$] (**41**, scheme **1.36.**). Complex **41** is a mixed valent U^{IV}/U^{V} dinuclear bridging nitride complex and is the only uranium nitride complex formed by the reductive cleavage of dinitrogen.



*Scheme **1.36.** Synthesis of **41**. Ethyl groups and the cationic fragment [K(DME)$_4$] omitted for clarity.*

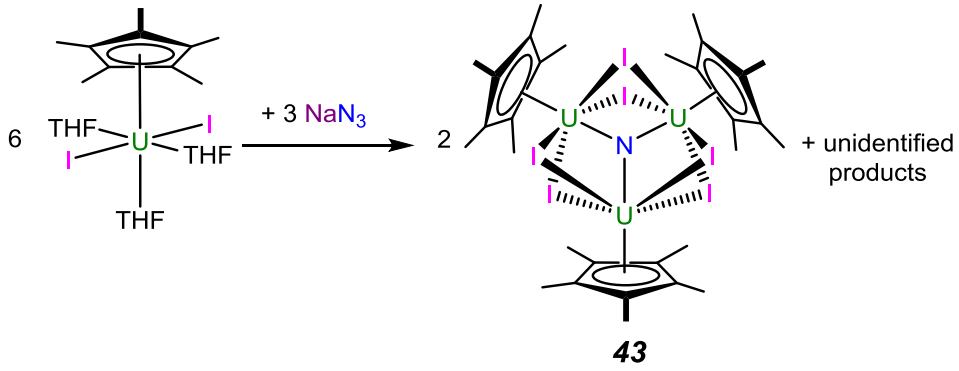
In 2005, Evans *et al*. reported the synthesis of an octauranium(IV) ring with alternating bridging nitride and azide ligands, [{$(C_5Me_4R)_2U(\mu$-N)U(μ-N_3)$(C_5Me_4R)_2\}_4$] (**42**, R = Me, H), by the reaction of [$U(C_5Me_4R)_2\{(\mu$-Ph)$_2BPh_2\}$] with NaN_3 (scheme **1.37.**).[137] Formally, eight U^{III} centres are oxidised to U^{IV} with the corresponding reduction of four azide ligands to

nitride ligands with concomitant dinitrogen elimination. Only half of the azide ligands are reduced as this process is a two-electron reduction, each reduction therefore requiring the one-electron oxidation of two uranium centres. This reactivity contrasted with the expected azide substitution product, "$[U(N_3)(C_5Me_4R)_2]$", which had been the anticipated product based on previous work.[137]



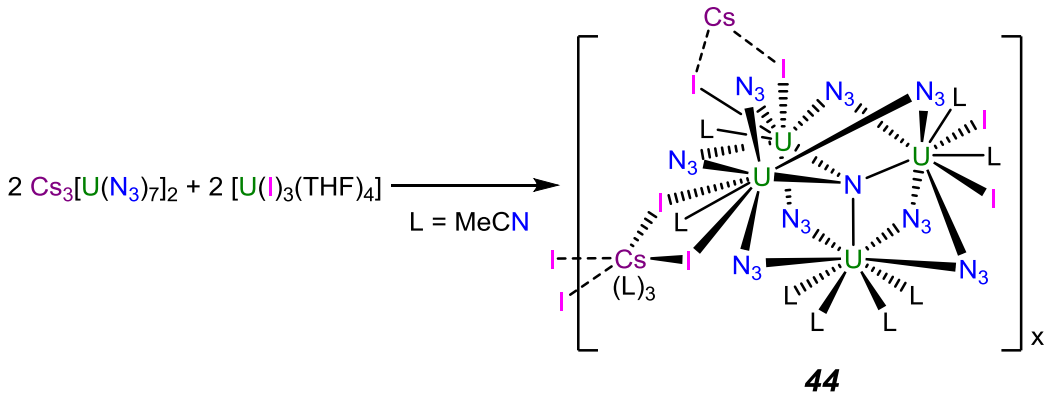
*Scheme **1.37.** Synthesis of **42.***

Evans *et al.* also reported the triuranium cluster $[\{U(Cp^*)(\mu\text{-}I)_2\}_3(\mu^3\text{-}N)]$ (**43**, Cp* = η^5-C_5Me_5), synthesised by the reduction of NaN_3 with $[U(Cp^*)(I)_2(THF)_3]$ (scheme **1.38.**).[138] The product incorporates bridging iodide ligands and a μ^3-nitrido centre. It was not possible to discern the nitride from an oxide or hydroxide *via* X-ray crystallographic analysis, though subsequent isotopic labelling and chemical ionisation mass spectrometry could confirm the identity of the central atom as nitrogen. Computational calculations were also used to discern the central atom, with an analysis of the spin density of the uranium centres leading to confirmation of three U^{IV} centres, which is in accordance with a nitride (N^{3-}) as the central atom.[139]



*Scheme **1.38.** Synthesis of **43**.*

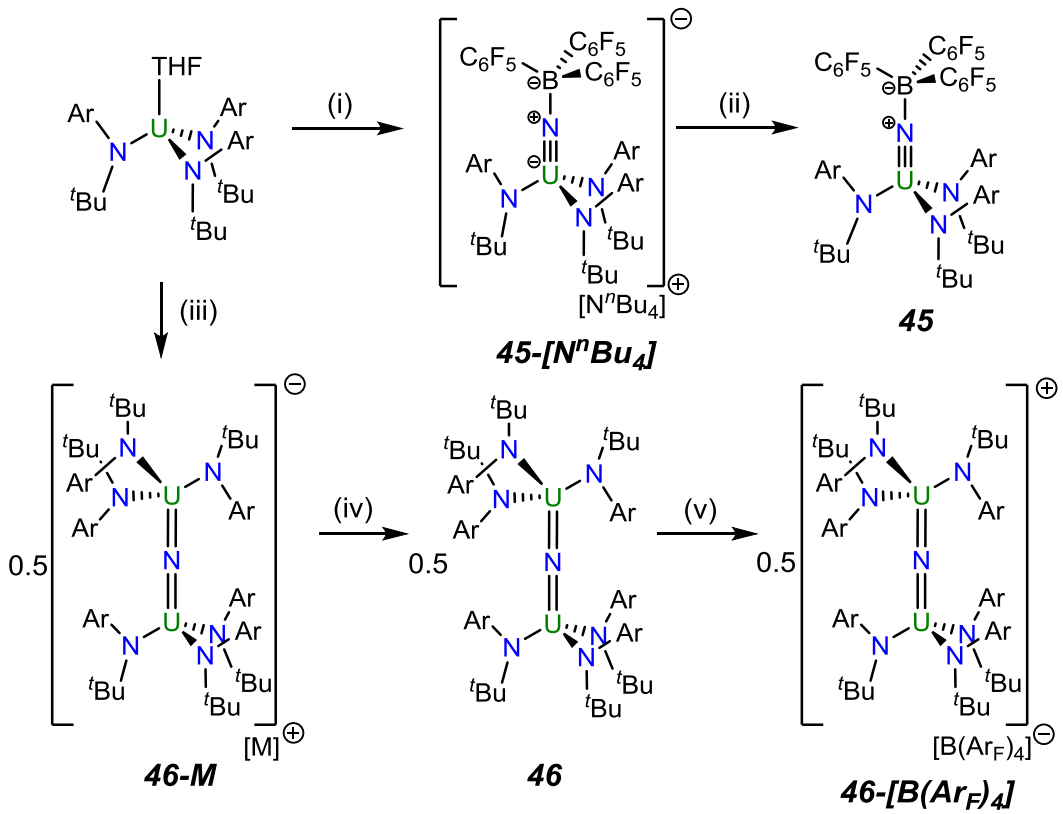
Mazzanti *et al*. also investigated uranium nitride clusters, reporting a tetrauranium cluster with a μ^4-nitrido centre and eight bridging azide ligands of formulation $\{[Cs(MeCN)_3][U_4(\mu^4\text{-}N)(\mu\text{-}N_3)_8(MeCN)_8(I)_6]\}_x$, **44**, in 2008.[140] The reaction of $[U(I)_3(THF)_4]$ with the homoleptic azide $[Cs_3][U(N_3)_7]$, resulted in a two-electron reduction of an azide by two U^{III} centres (see Scheme **1.39.**). It was proposed that the nitrido centre provides a templating role in cluster formation in this complex. Complex **44** is so far the only reported uranium nitride complex not to feature stabilising bulky ancillary ligands.



44

*Scheme **1.39.** Synthesis of **44**.*

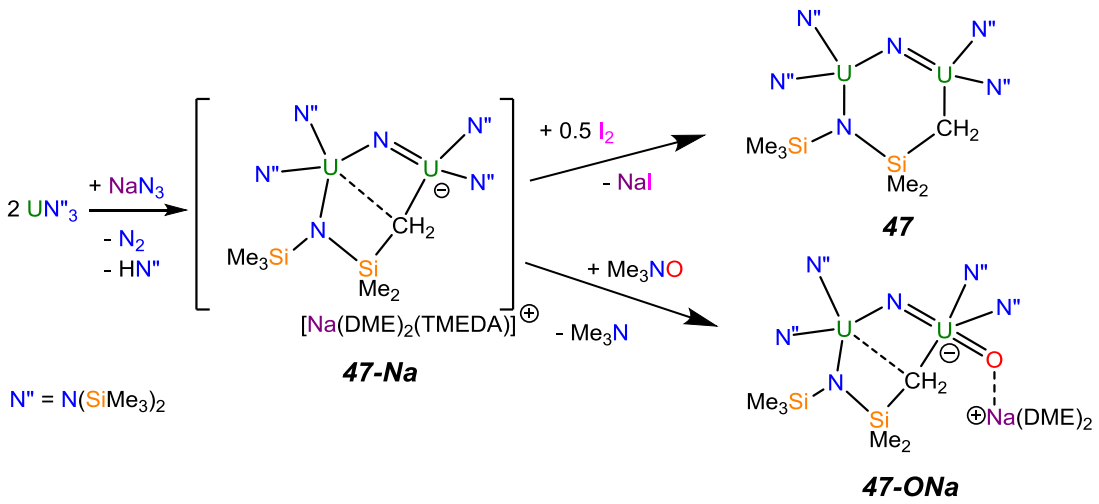
In 2009, Cummins *et al*. reported attempts to prevent cluster formation using relatively sterically demanding ligands. The reaction of **39** with $[N^nBu_4][(N_3)B(C_6F_5)_3]$ afforded the pentavalent uranium nitrido borate complex $[N^nBu_4][U\{N(Ar)^tBu\}_3\{\equiv NB(C_6F_5)_3\}]$, **45-[$N^nBu_4$]**, with the elimination of dinitrogen. This species was subsequently oxidised to the hexavalent neutral species $[U\{N(Ar)^tBu\}_3\{\equiv NB(C_6F_5)_3\}]$, **45**, using half an equivalent of elemental iodine (scheme **1.40.**, upper).[141] The U≡N bond length was reported as 1.880(4) Å, the shortest U-N bond reported at that time for a molecular system. However, the N-B bond was impervious to cleavage, and therefore syntheses utilising $[N^nBu_4][(N_3)B(C_6F_5)_3]$ do not afford a viable route to a terminal uranium nitride system.



i) + [N^{n}Bu$_4$][(N$_3$)B(C$_6$F$_5$)$_3$], - N$_2$, THF. ii) + 0.5 I$_2$, - [N^{n}Bu$_4$][I]. iii) +0.5 [MN$_3$], - N$_2$.
iv) + 0.5 [AgOTf], -0.5 Ag, 0.5 [MOTf]. v) 0.5 [Fe(Cp)$_2$][B(Ar$_F$)$_4$], -0.5 [Fe(Cp)$_2$].
M = Na, N^{n}Bu$_4$. Ar = 3,5-Me$_2$C$_6$H$_3$. Ar$_F$ = 3,5-(CF$_3$)$_2$C$_6$H$_3$.

*Scheme **1.40.** Synthesis of **45** and **46-[B(Ar$_F$)$_4$]**.*

As the cleavage of the borate group from the nitride in **45** had impeded the synthesis of terminal nitride systems, further work by Cummins *et al.* utilised unprotected azides in an attempt to avoid this cleavage step. However, addition of MN$_3$ (M = Na, N^{n}Bu$_4$) to **39** gave the nitride bridged bimetallic U^{IV}/U^{IV} system [M][{U(N[Ar]^{t}Bu)$_3$}$_2$(μ-N)] (**46-M**, Ar = 3,5-Me$_2$C$_6$H$_3$, scheme **1.40.**, lower).[142] By comparison of **45-[N^{n}Bu$_4$]** and **46-N^{n}Bu$_4$**, it can be seen that the presence of the borate has a considerable effect on the product synthesised. Addition of AgOTf oxidises **46-M** to the neutral, mixed valent uranium(IV/V) species [{U(N[^{t}Bu][Ar])$_3$}$_2$(μ-N)], **46**.[142] Further oxidation with [Cp$_2$Fe][BAr$_F$)$_4$] (Ar$_F$ = 3,5-(CF$_3$)$_2$C$_6$H$_3$) yields the U^V/U^V system [{U(N[^{t}Bu][Ar])$_3$}$_2$(μ-N)][B(Ar$_F$)$_4$], **46-[B(Ar$_F$)$_4$]**.[142]

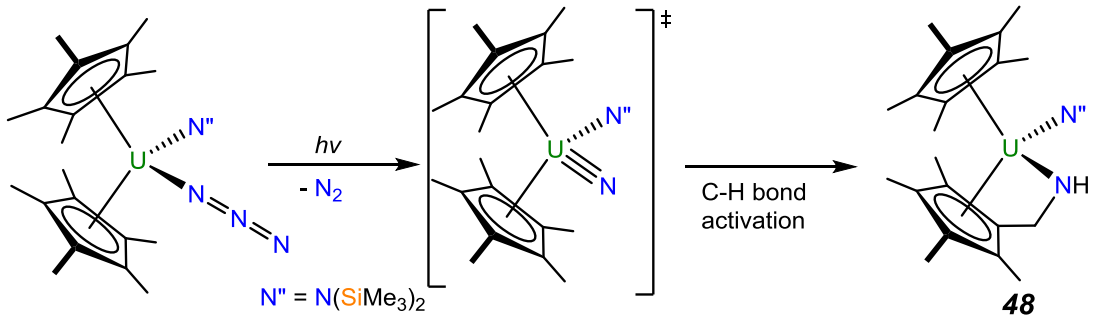


Scheme ***1.41.*** *Synthesis of* **47** *and* **47-ONa**.

All molecular examples of uranium nitride species thus far discussed have all contained a nitride bound to multiple uranium centres (or are borane capped, **45**), where the bond order of each U-N interaction is essentially equivalent. In 2010, Hayton *et al*. reported the first example of nitride species with inequivalent U-N bond distances. The complex $[Na(DME)_2(TMEDA)][U(N'')_2(\mu\text{-}N)(CH_2SiMe_2NSiMe_3)U(N'')_2]$ [**47-Na**, N″ = $N(SiMe_3)_2$, TMEDA = tetramethylethylenediamine, $Me_2NCH_2CH_2NMe_2$, scheme **1.41.**], was prepared by the reduction of NaN_3 with $[U(N'')_3]$.[122] Oxidation of **47-Na** with elemental iodine yielded the mixed valent U^{IV}/U^{V} complex $[U(N'')_2(\mu\text{-}N)(CH_2SiMe_2NSiMe_3)U(N'')_2]$ (**47**), which in addition to a bridged nitride motif also features a tuck-over cyclometallated alkyl ligand, using the same terminology as in Section 2.2.1. Complex **47-Na** was also reacted with Me_3NO, an oxo transfer reagent, which gave the U^{VI}/U^{IV} mono-oxo complex, $[Na(DME)_2][U(O)(\mu\text{-}N)(N'')_2(CH_2SiMe_2NSiMe_3)U(N'')_2]$, **47-ONa**. The bridging nitrides in **47**, **47-Na** and **47-ONa** each have two inequivalent bonds, where the difference is more pronounced in the neutral species **47** than in anionic **47-Na**. The U-N bond distances of 1.909(6) and 2.201(6) Å in **47** suggest a localised bonding scheme in which the core is best formulated as [U=N-U]. This single and double bond inequivalency of the nitride may be as a consequence of the non-linearity of the bonding: the U(1)-N(1)-U(2) bond angle in **47** is 123.5(5)°. Complex **47-ONa** has a great

similarity in both its geometry (sodium-capped oxo ligand *trans* to the nitride bridging ligand [O(1)-U(1)-N(1) 167.6(3)°]) and bond distances (short U(1)-N(1) and U(1)-O(1) bond distances [1.818(9) and 1.797(7) Å respectively]) to the uranyl ion, $[UO_2]^{2+}$.[143]

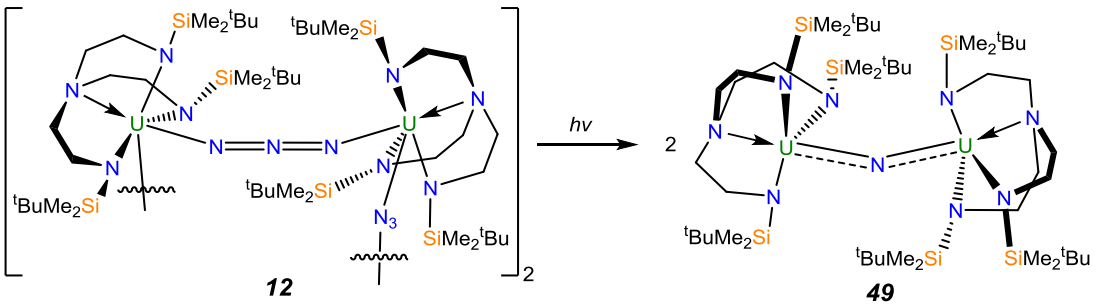
Photolysis of azide complexes is a well-known route to nitrides in transition metal chemistry,[64,144,145] however until 2010, the photochemistry of uranium azides had remained largely unexplored. Kiplinger *et al.* reported the photolytic C-H activation of the uranium(IV) species $[U(Cp^*)_2(N_3)(N'')]$ to form the cyclometallated complex $[U(Cp^*)(\kappa^1{:}\eta^5\text{-}C_5Me_4CH_2NH)(N'')]$, **48** (scheme **1.42.**).[146] Computational calculations hypothesised that a terminal uranium(VI)–nitride species is generated *in situ* before 1,1-insertion into a C-H bond on a Cp* ligand to yield the uranium(IV) cyclometallate. This work represents a close approach to a terminal system, with the decomposition of the azide ligand forming a uranium(VI)–nitride species before undergoing C-H activation as a result of the inherently high energy photolytic conditions.



*Scheme **1.42.** Synthesis of **48**.*

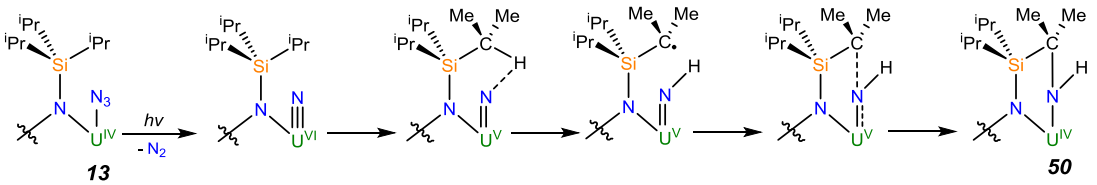
A salient structural point to note from these syntheses is that in all cases, the nitride atom is either bound to multiple electrophilic uranium centres, be that between two uranium centres (**41**, **42**, **46**, **47**), or as part of a cluster (**43**, **44**), or is capped by a borane group impervious to removal (**45**), or was only transiently formed by photolytic techniques which prepared a cyclometallated amide species (**48**). It is therefore appreciable how challenging a synthetic target the terminal uranium nitride was.

Unpublished work[37] from within the Liddle group also explored the behaviour of uranium–azide species under photolytic conditions. Exposure of [{U(Tren^{DMBS})(μ-N$_3$)}$_4$] (**12**) to photolytic conditions (7 hours, 125 W Hg photolysis lamp, room temperature) did not result in the desired terminal nitride species "[U(Tren^{DMBS})(N)]", instead affording the bridged nitride species [{U(Tren^{DMBS})}$_2$(μ-N)], **49** (scheme **1.43.**). This suggests that the Tren^{DMBS} framework is not sterically bulky enough to stabilise a monomeric terminal nitride, and hence the bimetallic species **49** is prepared.



*Scheme **1.43.** Synthesis of **49**.*

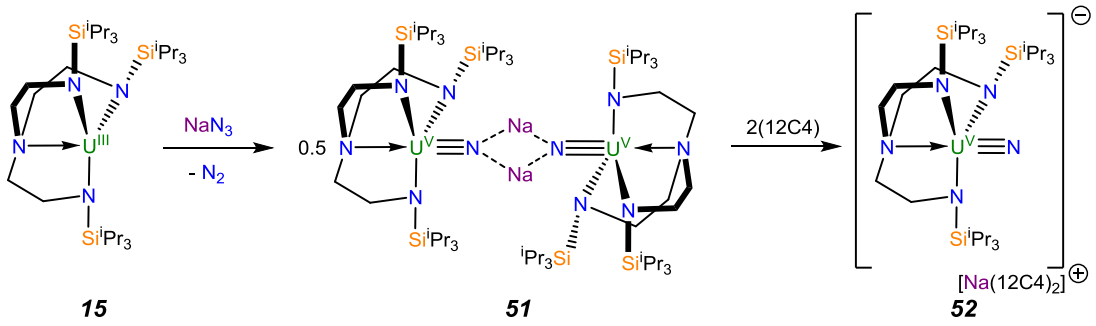
Following this, irradiation of the more sterically bulky [U(Tren^{TIPS})(N$_3$)], **13**, which is monomeric in the solid state (*cf.* **12**, which is tetranuclear) was also attempted. Exposure of **13** to photolytic conditions for 5 hours afforded a new colourless compound, with a ^{1}H NMR spectrum featuring paramagnetic resonances spanning +105 to –47 ppm, which was formulated as the cyclometallated amide compound [U{*N*(H)C(Me)$_2$Si(^{i}Pr)$_2$*N*CH$_2$CH$_2$*N*(CH$_2$CH$_2$*N*Si^{i}Pr$_3$)$_2$], **50**.[34] This reactivity parallels that described by Kiplinger (for the preparation of **48**).[146] A mechanism proposed for the transformation of **13** to **50**, *via* a transiently formed uranium–nitride, is illustrated in Scheme **1.44.**



*Scheme **1.44.** Proposed mechanism for the decomposition of **13** to **50**.*

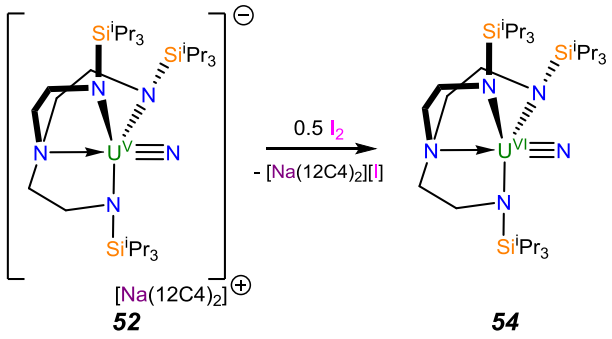
As the proposed mechanism for the high energy photolytic route which prepared **50** invokes a postulated transiently formed uranium nitride, other routes towards a nitride of {U(Tren^{TIPS})} were investigated. The reaction of [U(Tren^{TIPS})] (**15**) with NaN_3 in pyridine afforded the dinuclear species [{U(Tren^{TIPS})(μ-N)(μ-Na)}$_2$], **51**, with the concomitant elimination of dinitrogen (scheme **1.45.**).[31] The two electrons required for reduction of the azide fragment come from the uranium(III) centre, in reactivity paralleling that of the preparation of **42**.[137]

Reaction of **51** with two equivalents of 12-crown-4 ether (12C4) per sodium afforded [U(Tren^{TIPS})(N)][Na(12C4)$_2$], **52**, which was the first example of a terminal uranium–nitride species stable at ambient conditions (scheme **1.45.**).[31] It was also noted that using a slightly larger crown ether afforded a capped nitride: addition of 15-crown-5 ether (15C5) to **51** yields [U(Tren^{TIPS}){(μ-N)(μ-Na)(15C5)}] (**53**).[34]



*Scheme **1.45.** Synthesis of **52**.*

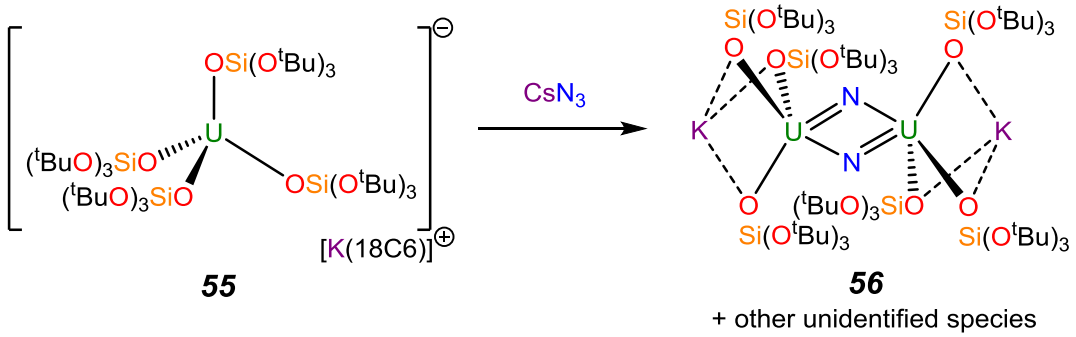
As was found for the preparation of **45** and **47** (from **45-N^{n}Bu$_4$** and **47-Na** respectively), oxidation of **52** is readily achieved using half an equivalent of elemental iodine to afford [U(Tren^{TIPS})(N)], **54** (scheme **1.46.**).[34]



*Scheme **1.46.** Synthesis of **54**.*

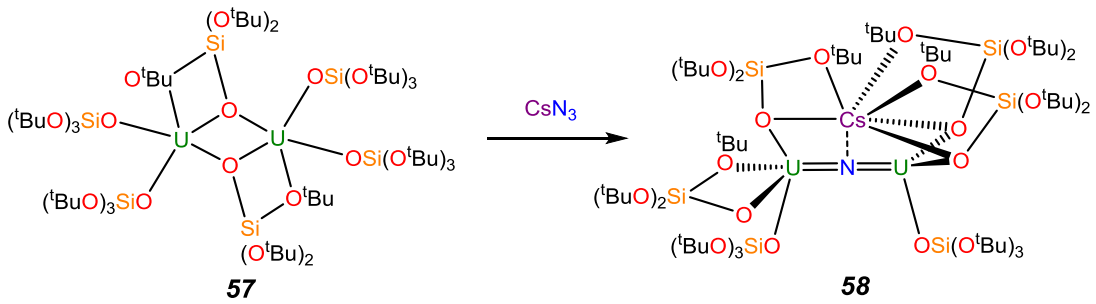
Since the initial publication of **52** in 2012, several further uranium nitrides have been published, though again, these are all dinuclear species, where the nitride resides between two electrophilic uranium centres, or capped species.

Mazzanti *et al*. reported reactions of several azide sources with uranium siloxide complexes in attempts to prepare nitride complexes.[147] They report several examples of imide formation, as well as two bridged uranium–nitride species. The reaction of [U{OSi(O^{t}Bu)$_3$}$_4$][K(18C6)] (**55**) with CsN_3 affords a complex mixture of compounds, from which the di-μ-nitrido diuranium(V) species [KU{OSi(O^{t}Bu)$_3$}$_3$(μ-N)]$_2$ (**56**) was crystallised (scheme **1.47.**).[147] Complex **56** features a U_2N_2 diamond shaped core, reminiscent of the structure reported for **41**.[136]



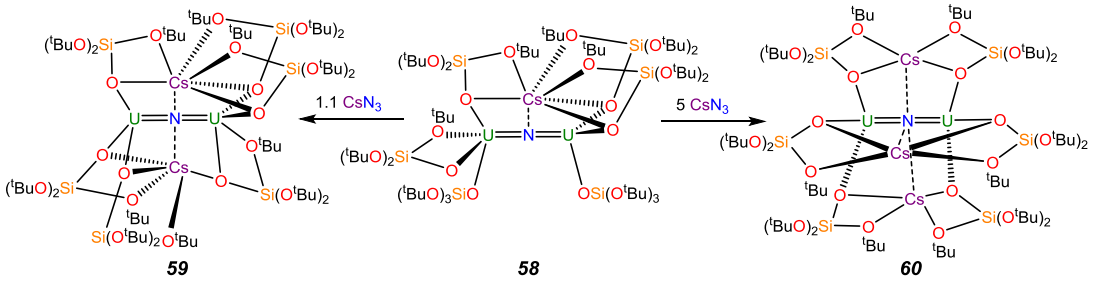
*Scheme **1.47.** Synthesis of **56**.*

Contrastingly, reaction of the homoleptic diuranium(III) species [{U(OSi[O^{t}Bu]$_3$)$_2$(μ-OSi[O^{t}Bu]$_3$)}$_2$] (**57**) with CsN_3 affords the bridged nitride species Cs[{U(OSi(O^{t}Bu)$_3$)$_3$}$_2$(μ-N)] (**58**, scheme **1.48.**).[147] Complex **58** contains two uranium(IV) centres, bridged by a nitride atom, and is the second example of a linear U^{IV}-N-U^{IV} motif (*cf*. **46**), though here there is a caesium atom in the apical position of the nitride ligand, between the siloxide ligands.



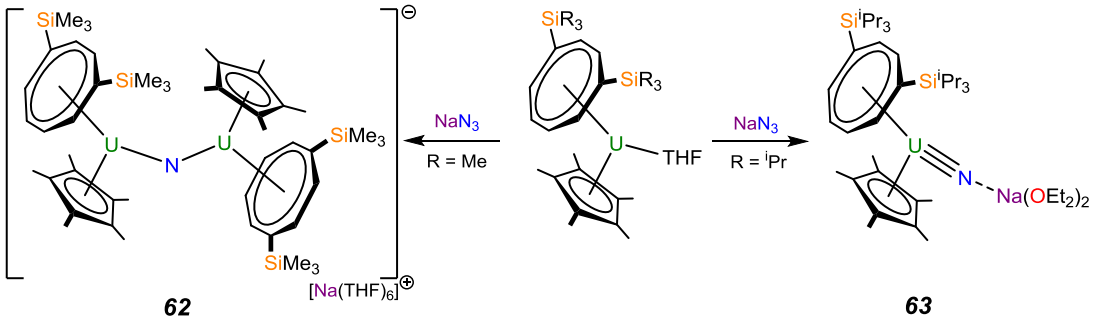
*Scheme **1.48.** Synthesis of **58**.*

Very recently, Mazzanti *et al.* have reported the further reduction of **58** with 1.1 equivalents of Cs to afford $Cs_2[\{U(OSi(O^tBu)_3)_3\}_2(\mu\text{-}N)]$ (**59**, scheme **1.49.**, left) or with 5 equivalents of Cs to afford $Cs_3[\{U(OSi(O^tBu)_3)_3\}_2(\mu\text{-}N)]$ (**60**, scheme **1.49.**, right), which are respectively the U^{III}-N-U^{IV} and U^{III}-N-U^{III} bridged nitrides.[148] The authors report that this is an extension of the set of molecular uranium nitrides to incorporate the uranium(III) oxidation state.



*Scheme **1.49.** Synthesis of **59** and **60**.*

Similarly, reaction of $[U\{(^{tBu2}ArO)_2Me_2\text{-cyclam}\}I]$ [$(^{tBu2}ArO)_2Me_2$-cyclam = $\{(1\text{-}O\text{-}2,4\text{-}^tBu_2\text{-}C_6H_2\text{-}6)\text{-}CH_2N(CH_2)_2N(Me)(CH_2)_3\}_2$] with CsN_3 gave the U^{IV}=N-U^{IV} bridged nitride complex $[\{\kappa^4\text{-}(^{tBu2}ArO)_2Me_2\text{-cyclam}\}(N_3)U(\mu\text{-}N)U\{\kappa^5\text{-}(^{tBu2}ArO)_2Me_2\text{-cyclam}\}]$ (**61**).[149] The authors report that **61** was prepared on a low scale in an NMR tube, and attempts at scale up were unsuccessful.



*Scheme **1.50.** Synthesis of **62** and **63**.*

Finally, the most recent example of uranium nitrides come from the reaction of $[U\{\eta^8\text{-}1,4\text{-}(Me_3Si)_2C_8H_6\}(Cp^*)(THF)]$ with NaN_3 which affords the bridging nitride complex $[\{U(\eta^8\text{-}1,4\text{-}[Me_3Si]_2C_8H_6)(Cp^*)\}_2(\mu\text{-}N)]$, **62** (scheme **1.50.**, left). Increasing the steric bulk of the COT ligand [from 1,4-$(SiMe_3)_2$ substituents to 1,4-$(Si^iPr_3)_2$

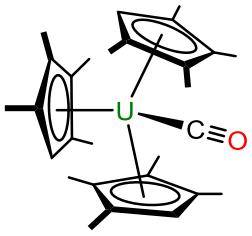
substituents] affords instead the capped nitride, [U{η^8-1,4-(^{i}Pr$_3$Si)$_2$C$_8$H$_6$}(Cp*){(μ-N)(μ-Na)(OEt$_2$)$_2$}], **63**, under the same conditions (scheme **1.50.**, right). [150]

1.6. Reactivity of uranium species towards small molecules

The reactivity of uranium towards a vast array of small molecules is a burgeoning field of research, and what follows is a brief overview of investigations to date. Special interest shall be paid to investigations towards CO and CE_2 (E = O, S), as these small molecules will be investigated in the body of this thesis. For further reading, the reader is directed towards reviews into the small molecule activation chemistry of uranium(III) species, by Liddle[14] and Meyer.[15]

1.6.1. Reactivity of uranium species towards CO

The reactivity of uranium complexes towards CO has been widely investigated, and a large number of these feature uranium in the +3 oxidation state.



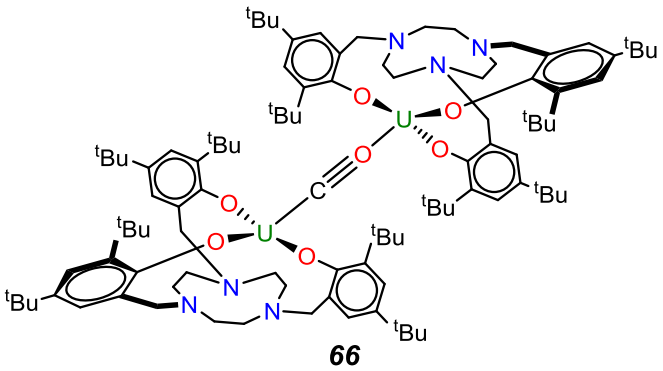
64

*Figure **1.14.** Complex **64**, the first crystallographically characterised uranium carbonyl.*

The first uranium carbonyl complex reported was [U(Me$_3$SiC$_5$H$_4$)$_3$(CO)], and was prepared by the reaction of [U(Me$_3$SiC$_5$H$_4$)$_3$] with CO.[151] The carbonyl unit, which was reversibly bound, had an absorption in the IR spectrum at 1976 cm^{-1}. The first isolable, crystallographically characterised uranium carbonyl was [U(Me$_4$C$_5$H)$_3$(CO)] (**64**, figure **1.14.**),[152] prepared in an analogous manner to [U(Me$_3$SiC$_5$H$_4$)$_3$(CO)]. The IR spectrum contains a broad absorption at 1880 cm^{-1}. A

third carbonyl complex, $[U(Cp^*)_3(CO)]$, has also been prepared by reaction of the homoleptic trivalent precursor with carbon monoxide (ν_{CO} = 1922 cm^{-1}).[153]

The reaction of $[U\{(^{tBu2}ArO)_3tacn\}]$ [($^{tBu2}ArO)_3tacn$ = *tris*(aryloxide)triazocyclononane, (1-*O*-2,4-$^tBu_2C_6H_2$-$CH_2)_3(NCH_2CH_2)_3$], **65-^{t}Bu$_2$**, with CO afforded the dinuclear bridged species $[\{U([^{tBu2}ArO]_3tacn)\}_2(\mu\text{-}\eta^1\text{:}\eta^1\text{-CO})]$ (**66**, figure **1.15.**), with a strong absorption at 2092 cm^{-1} in the FTIR spectrum.[154] Complex **66**, the first crystallographically characterised CO-bridged diuranium complex, is proposed to form by the nucleophilic attack of a charge separated carbonyl complex $[U^{IV}\{(^{tBu2}ArO)_3tacn\}(CO)^{\bullet-}]$ on a coordinatively unsaturated molecule of **65-^{t}Bu$_2$**.



66

*Figure **1.15.** Complex **66**.*

An interesting reactivity pattern described within the literature for CO activation involves the homologation of CO into ethynediolate $(OCCO)^{2-}$, deltate $(C_3O_3)^{2-}$ or squarate $(C_4O_4)^{2-}$units.

In 2006, Cloke *et al.* found that the reaction of $[U\{\eta^8\text{-}1,4\text{-}(^iPr_3Si)_2C_8H_6\}(\mu^5\text{-}C_5Me_5)(THF)]$ (**67**) with CO prepares the deltate complex $[\{U(\mu^8\text{-}1,4\text{-}[^iPr_3Si]_2C_8H_6)(\mu^5\text{-}C_5Me_5)\}_2(\mu\text{-}\kappa^1\text{:}\kappa^2\text{-}C_3O_3)]$ (**68**), by reductive cyclotrimerisation (figure **1.16.**, left).[155]

Reaction of $[U\{\eta^8\text{-}1,4\text{-}(^iPr_3Si)_2C_8H_6\}(\eta^5\text{-}C_5Me_4H)(THF)]$ (**69**), where there is a slight modification of the cyclopentadienyl ligand (when compared to **67**), with CO instead prepares the squarate complex

[{U(η^8-1,4-[^{i}Pr$_3$Si]$_2$C$_8$H$_6$)(η^5-C$_5$Me$_5$)}$_2$(μ-η^2:η^2-C$_4$O$_4$)] (**70**) by reductive cyclotetramerisation (figure **1.16.**, right).[156]

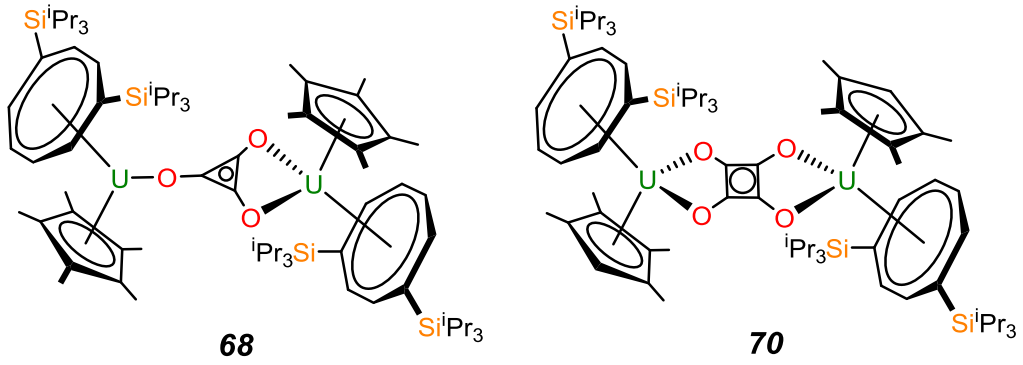


*Figure **1.16.** Complexes **68** and **70**.*

The mechanism for these reductive oligomerisations was investigated. The ethynediolate complex [{U(η^8-1,4-[^{i}Pr$_3$Si]$_2$C$_8$H$_6$)(η^5-C$_5$Me$_5$)}$_2$(μ-κ^1:κ^1-^{13}C$_2$O$_2$)] (**71**) was prepared by the reaction of **67** with 0.9 equivalents of ^{13}CO. The authors found that reaction of **71** with excess ^{13}CO did not prepare **68**-^{13}**C**, even after heating at 60 °C for 3 days, which implies that the mechanism for the formation of **68** and **70** does not proceed *via* **71**.

To investigate the formation of **71**, an FTIR spectrum was run immediately of a sample of **67** in d$_8$-toluene treated with CO, and a strong absorption was observed at 1920 cm^{-1} (comparable to the carbonyls described above, *cf.* **64**), which is attributed to [U{η^8-1,4-(^{i}Pr$_3$Si)$_2$C$_8$H$_6$}(μ^5-C$_5$Me$_5$)(CO)].

DFT calculations were then performed on the formation of **71** from **67** and CO (figure **1.17.**),[157] which indicate that [U{η^8-1,4-(^{i}Pr$_3$Si)$_2$C$_8$H$_6$}(η^5-C$_5$Me$_5$)(CO)], (figure **1.17.**, I) prepares a dimer, II, such that there are not only the initial U-C bonds, but also U-O bonds, through Lewis acidic binding. The C-C distance then shortens, passing through a transition state 9 kJ mol^{-1} above II, and the transition state to prepare **71** (IV) is 59 kJ mol^{-1} above III. This is consistent with the slow formation of **71** (hours by NMR spectroscopic analysis). The authors propose that III is a long lived intermediate, which prepares **68** or **70** in the presence of further CO reagent, but in the absence of further CO, U-C bond breaking allows the formation of **71**.

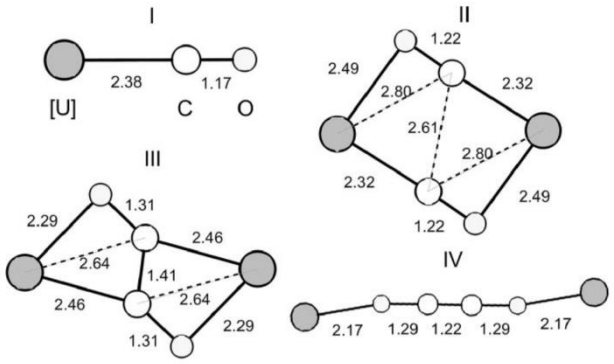


*Figure **1.17.** Calculated dimensions for U-CO units in I – IV.*

The reaction of [U{η^8-1,4-(^{i}Pr$_3$Si)$_2$C$_8$H$_6$}(η^5-C$_5$Me$_4$R)] (R = Et) with CO to give [{U(μ^8-1,4-[^{i}Pr$_3$Si]$_2$C$_8$H$_6$)(μ^5-C$_5$Me$_4$Et)}$_2$(μ-η^1:η^1-C$_2$O$_2$)].[158] The authors outline that for mixed sandwich complexes of uranium, the global sterics at uranium dictate whether reactivity with CO occurs, whilst sterics at the cyclopentadienyl ligand define which oxocarbon $(C_nO_n)^{2-}$ (n = 2, 3, 4) is formed. In the case of the compounds with more bulky substituents, [U{μ^8-1,4-(^{i}Pr$_3$Si)$_2$C$_8$H$_6$}(μ^5-C$_5$Me$_4$R)] (R = ^{i}Pr, SiMe$_3$), no reactivity was observed with CO. Finally, they also report the liberation of the squarate by reaction from **70** with Me$_3$SiCl to give the silylated ester of squaric acid, [C$_4$O$_2$(OSiMe$_3$)$_2$], in a similar manner to the liberation of silyl esters from **73** (see below).[158]

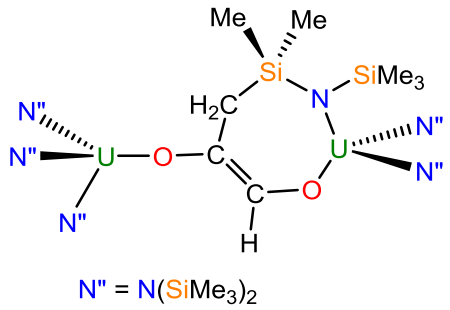
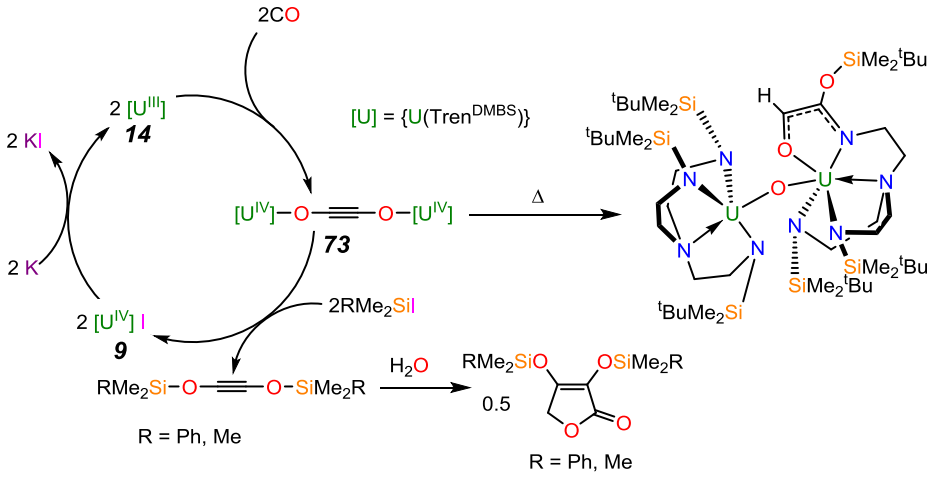


*Figure **1.18.** Complex [U(N")$_3${μ-OC(=CH-O)-CH$_2$Si(Me)$_2$N(SiMe$_3$)}U(N")$_2$], from the thermolytic decomposition of **72**.*

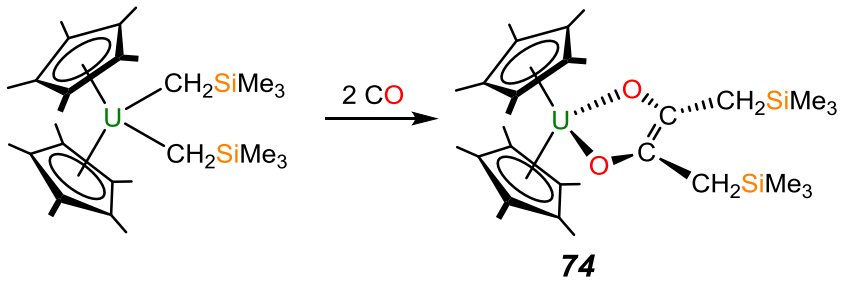
Ethynediolate formation is also observed in the reaction of the complexes [U(OAr)$_3$][159] (Ar = 2,6-^{t}Bu$_2$C$_6$H$_3$, 2,4,6-^{t}Bu$_3$C$_6$H$_2$), and [U(N″)$_3$] with CO.[160] Heating a sample of [{U(N″)$_3$}$_2$(μ-η^1:η^1-C$_2$O$_2$)] (**72**) in benzene affords the addition of C-H

across the alkyne group intramolecularly, giving [U(N″)$_3${μ-*O*C(=CH-*O*)-CH$_2$Si(Me)$_2$*N*(SiMe$_3$)}U(N″)$_2$], figure **1.18.**[160]



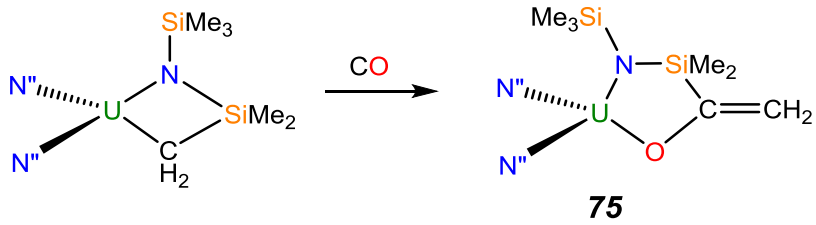
*Scheme **1.51.** Synthetic cycle for the functionalisation of CO to furanones.*

The Liddle group have also investigated CO homologation chemistry, and found that [U(Tren^{DMBS})] (**14**) reductively homologates CO to prepare [{U(Tren^{DMBS})$_3$}$_2$(μ-η^1:η^1-C$_2$O$_2$)] (**73**, scheme **1.51.**).[44] In contrast to **72**, heating **73** in benzene does not afford C-H addition across the C≡C bond, instead the ethynediolate inserts into an N-Si bond, and an oxo-bridged dinuclear species is formed, [U{κ^5-*O*C(H)=C(OSiMe$_2$^{t}Bu)*N*CH$_2$CH$_2$*N*(CH$_2$CH$_2$*N*SiMe$_2$^{t}Bu)$_2$}{(μ-O)U(Tren^{DMBS})}]. More notable, however, was the finding that the addition of silyl iodides (RMe$_2$SiI, R = Me, Ph) prepares **9**, liberating *bis*(organosiloxy)acetylenes, RMe$_2$SiOC≡COSiMe$_2$R. As **9** can be reduced to **14**, this is then a uranium mediated synthetic cycle for the functionalisation of CO. The liberated acetylene can be further functionalised by addition of water to prepare furanones [-OC(=O)C(OSiMe$_2$R)=C(OSiMe$_2$R)CH$_2$-], scheme **1.51.**, lower right.



*Scheme **1.52.** Synthesis of **74**.*

Somewhat analogous to the preparation of ethynediolate species, such as **71**, **72** and **73**, is the preparation of [U(Cp*)$_2${κ^2-*O*C(CH$_2$SiMe$_3$)=C(CH$_2$SiMe$_3$)*O*}], **74**, by the reaction of the *bis*(alkyl) complex [U(Cp*)$_2$(CH$_2$SiMe$_3$)$_2$] with CO (scheme **1.52.**).[161] Here, the CO fragments couple and are functionalised by the alkyl ligands.



75

*Scheme **1.53.** Synthesis of **75**.*

A common outcome for the reaction of uranium complexes with CO is the insertion into U-C ligand bonds. The reaction of cyclometallated species, such as [U(N″)$_2${*C*H$_2$Si(Me)$_2$*N*(SiMe$_3$)}],[162] [U(N″){*C*H$_2$Si(Me)$_2$*N*(SiMe$_3$)}$_2$][Na(THF)$_x$],[163] [U{η^5:η^1-C$_5$Me$_4$Si(Me)$_2$*C*H$_2$}$_2$],[164] [[U{η^5:η^1-C$_5$Me$_4$Si(Me)$_2$*C*H$_2$}(η^5-C$_5$Me$_4$SiMe$_3$){κ*(C)*:κ*(O)*-C$_5$H$_4$N-O}][165] or [U(N″)$_2${*O*C(Me)$_2$CH$_2$(1-*C*[NCH$_2$CH$_2$NAr])}] (Ar = 2,6-^{i}Pr$_2$C$_6$H$_3$),[114] prepare products of the form [U{OC(=CH$_2$)…}(L)$_x$] by insertion into U-C bonds, then rearrangement, for example [U(N″)$_2${OC(=CH$_2$)Si(Me)$_2$*N*(SiMe$_3$)}] (**75**, scheme **1.53.**).[162]

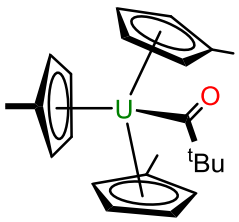
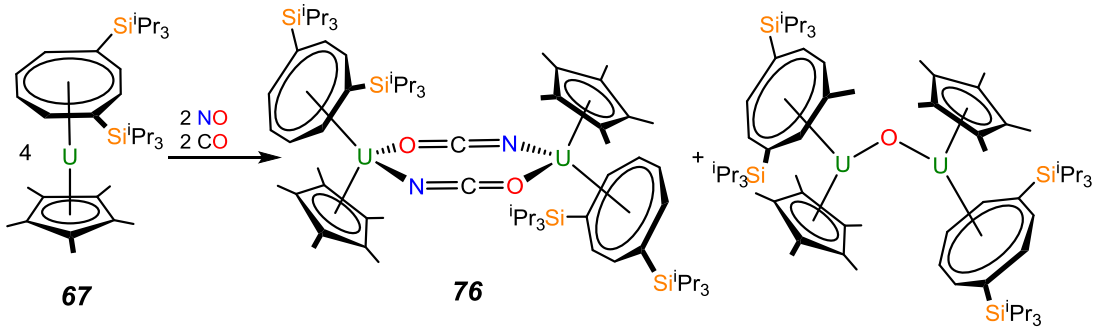


*Figure **1.19.** Complex [U(η^5-C$_5$H$_4$Me)$_2${C(O)^{t}Bu}].*

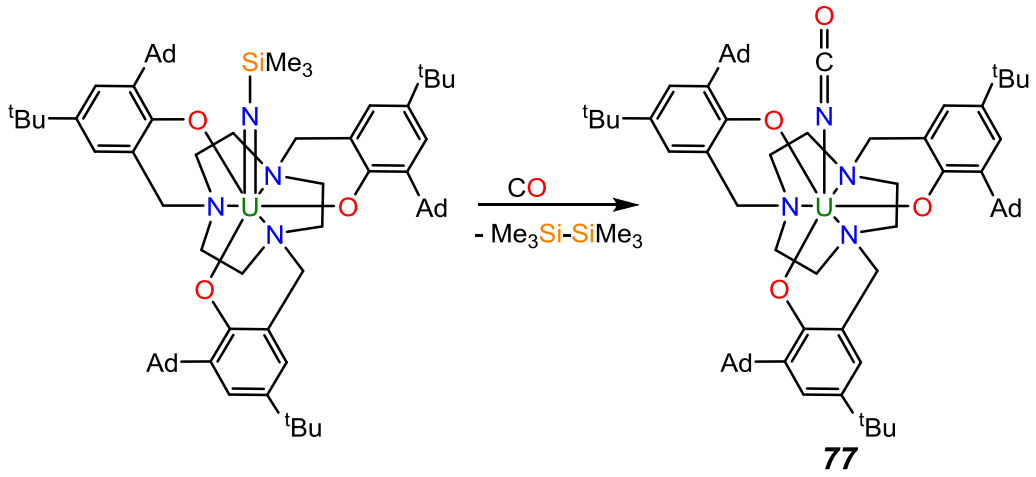
In the case of the non-cyclometallated alkyl complex [U(η^5-C$_5$H$_4$Me)$_3$(^{t}Bu)], reaction with CO instead affords 1,1 migratory insertion to prepare the uranium–acyl compound [U(η^5-C$_5$H$_4$Me)$_2${C(O)^{t}Bu}].[166] No rearrangement of the ligand coordination is observed. A strong absorption was found in the FTIR spectrum at 1490 cm^{-1}.

The assembly of cyanate functionalities (NCO) at uranium is also known upon reaction of uranium species with CO. Expanding on the work discussed earlier, of the reductive oligomerisation of CO, Cloke *et al.* expanded their research towards the preparation of nitrogen analogues of **68** with a deltate $\{CN_2O_3\}^{2-}$ unit. The reaction of **67** with NO and CO did not afford a cyclotrimerised product, instead preparing a bridging oxo complex $[\{U(\eta^8\text{-}1,4\text{-}[^iPr_3Si]C_8H_6)(Cp^*)\}_2(\mu\text{-}O)]$ and a bridging dicyanate complex $[\{U(\eta^8\text{-}1,4\text{-}[^iPr_3Si]C_8H_6)(Cp^*)\}_2(\mu\text{-}\kappa^1\text{:}\kappa^1\text{-}NCO)_2]$, **76** (scheme **1.54.**).[167] The mechanism was found to proceed *via* the initial attack of CO on a $\mu\text{-}\eta^2\text{:}\eta^2$-coordinated NO, bound side on between two uranium centres. From this intermediate is ejected a cyanate radical to afford the oxo-bridged dinuclear species. Coordination of the cyanate and dimerisation affords **76**.[168]



*Scheme **1.54.** Synthesis of **76** and [{U(1,4-[^{i}Pr$_3$Si]C$_8$H$_6$)(Cp*)}$_2$(μ-O)].*

A second route to cyanate formation was the reaction of the uranium(V)–imide species $[U\{(^{Ad}ArO)_3tacn\}(=NSiMe_3)]$ $[(^{Ad}ArO)_3tacn$ = $(1\text{-}O\text{-}2\text{-}Ad\text{-}4\text{-}^tBu_2C_6H_2\text{-}CH_2)_3(NCH_2CH_2)_3]$ with CO, which affords the homocoupling of two trimethylsilyl groups to give Si_2Me_6, and the formation of an isocyanate complex $[U\{(^{Ad}ArO)_3tacn\}(NCO)]$, **77** (scheme **1.55.**).[118]



*Scheme **1.55.** Synthesis of **77**.*

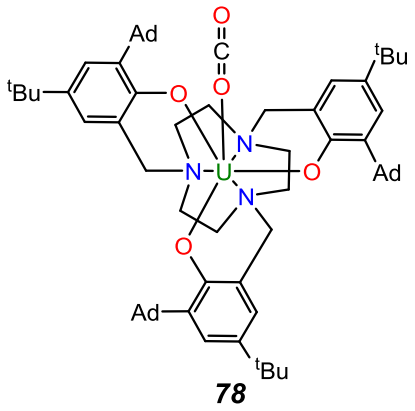
In a similar manner to the construction of cyanate ligands by the reaction of NO and CO with **67** to give **76**, the construction of a methoxide ligand at uranium in [U{η^8-1,4-(^{i}Pr$_3$Si)C$_8$H$_6$}](Cp*)(O^{13}CH$_3$)] was achieved by the treatment of **67** with subsequently ^{13}CO and two equivalents of H_2.[169] This reaction therefore reflects the use of syngas to hydrogenate carbon monoxide at subambient to ambient temperatures and pressures.

1.6.2. Reactivity of uranium species towards CO_2

The reactivity of uranium complexes towards CO_2 has been fairly widely studied, and in many cases the chemistry observed is insertion chemistry. Insertion chemistry has been observed for a wide range of uranium–ligand bonds, including U-H, U-C, U-N, U-O, and U-S bonds, which will be variously discussed below.

In contrast to the coordination of carbonyl monoxide to uranium centres, for which there are several examples, as discussed above (e.g. **64**), there is only known example of CO_2 binding in an η^1 fashion, through an oxygen atom. In 2004, Meyer *et al.* reported the binding of a linear OCO fragment to uranium in the complex [{(^{Ad}ArO)$_3$tacn}U(η^1-O$_\alpha$CO$_\beta$)] (**78**, figure **1.20.**).[170] The authors note that the O$_\alpha$-C bond is significantly shorter than that of the C-O$_\beta$ bond [O$_\alpha$-C 1.122(4), C-O$_\beta$ 1.277(4) Å], which might suggest that charge separated resonance structures may be applicable in representations of the bonding in this fragment. This charge separation

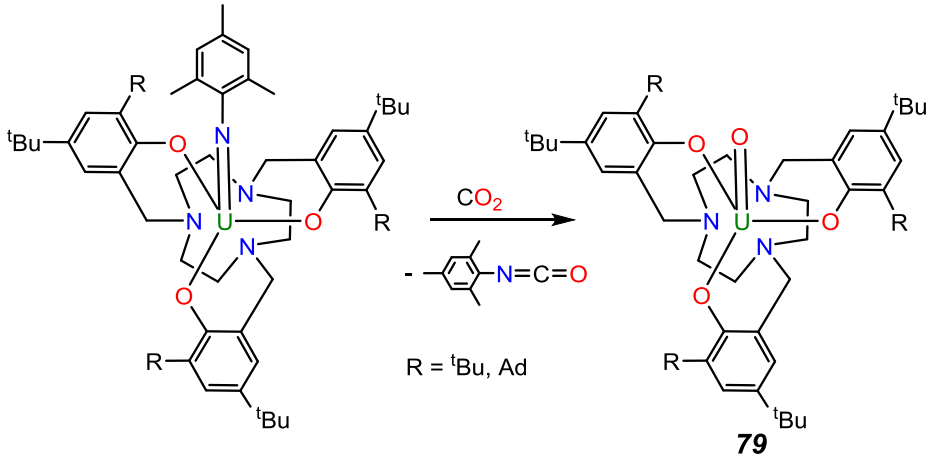
is reminiscent of the charge separated uranium–carbonyl species implicated in the formation of **66**.



78

*Figure **1.20.** Complex **78**.*

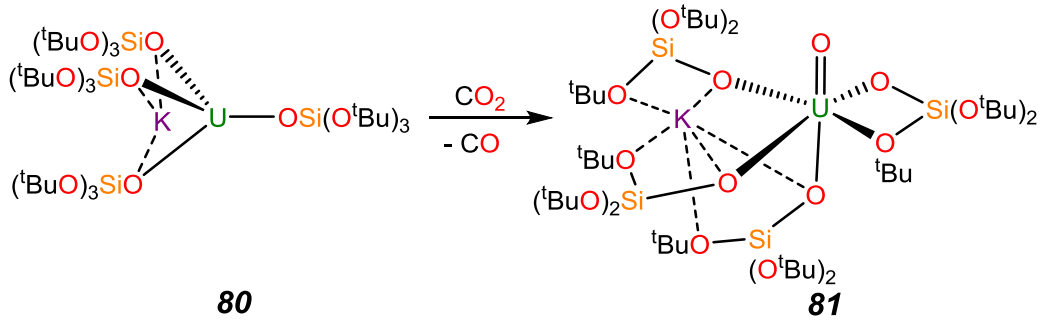
Somewhat rarer than CO_2 insertion into metal ligand bonds are examples of CO_2 splitting. There are several examples in the literature of terminal uranium–oxo formation by the reaction of either uranium–imides or uranium–siloxides. In the former case, the reaction of [U{(^{R,tBu}ArO)tacn}(=NMes)] (R = ^{t}Bu, Ad; Mes = 2,4,6-$Me_3C_6H_2$) with CO_2 affords the elimination of MesNCO and the formation of the oxo species [U{(^{R,tBu}ArO)tacn}(O)] (**79**, scheme **1.56.**).[119] Similarly, the reaction of [U{(^{nP,Me}ArO)tacn}(=NCPh$_3$)][K] [^{n}P = $CH_2C(CH_3)_3$] with CO_2 affords the uranium(IV)–oxo [U{(^{nP,Me}ArO)tacn}(O)][K] and eliminates trityl isocyanate (Ph_3CNCO).[171]



79

*Scheme **1.56.** Synthesis of **79**.*

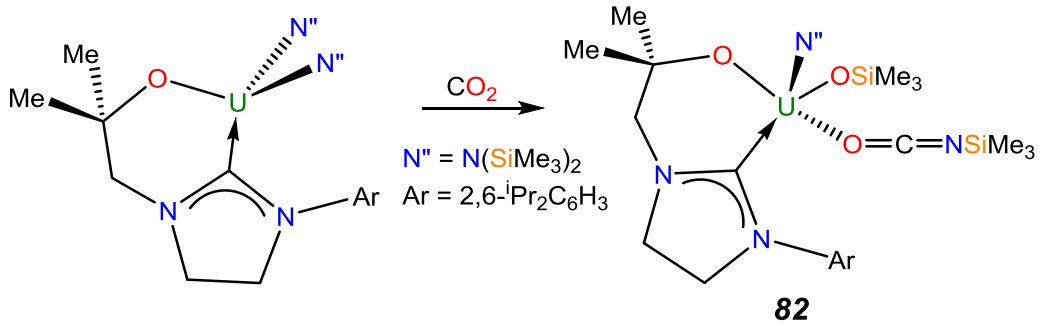
For the latter case, the reaction of K[U{OSi(O^{t}Bu)$_3$}$_4$] (**80**) with CO_2 prepares a uranium(V)–oxo, K[U{OSi(O^{t}Bu)$_3$}$_4$(O)], **81**, alongside the elimination of an equivalent of CO (scheme **1.57.**).[121] This is the first example of a terminal uranium(V)–oxo obtained by the two-electron reductive cleavage of CO_2 mediated by a uranium(III) complex. Alternatively, reaction of **80** with two equivalents of CO_2 gives a bridging carbonate, [U{OSi(O^{t}Bu)$_3$}$_4${(μ-κ^2:κ^1-O$_2$CO)K(18C6)}].



80 **81**

*Scheme **1.57.** Synthesis of **81**.*

CO_2 splitting was also observed for a uranium *N*-heterocyclic carbene complex, [U(N″)$_2${*O*C(Me)$_2$CH$_2$(1-*C*[NCH$_2$CH$_2$NAr])}] (Ar = 2,6-^{i}Pr$_2$C$_6$H$_3$), which prepares [U(N″)(OSiMe$_3$)(OCNSiMe$_3$){*O*C(Me)$_2$CH$_2$(1-*C*[NCH$_2$CH$_2$NAr])}] (**82**, scheme **1.58.**).[114] The mechanism proposed for N-Si bond cleavage alongside CO_2 splitting to afford siloxide and cyanate ligands is thought to be mediated by the hemi-labile *N*-heterocyclic carbene.

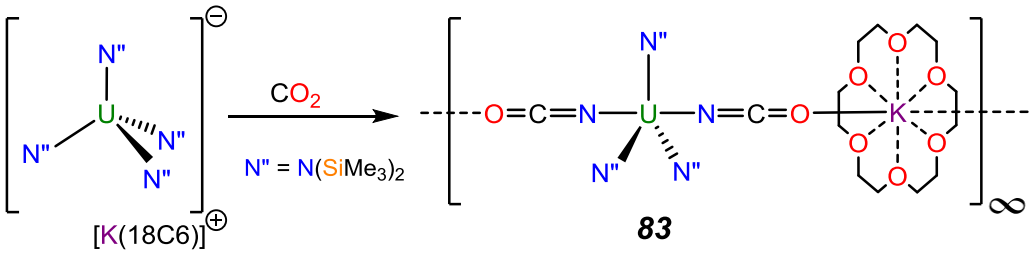


82

*Scheme **1.58.** Synthesis of **82**.*

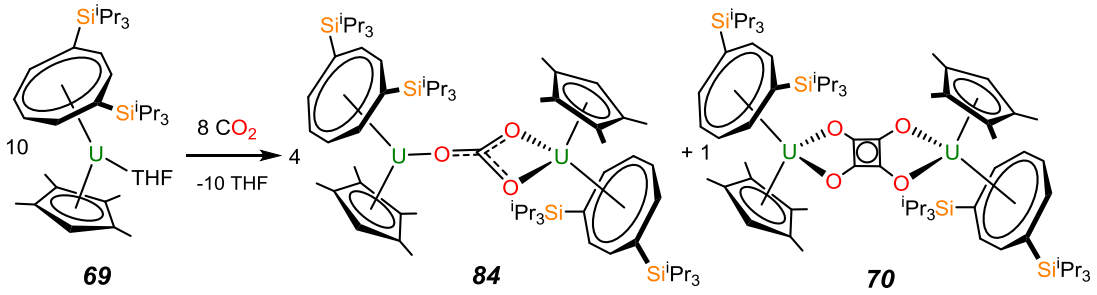
In addition to isocyanate formation by the reaction of uranium imides with CO (**77**)[118] or the coupling of NO and CO with mixed sandwich complexes (**76**),[167] (*vide supra*) a third example of formation of cyanate at uranium results from the reaction

of [U(N″)$_4$][K(18C6)] with CO_2,[172] which affords [(μ-OCN)U(N″)$_3$(μ-NCO){K(18C6)}$_\infty$ (**83**), a 1D coordination polymer, alongside other unknown products (scheme **1.59.**). As for the preparation of **82**, multiple N-Si bonds are broken in order to prepare **83**.



*Scheme **1.59.** Synthesis of **83**.*

The formation of carbonates is also observed for reactions of CO_2 with uranium complexes. The reaction of [U{η^8-1,4-(^{i}Pr$_3$Si)$_2$C$_8$H$_6$}(η^5-C$_5$Me$_4$R)] (R = H, **69**; Me, **67**) with CO_2 affords free CO and [{U(η^8-1,4-[^{i}Pr$_3$Si]$_2$C$_8$H$_6$)(η^5-C$_5$Me$_4$R)}$_2$(μ-η^1:η^2-CO$_3$)] (**84**).[173] These same starting materials prepare the squarate **70** (R = H)[156] and deltate **68** (R = Me)[155] oxocarbons upon reaction with CO. With the correct stoichiometry, both **84** and **70** could be prepared by the reaction of **69** with CO_2 (CO liberated by the reaction of **69** and CO_2 reacts with **69** to afford **70**), the first preparation of a carbocycle (**70**) derived from CO_2 (scheme **1.60.**).



*Scheme **1.60.** Synthesis of **84** and **70**.*

In a similar manner to the variation observed on the reaction of CO with mixed sandwich complexes of uranium, forming variously ethynediolate, deltate or squarate products (**71**, **68** and **70** respectively), small modifications of the ligand environment of mixed sandwich complexes impart differing reactivities with CO_2. Using instead

the series [{U(η^8-1,4-[Me$_3$Si]$_2$C$_8$H$_6$)(η^5-C$_5$Me$_4$R)}(THF)] (with trimethylsilyl substituents on the COT ligand), larger substituents (R = ^{t}Bu) afford carbonates analogous to **74**. When R = Et or ^{i}Pr, a mixture of carbonate and oxalate species [{U(η^8-1,4-[Me$_3$Si]$_2$C$_8$H$_6$)(η^5-C$_5$Me$_4$R)}$_2$(μ-η^2:η^2-C$_2$O$_4$)] (**85**) are formed. Finally, if R = Me, then a mixture of the oxalate and the bridging oxo species [{U(η^8-1,4-[Me$_3$Si]$_2$C$_8$H$_6$)(η^5-C$_5$Me$_5$)}$_2$(O)] (**86**) are prepared (figure **1.21.**).[174]

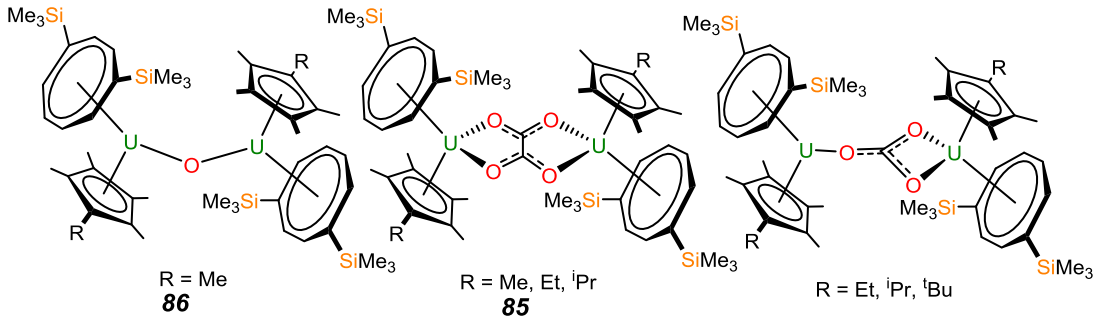
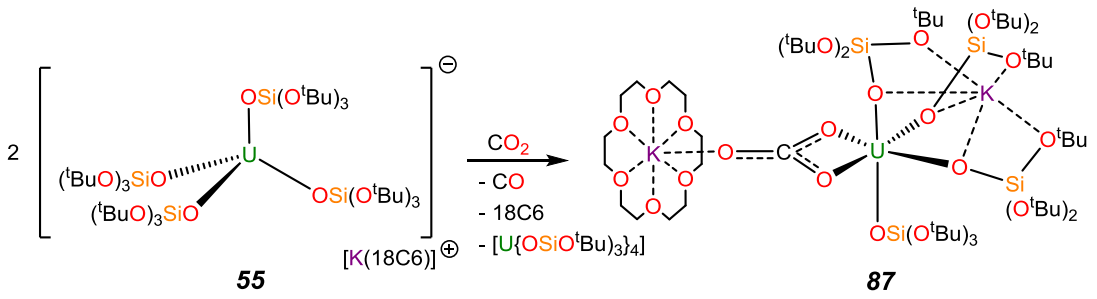


*Figure **1.21.** Complexes **86** and **85**.*

The formation of a carbonate species was also observed for reaction with uranium siloxide species. The reaction of dinuclear [{U(OSi[O^{t}Bu]$_3$)$_2$(μ-OSi[O^{t}Bu]$_3$)}$_2$] (**57**) or heterobimetallic [U{OSi(O^{t}Bu)$_3$}$_4$][K(18C6)] (**55**) with CO_2 affords [{U(OSi[O^{t}Bu]$_3$)$_3$}$_2$(μ-η^1:η^2-CO$_3$)][175] and K[U{OSi(O^{t}Bu)$_3$}$_4${(μ-η^2-O$_2$CO)K(18C6)}] (**87**),[121] respectively (scheme **1.61.**). This latter reactivity contrasts with the formation of an oxo species (**81**),[121] when the potassium ion is integrated into the structure of the starting material (that is, it is a contact ion pair, not a separated ion pair, complex **80**). Clearly, both the connectivity (steric bulk) and the nature of the metal species (heterobimetallic) involved in these uranium(III) species dictates the resultant chemistry upon reaction with CO_2.



*Scheme **1.61.** Synthesis of **87**.*

The Meyer group also report the synthesis of uranium–carbonates. The reaction of either [U{(^{tBu2}ArO)$_3$Mes}] (**88-^{t}Bu$_2$**) or [U{(^{AdMe}ArO)$_3$N}(DME)] (**89-AdMe**) with CO_2 forms the carbonates [{U([^{tBu2}ArO]$_3$Mes)}$_2$(μ-η^2:η^2-CO_3)] (**90**) or [{U([^{AdMe}ArO]$_3$N)}$_2$(μ-η^1:η^2-CO_3)] (**91**), see figure **1.22**.[176] The proposed mechanism for the formation of **90** and **91** is *via* an oxo bridged intermediate with the elimination of CO. This was tested for by the preparation of these oxo species by reaction of the trivalent starting materials (**88-^{t}Bu$_2$** or **89-AdMe**) with N_2O. Addition of CO_2 to these oxo species prepared the carbonates (**90** and **91**).

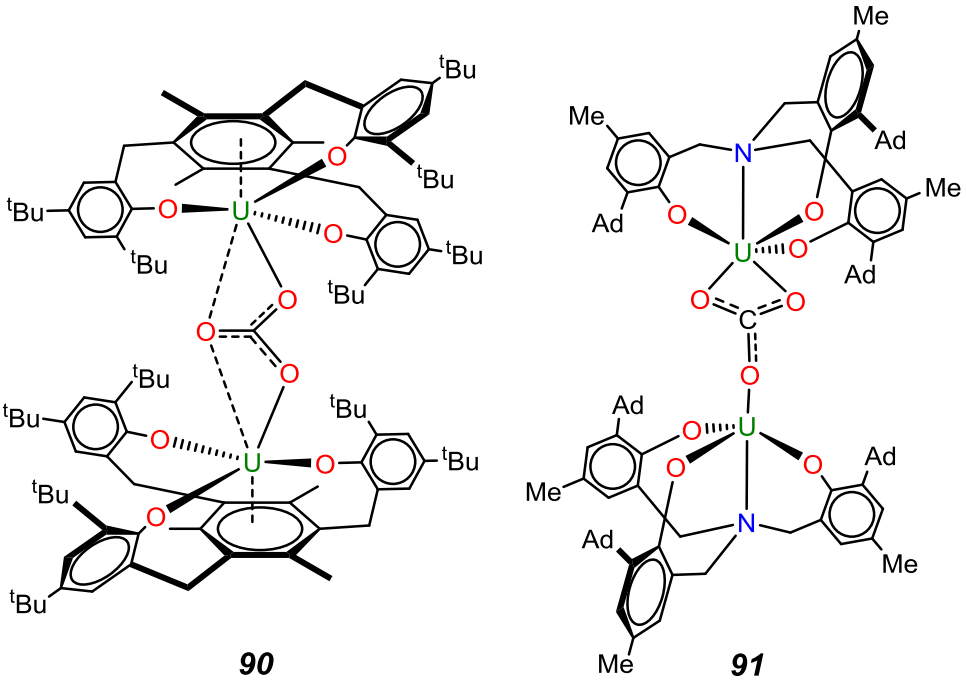
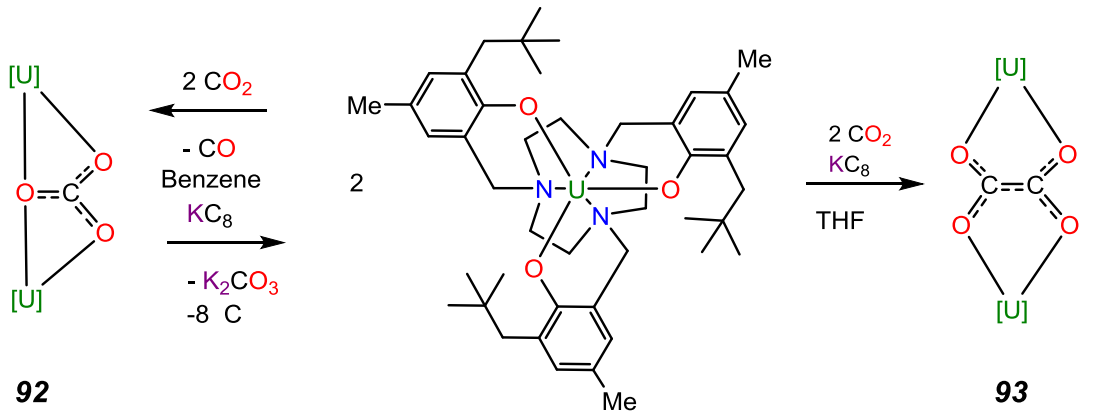


*Figure **1.22.** Complexes **90** and **91**.*

Similarly, the reaction of [U{(^{nP,Me}ArO)$_3$tacn}] (**65-nP,Me**) with CO_2 affords the corresponding carbonate, with a geometry paralleling that of **90**, [{U([^{nP,Me}ArO]$_3$tacn)}$_2$(μ-η^2:η^2-CO_3)], **92**.[177] The authors report that both **92**, and the bridging oxo intermediate (prepared by reaction with N_2O with **65-nP,Me**, analogously to the preparation of oxo-derivatives from **88-^{t}Bu$_2$** or **89-AdMe**), could be reduced back to **65-nP,Me** by addition of KC_8, with the elimination of graphite and K_2CO_3 or K_2O respectively (scheme **1.62**, left).[177] This reductive chemistry was not observed for **90** or **91**, nor their oxo-bridged intermediates. This therefore

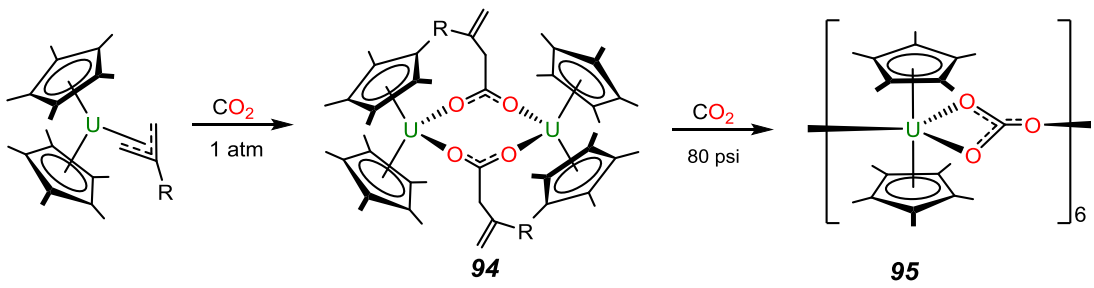
represents a closed synthetic cycle for the conversion of CO_2 to CO and potassium carbonate.



*Scheme **1.62.** Synthesis of **92** and **93**.*

When the reaction of **65-nP,Me** with CO_2 in the presence of KC_8 in THF was investigated by Meyer *et al.*, they found that they could prepare the uranium–oxalate, [{U([^{nP,Me}ArO]$_3$tacn)}$_2$(μ-η^2:η^2-C_2O_4)] (**93**, scheme **1.62.**, right).[178] This differs from the preparation of the carbonate **92**, which was prepared in benzene. The difference in end product results from the rate of reduction, where reduction of **92** in benzene is slow, affording **65-nP,Me**, but in THF is fast, and hence in the presence of a CO_2 atmosphere permits the formation of the oxalate **93**.

A nanometre sized uranium carbonate was prepared from the allylic uranium species [U(Cp*)$_2$(η^3-C_3H_4R)] (R = H, Me). The reaction of the allylic species with CO_2 at one atmosphere afforded the bridged species [{U(Cp*)$_2$}$_2$(μ-η^1:η^1-O_2CCH_2C(R)=CH_2)$_2$], **94**.[179] Under high pressure (80 psi), this then converts to [{U(Cp*)$_2$(μ-η^2:η^1-CO_3)}$_6$], **95** (scheme **1.63.**).[179]



*Scheme **1.63.** Synthesis of **94** and **95**.*

The most common form of reactivity observed of uranium complexes with CO_2 is that of insertion, which has been observed for a wide range of uranium–ligand bonds. Insertion into U-C bonds is most often seen, and insertion into alkyl bonds results in complexes of the form {U(κ^2-O_2CR)}. This has been seen for a wide variety of alkyl linkages, including R = Me,[180-182] CH_2Ph,[180,183] CH_2SiMe_3[180] and C≡CPh.[184,185] The reaction of the allylic fragments in [U(Cp*)$_2$(η^3-C_3H_5)$_2$] with CO_2 is accompanied by slippage to give [U(Cp*)$_2$(κ^2-OCCH$_2$CH=CH$_2$)$_2$], which differs from the preparation of **94** due to the oxidation state of uranium.[186] In some cases, the resultant connectivity is slightly altered, such that only one oxygen remains bound to the uranium centre, as for the reaction of [U(Cp*)$_2$(Me)$_2$] which prepares [U(Cp*)$_2$(OAc)$_2$],[187] or the cyclometallated complex [U(N″)(*C*H$_2$SiMe$_2$*N*SiMe$_3$)$_2${Na(THF)$_x$}] which affords [U(N″){*O*C(O)CH$_2$SiMe$_2$NSiMe$_3$}$_2$].[163]

An example of CO_2 insertion into U-O bonds comes from Arnold. The reaction of [{U(O-2,4,6-^{t}Bu$_3$C$_6$H$_2$)$_3$}$_2$(μ-η^2:η^2-N_2)] with CO_2 affords the reduction of a molecule of CO_2 to CO and O, wherein the O atom is incorporated into a U-O-U motif. Two molecules of CO_2 into then insert into two U-O ligand bonds, which rearrange to bridge the U-O-U motif, [{U(O-2,4,6-^{t}Bu$_3$C$_6$H$_2$)}$_2$(μ-η^1:η^1-O_2CO-2,4,6-^{t}Bu$_3$C$_6$H$_2$)$_2$(μ-O)], figure **1.23.**[159]

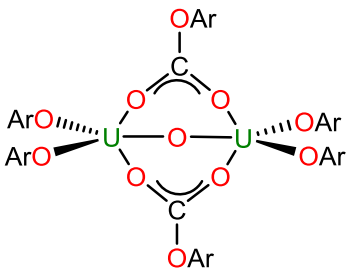


Figure ***1.23.*** *Complex [{U(O-2,4,6-^{t}Bu$_3$C$_6$H$_2$)}$_2$(μ-η^1:η^1-O_2CO-2,4,6-^{t}Bu$_3$C$_6$H$_2$)$_2$ (μ-O)].*

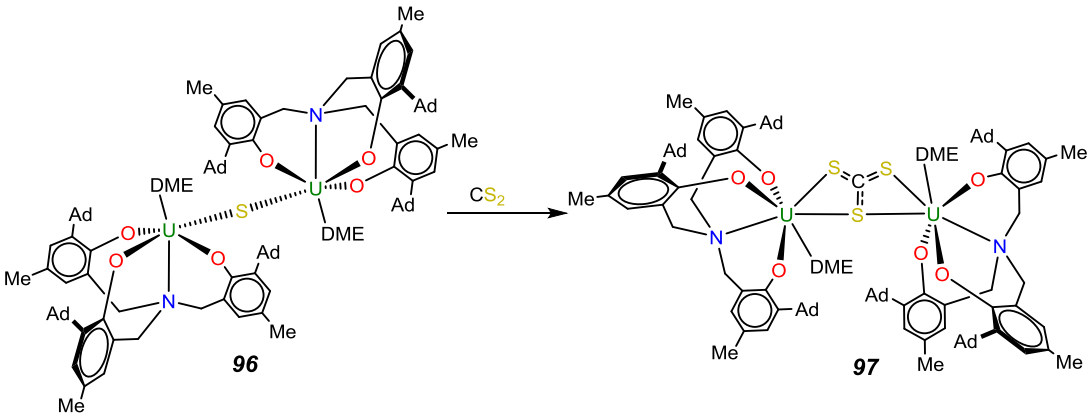
Similar insertion has been observed for U-E bonds, such as the U-N bonds in [U(Cp)$_2$(NEt$_2$)$_2$],[188] [U(Tp*)$_2$(NHPh)],[185] [U(Tp*)$_2$(NCH$_2$Ph)],[185] and [U{η^8-1,4-(^{i}Pr$_3$Si)$_2$C$_8$H$_6$}(Cp*)(NH$_2$)][189]; the U-S bonds in [U(Cp*)$_2$(S^{t}Bu)$_2$][190] and

[U(Tp*)$_2$(SPh)][185]; and the U-H bond of [U{η^8-1,4-(^{i}Pr$_3$Si)$_2$C$_8$H$_6$}(Cp*)(H)][180] to give carboxylate {U(κ^2-O$_2$CE)} derivatives [Tp* = HB{NC(Me)CHC(Me)*N*}$_3^-$].

1.6.3. Reactivity of uranium species towards CS_2

The reactivity of uranium compounds with CS_2 follows many similar trends to their reactivity with CO_2. Accordingly, the insertion of the CS_2 fragment into uranium–ligand bonds, including U-C[165,183] and U-N,[188] has been widely observed, alongside insertion into U-SR[190] bonds to afford alkyl capped trithiocarbonate ligands.

Similarly to the preparation of carbonates by addition of CO_2 to bridging oxides (**90**, **91**), bridging trithiocarbonates can be prepared by the addition of CS_2 to bridging sulfides, notably the preparation of [{U([^{Ad}ArO]$_3$N]}$_2$(μ-κ^2:κ^2-CS$_3$)] (**97**) from the corresponding bridged sulphide (**96**, scheme **1.64.**).[191]



*Scheme **1.64.** Synthesis of **96**.*

Mixed carbonates have also been prepared, by the addition of CS_2 across U-Se-U linkages[192] or insertion into U-E bonds (E = Se, Te).[193] Insertion into the U-Se-U bond of analogues of **96** (**96-Se**) affords the {U-μ-κ^2:κ^2-SC(Se)S-U} analogue of **97**; furthermore addition of COS (O=C=S) to **96-Se** affords the {U-μ-κ^2:κ^2-SC(Se)O-U} analogue of **97**.[192] Insertion into the U-E bonds of [U(Tp*)$_2$(EPh)], (E = Se, Te) gives mixed carbonates with aryl pendants.[193]

Further to this, there are some examples of complexes where there is activation of the CS_2 unit. Addition of CS_2 to $[U(Cp^{Me})_3(THF)_n]$ (n = 0, 1) resulted in the immediate formation of $[\{U(Cp^{Me})_3\}_2(\mu\text{-}\eta^1\text{:}\eta^2\text{-}CS_2)]$ (**98**, figure **1.24.**, left).[194] This complex has inequivalent C-S bonds [1.464(19) and 1.831(19) Å], which is suggestive of activation of the CS_2 unit to CS_2^{2-}. Similarly, addition of CS_2 to $[\{U(OSi[O^tBu]_3)_2\}_2\{\mu\text{-}OSi(O^tBu)_3\}_2]$ (**57**) affords $[\{U(OSi[O^tBu]_3)_3\}_2\{\mu\text{-}\eta^2(C,S)\text{:}\eta^2(S,S)\text{-}CS_2\}]$ (**99**, figure **1.24.**, right), with an asymmetric CS_2^{2-} unit [C-S bond lengths: 1.594(12) and 1.748(11) Å].[175] In some respects, **98** and **99** are most reminiscent of **78**, where there is a small amount of resonance in the η^1-OCO unit, as indicated by bond lengths,[170] though the bimetallic nature of these complexes invokes a far greater degree of activation than that observed for **78**.

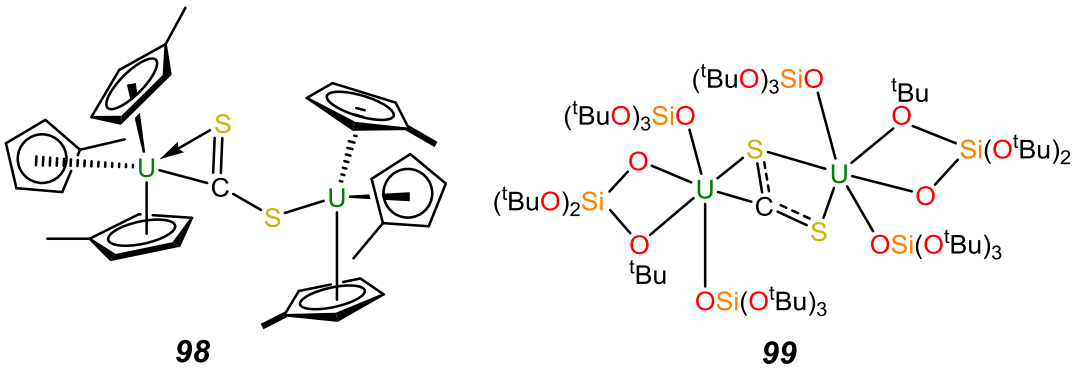
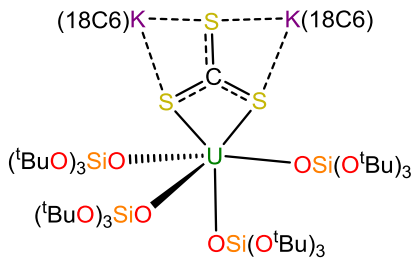


*Figure **1.24.** Complexes **98** and **99**.*

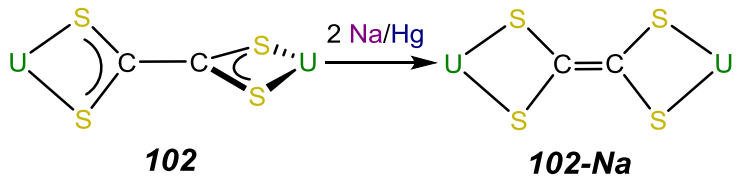
Reactivity of uranium siloxides with CS_2 is not always as clear cut as in the preparation of **99**. The reaction of $[U\{OSi(O^tBu)_3\}_4][K(18C6)]$ (**55**) with CS_2 affords multiple products.[195] Isolation of the reaction mixture after 30 minutes afforded crystals of the trithiocarbonate species $[U\{OSi(O^tBu)_3\}_4\{(\mu\text{-}\eta^2\text{:}\eta^2\text{:}\eta^2\text{-}CS_3)(K[18C6])_2\}]$, (**100,** figure **1.25.**), alongside $[U\{OSi(O^tBu)_3\}_4]$ (**101**), $[K(18C6)]_2[C_2S_4]$ and other unidentified species. Samples left for two days under the same conditions afforded **101** at the only uranium containing product, and CS_3^{2-} and $C_3S_5^{2-}$ salts in a 10:1 ratio.[195]



100

*Figure **1.25.** Complex **100**.*

Finally, C-C bond coupling was observed upon the reaction of **89-AdMe** with CS_2, to prepare [{U([^{AdMe}ArO]$_3$N)(DME)}$_2$(μ-κ^2:κ^2-C_2S_4)] (**102**).[196] This was the first example of the formation of a tetrathiooxalate complex through the reductive coupling of CS_2. Complex **102** features a new, non-planar, κ^2:κ^2 binding mode for $C_2S_4^{2-}$; normally five membered MSCCS rings enforce planarity. Reduction of **102** with two equivalents of sodium/mercury amalgam affords [{U([^{AdMe}ArO]$_3$N)}$_2$(μ-κ^2:κ^2-C_2S_4)][Na(DME)$_3$]$_2$, **102-Na**, which has a planar tetrathiooxalate unit and features a five membered USCCS ring, incorporating a formal C=C double bond (scheme **1.65.**).

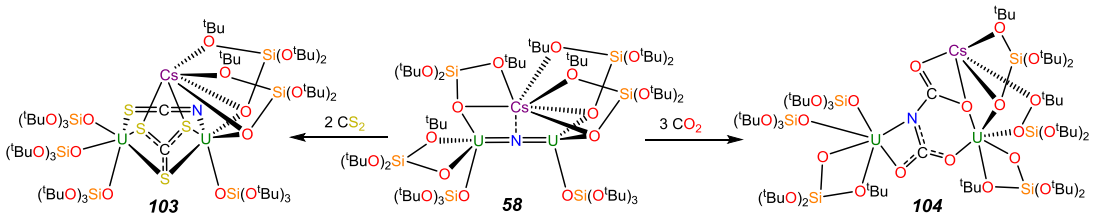


102 ***102-Na***

*Scheme **1.65.** Tetrathiooxalate centres of **102** and **102-Na**.*

1.6.4. Reactivity of uranium nitrides

Mazzanti *et al.* have very recently reported reactivity that they observed for their bridged uranium nitride systems (see Section 5), which has been developed concurrently to this work. Complex **58** undergoes thermal rearrangement (12 h, 80 °C) to afford the bridging imide species Cs[(μ-N^{t}Bu)(μ-O$_2$Si(O^{t}Bu)$_2$)U$_2$(OSi(O^{t}Bu)$_3$)$_3$}$_5$] by C-O bond cleavage with concomitant N-C bond formation.[197]



*Scheme **1.66.** Reactivity of **58** with CE_2 to prepare **103** and **104**.*

The authors also report reactivity of **58** with CE_2 (E = O, S). The reaction of **58** with CS_2 affords the diuranium(IV) complex $Cs[\{U(OSi[O^tBu]_3)_3\}_2(\mu^2\text{-}NCS)(\mu^3\text{-}\kappa^2\text{:}\kappa^2\text{:}\kappa^2\text{-}CS_3)]$ (**103**), which features bridging thiocyanate and trithiocarbonate ligands (scheme **1.66.**, left). Conversely, the reaction of **58** with CO_2 forms a dicarbamate $\{N(CO_2)_2\}^{3-}$ unit between the two uranium centres, $Cs[\{U(OSi[O^tBu]_3)_3\}_2(\mu^3\text{-}\kappa^2\text{:}\kappa^2\text{:}\kappa^2\text{-}NC_2O_4)]$ (**104**), where the six and four membered rings in this unit share an N-C bond (scheme **1.66.**, right). The authors also describe that in the presence of substoichiometric ratios of CO_2 (one equivalent), **58** does not form **104**, and instead affords $Cs[\{U(OSi[O^tBu]_3)_3\}_2(\mu^3\text{-}O)(\mu^2\text{-}\kappa^1\text{-}NCO)]$, **105** (figure **1.26.**), containing bridging oxo and cyanate units, though in contrast to the bridging cyanate units in **76** (which bind through both the oxygen and nitrogen atoms), in **105** both uranium centres are bound to the nitrogen atom.

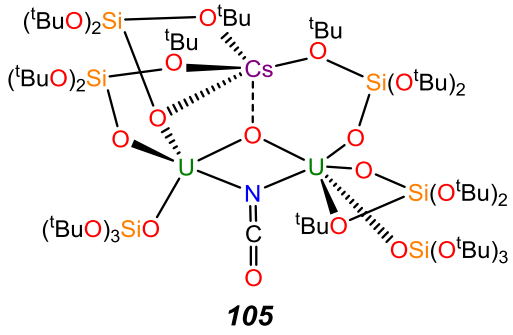


*Figure **1.26.** Complex **105**.*

The reaction of either **59** or **60** with CS_2 resulted in the extrusion of the thiocyanate anion as CsSCN to give the diuranium(IV)–disulfide complex $[Cs(THF)]_2[\{U(OSi[O^tBu]_3)_3\}_2(\mu\text{-}S)_2]$ (figure **1.27.**). Therefore, there is a demonstrable difference between the reactivity of bridged uranium nitrides with CS_2,

dependent upon the oxidation state of the uranium centres [U^{IV}-N-U^{IV}, **58** *vs* U^{II}-N-U^{IV}, **59** and U^{III}-N-U^{III}, **60**].

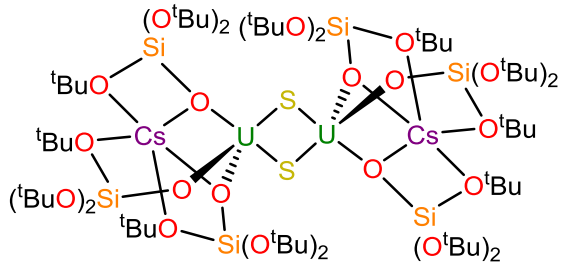


*Figure **1.27.** Product of the reaction of **59** or **60** with CS_2.*

1.7. Aims of Project

Terminal transition metal nitride systems have been prepared by a wide variety of synthetic methods, and their reactivity has been investigated towards small molecules. A terminal uranium–nitride was first isolated in 2012, though until now, no reactivity studies had been reported with this system towards small molecules.

In light of the isolation of the Tren–uranium nitride, [U($Tren^{TIPS}$)(N)][Na(12C4)$_2$] (**52**), alternative routes can be investigated for the installation of this functionality, by a reappraisal of the fundamental chemistry that is occurring. As such, the aforementioned route is described in equation 1, and a potential alternative synthetic strategy is outlined in equation 2.

$$U^{III} + N_3^- + Na^I \rightarrow U^V{\equiv}N^- + Na^I + N_2 \qquad \text{(Eqn 1)}$$

$$U^{IV}\text{-}N_3 + M^0 \rightarrow U^V{\equiv}N^- + M^I + N_2 \qquad \text{(Eqn 2)}$$

As has been demonstrated by examples of transition metal nitrides, the reactivity these systems undergo is not always immediately obvious. Transition metal nitrides can be either nucleophilic or electrophilic, and a wide range of factors can influence how any given system might react. Therefore, the reactivity displayed by the bridged uranium–nitride Cs[{U(OSi(O^{t}Bu)$_3$)$_3$}$_2$(μ-N)] (**58**), prepared concurrently to this work, is not by necessity reflective of the reactivity of all uranium–nitride systems towards small molecules (e.g. CO_2 and CS_2).

The reactivity of Tren-stabilised uranium nitrides must also be investigated to establish the behaviour of terminal systems, and broaden our collective understanding of this only recently isolated fragment. Tren–uranium nitrides will therefore be reacted with CO, CO_2 and CS_2, and comparisons can then be made to known transition metal nitrides, and an appraisal of the reactivity of uranium–nitrides can be made.

1.8. References

(1) World-Nuclear-Association; http://www.world-nuclear.org/information-library/nuclear-fuel-cycle/mining-of-uranium/uranium-mining-overview.aspx: accessed 22/03/2016.
(2) World-Nuclear-Association; http://www.world-nuclear.org/information-library/current-and-future-generation/thorium.aspx: accessed 22/03/2016.
(3) Klaproth, M. H. *Chem. Ann. Freunde. Naturl.* **1789**, *2*.
(4) A. F. Holleman, E. Wiberg *Inorganic Chemistry*; Walter de Gruyter: Berlin, 2001.
(5) Liddle, S. T. *Angew. Chem. Int. Ed.* **2015**, *54*, 8604.
(6) Patel, D.; Wooles, A. J.; Hashem, E.; Omorodion, H.; Baker, R. J.; Liddle, S. T. *New J. Chem.* **2015**, *39*, 7559.
(7) Winter, M.; http://winter.group.shef.ac.uk/orbitron/AOs/5f/index.html: accessed 22/03/2016.
(8) Winter, M.; http://winter.group.shef.ac.uk/orbitron/AOs/5f/index-gen.html: accessed 22/03/2016.
(9) Clark, D. L. *Los Alamos Science* **2000**, *26*, 364.
(10) Bursten, B. E.; Rhodes, L. F.; Strittmatter, R. J. *J. Am. Chem. Soc.* **1989**, *111*, 2756.
(11) Kaltsoyannis, N.; Scott, P. *The f elements*; Oxford University Press, 1999.
(12) MacDonald, M. R.; Fieser, M. E.; Bates, J. E.; Ziller, J. W.; Furche, F.; Evans, W. J. *J. Am. Chem. Soc.* **2013**, *135*, 13310.
(13) La Pierre, H. S.; Scheurer, A.; Heinemann, F. W.; Hieringer, W.; Meyer, K. *Angew. Chem. Int. Ed.* **2014**, *53*, 7158.
(14) Gardner, B. M.; Liddle, S. T. *Eur. J. Inorg. Chem.* **2013**, *2013*, 3753.
(15) La Pierre, H. S.; Meyer, K. In *Progress in Inorganic Chemistry Volume 58*; John Wiley & Sons, Inc.: 2014, p 303.
(16) Kindra, D. R.; Evans, W. J. *Chem. Rev.* **2014**, *114*, 8865.
(17) Orchard, A. F. *Magnetochemistry*; Oxford University Press, 2003.
(18) Verkade, J. G. *Accounts of Chemical Research* **1993**, *26*, 483.
(19) Eaborn, C.; Odell, K. J.; Pidcock, A.; Scollary, G. R. *J. Chem. Soc., Chem. Commun.* **1976**, 317.
(20) Jurkschat, K.; Tzschach, A.; Meunier-Piret, J.; van Meerssche, M. *J. Organomet. Chem.* **1986**, *317*, 145.

(21) Cummins, C. C.; Schrock, R. R.; Davis, W. M. *Organometallics* **1992**, *11*, 1452.
(22) Gudat, D.; Verkade, J. G. *Organometallics* **1989**, *8*, 2772.
(23) Schrock, R. R. *Acc. Chem. Res.* **1997**, *30*, 9.
(24) Smythe, N. C.; Schrock, R. R.; Müller, P.; Weare, W. W. *Inorg. Chem.* **2006**, *45*, 7111.
(25) Yandulov, D. V.; Schrock, R. R.; Rheingold, A. L.; Ceccarelli, C.; Davis, W. M. *Inorg. Chem.* **2003**, *42*, 796.
(26) Ritleng, V.; Yandulov, D. V.; Weare, W. W.; Schrock, R. R.; Hock, A. S.; Davis, W. M. *J. Am. Chem. Soc.* **2004**, *126*, 6150.
(27) Wünsche von Leupoldt, A.; Förster, C.; Fiedler, T. J.; Bings, N. H.; Heinze, K. *Eur. J. Inorg. Chem.* **2013**, *2013*, 6079.
(28) Wildman, E. P.; Ostrowski, J. P. A.; King, D. M.; Lewis, W.; Liddle, S. T. *Polyhedron*.
(29) Liddle, S. T.; McMaster, J.; Mills, D. P.; Blake, A. J.; Jones, C.; Woodul, W. D. *Angew. Chem., Int. Ed.* **2009**, *48*, 1077.
(30) Roussel, P.; Alcock, N. W.; Boaretto, R.; Kingsley, A. J.; Munslow, I. J.; Sanders, C. J.; Scott, P. *Inorg. Chem.* **1999**, *38*, 3651.
(31) King, D. M.; Tuna, F.; McInnes, E. J. L.; McMaster, J.; Lewis, W.; Blake, A. J.; Liddle, S. T. *Science* **2012**, *337*, 717.
(32) Scott, P.; Hitchcock, P. B. *Polyhedron* **1994**, *13*, 1651.
(33) Gardner, B. M.; McMaster, J.; Lewis, W.; Liddle, S. T. *Chem. Commun. (Cambridge, U. K.)* **2009**, 2851.
(34) King, D. M.; Tuna, F.; McInnes, E. J. L.; McMaster, J.; Lewis, W.; Blake, A. J.; Liddle, S. T. *Nat. Chem.* **2013**, *5*, 482.
(35) Gardner, B. M.; Lewis, W.; Blake, A. J.; Liddle, S. T. *Inorg. Chem.* **2011**, *50*, 9631.
(36) King, D. M.; McMaster, J.; Tuna, F.; McInnes, E. J. L.; Lewis, W.; Blake, A. J.; Liddle, S. T. *J. Am. Chem. Soc.* **2014**, *136*, 5619.
(37) King, D. M. *PhD Thesis* University of Nottingham, 2013.
(38) Roussel, P.; Hitchcock, P. B.; Tinker, N.; Scott, P. *Chem. Commun.* **1996**, 2053.
(39) Roussel, P.; Boaretto, R.; Kingsley, A. J.; Alcock, N. W.; Scott, P. *J. Chem. Soc., Dalton Trans.* **2002**, 1423.
(40) Roussel, P.; Scott, P. *J. Am. Chem. Soc.* **1998**, *120*, 1070.
(41) Kaltsoyannis, N.; Scott, P. *Chem. Commun.* **1998**, 1665.
(42) Gardner, B. M.; McMaster, J.; Moro, F.; Lewis, W.; Blake, A. J.; Liddle, S. T. *Chem. - Eur. J.* **2011**, *17*, 6909.
(43) Gardner, B. M.; Patel, D.; Cornish, A. D.; McMaster, J.; Lewis, W.; Blake, A. J.; Liddle, S. T. *Chem. - Eur. J.* **2011**, *17*, 11266.
(44) Gardner, B. M.; Stewart, J. C.; Davis, A. L.; McMaster, J.; Lewis, W.; Blake, A. J.; Liddle, S. T. *Proc. Natl. Acad. Sci. U. S. A.* **2012**, *109*, 9265.
(45) King, D. M.; Tuna, F.; McMaster, J.; Lewis, W.; Blake, A. J.; McInnes, E. J. L.; Liddle, S. T. *Angew. Chem., Int. Ed.* **2013**, *52*, 4921.
(46) Gardner, B. M.; Balázs, G.; Scheer, M.; Tuna, F.; McInnes, E. J. L.; McMaster, J.; Lewis, W.; Blake, A. J.; Liddle, S. T. *Angew. Chem., Int. Ed.* **2014**, *53*, 4484.

(47) Gardner, B. M.; Balázs, G.; Scheer, M.; Tuna, F.; McInnesEric, J. L.; McMaster, J.; Lewis, W.; Blake, A. J.; Liddle, S. T. *Nat Chem* **2015**, *7*, 582.
(48) Gardner, B. M.; Liddle, S. T. *Chem. Commun.* **2015**, *51*, 10589.
(49) Scott, P.; Hitchcock, P. B. *J. Chem. Soc., Dalton Trans.* **1995**, 603.
(50) Scott, P.; Hitchcock, P. B. *J. Chem. Soc., Chem. Commun.* **1995**, 579.
(51) Gardner, B. M.; Lewis, W.; Blake, A. J.; Liddle, S. T. *Organometallics* **2015**, *34*, 2386.
(52) Cummins, C. C.; Schrock, R. R.; Davis, W. M. *Organometallics* **1992**, *11*, 1452.
(53) Simpson, S. J.; Turner, H. W.; Andersen, R. A. *Inorg. Chem.* **1981**, *20*, 2991.
(54) Roering, A. J.; Maddox, A. F.; Elrod, L. T.; Chan, S. M.; Ghebreab, M. B.; Donovan, K. L.; Davidson, J. J.; Hughes, R. P.; Shalumova, T.; MacMillan, S. N.; Tanski, J. M.; Waterman, R. *Organometallics* **2009**, *28*, 573.
(55) Morton, C.; Munslow, I. J.; Sanders, C. J.; Alcock, N. W.; Scott, P. *Organometallics* **1999**, *18*, 4608.
(56) Gardner, B. M.; McMaster, J.; Lewis, W.; Blake, A. J.; Liddle, S. T. *J. Am. Chem. Soc.* **2009**, *131*, 10388.
(57) Schrock, R. R.; Seidel, S. W.; Mösch-Zanetti, N. C.; Shih, K.-Y.; O'Donoghue, M. B.; Davis, W. M.; Reiff, W. M. *J. Am. Chem. Soc.* **1997**, *119*, 11876.
(58) Boaretto, R.; Roussel, P.; Kingsley, A. J.; Munslow, I. J.; Sanders, C. J.; Alcock, N. W.; Scott, P. *Chem. Commun.* **1999**, 1701.
(59) Boaretto, R.; Roussel, P.; Alcock, N. W.; Kingsley, A. J.; Munslow, I. J.; Sanders, C. J.; Scott, P. *J. Organomet. Chem.* **1999**, *591*, 174.
(60) Pyykkö, P.; Atsumi, M. *Chem. -Eur. J.* **2009**, *15*, 186.
(61) Cordero, B.; Gomez, V.; Platero-Prats, A. E.; Reves, M.; Echeverria, J.; Cremades, E.; Barragan, F.; Alvarez, S. *Dalton Trans.* **2008**, 2832.
(62) Dehnicke, K.; Straehle, J. *Angew. Chem.* **1981**, *93*, 451.
(63) Dehnicke, K.; Straehle, J. *Angew. Chem.* **1992**, *104*, 978.
(64) Eikey, R. A.; Abu-Omar, M. M. *Coord. Chem. Rev.* **2003**, *243*, 83.
(65) Berry, J. F. *Comments Inorg. Chem.* **2009**, *30*, 28.
(66) Smith, J. M. In *Progress in Inorganic Chemistry Volume 58*; John Wiley & Sons, Inc.: 2014, p 417.
(67) Lyne, P. D.; Mingos, D. M. P. *J. Chem. Soc., Dalton Trans.* **1995**, 1635.
(68) Birk, T.; Bendix, J. *Inorg. Chem.* **2003**, *42*, 7608.
(69) Chen, S.; Chisholm, M. H.; Davidson, E. R.; English, J. B.; Lichtenberger, D. L. *Inorg. Chem.* **2009**, *48*, 828.
(70) Chisholm, M. H.; Davidson, E. R.; Pink, M.; Quinlan, K. B. *Inorg. Chem.* **2002**, *41*, 3437.
(71) Woo, L. K. *Chem. Rev.* **1993**, *93*, 1125.
(72) Johnson, M. J. A.; Lee, P. M.; Odom, A. L.; Davis, W. M.; Cummins, C. C. *Angew. Chem., Int. Ed. Engl.* **1997**, *36*, 87.
(73) Mindiola, D. J.; Cummins, C. C. *Angew. Chem.-Int. Edit.* **1998**, *37*, 945.
(74) Bolzati, C.; Cavazza-Ceccato, M.; Agostini, S.; Tisato, F.; Bandoli, G. *Inorg. Chem.* **2008**, *47*, 11972.
(75) Baldas, J.; Boas, J. F.; Bonnyman, J.; Williams, G. A. *J. Chem. Soc., Dalton Trans.* **1984**, 2395.

(76) Yam, V. W.-W.; Tam, K.-K.; Cheng, M.-C.; Peng, S.-M.; Wang, Y. *J. Chem. Soc., Dalton Trans.* **1992**, 1717.
(77) Reinerth, W. A.; Shapley, P. A. *Inorg. Chim. Acta* **1998**, *267*, 335.
(78) Shin, J. H.; Bridgewater, B. M.; Churchill, D. G.; Baik, M.-H.; Friesner, R. A.; Parkin, G. *J. Am. Chem. Soc.* **2001**, *123*, 10111.
(79) Tran, B. L.; Pink, M.; Gao, X. F.; Park, H.; Mindiola, D. J. *J. Am. Chem. Soc.* **2010**, *132*, 1458.
(80) Tran, B. L.; Krzystek, J.; Ozarowski, A.; Chen, C.-H.; Pink, M.; Karty, J. A.; Telser, J.; Meyer, K.; Mindiola, D. J. *Eur. J. Inorg. Chem.* **2013**, *2013*, 3916.
(81) Grapperhaus, C. A.; Mienert, B.; Bill, E.; Weyhermüller, T.; Wieghardt, K. *Inorg. Chem.* **2000**, *39*, 5306.
(82) Song, Y.-F.; Berry, J. F.; Bill, E.; Bothe, E.; Weyhermüller, T.; Wieghardt, K. *Inorg. Chem.* **2007**, *46*, 2208.
(83) Carroll, M. E.; Pinter, B.; Carroll, P. J.; Mindiola, D. J. *J. Am. Chem. Soc.* **2015**, *137*, 8884.
(84) Laplaza, C. E.; Cummins, C. C. *Science* **1995**, *268*, 861.
(85) Laplaza, C. E.; Johnson, M. J. A.; Peters, J. C.; Odom, A. L.; Kim, E.; Cummins, C. C.; George, G. N.; Pickering, I. J. *J. Am. Chem. Soc.* **1996**, *118*, 8623.
(86) Hebden, T. J.; Schrock, R. R.; Takase, M. K.; Muller, P. *Chem. Commun.* **2012**, *48*, 1851.
(87) Solari, E.; Da Silva, C.; Iacono, B.; Hesschenbrouck, J.; Rizzoli, C.; Scopelliti, R.; Floriani, C. *Angew. Chem. Int. Ed.* **2001**, *40*, 3907.
(88) Cherry, J.-P. F.; Johnson, A. R.; Baraldo, L. M.; Tsai, Y.-C.; Cummins, C. C.; Kryatov, S. V.; Rybak-Akimova, E. V.; Capps, K. B.; Hoff, C. D.; Haar, C. M.; Nolan, S. P. *J. Am. Chem. Soc.* **2001**, *123*, 7271.
(89) Odom, A. L.; Cummins, C. C.; Protasiewicz, J. D. *J. Am. Chem. Soc.* **1995**, *117*, 6613.
(90) Leung, W.-H.; Wilkinson, G.; Hussain-Bates, B.; Hursthouse, M. B. *J. Chem. Soc., Dalton Trans.* **1991**, 2791.
(91) Dehnicke, K.; Strahle, J. *Angew. Chem., Int. Ed. Engl.* **1992**, *31*, 955.
(92) Mersmann, K.; Horn, K. H.; Böres, N.; Lehnert, N.; Studt, F.; Paulat, F.; Peters, G.; Ivanovic-Burmazovic, I.; van Eldik, R.; Tuczek, F. *Inorg. Chem.* **2005**, *44*, 3031.
(93) Abram, U.; Hagenbach, A. *Z. Anorg. Allg. Chem.* **2002**, *628*, 1719.
(94) Fickes, M. G.; Odom, A. L.; Cummins, C. C. *Chem. Commun.* **1997**, 1993.
(95) Silvia, J. S.; Cummins, C. C. *J. Am. Chem. Soc.* **2009**, *131*, 446.
(96) Hills, A.; Hughes, D. L.; Leigh, G. J.; Prieto-Alcon, R. *J. Chem. Soc., Dalton Trans.* **1993**, 3609.
(97) Ju Chang, K.; Byung Min, L.; Jong, I. S. *Polyhedron* **1995**, *14*, 2145.
(98) Scepaniak, J. J.; Fulton, M. D.; Bontchev, R. P.; Duesler, E. N.; Kirk, M. L.; Smith, J. M. *J. Am. Chem. Soc.* **2008**, *130*, 10515.
(99) Bakir, M.; White, P. S.; Dovletoglou, A.; Meyer, T. J. *Inorg. Chem.* **1991**, *30*, 2835.
(100) Bagh, B.; Broere, D. L. J.; Siegler, M. A.; van der Vlugt, J. I. *Angew. Chem, Int. Ed.* **2016**, *55*, 8603.
(101) Cozzolino, A. F.; Silvia, J. S.; Lopez, N.; Cummins, C. C. *Dalton Trans.* **2014**, *43*, 4639.

(102) Scepaniak, J. J.; Bontchev, R. P.; Johnson, D. L.; Smith, J. M. *Angew. Chem., Int. Ed.* **2011**, *50*, 6630.
(103) Askevold, B.; Nieto, J. T.; Tussupbayev, S.; Diefenbach, M.; Herdtweck, E.; Holthausen, M. C.; Schneider, S. *Nat. Chem.* **2011**, *3*, 532.
(104) Walstrom, A.; Fan, H. J.; Pink, M.; Caulton, K. G. *Inorg. Chim. Acta* **2010**, *363*, 633.
(105) Brask, J. K.; Dura-Vila, V.; Diaconescu, P. L.; Cummins, C. C. *Chem. Commun. (Cambridge, U. K.)* **2002**, 902.
(106) Ruppa, K. B. P.; Desmangles, N.; Gambarotta, S.; Yap, G.; Rheingold, A. L. *Inorg. Chem.* **1997**, *36*, 1194.
(107) Silvia, J. S.; Cummins, C. C. *J. Am. Chem. Soc.* **2010**, *132*, 2169.
(108) *As evidenced by a search of the Cambridge Structural Database (CSD)*.
(109) Cramer, R. E.; Maynard, R. B.; Paw, J. C.; Gilje, J. W. *J. Am. Chem. Soc.* **1981**, *103*, 3589.
(110) Cramer, R. E.; Bruck, M. A.; Edelmann, F.; Afzal, D.; Gilje, J. W.; Schmidbaur, H. *Chemische Berichte* **1988**, *121*, 417.
(111) Fortier, S.; Walensky, J. R.; Wu, G.; Hayton, T. W. *J. Am. Chem. Soc.* **2011**, *133*, 6894.
(112) Gregson, M.; Wooles, A. J.; Cooper, O. J.; Liddle, S. T. *Comments on Inorganic Chemistry* **2015**, 1.
(113) Oldham, J. W. J.; Oldham, S. M.; Scott, B. L.; Abney, K. D.; Smith, W. H.; Costa, D. A. *Chem. Commun.* **2001**, 1348.
(114) Arnold, P. L.; Turner, Z. R.; Germeroth, A. I.; Casely, I. J.; Nichol, G. S.; Bellabarba, R.; Tooze, R. P. *Dalton Trans.* **2013**, *42*, 1333.
(115) Lu, E.; Cooper, O. J.; McMaster, J.; Tuna, F.; McInnes, E. J. L.; Lewis, W.; Blake, A. J.; Liddle, S. T. *Angew. Chem., Int. Ed.* **2014**, *53*, 6696.
(116) Brennan, J. G.; Andersen, R. A. *J. Am. Chem. Soc.* **1985**, *107*, 514.
(117) Burns, C. J.; Smith, W. H.; Huffman, J. C.; Sattelberger, A. P. *J. Am. Chem. Soc.* **1990**, *112*, 3237.
(118) Castro-Rodriguez, I.; Nakai, H.; Meyer, K. *Angew. Chem., Int. Ed.* **2006**, *45*, 2389.
(119) Bart, S. C.; Anthon, C.; Heinemann, F. W.; Bill, E.; Edelstein, N. M.; Meyer, K. *J. Am. Chem. Soc.* **2008**, *130*, 12536.
(120) Peters, R. G.; Warner, B. P.; Burns, C. J. *J. Am. Chem. Soc.* **1999**, *121*, 5585.
(121) Cooper, O.; Camp, C.; Pécaut, J.; Kefalidis, C. E.; Maron, L.; Gambarelli, S.; Mazzanti, M. *J. Am. Chem. Soc.* **2014**, *136*, 6716.
(122) Fortier, S.; Wu, G.; Hayton, T. W. *J. Am. Chem. Soc.* **2010**, *132*, 6888.
(123) Fortier, S.; Brown, J. L.; Kaltsoyannis, N.; Wu, G.; Hayton, T. W. *Inorg. Chem.* **2012**, *51*, 1625.
(124) Fortier, S.; Kaltsoyannis, N.; Wu, G.; Hayton, T. W. *J. Am. Chem. Soc.* **2011**, *133*, 14224.
(125) Evans, W. J.; Kozimor, S. A.; Ziller, J. W. *Polyhedron* **2004**, *23*, 2689.
(126) Brown, J. L.; Fortier, S.; Lewis, R. A.; Wu, G.; Hayton, T. W. *J. Am. Chem. Soc.* **2012**, *134*, 15468.
(127) Ephritikhine, M. *Coord. Chem. Rev.* **2016**, *319*, 35.
(128) Green, D. W.; Reedy, G. T. *J. Chem. Phys.* **1976**, *65*, 2921.
(129) Hunt, R. D.; Yustein, J. T.; Andrews, L. *J. Chem. Phys.* **1993**, *98*, 6070.
(130) Zhou, M. F.; Andrews, L. *J. Chem. Phys.* **1999**, *111*, 11044.

(131) Andrews, L.; Wang, X. F.; Lindh, R.; Roos, B. O.; Marsden, C. J. *Angew. Chem., Int. Ed.* **2008**, *47*, 5366.
(132) Wang, X. F.; Andrews, L.; Vlaisavljevich, B.; Gagliardi, L. *Inorg. Chem.* **2011**, *50*, 3826.
(133) Heinemann, C.; Schwarz, H. *Chem.-Eur. J.* **1995**, *1*, 7.
(134) Meyer, K.; Mindiola, D. J.; Baker, T. A.; Davis, W. M.; Cummins, C. C. *Angew. Chem.-Int. Edit.* **2000**, *39*, 3063.
(135) Odom, A. L.; Arnold, P. L.; Cummins, C. C. *J. Am. Chem. Soc.* **1998**, *120*, 5836.
(136) Korobkov, I.; Gambarotta, S.; Yap, G. P. A. *Angew. Chem., Int. Ed.* **2002**, *41*, 3433.
(137) Evans, W. J.; Kozimor, S. A.; Ziller, J. W. *Science* **2005**, *309*, 1835.
(138) Evans, W. J.; Miller, K. A.; Ziller, J. W.; Greaves, J. *Inorg. Chem.* **2007**, *46*, 8008.
(139) Todorova, T. K.; Gagliardi, L.; Walensky, J. R.; Miller, K. A.; Evans, W. J. *J. Am. Chem. Soc.* **2010**, *132*, 12397.
(140) Nocton, G.; Pecaut, J.; Mazzanti, M. *Angew. Chem., Int. Ed.* **2008**, *47*, 3040.
(141) Fox, A. R.; Cummins, C. C. *J. Am. Chem. Soc.* **2009**, *131*, 5716.
(142) Fox, A. R.; Arnold, P. L.; Cummins, C. C. *J. Am. Chem. Soc.* **2010**, *132*, 3250.
(143) Pyykko, P.; Zhao, Y. *Inorg. Chem.* **1991**, *30*, 3787.
(144) Vogel, C.; Heinemann, F. W.; Sutter, J.; Anthon, C.; Meyer, K. *Angew. Chem., Int. Ed.* **2008**, *47*, 2681.
(145) Berry, J. F.; Bill, E.; Bothe, E.; George, S. D.; Mienert, B.; Neese, F.; Wieghardt, K. *Science* **2006**, *312*, 1937.
(146) Thomson, R. K.; Cantat, T.; Scott, B. L.; Morris, D. E.; Batista, E. R.; Kiplinger, J. L. *Nat. Chem.* **2010**, *2*, 723.
(147) Camp, C.; Pécaut, J.; Mazzanti, M. *J. Am. Chem. Soc.* **2013**, *135*, 12101.
(148) Chatelain, L.; Scopelliti, R.; Mazzanti, M. *J. Am. Chem. Soc.* **2016**, *138*, 1784.
(149) Maria, L.; Santos, I. C.; Sousa, V. R.; Marçalo, J. *Inorg. Chem.* **2015**, *54*, 9115.
(150) Tsoureas, N.; Kilpatrick, A. F. R.; Inman, C. J.; Cloke, F. G. N. *Chem. Sci.* **2016**, *7*, 4624.
(151) Brennan, J. G.; Andersen, R. A.; Robbins, J. L. *J. Am. Chem. Soc.* **1986**, *108*, 335.
(152) Parry, J.; Carmona, E.; Coles, S.; Hursthouse, M. *J. Am. Chem. Soc.* **1995**, *117*, 2649.
(153) Evans, W. J.; Kozimor, S. A.; Nyce, G. W.; Ziller, J. W. *J. Am. Chem. Soc.* **2003**, *125*, 13831.
(154) Castro-Rodriguez, I.; Meyer, K. *J. Am. Chem. Soc.* **2005**, *127*, 11242.
(155) Summerscales, O. T.; Cloke, F. G. N.; Hitchcock, P. B.; Green, J. C.; Hazari, N. *Science* **2006**, *311*, 829.
(156) Summerscales, O. T.; Cloke, F. G. N.; Hitchcock, P. B.; Green, J. C.; Hazari, N. *J. Am. Chem. Soc.* **2006**, *128*, 9602.
(157) Frey, A. S.; Cloke, F. G. N.; Hitchcock, P. B.; Day, I. J.; Green, J. C.; Aitken, G. *J. Am. Chem. Soc.* **2008**, *130*, 13816.

(158) Tsoureas, N.; Summerscales, O. T.; Cloke, F. G. N.; Roe, S. M. *Organometallics* **2013**, *32*, 1353.
(159) Mansell, S. M.; Kaltsoyannis, N.; Arnold, P. L. *J. Am. Chem. Soc.* **2011**, *133*, 9036.
(160) Arnold, P. L.; Turner, Z. R.; Bellabarba, R. M.; Tooze, R. P. *Chem. Sci.* **2011**, *2*, 77.
(161) Manriquez, J. M.; Fagan, P. J.; Marks, T. J.; Day, C. S.; Day, V. W. *J. Am. Chem. Soc.* **1978**, *100*, 7112.
(162) Simpson, S. J.; Andersen, R. A. *J. Am. Chem. Soc.* **1981**, *103*, 4063.
(163) Bénaud, O.; Berthet, J.-C.; Thuéry, P.; Ephritikhine, M. *Inorg. Chem.* **2010**, *49*, 8117.
(164) Evans, W. J.; Siladke, N. A.; Ziller, J. W. *Chem. -Eur. J.* **2010**, *16*, 796.
(165) Siladke, N. A.; LeDuc, J.; Ziller, J. W.; Evans, W. J. *Chem. -Eur. J.* **2012**, *18*, 14820.
(166) Weydert, M.; Brennan, J. G.; Andersen, R. A.; Bergman, R. G. *Organometallics* **1995**, *14*, 3942.
(167) Frey, A. S. P.; Cloke, F. G. N.; Coles, M. P.; Hitchcock, P. B. *Chem.-Eur. J.* **2010**, *16*, 9446.
(168) Kefalidis, C. E.; Frey, A. S. P.; Roe, S. M.; Cloke, F. G. N.; Maron, L. *Dalton Trans.* **2014**, *43*, 11202.
(169) Frey, A. S. P.; Cloke, F. G. N.; Coles, M. P.; Maron, L.; Davin, T. *Angew. Chem., Int. Ed.* **2011**, *50*, 6881.
(170) Castro-Rodriguez, I.; Nakai, H.; Zakharov, L. N.; Rheingold, A. L.; Meyer, K. *Science* **2004**, *305*, 1757.
(171) Schmidt, A.-C.; Heinemann, F. W.; Maron, L.; Meyer, K. *Inorg. Chem.* **2014**, *53*, 13142.
(172) Camp, C.; Chatelain, L.; Kefalidis, C. E.; Pecaut, J.; Maron, L.; Mazzanti, M. *Chem. Commun.* **2015**, *51*, 15454.
(173) Summerscales, O. T. F., A. S. P.; Cloke, F. G. N.; Hitchcock, P. B. *Chem. Commun. (Cambridge, U. K.)* **2009**, 198.
(174) Tsoureas, N.; Castro, L.; Kilpatrick, A. F. R.; Cloke, F. G. N.; Maron, L. *Chem. Sci.* **2014**, *5*, 3777.
(175) Mougel, V.; Camp, C.; Pécaut, J.; Copéret, C.; Maron, L.; Kefalidis, C. E.; Mazzanti, M. *Angew. Chem., Int. Ed.* **2012**, *51*, 12280.
(176) Lam, O. P.; Bart, S. C.; Kameo, H.; Heinemann, F. W.; Meyer, K. *Chem. Commun.* **2010**, *46*, 3137.
(177) Schmidt, A.-C.; Nizovtsev, A. V.; Scheurer, A.; Heinemann, F. W.; Meyer, K. *Chem. Commun.* **2012**, *48*, 8634.
(178) Schmidt, A.-C.; Heinemann, F. W.; Kefalidis, C. E.; Maron, L.; Roesky, P. W.; Meyer, K. *Chem. -Eur. J.* **2014**, *20*, 13501.
(179) Webster, C. L.; Ziller, J. W.; Evans, W. J. *Organometallics* **2013**, *32*, 4820.
(180) Higgins, J. A.; Cloke, F. G. N.; Roe, S. M. *Organometallics* **2013**, *32*, 5244.
(181) Evans, W. J.; Siladke, N. A.; Ziller, J. W. *Comptes Rendus Chimie* **2010**, *13*, 775.
(182) Webster, C. L.; Ziller, J. W.; Evans, W. J. *Organometallics* **2014**, *33*, 433.
(183) Matson, E. M.; Forrest, W. P.; Fanwick, P. E.; Bart, S. C. *J. Am. Chem. Soc.* **2011**, *133*, 4948.
(184) Evans, W. J.; Walensky, J. R.; Ziller, J. W. *Organometallics* **2010**, *29*, 945.

(185) Matson, E. M.; Fanwick, P. E.; Bart, S. C. *Organometallics* **2011**, *30*, 5753.
(186) Webster, C. L.; Ziller, J. W.; Evans, W. J. *Organometallics* **2012**, *31*, 7191.
(187) Moloy, K. G.; Marks, T. J. *Inorg. Chim. Acta* **1985**, *110*, 127.
(188) Arduini, A. L.; Jamerson, J. D.; Takats, J. *Inorg. Chem.* **1981**, *20*, 2474.
(189) Higgins Frey, J. A.; Cloke, F. G. N.; Roe, S. M. *Organometallics* **2015**, *34*, 2102.
(190) Lescop, C.; Arliguie, T.; Lance, M.; Nierlich, M.; Ephritikhine, M. *J. Organomet. Chem.* **1999**, *580*, 137.
(191) Lam, O. P.; Castro, L.; Kosog, B.; Heinemann, F. W.; Maron, L.; Meyer, K. *Inorg. Chem.* **2012**, *51*, 781.
(192) Lam, O. P.; Franke, S. M.; Heinemann, F. W.; Meyer, K. *J. Am. Chem. Soc.* **2012**, *134*, 16877.
(193) Matson, E. M.; Breshears, A. T.; Kiernicki, J. J.; Newell, B. S.; Fanwick, P. E.; Shores, M. P.; Walensky, J. R.; Bart, S. C. *Inorg. Chem.* **2014**, *53*, 12977.
(194) Brennan, J. G.; Andersen, R. A.; Zalkin, A. *Inorg. Chem.* **1986**, *25*, 1756.
(195) Camp, C.; Cooper, O.; Andrez, J.; Pecaut, J.; Mazzanti, M. *Dalton Trans.* **2015**, *44*, 2650.
(196) Lam, O. P.; Heinemann, F. W.; Meyer, K. *Angew. Chem., Int. Ed.* **2011**, *50*, 5965.
(197) Falcone, M.; Chatelain, L.; Mazzanti, M. *Angew. Chem., Int. Ed.* **2016**, *55*, 4074.

Chapter Two

The Synthesis of Uranium Nitrides

Table of Contents

2.1. Introduction and Aims 88

2.2. Reactivity Studies of [U(Tren^{TIPS})(N$_3$)] Towards Reducing Agents 89

2.3. Reactivity Studies of [{U(Tren^{TIPS})(μ-N)(μ-M)}$_2$] (M = Li, Na, K, Rb, Cs) Towards Crown Ethers 99

2.3.1. Overview 99

2.3.2. Preparation of [U(Tren^{TIPS}){(μ-N)(μ-M)(crown)}] (M = Na, K, Rb, Cs) 100

2.3.3. Preparation of [U(Tren^{TIPS})(N)][M(crown)$_2$] (M = Na, K, Rb, Cs) 106

2.3.4. Reactivity studies of [{U(Tren^{TIPS}){(μ-N)(μ-Li)}$_2$] towards donor ligands 112

2.3.5. Solution phase electronic data for 52, 53, 111 – 121 118

2.4. Preparation of [U(Tren^{TIPS})(N)] (54) 124

2.5. Alternative Syntheses of [{U(Tren^{TIPS})(μ-N)(μ-K)}$_2$] (107) 124

2.5.1. Reactivity studies of [U(Tren^{TIPS})(N)] (54) towards reducing agents 124

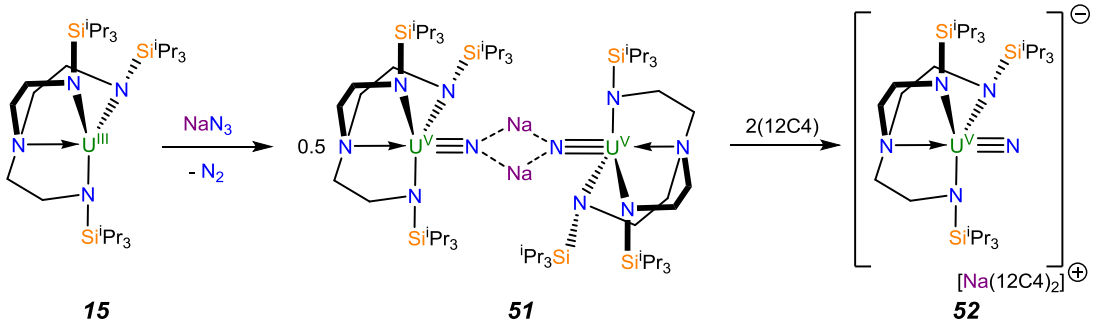
2.5.2. Transmetallation reactions of [{U(Tren^{TIPS})(μ-N)(μ-Na)}$_2$] (51) 125

2.6. Summary and Conclusions 126

2.7. References 127

2.1. Introduction and Aims

The synthesis of a terminal uranium nitride was achieved by Liddle *et al.*[1] in 2012, *via* the reaction of [U(Tren^{TIPS})] (**15**) with NaN_3, followed by the subsequent sequestration and encapsulation of the electrostatically bound sodium cations in [{U(Tren^{TIPS})(μ-N)(μ-Na)}$_2$] (**51**) with two equivalents of 12-crown-4 ether (12C4) to afford [U(Tren^{TIPS})(N)][Na(12C4)$_2$] (**52**).



*Scheme **2.1.** Synthesis of **51** and **52**.*

The methodology employed here, as discussed above,[1] employs the highly sterically demanding tripodal tetradentate ligand Tren^{TIPS} [{N(CH$_2$CH$_2$NSi^{i}Pr$_3$)$_3$}$^{3-}$], which allows only coordination of small and/or cylindrical ligands into an apical pocket, *trans* to the face-capping amine. Therefore, an azide anion can fit into this space and it coordinates to the uranium centre. The sodium cation can, due to the ionic nature of its bonding, provide electronic stabilisation during the reduction of the azide ligand. Two electrons from the uranium(III) centre are fed into the azide group, which promotes the elimination of dinitrogen, and this affords a uranium(V)–nitride fragment, which is stabilised by the sodium cations.

The initial aim of this work was then to prepare the group one metal analogues of **51**, i.e. [{U(Tren^{TIPS})(μ-N)(μ-M)}$_2$] (M = Li, K, Rb, Cs), and to treat the resultant species with various crown ethers (and other co-ligands) to afford analogues of [U(Tren^{TIPS})(N)][Na(12C4)$_2$] (**52**) and [U(Tren^{TIPS}){(μ-N)(μ-Na)(15C5)}] (**53**). The ultimate aim is then to investigate any differences in the uranium–nitride ligand that may arise from changing the alkali metal, which may be structural, electronic, or concerning reactivity.

The work discussed in this chapter was performed in collaboration with Dr D. M. King, Dr A. J. Wooles, Dr B. M. Gardner and Dr M. J. Gregson, and all results are discussed here for completeness, and to allow for a more complete discussion into the inherent properties of the prepared complexes.

2.2. Reactivity Studies of [U(Tren^{TIPS})(N$_3$)] Towards Reducing Agents

The first step was to replicate the published synthesis, with the goal of optimising the yields for the preparation of **51**.[1] However, whilst this methodology is sound in principle, we encountered some issues. Firstly, the reduction of sodium azide with **15** can be unreliable in multi-gram scale quantities. This is believed to be due to the low solubility of NaN_3 in pyridine. The choice of pyridine as the solvent for this reaction acts as a compromise between polar solvents which solubilise NaN_3, and the solvents tolerated by the uranium species, wherein the use of polar solvents results in decomposition. Heating the reaction mixture to promote reactivity is not viable, as this also results in decomposition. Pre-addition of 12-crown-4 ether to improve the solubility of NaN_3 by the formation of $[Na(12C4)_2][N_3]$ is also not a valid strategy, as the encapsulated cation cannot approach the uranium centre close enough to electrostatically stabilise the installation of the azide ligand, or in its subsequent reduction to a nitride functionality.

Similarly, reactions of **15** with KN_3 in pyridine to afford $[\{U(Tren^{TIPS})(\mu\text{-}N)(\mu\text{-}K)\}_2]$ were unsuccessful, resulting in intractable mixtures, which we believe is due to increased solubility problems of KN_3 compared to NaN_3.

Consequently, a reappraisal of the chemistry occurring at uranium suggested that alternative routes towards $[\{U(Tren^{TIPS})(\mu\text{-}N)(\mu\text{-}M)\}_2]$ might be feasible. The fundamental chemistry (i.e. electron transfer, bond breaking/ forming) employed in the initial strategy is shown in equation 1.

$$U^{III} + N_3^- + Na^I \rightarrow U^V{\equiv}N^- + Na^I + N_2 \qquad \text{(Eqn 1)}$$

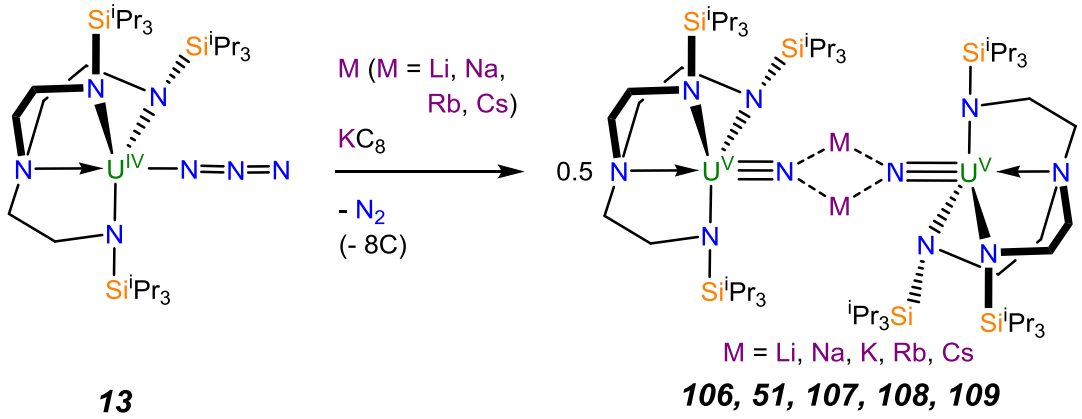
The uranium(III) ions provide two electrons to effect the ejection of dinitrogen and the installation of the trianionic nitride.

It was postulated that the addition of an external one-electron reductant (such as an alkali metal) to a pre-installed azide functionality such as in the known species [U(Tren^{TIPS})(N$_3$)] (**13**), might effect analogous reactivity to afford a nitride species, as described in equation 2. The second electron required for the reduction of the azide fragment would come from the oxidation of the uranium centre from U^{IV} to U^{V}. The oxidation state of uranium would need to be adjusted to avoid premature activation of the azide group, which might be anticipated for uranium(III) but not uranium(IV).[2]

$$U^{IV}\text{-}N_3 + M^0 \rightarrow U^{V}\equiv N^- + M^I + N_2 \qquad \text{(Eqn 2)}$$

The benefits of this methodology would include the pre-coordination of the azide ligand, which results in fewer sequential bond breaking and forming steps in the reaction pathway. That, in equation 1, there must be not only the formation of a U≡N triple bond, but also the breaking of a N=N double bond and the formation of an N≡N triple bond, as well as a two electron transfer from U^{III} to azide, suggests that the multitude of transformations that need to occur to effect nitride formation might reveal some insight as to the capriciousness of this reaction, any there are many routes towards decomposition available during reaction.

This methodology (the reduction of a terminal azide ligand) was also employed by Mindiola *et al*. to prepare the first titanium nitride complex (see Chapter 1, Section 3), in work that was completed concurrently to this.



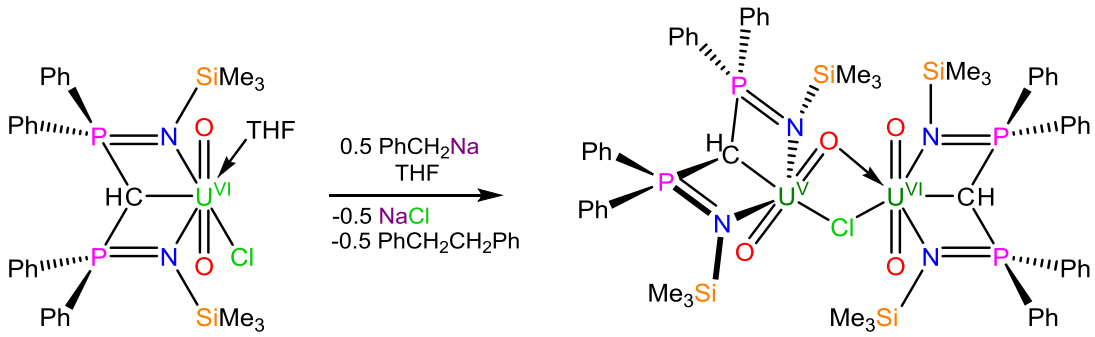
13 ***106, 51, 107, 108, 109***

*Scheme **2.2.** Syntheses of **51** and **106**, **107**, **108** and **109**.*

The reaction of **13** towards alkali metal reagents was investigated. A mixture of **13** and lithium or sodium powders, in toluene, were stirred at room temperature for 5 days. These mixtures were sonicated for one hour per day. After this period, a red solid formed in both cases, and complete consumption of the alkali metal was observed. Similarly, the reaction of **13** with elemental rubidium or caesium in toluene for one week afforded red solids with the concomitant consumption of the metal reagent observed. Extraction of each of these red solids into boiling aromatic solvent (toluene or benzene) afforded red crystals upon cooling to room temperature. Our initial formulation of the complexes was [{U(Tren^{TIPS})(μ-N)(μ-M)}$_2$] (M = Li, Na, Rb, Cs; respectively **106**, **51**, **108** and **109**).

In an analogous manner to the preparation of **51**, **106**, **108** and **109**, the reaction of **13** with KC_8 (potassium graphite) was also investigated. Stirring this mixture for four days resulted in a dark suspension. Filtration of the dark mixture afforded a brown black solid. Extraction of this solid into boiling aromatic solvent away from residual graphite allowed for the isolation of red crystals, formulated as [{U(Tren^{TIPS})(μ-N)(μ-K)}$_2$] (**107**).

Additionally, the reduction of **13** with KCH_2Ph was attempted. It was envisioned that the reduction would occur alongside the elimination of half an equivalent of bibenzyl ($PhCH_2CH_2Ph$), analogously to the reduction of [U(BIPMH^{TMS})(O)$_2$(Cl)(THF)] [BIPMH^{TMS} = {H*C*(PPh$_2$=*N*SiMe$_3$)$_2$}$^-$] to the mixed U^V-U^{VI} system [{U(BIPMH^{TMS})(O)(μ-O)}(μ-Cl){U(BIPMH^{TMS})(O)$_2$}], scheme **2.3.**[3] Instead, the only uranium containing product isolated was the cyclometallated species [U{*C*H$_2$CH(Me)Si(^{i}Pr)$_2$*N*CH$_2$CH$_2$*N*(CH$_2$CH$_2$NSi^{i}Pr$_3$)$_2$}], **110**. For further discussion of this reaction and the nature of **110**, see Chapter 3.



Scheme ***2.3.*** *Synthesis of [{U(BIPMH^{TMS})(O)(μ-O)}(μ-Cl){U(BIPMH^{TMS})(O)$_2$}].*[3]

Single crystal X-ray diffraction studies on **51**, **106**, **107**, **108** and **109** elucidated their structures, and these are illustrated in figures **2.1.** – **2.4.**, alongside selected bond lengths and angles. Though the molecular structure for **51** has been previously described (as prepared *via* the two electron reduction of NaN_3 with **15** in pyridine),[1,4] it is included here for completeness, and to aid structural comparisons (*vide infra*).

In the case of **106**, and **107** as prepared by *via* a different synthetic strategy (Chapter 2, Section 5), crystals of two different phases were obtained, and the solid state structures are depicted in figures **2.1.** (left and right), and **2.2.** (right) and **2.3.** (left), respectively, to allow comparison to be made.

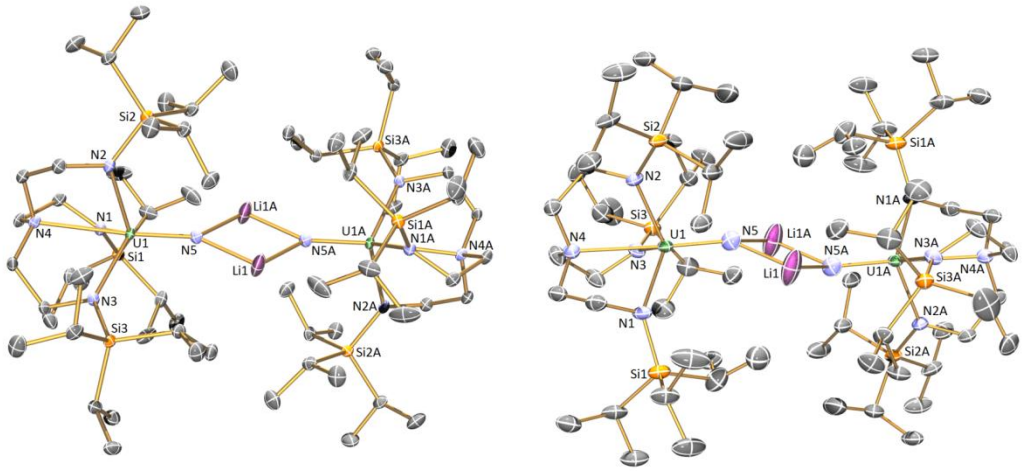


Figure ***2.1.*** *Molecular structures of [{U(Tren^{TIPS})(μ-N)(μ-Li)}$_2$],* ***106*** *(co-planar, left) and Trans-bent polymorphic molecular structure of [{U(Tren^{TIPS})(μ-N)(μ-Li)}$_2$],* ***106*** *(right). Thermal ellipsoids set at 40% probability. Hydrogen atoms are omitted for clarity. Selected distances (Å) and angles (°):* ***106*** *(co-planar) U(1)-N(1) 2.313(3), U(1)-N(2) 2.320(2), U(1)-N(3) 2.313(2), U(1)-N(4)*

2.683(2), U(1)-N(5) 1.885(2), N(5)-Li(1) 1.974(7), N(5)-Li(1A) 1.985(6), N(4)-U(1)-N(5) 172.67(9), N(5)-Li(1)-N(5A) 106.7(3), Li(1)-N(5)-Li(1A) 73.3(3); ***106*** *(trans-bent) U(1)-N(1) 2.320(5), U(1)-N(2) 2.305(5), U(1)-N(3) 2.311(6), U(1)-N(4) 2.671(5), U(1)-N(5) 1.912(6), N(5)-Li(1) 1.949(17), N(5)-Li(1A) 1.979(16), N(4)-U(1)-N(5) 175.9(2), N(5)-Li(1)-N(5A) 107.8(7), Li(1)-N(5)-Li(1A) 72.2(7).*

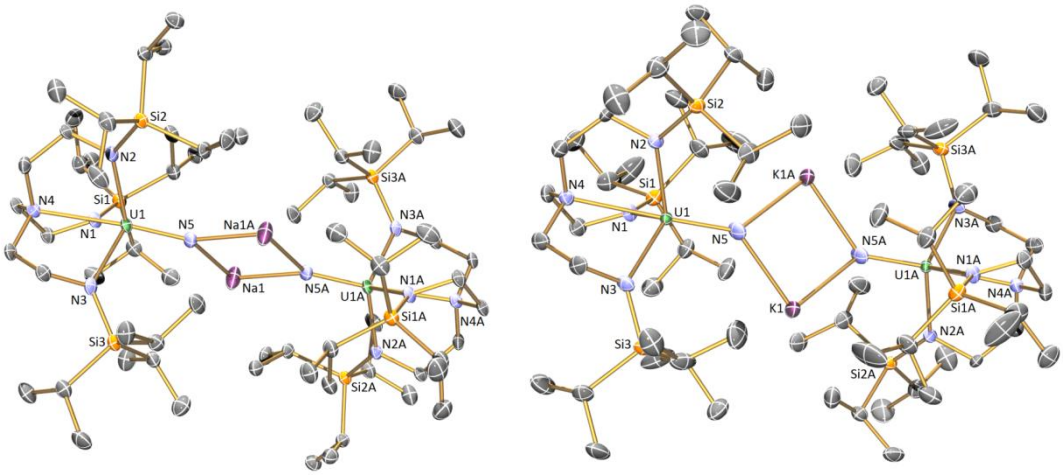


Figure ***2.2.*** *Molecular structures of [{U(Tren*^{TIPS}*)(μ-N)(μ-Na)}$_2$], **51**,*[1] *and [{U(Tren*^{TIPS}*)(μ-N)(μ-K)}$_2$], **107** (co-planar). Thermal ellipsoids set at 40% probability. Hydrogen atoms are omitted for clarity. Selected distances (Å) and angles (°):**51** U(1)-N(1) 2.333(4), U(1)-N(2) 2.322(4), U(1)-N(3) 2.328(4), U(1)-N(4) 2.654(4), U(1)-N(5) 1.883(4), N(5)-Na(1) 2.308(5), N(5)-Na(1A) 2.345(5), N(4)-U(1)-N(5) 174.12(16), N(5)-Na(1)-N(5A) 99.26(17), Na(1)-N(5)-Na(1A) 80.74(17);* ***107*** *(co-planar) U(1)-N(1) 2.349(5), U(1)-N(2) 2.317(6), U(1)-N(3) 2.333(6), U(1)-N(4) 2.666(6), U(1)-N(5) 1.929(6), N(5)-K(1) 2.702(6), N(5)-K(1A) 2.746(7), N(4)-U(1)-N(5) 177.3(2), N(5)-K(1)-N(5A) 96.37(17), K(1)-N(5)-K(1A) 83.64(17).*

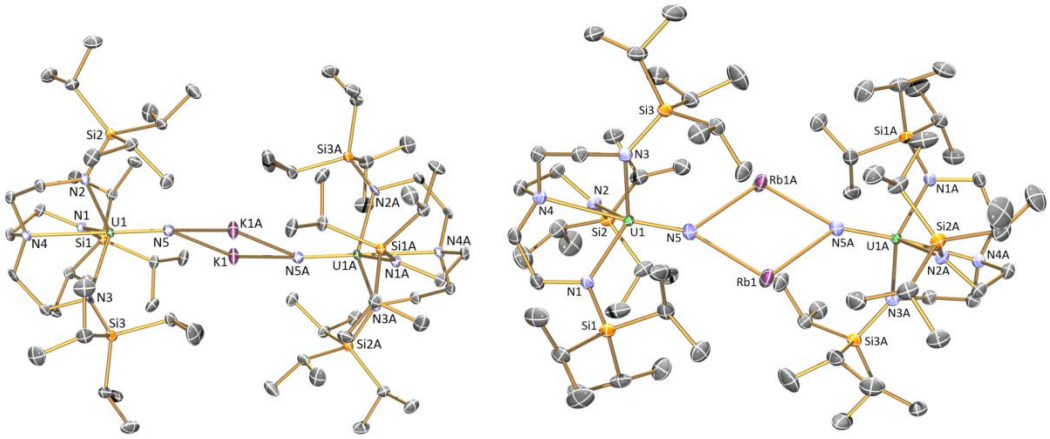


*Figure **2.3.** Molecular stuctures of [{U(Tren^{TIPS})(μ-N)(μ-K)}$_2$], **107** (trans-bent) and [{U(Tren^{TIPS})(μ-N)(μ-Rb)}$_2$], **108**. Thermal ellipsoids set at 30% probability. Hydrogen atoms are omitted for clarity. Selected distances (Å) and angles (°):**107** (trans-bent) U(1)-N(1) 2.341(3), U(1)-N(2) 2.344(3), U(1)-N(3) 2.327(3), U(1)-N(4) 2.635(3), U(1)-N(5) 1.861(4), N(5)-K(1) 2.687(4), N(5)-K(1A) 2.707(4), N(4)-U(1)-N(5) 174.78(13), N(5)-K(1)-N(5A) 101.32(10), K(1)-N(5)-K(1A) 78.68(10); **108** U(1)-N(1) 2.335(3), U(1)-N(2) 2.322(3), U(1)-N(3) 2.352(3), U(1)-N(4) 2.669(3), U(1)-N(5) 1.846(3), N(5)-Rb(1) 2.846(3), N(5)-Rb(1a) 2.882(3), N(4)-U(1)-N(5) 175.61(12), N(5)-Rb(1)-N(5A) 98.02(8), Rb(1)-N(5)-Rb(1A) 81.98(8).*

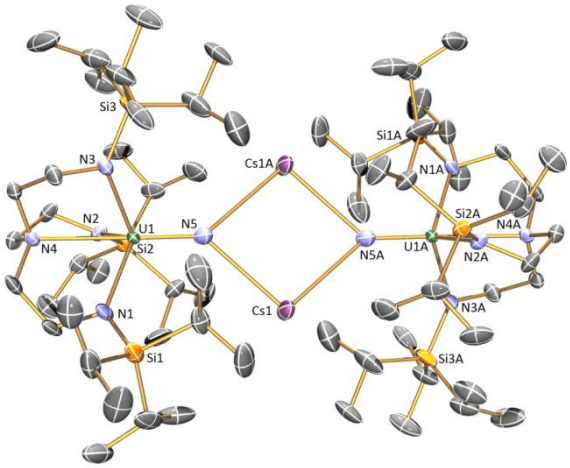


*Figure **2.4.** Molecular structure of [{U(Tren^{TIPS})(μ-N)(μ-Cs)}$_2$], **109**. Thermal ellipsoids set at 40% probability. Hydrogen atoms are omitted for clarity. Minor disorder component at caesium not shown. Selected distances (Å) and angles (°): U(1)-N(1) 2.339(5), U(1)-N(2) 2.351(5), U(1)-N(3) 2.329(5), U(1)-N(4) 2.655(4),*

U(1)-N(5) 1.860(5), N(5)-Cs(1) 2.956(5), N(5)-Cs(1A) 3.092(5), N(5A)-Cs(1) 2.979(6), N(5A)-Cs(1A) 3.064(6), N(4)-U(1)-N(5) 175.6(2), N(5)-Cs(1)-N(5A) 96.35(14), N(5)-Cs(1A)-N(5A) 96.50(14), Cs(1)-N(5)-Cs(1A) 83.65(14), Cs(1)-N(5A)-Cs(1A) 83.51(14).

The solid state structures of **106**, **107**, **108** and **109** confirm our initial assignment of [{U(Tren^{TIPS})(μ-N)(μ-M)}$_2$], and are analogues of the previously reported **51**.[1] The isolation of **51** and **106**, **107**, **108** and **109** confirms that the preparation of uranium nitrides *via* the addition of a one electron external reductant to the pre-installed azide in **13** is a valid strategy.

The uranium centres are five-coordinate, with a nitride ligand in the apical pocket of Tren^{TIPS}. The uranium centres adopt distorted trigonal bipyramidal geometries, with the nitride ligand and the face-capping amine in the apical positions. The trigonal bipyramidal geometry is confirmed by the τ values of **51** and **106**, **107**, **108** and **109**,[5] which range from 0.93 to 1.08.[6] In all cases, **51** and **106**, **107**, **108** and **109** are centrosymmetric, with an inversion centre at the centre of the [N-M-N-M] core. The nitride ligands are mutually bridged by two alkali metal cations, which, though apparently two-coordinate, are supported by a number of agostic-type interactions with nearby *iso*-propyl C-H bonds. Predictably, the length of these interactions increases proportionally to the size of the cation [six coordinate cation sizes: Li 0.76, Na 1.02, K 1.38, Rb 1.48, Cs 1.67 Å;[7] agostic-type interaction ranges: Li···H-C 2.059 – 2.328, Na···H-C 2.407 – 2.588, K···H-C 2.518 – 3.031, Rb···H-C 2.595 – 3.244, Cs···H-C 2.687 – 3.445 Å]. The number of interactions present depends on the geometry of the nitride core [U≡N-M$_2$-N≡U]. The geometry of the core can be assessed by the relationship between the two planes defined by each of the sets of bound amine, uranium and nitride atoms [N(4)-U(1)-N(5) and N(4A)-U(1A)-N(5A)]. These are either co-planar, and therefore the core is flat, or they are offset from one-another, resulting in a *trans*-bent core (figure **2.5.**).

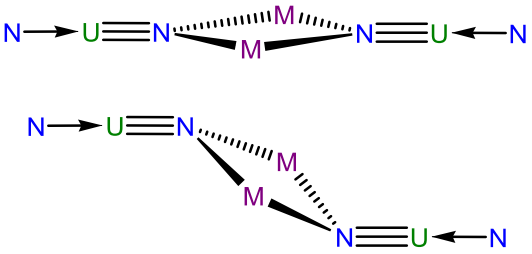


*Figure **2.5.** The two geometries possible for **51** and **106**, **107**, **108** and **109**: upper, co-planar; lower, trans-bent.*

The geometry observed in the structures of **51** and **106**, **107**, **108** and **109**, and correspondingly the nature of the nitride core, appears to be solely based upon crystal packing effects. This can be seen most readily though the isolation of polymorphs (one of each geometry) for lithium (figure **2.1.** left and right), and potassium (figures **2.2.**, right and **2.3.**, left). The potential energy surface for **51** and **106**, **107**, **108** and **109**, which governs the solid state conformation that is adopted, is relatively shallow. This is due to ionic bonding dominating the interactions between the nitride and the alkali metal cation. As a result, crystal packing effects, which are weak, possess a large enough energy to perturb the conformation, and thus allow the molecule to occupy a different local minimum, and hence adopt a differing geometry, be that co-planar or *trans*-bent. Accordingly, no obvious trends can be found to link the bent or flat polymorphs, be that with respect to the crystal parameters (a, b, c, β), or the variance in size of the cationic metal.

The uranium–nitride bond lengths vary considerably, from 1.846(3) to 1.929(6) Å (sum of covalent radii for U≡N 1.74 Å).[8] Whilst these distances are not as short as might be expected, due to a lack of covalency at the uranium centre, there is still evidence for multiple bond interactions. Broadly speaking, there is a vague trend towards longer U≡N bond lengths for those complexes with a greater distortion from co-planarity of the nitride core. This may be due to the degree of pyramidalisation of the nitrogen atom, that is, the sp-hybridised nitride atom must incorporate more p-orbital character to accommodate the deviation from linearity, which then weakens (lengthens) the U≡N interaction.

The uranium–amide [2.312(6) – 2.339(5) Å] and uranium–amine [2.635(3) – 2.683(2) Å] distances are all broadly the same, regardless of the alkali metal cation

present, and have all lengthened upon oxidation at the metal centre (*cf.* [U(Tren^{TIPS})(N$_3$)] **13**, 2.247(3) and 2.613(3) Å respectively). These data are illustrated in table **2.1.**

*Table **2.1.** Selected bond lengths for **13** and **106**, **51**, **107**, **108** and **109**.*

Compound	U(1)-N$_{amide(av)}$ (Å)	U(1)-N(4) (Å)	U(1)-N(5) (Å)	N(5)-M$_{(av)}$ (Å)
13	2.247(3)	2.613(3)	2.305(3)	n/a
106 – figure **2.1.**, left	2.315(3)	2.683(2)	1.885(2)	1.980(7)
106 – figure **2.1.**, right	2.312(6)	2.671(5)	1.912(6)	1.964(17)
51	2.320(4)	2.654(4)	1.883(4)	2.327(5)
107 – figure **2.2.**, right	2.333(6)	2.666(6)	1.929(6)	2.724(7)
107 – figure **2.3.**, left	2.337(3)	2.635(3)	1.861(4)	2.697(4)
108	2.336(3)	2.669(3)	1.846(3)	2.864(3)
109	2.339(5)	2.655(4)	1.860(5)	3.023(5)

The average nitride-alkali metal cation distance increases down the series as would be expected, and all are shorter than the mean N-M distances from the literature [M$_{group1}$-N distances when bound to M-N$_{amide}$, M=N$_{imide}$ and M≡N$_{nitride}$: mean N-M$_{group\ 1}$ distances: M-N-Li 2.076, M=N-Li 2.100, M≡N-Li 2.055; M-N-Na 2.504, M=N-Na 2.446, M≡N-Na 2.338; M-N-K 2.939, M=N-K 2.880, M≡N-K 2.763, M-N-Rb 3.031, M-N-Cs 3.282 Å. No structures found for M=N-Rb, M≡N-Rb, M=N-Cs or M≡N-Cs].[9] The shorter bond lengths indicate the electron deficient nature of the cations in this bonding environment, as well as that these nitride centres may be nucleophilic.

All of the isolated dinuclear species are highly insoluble in non-polar solvents once isolated, and therefore reliable solution phase data could not always be acquired. In spite of this, ^{1}H NMR spectroscopic analysis was performed on samples of **106** and **109** which were very sparingly soluble. However, due the broad, paramagnetic nature of the NMR spectra obtained, unambiguous assignment of these spectra is often difficult. The ^{1}H NMR spectrum previously reported for **51** spanned the range +4 to –7 ppm,[1] but this narrow range is in contrast to that observed for **106** (+34 to

–3 ppm), and **109** (+38 to –6 ppm) in this study. Due to the large inconsistency in reported data, we repeated ^{1}H NMR spectroscopic studies on a freshly prepared sample of **51**, and we believe the correct assignment for **51** is [δ 38.33 (s, 6H, CH_2), 7.70 (s, 6H, CH_2), −6.55 (s, 9H, CH(CH$_3$)$_2$), −6.82 (s, 54H, CH(CH_3)$_2$)]. This reappraisal of the data allows for spectroscopic analysis which is commensurate across the series.

FTIR spectra were collected for **51** and **106**, **107**, **108** and **109** as Nujol mulls. For **51**, a stretch at ~930 cm^{-1} was identified as the U≡N stretch.[1] Correspondingly, in the ^{15}N-labelled isotopomer, this stretch had shifted to ~900 cm^{-1}, though this was somewhat complicated by overlapping bands from 12-crown-4 ether. In the cases of [{U(Tren^{TIPS})(μ-N)(μ-M)}$_2$] (M = Li, K, Rb, Cs), the isotopomer shifts could not be observed *via* IR spectroscopy, as the fingerprint region contained more overlapping bands, preventing conclusive identification of the U≡^{15}N stretch.

Due to the insolubility of **51** and **106**, **107**, **108** and **109** in non-polar solvents, neither UV-Vis-NIR absorption nor Evans' method solution magnetic experiments could be performed. Solid state, variable temperature SQUID magnetometry, as well as EPR studies, for **51** and **106**, **107**, **108** and **109**, alongside the terminal uranium nitride derivatives of the type [U(Tren^{TIPS}){(μ-N)(μ-M)(crown)}] and [U(Tren^{TIPS})(N)][M(crown)$_2$] (see below), will be discussed in Chapter 4.

The yields for the preparations of **51** and **106**, **107**, **108** and **109** are outlined in table **2.2.** Whilst these yields are not an absolute improvement over the yield reported for the reaction of NaN_3 with **15** in pyridine (best yield 60%),[1] they are considerably more consistent, and therefore this represents an improvement upon that synthesis. Whilst the scale of these reductions of **13** appears to be limited to 3 mmol (at 3 mmol scales the yield was reliably 55 – 60%, attempts to scale up the synthesis to larger than 3 mmol batches became capricious), the reliability of this method makes it a viable route towards bulk scale synthesis, which should permit future reactivity studies (discussed below).

*Table **2.2.** Yields for [U(Tren^{TIPS})(μ-N)(μ-M)}$_2$] (M = Li, Na, K, Rb, Cs), **51** and **106**, **107**, **108** and **109**.*

[U(Tren^{TIPS})(μ-N)(μ-M)}$_2$] (M =)	Yield, %
Li	35
Na	50
K	60
Rb	50
Cs	36

2.3. Reactivity Studies of [{U(Tren^{TIPS})(μ-N)(μ-M)}$_2$] (M = Li, Na, K, Rb, Cs) Towards Crown Ethers

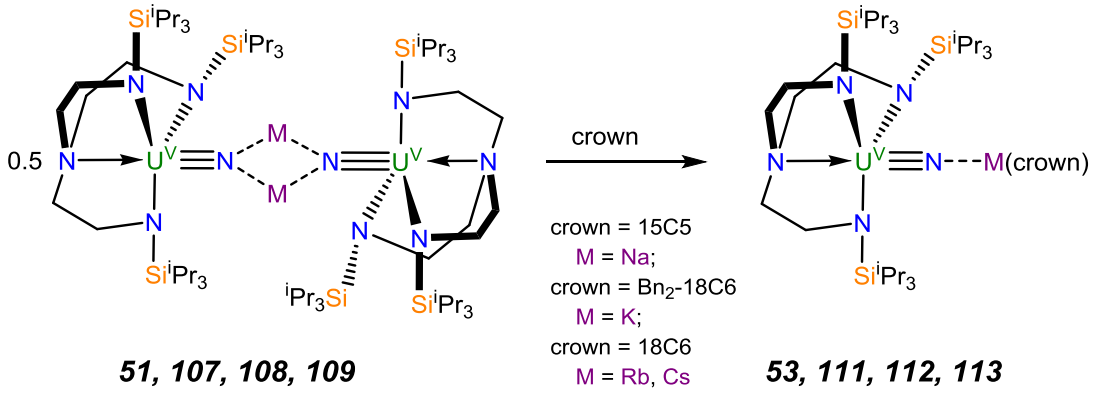
2.3.1. Overview

With a series of dinuclear uranium nitrides in hand, the next synthetic targets are their derivatisation towards terminal, mononuclear derivatives of the type [U(Tren^{TIPS})(N)][M(crown)$_2$]. It has previously been shown that crown ethers are suitable candidates as co-ligands for this purpose, and have demonstrated a large degree of tunability to enforce this role. The selection of the crown ether is therefore an important one, as was discussed in previous works.[1,4,10] For the sodium species **51**, it was found that addition of 15-crown-5 ether (15C5) afforded the capped species [U(Tren^{TIPS}){(μ-N)(μ-Na)(15C5)}] (**53**, a "masked" nitride), whilst the addition of the slightly smaller 12-crown-4 ether (12C4) resulted in the sequestration and encapsulation of the sodium ions to prepare **52**. The product that formed was determined not by stoichiometry, but instead solely by the size of the co-ligand used. It was also reported that other co-ligands (e.g. 2,2,2-Kryptofix, pentaglyme [Me(OCH$_2$CH$_2$)$_5$OMe] and 18-crown-6 ether) resulted in intractable mixtures and the only isolable product was co-ligand.

What follows will be a discussion of reactions of **107**, **108** and **109** (M = K, Rb, Cs) towards various crowns ethers, towards both products of the form [U(Tren^{TIPS}){(μ-N)(μ-M)(crown)}] and ultimately towards separated ion pair species

of the form [U(Tren^{TIPS})(N)][M(crown)$_2$]. Due to issues which will be discussed later, reactions with **106** form a special case, and are therefore discussed separately (see Section 3.4.).

2.3.2. Preparation of [U(Tren^{TIPS}){(μ-N)(μ-M)(crown)}] (M = Na, K, Rb, Cs)



*Scheme **2.4.** Syntheses of **53**, **111**, **112** and **113**.*

In an analogous manner to the reactivity of **51**, addition of one equivalent of a crown ether that is large enough to coordinate equatorially around the alkali metal ion results in cleavage of the dinuclear system and the formation of a capped uranium nitride species. In the case of **51**, addition of 15-crown-5 ether in toluene afforded **53**.[10]

Similarly, the reaction of appropriately sized crowns with **107**, **108** and **109** in toluene for one day afforded analogues of **53** in moderate yields (34 – 66% crystalline yields). Correspondingly the larger potassium congener required the use of dibenzo-18-crown-6, resulting in [U(Tren^{TIPS}){(μ-N)(μ-K)(Bn$_2$-18C6)}], **111**. Curiously, rubidium and caesium also prepare these capped uranium nitride species using 18-crown-6 ether, and do not require larger crown ethers, despite their larger ionic radii (six coordinate radii: K 1.38, Rb 1.48, Cs 1.67 Å).[7] The addition of these crown ethers to **107**, **108** and **109** resulted in a marked change in solubility from the highly insoluble dinuclear uranium nitrides, which was suggestive of a reaction having occurred.

The ^{1}H NMR spectra for **53**, **111**, **112** and **113** are all internally consistent, spanning the ranges **53** +41 to –8 ppm, **111** +40 to –7 ppm, **112** +42 to –7 ppm, and **113** +41 to –8 ppm, which represents a small shift from the dinuclear species (for which spectra could be collected, **51** +38 to –7 and **109** +38 to –6 ppm), and are consistent with the proposed formulation.

FTIR spectra were collected for the complexes as Nujol mulls. For **53**, a stretch at 856 cm^{-1} was identified as the U≡N stretch. In the ^{15}N-labelled isotopomer of **53**, this stretch was reduced in intensity by ~50%, and was accompanied by the growth of a stretch at 827 cm^{-1}. This reduction in intensity arises from the preparation of [U(Tren^{TIPS})($^{15}N_3$)] using sodium 1-^{15}N-azide, which has only one labelled nitrogen atom (i.e. the azide fragment is ^{15}N=^{14}N=^{14}N). Upon coordination to uranium, 50% of the molecules will have U-^{15}N interactions and the remainder will be U-^{14}N. Hence following reduction with one electron external reductants, 50% of the isotopically labelled nitrogen atoms will be lost as dinitrogen, and therefore a reduction in intensity of the band by 50% is anticipated. Corresponding studies were attempted for the heavier capped nitrides, **111**, **112** and **113**, however conclusive identification of these stretches, and the subsequent ^{15}N isotopomer band, is precluded by overlapping bands from the various crown ether C-C stretches in the fingerprint region, so the isotopomer shift could not unambiguously be assigned.

These data were not conclusive as to the formulation of these more soluble complexes, and so single crystal X-ray diffraction studies were carried out on red crystals grown from concentrated solutions of **111**, **112** and **113** in hexanes. The studies on **111**, **112** and **113** confirmed the extension of the set of masked nitrides to encompass alkali metals from sodium to caesium. These structures are illustrated in figures **2.6.** and **2.7.**, alongside selected bond lengths and angles. Though the molecular structure for **53** has been previously described it is included here for completeness, and to aid structural comparisons (*vide infra*).[4,10] As mentioned before, lithium containing analogues of **53**, **111**, **112** and **113** will be discussed separately (see Section 3.4.).

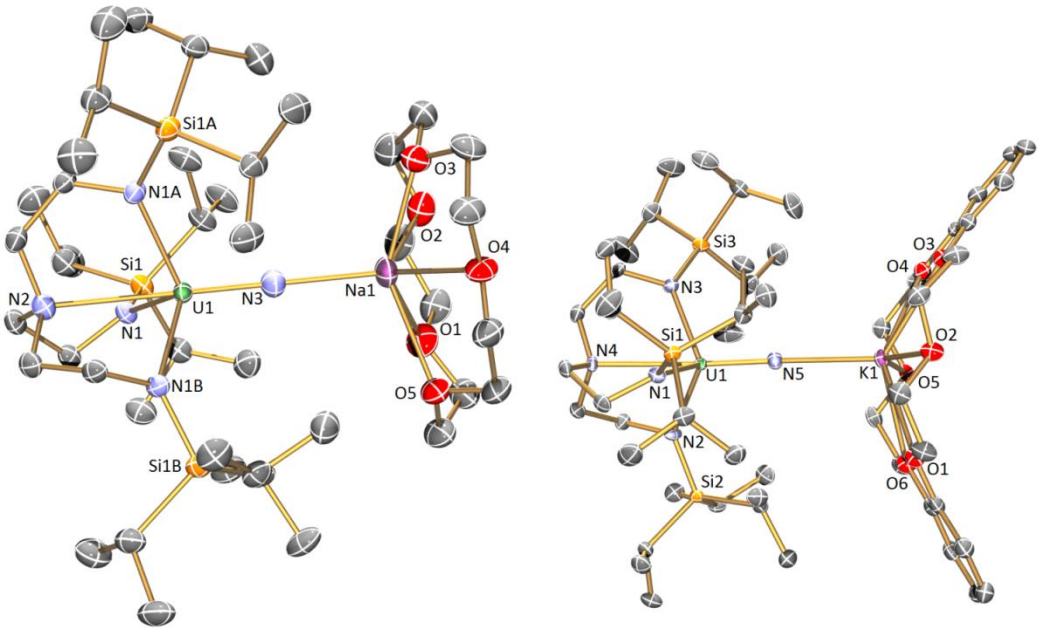


Figure ***2.6.*** *Molecular structures of [U(Tren^{TIPS}){(μ-N)(μ-Na)(15C5)}]•1.5(C_6H_{14}),* ***53****,[10] and [U(Tren^{TIPS}){(μ-N)(μ-K)(Bn$_2$-18C6)}],* ***111****. Thermal ellipsoids set at 40% probability. Hydrogen atoms and lattice solvent are omitted for clarity. Selected distances (Å) and angles (°):* ***53*** *U(1)-N(1) 2.335(3), U(1)-N(2) 2.742(5), U(1)-N(3) 1.810(5), N(3)-Na(1) 2.291(5), Na(1)-O(1) 2.423(10), Na(1)-O(2) 2.348(9), Na(1)-O(3) 2.408(8), Na(1)-O(4) 2.567(11), Na(1)-O(5) 2.617(10), N(2)-U(1)-N(3) 180.0(9), U(1)-N(3)-Na(1) 180.0(4);* ***111*** *U(1)-N(1) 2.369(3), U(1)-N(2) 2.347(3), U(1)-N(3) 2.343(3), U(1)-N(4) 2.712(2), U(1)-N(5) 1.840(3), N(5)-K(1) 2.735(3), K(1)-O(1) 2.958(3), K(1)-O(2) 2.862(3), K(1)-O(3) 2.965(3), K(1)-O(4) 2.915(3), K(1)-O(5) 2.798(2), K(1)-O(6) 2.871(3), N(4)-U(1)-N(5) 175.25(10), U(1)-N(5)-K(1) 162.76(16).*

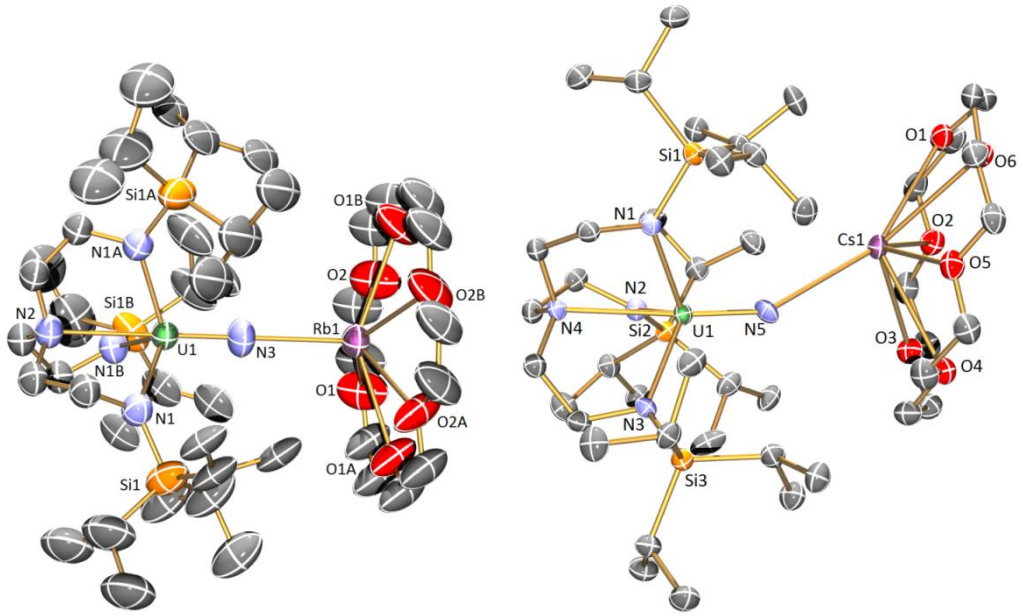


*Figure **2.7.** Molecular structures of [U(Tren^{TIPS}){(μ-N)(μ-Rb)(18C6)}]•(C_6H_{14}), **112** and [U(Tren^{TIPS}){(μ-N)(μ-Cs)(18C6)}], **113**. Thermal ellipsoids set at 40% probability. Hydrogen atoms and lattice solvent are omitted for clarity. Selected distances (Å) and angles (°): **112** U(1)-N(1) 2.352(7), U(1)-N(2) 2.940(15), U(1)-N(3) 1.804(13), N(3)-Rb(1) 2.777(13), Rb(1)-O(1) 2.972(12), Rb(1)-O(2) 2.845(11), N(2)-U(1)-N(3) 180.0(6), U(1)-N(3)-Rb(1) 180.0(10); **113** U(1)-N(1) 2.355(5), U(1)-N(2) 2.346(5), U(1)-N(3) 2.364(5), U(1)-N(4) 2.680(5), U(1)-N(5) 1.803(5), N(5)-Cs(1) 3.099(5), Cs(1)-O(1) 3.177(5), Cs(1)-O(2) 3.285(5), Cs(1)-O(3) 3.109(5), Cs(1)-O(4) 3.171(5), Cs(1)-O(5) 3.047(5), Cs(1)-O(6) 3.204(5), N(4)-U(1)-N(5) 175.3(2), U(1)-N(5)-Cs(1) 148.8(3).*

Complexes **53**, **111**, **112** and **113** adopt monomeric, five-coordinate, distorted trigonal bipyramidal geometries (τ = 0.99 – 1.15)[5,6] about the uranium centre, which is coordinated by Tren^{TIPS} and the nitride ligand. The salient feature is an alkali metal capped nitride fragment, which lies *trans* to the face-capping amine of Tren^{TIPS}. Whilst these ligands occupy the axial positions, and consequently have a near to linear or linear alignment [N_{amine}-U(1)-$N_{nitride}$: 175 – 180°], the angle between U(1)-$N_{nitride}$-M(1) is not consistent across the set. In **53** and **112**, which both crystallised in cubic space groups, this bond angle is defined as linear. Contrastingly, for **111** and **113**, which crystallised in lower symmetry space groups, there is a considerable distortion from linearity [U(1)-$N_{nitride}$-M(1): **111** 162.76(16), **113**

148.8(3)°]. Whether this deviation in linearity is due to crystal packing effects, or alternatively is due to the larger steric bulk of either the dibenzo-18-crown-6 ether or caesium, respectively, is uncertain. Furthermore, and perhaps coincidentally, the linear **53** and **112** both incorporate lattice solvent in the unit cell, which might influence the crystal packing of these compounds.

If polymorphs, or alternatively the analogous {K(18C6)} or {Rb(Bn_2-18C6)] species were crystallised, then this would go some way towards answering this question, but, as yet, attempts to prepare such species have been unsuccessful. Furthermore, the orientation of the metal-crown fragment for **111** and **113** differs. This geometry can be assessed by consideration of the N(1)-U(1)-N(5)-M(1) (M = K, Cs) torsion angles, where for **111**, this is 0.5(5)°, but for **113** it is 65.0(6)°.

*Table **2.3.** Selected bond lengths for **53**, **111**, **112** and **113**.*

Compound	U(1)-$N_{amide(av)}$ (Å)	U(1)-N_{amine} (Å)	U(1)-$N_{nitride}$ (Å)	N(5)-M(1) (Å)
53	2.335(3)	2.742(5)	1.810(5)	2.291(5)
111	2.353(7)	2.712(2)	1.840(3)	2.735(3)
112	2.352(7)	2.940(15)	1.804(13)	2.777(13)
113	2.355(5)	2.680(5)	1.803(5)	3.099(5)

The U(1)-N_{amine} bond distances decrease as the metal capping the nitride increases in size [the distance in **53** is longer than in **113**, 2.742(5) *vs* 2.680(5) Å]. A notable exception to this trend is **112**, which has a much longer U(1)-N_{amine} bond distance of 2.940(15) Å. We reason that this may be an artefact of **112** crystallising in a cubic space group (*P*a-3) and exhibiting heavy disorder. While the U-N_{amine} bond distance in **112** was not restrained, many other parameters within the model were restrained, which is reflected in the sizeable uncertainties in the metrical parameters of **112**. Consequently, this bond distance may not be reliable and may be a reflection of crystal quality rather than being a genuine outlier.

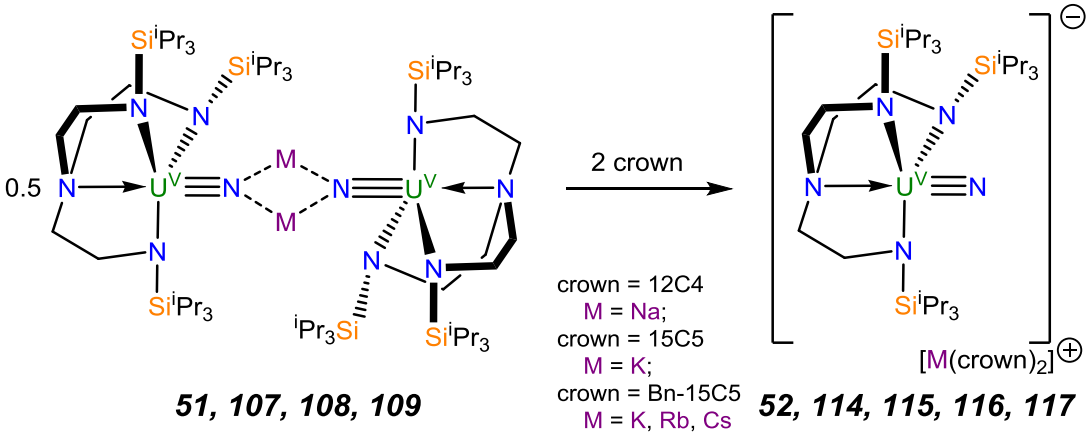
The uranium nitride distances are shorter in the capped species [range: 1.803(5) – 1.840(3) Å] than their dinuclear precursors [range: 1.846(3) – 1.929(6) Å]. The

decrease in bond distance is most noticeable for the potassium analogue: dependent on the polymorph of **111** considered, the decrease in U≡N bond length is either ~0.02 Å (from the flatter polymorph) or ~0.09 Å (from the *trans*-bent polymorph). The U≡N bond shortening is less dramatic for the other congeners (Na, ~0.07, Rb ~0.03, Cs ~0.05 Å). The $N_{nitride}$-M_{group1} distance increases down the group, in line with the increase in the ionic radii of the metal (six coordinate cation sizes: Li 0.76, Na 1.02, K 1.38, Rb 1.48, Cs 1.67 Å)[7] though the increase in bond length is not uniform. This may be attributed to the distortion from linearity of the U(1)-$N_{nitride}$-M(1) motif, as discussed earlier, which lengthens the N-M bond distance beyond that which might be expected, such that the N-K and N-Rb bond distances are statistically invariant. The geometry of the capped species determines whether the nitride-cation interaction lengthens or shortens on coordination of crown. The linear species **53** and **112** decrease in N-M bond length (by ~0.01 – ~0.03 Å), whilst the bent species experience an increase in N-M bond distance (for **113**, by ~0.05 Å, for **111**, this is polymorph dependent: only from the flatter polymorph can a bond lengthening of ~0.02 be distinguished as statistically significant). This series of capped nitrides can be considered as masked nitrides, with similarities to the uranium nitride borane adduct, $[N^nBu_4][U\{N(Ar)^tBu\}_3\{\equiv N\text{-}B(C_6F_5)_3\}]$ (Ar = 3,5-$Me_2C_6H_3$), which exhibits a U-N bond distance of 1.916(4) Å,[11] or the sodium capped uranium nitride $[U(\{\eta^8\text{-}1,4\text{-}(Si^iPr_3)_2C_8H_6\}(\eta^5\text{-}C_5Me_5)\{(\mu\text{-}N)Na(OEt_2)_2\}]$, which exhibits a U-N bond distance of 1.835(5) Å.[12]

The metal-crown oxygen distances [ranges: **53** Na-O 2.348(9) – 2.617(10), **111** K-O 2.734(7) – 2.970(7), **112** Rb-O 2.929(7) – 2.945(10), **113** Cs-O 3.047(5) – 3.285(5) Å] are consistent with the corresponding literature distances [mean distances: Na-O(15C5) 2.465, K-O(18C6) 2.840, Rb-O(18C6) 2.988, Cs-O(18C6) 3.228 Å].[9]

UV-vis-NIR electronic absorption spectra and room temperature solution magnetic measurements for **53**, **111**, **112** and **113** will be discussed in Section 3.5.

2.3.3. *Preparation of [U(Tren^{TIPS})(N)][M(crown)$_2$] (M = Na, K, Rb, Cs)*



*Scheme **2.5.** Syntheses of **52**, **114**, **115**, **116** and **117**.*

As was previously reported for **51**, addition of two equivalent of a crown ether that is slightly smaller than that required to coordinate equatorially around the alkali metal ion results in cleavage of the dinuclear system and the formation of an unsupported, terminal uranium nitride as a separated ion pair complex. In the case of **51**, addition of 12-crown-4 ether afforded **52**, which was the first terminal uranium nitride to be isolated and stable at ambient temperatures.

In attempts to prepare [U(Tren^{TIPS})(N)][M(crown)$_2$] (M = K, Rb, Cs), many different crown ethers were attempted, including benzo-15-crown-5 ether and 15-crown-5 ether. We were able to isolate complexes [U(Tren^{TIPS})(N)][M(Bn-15C5)$_2$] for K, Rb and Cs (**115**, **116** and **117** respectively), as well as [U(Tren^{TIPS})(N)][K(15C5)$_2$] (**114**). This suggests that here, again, it is the size of the crown ether which is most important, with benzo groups only acting to aid (or hinder) the resultant crystallinity of [U(Tren^{TIPS})(N)][M(crown)$_2$].

The addition of crown ethers (or equivalent co-ligands) not listed for the preparation of **53**, **111**, **112** and **113**, or **52**, **114**, **115**, **116** and **117**, resulted in intractable mixtures that could not be crystallised. This is attributed to the mismatching of cation to co-ligand size ratios, which appear to be pivotal in these reactions.

X-ray crystallographic studies on **114**, **115**, **116** and **117** elucidated their structure, expanding the set of terminal, separated ion pair (SIP) nitrides to encompass alkali metals from sodium to caesium. The structures **114**, **115**, **116** and **117** are illustrated

in figures **2.8.** – **2.12.**, alongside selected bond lengths and angles. Though the molecular structure for **52** has been previously described,[1,4] it is included here for completeness, and to aid structural comparisons (*vide infra*).

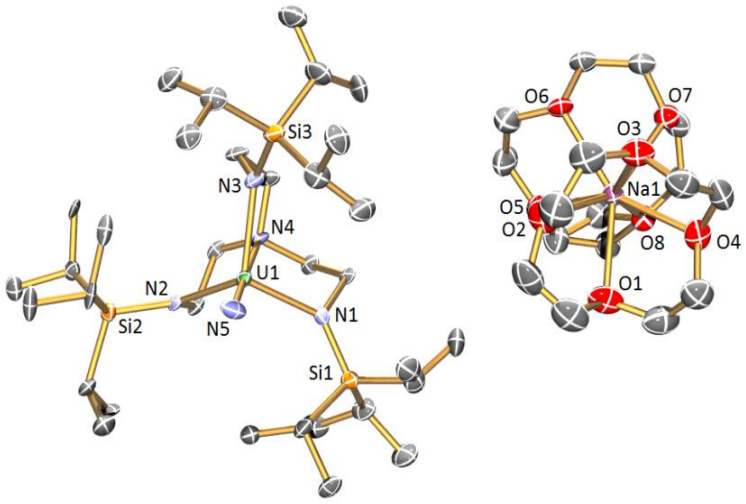


*Figure **2.8.** Molecular structure of [U(Tren^{TIPS})(N)][Na(12C4)$_2$], **52**.[1,4] Thermal ellipsoids set at 40% probability. Hydrogen atoms are omitted for clarity. Selected distances (Å) and angles (°): U(1)-N(1) 2.328(5), U(1)-N(2) 2.365(15), U(1)-N(3) 2.367(14), U(1)-N(4) 2.713(13), U(1)-N(5) 1.825(15), Na(1)-O(1) 2.468(19), Na(1)-O(2) 2.41(2), Na(1)-O(3) 2.445(19), Na(1)-O(4) 2.379(18), Na(1)-O(5) 2.432(16), Na(1)-O(6) 2.431(16), Na(1)-O(7) 2.504(16), Na(1)-O(8) 2.491(16), N(4)-U(1)-N(5) 178.0(7).*

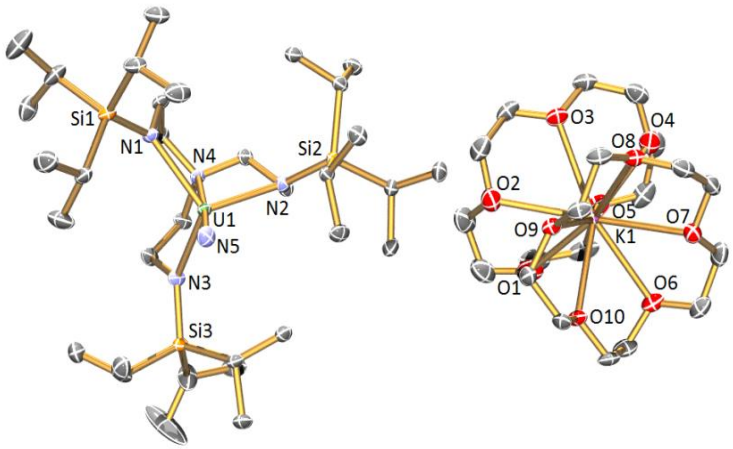


*Figure **2.9.** Molecular structure of [U(Tren^{TIPS})(N)][K(15C5)$_2$], **114**. Thermal ellipsoids set at 40% probability. Hydrogen atoms are omitted for clarity. Selected*

distances (Å) and angles (°): U(1)-N(1) 2.368(3), U(1)-N(2) 2.359(3), U(1)-N(3) 2.361(3), U(1)-N(4) 2.684(3), U(1)-N(5) 1.802(4), K(1)-O(1) 2.896(4), K(1)-O(2) 2.914(4), K(1)-O(3) 2.856(3), K(1)-O(4) 2.842(4), K(1)-O(5) 2.878(4), K(1)-O(6) 2.859(3), K(1)-O(7) 2.973(3), K(1)-O(8) 2.998(3), K(1)-O(9) 2.824(3), K(1)-O(10) 2.860(3), N(4)-U(1)-N(5) 176.12(13).

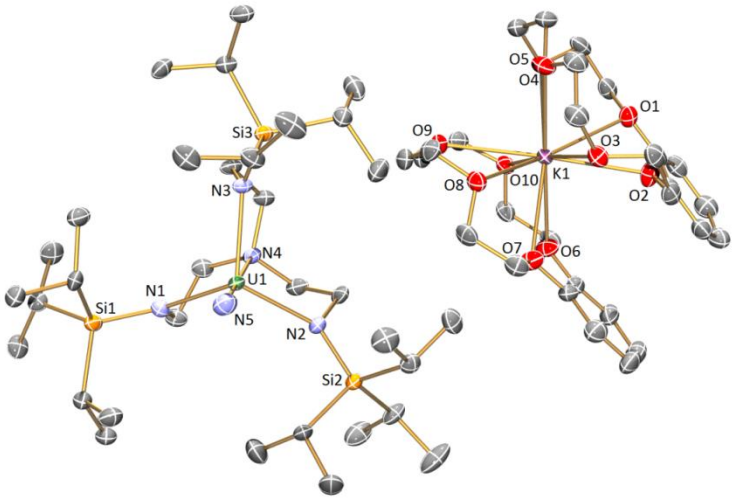


*Figure **2.10.** Molecular structure of [U(Tren^{TIPS})(N)][K(Bn-15C5)$_2$], **115**. Thermal ellipsoids set at 40% probability. Hydrogen atoms are omitted for clarity. Selected distances (Å) and angles (°): U(1)-N(1) 2.362(3), U(1)-N(2) 2.385(3), U(1)-N(3) 2.357(3), U(1)-N(4) 2.683(3), U(1)-N(5) 1.820(3), K(1)-O(1) 2.998(3), K(1)-O(2) 2.771(3), K(1)-O(3) 2.893(3), K(1)-O(4) 2.786(3), K(1)-O(5) 2.798(3), K(1)-O(6) 2.860(3), K(1)-O(7) 2.883(3), K(1)-O(8) 2.792(3), K(1)-O(9) 2.821(3), K(1)-O(10) 2.879(3), N(4)-U(1)-N(5) 178.81(13).*

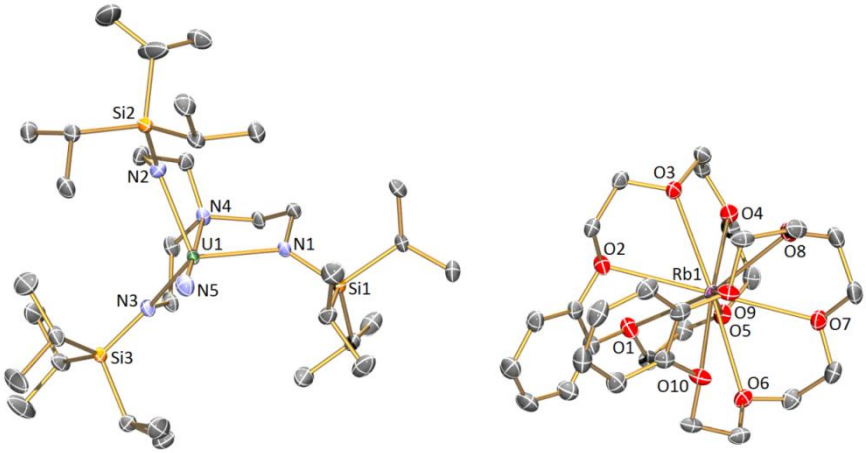


*Figure **2.11.** Molecular structure of [U(Tren^{TIPS})(N)][Rb(Bn-15C5)$_2$], **116**. Thermal ellipsoids set at 40% probability. Hydrogen atoms are omitted for clarity. Selected distances (Å) and angles (°): U(1)-N(1) 2.3722(18), U(1)-N(2) 2.3601(19), U(1)-N(3) 2.3922(19), U(1)-N(4) 2.687(2), U(1)-N(5) 1.810(2), Rb(1)-O(1) 2.990(2), Rb(1)-O(2) 2.9891(18), Rb(1)-O(3) 2.9272(18), Rb(1)-O(4) 2.9168(18), Rb(1)-O(5) 2.8762(19), Rb(1)-O(6) 2.9591(18), Rb(1)-O(7) 2.8936(19), Rb(1)-O(8) 2.8837(18), Rb(1)-O(9) 3.0728(19), Rb(1)-O(10) 2.8979(19), N(4)-U(1)-N(5) 178.93(9).*

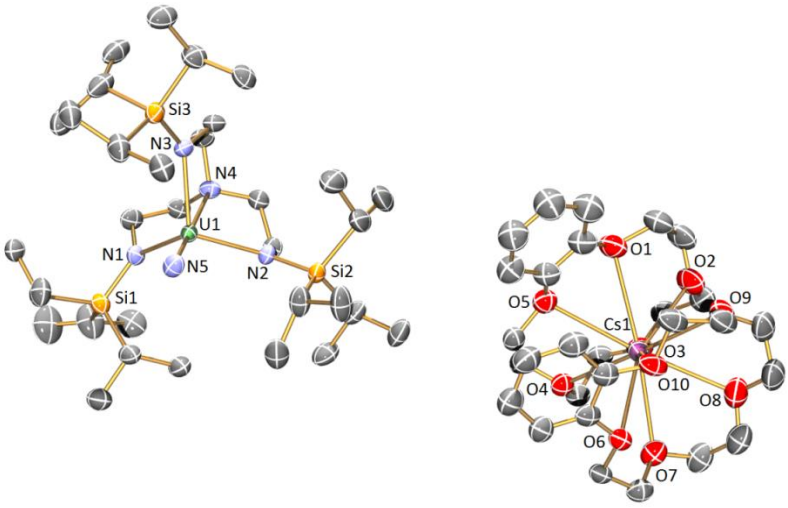


*Figure **2.12.** Molecular structure of [U(Tren^{TIPS})(N)][Cs(Bn-15C5)$_2$], **117**. Thermal ellipsoids set at 40% probability. Hydrogen atoms are omitted for clarity. Selected distances (Å) and angles (°): U(1)-N(1) 2.365(6), U(1)-N(2) 2.368(6), U(1)-N(3) 2.382(6), U(1)-N(4) 2.696(7), U(1)-N(5) 1.801(7), Cs(1)-O(1) 3.173(9), Cs(1)-O(2) 2.991(8), Cs(1)-O(3) 3.094(7), Cs(1)-O(4) 3.008(7), Cs(1)-O(5) 3.134(8),*

Cs(1)-O(6) 3.190(6), Cs(1)-O(7) 3.040(8), Cs(1)-O(8) 3.026(9), Cs(1)-O(9) 3.047(8), Cs(1)-O(10) 3.062(7), N(4)-U(1)-N(5) 178.3(3).

The molecular structures of **114**, **115**, **116** and **117** reveal analogues of **52**, which have crystallised as separated ion pair complexes, with five-coordinate distorted trigonal bipyramidal geometry at uranium (τ = 1.04 – 1.13).[5,6] The anionic fragments ([U(Tren^{TIPS})(N)]$^-$) of all the analogues (**52**, **114**, **115**, **116** and **117)** are isostructural, ligated by Tren^{TIPS} and the nitride ligand, where the nitride and face-capping amine are in the axial positions. All respective U-N distances [U-N_{amide} range 2.344(15) – 2.3748(19) Å, U-N_{amine} range 2.683(3) –2.713(13) Å, U-$N_{nitride}$ range 1.801(7) – 1.825(15) Å] are statistically indistinguishable (see table **2.4.**). The U(1)-N_{amide} average distances [range: 2.344(15) – 2.372(7) Å] are broadly similar to both the dinuclear and capped analogues [ranges: 2.320(4) – 2.339(5) and 2.335(3) – 2.355(5) Å respectively], despite the loss of an alkali metal coordinated to the nitride ligand. The U(1)-N_{amine} distances [range: 2.683(3) – 2.713(13) Å] have undergone a modest increase in bond length upon encapsulation of the alkali metal cation, of ~0.04 Å, [range for **52**, **107**, **108** and **109**, 2.635(3) – 2.669(3) Å] and reflects a corresponding change in the geometry at uranium, where in the terminal species the uranium atom sits slightly more out of the plane of the three amide atoms [U(1)-N_{amide} plane distances: **51** 0.791, **52** 0.824; **107** 0.788, **114** 0.831, **115** 0.839; **108** 0.800, **116** 0.839; **109** 0.801, **117** 0.840 Å]. The U(1)-$N_{nitride}$ distances [range: 1.801(7) – 1.820(3) Å] have also contracted with respect to the dinuclear species range: 1.846(3) – 1.929(6) Å], and are comparable to the equivalent distances in the capped analogues. The N_{amine}-U(1)-$N_{nitride}$ angles are near linear, and range from 176.12(13) to 178.93(9)°.

These bond distances can also be compared to the neutral complex [U(Tren^{TIPS})(N)] (**54**), [U(1)-$N_{amide(av)}$ 2.271(8), U(1)-N_{amine} 2.465(5), U(1)-$N_{nitride}$ 1.799(7), table **2.4.**]. The loss of the valence electron impacts upon the U(1)-N_{amide} and U(1)-N_{amine} distances, which contract by ~0.01 Å and ~0.22 Å respectively [from U(1)-N_{amide} 2.344(15) – 2.3748(19) and U(1)-N_{amine} 2.683(3) – 2.713(13) Å for **52**, **114**, **115**, **116** and **117**]). This is due to the smaller size of the uranium(VI) ion in comparison with the uranium(V) ion.[7] That the U(1)-N_{amine} distance is so much shorter in **54** is hypothesised to result from the inverse-*trans*-influence.[10] By contrast, the U≡N

distance in **52**, **114**, **115**, **116** and **117** does not undergo a reduction in bond length upon oxidation to **54**, with **52**, **114**, **115**, **116** and **117** and **54** having statistically invariant U(1)-$N_{nitride}$ bond lengths. This is believed to be due to the removal of a non-bonding 5f electron on oxidation to U^{VI}.

*Table **2.4.** Selected bond lengths for **52**, **114**, **115**, **116, 117** and **54**.*

Compound	U(1)-$N_{amide(av)}$ (Å)	U(1)-N_{amine} (Å)	U(1)-$N_{nitride}$ (Å)
52	2.344(15)	2.713(13)	1.825(15)
114	2.362(3)	2.684(3)	1.802(4)
115	2.368(3)	2.683(3)	1.820(3)
116	2.3748(19)	2.687(3)	1.810(3)
117	2.372(6)	2.696(7)	1.801(7)
54[10]	2.271(8)	2.465(5)	1.799(7)

The metal-crown oxygen distances in **52** and **114**, **115**, **116** and **117** [ranges: **52** Na-O 2.379(18) – 2.504(16), **114** and **115** K-O 2.771(3) – 2.998(3), **116** Rb-O 2.876(2) – 3.073(3), **117** Cs-O 2.991(8) – 3.189(6) Å] are consistent with the corresponding literature distances for crown-alkali metal interactions [mean distances: Na-O(12C4) 2.480, K-O(15C5) 2.908, Rb-O(15C5) 2.992, Cs-O(15C5) 3.167 Å].[9]

As was the case for **51**, **106** and **109**, unambiguous assignment of the ^{1}H NMR spectra can be problematic due to their broad paramagnetic nature resulting from the U^V $5f^1$ centre. The ^{1}H NMR spectrum previously reported for **52** spanned the range +12 to –6 ppm.[1] This narrow range is in contrast to that observed for **114** (+39 to –6 ppm), **115** (+39 to –6 ppm), **116** (+39 to –6 ppm) and **117** (+38 to –6 ppm) in this study. Due to this inconsistency in data, we repeated ^{1}H NMR spectroscopic studies on a freshly prepared sample of **52**, and we believe the correct assignment for this complex to be [δ 36.64 (s, 6H, CH_2), 12.29 (s, 6H, CH_2), 9.72 (s, 16H, OC$H_{2)}$, 3.82 (s, 16H, OCH_2), −5.18 (s, 9H, CH(CH_3)$_2$), −5.72 (s, 54H, CH(CH_3)$_2$)], which brings this analysis in line with the heavier alkali metal analogues.

The FTIR spectra for **52**, **114** and **115** feature a stretch at ~936 cm^{-1}, which is assigned to the U≡N stretch. The corresponding ^{15}N labelled spectra incorporate a stretch at 900 cm^{-1}, and see a reduction by ~50 % for the original bands' intensity. These data compare well to a calculated isotopomer shift to 906 cm^{-1} from reduced mass considerations for both compounds.[13] Contrastingly, overlapping band structures for the crown moieties for both **116** and **117** prevent the analogous comparisons being made with certainty.

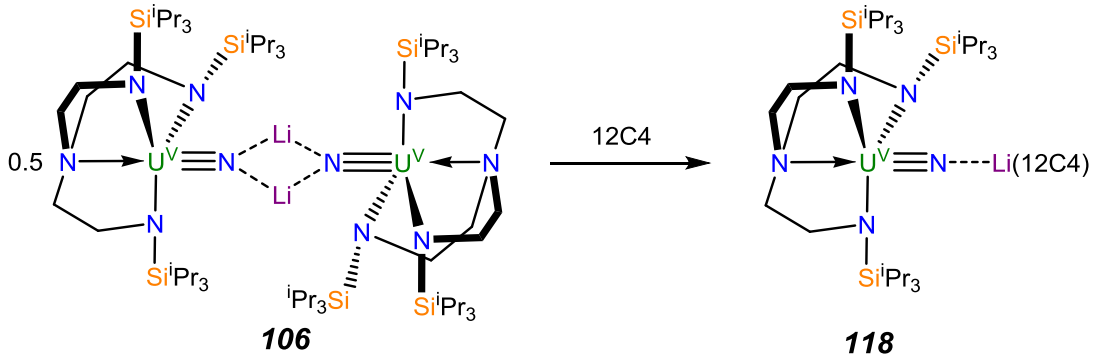
UV-vis-NIR electronic absorption spectra and room temperature solution magnetic measurements for **52**, **114**, **115**, **116** and **117** will be discussed in Section 3.5.

Here, a pragmatic point towards the synthesis of [{U(Tren^{TIPS})(μ-M)(μ-N)}$_2$] (**51**, **106**, **107**, **108** and **109**) can be made. The preparation of **107** by the reduction of **13** is higher yielding than for **51**, **106**, **108** and **109**, although graphite is a by-product. We discovered that the addition of crown ethers (15C5 or Bn-15C5) to the crude mixture allowed for the extraction of **114** or **115** from graphite *via* dissolution in toluene, thus the elimination of graphite in the preparation of **107** is not a hindrance to the yield of **114** or **115**.

2.3.4. Reactivity studies of [{U(Tren^{TIPS}){(μ-N)(μ-Li)}$_2$] towards donor ligands

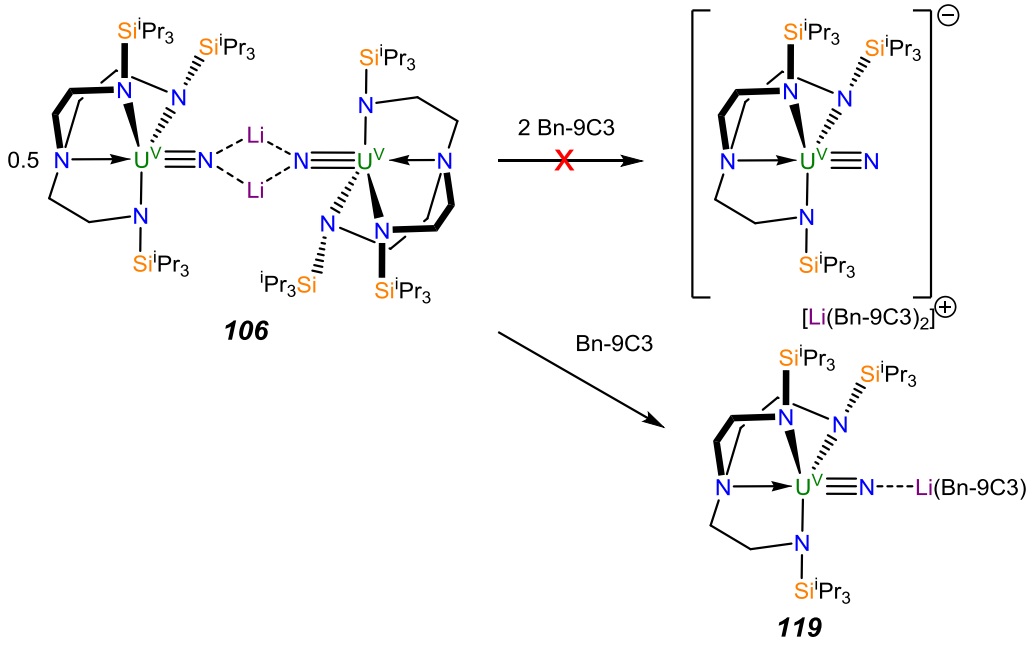
The reactions of **106** with a with range of donor ligands in toluene were attempted towards the targeted complexes [U(Tren^{TIPS}){(μ-N)(μ-Li)(crown)}] and [U(Tren^{TIPS})(N)][Li(crown)$_2$]. However we were only ever able to isolate complexes of the type [U(Tren^{TIPS}){(μ-N)(μ-Li)(L)$_n$}] (where L is a donor ligand). The reactions of **106** towards a wide range of donor ligands in toluene were attempted, including 12-crown-4 ether (12C4), benzo-9-crown-3 ether (Bn-9C3), 9-ane-S3 ($C_6H_{12}S_3$), tetraglyme [$Me(OCH_2CH_2)_4OMe$], hexamethylphosphoramide [HMPA, $OP(NMe_2)_3$], tetramethyl ethylene diamine [TMEDA, $Me_2NCH_2CH_2NMe_2$], pentamethylene diethylene triamine [PMDETA, $MeN(CH_2CH_2NMe_2)_2$], DME (dimethoxyethane) and pyridine. Following work-up, red single crystals suitable for XRD study were isolated from reactions with 12C4, Bn-9C3, tetraglyme and pyridine (**118**, **119**, **120** and **121** respectively). All other reagents gave

non-crystalline, intractable mixtures of products, so the product of these reactions is not known.



*Scheme **2.6.** Synthesis of **118**.*

The reaction of **106** towards 12C4 was investigated. It was anticipated that 12C4 would be of an appropriate size to cap the lithium ion, since lithium is smaller than sodium, therefore would not be encapsulated by two crown moieties [eight coordinate radii: Li 0.92(8), Na 1.32(8) Å].[7] Following work-up, red crystals were isolated from the reaction mixture. A single crystal XRD diffraction study was performed. The molecular structure is illustrated in figure **2.13.**, left, alongside selected bond lengths and angles.



*Scheme **2.7.** Synthesis of **119**.*

By analogy to the other group 1 metal species discussed so far, utilising a smaller crown was envisaged to enact the abstraction of the lithium cation of **106**, resulting in "[U(Tren^{TIPS})(N)][Li(Bn-9C3)$_2$]". To this end, two equivalents of benzo-9-crown-3 ether (Bn-9C3) were added to **106** in toluene. Following work-up, red crystals were obtained from a concentrated pentane solution, and these were subjected to a single crystal XRD study. The molecular structure, alongside selected bond lengths and angles, is illustrated in figure **2.13.**, right.

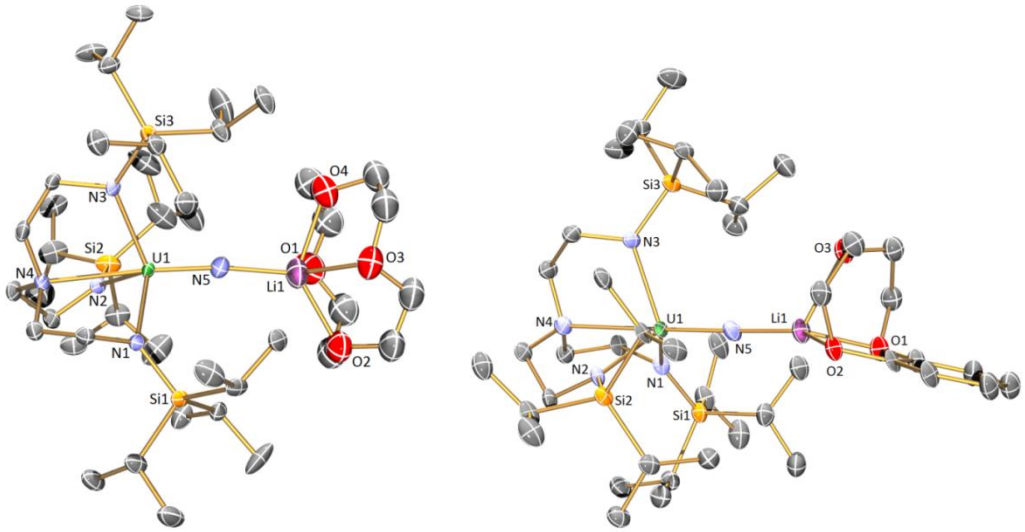


*Figure **2.13.** Molecular structures of [U(Tren^{TIPS}){(μ-N)(μ-Li)(12C4)}], **118**, left and [U(Tren^{TIPS}){(μ-N)(μ-Li)(Bn-9C3)}], **119**, right. Thermal ellipsoids set at 40% probability. Hydrogen atoms are omitted for clarity. Selected distances (Å) and angles (°): **118** U(1)-N(1) 2.341(6), U(1)-N(2) 2.364(5), U(1)-N(3) 2.346(5), U(1)-N(4) 2.665(5), U(1)-N(5) 1.815(6), N(5)-Li(1) 1.961(16), Li(1)-O(1) 2.162(12), Li(1)-O(2) 2.149(12), Li(1)-O(3) 2.138(12), Li(1)-O(4) 2.132(12), N(4)-U(1)-N(5) 175.8(2), U(1)-N(5)-Li(1) 172.1(5). **119** U(1)-N(1) 2.347(12), U(1)-N(2) 2.340(12), U(1)-N(3) 2.336(13), U(1)-N(4) 2.644(14), U(1)-N(5) 1.896(14), N(5)-Li(1) 1.85(3), Li(1)-O(1) 2.01(3), Li(1)-O(2) 1.99(3), Li(1)-O(3) 2.19(3), N(4)-U(1)-N(5) 178.5(6), U(1)-N(5)-Li(1) 175.0(14).*

The molecular structure of **118** (figure **2.13.**, left) reveals the complex to be the anticipated capped lithium nitride complex, [U(Tren^{TIPS}){(μ-N)(μ-Li)(12C4)}]. The solid state structure of **119** (figure **2.13.**, right) was revealed not to be the targeted "[U(Tren^{TIPS})(N)][Li(Bn-9C3)$_2$]", but instead the lithium cation remained bound to

the uranium nitride, resulting in a lithium capped nitride structure [U(Tren^{TIPS}){(μ-N)(μ-Li)(Bn-9C3)}], **119**, which is analogous to **118**. The metrical data of both **118** and **119** will be discussed shortly (*vide infra*).

Due to the failure to abstract the lithium cation from the uranium nitride ligand by use of crown ethers, we expanded our selection of donor ligands to encompass reactions with various other co-ligands in an attempt to prepare "[U(Tren^{TIPS})(N)][Li(L)$_n$}]". The addition of one equivalent of tetraglyme, or six equivalents of pyridine, based on the metal, to **106** in toluene afforded, following work-up and storage of concentrated hexanes solutions, red crystals suitable for single crystal X-ray diffraction studies. The molecular structures are illustrated in figure **2.14.**, alongside selected bond lengths and angles for **121**.

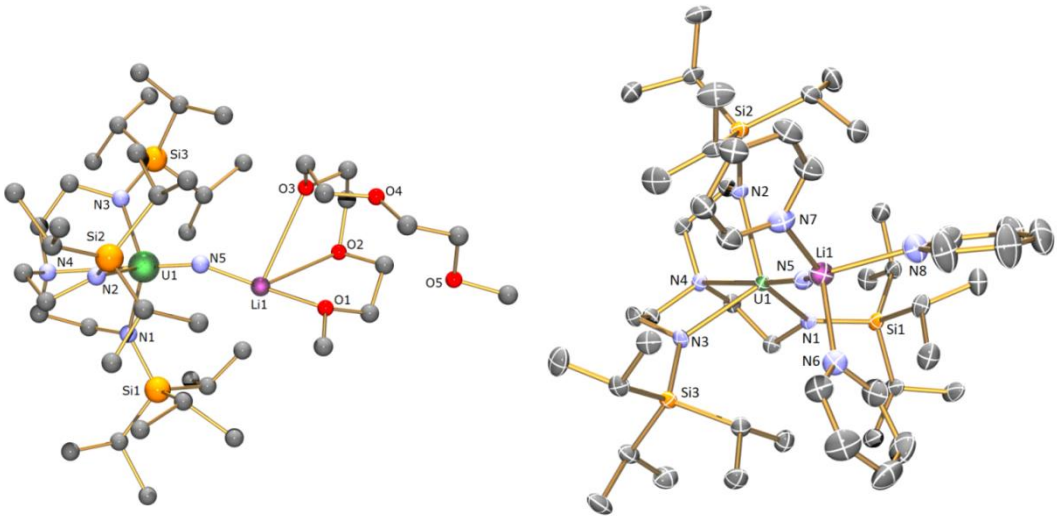


Figure ***2.14.*** *Molecular structures of [U(Tren^{TIPS}){(μ-N)(μ-Li)(η^3-tetraglyme)}]•(C_6H_6),* ***120****, left, and [U(Tren^{TIPS}){(μ-N)(μ-Li)(Py)$_3$}],* ***121****, right . Thermal ellipsoids for* ***121*** *set at 40% probability. Hydrogen atoms and lattice solvent are omitted for clarity. Selected distances (Å) and angles (°) for* ***121****: U(1)-N(1) 2.336(3), U(1)-N(2) 2.350(3), U(1)-N(3) 2.349(3), U(1)-N(4) 2.709(3), U(1)-N(5) 1.869(3), N(5)-Li(1) 1.983(8), Li(1)-N(6) 2.144(9), Li(1)-N(7) 2.127(9), Li(1)-N(8) 2.164(9), N(4)-U(1)-N(5) 175.14(14), U(1)-N(5)-Li(1) 159.3(3).*

Unfortunately, despite repeated attempts, a better X-ray data set could not be obtained for **120** (R_{int} 23.9%). This precludes assessment of metrical parameters for

120, (which are not discussed here), however the connectivity is clear cut. The complex has formed a capped nitride, not a SIP, which is the most pertinent thing to note from this reactivity. We can infer from the geometry of the tetraglyme ligand that it may be bound in an η^3 fashion, with the remaining ethereal oxygens not interacting with the lithium ion.

The molecular structure of **121** revealed a capped lithium nitride, [U(Tren^{TIPS}){(μ-N)(μ-Li)(py)$_3$}], **121**, in contrast to [U(Tren^{TIPS})(N)][Li(py)$_6$], which was a potential product for this reaction. All three compounds (**118**, **119** and **121**), for which reliable data are available, feature a distorted trigonal bipyramidal geometry at uranium (τ = 1.00 – 1.05),[5,6] in close agreement with **53**, **111**, **112** and **113**. The uranium centres are five-coordinate, with the face-capping amine of Tren^{TIPS} and the donor ligand capped nitride moiety in the axial positions.

The average U(1)-N$_{amide}$ distances [range: 2.341(13) – 2.350(6) Å] are statistically indistinguishable from each other, and as for the larger cations, these distances have increased when compared to **106** [2.285(3), 2.312(6) Å], which is accompanied by a change in geometry wherein the uranium atom sits further out of the plane formed by the three amide atoms [**106** 0.780, **118** 0.813, **119** 0.814, **121** 0.839 Å]. The length of the U(1)-N$_{nitride}$ and N$_{nitride}$-Li(1) bonds seems dependent upon the coordination at the lithium. Complexes **119** and **121**, which are coordinated by three donor atoms have longer uranium nitride distances [1.896(14) and 1.869(3) Å] than the corresponding distance in **118**, [1.815(6) Å] which is ligated by the tetradentate 12-crown-4 ether. In contrast, the length of the nitride lithium interaction appears to depend on the steric bulk of the co-ligands (where the longest N-Li bond correlates more steric congestion at lithium i.e. **121** > **118** > **119**).

*Table **2.5.** Selected bond lengths for [U(Tren^{TIPS}){(μ-N)(μ-Li)(co-ligand)}].*

Compound	U(1)-N$_{amide(av)}$ (Å)	U(1)-N$_{amine}$ (Å)	U(1)-N$_{nitride}$ (Å)	N(5)-M(1) (Å)
118	2.350(6)	2.665(5)	1.815(6)	1.961(16)
119	2.341(13)	2.644(14)	1.896(14)	1.85(3)
121	2.345(3)	2.709(3)	1.869(3)	1.983(8)

The lithium–crown oxygen distances [ranges: **118** 2.131(12) – 2.160(12), **119** 1.99(3) – 2.19(3) Å] are consistent with the corresponding literature distances [mean distances: Li-O(12C4) 2.314 Å; there are no crystallographically characterised examples of Bn-9C3 coordinated to lithium in the literature].[9] The lithium–pyridine nitrogen distances [**121** 2.127(9) – 2.164(9) Å] are also consistent with the corresponding literature distances [mean Li-N$(py)_3$ 2.120 Å].

Though more polar solvents, such as THF, might be the ideal reagents for preparing "[U($Tren^{TIPS}$)(N)][$Li(L)_n$]", as they might be anticipated to be better able to liberate the lithium cation from the nitride in **106**, it was not possible to investigate these reactions as the addition of polar solvents results in decomposition of **106**. As a result, we were unable to find a suitable co-ligand that would permit the encapsulation of the lithium cation to afford the target product "[U($Tren^{TIPS}$)(N)][$Li(L)_n$]", so a separated ion pair nitride with a lithium counter ion remains an elusive synthetic target.

We believe this to be due to the hard nature of both the lithium cation and the nitride ligand, therefore precluding the successful isolation of the desired complex. This suggests that Tren–uranium nitrides may be nucleophilic in nature, as they favour coordination by the very hard electropositive lithium cations. This hypothesis will be discussed in more detail in future chapters following reactivity studies to investigate the nature of the uranium nitride bond (see Chapter 5).

The ^{1}H NMR spectra for **118**, **119**, **120** and **121** span the ranges **118** +39 to –7 ppm, **119** +34 to –5 ppm, **121** +41 to –8 ppm, and **120** +38 to –24 ppm, which represents a small shift from **106**, are consistent with the proposed formulations. In contrast to the **53**, **111**, **112**, **113**, **118**, **119** and **121**, our current interpretation of the spectrum of **120** features resonances for the co-ligand spanning +32 to –24 ppm. We argue that this may be due the differing coordination environment (asymmetric co-ligand coordination, with an unbound pendant ether chain), which has had an unexpectedly large impact upon the ^{1}H NMR spectrum. Furthermore, analysis of the ^{1}H NMR spectrum for **119** reveals that whilst this species is the major product, there are several other uranium containing by-products also present. Those identifiable by comparison to reported spectroscopic data include [U($Tren^{TIPS}$)(N)][10] (**54**) and

[U(Tren^{TIPS})(O)][14] (**122**), which may arise from reactions with by-products present from the synthesis of benzo-9-crown-3 ether. Consequently, as **119** was only isolated in poor yield (18%), all analysis based on this sample will have to be considered as a mixed component sample.

FTIR spectra were collected for **118**, **119**, **120** and **121** as Nujol mulls. As was observed for **111**, **112** and **113**, absorptions corresponding to the lithium capped nitride stretch were not observed at ~850 cm^{-1}. The absence of these absorptions is attributed to overlapping absorptions from the co-ligands present. UV-vis-NIR electronic absorption spectra and room temperature solution magnetic measurements for **118**, **119**, **120** and **121** will be discussed in Section 3.5.

Though full data could not be collected for **119**, we are certain that by analogy to the data that could be collected for **118**, **120** and **121**, that all four compounds are capped uranium nitrides, and that unfortunately we have been unable to prepare "[U(Tren^{TIPS})(N)][Li(L)$_n$]".

2.3.5. Solution phase electronic data for 52, 53, 111 – 121

Electronic absorption spectroscopy can be a useful tool in identifying uranium(V) species. This is because studying the U^{V} 5f^{1} electronic ground state is possible by observing the *f-f* transitions, which occur in the near-IR region. The study of 5f^{1} U^{V} is simplified by having only one valence electron, in contrast to multi-electron U^{IV} (5f^{2}) and U^{III} (5f^{3}) centres which therefore require us to consider electron-electron repulsion. The ^{2}F orbital manifold for uranium(V) is first split by spin-orbit coupling into two *J* multiplets, the ground state $^{2}F_{5/2}$ and excited $^{2}F_{7/2}$ state terms. These are then further split by the C_{3v} ligand crystal field into (2*J* + 1)/2 doubly degenerate levels. $^{2}F_{5/2}$ splits into two μ = 1/2 ($^{2}\Gamma_4$) and one μ = 3/2 ($^{1}\Gamma_5$ + $^{1}\Gamma_6$) Kramers doublet; $^{2}F_{7/2}$ splits into three μ = 1/2 ($^{2}\Gamma_4$) and one μ = 3/2 ($^{1}\Gamma_5$ + $^{1}\Gamma_6$) Kramers doublet, where μ is the crystal quantum number. These levels are illustrated in figure **2.15.** Transitions less than 5000 cm^{-1} are often obscured by solvent overtones in UV-vis-NIR spectroscopy, and therefore we would expect to see four optical transitions arising from *f-f* transitions in uranium(V). Experimentally, more bands may be observed, and this is due to either vibronic transitions or as a result of a

lowering of symmetry within the molecule, which would split doubly degenerate states. In other symmetries, absorptions at higher energies may not be observable due to overlap of metal-ligand charge transfer (CT) or Laporte allowed *f-d* transitions ($\varepsilon > 10^3$ $M^{-1}cm^{-1}$), which tail in from the visible region.

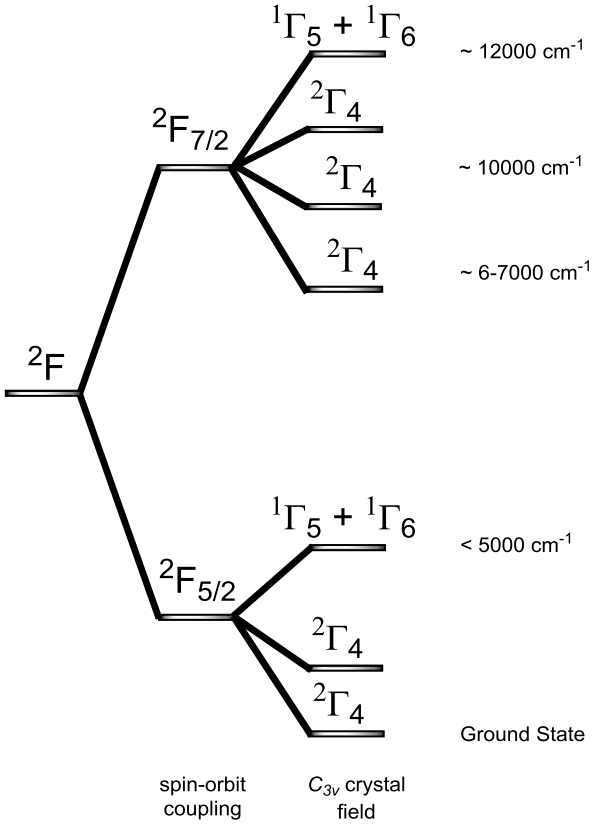


*Figure **2.15.** Schematic energy level diagram (not to scale) for the U^{5+} ion, showing the effect of spin-orbit and crystal field splitting upon the ^2F electronic ground state in C_{3v} symmetry.*

Solutions of complexes **53**, **111**, **112** and **113**; **52**, **114**, **115**, **116** and **117**; and **118**, **119**, **120** and **121** were analysed by UV-vis-NIR electronic absorption spectroscopy, and these spectra are illustrated in figures **2.16**, **2.17** and **2.18** respectively.

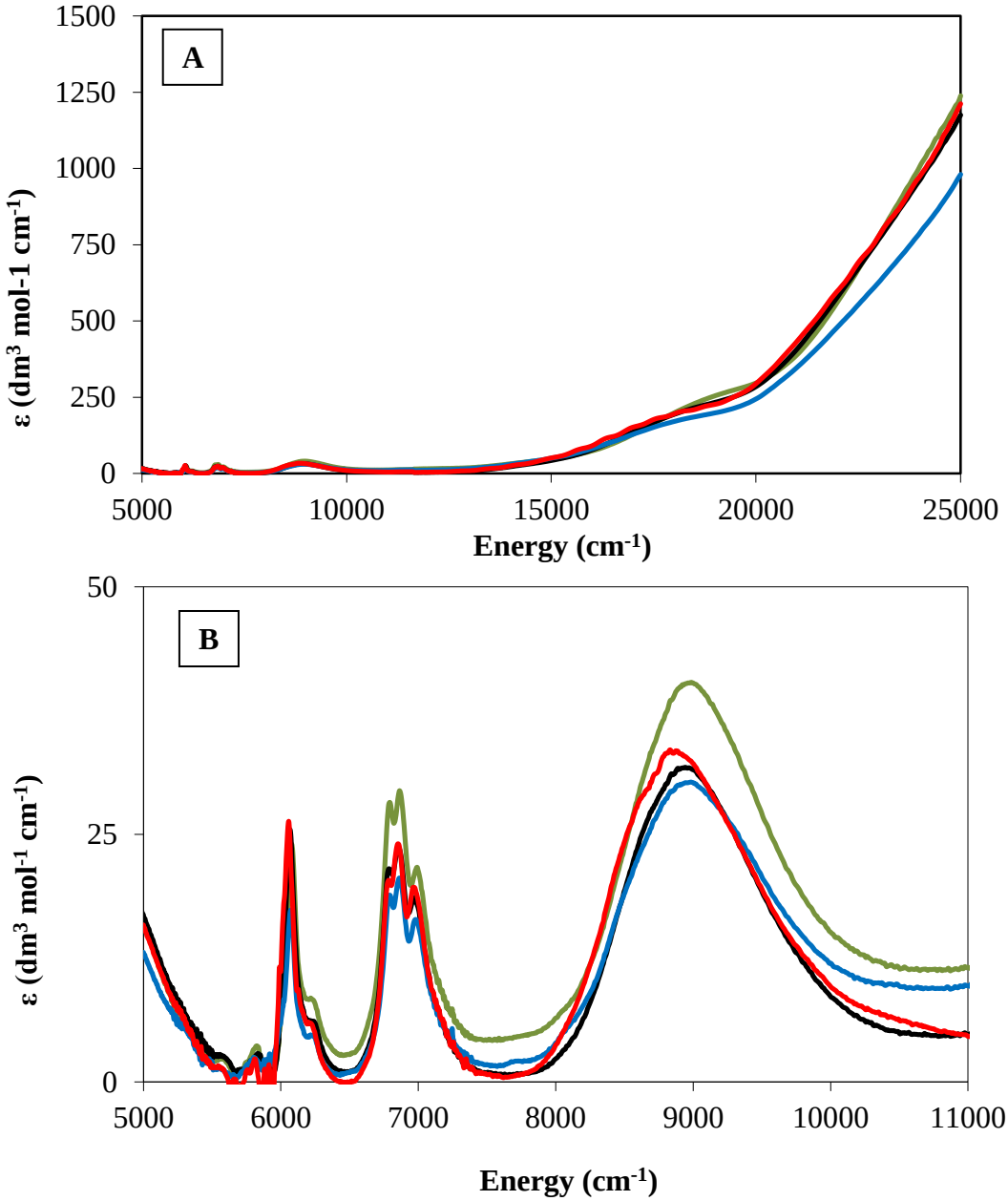


*Figure **2.16.** **A**: UV-vis-NIR electronic absorption spectra of **53** (green), **111** (black), **112** (blue), and **113** (red); **B**: zoom region.*

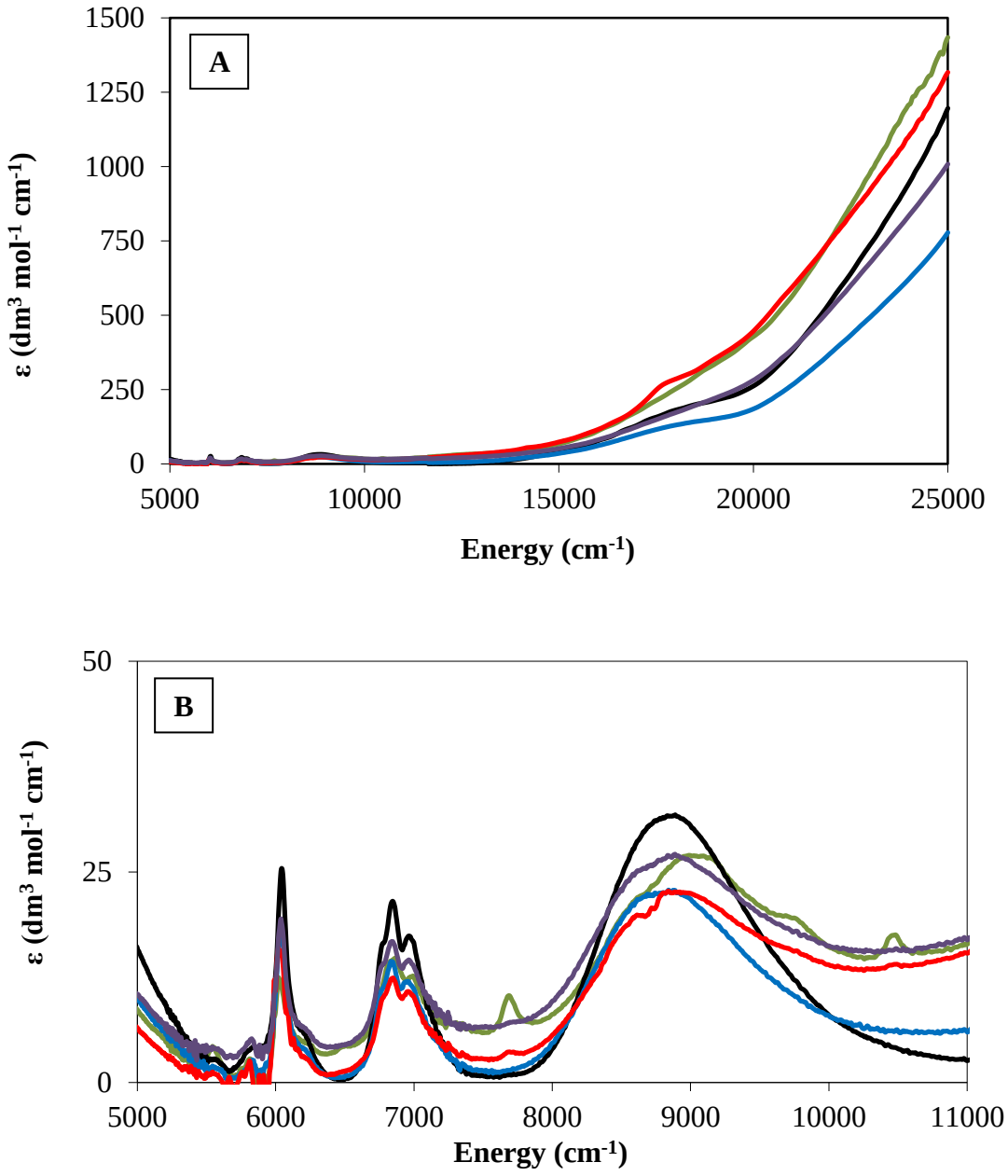


*Figure **2.17.** **A**: UV-vis-NIR electronic absorption spectra of **52** (green), **114** (black), **115** (purple), **116** (blue) and **117** (red); **B**: zoom region.*

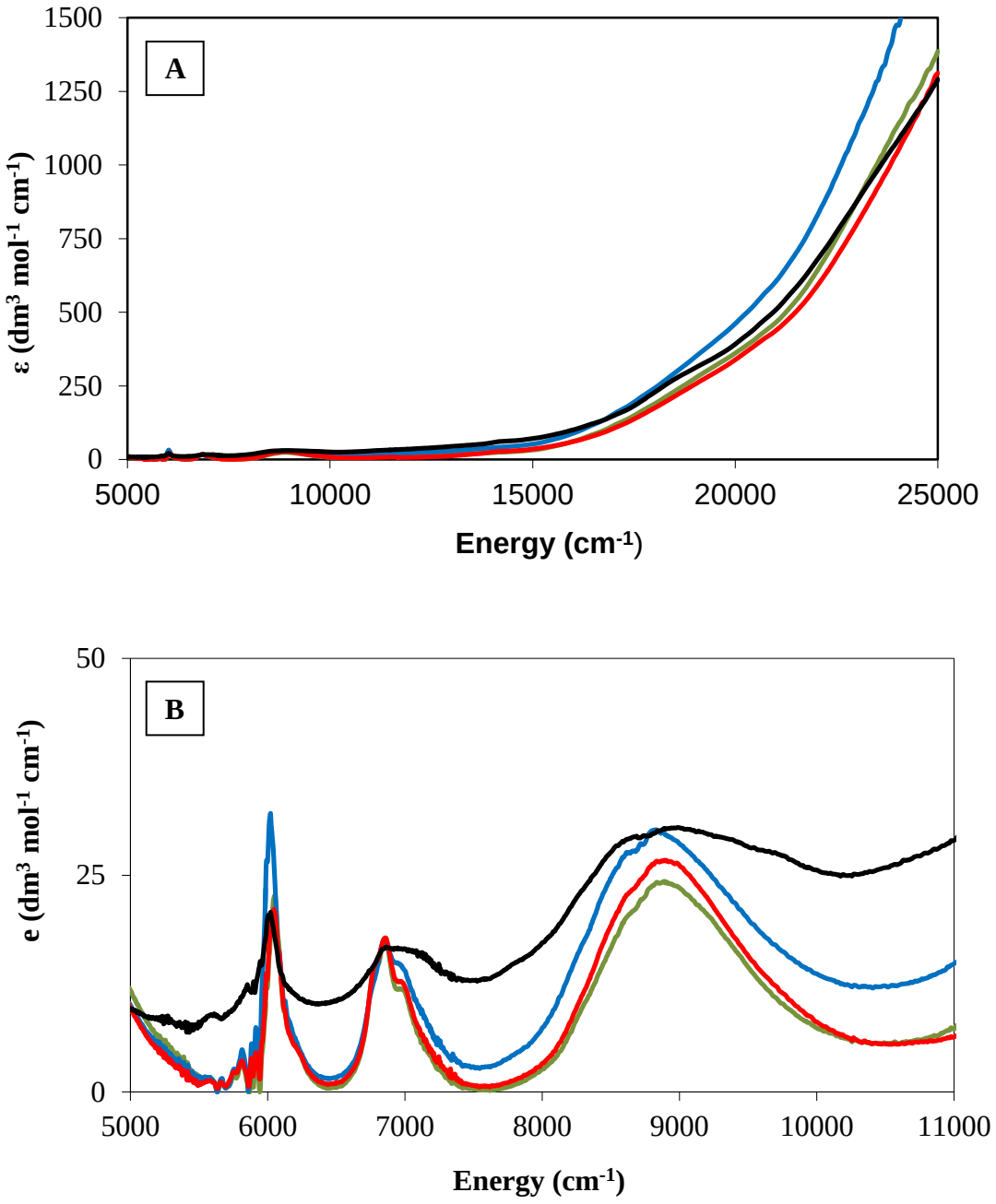


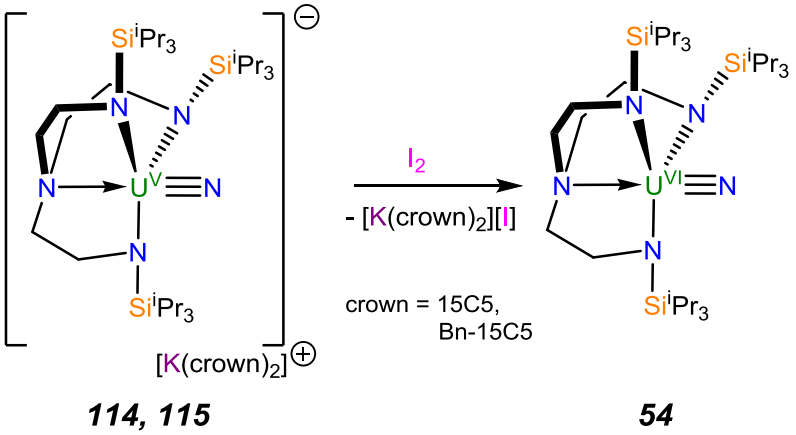
Figure ***2.18.*** ***A****: UV-vis-NIR electronic absorption spectra of* ***118*** *(green),* ***119*** *(black),* ***121*** *(blue)* ***120*** *(red);* ***B****: zoom region.*

The spectra for **53**, **111**, **112** and **113**; **52, 114**, **115**, **116** and **117**; and **118**, **119**, **120** and **121** were recorded as 25 mM solutions in toluene, and all are dominated by charge transfer (CT) bands which tail in from the ultraviolet region (down to ~13000 cm^{-1}, figures **2.16.a**, **2.17.a** and **2.18.a** respectively). Figures **2.16.b**, **2.17.b** and **2.18.b** illustrate the region of interest for uranium(V) electronic absorption spectra (5000 – 11000 cm^{-1}), featuring *f-f* transitions, as described above.[15] Inspection of the spectrum reveals well resolved absorptions which correspond to the transitions predicted by three μ = 1/2 ($^2\Gamma_4$) and one μ = 3/2 ($^1\Gamma_5$ + $^1\Gamma_6$) Kramers doublets which originate from $^2F_{7/2}$, with absorptions ranging from ε = 15 to 40 $M^{-1}cm^{-1}$.

All spectra obtained for **53**, **111**, **112** and **113**; **52, 114**, **115**, **116** and **117**; and **118**, **119**, **120** and **121** as similar, suggesting that neither alkali metal nor the coordination environment of that cation has an effect on the UV-vis properties of the uranium centre under these conditions. That being said, there are some additional features in the spectra for **52** and **117** at ~7700 and ~10500 cm^{-1}, which may result from vibronic coupling. Finally, the spectrum for **119** appears significantly broader than spectra for **118**, **119** and **121**. We attribute this to the presence of other compounds in the sample, as identified by ^{1}H NMR (see Section 3.4.), including **122** and **54**, as well as other, unknown, uranium containing compounds which may have had an adverse effect on the sharpness of the spectrum.

Evans' method[16] room temperature solution magnetic moments were determined for all complexes of the types [U($Tren^{TIPS}$){μ-N)(μ-M)(crown)}] (**53, 111, 112, 113**, **118**, **120** and **121**) and [U($Tren^{TIPS}$)(N)][M$(crown)_2$] (**52**, **114**, **115**, **116** and **117**) in benzene. The data are as follows: μ_{eff} = **53** 2.34, **111** 2.72, **112** 1.89, **113** 2.20, **118** 2.04, **120** 2.39, **121** 2.52, **52** 1.99, **114** 1.58, **115** 1.93, **116** 2.46, and **117** 2.09 μ_B. These values are near to, or somewhat lower than (for **52** and **114**, **115**, **116** and **117**) to the theoretical value of 2.54 μ_B for a uranium(V) $^2F_{5/2}$ ground state, and they are in agreement with experimentally derived values reported for uranium(V) complexes (1.4 – 3.2 μ_B).[17] No solution magnetic data are reported for **119** due to the presence of paramagnetic contaminants. Further discussion of these data, alongside variable temperature SQUID magnetometry and EPR studies for **106**, **51**, **107**, **108** and **109**; **118**, **53**, **111**, **112** and **113**; and **52**, **114**, **116** and **117**, will be made in Chapter 4.

2.4. Preparation of [U(Tren^{TIPS})(N)] (54)



114, 115 ***54***

*Scheme **2.8.** Synthesis of **54**.*

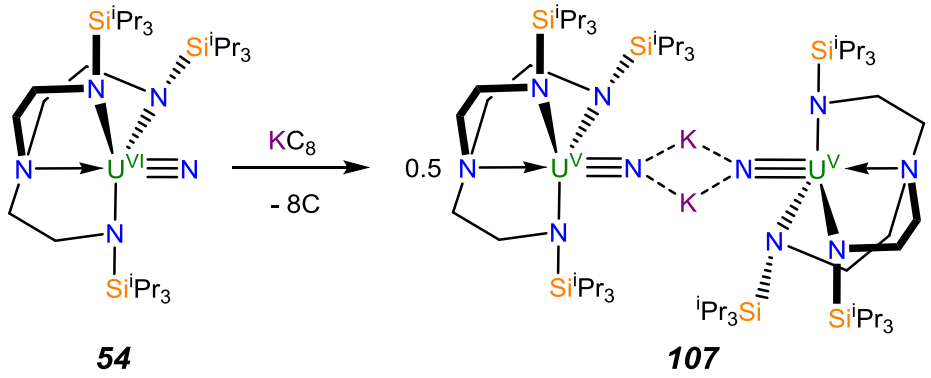
To test that this new route, *via* the addition of an external one electron oxidant to **13** and the subsequent sequestration with crown ethers, affords nitrides that are oxidisable, i.e. that it is a valid route towards the neutral **54**, both **114** and **115** were treated with iodine in toluene, in an analogous fashion as for the initial preparation of **54** from **52**.[10] As with all experiments involving **54**, the reaction vessels were shielded from light, as previous studies have shown that **54** decomposes photolytically *via* C-H activation to prepare the cyclometallated amide complex [U{*N*(H)C(Me)$_2$Si(^{i}Pr)$_2$*N*CH$_2$CH$_2$*N*(CH$_2$CH$_2$*N*Si^{i}Pr$_3$)$_2$}], **50**.[10] After 16 hours, the product could be isolated by extraction in toluene, followed by either washing with pentane or recrystallisation from hexanes. The preparation of **54** from **114** or **115** proceeded in good yield (59%), and therefore validates this new route as a higher yielding, more reliable route to uranium(V)–nitrides, which also leads to a simpler preparation of **54**.

2.5. Alternative Syntheses of [{U(Tren^{TIPS})(μ-N)(μ-K)}$_2$] (107)

2.5.1. Reactivity studies of [U(Tren^{TIPS})(N)] (54) towards reducing agents

As a proof of concept, several alternative synthetic routes were investigated towards the preparation of **107** from starting materials other than **13**. To this end, KC_8 was added to **54** in toluene. This reaction parallels that of the initial formation of **107**, though in this new reactivity, there is only a straightforward reduction of the uranium

centre, as opposed to a reduction of the azide ligand concurrent to an oxidation at the uranium centre and the elimination of dinitrogen.



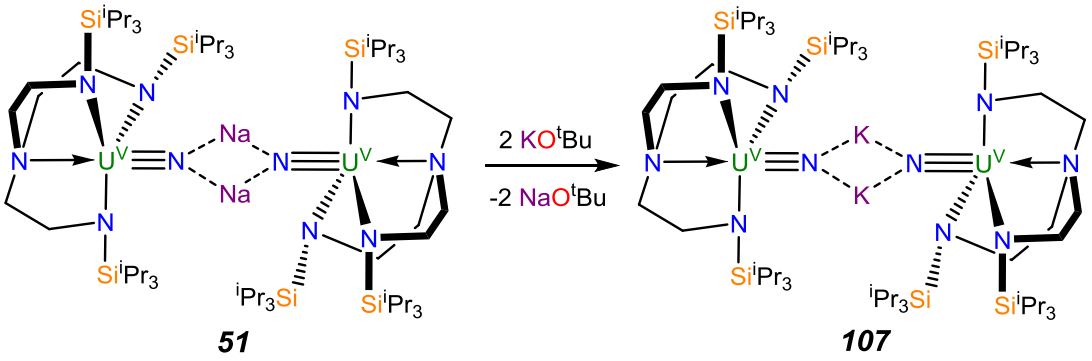
54 **107**

*Scheme **2.9.** Synthesis of **107**.*

Pleasingly, extraction of **107** into boiling benzene away from graphite afforded red crystals of **107**, as identified by a comparison of the crystal parameters in a preliminary single crystal XRD study. The yield was low (31 %), but this may be a consequence of the short reaction time (16 hours) in comparison to the several days allocated for the reduction of **13**. While better yields may have been achievable by stirring for a more prolonged period of time, the isolation of **107** from this reaction is evidence that this is a viable, if somewhat circuitous route to **107**.

2.5.2. Transmetallation reactions of [{U(Tren^{TIPS})(μ-N)(μ-Na)}$_2$] (51)

The reaction of **51** towards KO^{t}Bu was investigated. It was envisioned that under Hard Soft Acid Base (HSAB) principle, that the harder sodium ion would be preferred by the hard alkoxide anion to the softer potassium cation and hence this would provide a suitable driving force for the transmetallation of **51**.



*Scheme **2.10.** Synthesis of **107**.*

A stirring mixture of **51** and KO^{t}Bu in benzene was heated at reflux for 2 hours. Extraction of the resultant red solid into boiling benzene afforded red crystals of **107** on cooling to room temperature. A single crystal XRD study of these crystals confirmed their formulation as **107**.

As a result of these investigations, two further routes towards uranium nitrides have been identified, albeit that they are somewhat circuitous and longwinded. Whilst these reactions are unlikely to have much synthetic utility, they prove the point that it is possible to interconvert between these nitrides if it is so desired, for instance as part of a synthetic cycle.

2.6. Summary and Conclusions

The family of Tren^{TIPS} supported uranium nitrides has been expanded to encompass all the alkali metals by utilising an alternative synthetic route towards their synthesis. The one electron reduction of the pre-installed azide ligand of [U(Tren^{TIPS})(N$_3$)] (**13**) by alkali metals affords the facile syntheses of dinuclear uranium(V)–nitrides of the form [{U(Tren^{TIPS})(μ-N)(μ-M)}$_2$] (M = Li, Na, K, Rb, Cs; **106**, **51**, **107**, **108** and **109**). Careful selection of crown ether co-ligands has allowed the preparation of a range of monomeric alkali metal capped uranium(V)–nitrides of the form [U(Tren^{TIPS}){(μ-N)(μ-M)(crown)}] (M = Li, Na, K, Rb, Cs; **118**, **119**, **53**, **111**, **112** and **113**) and also, by sequestration and encapsulation of the cation, separated ion pair terminal uranium(V)–nitrides of the form [U(Tren^{TIPS})(N)][M(crown)$_2$], (M = Na, K, Rb, Cs; **114**, **115**, **116** and **117**). Oxidation of these SIP nitrides (M = Na, K;

52, **114**, **115**) to afford the neutral terminal uranium(VI)–nitride [U(Tren^{TIPS})(N)] (**54**) suggests that the reactivity of this set is broadly similar, and therefore reactivity studies can be performed on the highest yielding of these compounds (M = K, **107** and subsequently **115**, crown = Bn-15C5) and extrapolated in order to characterise the behaviour of this moiety.

It was not possible to prepare [U(Tren^{TIPS})(N)][M(crown)$_2$] for M = Li, and this is hypothesised to result from the hard nature of both the lithium ion and the nitride, which may indicate a nucleophilic linkage which cannot be broken by donor solvents.

The alternative syntheses of [{U(Tren^{TIPS})(μ-N)(μ-K)}$_2$] (**107**) from either [{U(Tren^{TIPS})(μ-N)(μ-Na)}$_2$] (**51**) or [U(Tren^{TIPS})(N)] (**54**) suggest that interconversion between these species is possible.

106, **51**, **107**, **108** and **109; 118**, **119**, **53**, **111**, **112** and **113**; and **52**, **114**, **115**, **116** and **117** have been characterised by ^{1}H NMR, FTIR and UV-vis-NIR spectroscopies, where possible. Further characterisation data pertaining to the magnetic character of [{U(Tren^{TIPS})(μ-N)(μ-M)}$_2$] (**106**, **51**, **107**, **108** and **109**), [U(Tren^{TIPS}){(μ-N)(μ-M)(crown)}] (**118**, **53**, **111**, **112** and **113**) and [U(Tren^{TIPS})(N)][M(crown)$_2$] (**52**, **114**, **116** and **117**) (i.e. SQUID, EPR), will be discussed in Chapter 4.

2.7. References

(1) King, D. M.; Tuna, F.; McInnes, E. J. L.; McMaster, J.; Lewis, W.; Blake, A. J.; Liddle, S. T. *Science* **2012**, *337*, 717.

(2) Evans, W. J.; Kozimor, S. A.; Ziller, J. W. *Science* **2005**, *309*, 1835.

(3) Mills, D. P.; Cooper, O. J.; Tuna, F.; McInnes, E. J. L.; Davies, E. S.; McMaster, J.; Moro, F.; Lewis, W.; Blake, A. J.; Liddle, S. T. *J. Am. Chem. Soc.* **2012**, *134*, 10047.

(4) King, D. M. *PhD Thesis* University of Nottingham, 2013.

(5) Addison, A. W.; Rao, T. N.; Reedijk, J.; van Rijn, J.; Verschoor, G. C. *J. Chem. Soc., Dalton Trans.* **1984**, 1349.

(6) *τ is a measure of how trigonal bipyramidal the complex is:*

τ = (β – α)/60, where β is the largest angle, and α is the second largest angle; a perfect square based pyramid has a value of 0, whilst a perfect trigonal

bipyramid has a value of 1; values larger than 1 arise due to distortion from the ideal angles of 180 and 120°, due to steric constraints of the ligand.
(7) Shannon, R. *Acta Crystallographica Section A* **1976**, *32*, 751.
(8) Pyykkö, P.; Riedel, S.; Patzschke, M. *Chem. -Eur. J.* **2005**, *11*, 3511.
(9) *As evidenced by a search of the Cambridge Structural Database (CSD)*.
(10) King, D. M.; Tuna, F.; McInnes, E. J. L.; McMaster, J.; Lewis, W.; Blake, A. J.; Liddle, S. T. *Nat. Chem.* **2013**, *5*, 482.
(11) Fox, A. R.; Cummins, C. C. *J. Am. Chem. Soc.* **2009**, *131*, 5716.
(12) Tsoureas, N.; Kilpatrick, A.; Inman, C.; Cloke, F. G. *Chem. Sci.* **2016**.
(13) *Using the harmonic oscillator formula ν = (1/2π)(k/μ)^1/2*.
(14) King, D. M.; Tuna, F.; McMaster, J.; Lewis, W.; Blake, A. J.; McInnes, E. J. L.; Liddle, S. T. *Angew. Chem.-Int. Edit.* **2013**, *52*, 4921.
(15) Graves, C. R.; Vaughn, A. E.; Schelter, E. J.; Scott, B. L.; Thompson, J. D.; Morris, D. E.; Kiplinger, J. L. *Inorg. Chem.* **2008**, *47*, 11879.
(16) Evans, D. F. *J. Chem. Soc. (Res.)* **1959**, 2003.
(17) Kindra, D. R.; Evans, W. J. *Chem. Rev.* **2014**, *114*, 8865.

Chapter Three

The Reactivity of Actinide Cyclometallates

Table of Contents

3.1. Introduction and Aims 130

3.1.1. Bonding differences in uranium and thorium complexes 130

3.1.2. Aims 131

3.2. Actinide Cyclometallates 133

3.2.1. Uranium cyclometallates 133

3.2.2. Thorium cyclometallates 136

3.2.3. Computational investigations into actinide cyclometallates 140

3.3. Summary and Conclusions 146

3.4. References 147

3.1.Introduction and Aims

3.1.1. Bonding differences in uranium and thorium complexes

The extent to which f orbital bonding interactions occur at uranium is still hotly debated. Studies have shown that uranium can involve moderate 5f orbital participation leading to modification of reactivity with consequences for the chemical outcome.[1-3] In contrast, the thorium(IV) ion is generally perceived as being unable to significantly access the 5f orbital manifold. Thus, its bonding is viewed as being restricted to electrostatics, which results in thorium–ligand bonds that are generally more labile than their uranium(IV) counterparts. Added to this, the greater ionic radius of Th^{IV} [six coordinate radii: Th^{IV} 94, U^{IV} 89 pm][4] means that thorium–ligand bonds are generally expected to be more reactive in comparison to uranium–ligand bonds.

The above arguments suggest that the reactivity of thorium and uranium should be different, but the picture is complicated and not well understood, and reports showing divergent experimental reactivity patterns of closely comparable uranium and thorium systems are rare.[1,5-8] Intramolecular amino-alkene hydroamination reactions tend to find thorium systems are more reactive than uranium systems. As similar trends have been observed for lanthanide complexes, this suggest that f orbital participation is not a key factor (the 4f orbitals are "core-like").[2,9]

Studies by Marks *et al.* found *bis*(cyclopentadienyl) thorium–dialkyls to be more stable than their uranium counterparts, however a decomposition pathway for these compounds is the reduction of uranium(IV) to uranium(III) which is unavailable for the thorium congeners. Whilst bond polarities were considered alongside these accessible oxidation states, f orbital participation was not examined, so no insight could be made in this regard.[10,11] Studies by Kiplinger *et al*. on similar systems have shown varying reactivity trends for thorium *vs* uranium, but their origins were not resolved.[6,12,13]

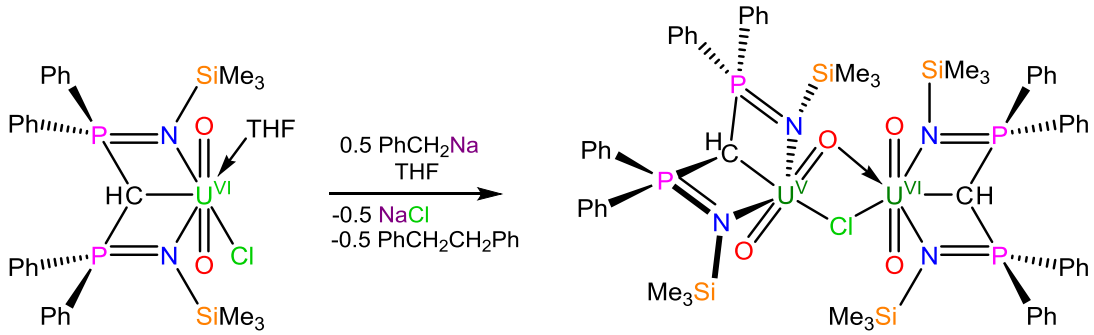
Moreover, there are a multitude of factors which can contribute to an isostructural pair of uranium and thorium complexes exhibiting similar or different reactivities, such as common geometries of products, adducts and agostic-type transition states, and the relative activation energies, and a recent computational study could not

derive a clear conclusion.[14] Where f orbital participation has been probed, this has been to compare the differences between f-block and d-block systems, as opposed to Th^{IV} *vs* U^{IV}.[3]

Recently, the formation of a uranium benzyne complex *vs* a thorium tetraaryl derivative was reported.[1] In that report, greater f orbital participation in the uranium product was found and it was postulated that this provided kinetic facilitation of the benzyne.

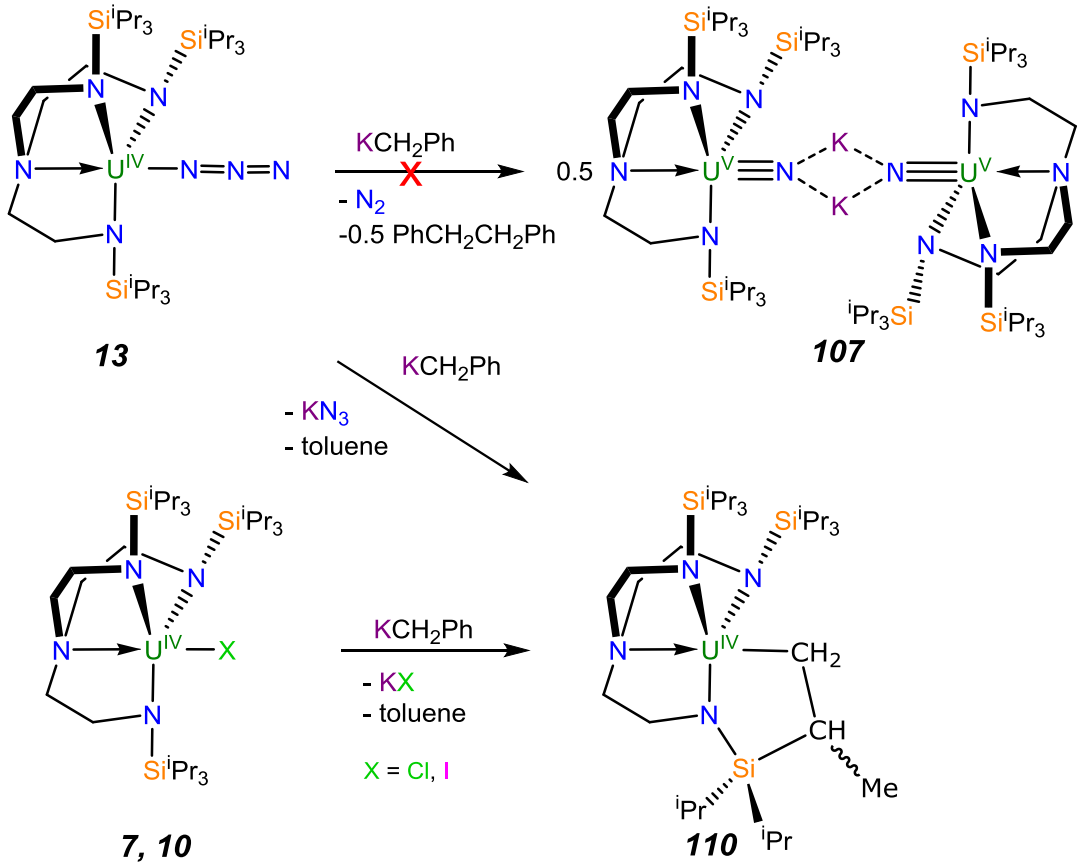
3.1.2. Aims

As was discussed previously (see Chapter 2), the reduction of [U(Tren^{TIPS})(N_3)] (**13**) with KCH_2Ph was attempted. It was envisioned [{U(Tren^{TIPS})(μ-N)(μ-K)}$_2$] (**107**) would be prepared with the concomitant elimination of half an equivalent of bibenzyl ($PhCH_2CH_2Ph$) and dinitrogen, similarly to the reduction of [U(BIPMH^{TMS})$(O)_2$(Cl)(THF)] [BIPMH^{TMS} = {H*C*(PPh_2=*N*$SiMe_3$)$_2$}$^-$] to the mixed U^V-U^{VI} system [{U(BIPMH^{TMS})(O)(μ-O)}(μ-Cl){U(BIPMH^{TMS})$(O)_2$}], scheme **3.1.**[15]



*Scheme **3.1.** Synthesis of [{U(BIPMH^{TMS})(O)(μ-O)}(μ-Cl){U(BIPMH^{TMS})$(O)_2$}].*[15]

Instead, the only uranium containing product isolated from the reaction of **13** with KCH_2Ph was the cyclometallated species [U{*C*H_2CH(Me)Si(^{i}Pr)$_2$*N*CH_2CH_2*N*(CH_2CH_2*N*Si^{i}Pr$_3$)$_2$}] (**110**), with the elimination of KN_3 and toluene, scheme **3.2.** In this case, the azide functionality behaves like a halide group, therefore following the reactivity described by Scott *et al.*,[16] rather than the chemistry observed in the reduction of [U(BIPMH^{TMS})$(O)_2$(Cl)(THF)].



*Scheme **3.2.** Syntheses of **110**.*

Cyclometallated actinide complexes,[17-21] for which those of triamidoamine ligands have been discussed previously (see Chapter 1, Section 2.3),[16,22-24] can have novel properties. Whilst many Tren N-silyl derived metal complexes are known,[25,26] only one benzyl derivative has been structurally authenticated, namely [Zr(Tren^{DMBS})(CH$_2$Ph)] (**19**),[27] which makes this ligand combination exceedingly rare. Stable actinide benzyl derivatives are known, but only in combination with ligands that do not cyclometallate,[8,17,28-35] and it seems evident that Tren N-silyl groups help promote this cyclometallation, hence the paucity of authenticated derivatives. Moreover, stabilisation of the metallocyclic alkyl groups occurs *via* negative hyperconjugation to the silicon. It is for these reasons that these complexes shall be explored further, as their inherent reactivity may lead to useful insights into actinide chemistry.

For reasons of synthetic efficacy, reactions towards the cyclometallated complex **110** from the halide precursors [U(Tren^{TIPS})(X)] (X = Cl **7**, I **10**) were also investigated.

What follows will be a comparative investigation into the preparation of both **110** and its thorium congener, and the unusual reactivity trend which was found during this study. The work discussed in this Chapter was performed in collaboration with Dr B. M. Gardner whilst at the University of Nottingham, Dr C. E. Kefalidis and Prof. L. Maron of Université Paul Sabatier, Toulouse, and Dr J. Fang, of Université Paul Sabatier, Toulouse and Lanzhou University, China.

3.2.Actinide Cyclometallates

3.2.1. Uranium cyclometallates

The reaction of uranium(IV)–halides or pseudohalides [U(Tren^{TIPS})(X)] (X = Cl **7**, I **10**, N_3 **13**) with benzyl potassium at room temperature afforded the cyclometallated uranium(IV)–alkyl complex [U{*C*H_2CH(Me)Si(^{i}Pr)$_2$*N*CH_2CH_2*N*($CH_2CH_2NSi^iPr_3$)$_2$}] (**110**) in moderate (60%) yield (scheme **3.2.**). Orange crystals of **110** suitable for single crystal XRD studies were grown from a concentrated solution in hexanes. The molecular structure of **110** is illustrated in figure **3.1.**, alongside selected bond lengths and angles.

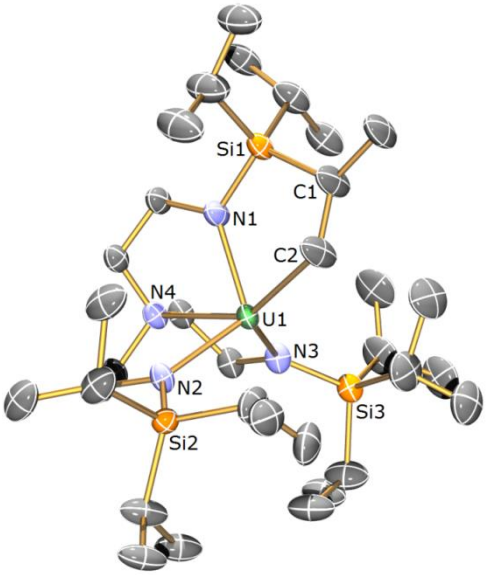


*Figure **3.1.** Molecular structure of [U{$CH_2CH(Me)Si(^iPr)_2NCH_2CH_2N(CH_2CH_2NSi^iPr_3)_2$}], **110**. Thermal ellipsoids set at 40% probability. Hydrogen atoms are omitted for clarity. Selected distances (Å)*

and angles (°): U(1)-N(1) 2.258(16), U(1)-N(2) 2.298(15), U(1)-N(3) 2.289(15), U(1)-N(4) 2.514(15), U(1)-C(2) 2.55(2), N(4)-U(1)-C(2) 146.1(7), N(1)-U(1)-C(2) 76.1(7).

The coordination sphere of uranium in **110** features the typical U-N_{amide} and U-N_{amine} bonds as expected for a Tren complex, in addition to a uranium–alkyl bond arising from the cyclometallation of one arm of $Tren^{TIPS}$. Whilst **110** could be considered to have a severely distorted trigonal bipyramidal geometry with the cyclometallated carbon and the face-capping amine of $Tren^{TIPS}$ occupying the axial positions, the τ value (0.31)[36] suggests that instead the geometry is better described as distorted square based pyramidal.[37] Under this description, the apex of the pyramid can be either of the amide nitrogens not part of the five-membered metallocyclic ring U(1)-N(1)-Si(1)-C(1)-C(2) i.e. N(2) or N(3).

The U(1)-N_{amide} [av. 2.282(16) Å] and U(1)-N(4) distances [2.514(15) Å] in **110** are typical for Tren–uranium complexes [*cf*. **7**: 2.245(2), 2.623(2); **13**: 2.247(3), 2.613(3) Å respectively]. The U(1)-C(2) bond distance of 2.55(2) Å is within the reported range of U-C single bonds [2.40-2.55 Å],[38] and this distance is considerably shorter than the corresponding distance in the $Tren^{DMBS}$ analogue, [U{*C*H_2Si(Me)(^{t}Bu)*N*CH_2CH_2*N*($CH_2CH_2NSi(Me)_2{}^t Bu)_2$}] (**22**), reported by Scott *et al*., [2.752(11) Å].[23] This can be attributed to the increased geometric strain in the $Tren^{DMBS}$ system, *vs* $Tren^{TIPS}$, as a result of the incorporation of the uranium–alkyl bond into a four membered ring [U-N-Si-C]. The $Tren^{TIPS}$ system has a five membered ring [U-N-Si-C-C], which releases this strain and permits a shorter bond length. Further evidence for the strain arises on consideration of the bite angle [the N(1)-U(1)-C(2) angle] for **110** and **22**, where in **110**, ∠N(1)-U(1)-C(2) is 76.1(7)°, which is less acute than the comparable angle in **22**, at 66.1(2)°.

Whilst the C(1) atom in **110** is chiral, **110** crystallised in a centrosymmetric space group which contains an inversion centre, and therefore **110** is inherently racemic in the solid state.

The ^{1}H NMR spectrum of **110** consists of 27 resonances and spans the range +47 to –35 ppm. This is consistent with the expected asymmetric C_1 Tren environment, as is the observance of three resonances in the $^{29}Si\{^1H\}$ NMR spectrum which

corroborate the presence of a uranium(IV) centre.[39] The broad range of resonances indicates the complex is paramagnetic, and this is corroborated by the Evans' method room temperature solution magnetic moment,[40] which reveals a μ_{eff} of 2.90 μ_B. Whilst this is lower than the theoretical free ion for the formal $^3H_4$ ground state of $5f^2$ U^{IV} of 3.58 μ_B, it is consistent with previously reported uranium(IV) species, which usually fall in the range 2.50 to 3.20 μ_B.[41]

A solution of **110** in toluene was analysed by UV-vis-NIR electronic absorption spectroscopy, and the spectrum obtained is illustrated in figure **3.2.**

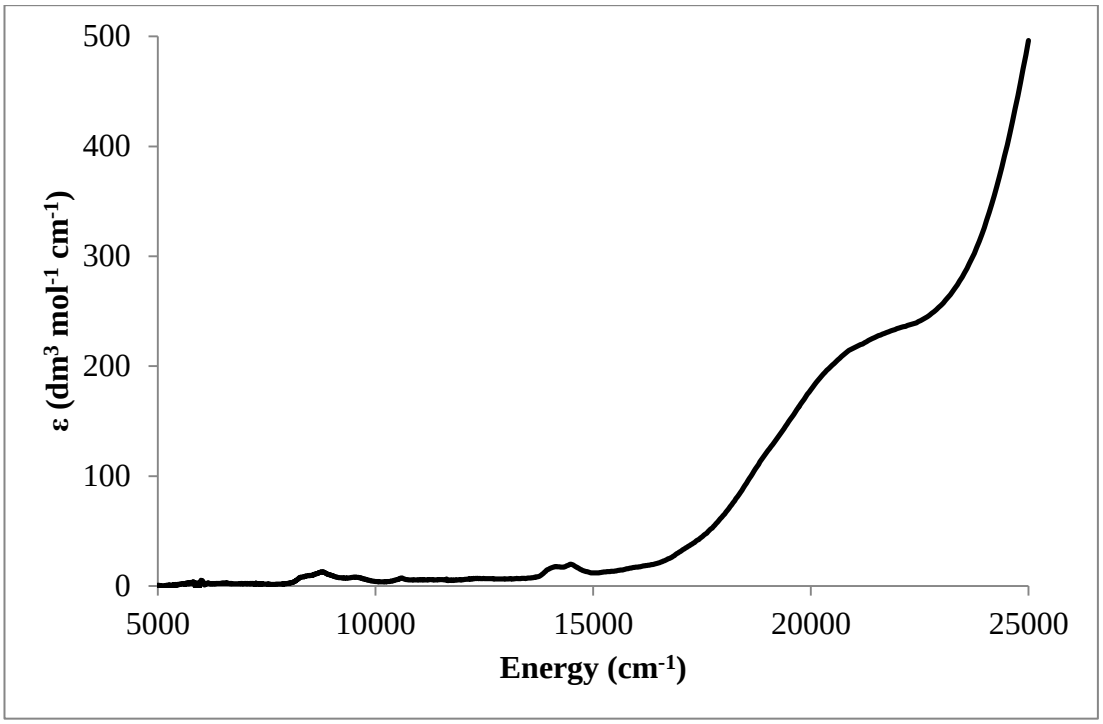
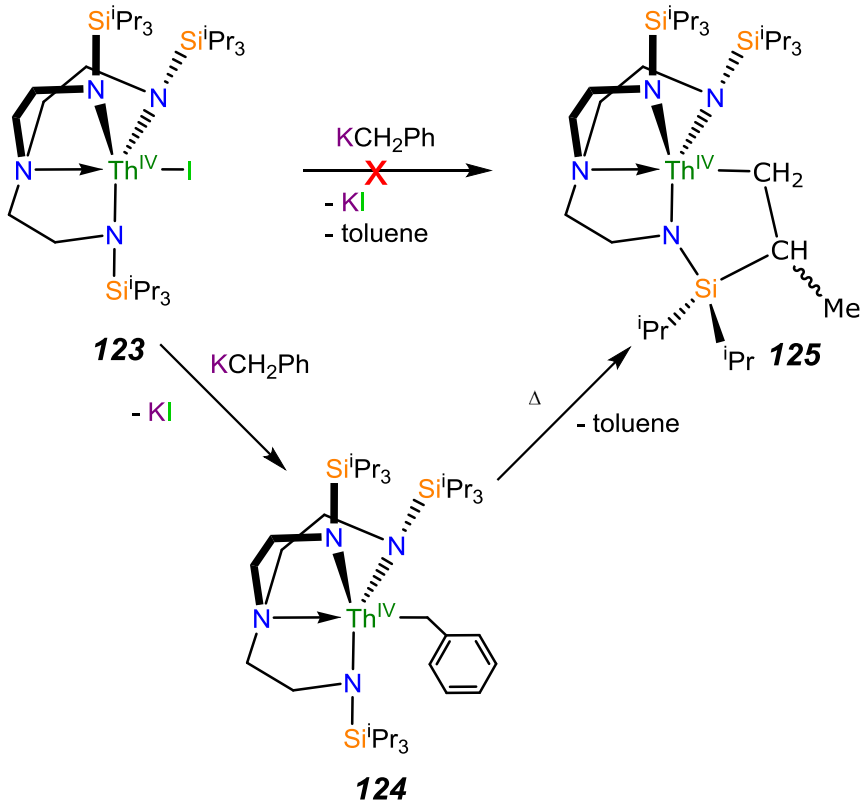


*Figure **3.2.** UV-vis-NIR electronic absorption spectrum of **110**.*

The spectrum is dominated by charge transfer (CT) bands tailing in from the high energy region (15000 – 25000 cm^{-1}), with a broad shoulder at ~22000 cm^{-1} (ε = ~250 dm^3 mol^{-1} cm^{-1}) which accounts for the orange-red colour of **110**. At lower energies weak Laporte forbidden *f-f* transitions are present (λ = 1100 nm, ε = 10 dm^3 mol^{-1} cm^{-1}; 700 nm, ε = 20 dm^3 mol^{-1} cm^{-1}), which is in-line with uranium(IV) complexes that have broad and unresolved spectra.

3.2.2. Thorium cyclometallates



*Scheme **3.3.** Synthesis of **124** and **125**.*

The reaction of a Tren–thorium halide with benzyl potassium was also investigated. The reaction of [Th(Tren^{TIPS})(I)] (**123**) with KCH$_2$Ph afforded, following work-up, colourless crystals of **124** (30% crystalline yield). The ^{1}H NMR spectrum of **124** contained 8 resonances spanning 0 – 10 ppm, which indicated that **124** has near C_{3v} symmetry, and not the C_1 symmetry anticipated for a cyclometallated thorium analogue of **110**. A single crystal XRD study elucidated the molecular structure of **124**, which is illustrated in figure **3.3.**, alongside selected bond lengths and angles.

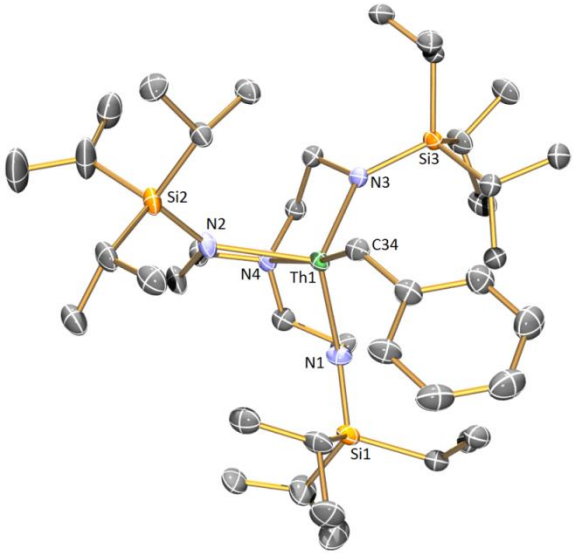


*Figure **3.3.** Molecular structure of [Th(Tren^{TIPS})(CH$_2$Ph)], **124**. Thermal ellipsoids set at 40% probability. Hydrogen atoms are omitted for clarity. Selected distances (Å) and angles (°) for one of the molecules in the asymmetric unit: Th(1)-N(1) 2.262(6), Th(1)-N(2) 2.309(6), Th(1)-N(3) 2.313(6), Th(1)-N(4) 2.701(6), Th(1)-C(34) 2.590(8), N(4)-Th(1)-C(34) 170.2(2).*

The molecular structure of **124** revealed the complex to be [Th(Tren^{TIPS})(CH$_2$Ph)], and not the anticipated thorium analogue of cyclometallated **110**. There are four crystallographically independent molecules in the asymmetric unit of the unit cell, for which the dimensions. In each case, the thorium centre has a distorted trigonal bipyramidal geometry ($\tau = 0.86$),[36,37] with the face-capping amine of Tren^{TIPS} being *trans* to the alkyl carbon of the η^1-benzyl group (i.e. in the axial positions). The Th-N$_{amide}$ bond distances range from 2.262(6) – 2.318(7) Å [mean 2.281(8) Å], and the four Th-N$_{amine}$ bond distances are statistically invariant [range 2.701(8) – 2.714(7), mean 2.708(8) Å]. The Th-C bond lengths range from 2.536(8) – 2.622(7) Å [mean 2.590(8) Å], with a mean Th-C-C$_{ipso}$ bond angle of 123.2(6)°. All Th-N$_{amide}$, Th-N$_{amine}$ and Th-C$_{alkyl}$ distances lie within reported ranges for Th^{IV} complexes.[42]

The $^{13}C\{^1H\}$ NMR contains 9 resonances. The benzyl-CH$_2$ group is observed at 1.62 and 113.7 ppm in the ^{1}H and $^{13}C\{^1H\}$ NMR spectra respectively. This compares to 2.63 and 63.95 ppm for the comparable benzyl-CH$_2$ in [Zr(Tren^{DMBS})(CH$_2$Ph)] (**19**).

These values differ despite their respective diamagnetic $5f^0/4d^0$ electronic configurations as a result of the slightly different electronic environment [*cf.* M-C bond lengths **124** 2.590(8), **19** 2.3243(18) Å] despite their closed-shell configurations.

It was envisioned that C-H activation of the TIPS group to prepare the desired Tren–thorium metallocycle might require thermolytic activation, as a benzyl species has been proposed as an intermediate *en route* to reported Tren–uranium cyclometallates in previous reports.[22,23]

To this end, a solution of **124** in toluene was heated to 80 °C for one hour, and following work-up, colourless crystals of a new product were isolated. A single crystal XRD study revealed this product to be the cyclometallated complex [Th{*C*H_2CH(Me)Si(^{i}Pr)$_2$*N*CH_2CH_2*N*($CH_2CH_2NSi^iPr_3$)$_2$}] (**125**). The molecular structure of **125** is illustrated in figure **3.4.**, alongside selected bond lengths and angles.

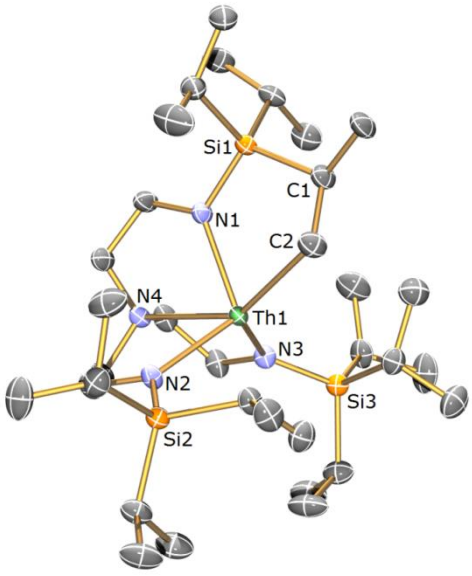


*Figure **3.4.** Molecular structure of [Th{$CH_2CH(Me)Si(^iPr)_2NCH_2CH_2N(CH_2CH_2NSi^iPr_3)_2$}], **125**. Thermal ellipsoids set at 40% probability. Hydrogen atoms are omitted for clarity. Selected distances (Å) and angles (°): Th(1)-N(1) 2.309(3), Th(1)-N(2) 2.337(3), Th(1)-N(3) 2.339(3),*

Th(1)-N(4) 2.607(3), Th(1)-C(2) 2.563(4), N(4)-Th(1)-C(2) 145.64(11), N(1)-Th(1)-C(2) 77.71(12).

Whilst the geometry of the cyclometallated **125** could be considered to be trigonal bipyramidal, analogous to the benzyl precursor (**124**), with the face-capping amine of $Tren^{TIPS}$ and the cyclometallated alkyl carbon in the axial positions, it may be better described as a distorted square based pyramid, with a non-cyclometallated amine [i.e. N(2) or N(3)] at the apex ($\tau = 0.31$).[36,37] Further to this, **125** is essentially isostructural to **110**, with any significant deviations of metal ligand bond distances ascribed to the smaller radius of U^{IV} *vs* Th^{IV} (six coordinate ionic radii: 89 *vs* 94 pm,[4] or covalent radii 170 *vs* 175 pm Pyykkö[43] or 196 *vs* 206 pm Alvarez[44]).

It would be expected that 27 resonances would be observed in the ^{1}H NMR spectrum of **125**, akin to **110**. However, the ^{1}H NMR spectrum of **125** reveals 16 resonances spanning the narrow range 0.68 – 3.90 ppm. The reason for this is likely due to multiple overlapping resonances reducing the number of resonances, which is consistent with multiplets being observed. The $^{13}C\{^{1}H\}$ NMR spectrum exhibits the expected downfield chemical shift (105.7 ppm) for the cyclometallated carbon [C(2)], and three resonances are observed in the $^{29}Si\{^{1}H\}$ spectrum, as was found to be the case for **110**, indicative of the breaking of approximate C_{3v} symmetry.

Again, the NMR spectra for **125** can be compared with the diamagnetic zirconium analogue, [Zr{$CH_2Si(Me)(^tBu)NCH_2CH_2N(CH_2CH_2NSiMe_2{}^tBu)_2$] (**20**).[27] Scott *et al.* observed 12 resonances spanning 0.15 – 3.68 ppm in the ^{1}H NMR spectrum, and the range reported for the $^{13}C\{^{1}H\}$ NMR spectrum spans –4.97 to 57.49 ppm, with the cyclometallated carbon appearing at 28.67 ppm. No $^{29}Si\{^{1}H\}$ spectrum was reported. The disparity between the ranges observed in the spectra for **125** and **20** might be best explained by the differing ring strain within these two complexes, wherein **20** (a four membered ring with $Tren^{DMBS}$) spans a smaller range than **125** (a five membered ring with $Tren^{TIPS}$). This is corroborated by the $^{13}C\{^{1}H\}$ NMR shifts reported for **24** (a dinuclear thorium $Tren^{DMBS}$ system), which range –6.58 to 56.84 ppm.[24]

The thermolytic conversion of **124** to **125** was probed by a kinetic NMR spectroscopic study. Experiments were conducted in C_7D_8 with a Mes*H standard

(Mes*H = 1,3,5-$^{t}Bu_3C_6H_3$) across the temperature range 40 to 70 °C. The mechanistic study revealed that the reaction follows first order kinetics with respect to **124**, with an activation energy (E_a) of 22.3 ± 0.1 kcal mol^{-1} (derived by Arrhenius analysis), an enthalpy of transition ($\Delta H^{\ddagger}$) of 21.7 ± 3.6 kcal mol^{-1} and an entropy of transition ($\Delta S^{\ddagger}$) of –10.5 ± 3.1 cal K^{-1} mol^{-1}(derived by Eyring analysis).

Low temperature variable temperature NMR spectroscopic experiments to assess whether a "[U(Tren^{TIPS})(CH_2Ph)]" intermediate would be observable for the conversion of **10** to **110**, found that no benzyl intermediate was observed (range 193 to 298 K). Consequently, no experimental mechanistic data can be reported. This is not unsurprising, as the (Tren^{TMS}) and (Tren^{DMBS}) uranium analogues of **110** both report smooth conversion from halide precursors to cyclometallates with the concomitant formation of toluene, and in neither case was a benzyl intermediate observed.[22,16]

3.2.3. Computational investigations into actinide cyclometallates

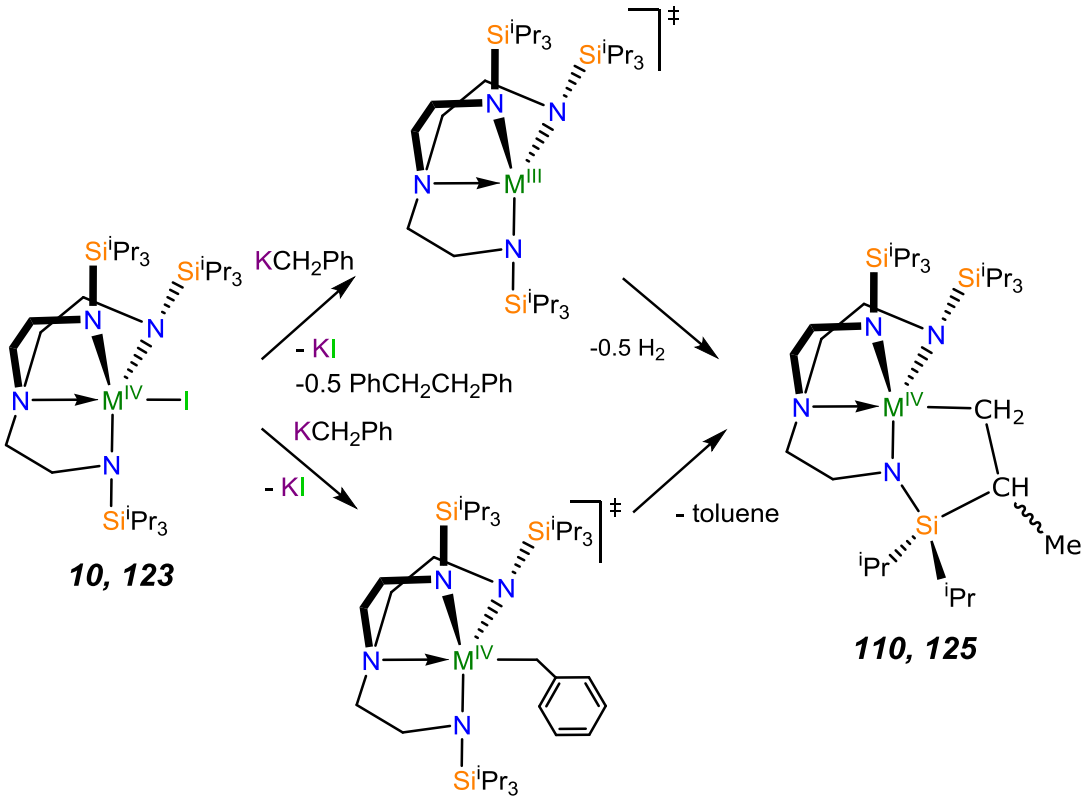
As alluded to above, **123** would be expected to be more ionic than **10** and therefore more reactive. However in this case the thorium system is less reactive and the benzyl intermediate (**124**) can be isolated, in contrast to the uranium analogue for which this is not the case. The cyclometallation of **10** and **123** therefore display inverted reactivity trends. Furthermore, the stability of **124** in the presence of silyl groups which can cyclometallate is notable, as there is only one example of an isolable silyl-Tren benzyl compound, [Zr(Tren^{DMBS})(CH_2Ph)],[27] and all other actinide benzyl species do not possess silyl substituents (which seem to facilitate cyclometallation by stabilising the metallocyclic alkyl groups *via* negative hyperconjugation to the silicon).[22]

We hypothesised that the reversal of anticipated reactivity is due to the σ-bond metathesis transition state for uranium being stabilised by 5f orbital participation. As was demonstrated in figure **1.2.** (by [An(Cp)$_3$] complexes, see Chapter 1, Section 1.), the relative 6d and 5f orbital energies vary across the actinide series.[45] This means that for thorium, the 5f orbitals are higher in energy, and therefore bonding at

thorium favours the use of (lower energy) 6d orbitals. This is in contrast to uranium, where these orbitals have more similar energies, and therefore can employ both in bonding. Consequently, the more energetically accessible vacant 5f orbitals at enhances the reactivity of the uranium system, by stabilising the transition state. Computational studies were performed to investigate this stabilisation, as well as the mechanistic route for the preparation of cyclometallated $Tren^{TIPS}$ species (**110** and **125**).

Calculations at the B3PW91 level of theory were firstly used to assess the preparation of the cyclometallated species by the reductive extrusion of bibenzyl ($PhCH_2CH_2Ph$) from "[$U(Tren^{TIPS})(CH_2Ph)$]" to afford [$U(Tren^{TIPS})$] (**15**), followed by the elimination of half an equivalent of dihydrogen (scheme **3.4.**, upper mechanism), a mechanism that has parallels in transition metal species where hydride species are implicated (see Section 1.2).[17] It was found that whilst the reductive extrusion step was favourable (–12 kcal mol^{-1}), the subsequent elimination of dihydrogen is disfavoured (+16 kcal mol^{-1}). Therefore, this route, which has no experimental support, can be ruled out from a computational standpoint.

The reaction profile *via* a benzyl intermediate, which does have experimental support in the isolation of **124**, was then probed (figure **3.5.**). It can be seen that there is little thermodynamic preference for the formation of the benzyl species (U –1.7, Th –0.6 kcal mol^{-1}), therefore the isolation of **124** but not the analogous uranium intermediate must originate from kinetic factors which are derived from orbital facilitation present for uranium but not for thorium. The cyclometallation step was found to be slightly exothermic for uranium (–2.8 kcal mol^{-1}), but near athermic for thorium (–0.8 kcal mol^{-1}).



Scheme ***3.4.*** *The two mechanistic routes investigated for the formation of cyclometallated species (M = U, Th).*

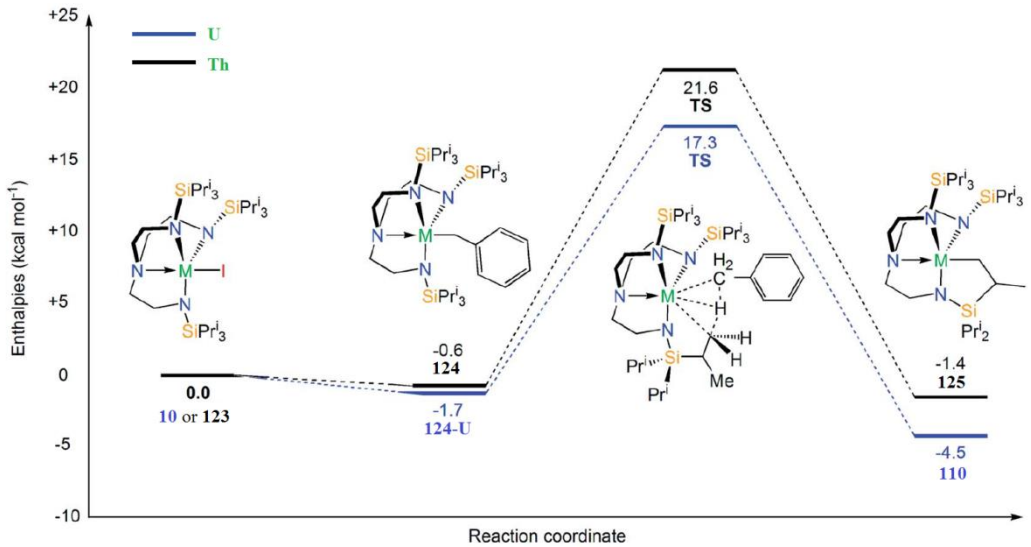


Figure ***3.5.*** *Enthalpy energy profiles (at 298 K) for the gas phase cyclometallation reactions for* ***10*** *(blue profile) and* ***123*** *(black profile), computed at the B3PW91 level of theory.*

The cyclometallation transition states (TS) were located on the potential energy surface and are illustrated in figure **3.6.** The geometry of the TSs are essentially identical to the classical σ-bond metathesis arrangement,[46] with the hydrogen atom that is ultimately transferred lying between the two alkyl groups as reported in previous studies of σ-bond metathesis for uranium and thorium catalysed C-H activation.[47] In particular, the M-H distance is short and the C-H-C angle is near linear (**110** 176°, **125** 172°). Interestingly, Natural Bond Orbital (NBO) analyses at the TS indicate that the metal-benzyl bonds are already broken (no interactions are found at either the first or the second order donor-acceptor level) and that an M-CH_2 bond is formed (which is found at the first order NBO level).

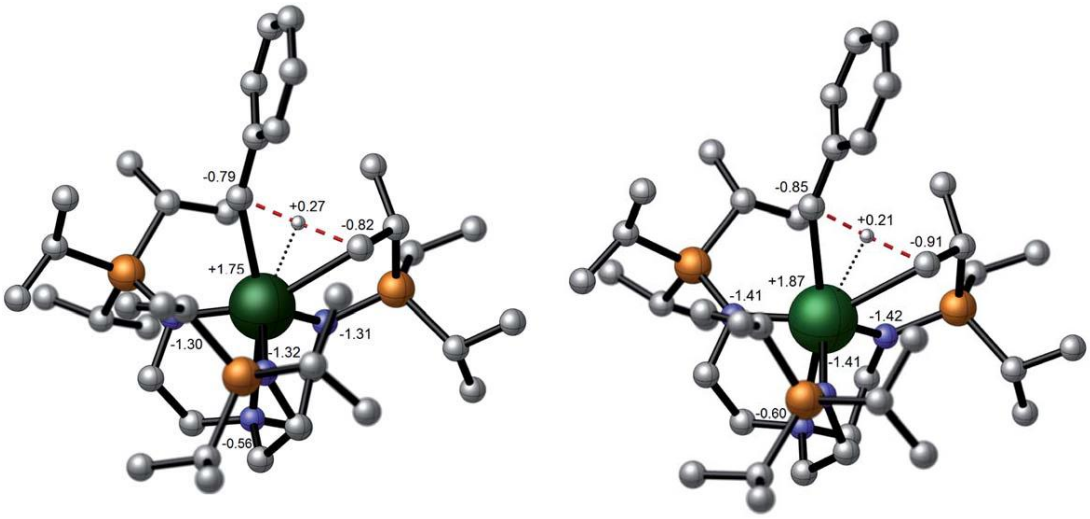


*Figure **3.6.** Calculated transition states for the cyclometallation step for uranium (left) and thorium systems (right). Selected atom natural population charge labelling and peripheral hydrogens omitted for clarity.*

The activation barriers were computed to be 19.0 and 22.2 kcal mol^{-1} for uranium and thorium cases, respectively. A salient point here is that the calculated activation barrier for the thorium case is in strong agreement with the experimentally derived value (22.3 ± 0.1 kcal mol^{-1}), which was derived through Arrhenius analysis of a kinetic ^{1}H NMR spectroscopic study.

Natural Population Analysis (NPA) was carried out to rationalise the kinetic preference for uranium over thorium (figure **3.6.**). The charge is slightly lower at uranium than thorium, which is consistent with a more ionic TS for thorium. This is

further highlighted by scrutinising the natural charges of the carbon centres of the alkyl groups, which are somewhat higher in the thorium case. Overall, the description of charge distribution shows the characteristic hallmarks of a σ-bond metathesis TS.[48]

It had been proposed that the observed difference in reactivity between uranium and thorium in this case could be attributed to the lack of 5f orbital involvement in the bonding of thorium systems, due to the higher energy of the 5f orbitals *vs* the 6d orbitals. This induces a greater degree of covalency for the uranium system.[1] To test this, the molecular orbitals (MOs) of the TSs were analysed. In the uranium case, four MOs were found (which mainly employed 5f orbitals), whereas only two were found in the thorium case (which mainly employed 6d orbitals), which might be expected based on the relative energies of the orbitals as described by Bursten.[45] This is in agreement with reports of the 5f orbital involvement in bonding,[1,3] but this does not translate to a clear difference in covalency of the bonding of these metal centres.

This reactivity has two possible explanations: (i) steric hindrance around the metal centre (sterically induced reactivity); or (ii) 5f orbital participation. Energy profiles for both metals, without 5f electrons and orbitals in the calculations, using large core relativistic effective core potentials (large core RECPs) were prepared to test the importance of the 5f orbitals (figure **3.7.**). These conditions essentially treat the systems as 6d transition metals. The use of large core RECPs has been demonstrated to be appropriate to describe U^{IV} and Th^{IV} chemistry.[49-51] With 5f orbitals and electrons excluded, the profiles for the two systems are found to be the same, with the same energy barrier (22 kcal mol^{-1}). Importantly, the barrier is unchanged for thorium (which has no 5f electrons) by both approaches, whereas for uranium the barrier is approximately 3 kcal mol^{-1} higher when 5f electrons are excluded. This suggests that the lack of accessible 5f orbitals makes these bonds more ionic.

To test that steric hindrance was not also a factor, calculations on the hypothetical zirconium and hafnium analogues of these systems were performed. The computed barriers were found to be 24 – 26 kcal mol^{-1}, again higher than the uranium case. As the steric congestion is enhanced for these smaller metals (4d and 5d respectively),

these results preclude sterically induced reactivity, as such factors would be expected to lower the energy barriers for these systems.

These calculations therefore strongly suggest that 5f orbital participation in bonding induces a clear change in that bonding, which could be interpreted as covalency,[52-54] and this in turn has a profound effect on experimentally observed reactivities.

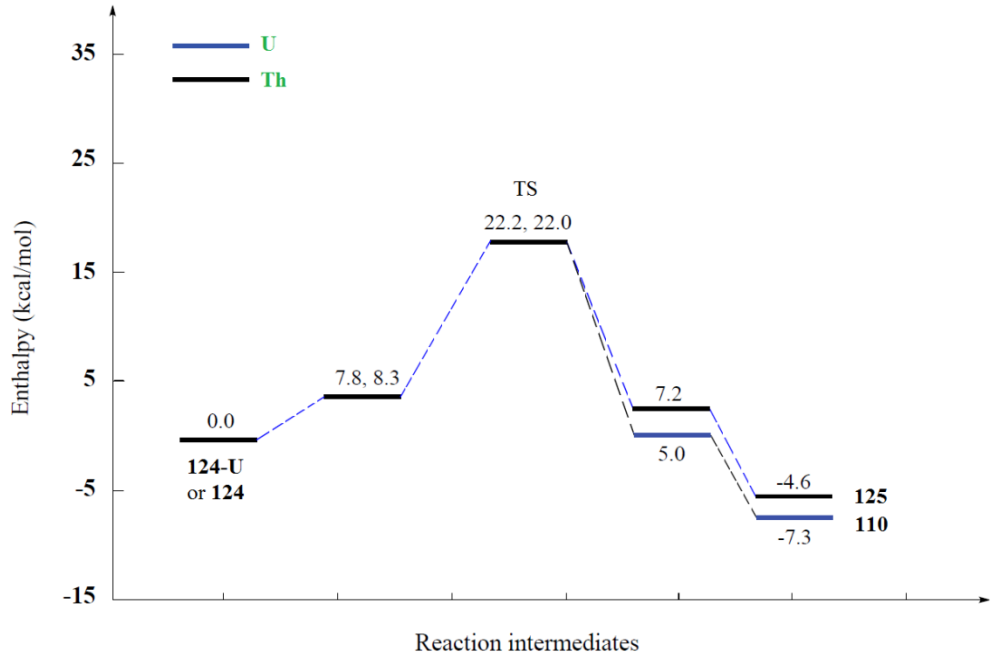


*Figure **3.7.** Energy profiles (at 298 K) for the gas phase cyclometallation reactions for **10** (blue profile) and **123** (black profile), computed using f-in-core RECPs.*

Finally, interesting multiple bond chemistry, performed by other members of the Liddle group, has arisen from the use of {M(Tren^{TIPS})} cyclometallates, **110** and **125**, as starting materials. For **110**, reaction with [HNEt$_3$][BPh$_4$] in THF affords the separated ion pair complex, [U(Tren^{TIPS})(THF)][BPh$_4$]. Addition of [NaPH$_2$] to [U(Tren^{TIPS})(THF)][BPh$_4$] affords the preparation of the first uranium phosphide complex [U(Tren^{TIPS})(PH$_2$)]. Subsequent reaction of [U(Tren^{TIPS})(PH$_2$)] with KCH$_2$Ph and the appropriate co-ligand prepares variously the capped phosphinidene [U(Tren^{TIPS}){(μ-PH)(μ-K)(2,2,2-crypt)] or separated ion pair phosphinidene [U(Tren^{TIPS})(PH)][K(Bn-15C5)$_2$].[55] Similarly, the arsenide [U(Tren^{TIPS})(AsH$_2$)] was prepared from the reaction of [U(Tren^{TIPS})(THF)][BPh$_4$] with [KAsH$_2$]. Subsequent addition of KCH$_2$Ph and benzo-15-crown-5 ether to [U(Tren^{TIPS})(AsH$_2$)] over two

hours affords [U(Tren^{TIPS})(AsH)][K(Bn-15C5)$_2$], while stirring for two days affords [{U(Tren^{TIPS})}$_2$(μ-η^3:η^3-As)] as a minor product. Reaction of [U(Tren^{TIPS})(AsH$_2$)] with KCH$_2$Ph in the absence of co-ligand affords the tetranuclear complex [{U(Tren^{TIPS})(μ-As)(μ-K)$_2$}$_4$], subsequent addition of 2,2,2-crypt affords [U(Tren^{TIPS}){(μ-AsH)(μ-K)(2,2,2-crypt)].[56] Multiple bond chemistry at thorium can be directly accessed from **125**. Reaction of **125** with NaPH$_2$ and 12-crown-4 ether affords either [{Th(Tren^{TIPS})}$_2$(μ-P)][Na(12C4)$_2$] or [Th(Tren^{TIPS})(PH)][Na(12C4)$_2$] dependent upon the ratio of reagents.[57]

3.3. Summary and Conclusions

Comparative investigations were carried out on the preparation of the cyclometallated uranium and thorium alkyl complexes [M{*C*H$_2$CH(Me)Si(^{i}Pr)$_2$*N*CH$_2$CH$_2$*N*(CH$_2$CH$_2$NSi^{i}Pr$_3$)$_2$}] (M = U, **110**, M = Th, **125**). In the case of the preparation of **125**, the presence of a benzyl species (**124**) was observed and thermolytic activation was required to prepare the cyclometallated species (**125**). In contrast, the benzyl intermediate was found to be non-isolable in the case of uranium, and the preparation of **110** was extremely facile, even at low temperatures. This reactivity is the inverse of that which might be anticipated, as the more ionic thorium system may be predicted to be more reactive than the uranium analogue; however this is not the case.

Computational calculations suggest that this inversion of reactivity can be attributed to the stabilisation of the σ-bond metathesis TS for uranium by 5f orbital participation. As thorium lacks 5f orbital stabilisation the transition state is more ionic and kinetically less accessible, and therefore less reactive. Hence, greater covalency in the uranium system does not stabilise the benzyl intermediate, instead facilitating the TS and affording greater reactivity.

Further calculations discount cyclometallation *via* redox chemistry as well as a steric dependence for this chemistry. This study represents an example of how 5f orbital participation can steer chemical reactivity in an unexpected yet profound manner.

3.4. References

(1) Seaman, L. A.; Pedrick, E. A.; Tsuchiya, T.; Wu, G.; Jakubikova, E.; Hayton, T. W. *Angew. Chem., Int. Ed.* **2013**, *52*, 10589.

(2) Hayes, C. E.; Platel, R. H.; Schafer, L. L.; Leznoff, D. B. *Organometallics* **2012**, *31*, 6732.

(3) Cantat, T.; Graves, C. R.; Jantunen, K. C.; Burns, C. J.; Scott, B. L.; Schelter, E. J.; Morris, D. E.; Hay, P. J.; Kiplinger, J. L. *J. Am. Chem. Soc.* **2008**, *130*, 17537.

(4) Shannon, R. *Acta Crystallographica Section A* **1976**, *32*, 751.

(5) Grant, D. J.; Stewart, T. J.; Bau, R.; Miller, K. A.; Mason, S. A.; Gutmann, M.; McIntyre, G. J.; Gagliardi, L.; Evans, W. J. *Inorg. Chem.* **2012**, *51*, 3613.

(6) Pool, J. A.; Scott, B. L.; Kiplinger, J. L. *J. Am. Chem. Soc.* **2005**, *127*, 1338.

(7) Morris, D. E.; Da Re, R. E.; Jantunen, K. C.; Castro-Rodriguez, I.; Kiplinger, J. L. *Organometallics* **2004**, *23*, 5142.

(8) Jantunen, K. C.; Burns, C. J.; Castro-Rodriguez, I.; Da Re, R. E.; Golden, J. T.; Morris, D. E.; Scott, B. L.; Taw, F. L.; Kiplinger, J. L. *Organometallics* **2004**, *23*, 4682.

(9) Stubbert, B. D.; Marks, T. J. *J. Am. Chem. Soc.* **2007**, *129*, 6149.

(10) Marks, T. J. *Acc. Chem. Res.* **1976**, *9*, 223.

(11) Fagan, P. J.; Manriquez, J. M.; Maatta, E. A.; Seyam, A. M.; Marks, T. J. *J. Am. Chem. Soc.* **1981**, *103*, 6650.

(12) Pool, J. A.; Scott, B. L.; Kiplinger, J. L. *J. Alloy. Compd.* **2006**, *418*, 178.

(13) Kiplinger, J. L.; Scott, B. L.; Schelter, E. J.; Pool Davis Tournear, J. A. *J. Alloy. Compd.* **2007**, *444–445*, 477.

(14) Yang, P.; Warnke, I.; Martin, R. L.; Hay, P. J. *Organometallics* **2008**, *27*, 1384.

(15) Mills, D. P.; Cooper, O. J.; Tuna, F.; McInnes, E. J. L.; Davies, E. S.; McMaster, J.; Moro, F.; Lewis, W.; Blake, A. J.; Liddle, S. T. *J. Am. Chem. Soc.* **2012**, *134*, 10047.

(16) Boaretto, R.; Roussel, P.; Kingsley, A. J.; Munslow, I. J.; Sanders, C. J.; Alcock, N. W.; Scott, P. *Chem. Commun.* **1999**, 1701.

(17) Simpson, S. J.; Turner, H. W.; Andersen, R. A. *Inorg. Chem.* **1981**, *20*, 2991.

(18) Fortier, S.; Walensky, J. R.; Wu, G.; Hayton, T. W. *J. Am. Chem. Soc.* **2011**, *133*, 6894.

(19) Bruno, J. W.; Marks, T. J.; Day, V. W. *J. Organomet. Chem.* **1983**, *250*, 237.

(20) Fendrick, C. M.; Marks, T. J. *J. Am. Chem. Soc.* **1984**, *106*, 2214.

(21) Bruno, J. W.; Smith, G. M.; Marks, T. J.; Fair, C. K.; Schultz, A. J.; Williams, J. M. *J. Am. Chem. Soc.* **1986**, *108*, 40.

(22) Gardner, B. M.; McMaster, J.; Lewis, W.; Blake, A. J.; Liddle, S. T. *J. Am. Chem. Soc.* **2009**, *131*, 10388.

(23) Boaretto, R.; Roussel, P.; Alcock, N. W.; Kingsley, A. J.; Munslow, I. J.; Sanders, C. J.; Scott, P. *J. Organomet. Chem.* **1999**, *591*, 174.

(24) Gardner, B. M.; Lewis, W.; Blake, A. J.; Liddle, S. T. *Organometallics* **2015**, *34*, 2386.

(25) Schrock, R. R. *Acc. Chem. Res.* **1997**, *30*, 9.

(26) Gardner, B. M.; Liddle, S. T. *Chem. Commun.* **2015**, *51*, 10589.

(27) Morton, C.; Munslow, I. J.; Sanders, C. J.; Alcock, N. W.; Scott, P. *Organometallics* **1999**, *18*, 4608.

(28) Kraft, S. J.; Fanwick, P. E.; Bart, S. C. *J. Am. Chem. Soc.* **2012**, *134*, 6160.
(29) Fortier, S.; Melot, B. C.; Wu, G.; Hayton, T. W. *J. Am. Chem. Soc.* **2009**, *131*, 15512.
(30) Edwards, P. G.; Andersen, R. A.; Zalkin, A. *Organometallics* **1984**, *3*, 293.
(31) Cruz, C. A.; Emslie, D. J. H.; Harrington, L. E.; Britten, J. F. *Organometallics* **2008**, *27*, 15.
(32) Cruz, C. A.; Emslie, D. J. H.; Robertson, C. M.; Harrington, L. E.; Jenkins, H. A.; Britten, J. F. *Organometallics* **2009**, *28*, 1891.
(33) Hayes, C. E.; Leznoff, D. B. *Organometallics* **2010**, *29*, 767.
(34) Broderick, E. M.; Gutzwiller, N. P.; Diaconescu, P. L. *Organometallics* **2010**, *29*, 3242.
(35) Monreal, M. J.; Diaconescu, P. L. *J. Am. Chem. Soc.* **2010**, *132*, 7676.
(36) Addison, A. W.; Rao, T. N.; Reedijk, J.; van Rijn, J.; Verschoor, G. C. *J. Chem. Soc., Dalton Trans.* **1984**, 1349.
(37) *τ is a measure of how trigonal bipyramidal the complex is:*

τ = (β – α)/60, where β is the largest angle, and α is the second largest angle; a perfect square based pyramid has a value of 0, whilst a perfect trigonal bipyramid has a value of 1; values larger than 1 arise due to distortion from the ideal angles of 180 and 120°, due to steric constraints of the ligand.
(38) Allen, F. *Acta Crystallographica Section B* **2002**, *58*, 380.
(39) Windorff, C. J.; Evans, W. J. *Organometallics* **2014**, *33*, 3786.
(40) Evans, D. F. *J. Chem. Soc. (Res.)* **1959**, 2003.
(41) Kindra, D. R.; Evans, W. J. *Chem. Rev.* **2014**, *114*, 8865.
(42) *As evidenced by a search of the Cambridge Structural Database (CSD).*
(43) Pyykkö, P.; Atsumi, M. *Chem. -Eur. J.* **2009**, *15*, 186.
(44) Cordero, B.; Gomez, V.; Platero-Prats, A. E.; Reves, M.; Echeverria, J.; Cremades, E.; Barragan, F.; Alvarez, S. *Dalton Trans.* **2008**, 2832.
(45) Bursten, B. E.; Rhodes, L. F.; Strittmatter, R. J. *J. Am. Chem. Soc.* **1989**, *111*, 2756.
(46) Waterman, R. *Organometallics* **2013**, *32*, 7249.
(47) Yahia, A.; Maron, L. *Organometallics* **2009**, *28*, 672.
(48) Lin, Z. *Coord. Chem. Rev.* **2007**, *251*, 2280.
(49) Castro, L.; Yahia, A.; Maron, L. *Dalton Trans.* **2010**, *39*, 6682.
(50) Castro, L.; Yahia, A.; Maron, L. *Comptes Rendus Chimie* **2010**, *13*, 870.
(51) Castro, L.; Yahia, A.; Maron, L. *ChemPhysChem* **2010**, *11*, 990.
(52) Kaltsoyannis, N. *Inorg. Chem.* **2013**, *52*, 3407.
(53) Neidig, M. L.; Clark, D. L.; Martin, R. L. *Coord. Chem. Rev.* **2013**, *257*, 394.
(54) Walensky, J. R.; Martin, R. L.; Ziller, J. W.; Evans, W. J. *Inorg. Chem.* **2010**, *49*, 10007.
(55) Gardner, B. M.; Balazs, G.; Scheer, M.; Tuna, F.; McInnes, E. J. L.; McMaster, J.; Lewis, W.; Blake, A. J.; Liddle, S. T. *Angew. Chem., Int. Ed.* **2014**, *53*, 4484.
(56) Gardner, B. M.; Balázs, G.; Scheer, M.; Tuna, F.; McInnesEric, J. L.; McMaster, J.; Lewis, W.; Blake, A. J.; Liddle, S. T. *Nat Chem* **2015**, *7*, 582.
(57) Wildman, E. P.; Balázs, G.; Wooles, A. J.; Scheer, M.; Liddle, S. T., *Nat. Commun.*, **2016**, *7*, doi: 10.1038/ncomms12884 .

Chapter Four

The Electronic Structure of Uranium Nitrides

Table of Contents

4.1. Introduction and Aims 150

4.1.1. An Introduction to Single Molecule Magnets (SMMs) 150

4.1.2. Highlights from the Literature 151

4.1.2.1. Transition Metal SMMs 151

4.1.2.2. Lanthanide SMMs 153

4.1.2.3. Actinide SMMs 156

4.1.3. Aims 158

4.2. Electronic Structure of Uranium(V)-Nitrides 159

4.2.1. Background 159

4.2.2. Ab initio modelling of $[U{\equiv}N]^{2+}$ 160

4.2.3. Ab initio modelling of $[U(NH_3)(NH_2)_3(N)]^-$ 164

4.2.4. Ab initio modelling of $[U(Tren^{TIPS})(N)]^-$ 169

4.3. Magnetic Structure of Uranium(V)-Nitrides 172

4.3.1. Magnetic measurements of uranium(V)-nitrides 172

4.3.2. EPR studies of uranium(V)-nitrides 178

4.3.3. Comparison of uranium(V)-nitrides with $[U(Tren^{TIPS})(O)]$*, 122* 183

4.3.4. Uranium(V)-nitrides as SMMs 185

4.4. Summary and Conclusions 188

4.5. References 190

4.1.Introduction and Aims

4.1.1. An Introduction to Single Molecule Magnets (SMMs)

Single Molecule Magnets (SMMs) are complexes that retain magnetisation (relax slowly) in the absence of an applied magnetic field.[1] This relaxation is purely of molecular origin, and originates from molecules that possess well isolated high spin ground states, with a strong easy axis type anisotropy, where the magnetisation aligns preferentially in one direction (the easy axis).[2] These factors mean that a (thermal) energy barrier to the relaxation of magnetisation is formed, which gives rise to magnetic bistability at liquid helium temperatures. This energy barrier can be surmounted by Quantum Tunnelling of the Magnetisation (QTM) between degenerate spin states of opposite sign through the energy barrier, which reduces the relaxation time.

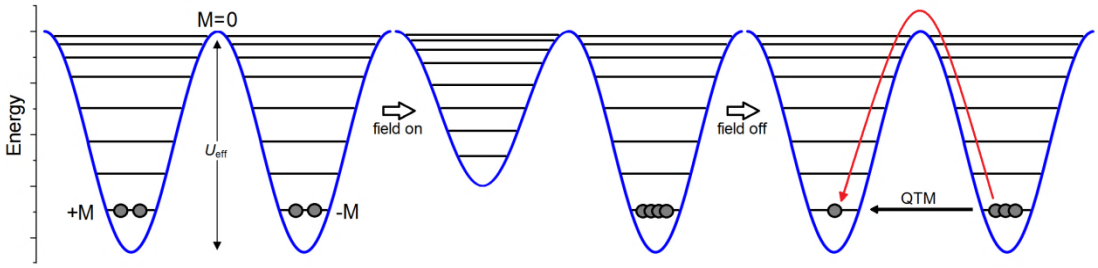
There are three parameters by which SMMs are often compared. The most commonly reported parameter is the effective energy (anisotropy) barrier, U_{eff}, which is the energy required to convert an SMM to a paramagnet. U_{eff} is variously reported in either cm^{-1} or K. The second parameter is the blocking temperature, T_B, which is the highest (sweep rate dependent) temperature at which an SMM maintains hysteresis in a plot of magnetisation (M) *vs* magnetic field (H). Sweep rates are discussed in terms of a T_B that corresponds to a relaxation time (τ). Finally, the coercive magnetic field, H_c, is the strength of the magnetic field required to return the magnetisation of an SMM back to zero (following saturation).

Whilst SMMs show great promise for a wide range of practical applications, (including high density data storage, quantum information processing, spintronics and magnetocaloric refrigeration),[3-6] the necessity for liquid helium temperatures to maintain these properties renders them impractical. Therefore, a key target for SMM research is to prepare complexes that retain their magnetisation at more practical temperatures.

4.1.2. Highlights from the Literature

4.1.2.1. Transition Metal SMMs

The energy barrier for transition metal SMMs can be expressed as $U_{eff} = |D|S^2$ for integer spins or $U_{eff} = |D|(S^2\text{-}0.25)$ for non-integer spins, where S is the total spin of the molecule and D is the axial zero-field splitting (ZFS) parameter. ZFS is a measure of the anisotropy of a molecule and should be large and negative. There are then $[2S + 1]$ m_s microstates, which are split in zero field, where $m_s = \pm S$ are the lowest in energy (for $D < 0$). For the magnetisation to relax, the energy barrier must be overcome. This can be achieved in ±1 steps in the m_s states until equilibrium is attained. QTM through the barrier between degenerate m_s states minimises this barrier.



*Scheme **4.1.** The magnetisation and relaxation of an SMM. Left, in zero field (M = 0), the two wells (±S) are equally populated, separated by an energy barrier (U_{eff}). Centre, application of a magnetic field selectively populated the right well. Right, on removal of the field, return to the equilibrium state occurs through a series of steps over the energy barrier (red arrow), or through quantum tunnelling of the magnetisation (QTM, black arrow).*

The first complex to display SMM behaviour, reported in 1993, was the manganese(III/IV) cluster $[Mn_{12}(O)_{12}(CH_3COO)_{16}(H_2O)_4]$ (**126**), which has a total spin of S = 10 and ZFS of $D = –0.51$ cm^{-1}, was shown to possess a U_{eff} of 51 cm^{-1}.[7,8]

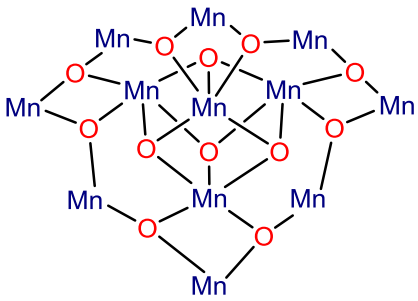


*Figure **4.1.** Complex **126**, acetyl and water ligands omitted for clarity.*

Further efforts to prepare SMMs focussed initially on manganese cluster compounds with an aim to increase the total spin of these systems. To this end, $[Mn_{19}O_8(N_3)_8(HL)_{12}(MeCN)_6]^{2+}$ [HL = 2,6-*bis*(hydroxylmethyl)-4-methylphenol, 1-HO-2,6-$(HOCH_2)_2$-4-MeC_6H_2], which has a maximum spin of S = 83/2, was prepared. However, this high total spin did not translate into a high energy barrier, with a U_{eff} of 4 cm^{-1} being observed.[9] The low energy barrier arises as the high overall symmetry cancels out the anisotropies of the manganese centres, and hence a ZFS of $D \sim 0$ is present in this species.[10]

In light of these findings, complexes with large anisotropies were instead targeted. The iron(I) compound $[Fe\{C(SiMe_3)_3\}_2][K(2,2,2\text{-crypt})]$ (**127**), which has two bulky alkyl groups in axial positions, promotes a large anisotropy and subsequently led to a U_{eff} of 226 cm^{-1}, despite a low total spin of S = 3/2.[11] This is the largest energy barrier yet reported for a transition metal SMM.

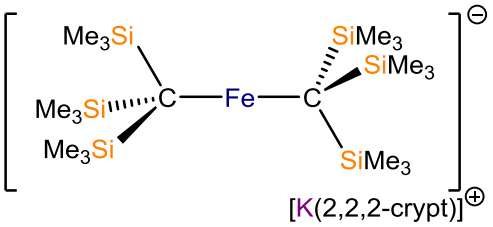


*Figure **4.2.** Complex **127**.*

4.1.2.2. Lanthanide SMMs

Complexes incorporating lanthanide (Ln) elements have the potential to be good SMMs. This is as a result of their large magnetic moments, which arise from large orbital contributions. These are essentially unquenched due to weak ligand field effects resulting from the core-like nature of 4f orbitals. Magnetic properties in Ln-SMMs are limited to the electronic ground multiplet, as large spin-orbit coupling (SOC) makes excited states thermally inaccessible for most of the lanthanides. The ground state is a combination of spin (*S*) and orbital (*L*) angular momenta, i.e. *J*, the total orbital angular momentum. From this are derived $[2J + 1]$ m_j microstates, which are influenced by ligand field effects. For lanthanides with $4f^n$, $n > 7$, the $m_j = \pm J$ state lies lowest in energy. At low temperatures, one state is favoured over the other, and repopulation is blocked by the energy barrier. When there are an odd number of valence electrons, the m_j states are doubly degenerate in the absence of a magnetic field. These states are Kramers doublets.[12]

The lowest energy doublet facilitates QTM through the energy barrier and hence repopulation of the m_j states and relaxation. QTM is diminished by axial anisotropy, though alternative relaxation processes are then employed. In order to return to the lower energy state (relax) energy must be exchanged with the lattice (following the law of the conservation of energy) by one of several ways. These include the direct process (where the energy difference is directly taken up by the lattice by a vibration or phonon), the Orbach mechanism (energy absorbed from phonons excites to the first excited state, which decays to either m_j sublevel), and the Raman process (phonons cause a spin-flip within the ground doublet using a virtual excited state).

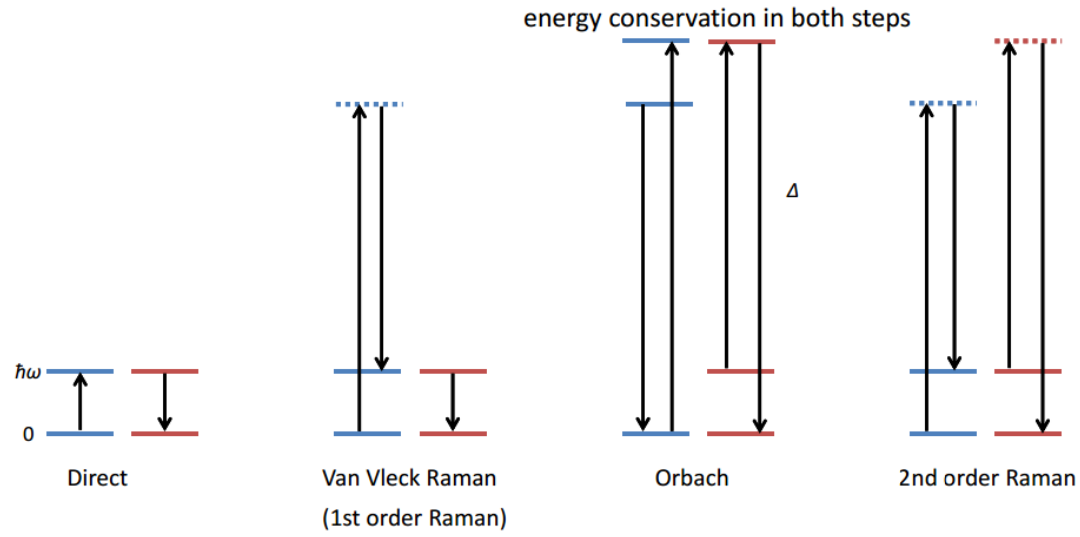


*Figure **4.3.** Relaxation processes. Adapted from [13].Blue lines represent energy levels of the lattice, and red lines the energy levels of the crystal field.*

The terbium-*bis*(phthalocyanine) sandwich complex $[Tb(Pc)_2][N(C_4H_9)_4]$ [Pc = $(C_6H_4C_2N)_4N_4$], reported in 2003, represented a breakthrough in SMM design, with a large U_{eff} of 230 cm^{-1} (*cf.* $[Fe\{C(SiMe_3)_3\}_2][K(2,2,2\text{-crypt})]$, which was reported in 2013).[14] By contrast, the dysprosium analogue has a U_{eff} of 28 cm^{-1}, due to quenching from low-lying excited states.[14] The related Tb mixed sandwich complex $[Tb(Pc)\{[p\text{-}^tBuC_6H_4O]_2C_6H_2C_2N)_4N_4\}]$ (**128**) was prepared, and has an increased energy barrier at 652 cm^{-1}, the highest observed for any SMM to date.[15]

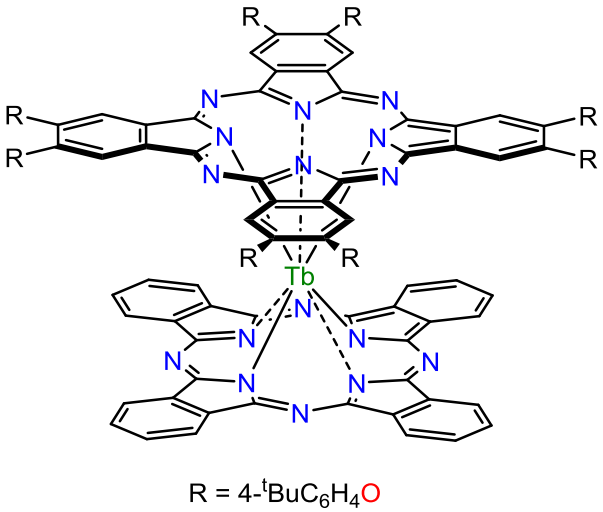


*Figure **4.4.** Complex **128**.*

The preparation of strongly axial complexes often leads to good SMMs, as has been demonstrated in the d-block (i.e. the axial, anisotropic nature of [Fe{C(SiMe$_3$)$_3$}$_2$][K(2,2,2-crypt)]). The extension of these low coordination environments to lanthanides is challenging due to their large, electropositive nature. Recently, a two coordinate samarium(II) *bis*(amide) complex has been prepared, [Sm{N(Si^{i}Pr$_3$)$_2$}$_2$] (**129**), which exhibits a linear geometry.[16] Theoretical calculations of a dysprosium analogue of this complex, [Dy{N(Si^{i}Pr$_3$)$_2$}$_2$][NCA] (**130**, NCA = non-coordinating anion), suggest that this Dy^{III} complex could have an energy barrier of *ca.* 1800 cm^{-1}. This is due to the axial geometry which prevents effective QTM, and so relaxation must occur *via* higher energy pathways. Exchange of the amide ligands to dianionic methanediide ligands, [Dy{C(Si^{i}Pr$_3$)$_2$}$_2$]$^-$ (**131**), could increase the observed energy barrier by a further factor of ~1.2 to 1.3.

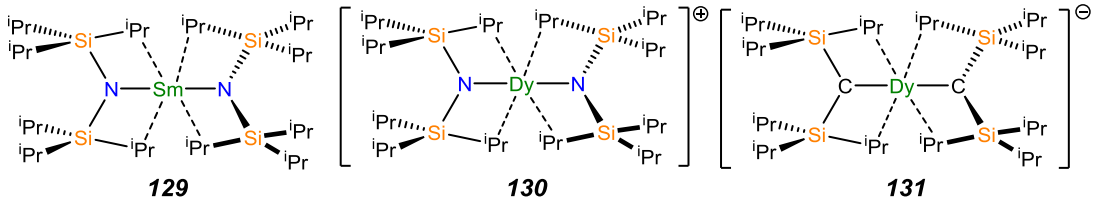


*Figure **4.5.** Complex **129** and theoretical complexes **130** and **131**.*

Whilst there has been a drive to prepare complexes with higher energy barriers, there is also a drive towards complexes with higher blocking temperatures (T_B). Currently, SMMs require liquid helium temperatures to maintain hysteresis, and it is a target within the SMM community to prepare an SMM that has a T_B at liquid nitrogen temperatures, which would begin to enable the development of SMMs towards practical applications. The more recent highest blocking temperatures were reported for the radical bridged terbium complex [{Tb(N[SiMe$_3$]$_2$)$_2$(THF)}$_2$(μ-η^2:η^2-N$_2$)][K(18C6)(THF)$_2$] (which has a T_B of 13.9 K where τ = 100 s),[17] for [Dy(BIPM^{TMS})$_2$][K(18C6)(THF)$_2$] (which has a T_B of 12 K for τ = 100 s, but clear divergence of magnetic susceptibility is maintained to 16 K)[18] and most recently for [Dy(Cy$_3$PO)$_2$(H$_2$O)$_5$]Br$_3$•2(Cy$_3$PO)•2(H$_2$O)•2(EtOH), (**132**, Cy = cyclohexyl) which maintains magnetic hysteresis to 20 K.[19] As described above, there are several measures to quantify SMMs, where different systems perform better by differing standards.

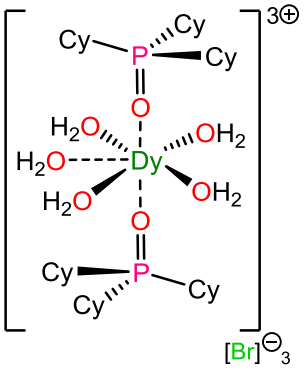


*Figure **4.6.** Complex **132**, co-crystallised molecules omitted.*

4.1.2.3. Actinide SMMs

The 5f orbitals available to actinide complexes are more radially extended than the corresponding 4f orbitals for lanthanides. This leads to larger crystal field splitting and potentially stronger exchange interactions between the actinide and other ions. However, spin-phonon coupling also becomes stronger, so there is faster spin-lattice relaxation. SMM behaviour should only possible for U^{III} and U^{V}, as U^{VI} has no valence electrons, and the $5f^2$ electron configuration for U^{IV} spin pairs at low temperature.

Initial reports of SMM behaviour for uranium were reported for uranium(III) species. The first actinide SMM reported was $[U(Ph_2BPz_2)_3]$ [**133**, Ph_2BPz_2 = diphenyl-*bis*(pyrazoyl)borate] which had an energy barrier of U_{eff} = 20 cm^{-1}.[20]

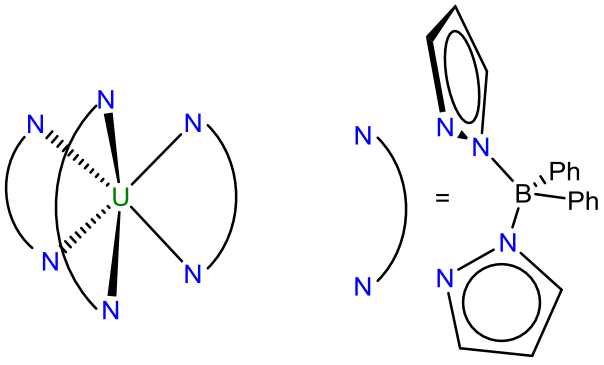


*Figure **4.7.** Complex **133**.*

Following this, the polyatomic actinide complex, [{U(BIPMH^{TMS})(I)}$_2$(μ-η^6:η^6-C_6H_5Me)] was prepared (BIPMH^{TMS} = HC{P(Ph)$_2$=*N*SiMe$_3$}$_2^-$).[21] Other uranium(III) compounds were also investigated, such as [U(I)$_3$(THF)$_4$] (U_{eff} = 13 cm^{-1}), [U{N(SiMe$_3$)$_2$}$_3$] (U_{eff} = 21.5 cm^{-1}) and [U(BIPMH^{TMS})(I)$_2$(THF)] (U_{eff} = 16.3 cm^{-1}) to investigate the effect of the ligand field on the magnetic properties of uranium(III) species.[22] These are all field induced SMMs with slow relaxation that persists in solution, with idealised symmetries of C_s, C_{3v} and C_1 respectively. These data suggest that uranium(III) complexes may inherently have SMM properties, regardless of the symmetry and ligand environment of the compound.

The uranyl(V)/manganese(II) cluster [{(U[O]$_2$[salen])$_{12}$Mn(Py)$_3$}$_6$] (**134**, salen = {CH$_2$*N*CHC$_6$H$_4$*O*}$_2^{2-}$) was prepared, and was found to have an energy barrier of U_{eff} = 98.7 cm^{-1}.[23] The SMM behaviour of the cluster is thought to originate from exchange coupling, and not necessarily as a consequence of the presence of uranyl(V) centres.

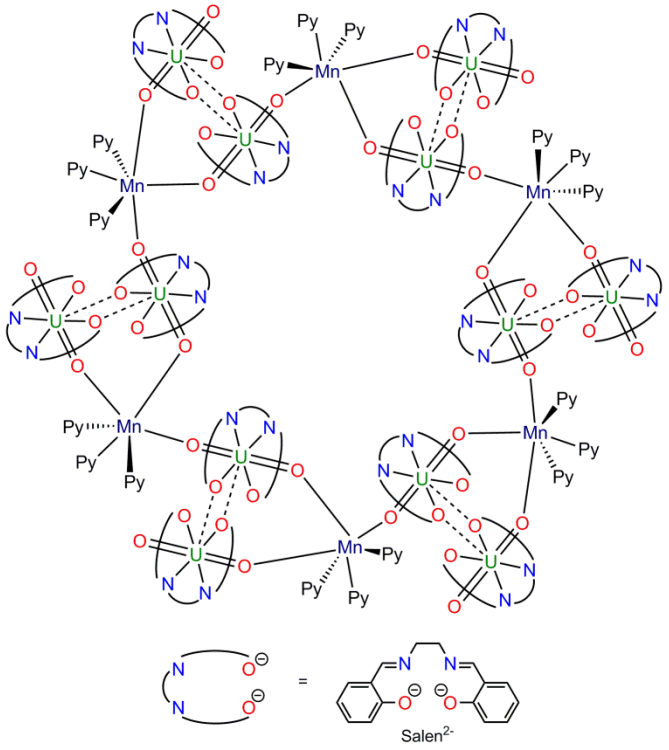


*Figure **4.8.** Complex **134**.*

Therefore, it was hypothesised that uranium(V), which has less total angular momentum than uranium(III) (ground states of $^2F_{5/2}$ and $^4I_{9/2}$ respectively), could exhibit SMM behaviour in a strongly axial environment, which would induce anisotropy. [U(Tren^{TIPS})(O)] (**122**) was the first example of a monometallic uranium(V) SMM (U_{eff} = 15 cm^{-1}),[24] which unambiguously confirms that uranium(V) complexes can be SMMs.

4.1.3. Aims

In light of the preparation of a mononuclear uranium(V) nitride, we were then interested in investigating the magnetic behaviour of our Tren–uranium(V) nitride systems, to see if they might exhibit SMM behaviour also. As these systems also feature the same strong axial ligand environment as [U(Tren^{TIPS})(O)] (**122**), these uranium(V) nitrides should also be SMMs, and therefore may also help our understanding of the magnetic behaviour of U^V centres.

What follows will therefore be an exploration of the electronic and magnetic structure of the Tren–uranium(V) nitrides, the syntheses of which were discussed in Chapter 2. Due to the time constraints required to fully characterise a compound's magnetic behaviour utilising SQUID magnetometry and EPR spectroscopy, only one congener of each crown containing formulation has been investigated. Therefore, the compounds analysed are [{U(Tren^{TIPS})(μ-N)(μ-M)}$_2$] (M = Li **106**, Na **51**, K **107**, Rb **108** and Cs **109**), [U(Tren^{TIPS})(N)[M(crown)$_2$] [M(crown)$_2$ = Na(12C4)$_2$ **52**, K(15C5)$_2$ **114**, Rb(Bn-15C5)$_2$ **116** and Cs(Bn-15C5)$_2$ **117**] and [U(Tren^{TIPS}){(μ-N)(μ-M)(crown)}] [M(crown) = Li(12C4) **118**, Na(15C5) **53**, K(Bn$_2$-18C6) **111**, Rb(18C6) **112** and Cs(18C6) **113**]. Other complexes with varying crowns (discussed in Chapter 2) have not been investigated by solid state magnetometry and EPR spectroscopy.

The magnetic data reported here was recorded, calculated and analysed by Dr N. F. Chilton, Dr F. Tuna and Prof. E. J. L. McInnes, of the Photon Science Institute at the University of Manchester.

4.2. Electronic Structure of Uranium(V)–Nitrides

4.2.1. Background

The uranium(V) ion has one unpaired electron ($5f^1$), and so does not suffer from 5f inter-electron repulsion, and therefore this series of uranium(V)–nitrides, alongside the isoelectronic oxo species [U(Tren^{TIPS})(O)], **122**,[24] are ideal candidates for the study of the electronic structure of uranium.

For this reason, the electronic structure of the published nitrides, **51**, **52** and **54** were probed with Density Functional Theory (DFT), Natural Bond Order (NBO) and Quantum Theory of Atom In Molecules (QTAIM) methods.[25,26] However, DFT suffers from static electron correlation and self-interaction errors.[27] This means that while these methods yielded results that are internally consistent, they are limited to a qualitative description.

Consequently, in order to fully understand the electronic structure of uranium(V)–nitrides, a quantitative picture needs to be developed. In order to do this, *ab initio* modelling was performed on simplified structures, and subsequently built up to the whole anion [U(Tren^{TIPS})(N)]$^-$. To do this, first the electronic structure is modelled with *ab initio* calculations, then is split by the crystal field (CF) using Complete Active Space Self-Consistent Field (CASSCF) calculations, then by spin orbit coupling (SOC).

The ground state of the uranium(V) ion ($5f^1$) is well separated (~100,000 cm^{-1}) from the first excited state ($6d^1$), with a SOC constant of $\lambda \sim 2174$ cm^{-1}.[28] As a free ion, all seven 5f orbitals are degenerate, and the excited $^2F_{7/2}$ SOC multiplet is approximately 7600 cm^{-1} above the ground multiplet ($^2F_{5/2}$). Following Hund's rule, the lowest energy *j* state, for electronic subshells that are less than half full, is the one with the lowest value of *j*, hence $^2F_{5/2}$ is the ground state, and lies below the $^2F_{7/2}$ excited state. As there is no inter-electronic repulsion, both the Russell-Saunders (*LS*) and *j-j* coupling schemes are equivalent.

4.2.2. Ab initio modelling of $[U{\equiv}N]^{2+}$

The dominant perturbation to the electronic structure of the uranium ion in the nitride complexes is the formal triple bond to the nitride ion, which has an average U≡N bond length of 1.84(4) Å. This perturbation splits the seven degenerate 5f orbitals (of the free ion). An idealised molecular orbital (MO) model for the ground state of a $[U{\equiv}N]^{2+}$ species consists of:

- two π-bonds between filled p-orbitals of the nitride ion and the two $l_z = \pm1$ ($5f_\pi$) orbitals,
- a σ-bond between a filled sp-hybridised nitride orbital and a metal-based $l_z = 0$ ($5f_\sigma$) orbital,
- a pair of non-bonding $l_z = \pm3$ ($5f_\varphi$) orbitals containing one electron,
- two non-bonding, empty $l_z = \pm2$ ($5f_\delta$) orbitals,
- two empty π* anti-bonding orbitals, and
- one empty σ* anti-bonding orbital.

These can be visualised as follows:

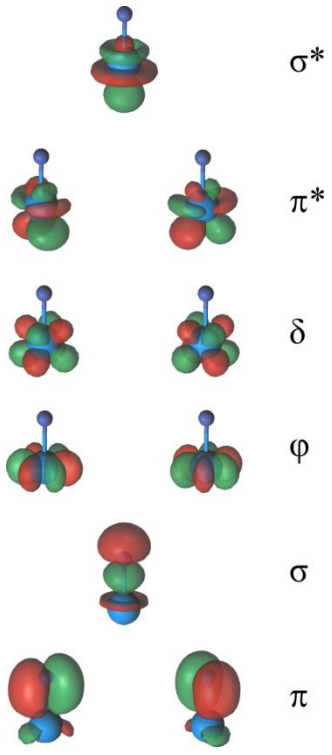


*Figure **4.9.** MOs for the $[U{\equiv}N]^{2+}$ species from ab initio calculations. U = light blue (lower), N = dark blue (upper).*

A result of the short U≡N interaction is that the π bonding orbitals are lower in energy than the σ bond combination in the MO. This arises due to partial anti-bonding character in the σ MO as a result of the annular lobes of the $5f_\sigma$ orbital.[29] This has also been observed in the uranyl dication, $[U(O)_2]^{2+}$.[30] This simplified description neglects mixing between 5f and 6d orbitals at uranium, and between U(5f) and N(2sp) orbitals, but despite this, the four non-bonding orbitals (labelled as φ and δ in figure **4.9.**) and the three anti-bonding orbitals (labelled as π* and σ* in figure **4.9.**) are mostly of metal character (> 80%). These seven orbitals can be considered metal-based,[31] and hence the states derived from $l_z = \pm1$ and 0 can represent the π* and σ* orbitals respectively (hence their description as such in figure **4.9.**).

In an axial crystal field of $C_{\infty v}$, the ordering of the metal based orbital energies results from the equatorial electron density. The order of the energies of the orbitals ($l_z = \pm3$, $l_z = \pm2$, $l_z = \pm1$, $l_z = 0$) is $E_{\pm3} < E_{\pm2} < E_{\pm1} < E_0$, and these orbitals are depicted in that order in figure **4.10.** (left, $\hat{H}_{CF(ax)}$) and in figure **4.11.a**.

The energies of these orbitals can then be estimated using CASSCF, using the average experimental bond length of 1.84(4) Å. As there is only one electron in the 5f manifold, the seven configuration state functions (CSFs) directly represent the relative orbital energies. Setting $E_z = \pm3$ to 0 cm^{-1}, $E_z = \pm2$ is found at ~1300 cm^{-1}, then $E_z = \pm1$ at ~4800 cm^{-1} and $l_z = 0$ at 6300 cm^{-1}. More precisely, these values are as follows:

*Table **4.1.** Relative energies of the seven 5f orbitals for the $[UN]^{2+}$ complex from ab initio calculations.*

CSF	$\|l_z\|$	Relative energy (cm^{-1})
1	3	0
2	3	9
3	2	1301
4	2	1302
5	1	4787
6	1	4788
7	0	6270

Combining these values with a SOC contribution ($\hat{H}_{SO}$, figure **4.10.**, i.e. coupling to ground state $^2F_{5/2}$ and excited state $^2F_{7/2}$) gives rise to 14 states ($\hat{H}_{CF(ax)+SO}$) which are all Kramers doublets (as discussed above, these are doubly degenerate m_j states in the absence of a magnetic field when occupied by an odd number of electrons).[12] These can be labelled with the j_z quantum number, which is allowed as the ligand field is uniaxial (where j is the total angular momentum quantum number, which is a combination of s and l, and j_z is the projection of j as a vector in the z axis, which requires an axial field). This coupling is visualised in figure **4.10.** The dotted red lines and dashed green lines will be discussed later on. The energies associated with those states can be found in table **4.2.**

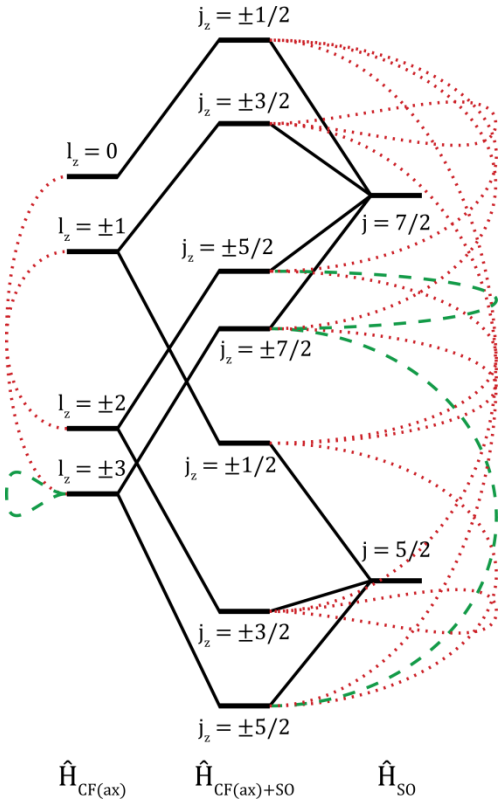


*Figure **4.10.** States arising from the $\hat{H}_{CF(ax)}$ (left), $\hat{H}_{SO}$ (right) and combined $\hat{H}_{CF(ax)+SO}$ (centre) Hamiltonians. Green dashed lines indicate states that have Δl_z or $\Delta j_z = 6$ and red dotted lines indicate states that have Δl_z or $\Delta j_z = 3$, corresponding to states that are mixed upon lowering to C_3 symmetry (vide infra).*

As can be seen by inspection of the relative energies for the seven doublets that arise from the combination of CF and SOC (table **4.2.**), the $j_z = \pm 5/2$ ground state (doublet

1) is well isolated (1934 cm^{-1}) from the j_z = ±3/2 excited state (doublet 2). The effective g_z value of the ground doublet (employing the effective *s* = 1/2 formalism) is calculated to be 4.20 (whereas g_{xy} is 0).

*Table **4.2.** Relative SO energies and effective g-values for the $[UN]^{2+}$ complex from ab initio calculations.*

Doublet	**Relative energy (cm^{-1})**	j_z	g_{xy}	g_z
1	0	±5/2	0.00	4.20
2	1934	±3/2	0.00	2.26
3	5129	±1/2	2.14	0.65
4	6866	±7/2	0.01	8.00
5	7990	±5/2	0.01	5.80
6	10876	±3/2	0.00	3.74
7	12504	±1/2	4.14	1.35

These data can be parameterised using a Hamiltonian. This is not a complex solution to the time independent Schrödinger equation, but just an effective parameterisation, which considers the one unpaired electron in this system. This electron is restricted to only 5f orbitals (i.e. $5f^1$). The Hamiltonian employed is therefore:

$$\widehat{H}_{CF(ax)+SO} = B_2^0\hat{O}_2^0 + B_4^0\hat{O}_4^0 + B_6^0\hat{O}_6^0 + \lambda\hat{l}\cdot\hat{s}$$

The Hamiltonian has uniaxial symmetry (as appropriate for $C_{\infty v}$ $[U{\equiv}N]^{2+}$), and $\hat{O}_k^q$ are Stevens Operator equivalents. K takes even values up to 2L ($^2F_{5/2}$ has L ≡ F = 3, therefore 2L = 6), and q = 0 for axial systems. The first three terms describe the crystal field, whilst the final term describes the SOC, (λ = spin-orbit coupling constant, $\hat{l}$ and $\hat{s}$ are the orbital and spin operators). This Hamiltonian predicts the energies of the orbitals based upon the following simultaneous equations, where $E_{\pm3} = 0$.

$$-15B_2^0 - 600B_4^0 - 1260B_6^0 = E_{\pm2}$$

$$-24B_2^0 - 120B_4^0 + 2520B_6^0 = E_{\pm1}$$

$$-27B_2^0 + 180B_4^0 - 3780B_6^0 = E_0$$

From the solution of those simultaneous equations, the following values are derived:

*Table **4.3.** Parameters derived from CF parameterisation of ab initio results for the $[U{\equiv}N]^{2+}$ complex.*

Parameter	Value (cm^{-1})
B_2^0	-211.8
B_4^0	3.012
B_6^0	0.008225
λ	2000

Fitting the SOC Hamiltonian then gives λ = 2000 cm^{-1} and the ground state doublet has g_z = 4.20.

4.2.3. Ab initio modelling of $[U(NH_3)(NH_2)_3(N)]^-$

Considering now the orbitals (i.e. l_z energies, without SOC), the second perturbation of the 5f orbitals (after the U≡N linkage) is the three-fold symmetric $Tren^{TIPS}$ ligand. For **106** and **108**, there is exact crystallographic three-fold symmetry, but for the other nitrides considered, this symmetry is an approximation in the solid state. To begin to model the Tren-ligand system, C_3 symmetrised $[U(NH_3)(NH_2)_3(N)]^-$ was modelled. The ammonia and three parent amide ligands mimic the face-capping amine and three pendant amide arms of $Tren^{TIPS}$.

The effects of the second perturbation are visualised in figure **4.11.**, where **a** (the energies listed in table **4.1.**, see above) represents $[U{\equiv}N]^{2+}$, whilst **b** represents symmetrised $[U(NH_3)(NH_2)_3(N)]^-$ (the energies listed in table **4.4.**).

*Table **4.4.** Relative energies of the seven 5f orbitals for the C_3 symmetrised $[U(NH_3)(NH_2)_3(N)]^-$ complex from ab initio calculations.*

CSF	$\|l_z\|$	Relative energy (cm^{-1})
1	2	0
2	2	1
3	3	43
4	3	1166
5	1	2176
6	1	2176
7	0	9649

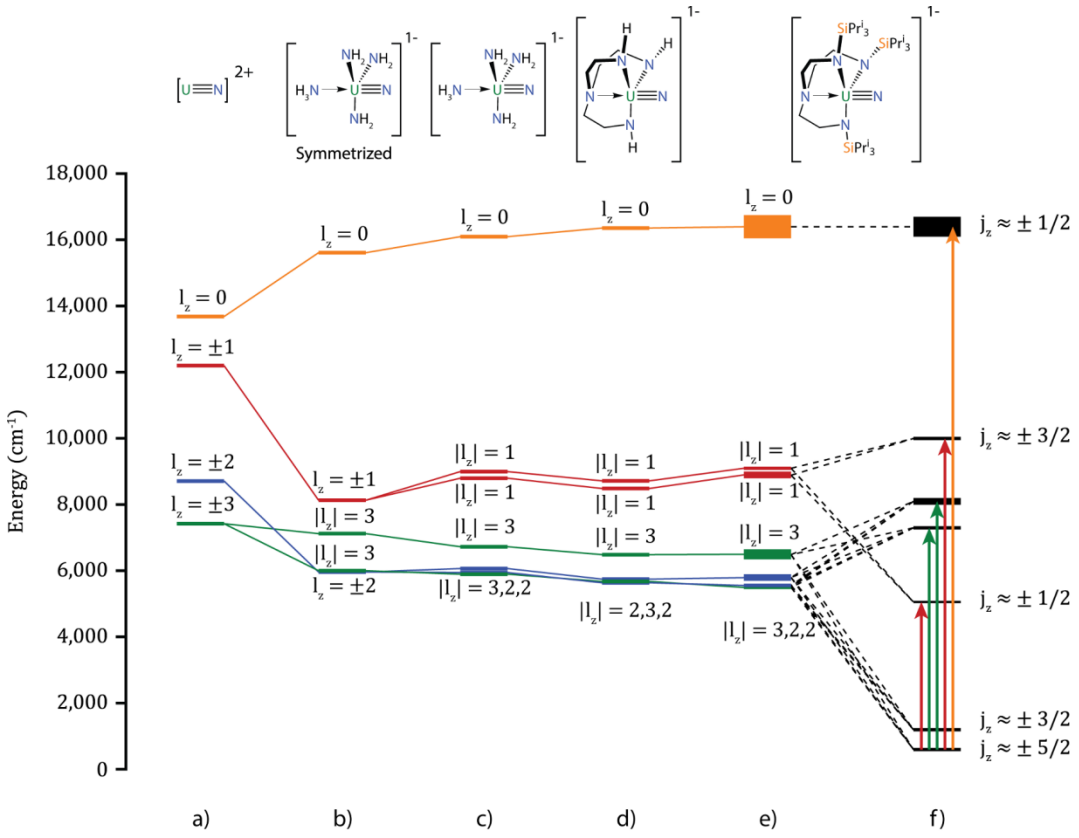


*Figure **4.11.** 5f Orbital energy diagram for model uranium(V) complexes from ab initio calculations; a) $[UN]^{2+}$, b) symmetrised $[U(NH_3)(NH_2)_3(N)]^-$, c) low symmetry $[U(NH_3)(NH_2)_3(N)]^-$, d) $[U(Tren^H)(N)]^-$, e) average dinuclear, SIP and capped nitride series for $[U(Tren^{TIPS})(N)]^-$, f) average dinuclear, SIP and capped nitride series for $[U(Tren^{TIPS})(N)]^-$ with SOC. The arrows refer to transitions within the j_z*

electronic manifold from ground to excited states and the colour references the orbital l_z parentage of the given transition.

There are three effects that can be seen on changing the environment from the axial $[U{\equiv}N]^{2+}$ to the symmetrised $[U(NH_3)(NH_2)_3(N)]^-$. Firstly, the spread of energy values is greater (l_z = 0 was 6270 cm^{-1} for $C_{\infty v}$, which increases to 9649 cm^{-1} for C_3). This is due to the additional axial amine ligand, *trans* to the nitride. Second, $l_z = \pm 3$ has split (i.e. the two orbitals are no longer degenerate) such that the two $|l_z| = 3$ are 1123 cm^{-1} apart. This is due to the mixing of the three-fold equatorial field with the $l_z = \pm 3$ orbitals (consider the shape of the $5f_\varphi$ orbitals as depicted in figure **4.9.**). Finally, $l_z = \pm 2$ (which remains degenerate) falls below $|l_z| = 3$, as a result of the destabilisation of the in-plane $l_z = \pm 3$.

These trends are carried into the orbital energies upon introduction of SOC, which again gives 7 Kramers doublets, as is the case for $[U{\equiv}N]^{2+}$. However, the first excited state for the C_3 system (still $j_z \approx 3/2$) is much less isolated than in the axial case (278 *vs* 1934 cm^{-1}). The ground state magnetism (for $j_z \approx 5/2$) is reduced to $g_z = 3.80$ (previously 4.20), and g_{xy} is no longer zero. These data are illustrated in table **4.5.**

*Table **4.5.** Relative SO energies and effective g-values for the C_3 symmetrised $[U(NH_3)(NH_2)_3(N)]^-$ complex from ab initio calculations.*

Doublet	**Relative energy (cm^{-1})**	**Approximate j_z**	**g_{xy}**	**g_z**
1	0	±5/2	0.03	3.80
2	278	±3/2	0.00	2.26
3	3334	±1/2	1.53	0.10
4	6624	-	2.21	3.40
5	7436	-	2.17	5.25
6	8155	±3/2	0.00	3.59
7	14506	±1/2	3.51	1.89

It should be noted that as $[U(NH_3)(NH_2)_3(N)]^-$ does not have $C_{\infty v}$ symmetry, j_z is no longer a good quantum number, as m_j microstates are only compatible with linear

combinations. However, we will continue to use it to describe the states resulting from SOC, as the strong axial potential of $[U(NH_3)(NH_2)_3(N)]^-$ and the subsequent compounds modelled (see below) mean that j_z is still a good approximation for these states. That being said, the third and fourth excited states (doublets 4 and 5) are not assigned approximate j_z labels due to inferences from the nitride complexes. The composition of these states, as will be discussed for models of $[U(Tren^{TIPS})(N)]^-$ (figure **4.11.f**) vary greatly across the dinuclear, SIP and capped nitride series (i.e. complexes **106**, **51**, **107**, **108** and **109**; **52**, **114**, **116** and **117;** and **118**, **53**, **111**, **112** and **113**), and therefore cannot be sufficiently well described by j_z labels.

As before we can now parameterise these states using a Hamiltonian. The first thing to consider is the loss of symmetry ($C_{\infty v}$ to C_3). In this case, we then add a B_6^6 term, as follows:

$$\hat{H} = B_2^0\hat{O}_2^0 + B_4^0\hat{O}_4^0 + B_6^0\hat{O}_6^0 + B_6^6\hat{O}_6^6 + \lambda\hat{l}\cdot\hat{s}$$

There would also be a B_6^{-6} term, however by setting our axes such that they align with the three-fold symmetry, we can remove this term (i.e. $B_6^{-6} = 0$). We would also expect to see terms with q = 3 (e.g. B_4^3, B_4^{-3}, B_6^3 and B_6^{-3}), though these become absorbed into q = 0 terms (see below).

The B_6^6 term has implications for the mixing of electronic states. Whereas before we had only q = 0 terms, we now allow q = 3 and q = 6 terms. This then allows mixing when the change in l_z or j_z (Δl_z, Δj_z) is equal to 0, 3 or 6 (e.g. $|l_z| + |l_z| = 3$). This is depicted in figure **4.10.** by the red dotted lines (Δl_z or $\Delta j_z = 3$) and the green dashed lines (Δl_z or $\Delta j_z = 6$).

For example, considering only the mixing of the axial crystal field states ($\hat{H}_{CF(ax)}$, figure **4.10.**, left), there is mixing between $l_z = \pm3$ and $l_z = 0$ ($\Delta l_z = 3$), between $l_z = \pm2$ and $l_z = \mp1$ ($\Delta l_z = 3$), and between $l_z = +3$ and $l_z = -3$ ($\Delta l_z = 6$). Mixing between the $\hat{H}_{CF(ax)+SO}$ follows the same rules, and there are many more transitions.

Figure **4.10.** is a simplified picture and does not depict mixing for Δl_z or $\Delta j_z = 0$. For example, there would be mixing between the lowest $j_z = \pm5/2$ state and the upper

$j_z = \pm 5/2$ state. This means that the lower $j_z = \pm 5/2$ state, which under $C_{\infty v}$ symmetry is derived only from $l_z = \pm 3$ and $j = 5/2$, will also be partially derived from the $j = 7/2$ SOC state and the $l_z = \pm 2$ CF state when the symmetry is lowered to C_3.

If we fit the *ab initio* orbital energies (table **4.4.**, i.e. $\lambda = 0$), then we get the CF parameters as follows:

*Table **4.6.** Parameters derived from CF parameterisation of ab initio results for the C_3 symmetrised $[UN(NH_3)(NH_2)_3]^-$ complex.*

Parameter	Value (cm^{-1})
B_2^0	-181.0
B_4^0	7.128
B_6^0	-0.7606
$\lvert B_6^6 \rvert$	1.560

We can see that B_6^6 is approximately 1% of the value of $|B_2^0|$. Using these parameters, and then varying λ so that it fits the *ab initio* SOC doublet gives $\lambda = 2022$ cm^{-1}. This gives a ground doublet g_z of 4.27 which is larger than the calculated value of 3.80 (table **4.5.**). Attempts to remedy this by inclusion of q = 3 terms (see above) gives unfeasibly large parameters. This is likely because of the large energy gap between the states being coupled by q = 3 (red dotted lines, figure **4.10.**), most of which couple to $l_z = 0$.

It is then more likely that the inconsistencies arise from the use of pure 5f orbitals, whereas the MOs have some ligand character ($\leq$ 20%, see above). This can be treated by the inclusion of an orbital reduction parameter, $0 \leq \kappa \leq 1$.[32] This results in the following Hamiltonian, with the inclusion of a Zeeman term to allow a consideration of the field dependency:

$$\hat{H} = \kappa^2 B_2^0 \hat{O}_2^0 + \kappa^4 B_4^0 \hat{O}_4^0 + \kappa^6 \left(B_6^0 \hat{O}_6^0 + B_6^6 \hat{O}_6^6 \right) + \kappa\lambda \hat{l} \cdot \hat{s} + \mu_B \left(\kappa \hat{l} + 2\hat{s} \right) \cdot B$$

If we then fix $\kappa^6 B_6^6$ (the off-axial CF term) to 1.560 (derived when $\lambda = 0$, table **4.6.**), and vary κ in order to reproduce the ground state value of g_z (4.20), we find $\kappa = 0.92$.

*Table **4.7.** Parameters derived from CF parameterisation of ab initio results for the C_3 $[UN(NH_3)(NH_2)_3]^-$ complex, including orbital reduction.*

Parameter	Value (cm^{-1})
B_2^0	-212.1
B_4^0	9.610
B_6^0	-1.335
$\lvert B_6^6 \rvert$	2.571
λ	2195
κ	0.9201

4.2.4. Ab initio modelling of [U(Tren^{TIPS})(N)]$^-$

Having now modelled the axial, $C_{\infty v}$ symmetric $[U{\equiv}N]^{2+}$ and the symmetrised $[U(NH_3)(NH_2)_3(N)]^-$, we can now calculate larger models. The models then investigated, and their corresponding orbital energies (as depicted in figure **4.11.**), were the non-symmetrised $[U(NH_3)(NH_2)_3(N)]^-$ (figure **4.11.c**), $[U(Tren^H)(N)]^-$ (figure **4.11.d**), and $[U(Tren^{TIPS})(N)]^-$ (figure **4.11.e**).

The further lowering of the symmetry (from figure **4.11.b** to **4.11.e**) does not significantly impact the orbital energies, with only small splittings being introduced to $l_z = \pm 2$ and $l_z = \pm 1$, in comparison to the large splitting observed for $l_z = \pm 3$ (figure **4.11.a** to **4.11.b**).

Combination of the orbital energies for $[U(Tren^{TIPS})(N)]^-$ (figure **4.11.e**) with the SOC contribution (figure **4.11.f**) shows remarkably little variation across the series of complexes (**106**, **51**, **107**, **108** and **109**; **52**, **114**, **116** and **117;** and **118**, **53**, **111**, **112** and **113**), except for the energies of the third and fourth excited states (as alluded to earlier). This is depicted in figure **4.11.** by the thickness of these levels for **e** and **f**, which indicates the standard deviation around the average positions across the nitride series. The variance in energies for these states comes as a result of direct mixing by the three-fold equatorial field. Consequently, these states are sensitive to mixing *via*

low symmetry CF components, i.e. small structural changes have a large impact on their energy. The energies of these states are illustrated in table **4.8.**

*Table **4.8.** Comparison between average ab initio predictions and average experimental observations of the SOC states for the series of dinuclear, SIP and capped nitride series for [U(Tren^{TIPS})(N)]$^-$. Standard deviations are given in brackets.*

SO State	***ab initio***			**Experimental**	
	Energy (cm^{-1})	**g_z**	**$g_{x,y}$**	**Energy (cm^{-1})[a]**	**g_z[b]**
$j_z \approx \pm 5/2$	0(100)	3.84(8)	0.3(2)	-	3.74(9)
$j_z \approx \pm 3/2$	600(100)	2.4(3)	0.3(2)	-	-
$j_z \approx \pm 1/2$	4460(70)	0.25(5)	1.7(1)	4700(100)	-
-	6700(100)	-	-	6060(20)	-
-	7500(200)	-	-	6900(200)	-
$j_z \approx \pm 3/2$	9400(100)	3.7(1)	0.1(1)	8900(500)	-
$j_z \approx \pm 1/2$	15800(600)	1.84(2)	3.5(1)	18000(1000)	-

[a] from UV-vis-NIR; [b] from EPR.

These predicted data can then be linked back to the experimental data collected. The collected electronic absorption spectra for terminal uranium(V)–nitrides **52**, **114**, **116** and **117**; and capped uranium(V)–nitrides **118**, **53**, **111**, **112** and **113** are plotted in figure **4.12.**, alongside vertical lines denoting the energies of the *ab initio* calculated absorptions. These spectra are also presented with a zoomed in view of the lower energy transitions in Chapter 2, Section 3.5.

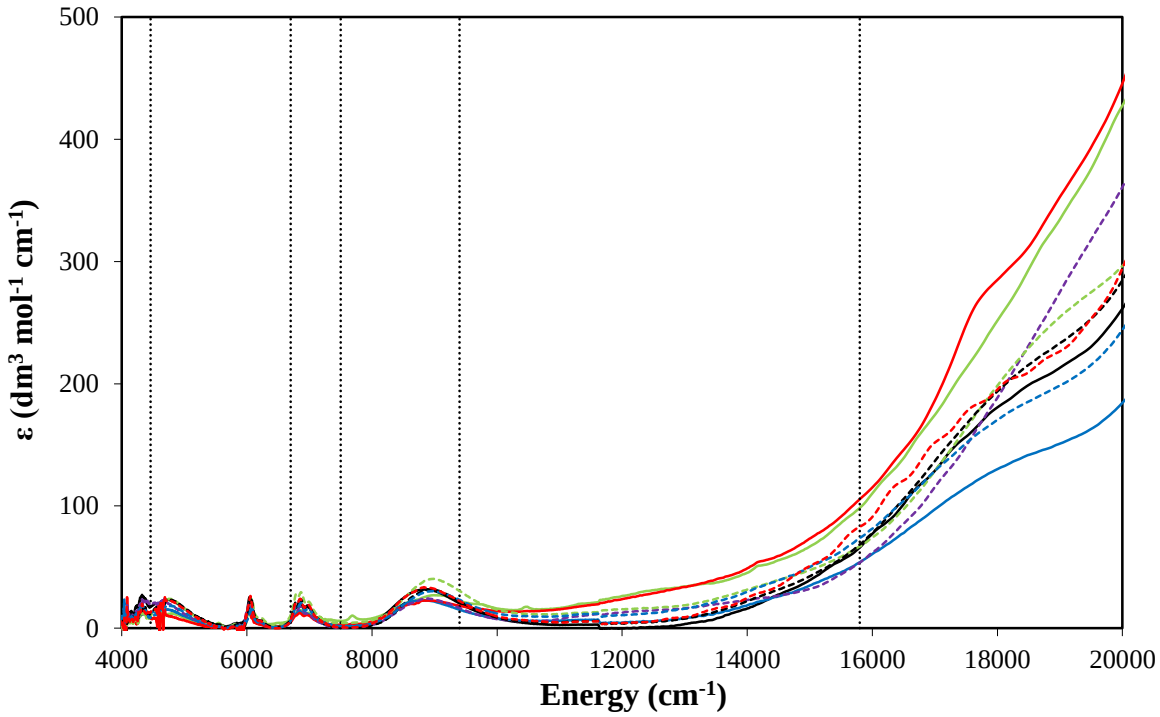


Figure ***4.12.*** *UV-vis-NIR electronic absorption spectra of terminal nitrides* ***53*** *(green),* ***111*** *(black),* ***112*** *(blue), and* ***113*** *(red); capped nitrides* ***118*** *(purple dashed)* ***52*** *(green dashed),* ***114*** *(black dashed),* ***116*** *(blue dashed) and* ***117*** *(red dashed); and the five ab initio calculated f-f transitions (black dotted).*

There is a significant degree of correlation between the calculated absorptions, and those measured experimentally, with deviations of up to *ca*. 10^3 cm^{-1} (2.9 kcal mol^{-1}). The discrepancies between these data can be attributed to the subtle differences arising from the calculation of these transitions in the gas phase, *versus* their experimental origin in the solution phase. Poor quality data (< 4500 cm^{-1}) are due to solvent subtraction errors.

The transitions that are observed are depicted as arrows in figure **4.11.f**. The reader is invited to recall the MO diagram presented in Chapter 2 (see Section 3.5., figure **2.15.**), and now it can be seen how such an MO was derived. As was discussed in Chapter 2, the transition of the smallest energy does not fall within the UV-vis-NIR range, and therefore is not observed (transition to $j_z \approx \pm 3/2$, 600(100) cm^{-1}).

The linewidths of all the nitrides investigated follow a consistent pattern, from low to high energy, of broad, sharp, sharp, broad, and very broad (a shoulder on the

charge transfer band). As calculated by *ab initio* methods (and depicted in figure **4.11.e** and **4.11.f**), these are transitions to excited SO states derived from $|l_z| = 1$ ($j_z \approx \pm 1/2$), $|l_z| = 2$ or 3 (unlabelled), $|l_z| = 2$ or 3 (unlabelled), $|l_z| = 1$ ($j_z \approx \pm 3/2$), and $|l_z| = 0$ ($j_z \approx \pm 1/2$). Broad transitions in figure **4.12.** are to excited states with $|l_z| = 1$ or 0 parentage (which represent formal anti-bonding interactions with respect to the nitride, figure **4.9.**). Sharp transitions involve $|l_z| = 2$ or 3, which are non-bonding. These anti-bonding interactions would be expected to be more susceptible to vibrational broadening (more so for $l_z = 0$ than $l_z = \pm 1$) than the non-bonding interactions, and hence these transitions are broader, and the theoretical picture is consistent with the theory.

From these results, we can see that there are two low-lying SO coupled doublets, $j_z \approx \pm 5/2$ and $j_z \approx \pm 3/2$, which are within a few hundred wavenumbers of each other, though separated from the other doublets by ~4000 cm^{-1}. This small calculated energy gap is of the same order of magnitude as the standard deviations calculated for some of these states (table **4.8.**). It is therefore possible that the actual ordering could be reversed, when compared to that derived by *ab initio* methods.

The lowest three orbital energies were found to be extremely close. Consequently, small inaccuracies in computational method afford exaggerated errors upon combination with SOC. It is then possible for the ground doublet to vary across the investigated nitrides. In order to determine the ground state of these nitrides, their magnetic data must be investigated.

4.3. Magnetic Structure of Uranium(V)–Nitrides

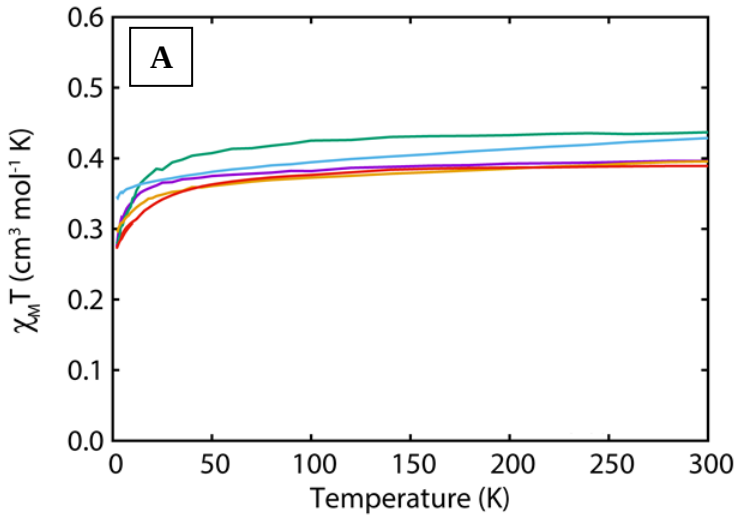
4.3.1. Magnetic measurements of uranium(V)–nitrides

All compounds (dinuclear nitrides **106**, **51**, **107**, **108** and **109**, terminal nitrides **52**, **114**, **116** and **117**, and capped nitrides **118**, **53**, **111**, **112** and **113**) were investigated by SQUID (Super-conducting QUantum Interference Device) methods, and at room temperature their $\chi_M T$ values per uranium are all within the narrow range of 0.38 – 0.49 cm^3 K mol^{-1}, where χ_M is the molar magnetic susceptibility, and T is the temperature. Values were recorded at 0.1 T applied magnetic field, and correspond to 1.7 – 2.0 μ_B mol^{-1} (for comparison to the Evans' method room temperature

solution magnetic moments reported in Chapter 2, Section 3.5., which range 1.58 – 2.72 μ_B mol^{-1}). As was discussed previously, these values are towards the lower end of magnetic moments associated with uranium(V) species, where literature values range from 0.25 – 1.3 cm^3 K mol^{-1} (1.4 – 3.2 μ_B mol^{-1}).[33] These values are lower as a result of the strong crystal field imposed by the nitride.

The χ_MT values decrease slowly on cooling (in the high temperature range). The terminal nitride complexes (**52**, **114**, **116** and **117,** figure **4.13.b**) then decrease more rapidly below *ca.* 50 K, reaching 0.1 – 0.2 cm^3 K mol^{-1} at 2 K. The dinuclear and capped nitrides (**106**, **51**, **107**, **108** and **109**, figure **4.13.a,** and **118**, **53**, **112** and **113,** figure **4.13.c**) decrease more slowly, reaching only 0.3 – 0.4 cm^3 K mol^{-1} at 2 K. This is most noticeable for **107** (figure **4.13.a**) and **53** (figure **4.13.c**), which exhibit very little temperature dependence (only a very small reduction in χ_MT). Complex **111** (figure **4.13.c**) is an outlier to this trend, which although a capped nitride, behaves more like the terminal nitride series (i.e. χ_MT decreases more rapidly below 50 K).

These magnetisation data are illustrated in figure **4.13.**



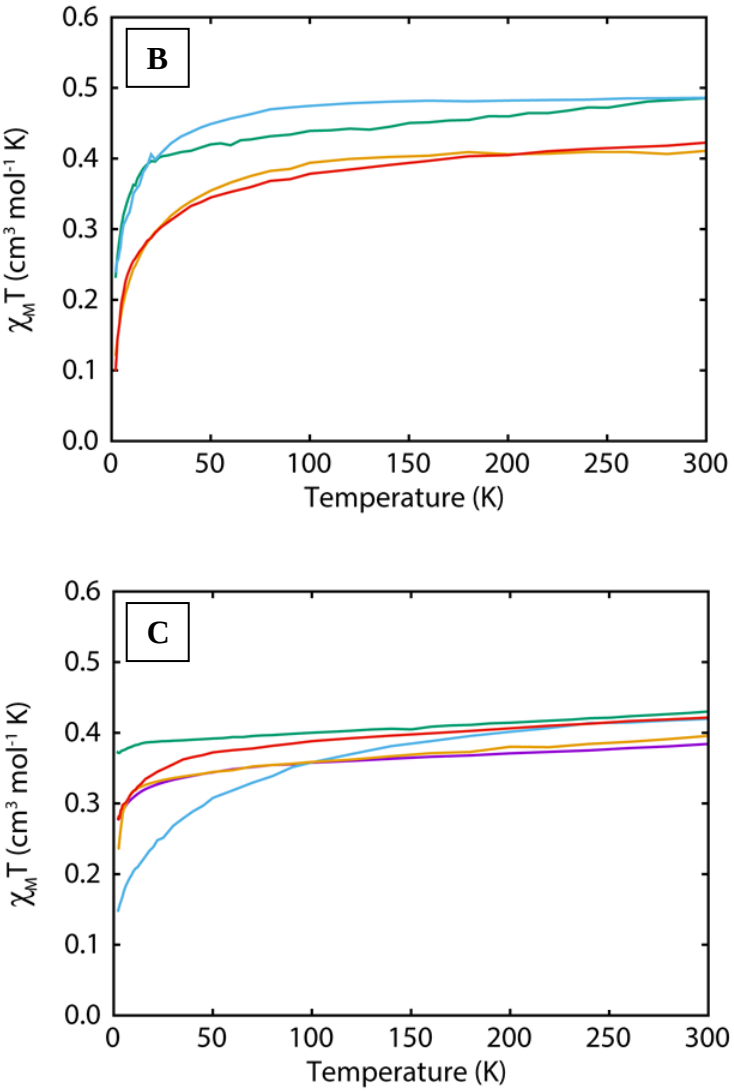


*Figure **4.13.** Experimental $\chi_M T$ vs T curves in a 0.1 T DC field; **A**: **106** (purple), **51** (green), **107** (blue), **108** (orange) and **109** (red), **B**: **52** (green), **114** (blue), **116** (orange) and **117** (red), and **C**: **118** (purple), **53** (green), **111** (blue), **112** (orange) and **113** (red). All data is shown per uranium.*

As we know from the *ab initio* calculations described above, low-lying excited states exist for these uranium(V)–nitrides. A more accurate measurement of $\chi_M T$, when such states exist, can be gained from the in-phase component of the ac susceptibility $\chi_M' T$. This is because the differential susceptibility is measured directly by the small oscillating field (*ca*. 1.5 G), i.e. magnetism can be derived from the initial gradient of the plots of M(H), as at small field the plots are assumed to be linear, and hence the gradient of M corresponds to χ (i.e. $\chi = \delta M/\delta H$).

The frequency independent part of $\chi_M'T(T)$ for these complexes in these plots falls into three groups. For the **107**, **108**, **109**, **118**, **53**, **112** and **113** (i.e. the heavier dinuclear complexes and capped nitrides excluding **111**), the frequency independent part of $\chi_M'T(T)$ plateaus at low temperatures in the range 0.27 – 0.37 cm^3 K mol^{-1}. This implies that the ground Kramers doublet is isolated under these conditions. A representative plot for group one is illustrated in figure **4.14.**

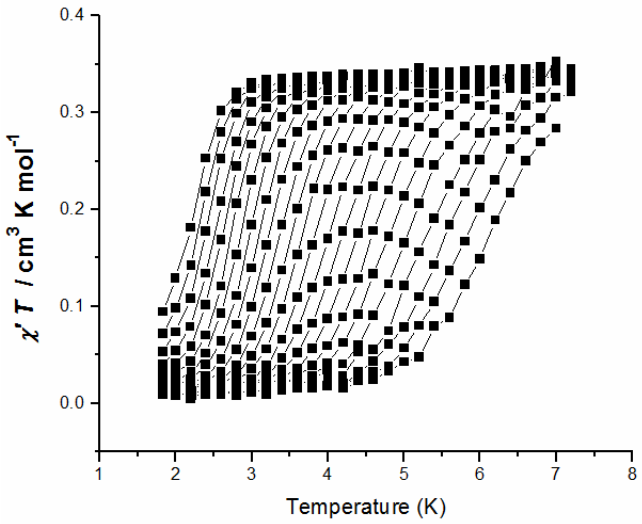


*Figure **4.14.** Experimental $\chi_M'T$ for **113** recorded under a 0.1 T field. Lines just join the points.*

A second group includes **52**, **114**, **116**, **117** and **111** (i.e. the terminal uranium nitrides and **111**), which do *not* plateau at low temperatures. This indicates that the ground Kramers is less well isolated, and therefore that the first excited doublet is closer in energy. Extrapolation of the data to 0 K for the second group gives significantly lower values (*ca.* 0.1 – 0.2 cm^3 K mol^{-1}) than for the first group (which plateaued at 0.27 – 0.37 cm^3 K mol^{-1}). This implies that the lowest doublet in the second group is less magnetic than the lowest doublet in the first group. A representative plot for group two is illustrated in figure **4.15.**

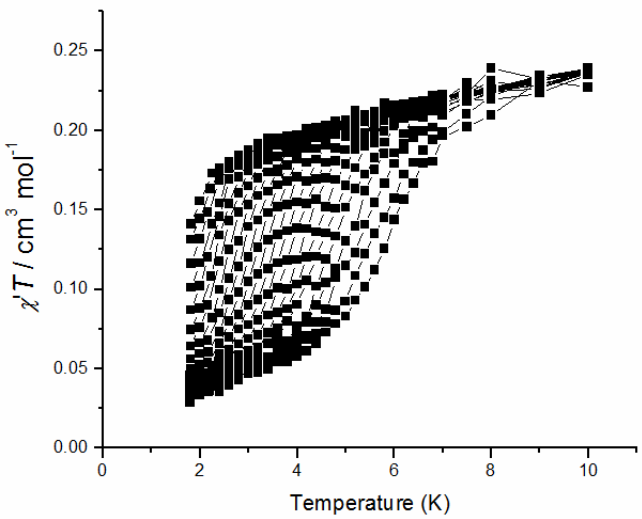
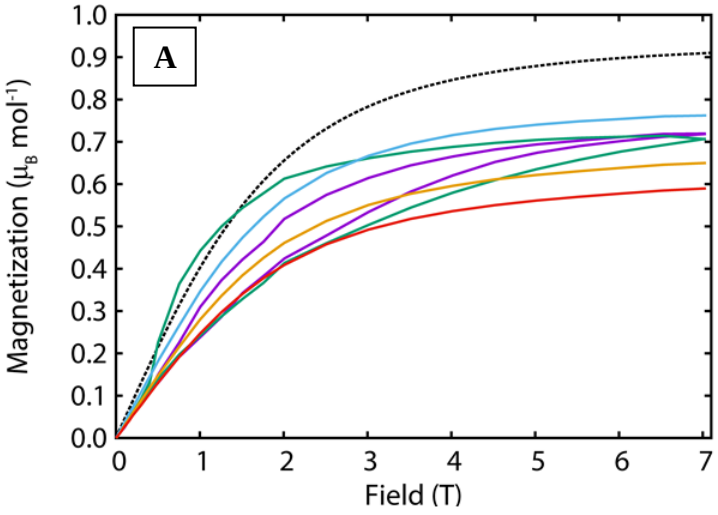


*Figure **4.15.** Experimental χ_M'T for **117** recorded under a 0.1 T field. Lines just join the points.*

The third group includes **106** and **51**. These behave differently to the other dinuclear species (i.e. **107**, **108**, **109**, which are in group one). There is no plateau in χ_M'T(T), which is highly sloped (tending towards 0.29 cm^3 K mol^{-1}, higher than for group two), and the magnetisation data exhibits hysteresis which collapses below 0.5 T.

These trends, and allocation of these complexes into three groups, are also visible in the plots of low temperature magnetisation as a function of applied field (figure **4.16.**). Complexes in group one reach 0.6 – 0.8 μ_B mol^{-1} at 1.8 K and 7 T, whilst group two reach lower values, between 0.3 – 0.6 μ_B mol^{-1}. The hysteresis described for group three can be observed in these plots (figure **4.16.a**). These magnetisation data are illustrated in figure **4.16**.



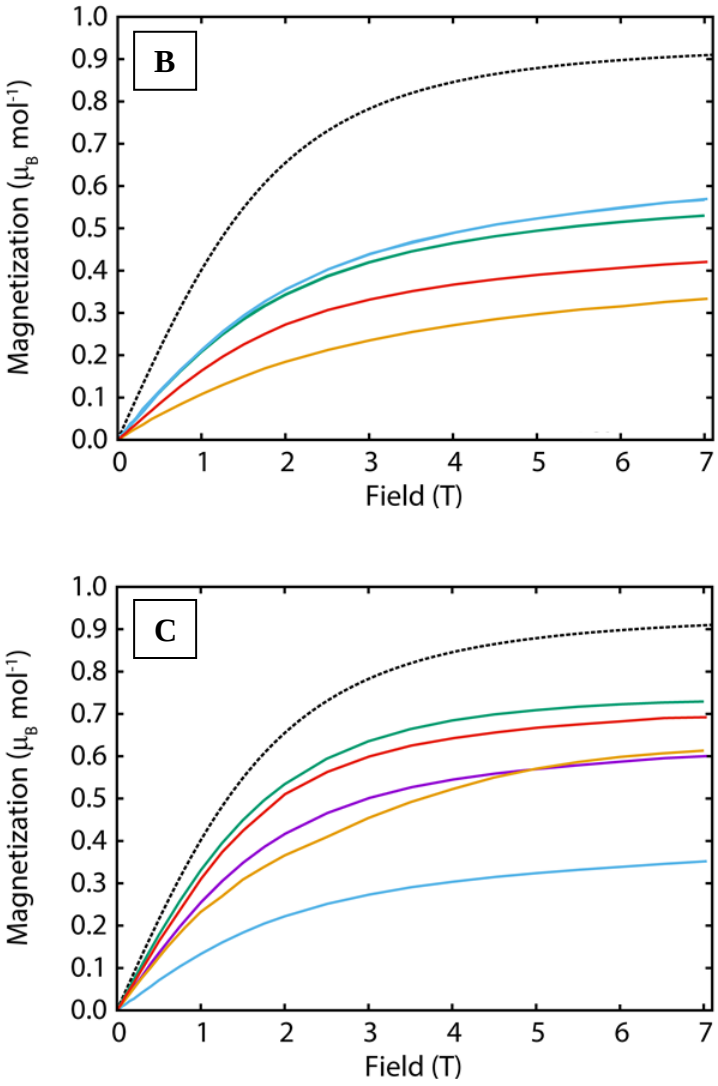


Figure ***4.16.*** *Experimental magnetization curves at 1.8 K;* ***A****:* ***106*** *(purple),* ***51*** *(green),* ***107*** *(blue),* ***108*** *(orange) and* ***109*** *(red),* ***B****:* ***52*** *(green),* ***114*** *(blue),* ***116*** *(orange) and* ***117*** *(red), and* ***C****:* ***118*** *(purple),* ***53*** *(green),* ***111*** *(blue),* ***112*** *(orange) and* ***113*** *(red). The black dashed curves gives expected magnetization for* $j_z \approx \pm 5/2$ *state with* $g_{xy} = 0$ *and* $g_z = 3.74$*. All data is shown per uranium.*

Inspection of the out-of-phase susceptibility (χ_M'') plots as a function of frequency and temperature show clear peaks. This is indicative of slow relaxation of the magnetisation, and therefore these materials are behaving as SMMs. A representative plot is illustrated in figure **4.17.**

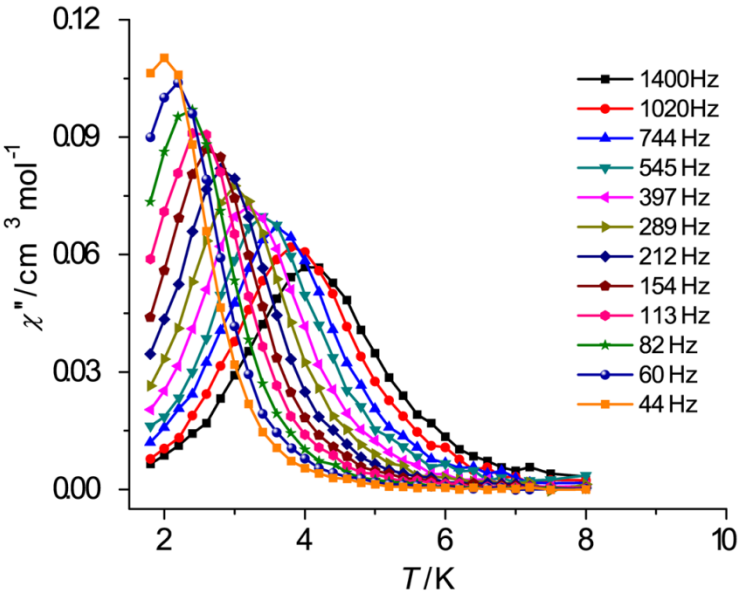


*Figure **4.17.** Experimental χ_M"T for **109** recorded under a 0.1 T field. Lines just join the points.*

Hysteresis is only observed in M(H) experiments for compounds in group three **(106** and **51**), as described above (figure **4.16.a**). This is thought to be related to the U···U exchange interactions observed by EPR spectroscopy (the observance of two transitions in the spectrum, figure **4.18.**).

4.3.2. EPR studies of uranium(V)–nitrides

Low temperature EPR studies allow us to determine the nature of the ground state, which, as discussed above, is predicted by *ab initio* calculations to be $j_z \approx \pm 5/2$, though $j_z \approx \pm 3/2$ is low-lying and within the errors of these calculations, and could therefore feasibly be the ground state. As these doublets are well isolated from the other excited state doublets (1000s of wavenumbers), they will dominate the magnetic properties of these uranium(V)–nitrides.

The low temperature EPR for terminal nitrides **52**, **114**, **116** and **117**, capped nitrides **118**, **53**, **111**, **112** and **113**, and dinuclear nitrides **107**, **108** and **109** give a $g_z \approx 3.74(9)$ (table **4.8.**), with $g_{xy} < 0.5$. A representative EPR spectrum is shown in figure **4.18.** for **53** ($g_z = 3.747$).

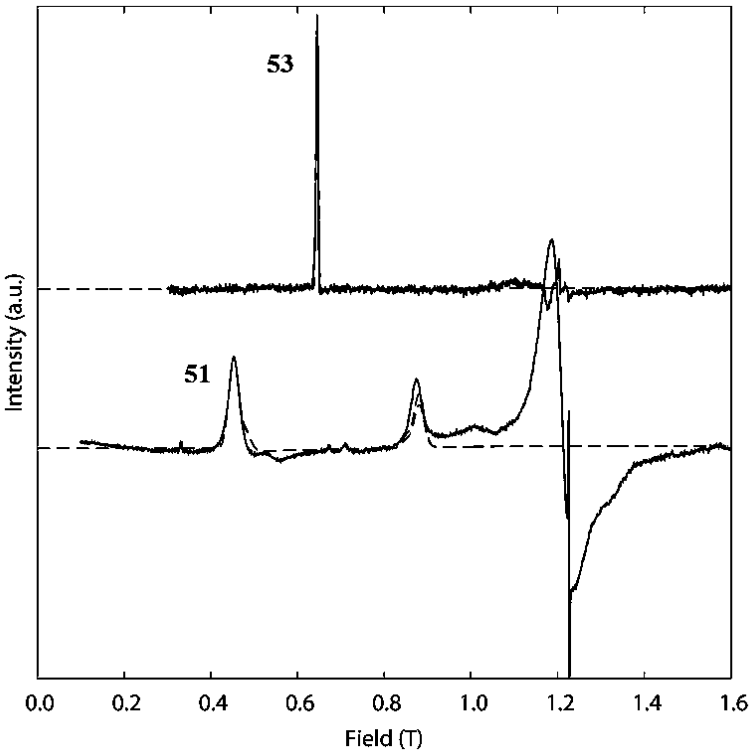


*Figure **4.18.** Q-band EPR spectra of **53** recorded at 5 K at a frequency of 33.937 GHz and **51** recorded at 7 K and 33.0787 GHz. Dotted lines represent the simulated fittings of the spectra, using the Hamiltonian equations described above.*

As described above, the EPR spectra for **106** and **51** feature two transitions, in contrast to the one transition observed for other EPR spectra (figure **4.18.**). This is assigned to exchange coupling between the two co-linear U≡N units in these complexes.

The *ab initio* calculations predicted g_z of 3.84(8) for $j_z \approx \pm 5/2$, and g_z of 2.4(3) for $j_z \approx \pm 3/2$ (table **4.8.**). We therefore assume that the EPR spectra arise from the $j_z \approx \pm 5/2$ state, which we also assumed to be the ground state. However, assignment of $j_z \approx \pm 5/2$ as the ground state does not agree with the magnetic data in all cases, which shows that magnetisation decreases with decreasing temperature. If $j_z \approx \pm 5/2$ were the ground state, then as it becomes more populated with decreasing temperature (i.e. low-lying $j_z \approx \pm 3/2$ becomes depopulated), then it should become more magnetic.

The calculated powder magnetisation for an isolated $j_z \approx \pm 5/2$ ground state doublet, with $g_z = 3.74$, $g_{xy} = 0$, is 0.90 μ_B mol^{-1} (black dotted curves, figure **4.16.**). The

powder $\chi_M'T$ value is 0.44 cm^3 K mol^{-1}. By comparison, the values for an isolated $j_z \approx \pm 3/2$ doublet with $g_z = 2.40$, $g_{xy} = 0$, are 0.55 μ_B mol^{-1} and 0.18 cm^3 K mol^{-1}. The calculated data for isolated $j_z \approx \pm 3/2$ agree well the spectra for group two, which range 0.33 – 0.53 μ_B mol^{-1}, and have extrapolated 0 K $\chi_M'T$ values of 0.12 – 0.22 cm^3 K mol^{-1}. If an uncertainty in g_z is included in the calculation, such that $g_z = 2.0$, then the calculated values fall to 0.45 μ_B mol^{-1} and 0.13 cm^3 K mol^{-1}. As the values for group two coincide with those predicted for $j_z \approx \pm 3/2$, it would appear that $j_z \approx \pm 3/2$ is the ground state for group two, and not $j_z \approx \pm 5/2$, as was previously predicted by *ab initio* calculations.

However, $j_z \approx \pm 5/2$ must still be low-lying, to the order of only 10s of cm^{-1} higher than $j_z \approx \pm 3/2$, as there is a temperature dependence in the plots of $\chi_M T$. Therefore, as the EPR spectra are all the same (across **52**, **114**, **116** and **117**, capped nitrides **118**, **53**, **111**, **112** and **113**, and dinuclear nitrides **107**, **108** and **109**), $j_z \approx \pm 5/2$ must be substantially populated at temperatures less than 10 K.

Considering then the compounds in group one, which range 0.6 – 0.75 μ_B mol^{-1} [from M(H) plots], and have extrapolated 0 K $\chi_M'T$ values of 0.26 – 0.37 cm^3 K mol^{-1} per uranium [from $\chi_M'T$(T) plots], there are only two compounds which do not show a temperature dependence in $\chi_M T$: **107** and **53**. These compounds have the highest magnetic moments in figure **4.16.** (**a** and **c**, respectively), and therefore approach the calculated value of 0.90 μ_B mol^{-1} (black dotted lines in M(H) plots). Coupled with the absence of temperature dependence, these compounds must therefore have a $j_z \approx \pm 5/2$ ground state.

As a result of the temperature dependent nature of the rest of the compounds in group one, (**108**, **109**, **118**, **112** and **113**), and also group two, the $j_z \approx \pm 3/2$ doublet is therefore the suggested ground state. The $j_z \approx \pm 5/2$ doublet must however be a very low-lying excited state. This means that despite the differing $\chi_M'T$(T) plots, which either plateau or are sloping, all compounds in groups 1 and 2, except **107** and **53**, have the same ground state: $j_z \approx \pm 3/2$.

We estimated the separation of the two lowest lying doublets by simultaneously fitting the temperature dependent $\chi_M T$ data (figure **4.11.**), with the experimental data (EPR, optical and magnetic) and the CF Hamiltonian, (as described in Section 2.3.):

$$\hat{H} = \kappa^2 B_2^0 \hat{O}_2^0 + \kappa^4 B_4^0 \hat{O}_4^0 + \kappa^6 \left(B_6^0 \hat{O}_6^0 + B_6^6 \hat{O}_6^6 \right) + \kappa\lambda \hat{l} \cdot \hat{s} + \mu_B \left(\kappa \hat{l} + 2\hat{s} \right) \cdot B$$

Using the PHI software,[34] we were able to find fits with small B_6^6 values (0.01 cm^{-1}) though considering the mixing of l_z = ±3 from the *ab initio* calculations, such values seem unlikely. Therefore, as had been observed previously (table **4.6.**), we set B_6^6 to be 1% of the value of B_2^0. The following parameters (table **4.9.**) were derived from the equation above.

*Table **4.9.** Parameters derived from fitting experimental data with CF and SO model. [a] Fixed at 1% of $|B_2^0|$; [b] Fixed at the values derived from the EPR with an effective s = 1/2 model (except for **51** and **114**).*

	Dinuclear Nitrides				**Terminal Nitrides**	
Parameter	**51**	**107**	**108**	**109**	**52**	**114**
B_2^0 (cm^{-1})	-353.7	-341.7	-331.8	-332.1	-322.6	-322.8
B_4^0 (cm^{-1})	17.36	14.89	15.75	15.78	15.11	15.36
B_6^0 (cm^{-1})	-2.138	-2.009	-1.910	-1.916	-1.810	-1.835
$\|B_6^6\|$ (cm^{-1})[a]	3.537	3.417	3.318	3.321	3.226	3.228
λ (cm^{-1})	2121	2078	2112	2111	2110	2112
κ	0.8845	0.9004	0.9027	0.9025	0.9112	0.9011

	Terminal Nitrides		**Capped Nitrides**				
Parameter	**116**	**117**	**118**	**53**	**111**	**112**	**113**
B_2^0 (cm^{-1})	-274.9	-325.8	-340.0	-331.7	-324.5	-319.0	-321.7
B_4^0 (cm^{-1})	11.54	15.60	16.11	14.14	15.42	15.03	15.34
B_6^0 (cm^{-1})	-1.182	-1.874	-2.051	-1.761	-1.781	-1.699	-1.753
$\|B_6^6\|$ (cm^{-1})[a]	2.749	3.258	3.400	3.317	3.245	3.190	3.217
λ (cm^{-1})	1956	2118	2107	2054	2115	2117	2121
κ	0.9681	0.8994	0.9072	0.9288	0.9030	0.9032	0.8968

As we can model all the experimental data with a single model (table **4.9.**), we can now compare our experimental electronic structure to our theoretical electronic structure (table **4.8.**, Section 2.4.). In terms of orbital energies (*cf.* figure **4.11.e**, Section 2.3.), the barycentre of l_z = ±3 is 800(200) cm^{-1} above the barycentre of the

$l_z = \pm 2$ pair. The $l_z = \pm 1$ pair are at 3500(200) cm^{-1}, and $l_z = 0$ is at 13800(400) cm^{-1}. The large uncertainties listed account for the variation of these experimentally derived values, and this is illustrated in figure **4.11.e** by the thickness of the lines representing these orbitals. The splitting of the $l_z = \pm 3$ pair is 1290(70) cm^{-1}, except for **116**, where it is 1630 cm^{-1}. This then means that the energy gap between the lowest lying orbitals is only 200 – 300 cm^{-1} (0.6 – 0.9 kcal mol^{-1}).

Addition of SOC (*cf.* figure **4.11.f**, Section 2.3.) then brings us to the two different ground states. For **107** and **53**, the ground state is $j_z \approx \pm 5/2$, with $j_z \approx \pm 3/2$ at 300 – 400 cm^{-1} (as determined above). The energy of $j_z \approx \pm 3/2$ is poorly defined as there is no direct experimental handle (as it is EPR silent, see below, and of too low an energy to be observed by UV-vis-NIR electronic absorption spectra, see above, Section 2.4.). For the other nitrides (from group one: **108**, **109**, **118**, **112** and **113**, and group two: **52**, **114**, **116**, **117** and **111**), which have a $j_z \approx \pm 3/2$ ground state doublet, the $j_z \approx \pm 5/2$ first excited state doublet lies at 7 – 46 cm^{-1}. This value is defined by the temperature dependence of $\chi_M T$ *vs* T plots (figure **4.13.**). The experimentally determined energies of the higher energy excited states, whose ordering is discussed above, are listed in table **4.8.**, (see Section 2.4.).

The EPR selection rule is $\Delta m_j = \pm 1$. If you consider the doublet $j_z \approx \pm 5/2$, it has two states, α and β. As a result of mixing under q = 6 (figure **4.10.**, green dashes), $\alpha \approx a|+5/2\rangle + b|-7/2\rangle$ and $\beta \approx c|-5/2\rangle + d|+7/2\rangle$ (where $|m_j\rangle$ represents a pure state). There can therefore be a transition between α and β, as there are terms that are separated by $\Delta m_j = \pm 1$ (those with a factor of a and d, and b and c). Consequently, $j_z \approx \pm 5/2$ is EPR active. By contrast, $j_z \approx \pm 3/2$ is EPR silent as it does not mix under q = ±6, and under q = ±3, the $j_z \approx \pm 3/2$ doublet only mixes with the other $j_z \approx \pm 3/2$ doublet (red dots, figure **4.10.**). No further mixing arises on addition of SOC. There is therefore no $\Delta m_j = \pm 1$ component, which is required for a state to be EPR active, and so $g_{xy} = 0$, and the state is EPR silent.

We can compare the range of energies of the 5f orbitals of our series of uranium(V)–nitrides [13800(400) cm^{-1}] to well-characterised uranium(V) octahedral species, $[U(X)_6]^-$. For the literature species, the 5f orbitals span 11361 (X = F), 6307 (X =

Cl), 5310 (X = Br), 6800 (X = R, alkyl), 8500 (X = OR, alkoxide), 7400 (X = NR_2, amide) and 6900 cm^{-1} (X = NCR_2, ketimide).[35,36] The 5f orbitals of the nitride series span a considerably larger range than the octahedral complexes, which results from the stronger axial crystal field present in the nitride complexes. As our Hamiltonian includes an orbital reduction term (κ), we compare our κλ [table **4.9.**, 1900(20) cm^{-1}] to the reported ζ values [1910(70) cm^{-1}], and find that despite the difference in 5f orbital energy span, the SOC coupling constants are nearly identical.[35,36]

The EPR values predicted by the model for $j_z \approx \pm 5/2$ are $3.7 < g_z < 4.0$ and $0.14 < g_{xy} < 0.18$, and so as g_{xy} is non-zero, $j_z \approx \pm 5/2$ is predicted to be EPR active (see above). Contrastingly, for $j_z \approx \pm 3/2$, the values are $1.9 < g_z < 2.2$ and $g_{xy} = 0$, so this doublet is predicted to be EPR silent. The *ab initio* calculations (table **4.8.**), predicted a non-zero value for g_{xy} for $j_z \approx \pm 3/2$, and this is due to low symmetry effects. These g values are consistent with experiment, as we see no EPR features corresponding to the $j_z \approx \pm 3/2$, regardless of the ground state.

4.3.3. Comparison of uranium(V)–nitrides with [U(Tren^{TIPS})(O)], 122

The series of uranium(V)–nitride complexes, [U(Tren^{TIPS})(N)]$^-$, can be compared to the known uranium(V)–oxo complex, [U(Tren^{TIPS})(O)] (**122**), with which it is isoelectronic.[24] The χ_M′T(T) plot for **122** plateaus at 0.18 cm^3 K mol^{-1} (like the nitrides in group one, see for example the plot for **113**, figure **4.14.**), and the M(H) plot for **122** saturates at M = 0.52 μ_B mol^{-1} at 1.8 K and 7K (*cf.* figure **4.16.**). Complex **122** is EPR silent, which indicates that the ground state is the well isolated $j_z \approx \pm 3/2$ doublet, in contrast to the nitrides, which have a ground state of $j_z \approx \pm 5/2$ (**107** and **53**), or $j_z \approx \pm 3/2$, where the $j_z \approx \pm 5/2$ first excited state is near degenerate (all other nitrides investigated).

This can be explained in terms of the CF. Complex **122** has a weaker axial field than the nitrides as a result of the U=O double bond strength in comparison to the U≡N triple bond in the nitrides, whilst the equatorial field remains unchanged as the Tren^{TIPS} ligand is unchanged. This means that the $l_z = \pm 2$ orbitals will be stabilised relative to the $l_z = \pm 3$ as a result of the weaker axial field (figure **4.19.h**), and

subsequently, the $j_z \approx \pm 3/2$ Kramers doublet will be stabilised relative to $j_z \approx \pm 5/2$ after SOC (figure **4.19.g**).

Ab initio calculations were performed on **122** in an analogous manner to the uranium(V)–nitrides discussed previously (see Section 2), and these are listed in table **4.10.**, and illustrated in figure **4.19.** Figures **4.19.g** and **4.19.h** can therefore be compared directly to figures **4.11.f** and **4.11.e** (see Section 2.3.), which are the averaged uranium(V)–nitride orbital energies, both with and without SOC (respectively).

The *ab initio* calculations reveal that the ground state of **122** is $j_z \approx \pm 3/2$, with $g_z = 2.27$. The first excited state is $j_z \approx \pm 5/2$, with $g_z = 3.89$. This first excited state is well-isolated from the ground state, at 683 cm^{-1}. The next excited state lies several thousand wavenumbers above this, at 4417 cm^{-1}. Relative to the nitride series, the $j_z \approx \pm 3/2$ doublet in **122** has been stabilised by *ca.* 1500 cm^{-1}. Although there is some variation in the energies of the states within the nitride series, these differences are subtle in comparison to the difference between the uranium(V)–oxo and the uranium(V)–nitrides.

*Table **4.10.** Relative SO energies, and effective g-values, for [U(Tren^{TIPS})(O)] from ab initio calculations.*

Doublet	**Relative energy (cm^{-1})**	**g_1**	**g_2**	**g_3**
1	0	2.27	0.12	0.08
2	683	3.89	0.16	0.12
3	4417	0.10	1.43	1.53
4	6648	4.80	1.26	1.30
5	8391	6.74	1.09	1.39
6	9101	3.70	0.05	0.16
7	16819	1.87	3.50	3.47

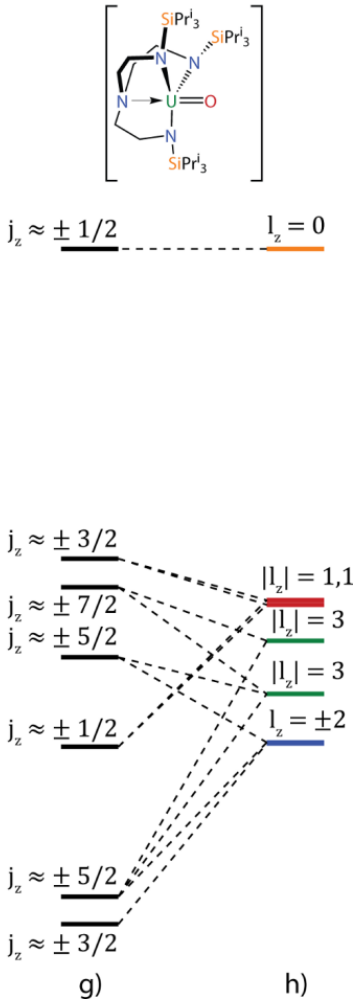


*Figure **4.19.** 5f Orbital energy diagram for model uranium(V) complexes from ab initio calculations, g) terminal mono(oxo) complex [U(Tren^{TIPS})(O)] (**122**) with SOC and h) **122** without SOC.*

4.3.4. Uranium(V)–nitrides as SMMs

The dynamic magnetic behaviour of the uranium(V)–nitrides was briefly discussed above (Section 3.1.). All complexes (except **106**), have peaks in their out-of-phase susceptibility (χ_M'') plots as a function of frequency and temperature (see figure **4.17.** above for an example, **109**).

Fitting the data using a generalised Debye model allows for the extraction of magnetisation relaxation times (τ). These relaxation times are slow for the nitride complexes on the experimental time scale (τ = 1 – 100 ms at 1.8 K), and this

indicates that these nitrides are SMMs. Literature examples of uranium centres having SMM behaviour are described previously in Section 1.2.3.

The usual way of interpreting the magnetic data is to find the energy barrier (U_{eff}). This is achieved by assuming that the Orbach mechanism (wherein relaxation occurs *via* an excited state by exchange of phonons with the lattice, see figure **4.3.**, Section 1.2.2.) is dominant. Under this assumption, U_{eff} is the gradient of the Arrhenius plot of ln(τ) *vs* T^{-1} in the high temperature regime.

Interpretation of the data would afford U_{eff} values for the nitrides ranging 20 – 40 K, for which **53** would have the highest blocking temperature. This would be the highest blocking temperature reported for a uranium complex to date. These values are higher than the value reported for **122**, with a U_{eff} of 22 K.[24]

The Orbach mechanism is feasible for the uranium(V)–nitrides, as 20 – 40 K is in the range of the low-lying first excited states, as determined above by *ab initio* calculations. However, Arrhenius plots have an intrinsic bias towards the Orbach mechanism. Linear behaviour is also observed in the higher temperature regime for the Raman mechanism.

By presenting the data in different ways, we can distinguish between the Orbach and Raman mechanisms. In the Arrhenius plot of ln(τ) *vs* T^{-1}, the Orbach mechanism affords a linear plot, and the Raman mechanism affords a curved trace. If instead the $\log_{10}$-$\log_{10}$ plot of τ^{-1} *vs* T is considered, then these profiles are switched, with the Orbach mechanism affording a curve, and the Raman mechanism giving a linear trace (figure **4.20.**). The energy barrier (U_{eff}) can be extracted from these plots, as the dependence of temperature and field for the Orbach mechanism is $\tau^{-1} = {\tau_0}^{-1} e^{-U_{eff}/T}$. The energy barrier is meaningless parameter for Raman mechanism relaxation as it is not present in the field or temperature dependencies, which follow $\tau^{-1} = CT^n$.

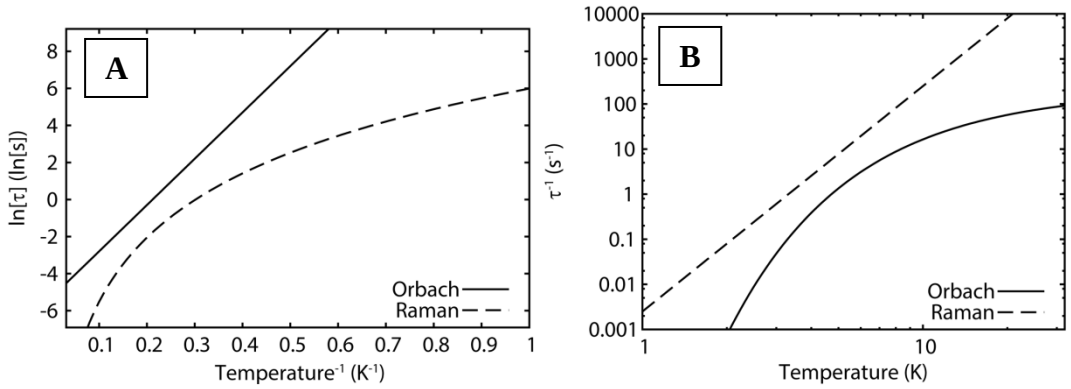
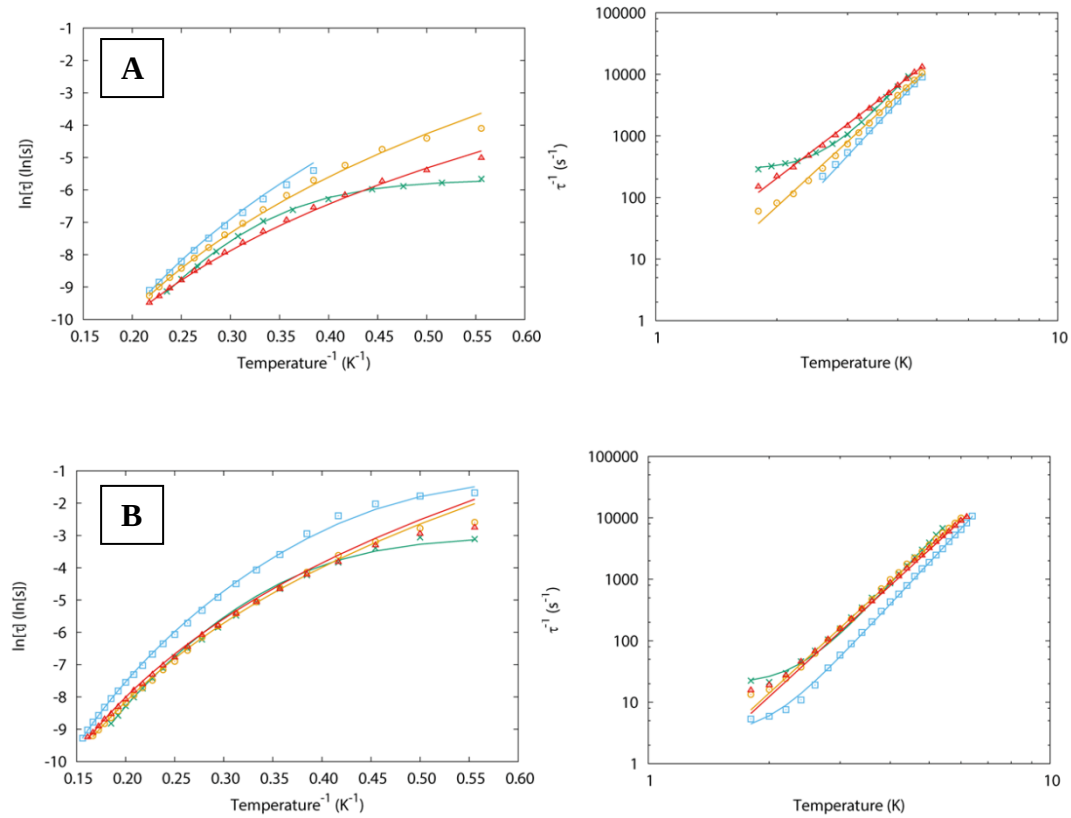


*Figure **4.20.** Theoretical temperature dependence for the Orbach and Raman relaxation mechanisms: a) an Arrhenius plot, and b) the log_{10}-log_{10} plot.*

The corresponding plots for the dinuclear nitride complexes (**51**, **107**, **108** and **109**) are illustrated in figure **4.21.a**, the terminal nitrides (**52**, **114**, **116** and **117**) in figure **4.21.b**, and the capped nitrides (**118**, **53**, **111**, **112** and **113**) in figure **4.21.c**.



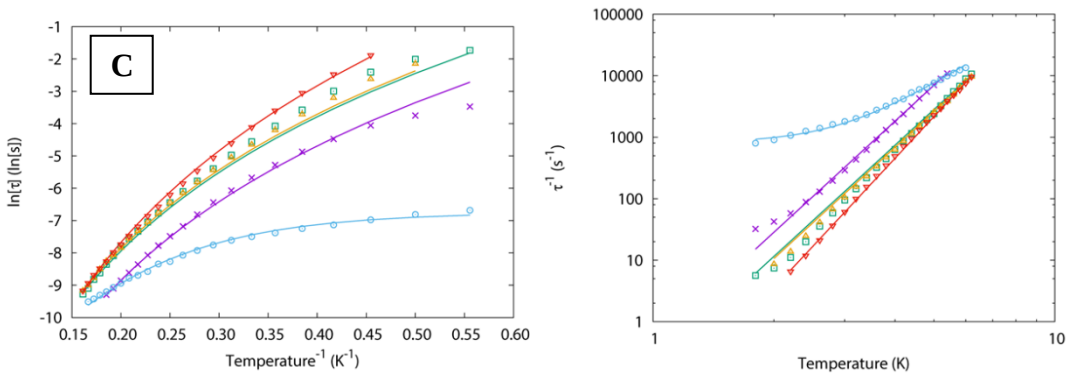


*Figure **4.21.** Experimental (points) and fitted (curves) magnetisation relaxation data as Arrhenius (left) and log_{10}-log_{10} (right) plots of **A**: **51** (green), **107** (blue), **108** (orange) and **109** (red), **B**: **52** (green), **114** (blue), **116** (orange) and **117** (red), **C**: **118** (purple), **53** (green), **111** (blue), **112** (orange) and **113** (red).*

Examination of these plots clearly shows that for all cases, the relaxation follows the Raman mechanism profile (i.e. a curved trace for the Arrhenius plot, and a linear relationship when plotted as a log_{10}-log_{10} plot). There are some examples where temperature independent behaviour is observed at temperatures less than 2 K. Fitting of the data in all cases did not require an exponential component, and therefore the fits are consistent with the Raman mechanism, and do not need to invoke Orbach relaxation. Therefore, U_{eff} values for the nitrides ranging 20 – 40 K are not strictly relevant, as this is attempting to fit a linear best fit to a curve plot (in the Arrhenius plots above). There is no simple correlation between the relaxation and the CF states described previously.

4.4. Summary and Conclusions

The range of uranium(V)–nitrides, for which the syntheses were described in Chapter 2, represent ideal candidates for detailed electronic structure studies. Such studies began with the use of CASSCF *ab initio* methods to investigate the 5f orbitals involved in the bonding of $[U{\equiv}N]^{2+}$, $[U(NH_3)(NH_2)_3(N)]^-$, $[U(Tren^{H})(N)]^-$ and $[U(Tren^{TIPS})(N)]^-$, and the effect of SOC on these orbitals. This allows us to predict the states involved and the transitions between them: transitions to the 2nd to

6th SO coupled excited states correlate well with those observed by UV-vis-NIR electronic absorption spectroscopy.

The calculations do not capture the subtlety of the ground state for the nitride complexes, however, as the first excited state is close in energy to the ground state (< 100 cm^{-1}). EPR spectroscopy afforded resonances consistent with a $j_z \approx \pm 5/2$ SO state, and an absence of resonances consistent with $j_z \approx \pm 3/2$, which is in agreement with previous studies on [U(Tren^{TIPS})(O)] (**122**), which was EPR silent. EPR cannot determine if the ground state is $j_z \approx \pm 5/2$ or $j_z \approx \pm 3/2$, as they are close enough in energy to both be thermally populated at temperatures < 10 K.

Magnetic measurements suggest that only two complexes have a $j_z \approx \pm 5/2$ ground state doublet ([{U(Tren^{TIPS})(μ-N)(μ-K)}$_2$] (**107**) and [U(Tren^{TIPS}){(μ-N)(μ-Na)(15C5)}]) (**53**). Other magnetic data group the nitrides into two groups, with χ_M′T(T) plots that either plateau or are sloping. These plots, in addition to temperature dependent χ_MT plots, indicate that these nitrides have a $j_z \approx \pm 3/2$ ground state, with a low-lying $j_z \approx \pm 5/2$ first excited state.

Temperature dependence of χ_MT allows for the prediction of the energies of nitrides with a $j_z \approx \pm 5/2$ first excited state, but the energy of the first excited state for complexes with a $j_z \approx \pm 5/2$ ground state (i.e. the $j_z \approx \pm 3/2$ state) remains ambiguous as there is no direct experimental handle. As the $j_z \approx \pm 3/2$ and $j_z \approx \pm 5/2$ states are so close (10s of cm^{-1}, ~0.1 kcal mol^{-1}), each complex must be examined independently.

All nitrides examined exhibit slow relaxation of their magnetisations, which is consistent with SMM behaviour. Conventional Arrhenius analysis suggests that [U(Tren^{TIPS}){(μ-N)(μ-Na)(15C5)}] (**53**) has the highest energy barrier (U_{eff}) for a uranium complex to date. Careful analysis however suggests that the complexes are instead dominated by Raman (not Orbach) relaxation, and hence U_{eff} is a meaningless parameter.

By probing the 14 uranium(V)–nitride complexes and the isoelectronic uranium(V)–oxo complex [U(Tren^{TIPS})(O)] (**122**) by EPR and UV-vis-NIR spectroscopies, SQUID magnetometry and modelling with CF and *ab initio* calculations, we can quantify a clear difference between O^{2-} and N^{3-} ligand sets. For O^{2-}, $j_z \approx \pm 3/2$ is

clearly the ground state, but the ground state for N^{3-} is more nuanced. From this data, a more coherent picture of the electronic structure for this series of complexes has emerged, with implications for the understanding of SMM behaviour and the orbital parentage of SO coupled states.

4.5. References

(1) Layfield, R. A. *Organometallics* **2014**, *33*, 1084.
(2) Sorace, L.; Benelli, C.; Gatteschi, D. *Chem. Soc. Rev.* **2011**, *40*, 3092.
(3) Affronte, M. *Journal of Materials Chemistry* **2009**, *19*, 1731.
(4) van Slageren, J. In *EPR Spectroscopy: Applications in Chemistry and Biology*; Drescher, M., Jeschke, G., Eds.; Springer Berlin Heidelberg: Berlin, Heidelberg, 2012, p 199.
(5) Bogani, L.; Wernsdorfer, W. *Nat Mater* **2008**, *7*, 179.
(6) Evangelisti, M.; Brechin, E. K. *Dalton Trans.* **2010**, *39*, 4672.
(7) Sessoli, R.; Gatteschi, D.; Caneschi, A.; Novak, M. A. *Nature* **1993**, *365*, 141.
(8) Sessoli, R.; Tsai, H. L.; Schake, A. R.; Wang, S.; Vincent, J. B.; Folting, K.; Gatteschi, D.; Christou, G.; Hendrickson, D. N. *J. Am. Chem. Soc.* **1993**, *115*, 1804.
(9) Ako, A. M.; Hewitt, I. J.; Mereacre, V.; Clérac, R.; Wernsdorfer, W.; Anson, C. E.; Powell, A. K. *Angew. Chem., Int. Ed.* **2006**, *45*, 4926.
(10) Neese, F.; Pantazis, D. A. *Faraday Discussions* **2011**, *148*, 229.
(11) Zadrozny, J. M.; Xiao, D. J.; Atanasov, M.; Long, G. J.; Grandjean, F.; Neese, F.; Long, J. R. *Nat Chem* **2013**, *5*, 577.
(12) Blagg, R. J.; Ungur, L.; Tuna, F.; Speak, J.; Comar, P.; Collison, D.; Wernsdorfer, W.; McInnes, E. J. L.; Chibotaru, L. F.; Winpenny, R. E. P. *Nat Chem* **2013**, *5*, 673.
(13) Liddle, S. T.; van Slageren, J. *Chem. Soc. Rev.* **2015**, *44*, 6655.
(14) Ishikawa, N.; Sugita, M.; Ishikawa, T.; Koshihara, S.-y.; Kaizu, Y. *J. Am. Chem. Soc.* **2003**, *125*, 8694.
(15) Ganivet, C. R.; Ballesteros, B.; de la Torre, G.; Clemente-Juan, J. M.; Coronado, E.; Torres, T. *Chem. -Eur. J.* **2013**, *19*, 1457.
(16) Chilton, N. F.; Goodwin, C. A. P.; Mills, D. P.; Winpenny, R. E. P. *Chem. Commun.* **2015**, *51*, 101.
(17) Rinehart, J. D.; Fang, M.; Evans, W. J.; Long, J. R. *J. Am. Chem. Soc.* **2011**, *133*, 14236.
(18) Gregson, M.; Chilton, N. F.; Ariciu, A.-M.; Tuna, F.; Crowe, I. F.; Lewis, W.; Blake, A. J.; Collison, D.; McInnes, E. J. L.; Winpenny, R. E. P.; Liddle, S. T. *Chem. Sci.* **2016**, *7*, 155.
(19) Chen, Y.-C.; Liu, J.-L.; Ungur, L.; Liu, J.; Li, Q.-W.; Wang, L.-F.; Ni, Z.-P.; Chibotaru, L. F.; Chen, X.-M.; Tong, M.-L. *J. Am. Chem. Soc.* **2016**, *138*, 2829.
(20) Rinehart, J. D.; Long, J. R. *J. Am. Chem. Soc.* **2009**, *131*, 12558.

(21) Mills, D. P.; Moro, F.; McMaster, J.; van Slageren, J.; Lewis, W.; Blake, A. J.; Liddle, S. T. *Nat. Chem.* **2011**, *3*, 454.
(22) Moro, F.; Mills, D. P.; Liddle, S. T.; van Slageren, J. *Angew. Chem., Int. Ed.* **2013**, *52*, 3430.
(23) Mougel, V.; Chatelain, L.; Pécaut, J.; Caciuffo, R.; Colineau, E.; Griveau, J.-C.; Mazzanti, M. *Nat Chem* **2012**, *4*, 1011.
(24) King, D. M.; Tuna, F.; McMaster, J.; Lewis, W.; Blake, A. J.; McInnes, E. J. L.; Liddle, S. T. *Angew. Chem., Int. Ed.* **2013**, *52*, 4921.
(25) King, D. M.; Tuna, F.; McInnes, E. J. L.; McMaster, J.; Lewis, W.; Blake, A. J.; Liddle, S. T. *Science* **2012**, *337*, 717.
(26) King, D. M.; Tuna, F.; McInnes, E. J. L.; McMaster, J.; Lewis, W.; Blake, A. J.; Liddle, S. T. *Nat. Chem.* **2013**, *5*, 482.
(27) Cohen, A. J.; Mori-Sánchez, P.; Yang, W. *Chem. Rev.* **2012**, *112*, 289.
(28) Kaufman, V.; Radziemski, L. J. *J. Opt. Soc. Am.* **1976**, *66*, 599.
(29) Kaltsoyannis, N.; Scott, P. *The f elements*; Oxford University Press, 1999.
(30) Pepper, M.; Bursten, B. E. *Chem. Rev.* **1991**, *91*, 719.
(31) Eisenstein, J. C.; Pryce, M. H. L. *Proc. R. Soc. Lond. A, Math. Phys. Eng. Sci.* **1955**, *229*, 20.
(32) Gerloch, M.; Miller, J. R. In *Prog. Inorg. Chem.*; John Wiley & Sons, Inc.: 2007, p 1.
(33) Kindra, D. R.; Evans, W. J. *Chem. Rev.* **2014**, *114*, 8865.
(34) Chilton, N. F.; Anderson, R. P.; Turner, L. D.; Soncini, A.; Murray, K. S. *J. Comput. Chem.* **2013**, *34*, 1164.
(35) Edelstein, N.; Brown, D.; Whittaker, B. *Inorg. Chem.* **1974**, *13*, 563.
(36) Lukens, W. W.; Edelstein, N. M.; Magnani, N.; Hayton, T. W.; Fortier, S.; Seaman, L. A. *J. Am. Chem. Soc.* **2013**, *135*, 10742.

Chapter Five

The Reactivity of Uranium Nitrides Towards Carbon Monoxide

Table of Contents

5.1. Introduction and Aims 194

5.2. Reactivity Studies of Uranium Nitride Complexes Towards CO 195

5.2.1. ***Tren–uranium(VI) nitride*** **(54)** 195

5.2.2. ***Tren–uranium(V) nitrides*** 199

5.2.2.1. ***Reactivity study of [U(Tren^{TIPS})(N)][K(Bn-15C5)$_2$] (115) towards CO*** 199

5.2.2.2. ***Reactivity study of [U(Tren^{TIPS}){(μ-N)(μ-K)(18C6)}] (111) towards CO*** 203

5.2.3. ***Towards a synthetic cycle for the conversion of NaN$_3$ to NaOCN*** 207

5.2.4. ***Computational analysis*** 211

5.2.5. ***Reactivity of Tren–uranium nitrides towards phosphines*** 213

5.3. Summary and Conclusions 214

5.4. References 215

5.1. Introduction and Aims

With a new, efficient route to uranium nitrides now established, in order to further assess the properties of the U≡N linkage, a series of reactivity studies towards small molecules must be undertaken. Whilst preliminary findings (as discussed in Chapter 2) indicate that these nitrides might be nucleophilic in nature, choosing an ambiphilic reagent such as carbon monoxide as the first small molecule to investigate reactivity towards permits for either nucleophilic or electrophilic reactivities to be probed. This will then allow us to develop our understanding of the electronic behaviour of this novel class of compounds.

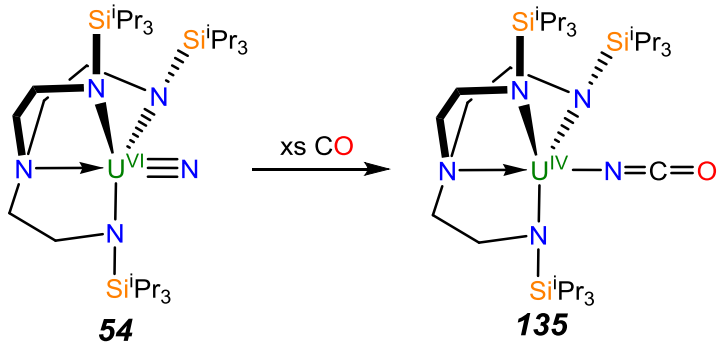
The next chapters will therefore be dedicated to understanding the reactivity of uranium nitrides towards small molecules starting with their reactivity towards CO. Computational analysis will afford an understanding of the mechanistic implications of these findings and whether these uranium nitrides are indeed nucleophilic.

As discussed in Chapter 1, transition metal nitrides have been shown to react with CO to afford isocyanate derivatives,[1-5] and complete nitrogen atom transfer to CO has been observed.[6] The activation of CO by uranium complexes is a burgeoning field, with reactive pathways including coordination, insertion into uranium–alkyl bonds and reductive homologation. The reaction of uranium imides with CO affords isocyanates.[7]

The computational chemistry reported in the chapter was performed by Dr C. E. Kefalidis and Prof. L. Maron of Université Paul Sabatier, Toulouse.

5.2. Reactivity Studies of Uranium Nitride Complexes Towards CO

5.2.1. Tren–uranium(VI) nitride (54)



*Scheme **5.1.** Synthesis of **135**.*

A degassed solution of [U(Tren^{TIPS})(N)] (**54**) in toluene was exposed to one atmosphere of CO for 16 hours. Upon work-up, pale green single crystals were isolated of the isocyanate species [U(Tren^{TIPS})(NCO)] (**135**). The molecular structure of **135** is illustrated in figure **5.1.**, alongside selected bond lengths and angles.

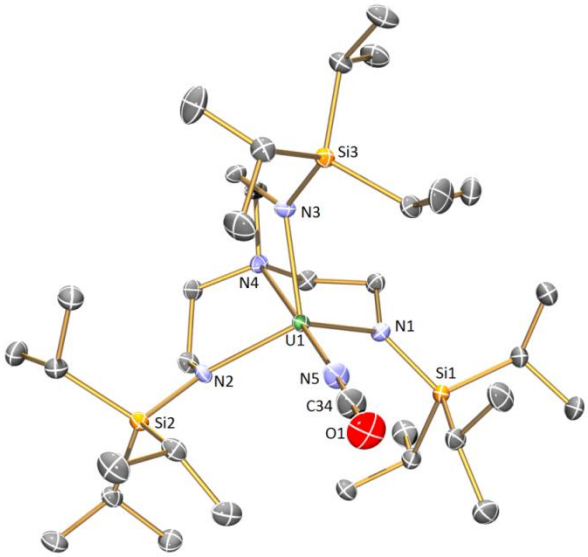


*Figure **5.1.** Molecular structure of [U(Tren^{TIPS})(NCO)], **135**. Thermal ellipsoids set at 40% probability. Minor disorder components of the isocyanate unit and hydrogen atoms are omitted for clarity. Selected distances (Å) and angles (°): U(1)-N(1) 2.255(3), U(1)-N(2) 2.253(3), U(1)-N(3) 2.245(3), U(1)-N(4) 2.620(3), U(1)-N(5) 2.338(3), N(5)-C(34)$_{av}$ 1.190(9), C(34)-O(1)$_{av}$ 1.192(9), N(4)-U(1)-N(5) 175.94(11), U(1)-N(5)-C(34)$_{av}$ 173.2(15), N(5)-C(34)-O(1)$_{av}$ 178(3).*

The molecular structure of **135** reveals a uranium(IV)–isocyanate, [U(Tren^{TIPS})(NCO)] which retains a distorted trigonal bipyramidal geometry at uranium (τ = 1.06),[8,9] with an *N*-bound isocyanate unit and the face-capping amine of Tren^{TIPS} occupying the axial positions. The isocyanate unit is disordered over two positions, but is essentially linear, with an average U(1)-N(5)-C(34) angle of 173.1°. The U(1)-$N_{isocyanate}$ bond is 2.338(3) Å, which compares with the U(1)-N_{amide} average distance of 2.251(3) Å and a U(1)-N_{amine} distance of 2.620(3) Å. These correlate well with distances in the analogous [U(Tren^{TIPS})(N_3)] (**13**), though the U(1)-$N_{isocyanate}$ bond in **135** is longer than the U(1)-N_{azide} bond length in **13** [2.305(3) Å] by ~0.03 Å.[10] The U(1)-$N_{isocyanate}$ bond distance [2.338(3) Å] compares well to literature values for uranium(IV)–isocyanates which range from 2.337(3) to 2.389(6) Å.[7,11-13]

The presence of an *N*-bound cyanate isomer as opposed to the *O*-bound isomer is confirmed by competitive crystallographic refinement of the two isomers, alongside DFT calculations, which show that the *N*-bound isomer is more stable than the *O*-bound isomer by 15.4 kcal mol^{-1}.

The ^{1}H NMR spectrum of **135** spans the range +8 to –31 ppm, which is consistent with Tren–uranium(IV) species. The ^{29}Si{^{1}H} spectrum contains one resonance at –4.7 ppm, which is consistent with a C_{3v} symmetric complex with a uranium(IV) centre.[14] The FTIR (Nujol) spectrum exhibits a strong absorption at 2187 cm^{-1}, which is assigned as a cyanate stretch. This is typical of uranium(IV)–isocyanates, with reported values ranging from 2172 – 2201 cm^{-1}.[7,11-13,15]

A solution of **135** in toluene was analysed by UV-vis-NIR electronic absorption spectroscopy, and this spectrum is illustrated in figure **5.2.**

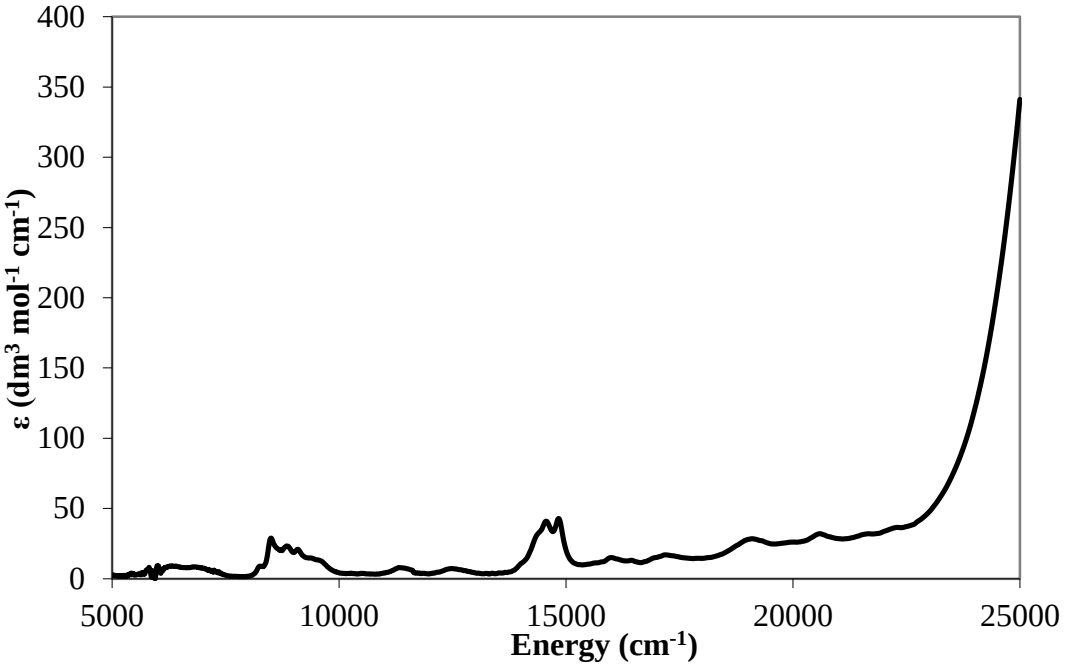


*Figure **5.2.** UV-vis-NIR electronic absorption spectra of **135**.*

The spectrum is dominated by charge transfer (CT) bands tailing in from the high energy region. The U^{IV}, $5f^2$ electronic configuration gives rise to weak, Laporte forbidden *f-f* transitions, which are visible in the lower energy portion of the spectrum. As is common for uranium(IV) electronic absorption spectra, however, these are broad and poorly resolved.

The Evans' method[16] room temperature solution magnetic moment for **135** was found to be 2.50 μ_B. Whilst this is lower than the theoretical value for a uranium(IV) $^3H_4$ ground state, it is within the range of experimentally observed values of U^{IV} complexes μ_{eff} (1.8 – 3.6 μ_B),[17] and correlates well to the magnetic moment observed in the solid state (figure **5.3.**), which is 2.41 μ_B at 298 K. The solid state magnetic moment then decreases to 0.44 μ_B at 2.0 K (tending to zero), as would be anticipated for a uranium(IV) complex that is a magnetic singlet at low temperature.

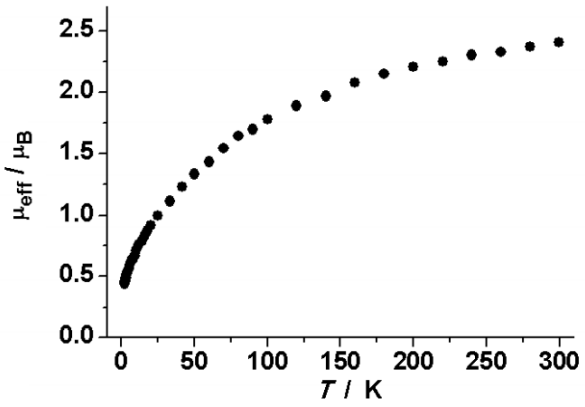
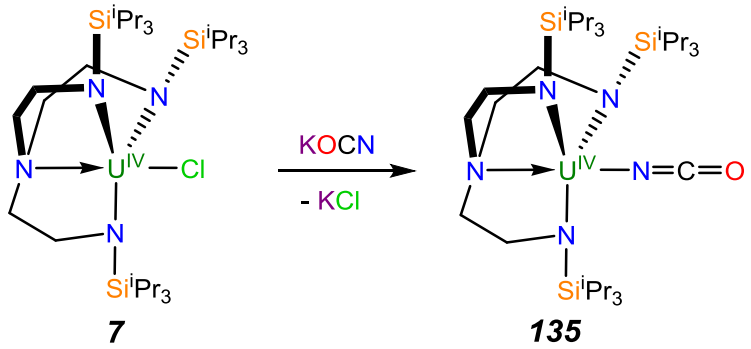


*Figure **5.3.** Magnetic susceptibility data [μ_{eff} (μ_B) vs T (K)] for **135**.*

Taken together, these data constitute strong evidence for the formation of a uranium(IV)–isocyanate species, which would result from the two electron reductive carbonylation of a uranium(VI)–nitride. This reactivity parallels that of transition metal nitrides, yet it is still a rare reaction, as although these are electron rich bonds, they are also strong, and therefore not very reactive.[1,2,4,6]

Examples of cyanate formation at uranium have been accomplished *via* different synthetic routes. In [U{(^{Ad}ArO)$_3$tacn}(NCO)] (**77**), NCO$^-$ was prepared *via* the reaction of CO with a uranium imide precursor;[7] in the polymeric [U(N″$_3$)(μ-NCO)$_2${μ-K(18C6)}]$_\infty$ (**83**), NCO$^-$ was prepared by multiple N-Si bond cleavage with CO_2;[12] and in [{U(η^8-1,4-[Si^{i}Pr$_3$]$_2$C$_8$H$_6$)(η^5-C$_5$Me$_5$)}$_2$(μ-NCO)$_2$] (**76**), cyanate was formed by bimetallic reductive activation of NO and CO.[15,18] The formation of **135** thus represents a novel pathway towards isocyanate formation at a uranium centre.

Mechanistic details for the reductive carbonylation of **54**, based upon computational studies, will be discussed in a later section.

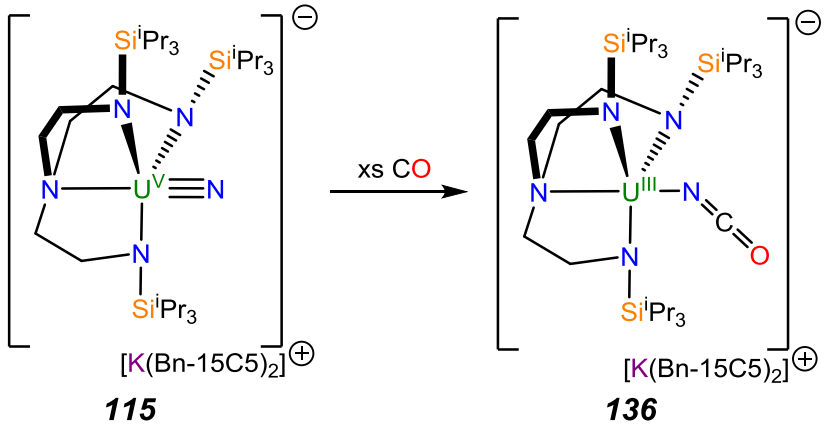


*Scheme **5.2.** Alternative synthetic route to **135**.*

For comparative purposes, and to confirm its formulation, **135** was also prepared *via* a salt elimination strategy. The reaction of [U(Tren^{TIPS})(Cl)] (**7**) with KOCN afforded **135** as anticipated, with all data in good agreement, and this confirmed the identity of the product of the reactivity study.

5.2.2. Tren–uranium(V) nitrides

5.2.2.1. Reactivity study of [U(Tren^{TIPS})(N)][K(Bn-15C5)$_2$] (115) towards CO



*Scheme **5.3.** Synthesis of **136**.*

A cold (–78°C) degassed solution of [U(Tren^{TIPS})(N)][K(Bn-15C5)$_2$] (**115**) in toluene was exposed to one atmosphere of CO. An immediate colour change from red-brown to dark green was observed; a comparison of the rates of reaction of **54** and **115** with CO will be discussed in a later section (2.4). Upon work-up, dark green single crystals were isolated of the species formulated as the isocyanate complex [U(Tren^{TIPS})(NCO)][K(Bn-15C5)$_2$] (**136**). The molecular structure is illustrated in

figure **5.4.**, alongside selected bond lengths and angles, as ascertained by a single crystal XRD study.

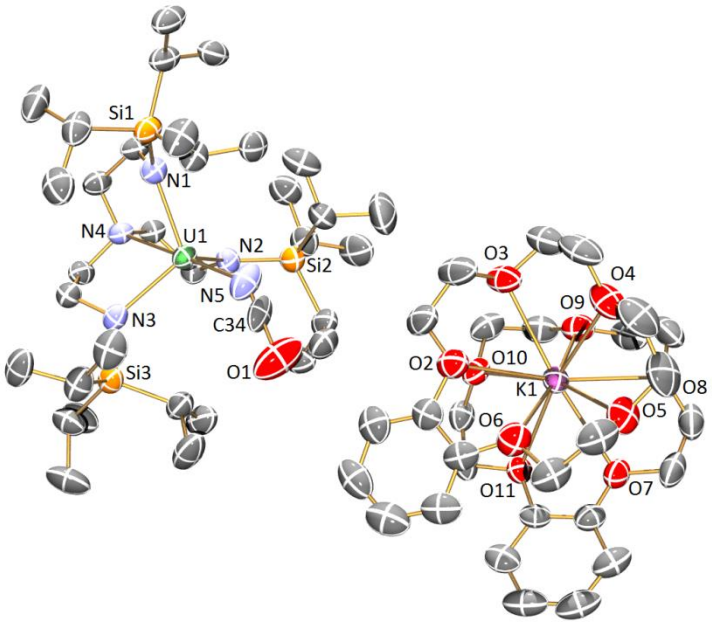


*Figure **5.4.** Molecular structure of [U(Tren^{TIPS})(NCO)][K(Bn-15C5)$_2$], **136**. Thermal ellipsoids set at 40% probability. The minor disorder component of the isocyanate unit and hydrogen atoms are omitted for clarity. Selected distances (Å) and angles (°): U(1)-N(1) 2.364(6), U(1)-N(2) 2.346(6), U(1)-N(3) 2.567(6), U(1)-N(4) 2.685(5), U(1)-N(5) 2.456(7), N(5)-C(34)$_{av}$ 1.023(15), C(34)-O(1)$_{av}$ 1.351(18), K(1)-O(2) 2.938(5), K(1)-O(3) 2.834(6), K(1)-O(4) 2.750(6), K(1)-O(5) 2.826(6), K(1)-O(6) 2.829(6), K(1)-O(7) 2.990(5), K(1)-O(8) 2.844(5), K(1)-O(9) 2.784(6), K(1)-O(10) 2.794(5), K(1)-O(11) 2.912(5), N(4)-U(1)-N(5) 178.8(2), U(1)-N(5)-C(34)$_{av}$ 138.1(12), N(5)-C(34)-O(1)$_{av}$ 177(2).*

The molecular structure of **136** confirms the formulation of a uranium(III)–isocyanate species, the first crystallographically characterised example of this linkage for that oxidation state.[19] The complex retains a distorted trigonal bipyramidal geometry at uranium (τ = 1.11),[8,9] with an isocyanate unit and the face-capping amine of Tren occupying the axial positions and the N(4)-U(1)-N(5) angle is near linear [178.8(2)°]. The isocyanate unit is disordered over two positions, and in contrast to **135**, is bent, with an average U-N-C bond angle of 138.1(12)° (*vide infra*).

As for **135**, the *N*-bound cyanate isomer (as opposed to the *O*-bound isomer) is supported by competitive crystallographic refinement of the two isomers, alongside DFT calculations, which show that the *N*-bound isomer of **136** is more stable than the *O*-bound isomer by 12.6 kcal mol^{-1}.

The ^{1}H NMR spectrum of **136** spans the range +9 to 0 ppm. The $^{29}Si\{^{1}H\}$ NMR spectrum is consistent with a uranium(III)[14] C_{3v} symmetric complex (one resonance at –16.4 ppm), though the ^{1}H NMR spectrum suggests that there may be a breaking of this symmetry based on the relative integrations of the resonances. The FTIR (Nujol) spectrum exhibits a strong absorption at 2172 cm^{-1}, which is assigned as a cyanate stretch.

The UV-vis-NIR electronic absorption of **136** was recorded, and this is illustrated in figure **5.7**. The spectrum will be discussed later alongside that of the product of the reductive carbonylation of [U(Tren^{TIPS}){(μ-N)(μ-K)(18C6)}] (see Chapter 5, Section 2.2.2.).

The Evans' method[16] room temperature solution magnetic moment of **136** is 2.76 μ_B. Though this is lower than the theoretical value of 3.62 for the U^{III} $^{4}I_{9/2}$ ground state, it is within the range of experimentally observed values for uranium(III) solution magnetic moments (2.4 – 3.8 μ_B).[17]

Variable temperature solid state magnetic measurements were also recorded for **136** (figure **5.5.**, left). At 298 K, the magnetic moment is 2.59 μ_B, which correlates well to the solution phase data. This decreases to 1.13 μ_B at 2.0 K. This suggests the uranium(III) formulation that is a magnetic doublet a low temperature.

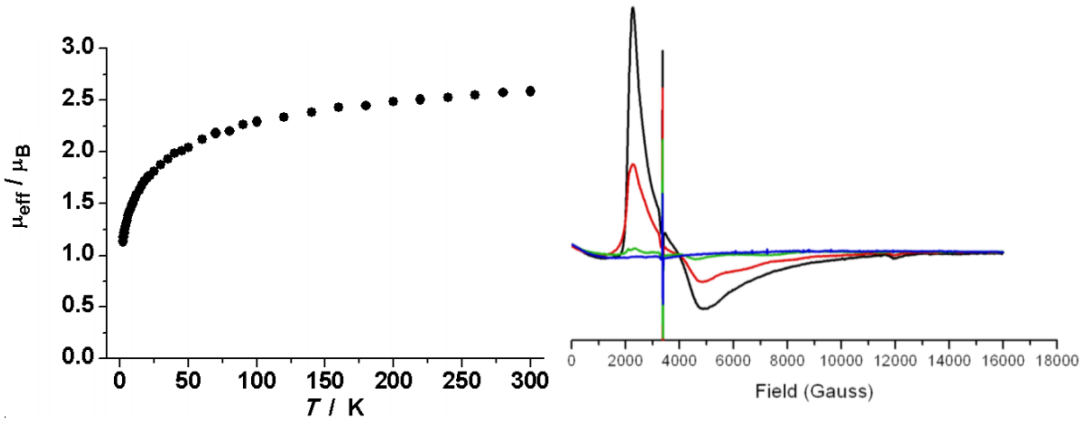


*Figure **5.5.** Magnetic susceptibility data [μ_{eff} (μ_B) vs T (K)], left, and solid state X-band EPR spectra, at 5 (black), 10 (red), 20 (green) and 40 K (blue), right, for **136**.*

The temperature dependent EPR spectrum of **136** (figure **5.5.**, right). shows one transition which corresponds to the presence of only one unpaired electron at low temperatures. This corroborates the assignment of a uranium(III) $5f^3$ centre, as this is a magnetic doublet at low temperature due to the spin pairing of two 5f electrons. By contrast, a uranium(IV) system would be expected to be EPR silent under these measurement conditions.[20]

Comparison of the structural data for **135** and **136** reveal some stark differences. In contrast to the **135**, the U(1)-$N_{isocyanate}$ bond is shorter in **135** relative to **136** [**136** 2.456(7), **135** 2.338(3) Å]. This is a result of both the higher oxidation state and the overall charge of zero of **135**, compared with the anionic separated ion pair structure for **136**. More notably, the isocyanate fragment adopts a near linear geometry in **135**, but is bent in **136** [**135** 176.1(15), **136** 138.1(12)°]. This is almost certainly due to an additional π-donor interaction from the $N_{isocyanate}$ to the uranium in **135**. The linear geometry is required to facilitate such an interaction. By contrast, **136** is more electron rich ($5f^3$) than **135** ($5f^2$) and therefore the U(1)-N(5) bond is more ionic, and so does not require a π-donor interaction to stabilise the U(1)-N(5) bond in **136**.

A combination of these factors also manifest themselves as a variance in the internal isocyanate unit distances. In the **135**, the N-C and C-O bond lengths are 1.190(9) and 1.191(9) Å respectively, whereas in **136**, the corresponding bond lengths are 1.023(15) and 1.351(18) Å respectively. The N-C bond in **136** shortens relative to

135, and the C-O bond is extended relative to **135**. For **135**, the linear U-NCO alignment is observed due to the additional π-donor interaction, which acts to polarise electron density out of the NCO^- π-system causing the observed variation in N-C and C-O bond lengths relative to **136**. Such an interaction does not occur for **136**, and so the N-C and C-O bond distances are largely unaffected.

In addition to the longer U(1)-$N_{isocyanate}$ bond distance in **136** *vs* **135**, the U(1)-N_{amide} and U(1)-N_{amine} bond distances have also increased by ~0.1 Å in **136** when compared to **135**, arising from the larger, anionic, electron rich uranium(III) centre in **136**. The potassium–oxygen interactions [K-O 2.750(6) – 2.938(5) Å] are unremarkable [literature mean K-O(15C5) distance 2.908 Å].[19]

Taken together, the oxidation state of the uranium centre in **136** is formally assigned as +3.

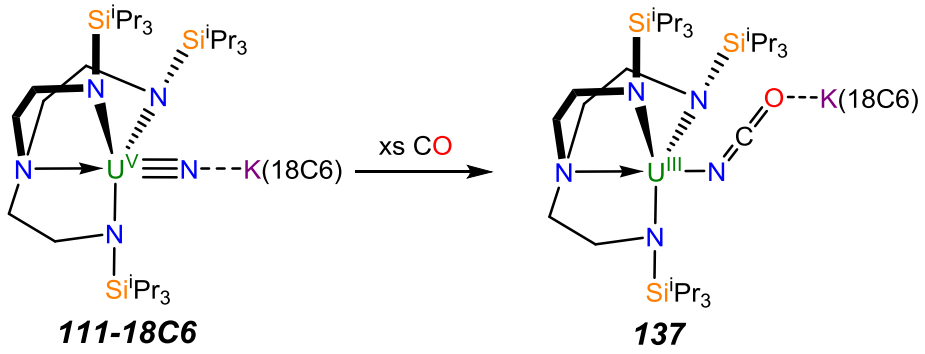
Mechanistic details, based upon computational studies, for the reductive carbonylation of **115** will be discussed in a later section.

5.2.2.2. Reactivity study of [U(Tren^{TIPS}){(μ-N)(μ-K)(18C6)}] (111) towards CO

The reaction of a crown ether capped nitride with CO was also investigated. The reaction of the potassium capped nitride [U(Tren^{TIPS}){(μ-N)(μ-K)(Bn_2-18C6)}$_2$] (**111**) with CO, analogously to **115** (as discussed), instantaneously changed colour from red-brown to dark green. Unfortunately, we were unable to isolate crystals of the product, the postulated uranium(III)–isocyanate species [U(Tren^{TIPS}){(μ-NCO)(μ-K)(Bn_2-18C6)}$_2$].

In light of our previous work, which indicated that the choice of crown can be pivotal for this kind of chemistry (see Chapter 2), a sample of [U(Tren^{TIPS}){(μ-N)(μ-K)(18C6)}] (**111-18C6**, a non-structurally authenticated analogue of **111**) was prepared by the reaction of **107** with two equivalents of 18-crown-6 ether. This compound was not isolated, but reacted with one atmosphere of CO (scheme **5.4.**). An instantaneous colour change from red-brown to dark green was observed, suggestive of the preparation of [U(Tren^{TIPS}){(μ-NCO)(μ-K)(18C6)}] (**137**). Crystals suitable for a single crystal XRD study were grown from a mixture of

toluene and pentane. The molecular structure is illustrated in figure **5.6.**, alongside selected bond lengths and angles.



111-18C6 **137**

*Scheme **5.4.** Synthesis of **137**.*

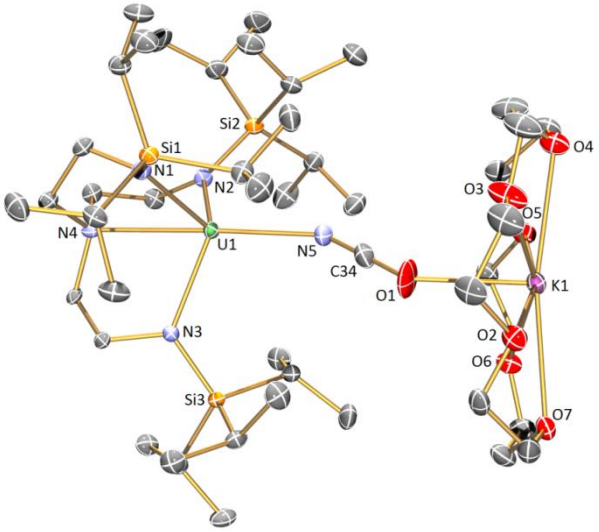


*Figure **5.6.** Molecular structure of [U(Tren^{TIPS}){(μ-NCO)(μ-K)(18C6)}], **137**. Thermal ellipsoids set at 40% probability. Hydrogen atoms are omitted for clarity. Selected distances (Å) and angles (°): U(1)-N(1) 2.405(4), U(1)-N(2) 2.326(3), U(1)-N(3) 2.349(6), U(1)-N(4) 2.710(5), U(1)-N(5) 2.451(7), N(5)-C(34) 1.181(7), C(34)-O(1) 1.208(7), O(1)-K(1) 2.604(4), K(1)-O(2) 2.813(4), K(1)-O(3) 2.700(5), K(1)-O(4) 2.888(5), K(1)-O(5) 2.793(4), K(1)-O(6) 2.709(4), K(1)-O(7) 2.934(4), N(4)-U(1)-N(5) 177.75(12), U(1)-N(5)-C(34) 149.0(4), N(5)-C(34)-O(1) 179.2(6), C(34)-O(1)-K(1) 136.3(4).*

The X-ray data confirms the anticipated capped uranium(III)–isocyanate structure of **137**, which adopts a distorted trigonal bipyramidal geometry at uranium ($\tau = 1.08$),[8,9]

with the isocyanate unit and face-capping amine in the axial positions. Like **136**, the N(4)-U(1)-N(5) angle is near linear [177.75(12)°] and the isocyanate unit is bent [U(1)-N(5)-C(34) 149.0(4)°], though to a lesser degree than in the terminal analogue [141.1(11)°]. The isocyanate unit itself is linear, and unlike **136**, the N-C and C-O bond lengths, of 1.181(7) and 1.208(7) Å respectively, are almost identical to those observed in the uranium(IV)–isocyanate complex (**135**). This is suggestive of significant polarisation of electron density from the π-manifold of the NCO^- ligand by the potassium cation in **137**.

The U(1)-$N_{isocyanate}$ distance and U(1)-N_{amine} distance are statistically indistinguishable between the two uranium(III)–isocyanate species (**136** and **137**), though the average U(1)-N_{amide} distances are shorter in the capped complex [**137** 2.360(6) *vs* **136** 2.426(6) Å]. The potassium–crown oxygen distances [range 2.700(5) – 2.934(4) Å] are unremarkable [literature K-O(18C6) average distance 2.840 Å].[19]

The ^{1}H NMR spectrum spans the range +8 to –1 ppm, and the $^{29}Si\{^1H\}$ NMR spectrum contains one resonance at –12.7 ppm.[14] Unlike **136**, both spectra are consistent with a C_{3v} symmetric structure in solution in spite of the bent interaction of the potassium crown capped isocyanate unit within the apical pocket of $Tren^{TIPS}$.

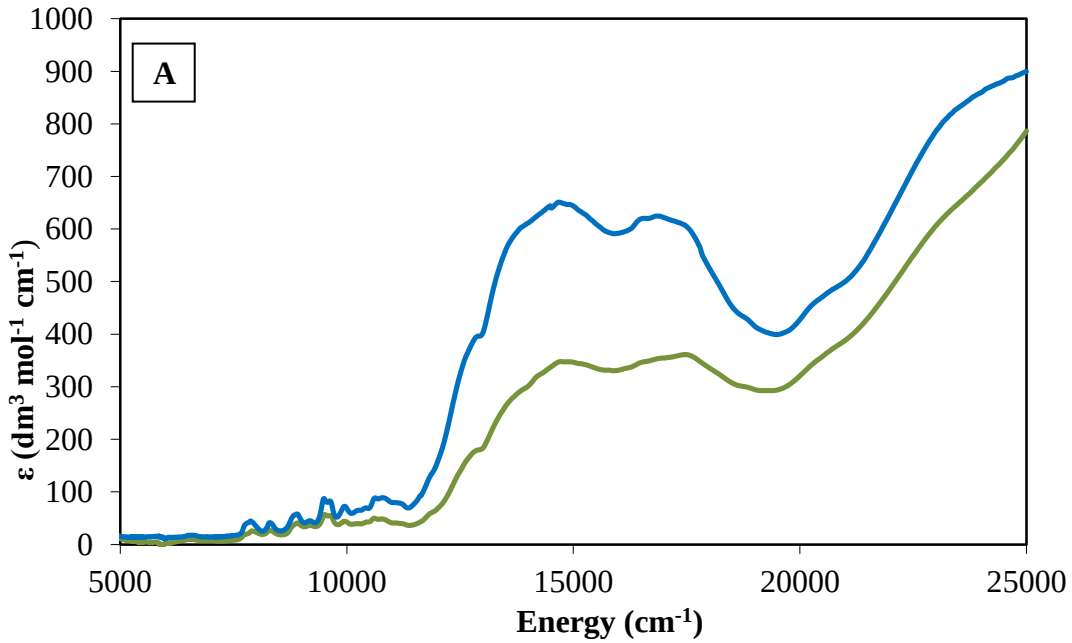
The FTIR (Nujol) spectrum features a strong absorption at 2180 cm^{-1}, which is assigned to the isocyanate stretch. This value lies between the absorptions for **135** (2187 cm^{-1}) and **136** (2172 cm^{-1}). This suggests that the degree to which there is polarisation of electron density of the π-manifold of the NCO^- ligand can be seen not only by single crystal XRD studies, but also by an assessment of the FTIR stretches of cyanate species. This trend therefore indicates that we may be able to infer by analytical techniques the variation in bonding in uranium–isocyanates.

The Evans' method[16] room temperature solution magnetic moment is 2.85 μ_B. This is lower than the theoretical value of 3.62 for the U^{III} $^4I_{9/2}$ ground state, though it is within the range of experimentally observed values for uranium(III) solution magnetic moments (2.4 – 3.8 μ_B).[17]

No further characterisation data (i.e. SQUID, EPR) that could confirm the oxidation state of **137** were collected, though by strong analogy to **136**, through the molecular structure and subsequent characterisation, the assignment of a uranium(III) oxidation state seems entirely reasonable. Furthermore, no computational analysis has been performed on the reductive carbonylation of **111-18C6**, though qualitatively, it can be argued that these results will be very similar to those reported below for the reaction of **115** with CO.

A solution of **137** in toluene was analysed by UV-vis-NIR electronic absorption spectroscopy. This spectrum, alongside that of **136**, is illustrated in figure **5.7.**

High energy CT bands tail in from the high energy region (20000 – 25000 cm^{-1}). In the 12000 – 20000 cm^{-1} region there are prominent *d-f* transitions (ε = 300 – 600 $dm^3\ mol^{-1}\ cm^{-1}$), which account for the dark green colour of these complexes. Finally, in the lower energy region (7000 – 11000 cm^{-1}) there are weak (ε = 20 – 100 $dm^3\ mol^{-1}\ cm^{-1}$) *f-f* Laporte forbidden transitions (figure **5.7.b**).



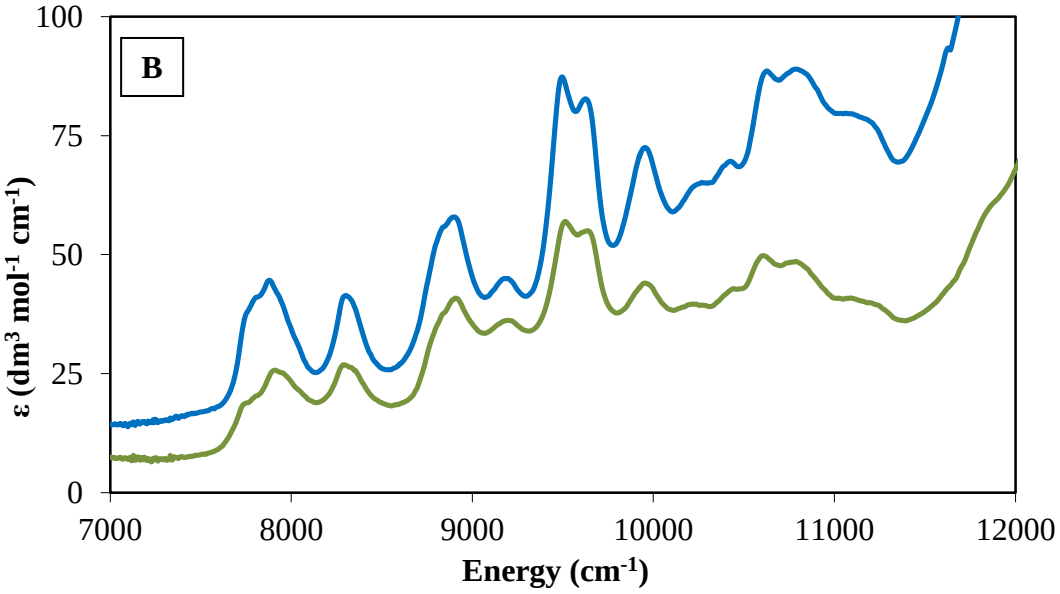
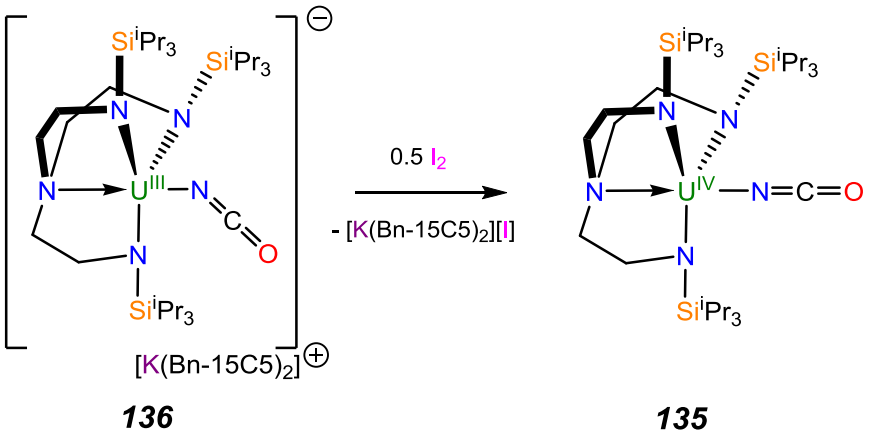


*Figure **5.7.** **A**: UV-vis-NIR electronic absorption spectra of **136** (green) and **137** (blue); **B**: zoom region.*

5.2.3. Towards a synthetic cycle for the conversion of NaN_3 to NaOCN

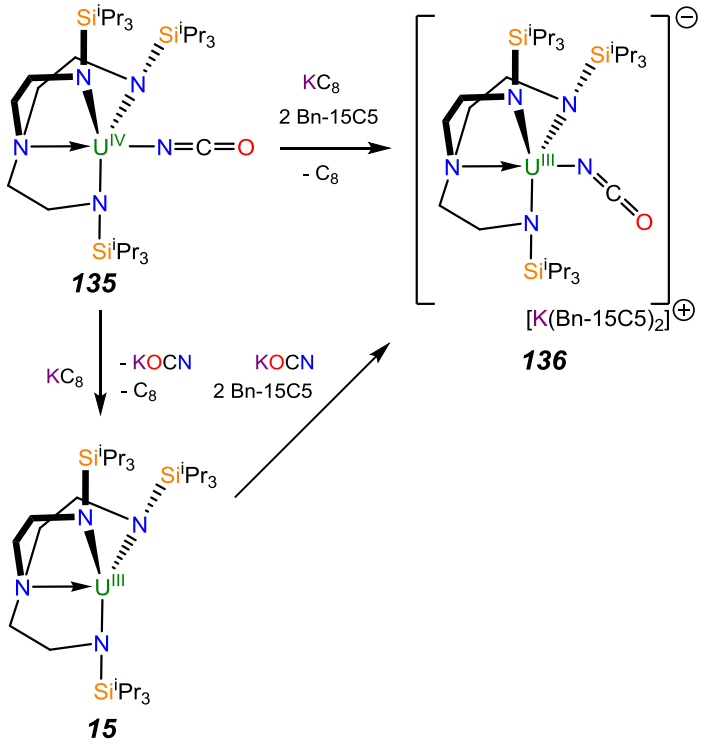
As it is possible to interconvert between uranium nitrides by oxidative and reductive methods (*vide infra*), we sought to interconvert between the uranium isocyanate species that had been prepared by the reductive carbonylation of uranium nitrides.



136 ***135***

*Scheme **5.5.** Alternative synthetic route to **135**.*

Addition of half an equivalent of elemental iodine to **136** resulted in oxidation of the uranium centre to **135**, in an analogous manner to the reported oxidation of **52** to **54**.[10]



*Scheme **5.6.** Alternative synthetic routes to **136**.*

We then investigated the reverse process, i.e. the reduction of **135** to prepare **136**. The one electron reduction of **135** with KC_8 followed two divergent routes, dependent on the reaction conditions (i.e. the presence or absence of benzo-15-crown-5 ether – scheme **5.6.**). In the presence of this crown ether, these solutions turned dark green, suggesting the desired uranium(III)–isocyanate species was prepared. Similarly, reduction in the presence of 18-crown-6 ether prepares **137**, as ascertained by ^{1}H NMR spectroscopy. In the absence of crown ethers the solution turns dark purple, which is characteristic of [U(Tren^{TIPS})] (**15**), with the concomitant elimination of KOCN (ν_{NCO} 2130 cm^{-1}).

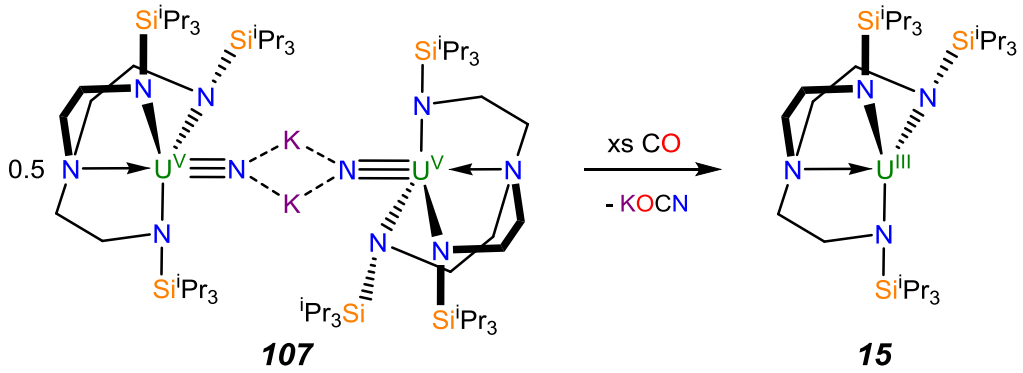
This denitrification is reminiscent of the reactivity reported for a vanadium–nitride (**33**), which under an atmosphere of CO prepares the trivalent **32** (see Chapter 1, Section 4.2.).[1] Notably, neither of these reaction conditions afford the decarbonylation of the isocyanate species as was uniquely observed for a niobium–

isocyanate (**29**) which was reduced to afford **30**.[21,22] The analogous decarbonylation of **135** would have resulted in the preparation of **107**. Moreover, the preparation of **15** by the reduction of **135** (and elimination of KOCN) is reminiscent of the reduction of the vanadium analogue of **29**, which when reduced with a sodium/ mercury amalgam affords **32** (see Chapter 1, Section 3.5.).[1]

The identity of **15** prepared by denitrification was confirmed by comparison of analytical data with an authenticated sample. Both KOCN and **15** were prepared in essentially quantitative yields by this method, as determined by ^{1}H NMR and IR spectroscopies and isolated mass.

Addition of KOCN and benzo-15-crown-5 ether to **15**, or the addition of crown to the crude mixture resulting from the reduction of **135** in the absence of crown, afforded dark green solutions indicative isocyanate binding to afford **136**, and was confirmed by ^{1}H NMR spectroscopy.

Finding that the reduction of **135** with KC_8 in the absence of crown ethers affords **15**, we then investigated the analogous reaction between the dinuclear species [{U(Tren^{TIPS})(μ-N)(μ-K)}$_2$], **107**, which does not contain any crown moieties, and CO.



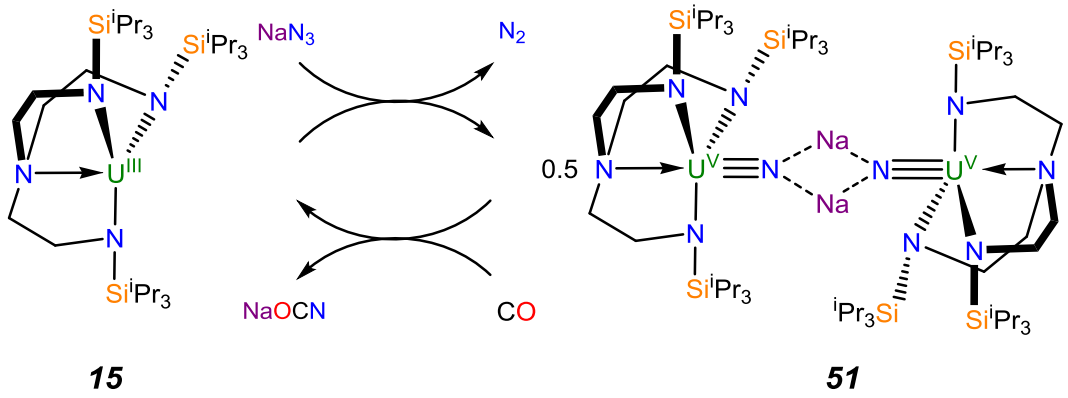
107 ***15***

*Scheme **5.7.** Synthesis of **15**.*

As judged by IR and ^{1}H NMR spectroscopies, the reaction proceeds as anticipated to afford **15** and KOCN, *via* two electron reductive carbonylation/denitrification. This transformation is reminiscent of the initial route to the preparation of the [{U(Tren^{TIPS})(μ-N)(μ-Na)}$_2$] (**51**). That is to say, the product of the reductive

carbonylation/denitrification of **107** (**15**) is one of the reagents in preparation of **51** (by the two electron reduction of NaN_3 in pyridine).

Our other studies had revealed that unlike [U(Tren^{DMBS})] (**14**), which reductively homologates CO to ethynediolate (**73**),[23] **15** does not react with CO. Furthermore, efforts to prepare **107** *via* reaction of **15** with KN_3 in pyridine had been unsuccessful. With this in mind, we sought to couple these known reactivities to effect a synthetic cycle for the conversion of sodium azide to sodium–bridged uranium–nitride to sodium cyanate utilising the two electron U^{III}-U^{V} redox couple.



*Scheme **5.8.** A two-step synthetic cycle for azide to nitride to cyanate conversion.*

A degassed mixture of **15** and NaN_3 in pyridine was exposed to one atmosphere of CO. As judged by IR spectroscopy, conversion of azide to nitride and then cyanate *via* reductive carbonylation/denitrification was observed (NaOCN ν_{NCO} 2228 cm^{-1}). Unfortunately, irrespective of the amount of NaN_3 present, only one turnover was achieved.

Although this two-step cycle is stoichiometric, and is the simplest cycle for this process reported to date, we believe that the limitation of this chemistry (as described in Chapter 2) is the requirement to use pyridine to prepare **51**, as NaN_3 is poorly soluble in the hydrocarbon solvents more commonly used for this chemistry. In light of the challenges in balancing solubility and compatibility issues and the preparation of **51** *via* this synthetic strategy, we have not yet been able to make this cycle catalytic.

However, reductive carbonylation of metal nitrides remains a rare transformation,[1,2,6] and newly formed substrates often remain bound to the metal,[6] with only three examples of denitrification to afford complete N atom transfer known for p- or d-block compounds.[1,5,24] Therefore, the reactivity demonstrated here represents a new precedent in f-block chemistry, and serves to highlight the surprising similarities between uranium nitrides and d- and p-block analogues.

5.2.4. Computational analysis

Density Functional Theory (DFT) was used to probe the difference in the rates of reaction for the reductive carbonylation of **115** and **54**.

The reactivity described puts **115** as more reactive than **54** which is contrary to reactivity already assessed, i.e. the photolytic decomposition of **54**. It had been observed that **54** undergoes C-H bond activation under photolytic conditions (sunlight $t_{1/2}$ ~ 7 days or 20 mins with 125 W medium pressure mercury lamp) to afford [U{NHCH(Me)$_2$Si(^{i}Pr)$_2$*N*CH$_2$CH$_2$*N*(CH$_2$CH$_2$*N*Si^{i}Pr$_3$)$_2$}] (**50**), whereas **115** is photolytically stable.

The reaction profiles for the reductive carbonylation of **115** and **54** were modelled using DFT calculations at the B3PW91 level of theory. In both cases, the reactions are kinetically accessible and thermodynamically favourable.

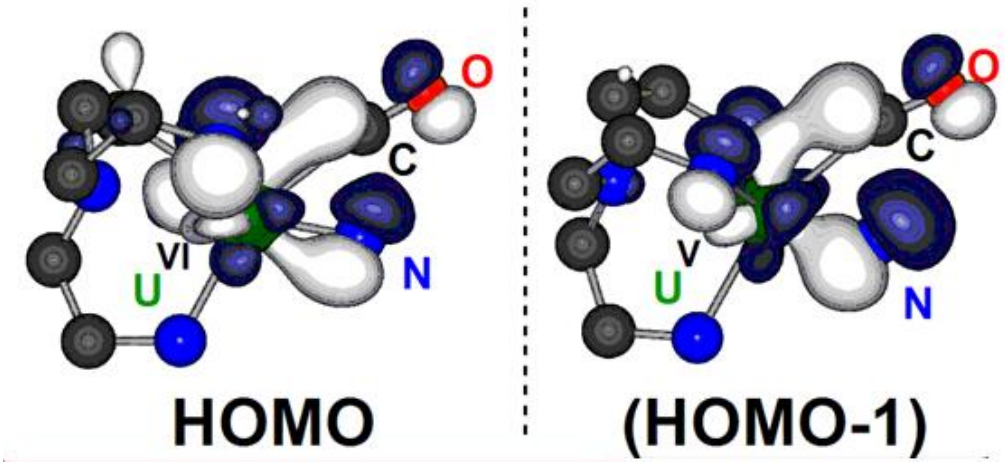


*Figure **5.8.** Kohn-Sham representations of the HOMO of **54** (left) and HOMO-1 of **115** (right) for the transition states of the reductive carbonylation of uranium*

nitrides. Full models were calculated but peripheral substituents have been omitted for clarity.

The reactions of uranium–nitrides towards carbon monoxide can be described as the nucleophilic attack of the nitride on an incoming CO molecule, which is revealed by the molecular orbitals of the transition states (figure **5.8.**). The HOMO for the uranium(VI) system, and the HOMO-1 for the uranium(V) system both exhibit an overlap between the nitride *p*-lone pair and the π* orbital of CO. This is somewhat different from a [2 + 2]-addition reaction, which may be interpreted as CO addition to the nitride. The nucleophilic behaviour of these Tren–uranium nitrides is in-line with experiment, as **115** and **54** do not undergo electrophilic addition with phosphines (see Chapter 5, Section 2.5). An important feature of these reactions is that the spin-state change only occurs after the TS. Indeed for **54**, a TS in the triplet state was located 20 kcal mol^{-1} higher than the TS reported here (figure **5.9.**).

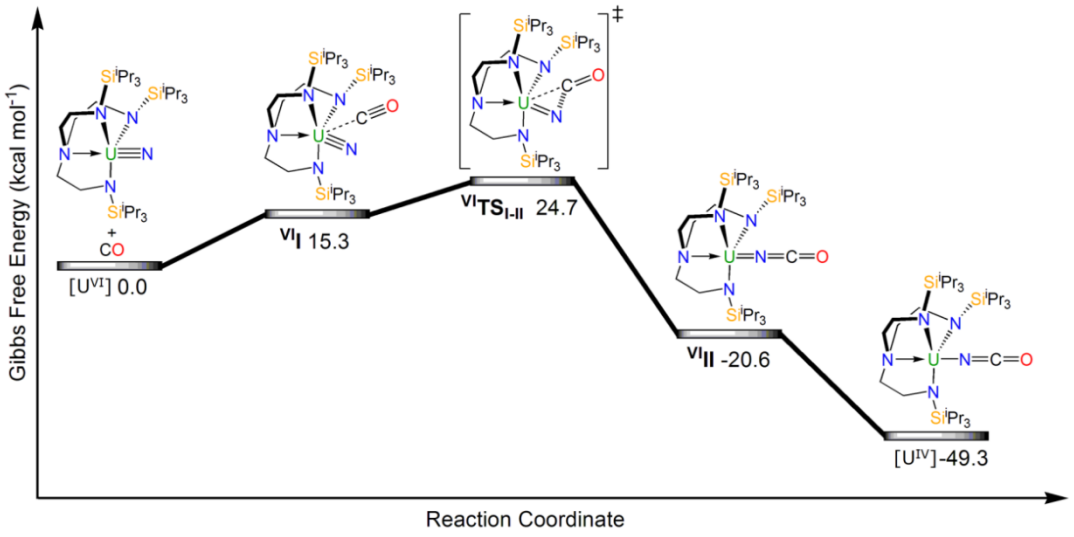


*Figure **5.9.** Gibbs free energy profile (at 298 K) for the reaction of CO with [U(Tren^{TIPS})(N)] (**54**) computed at the B3PW91 level of theory.*

The experimentally observed difference in reaction rates of **54** and **115** is corroborated theoretically, and can be explained by CO pre-coordination to uranium. For **54**, the CO molecule must approach closer to the uranium centre in order to coordinate than for **115**, as the ionic radius of uranium(VI) is smaller than for

uranium(V).[25] This coordination is energetically costly for **54** (endergonic by 15.3 kcal mol^{-1}, figure **5.9.**), which makes the barrier higher for **54** than **115**.

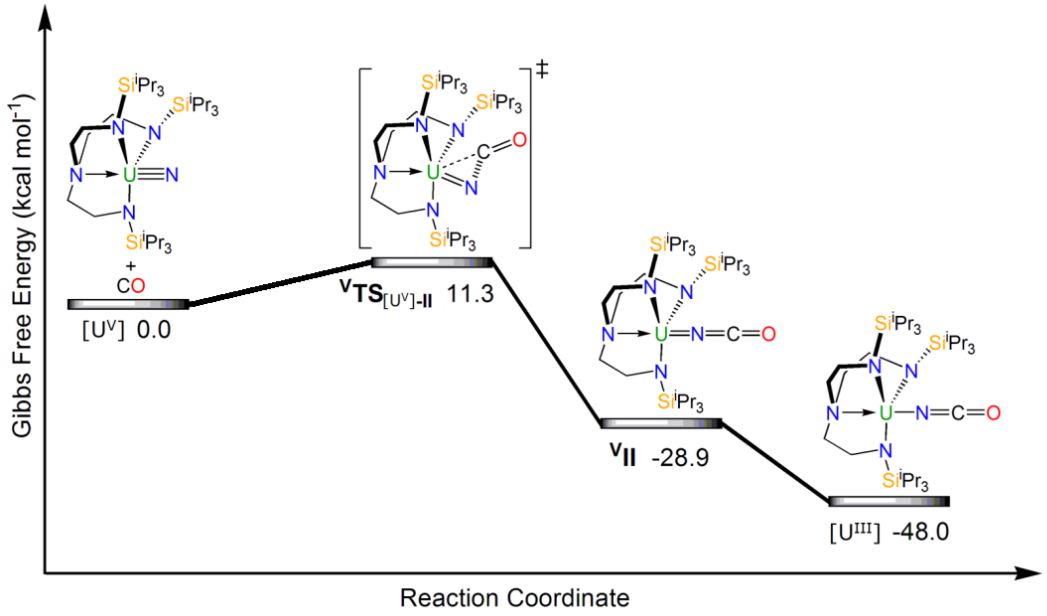


*Figure **5.10.** Gibbs free energy profile (at 298 K) for the reaction of CO with [U(Tren^{TIPS})(N)][K(Bn-15C5)$_2$] (**115**) computed at the B3PW91 level of theory.*

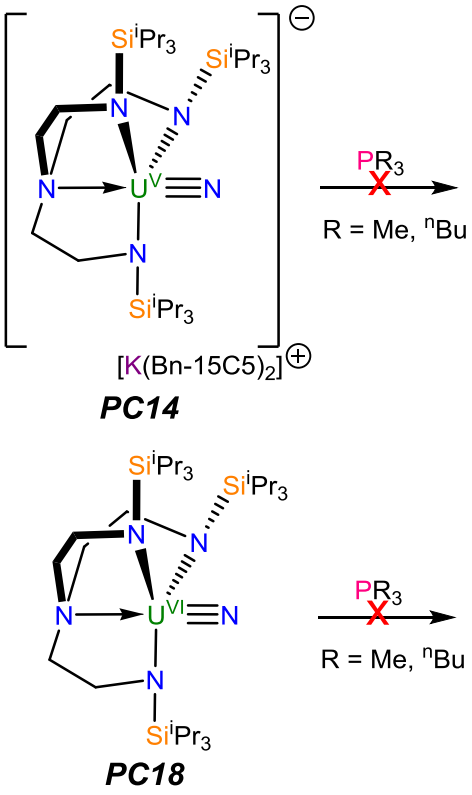
Finally, whilst there is CO-adduct formation described for **54** (figure **5.9.**), no such complex forms for **115** (figure **5.10.**). It can be inferred that uranium to CO back-bonding appears to play no role in the observed reactivity due to the absence of 5f electrons for uranium(VI).

5.2.5. Reactivity of Tren–uranium nitrides towards phosphines

Given that Tren–uranium nitrides have been shown to react with carbon monoxide in a nucleophilic manner, it is then instructive to test this by reaction with nucleophiles, such as phosphines, anticipating that there should be no reaction.

No reaction is observed when phosphines (PMe_3 or P^nBu_3) are added to either **115** or **54**, even with heating to 50°C, as judged by ^1H and $^{31}P\{^1H\}$ NMR spectra. This negative result verifies that **115** and **54** react in a nucleophilic manner, and allows us

to conclude this experimentally. This allows the targeting of further work can then be towards reactions with electrophilic molecules.



*Scheme **5.9.** Reaction of **115** and **54** with phosphine nucleophiles.*

5.3. Summary and Conclusions

A reactivity study of uranium(VI)– (**54**) and uranium(V)– (**115** and **111**) nitrides towards ambiphilic CO was carried out. Two electron reductive carbonylation of these species afforded uranium(IV)– (**135**) and uranium(III)– (**136** and **137**) isocyanates, [U(Tren^{TIPS})(NCO)], [U(Tren^{TIPS})(NCO)][K(Bn-15C5)$_2$] and [U(Tren^{TIPS}){(μ-NCO)(μ-K)(18C6)}], respectively.

Reduction of [U(Tren^{TIPS})(NCO)] (**135**) with KC_8 in the presence of crown ethers afforded uranium(III)–isocyanates (**136** and **137**). In the absence of crown ethers, one electron reduction with KC_8 of [U(Tren^{TIPS})(NCO)] (**135**) or the two electron reductive carbonylation of [{U(Tren^{TIPS})(μ-N)(μ-K)}$_2$] (**107**) resulted in the complete N atom transfer and denitrification of these species to afford KOCN and

[U(Tren^{TIPS})] (**15**). A synthetic cycle for the conversion of NaN_3 to NaOCN utilising a U^{III}-U^{V} redox couple was demonstrated to undergo one turnover. The absence of further turnovers we believe to arise from the poor solubility of NaN_3 in pyridine, which had previously caused us to investigated alternative syntheses for uranium–nitrides (Chapter 2).

DFT calculations were performed to model the reactions of [U(Tren^{TIPS})(N)] (**54**) and [U(Tren^{TIPS})(N)][K(Bn-15C5)$_2$] (**115**) with CO. Calculated reaction profiles reproduce experimental outcomes, provided evidence that these nitrides react nucleophilically, and uncovered reasons for the difference in the rate of reactions between uranium(V)– and uranium(VI)–nitrides.

Finally, the absence of reactions of **115** or **54** with phosphine nucleophiles is consistent with Tren–uranium nitrides reacting in a nucleophilic manner.

5.4. References

(1) Silvia, J. S.; Cummins, C. C. *J. Am. Chem. Soc.* **2009**, *131*, 446.
(2) Askevold, B.; Nieto, J. T.; Tussupbayev, S.; Diefenbach, M.; Herdtweck, E.; Holthausen, M. C.; Schneider, S. *Nat. Chem.* **2011**, *3*, 532.
(3) Knobloch, D. J.; Lobkovsky, E.; Chirik, P. J. *Nat. Chem.* **2010**, *2*, 30.
(4) Cozzolino, A. F.; Silvia, J. S.; Lopez, N.; Cummins, C. C. *Dalton Trans.* **2014**, *43*, 4639.
(5) Scepaniak, J. J.; Bontchev, R. P.; Johnson, D. L.; Smith, J. M. *Angew. Chem., Int. Ed.* **2011**, *50*, 6630.
(6) Tran, B. L.; Pink, M.; Gao, X. F.; Park, H.; Mindiola, D. J. *J. Am. Chem. Soc.* **2010**, *132*, 1458.
(7) Castro-Rodriguez, I.; Nakai, H.; Meyer, K. *Angew. Chem., Int. Ed.* **2006**, *45*, 2389.
(8) Addison, A. W.; Rao, T. N.; Reedijk, J.; van Rijn, J.; Verschoor, G. C. *J. Chem. Soc., Dalton Trans.* **1984**, 1349.
(9) *τ is a measure of how trigonal bipyramidal the complex is:*

τ = (β – α)/60, where β is the largest angle, and α is the second largest angle; a perfect square based pyramid has a value of 0, whilst a perfect trigonal bipyramid has a value of 1; values larger than 1 arise due to distortion from the ideal angles of 180 and 120°, due to steric constraints of the ligand.
(10) King, D. M.; Tuna, F.; McInnes, E. J. L.; McMaster, J.; Lewis, W.; Blake, A. J.; Liddle, S. T. *Nat. Chem.* **2013**, *5*, 482.
(11) Camp, C.; Settineri, N.; Lefevre, J.; Jupp, A. R.; Goicoechea, J. M.; Maron, L.; Arnold, J. *Chem. Sci.* **2015**, *6*, 6379.

(12) Camp, C.; Chatelain, L.; Kefalidis, C. E.; Pecaut, J.; Maron, L.; Mazzanti, M. *Chem. Commun.* **2015**, *51*, 15454.
(13) Thomson, R. K.; Scott, B. L.; Morris, D. E.; Kiplinger, J. L. *Comptes Rendus Chimie* **2010**, *13*, 790.
(14) Windorff, C. J.; Evans, W. J. *Organomet.* **2014**, *33*, 3786.
(15) Frey, A. S. P.; Cloke, F. G. N.; Coles, M. P.; Hitchcock, P. B. *Chem.-Eur. J.* **2010**, *16*, 9446.
(16) Evans, D. F. *J. Chem. Soc. (Res.)* **1959**, 2003.
(17) Kindra, D. R.; Evans, W. J. *Chem. Rev.* **2014**, *114*, 8865.
(18) Kefalidis, C. E.; Frey, A. S. P.; Roe, S. M.; Cloke, F. G. N.; Maron, L. *Dalton Trans.* **2014**.
(19) *As evidenced by a search of the Cambridge Structural Database (CSD)*.
(20) Patel, D.; Tuna, F.; McInnes, E. J. L.; McMaster, J.; Lewis, W.; Blake, A. J.; Liddle, S. T. *Dalton Trans.* **2013**, *42*, 5224.
(21) Fickes, M. G.; Odom, A. L.; Cummins, C. C. *Chem. Commun.* **1997**, 1993.
(22) Silvia, J. S.; Cummins, C. C. *J. Am. Chem. Soc.* **2010**, *132*, 2169.
(23) Gardner, B. M.; Stewart, J. C.; Davis, A. L.; McMaster, J.; Lewis, W.; Blake, A. J.; Liddle, S. T. *Proc. Natl. Acad. Sci. U. S. A.* **2012**, *109*, 9265.
(24) Dielmann, F.; Back, O.; Henry-Ellinger, M.; Jerabek, P.; Frenking, G.; Bertrand, G. *Science* **2012**, *337*, 1526.
(25) Shannon, R. *Acta Crystallographica Section A* **1976**, *32*, 751.

Chapter Six

The Reactivity of Uranium Nitrides Towards Heteroallenes

Table of Contents

6.1. Introduction and Aims 218

6.2. Reactivity Studies of Uranium Nitride Complexes Towards CE_2 219

6.2.1. CO_2 219

6.2.1.1. Tren–uranium(V) nitrides 219

6.2.1.1.1. Reactivity study of [U(Tren^{TIPS})(N)][K(Bn-15C5)$_2$] (115) towards CO_2 219

6.2.1.1.2. Reactivity study of [U(Tren^{TIPS}){(μ-N)(μ-K)(Bn$_2$-18C6)}] (111) towards CO_2 226

6.2.1.1.3. Reactivity study of [{U(Tren^{TIPS})(μ-N)(μ-K)}$_2$] (107) towards CO_2 227

6.2.1.2. Tren–uranium(VI) nitride (54) 227

6.2.2. CS_2 233

6.2.2.1. Tren–uranium(V) nitrides 233

6.2.2.1.1. Reactivity study of [U(Tren^{TIPS})(N)][K(Bn-15C5)$_2$] (115) towards CS_2. 233

6.2.2.1.2. Reactivity study of [U(Tren^{TIPS}){(μ-N)(μ-K)(Bn-15C5)}] (111) towards CS_2 238

6.2.2.1.3. Reactivity study of [{U(Tren^{TIPS})(μ-N)(μ-K)}$_2$] (107) towards CS_2 241

6.2.2.2. Tren–uranium(VI) nitride (54) 242

6.2.3. Computational Analysis 247

6.2.3.1. [U(Tren^{TIPS})(N)][K(Bn-15C5)$_2$] (115) + CO_2 247

6.2.3.2. [U(Tren^{TIPS})(N)] (54) + CO_2 248

6.2.3.3. [U(Tren^{TIPS})(N)][K(Bn-15C5)$_2$] (115) + CS_2 249

6.2.3.4. [U(Tren^{TIPS})(N)] (54) + CS_2 251

6.2.4. Discussion of mechanistic insights 252

6.3. Summary and Conclusions 256

6.4. References 258

6.1. Introduction and Aims

Having now established that the nitride functionalities in [U(Tren^{TIPS})(N)][K(Bn-15C5)$_2$] (**115**) and [U(Tren^{TIPS})(N)] (**54**) are both nucleophilic, by a combined experimental and theoretical study with carbon monoxide, and uncovered reasons that account for the difference in the rate of reactions with different oxidation states of uranium (see Chapter 5), we sought to investigate the reactivity of **115** and **54** towards the small heteroallenes, CE_2 (E = O, S), which contain electrophilic carbon centres.

In terms of their wider utility, CO_2 is an abundant, low cost, renewable C_1-source for fine chemicals and fuels production, whilst CS_2 is a versatile building block in organic chemistry and is often used to model CO_2 reactivity.

Whilst the activation of CO_2 and CS_2 by uranium has become more widespread recently, there are still far fewer examples in comparison to transformations promoted by transition metals (see Chapter 1). Often, due to the strong C=O bond in CO_2 (and to a lesser extent the C=S bond in CS_2), activation of these molecules occurs by the reductive cleavage of the C=E linkage, followed by insertion or coupling to afford $(CE_3)^{2-}$ and $(E_2CCE_2)^{2-}$ motifs. When activation does not occur by redox processes, insertion into metal-ligand linkages is the classical mode of reactivity. Redox-free σ-bond metathesis of CE_2 is relatively rare, being documented in only a few cases, usually involving terminal imide or nitride complexes.[1-7]

As there are relatively few examples of transition metal nitride reactivity with heteroallenes, and the only examples thus far for uranium systems incorporating U-N multiple bond interactions involve uranium–imides[1,2] or bridged nitrides,[3] we sought to investigate the reactions of our Tren–uranium(V) and (VI) nitrides with CE_2 (E = O, S) to discern if any unusual reactivity modes might be unlocked. What follows is an investigation into this area, followed by mechanistic insights from a computational standpoint.

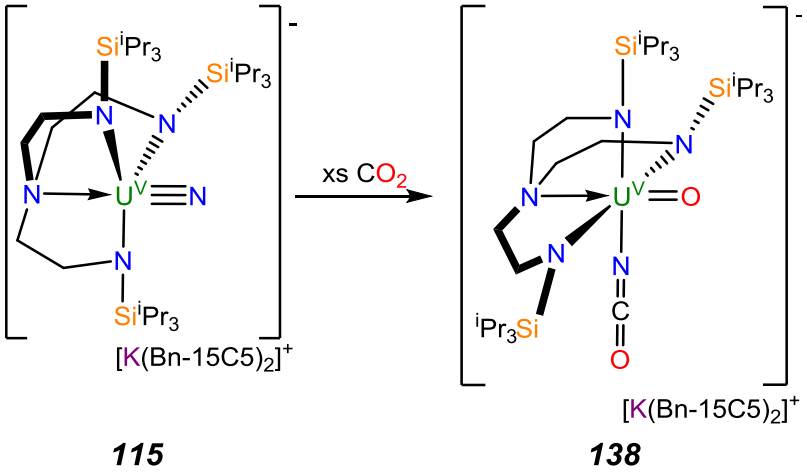
The computational chemistry reported in the chapter was performed by Dr C. E. Kefalidis and Prof. L. Maron of Université Paul Sabatier, Toulouse.

6.2. Reactivity Studies of Uranium Nitride Complexes Towards CE_2

6.2.1. CO_2

6.2.1.1. Tren–uranium(V) nitrides

6.2.1.1.1. Reactivity study of [U(Tren^{TIPS})(N)][K(Bn-15C5)$_2$] (115) towards CO_2



115 ***138***

*Scheme **6.1**. Synthesis of **138**.*

A cold (–78°C), degassed solution of [U(Tren^{TIPS})(N)][K(Bn-15C5)$_2$] (**115**) in toluene was exposed to one atmosphere of CO_2. After three minutes, a modest colour change from yellow-brown to red-brown was observed. Upon work-up, orange crystals were isolated of material formulated as oxo-isocyanate species [U(Tren^{TIPS})(O)(NCO)][K(Bn-15C5)$_2$], **138** (crystalline yield 36 %).

The optimal experimental conditions required to isolate **138** were found to be a reaction time of three minutes. Stirring a cold solution of **115** under one atmosphere of CO_2 for times much shorter than this resulted in no significant reaction, whilst reaction times of five minutes or longer resulted in decomposition of the sample, as confirmed by ^{1}H NMR spectroscopy which showed only diamagnetic resonances attributable to free pro-ligand and crown ether in spectra of reaction mixtures.

The molecular structure is of **138** illustrated in figure **6.1.**, alongside selected bond lengths and angles.

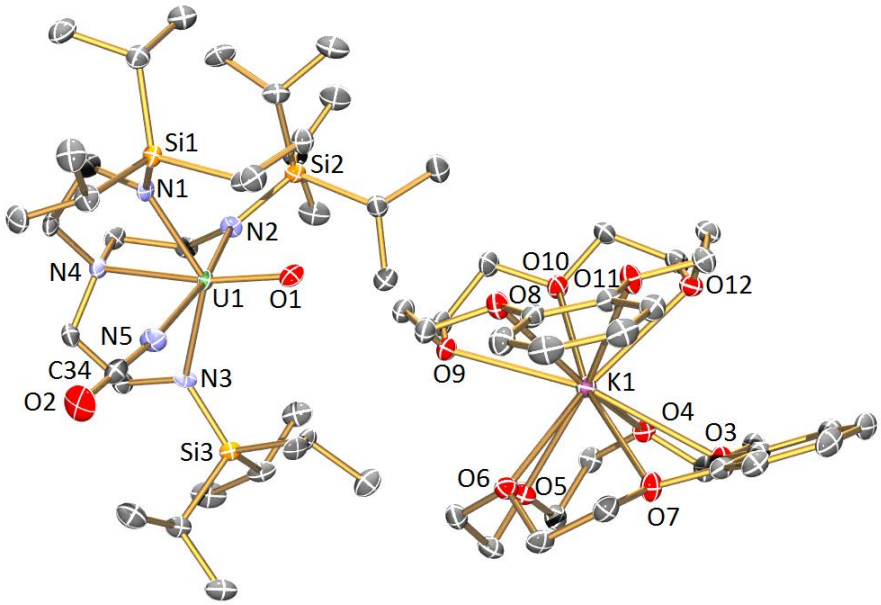


*Figure **6.1.** Molecular structure of [U(Tren^{TIPS})(O)(NCO)][K(Bn-15C5)$_2$]•(C_6H_6), **138**. Thermal ellipsoids set at 40% probability. Hydrogen atoms and lattice solvent are omitted for clarity. Selected distances (Å) and angles (°) for one of the crystallographically independent uranium and potassium fragments: U(1)-N(1) 2.316(7), U(1)-N(2) 2.302(7), U(1)-N(3) 2.342(7), U(1)-N(4) 2.517(7), U(1)-O(1) 1.848(7), U(1)-N(5) 2.404(8), N(5)-C(34) 1.199(13), C(34)-O(2) 1.163(13), K(1)-O(3) 2.925(7), K(1)-O(4) 2.886(7), K(1)-O(5) 2.775(7), K(1)-O(6) 2.832(7), K(1)-O(7) 2.879(7), K(1)-O(8) 3.022(7), K(1)-O(9) 2.806(6), K(1)-O(10) 2.770(7), K(1)-O(11) 2.875(7), K(1)-O(12) 2.896(7), N(4)-U(1)-O(1) 168.0(3), N(2)-U(1)-N(5) 168.3(3), U(1)-N(5)-C(34) 168.1(8), N(5)-C(34)-O(2) 179.1(12).*

The solid state structure of **138** reveals there are two crystallographically independent, separated ion pairs in the asymmetric unit. One of these pairs is considerably less disordered than the other, and it is the metrical parameter of this pair that will be discussed. Complex **138** adopts a distorted octahedral geometry at uranium with the oxo group being *trans* to the face-capping amine of Tren^{TIPS}, and the isocyanate group *trans* to one amine of Tren^{TIPS} and mutually *cis* to the oxo ligand. The deviation from ideal octahedral geometry, due to the large steric demands of the Tren^{TIPS} ligand, is demonstrated by the angles O(1)-U(1)-N(4) 168.0(3) and N(2)-U(1)-N(5) 168.3(3)°. This structure represents the first instance of a distorted octahedral geometry about uranium containing a {U(Tren^{TIPS})} motif, and

suggests that the apical pocket of $Tren^{TIPS}$, which had been considered only suitable for coordination of one small or cylindrical ligand, can in fact accommodate two such ligands in certain circumstances.

Competitive refinement of the diffraction data suggest that the cyanate unit is *N*-bound, not *O*-bound, which is in agreement with the isocyanate data discussed previously (**135** and **136**, Chapter 5). This is supported by DFT calculations, which indicate that the *N*-bound isomer is more stable that the *O*-bound isomer by 9 kcal mol^{-1}. The N-C and C-O bond distances within the isocyanate unit of **138** are statistically indistinguishable from the corresponding distances in **135**. This suggests that, as was the case for the uranium(IV) system (**135**), there is a significant polarisation of the electron density from the π-manifold of the NCO^- ligand by the uranium(V) centre. This is facilitated by the near linear geometry of the U-N-C angle of **138** [U(1)-N(5)-C(34) 168.1(8), *cf.* **135** U(1)-N(5)-$C(34)_{av}$ 173.2(15)°].

The U-O, U-$N_{isocyanate}$ and U-N_{amine} distances [U(1)-O(1) 1.848(7), U(1)-N(5) 2.404(8), U(1)-N(4) 2.517(7) Å respectively] are typical of such linkages [literature terminal uranium(V) mono-oxo distances range 1.805(2) – 1.859(6) Å, uranium(IV)–isocyanate distances range 2.337(3) – 2.389(6) Å][8] though the U-N_{amine} bond length is towards the lower end for TrenN_{amine}-U distances [*cf.* **115** U(1)-N(4) 2.683(3) Å], and is statistically indistinguishable from the corresponding U(1)-N_{amine} distance in [U($Tren^{TIPS}$)(O)] (**122**) of 2.482(6) Å,[9] despite the differing coordination geometries. In both **138** and **122**, the oxo ligand is *trans* to the amine nitrogen, and this suggests that there may be a weak inverse *trans* influence in the N→U=O unit of **138**, which was also implicated in the bonding of **122**.[9]

The metal-crown oxygen distances [K-O 2.770(7) – 3.022(7) Å] are consistent with other complexes of this form previously reported, as well as the corresponding literature distances [mean K-O(15C5) distance 2.908 Å],[8] and are otherwise unremarkable.

Complex **138** may be most directly comparable to **105**. Complex **105** was prepared by the reaction of the bridging nitride **58** with one equivalent of CO_2, and although it has two uranium(IV) centres it does contain both oxo and isocyanate ligands, in a bridging configuration.[3] As a result of this configuration, both U-O and U-N bonds

lengths [av. 2.559(9) and 2.123(5) Å respectively] are considerably longer than their terminal equivalents in **138**. There is one other example of a uranium–cyanate derived from CO_2, namely **83**, which results from the multiple N-Si bond cleavage of $[U(N'')_4][K(18C6)]$ on reaction with CO_2.[10]

The ^{1}H NMR spectrum of **138** spans the range +16 to –2 ppm, which is concordant with uranium(V) species of this form (such as for **122**, which spans +15 to –2 ppm).[9] The presence of two signals in the ^{29}Si{^{1}H} NMR spectrum (at –27.1 and –27.8 ppm) indicate that this complex does not possess C_{3v} symmetry, which is consistent with the ratios present upon integration of the resonances in the ^{1}H NMR spectrum [δ 15.63 (br, 6H, CH_2), 12.96 (br, 6H, CH_2), 7.06 – 6.90 (m, 8H, Ar-*H*), 3.98 – 3.76 (m, 32H, crown-CH_2), 1.95 (br, 18H, CH(CH_3)$_3$), 1.43 (br, 3H, C*H*(CH$_3$)$_3$), –1.36 (br, 36H, CH(CH_3)$_3$) –2.19 (br, 6H, C*H*(CH$_3$)$_3$) ppm] and by inspection of the geometry of the molecular structure as detailed above. The ^{29}Si{^{1}H} spectrum is also in agreement with literature values for uranium(V) species.[11]

The FTIR spectrum for **138** corroborates the formation of oxo and isocyanate functional groups, with absorptions at 742 and 800, and 2194 cm^{-1} being attributed to stretches of oxo and cyanate ligands respectively. These compare well to calculated frequencies of 747, 799 and 2195 cm^{-1}, as well as to literature values for uranium isocyanates [range 2172 – 2201 cm^{-1}].[8] Two stretches are calculated for the oxo, and these arise due to coupling with the U-N$_{amine}$ stretch resulting in both symmetric and asymmetric combinations. The isocyanate stretch also compares well to [U(Tren^{TIPS})(NCO)] (**135**, 2187 cm^{-1}, Chapter 5), in spite of the differing geometries of these compounds (wherein **135** is trigonal bipyramidal and the isocyanate is *trans* to an amine, and **138** is octahedral and the isocyanate is *trans* to an amide). Furthermore, this extends the trend that was established previously, where the wavenumber of the isocyanate stretch increases with increasing oxidation state [U^{III} (**136**) 2172, U^{III} (**137**) 2180, U^{IV} (**135**) 2187, U^{V} (**138**) 2194 cm^{-1}].

A solution of **138** in toluene was analysed by UV-vis-NIR electronic absorption spectroscopy, and the observed spectrum is illustrated in figure **6.2.**

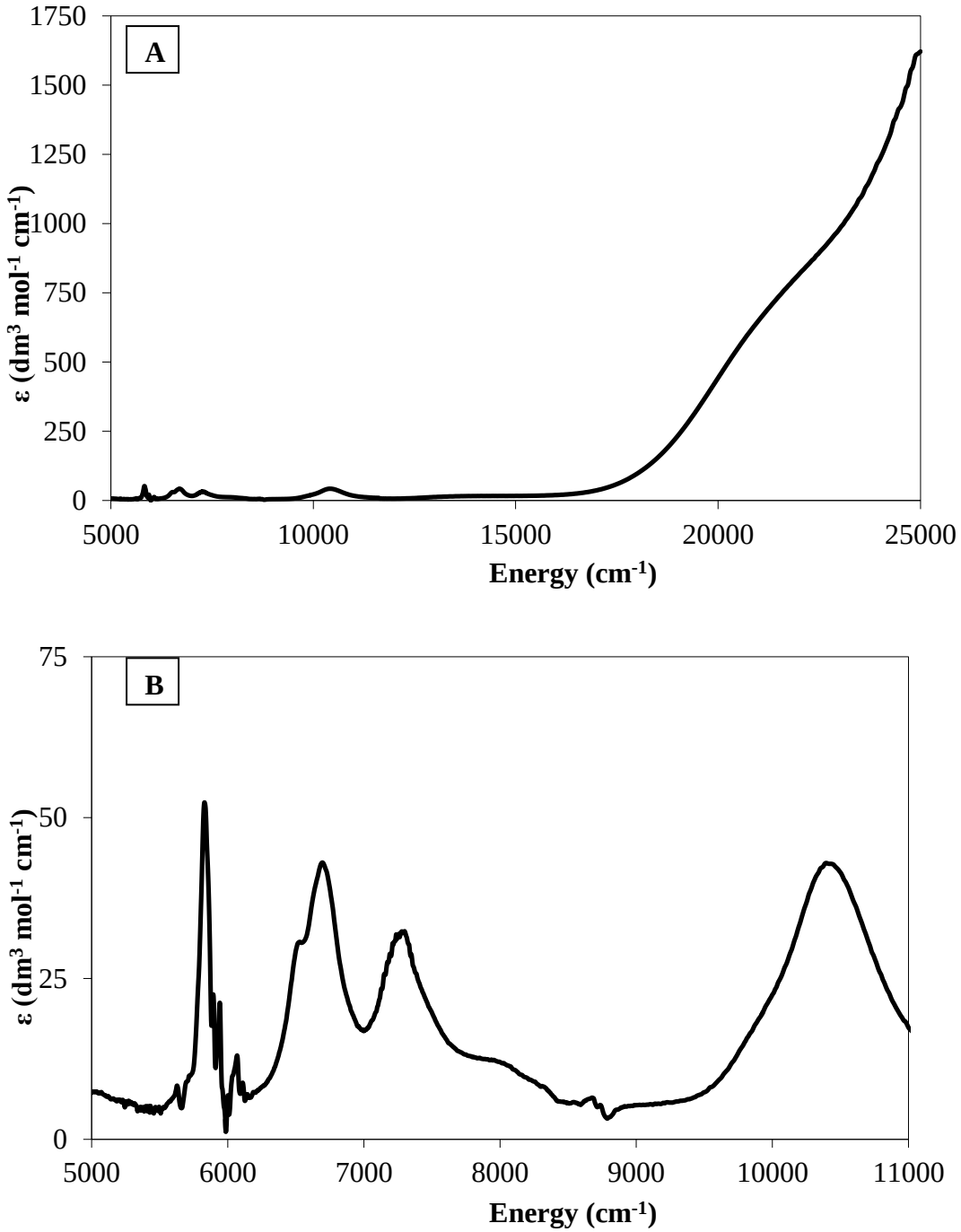


Figure ***6.2.*** ***A****: UV-vis-NIR electronic absorption spectrum of [U(Tren^{TIPS})(O)(NCO)][K(Bn-15C5)$_2$];* ***B****: zoom region.*

The spectrum of **138** can most readily be compared to other Tren–uranium(V) species, such as those of the form [U(Tren^{TIPS})(N)][M(crown)$_2$], (**52**, **114**, **115**, **116** and **117**) as discussed previously (Chapter 2, Section 3.5., figure **2.17.**). As with those data, the spectrum is dominated by charge transfer (CT) bands tailing in from

ultraviolet region. In the lower energy region (5000 – 11000 cm^{-1}), we again observe sharper absorptions as a result of *f-f* transitions. In an octahedral manifold, the ground state $^2F_{5/2}$ and excited $^2F_{7/2}$ terms are further split into $(2J + 1)/2$ doubly degenerate levels. $^2F_{5/2}$ splits into Γ_7 and Γ_8, which is double orbitally degenerate, $^2F_{7/2}$ splits into Γ_7', the double orbitally degenerate Γ_8', and Γ_6. Lowering of the symmetry further still to approximate C_s symmetry splits these degenerate Γ_8 and Γ_8' states, as illustrated in figure **6.3.**

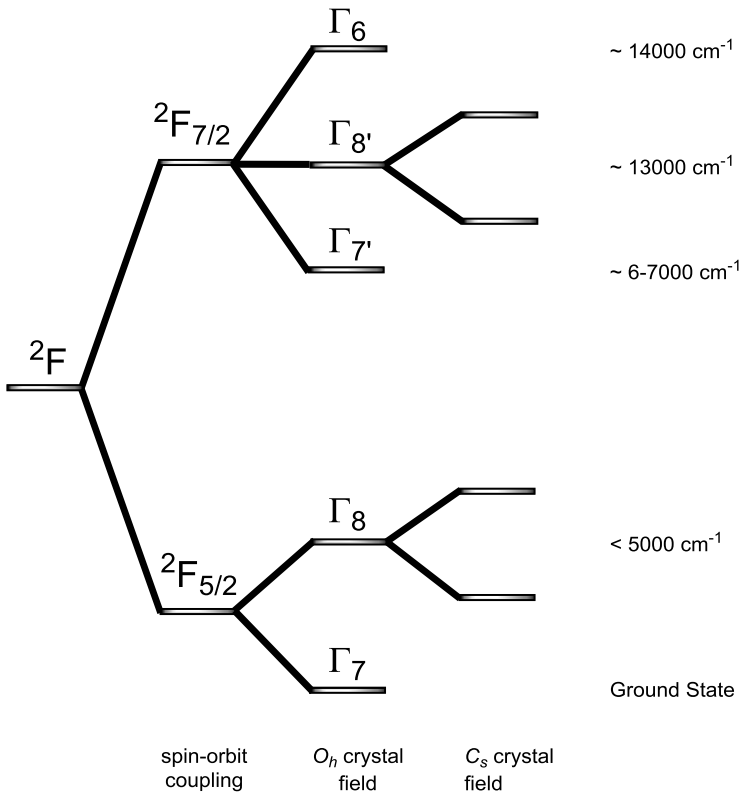


*Figure **6.3.** Schematic energy level diagram (not to scale) for the U^{5+} ion, showing the effect of spin-orbit and crystal field splitting upon the ^2F electronic ground state in O_h and C_s symmetries.*

The difference in symmetry between the C_{3v} and O_h geometries of **52** (for example) and **138**, and the subsequent effect this has of the splitting of the energy levels (see Chapter 2, figure **2.15.**), accounts for the differences between the spectrum observed for **138** and the spectra for **52**, **114**, **115**, **116** and **117**. The absorptions detailed in figure **6.3.** correspond well to four predicted transitions, as illustrated above, from Γ_7

to Γ_7', 2 x Γ_8' and Γ_6, which suggests that the strong distortion from the octahedral ideal imposes C_s symmetry.

The Evans' method[12] room temperature solution magnetic moment in benzene was determined for **138**, and found to be 1.69 μ_B. Whilst this is lower than the theoretical value of 2.54 μ_B for a uranium(V) $^2F_{5/2}$ ground state, it correlates well to experimentally observed values for μ_{eff} (1.4 – 3.2 μ_B).[13] Variable temperature SQUID magnetometry of **138** (Figure **6.4.**, left) reveals a magnetic moment of 1.86 μ_B at 298 K, that compares reasonably well to the solution magnetic moment (1.69 μ_B), considering the different phases for the measurements and weighing errors. The magnetic moment changes little until 50 K, where it falls more rapidly to 1.20 μ_B at 2 K consistent with the presence of uranium(V) that is a magnetic doublet at all temperatures.[13]

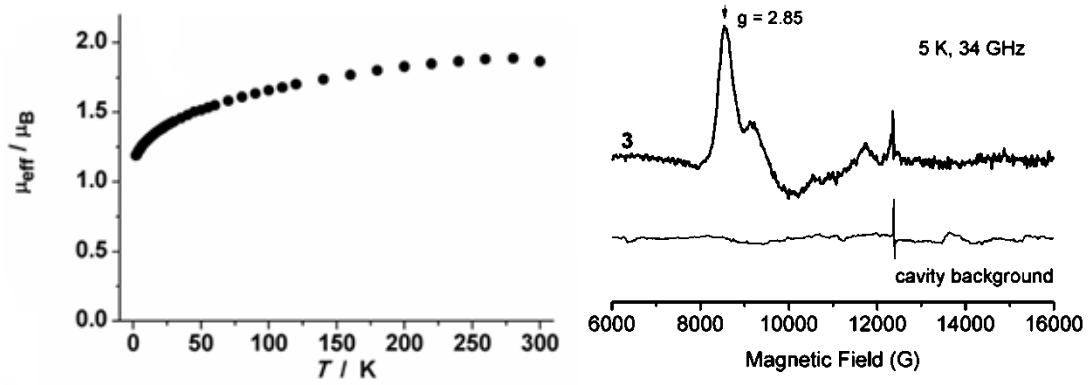
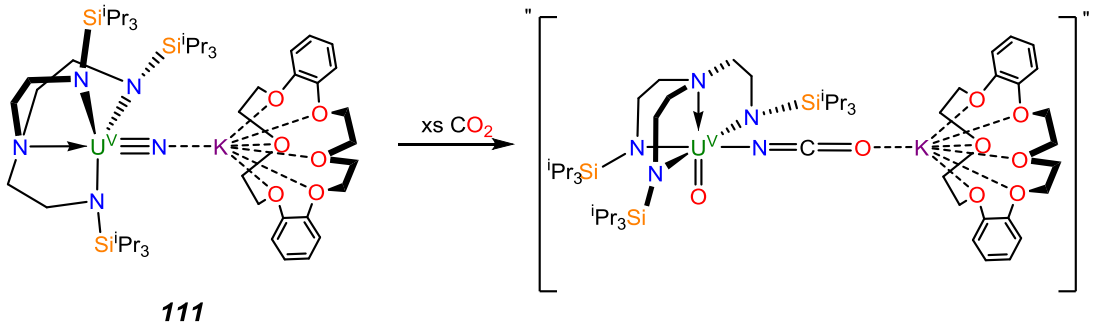


*Figure **6.4.** Left, magnetic susceptibility data [μ_{eff} (μ_B) vs T (K)] for **138**; Right, Q-band (34 GHz) EPR spectra of a powder sample of **138** and background at 5 K.*

Final confirmation of the presence of a uranium(V) centre in **138** is provided by EPR spectroscopy (figure **6.4.**, right) which reveals a strong absorption at near g = 2.85 at 5 K, which is consistent with a Kramers uranium(V) ion. By contrast, both uranium(IV) and uranium(VI) would be expected to be EPR-silent under these measurement conditions.[14]

6.2.1.1.2. Reactivity study of [U(Tren^{TIPS}){(μ-N)(μ-K)(Bn$_2$-18C6)}] (111) towards CO$_2$



111

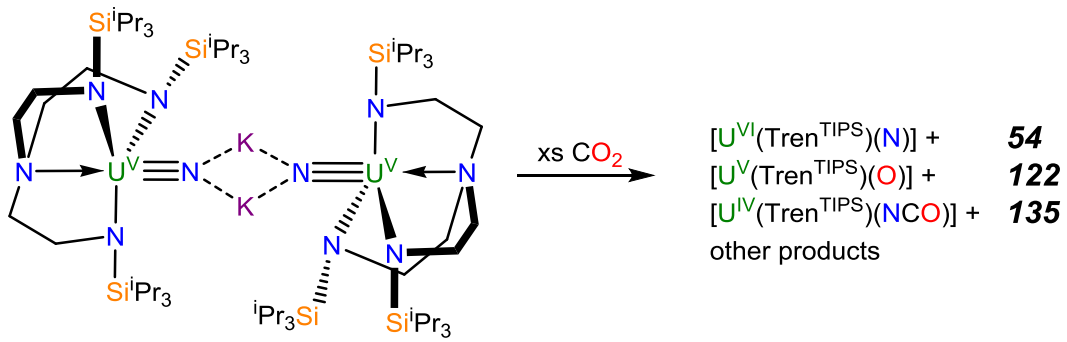
Scheme ***6.2.*** *Proposed synthesis of "[U(Tren^{TIPS})(O){(μ-NCO)(μ-K)(Bn$_2$-18C6)}]".*

The reaction of [U(Tren^{TIPS}){(μ-N)(μ-K)(Bn$_2$-18C6)}] (**111**), with CO_2 was also investigated. After stirring a solution under one atmosphere of CO_2 for 3 minutes, a colour change to orange-brown was observed. Analysis of the reaction mixture by ^{1}H NMR spectroscopy suggested that a reaction had occurred, with resonances attributable to [U(Tren^{TIPS})(O)] (**122**) and a new product present in the spectrum. By analogy to previous reactivities already discussed, (i.e. the preparation of a uranium(V)–oxo–isocyanate (**138**) from the reaction of **115** with CO_2, and a potassium uranium(III)–isocyanate (**137**) from **111-18C6** with CO), this new product from the reaction of **111** with CO_2 could be formulated as [U(Tren^{TIPS})(O){(μ-NCO)(μ-K)(Bn$_2$-18C6)}], however, as we were unable to cleanly isolate this species, this assignment is by no means unequivocal.

Analysis of the ATR spectrum for the product of the reaction of **111** with CO_2 is in agreement with this postulated species, with a strong absorption at 2181 cm^{-1}. This absorption is remarkably similar to that observed for **137** (2180 cm^{-1}), which features a capped isocyanate fragment, and therefore [U(Tren^{TIPS})(O){(μ-NCO)(μ-K)(Bn$_2$-18C6)}] seems a credible product for this reaction.

6.2.1.1.3. Reactivity study of [{U(Tren^{TIPS})(μ-N)(μ-K)}$_2$] (107) towards CO_2

Furthermore, the reaction of CO_2 with [{U(Tren^{TIPS})(μ-N)(μ-K)}$_2$] (**107**) lead to a mixture of products. Amongst these, as identified by ^{1}H NMR spectroscopy, were **54**, **122** and **135**. As no intermediates could be isolated, mechanistically it is unclear how these reactions proceed to afford the observed products. The picture is muddied further by the absence of any KOCN by-product as judged by FTIR spectroscopy (ν_{NCO} 2130 cm^{-1}). KOCN might be an anticipated product by analogy to the reductive carbonylation of **107**, which extruded KOCN in the absence of crown ethers, and hence in this system would explain the formation of **122**. This suggests that there may be multiple potential reaction pathways present, and that this may warrant further investigation.



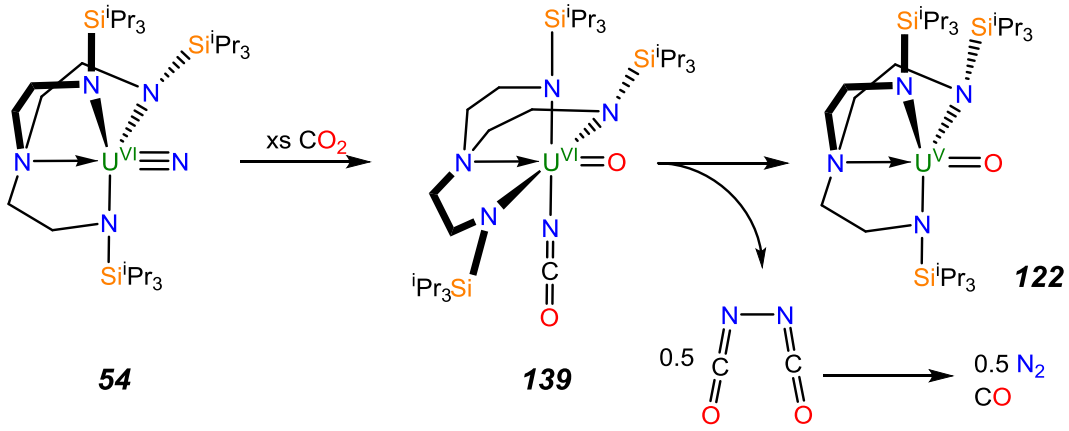
107

*Scheme **6.3.** Proposed reactivity for **107** with CO_2.*

6.2.1.2. Tren–uranium(VI) nitride (54)

In an analogous manner to the preparation of **138**, a cold (–78 °C) degassed solution of [U(Tren^{TIPS})(N)] (**54**) in toluene was exposed to one atmosphere of CO_2. As had been observed previously for reactivity studies of Tren–uranium nitrides with CO (Chapter 5), the rate of reaction for **54** was slower than for **115**. Whilst the reaction of **115** with CO_2 had gone to completion in 3 minutes, for **54**, a colour change to wine red was observed and the reaction complete after 22 minutes. Further reaction times in excess of 30 minutes resulted in decomposition of the sample. After quick work-up, a red solid was obtained, with a ^{1}H NMR spectrum spanning 0 – 10 ppm

(figure **6.5.**). Unfortunately, we were not able to obtain crystals of this red solid, as samples of this compound readily decomposed to **122** both in the solid state and as solutions in either benzene or toluene.



54 ***139***

*Scheme **6.4.** Synthesis of **139** and proposed decomposition pathway to **122**, N_2 and CO.*

By analogy to the preparation of **138**, and as the ^{1}H NMR spectrum for the crude mixture of **54** + CO_2 only has resonances only in the diamagnetic range (figure **6.5.**), we postulate that the product of this reaction is the neutral, uranium(VI) species, [U(Tren^{TIPS})(O)(NCO)], **139**. We believe **139** then undergoes decomposition to [U(Tren^{TIPS})(O)] (**122**), which explains the presence of resonances attributable to this complex in the crude ^{1}H NMR spectrum.[9]

The ^{29}Si{^{1}H} NMR spectrum, which might have been more informative than the ^{1}H NMR spectrum, as was the case for **138**, could not be obtained due to decomposition of **139** to **122** before the spectrum could be collected.

Further evidence towards a neutral oxo-isocyanate species can be found in the FTIR spectrum, which features strong absorptions at 827 and 2176 cm^{-1} (figure **6.6.**, as a Nujol mull this second absorption shifts to 2179 cm^{-1}), which can be assigned to the oxo and isocyanate fragments respectively [*cf.* literature values for uranium isocyanates: range 2172 – 2201 cm^{-1}].[8] These data are supported by calculated stretching frequencies, which predict absorptions at 812 and 2198 cm^{-1}. Interestingly, the oxo stretch is now decoupled from the U-N_{amide} stretch (*cf.* **137** which was

coupled), and therefore only one absorption is observed, which is reproduced by the frequency calculation.

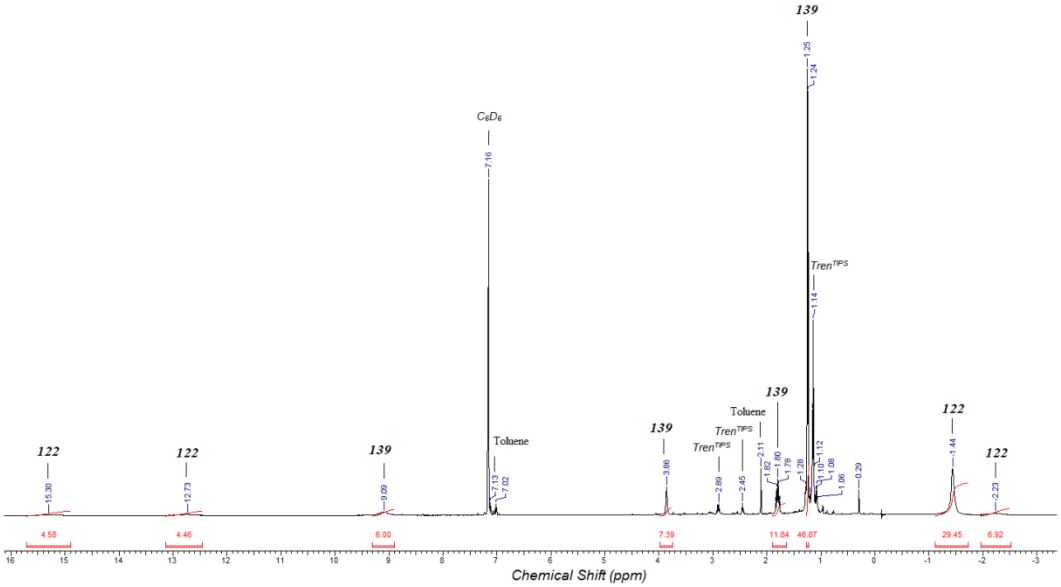


Figure ***6.5.*** *^1H NMR (d_6-benzene) spectrum of* ***54*** *+ CO_2, containing resonances assigned to* ***122*** *and free pro-ligand alongside a new product formulated as [U(Tren^{TIPS})(O)(NCO)] (**139**).*

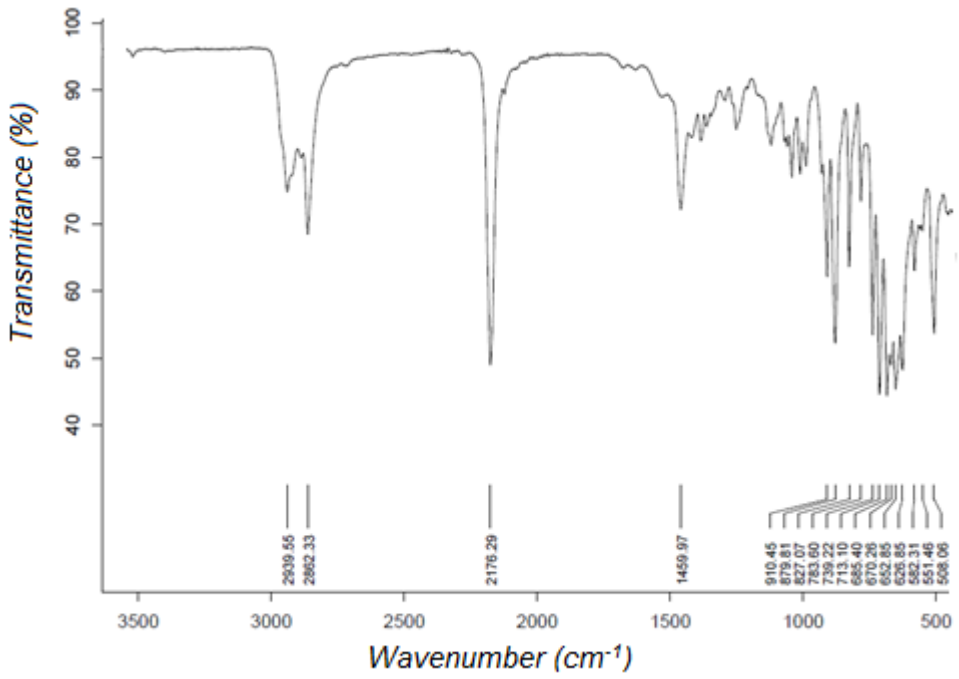


Figure ***6.6.*** *FTIR-ATR spectrum of* ***139****.*

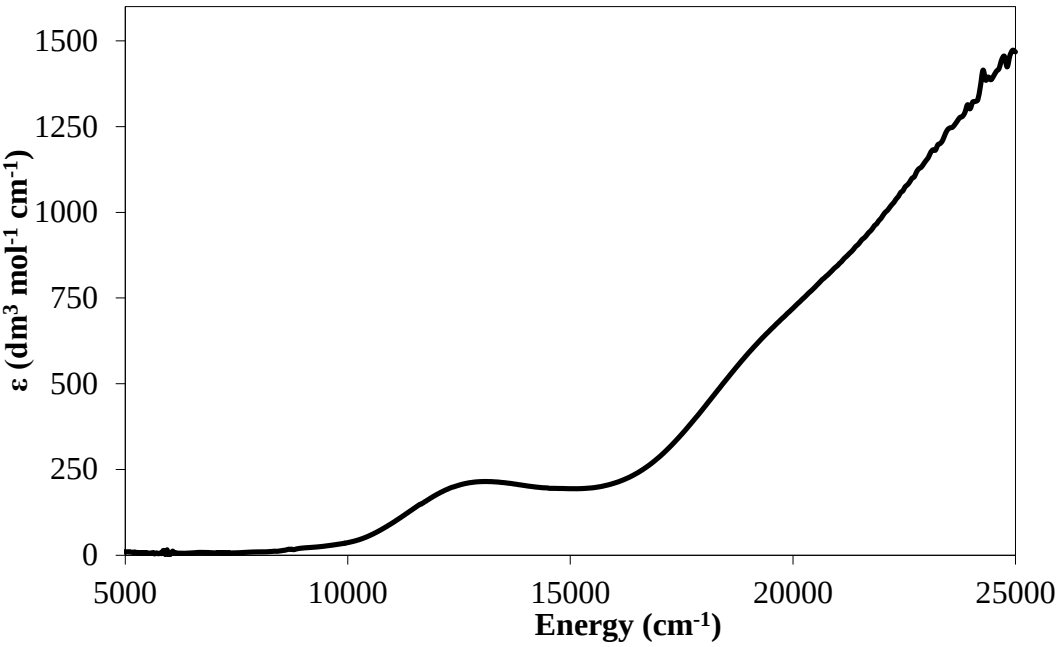


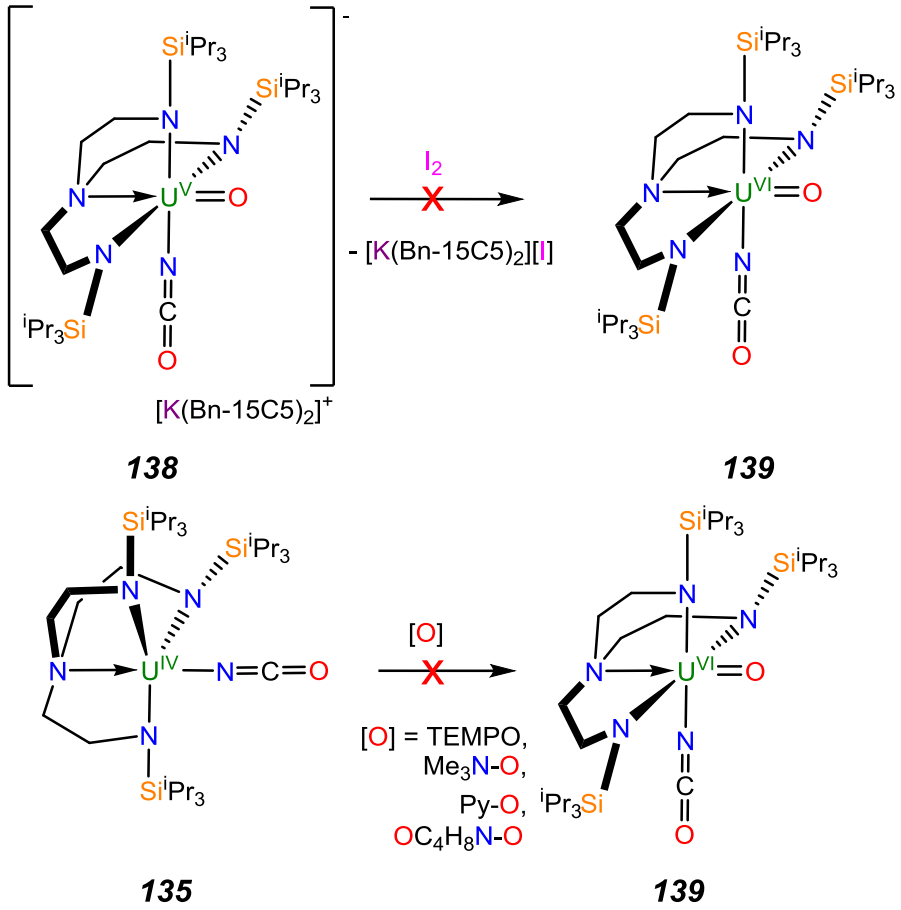
*Figure **6.7.** UV-vis-NIR electronic absorption spectrum of **139**.*

Due to the ready decomposition of **139** to **122**, the only other data which could be obtained was a UV-vis-NIR electronic absorption spectrum (figure **6.7.**). The spectrum of **139** is broad and featureless, which is consistent with the assignment of a neutral uranium(VI) $5f^0$ which has no valence *f* electrons, and therefore no *f-f* transitions. A broad absorption at ~13000 cm^{-1} arises from ligand to metal charge transfer.

The isolation of **122** as a decomposition product suggests that a cyanate radical has been ejected from the coordination sphere of uranium. Such a radical might be expected to dimerise to diisooxocyan [O=C=N–N=C=O], which would be followed by facile decomposition to N_2 and CO.[15] To test this hypothesis, we condensed the gases evolved from the reaction onto a frozen sample of vanadocene in toluene. This solution was allowed to thaw, stirred for 30 minutes, and following work-up, FITR studies were performed. These studies revealed a very weak band at 1895 cm^{-1}, which is consistent with the formation of vanadocene carbonyl $[V(Cp)_2(CO)]$.[16,17]

Other routes towards **139** were attempted. The methodology employed was to attempt to mitigate the capriciousness of the reaction of **54** with CO_2, wherein the reaction times must be strictly controlled. It was hypothesised that if **139** were stable,

and that the instability previously observed was merely due to the heterogeneous reaction conditions employed, then perhaps an oxidative route might help access this compound in a more controllable manner. Two possible synthetic pathways towards **139** were envisioned, namely the one electron oxidation of **138** with concomitant salt elimination, and the two electron oxidation of **135** with an oxide source (scheme **6.5.**).



*Scheme **6.5.** Proposed alternative syntheses of **139**.*

The addition of half an equivalent of diiodine to effect the oxidation of **138** with the concomitant elimination of $[K(Bn\text{-}15C5)_2][I]$, a pathway closely mirroring the oxidation of **115** to afford **54**, did not oxidise to afford the desired product. Whilst some change was observed in the FTIR-ATR spectrum (from 2194 cm^{-1} to 2170 and 2184 cm^{-1}), only diamagnetic decomposition products could be identified in the ^{1}H NMR spectrum (i.e. free pro-ligand).

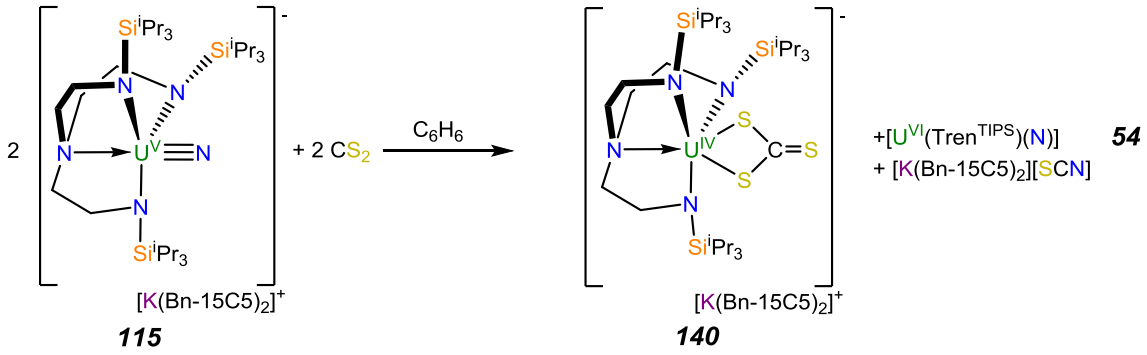
Several known oxygen transfer reagents were also tested, to see if they could effect the two electron oxidation of **135**. The addition of TEMPO [(2,2,6,6-tetramethylpiperidin-1-yl)oxyl] to **135** in d_6-benzene gave no reaction, even with heating to 60°C for 16 hours. Contrastingly, NMR scale reactions with either 4-methylmorpholine N-oxide, pyridine N-oxide or trimethylamine N-oxide as the oxide source all immediately underwent a colour change to wine red and afforded ^{1}H NMR spectra containing resonances assigned to **139**, alongside both unreacted **135** and the decomposition product, **122**. In the case of the reaction with pyridine N-oxide, there were a great many other resonances also present, spanning the range +36 to –50 ppm. However, on scale up these reactions did not permit the isolation of the desired product, instead giving only limited conversion to **122**.

From these reactivities, we might then conclude that the hypothesised product is indeed [U(Tren^{TIPS})(O)(NCO)] (**139**), as it is the logical product of the multiple synthetic routes attempted. Furthermore, we can infer that it is an inherently unstable complex, and that this instability is not due solely to the conditions of its preparation (i.e. heterogeneous reaction of solution phase **54** and gaseous CO_2). That this neutral species is less stable than the anionic analogue **138** might be ascribed to the steric congestion around the uranium centre and the more oxidising nature of uranium(VI). As the uranium(VI) is smaller than the uranium(V) ion,[18] the coordination sphere of the uranium centre becomes congested, which then enforces the elimination of the cyanate radical. These findings will be discussed in reference to computational findings in a later section (see Section 2.3.).

6.2.2. CS_2

6.2.2.1. Tren–uranium(V) nitrides

6.2.2.1.1. Reactivity study of [U(Tren^{TIPS})(N)][K(Bn-15C5)$_2$] (115) towards CS_2



*Scheme **6.6.** Synthesis of **140**.*

In light of the reaction of CO_2 with **115** which afforded the oxo-isocyanate species, **138**, the corresponding reactivity with the heavier heteroallene CS_2 was investigated. To this end CS_2 was reacted with **115** in toluene. Whilst the expected product might be the analogue of **138**, i.e. a uranium(V)–sulfide–isothiocyanate complex, analysis of the crude ^{1}H NMR spectrum revealed resonances assigned to **54**. Furthermore, there was a strong absorbance at 2052 cm^{-1} in the FTIR-ATR, which strongly suggested that a thiocyanate moiety might be present.

Extraction of the brown solid into aromatic solvents (benzene or toluene) afforded orange crystals of a proposed uranium(IV)–trithiocarbonate species, [U(Tren^{TIPS})(κ^2-CS$_3$)][K(Bn-15C5)$_2$], **140**. The molecular structure is illustrated in figure **6.8.**, alongside selected bond lengths and angles.

Further extraction into hexanes afforded brown crystals, and a single crystal XRD study revealed these to be **54**, This therefore represents another, albeit unusual, method to prepare **54**.

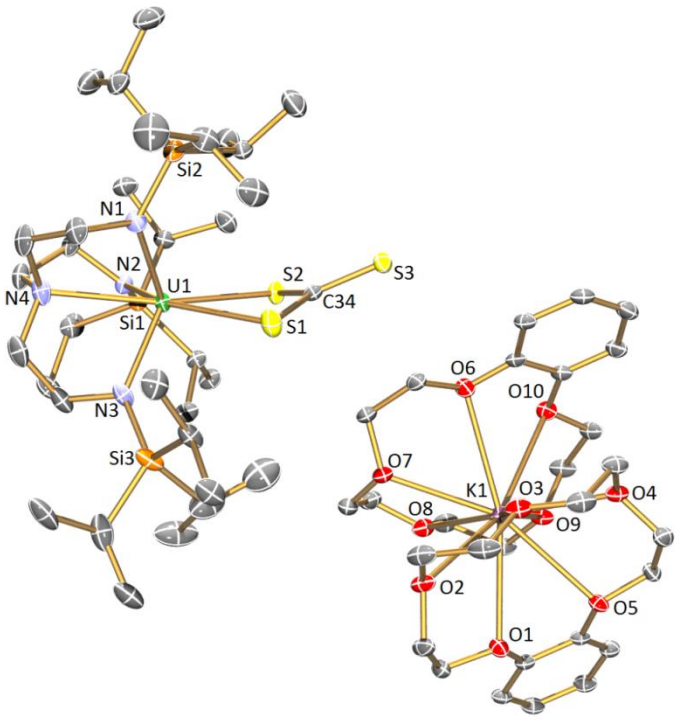


*Figure **6.8.** Molecular structure of [U(Tren^{TIPS})(κ^2-CS_3)][K(Bn-15C5)$_2$]•(C_6H_6), **140**. Thermal ellipsoids set at 40% probability. Lattice solvent and hydrogen atoms are omitted for clarity. Selected distances (Å) and angles (°): U(1)-N(1) 2.277(3), U(1)-N(2) 2.290(3), U(1)-N(3) 2.295(3), U(1)-N(4) 2.670(3), U(1)-S(1) 2.8520(10), U(1)-S(2) 2.8415(8), S(1)-C(34) 1.729(4), S(2)-C(34) 1.731(4), C(34)-S(3) 1.665(4), K(1)-O(1) 3.047(3), K(1)-O(2) 2.891(3), K(1)-O(3) 2.815(3), K(1)-O(4) 2.849(3), K(1)-O(5) 3.032(3), K(1)-O(6) 3.017(3), K(1)-O(7) 2.849(3), K(1)-O(8) 2.825(3), K(1)-O(9) 2.866(3), K(1)-O(10) 3.037(3), N(4)-U(1)-S(1) 142.38(8), N(4)-U(1)-S(2) 155.28(8), U(1)-S(1)-C(34) 89.00(12), U(1)-S(2)-C(34) 89.30(12), S(1)-U(1)-S(2) 61.82(3), S(1)-C(34)-S(2) 115.4(2).*

A single crystal XRD study revealed that the resultant product was [U(Tren^{TIPS})(κ^2-CS_3)][K(Bn-15C5)$_2$]•(C_6H_6), **140**. In the solid state **140** exhibits a separated ion pair structure, with a uranium based anion and a potassium cation encapsulated by crown ethers. The uranium centre is six coordinate, and if the CS_3 ligand is considered as a point charge [S(1)-U(1)-S(2) bite angle 61.82(3)°] then the geometry could be described as distorted trigonal bipyramidal (τ = 0.85).[19,20] The apical pocket at uranium contains a trithiocarbonate $(CS_3)^{2-}$ unit which aligns itself with one arm of the Tren^{TIPS} backbone. The CS_3 unit is planar, and like most other

complexes of $Tren^{TIPS}$ the angle between the N_{amine} and the ligand in the apical pocket is near linear [N(4)-U(1)-{plane:U(1)-S(1)-S(2)} 172.23(7)°], but the trithiocarbonate ligand itself is bent, and not in that same plane [the angle between the U(1)-S(1)-S(2) and S(1)-S(2)-S(3) planes is 25.50(4)°].

Complex **140** is the first example of this a trithiocarbonate dianion functionality being terminally bound to an f-block metal. This κ^2-coordination mode appears to have localised negative charges on the two sulfur atoms bound to uranium, which results in more double bond character between the central carbon (C34) and the unbound sulfur (S3), which is evidenced by a shorter C-S bond length [S(1)-C(34) 1.729(4) and S(2)-C(34) 1.731(4) *versus* C(34)-S(3) 1.665(4) Å]. The uranium–sulfur bonds [2.8415(8) and 2.8520(10) Å] are shorter than the equivalent bonds in analogous compounds, in which this fragment bridges several uranium centres, such as in **97** and **103**, or is bridged such as in the heterobimetallic **100** [range: 2.881(4) – 3.130(2) Å].[3,21-24] The bond distances are more comparable to systems capped by organic fragments prepared by insertion of CS_2 into U-SR bonds, such as in [U(Cp*)2(κ^2-S_2CS^tBu)(S^tBu)] which has U-S bond lengths of 2.885(4) and 2.821(5) Å, and two distinct C-S bond lengths within the trithiocarbonate unit [1.72(1), 1.73(2) and 1.66(2) Å].[23]

The U(1)-N_{amine} [2.670(3) Å] and U(1)-N_{amide} [range: 2.277(3) – 2.296(3) Å] bond distances are typical for Tren–uranium(IV) complexes [compare **7**,[25] **13**[26] and **135**, U(1)-N_{amine} range 2.613(3) – 2.623(2), U(1)-N_{amide} range 2.231(2) – 2.255(3) Å]. The potassium–oxygen interactions [K-O 2.815(3) – 3.047(3) Å] are also unremarkable [literature mean K-O(15C5) distance 2.908 Å],[8] and in line with other separated ion pair type complexes reported elsewhere in this thesis.

The ^{1}H NMR spectrum of **140** spans the range +9 to –26 ppm, which is consistent with the uranium(IV) assignment of **140** (*cf* **7** +9 to –36,[25] **13** +8 to –30[26] and **135** +7 to –30 ppm). No resonances were observed in the $^{29}Si\{^1H\}$ NMR spectrum of **140**, and attempts to observe these resonances were hampered by the poor solubility of **140** once isolated.

The FTIR-ATR data for **140** reveals a spectrum that has many absorptions present in the characteristic regions for C=S bonds (1025 – 1225 cm^{-1})[27] and similar to those

reported for K_2CS_3 (904 and 886 cm^{-1}).[28] However, it has not been possible to definitively state which absorptions result from these stretches, as there may be a sizeable change in the frequencies of these stretches as a result of the proximity of the trithiocarbonate ligand to the uranium centre.

A solution of **140** in THF was analysed by UV-vis-NIR electronic absorption spectroscopy, and this spectrum is illustrated in figure **6.9.**

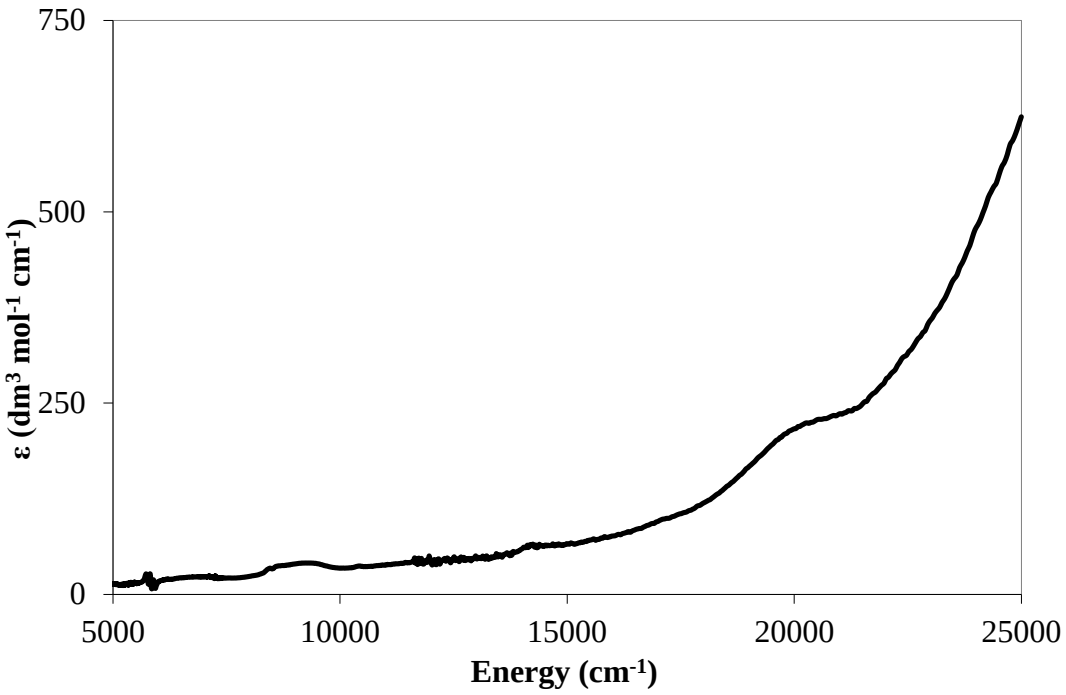


*Figure **6.9.** UV-vis-NIR electronic absorption spectrum of **140**.*

Poor solubility once isolated prevents a quantitative discussion of the UV-vis-NIR spectrum of **140**, though qualitatively we can say that it is dominated by CT bands tailing in from the high energy region. There are some weak, Laporte forbidden *f-f* transitions visible, which arise from the U^{IV} $5f^2$ electronic configuration, but these are broad and poorly resolved, in-line with uranium(IV) electronic absorption spectra. As described previously, poor solubility of **140** once isolated precluded the collection of meaningful solution phase magnetic data, however we were able to obtain solid phase data for **140** (figure **6.10.**).

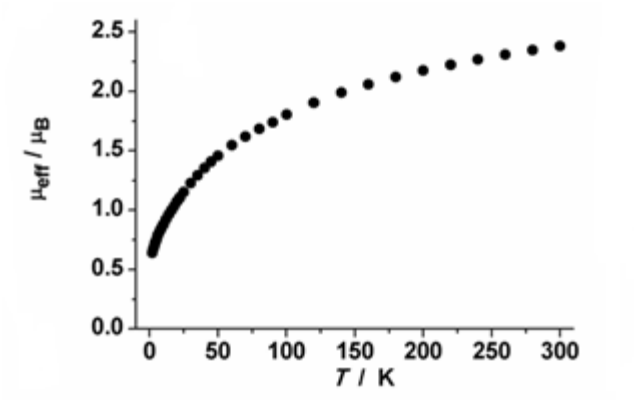


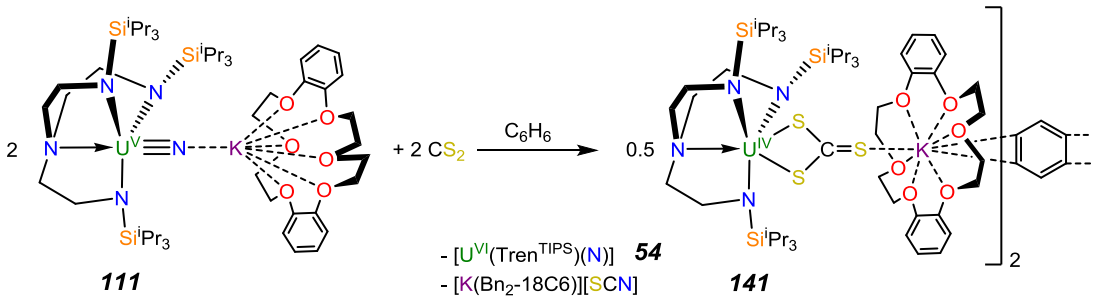
*Figure **6.10.** Magnetic susceptibility data [μ_{eff} (μ_B) vs T (K)] for **140**.*

Solid-state SQUID magnetometry of **140** reveals a magnetic moment of 2.4 μ_B at 298 K, whose value decreases with decreasing temperature to 0.6 μ_B at 2 K and tending to zero, as expected for a uranium(IV) centre, which is a magnetic singlet at low temperatures.[13]

By mass balance, isolation of one equivalent of each **140** and **54** (as identified by single crystal XRD studies alongside further analysis described above) suggests the elimination of [K(Bn-15C5)$_2$][SCN] as a third product. FTIR-ATR of the aromatic solvent insoluble product revealed a strong absorption at 2052 cm^{-1}, which was attributed to a thiocyanate stretch. An authenticated sample of [K(Bn-15C5)$_2$][SCN] was prepared by heating a mixture of KSCN (commercial sample) with two equivalents of benzo-15-crown-5 ether in THF. Upon removal of volatiles, the absorption for the thiocyanate had shifted from 2061 cm^{-1} to 2052 cm^{-1}, which corroborates the formation of [K(Bn-15C5)$_2$][SCN] as a by-product of this reaction.

The isolation of uranium(IV) (**140**) and uranium(VI) (**54**) species indicates a disproportionation mechanism is being employed here. Mechanistic details for the formation of these species will be discussed in Section 2.3.3., based upon computational studies performed by our collaborators in Toulouse.

6.2.2.1.2. Reactivity study of [U(Tren^{TIPS}){(μ-N)(μ-K)(Bn-15C5)}] (111) towards CS_2



*Scheme **6.7.** Synthesis of **141**.*

In light of the observed reactivity for **115** with CS_2, the analogous reaction was investigated for [U(Tren^{TIPS}){(μ-N)(μ-K)(Bn$_2$-18C6)}] (**111**). As was the case for **115**, orange crystals suitable for single crystal XRD study were isolated from a benzene extraction of the crude reaction mixture. The molecular structure is illustrated in figure **6.11.**, alongside selected bond lengths and angles.

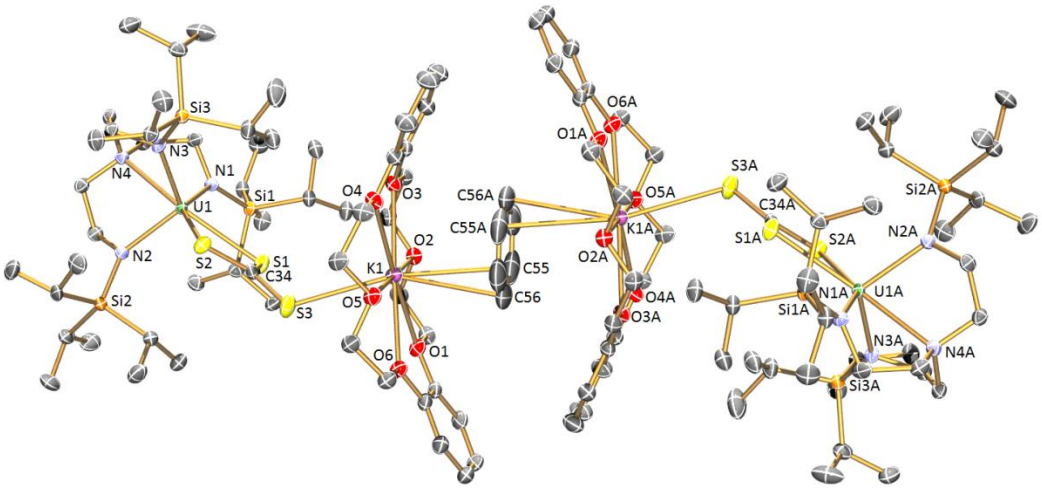


*Figure **6.11.** Molecular structure of [{U(Tren^{TIPS})(μ-κ^2-CS$_3$)[μ-K(Bn$_2$-18C6)]}$_2$(μ-η^2:η^2-C$_6$H$_6$)]•4(C$_6$H$_6$), **141**. Thermal ellipsoids set at 40% probability. Lattice solvent and hydrogen atoms are omitted for clarity. Selected distances (Å) and angles (°): U(1)-N(1) 2.278(3), U(1)-N(2) 2.295(3), U(1)-N(3) 2.299(3), U(1)-N(4) 2.665(3), U(1)-S(1) 2.8672(11), U(1)-S(2) 2.8762(10), S(1)-C(34) 1.720(4), S(2)-C(34) 1.726(4), C(34)-S(3) 1.678(4), S(3)-K(1) 3.1864(16), K(1)-O(1) 2.751(3), K(1)-O(2) 2.757(3), K(1)-O(3) 2.742(3),*

K(1)-O(4) 2.756(3), K(1)-O(5) 2.707(3), K(1)-O(6) 2.769(3), K(1)-C(55) 3.344(7), K(1)-C56) 3.290(7), N(4)-U(1)-S(1) 155.69(8), N(4)-U(1)-S(2) 142.83(8), U(1)-S(1)-C(34) 91.05(15), U(1)-S(2)-C(34) 90.64(14), S(1)-U(1)-S(2) 61.48(3), S(1)-C(34)-S(2) 116.8(2), C(34)-S(3)-K(1) 121.02(15).

Analogously to the preparation of **140**, the reaction of **111** with CS_2 affords a uranium(IV)–trithiocarbonate species. Similarly to the reaction of [U(Tren^{TIPS}){(μ-N)(μ-K)(18C6)}] (**111-18C6**) with CO, which afforded [U(Tren^{TIPS}){μ-NCO)(μ-K)(18C6)}] (**137**), the capped nature of the complex is retained upon reaction with the small molecules, at least in the solid state. Here, the coordination geometry for the potassium cations is not satiated by the crown interactions and the cyanate unit (in the apical pocket of Tren^{TIPS}), and in this case a benzene molecule bridges the two potassium centres in a μ-η^2:η^2 fashion, with and inversion centre present in the centre of the benzene ring. This dinuclear structure is in contrast to the product of reductive carbonylation of **111-18C6**, which maintained a mononuclear structure on the preparation of **137**.

As for **140**, the uranium centre of **141** is six coordinate, and if the $(CS_3)^{2-}$ ligand is considered as a point charge [S(1)-U(1)-S(2) bite angle 61.48(3)°] then the geometry could be described as distorted trigonal bipyramidal, with the trithiocarbonate and the face-capping amine of Tren^{TIPS} in the axial positions (τ = 0.96).[19,20] The apical pocket contains a trithiocarbonate $(CS_3)^{2-}$ unit which is planar, and the angle between the N_{amine}, uranium and CS_3 is near linear [N(4)-U(1)-{plane:U(1)-S(1)-S(2)} 173.52(8)°]. In contrast to **140**, however, the trithiocarbonate itself is in the same plane in **141** [the angle between the U(1)-S(1)-S(2) and S(1)-S(2)-S(3) planes is 0.90(5)°]. This may result from further interactions with the potassium cation. The potassium fragment is offset from this linearity [C(34)-S(3)-K(1) 121.02(15)°].

Consistent with the difference in coordination between a terminal trithiocarbonate and a bridged structure, the uranium sulfur distances have also increased [mean U(1)-S: **140**, 2.8468(10); **141**, 2.8717(11) Å], bringing these interactions into better agreement with other examples in the literature [U-S range: 2.9488(19) – 3.130(2) Å].[21-23] Interaction of the $(CS_3)^{2-}$ unit with the potassium ion has induced a degree of delocalisation of electrons around the trithiocarbonate unit, with C(34)-S(1) and

C(34)-S(2) bond lengths shorter in **141** than **140** and the C(34)-S(3) bond lengths longer in **141** than **140** [C(34)-S(1)/S(2), C(34)-S(3): **140**, 1.730(4), 1.665(4); **141**, 1.723(4), 1.678(4) Å]. The sulfur potassium interaction is also longer than the comparable example from the uranium literature,[22] which can be ascribed to the bridging nature of the potassium centres in [U{OSi(O^{t}Bu)$_3$}$_4$(μ^3-κ^2:κ^2:κ^2-CS$_3$){μ^2-K(18C6)}$_2$] (**100**), which shortens these bonds relative to **141** [**141** S(3)-K(1) 3.1864(16); **100** S(3)-K(1) 3.159(3), S(3)-K(2) 3.179(4) Å].[22]

The ^{1}H NMR spectrum of **141** contains resonances spanning the range +9 to –27 ppm, and is commensurate with the assignment of a uranium(IV) centre. As for **140**, the FTIR spectrum for **141** contains absorptions that could arise from C---S stretches, however, as this would be speculative, conclusive assignments will not be made here.

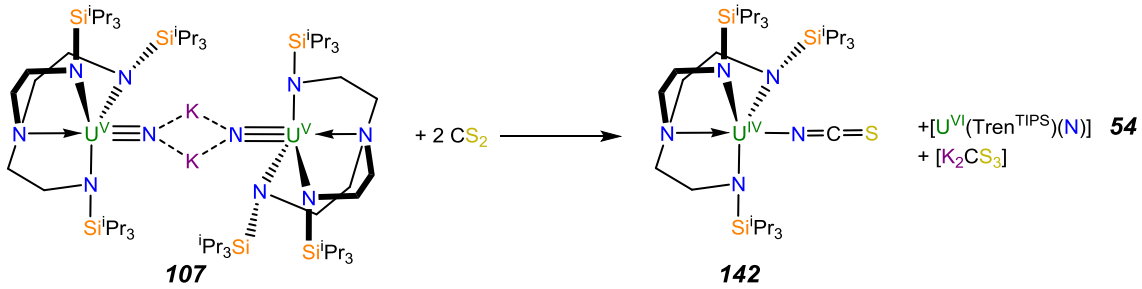
Further spectroscopic data could not be collected due to the insolubility of **141** once isolated, and therefore neither ^{29}Si{^{1}H} NMR spectroscopy, Evans' method solution phase magnetic data nor UV-vis-NIR electronic absorption spectroscopy shall be reported here. Variable temperature solid phase magnetic data (SQUID) were not collected for this compound, due to time constraints associated with utilising the magnetism facilities.

Analogously to the disproportionation that was observed in the preparation of **140** from **111** and CS_2, **54** was an anticipated by-product from the reaction of **111** with CS_2. Indeed, from a hexanes extraction of the crude mixture, brown crystals of **54** suitable for single crystal XRD study could be isolated, which confirmed that this by-product was present.

Finally, the third anticipated reaction by-product was the thiocyanate, [K(Bn$_2$-18C6)][SCN], analogous to the isolation of [K(Bn-15C5)$_2$][SCN] from the reaction of **115** with CS_2. Analysis of the benzene insoluble material revealed two absorptions in the thiocyanate regions (at 2064 and 2056 cm^{-1}). To confirm this assignment an authenticated sample of [K(Bn$_2$-18C6)][SCN] was prepared by the reaction of KSCN with 18-crown-6 ether in THF. The FTIR spectrum of this prepared species mirrors that of the compound isolated as a result of the reactivity study of **115** with CS_2 (*cf.* KSCN: 2061 cm^{-1}).

Due to the similarity in the products prepared from the reaction of CS_2 with either **115** or **111**, only the former shall be discussed in greater mechanistic detail (see Section 2.3.3.). By strong analogy to the preparation of **140**, we feel confident in our assignment of **141** as a Tren–uranium(IV) species, and that the reactivity it displays closely parallels that of **140**.

6.2.2.1.3. Reactivity study of [{U(Tren^{TIPS})(μ-N)(μ-K)}$_2$] (107) towards CS_2



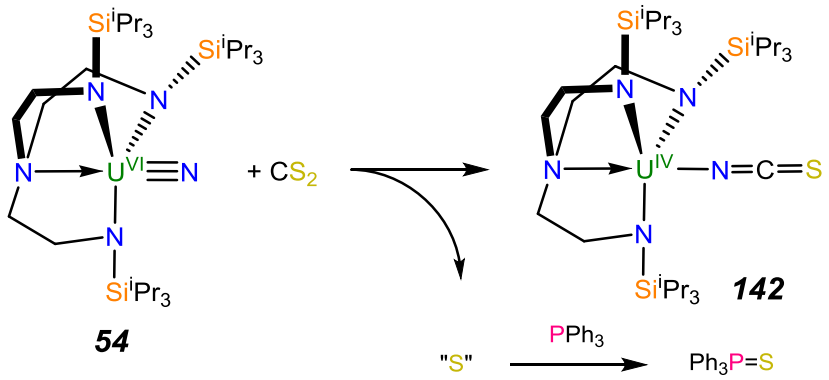
Scheme ***6.8.*** *Synthesis of* ***142****.*

The corresponding reactivity was also attempted for the dinuclear species, [{U(Tren^{TIPS})(μ-N)(μ-K)}$_2$] (**107**) with CS_2. Unfortunately no uranium containing species could be crystallographically characterised from the reaction mixture, however, inspection of the resultant crude ^{1}H NMR spectrum reveals the presence of resonances attributed to **54**, which might be anticipated based on the disproportionation chemistry observed for other uranium(V)–nitrides, as well as a new product, formulated as [U(Tren^{TIPS})(NCS)] (**142**), which is discussed in much greater detail below. On the basis of mass balance, this reaction would also prepare K_2CS_3 as a by-product.

In contrast to the reactivity observed for **107** with CO, whereupon reductive carbonylation affords **15** in the absence of crown ethers, there are no resonances attributable to **15** in the ^{1}H NMR spectrum of the crude reaction mixture of **107** and CS_2. Analysis of this ^{1}H NMR spectrum suggests fairly clean conversion of **107** and CS_2 to **54** and **142**, however complete conversion from **107** cannot be adjudged by inspection of the ^{1}H NMR spectrum, as **107** is highly insoluble in non-polar solvents (as discussed in Chapter 2). Analysis of the FTIR spectrum of the crude mixture

from the reaction of **107** with CS_2 (in Nujol) reveals a resonance commensurate with that of [U(Tren^{TIPS})(NCS)] (2012 cm^{-1}, see Section 2.2.2.). Furthermore, inspection of the IR spectrum (in Nujol) also revealed peaks that might correspond to K_2CS_3 at 914 and 883 cm^{-1},[28] whilst the FTIR-ATR spectrum contained resonances at 911 and 880, with a shoulder at 895 cm^{-1} [*cf.* literature values for K_2CS_3 of 904 and 886 cm^{-1} prepared a KBr pellets, the small discrepancies arise from the usage of differing techniques].[28] Whilst this IR data is not as conclusive as the comparable data for the elimination of cyanates (Chapter 5) or thiocyanates (*vide supra*), for which absorptions are in a distinct part of the spectrum (i.e. not overlapped by bands in the fingerprint region), this does lend some credence to the proposed synthetic pathway.

6.2.2.2. Tren–uranium(VI) nitride (54)



*Scheme **6.9.** Synthesis of **142** and sulfur capture reactivity.*

Since Tren–uranium(V) nitrides undergo, overall, disproportionation reactivity towards CS_2, we were interested in determining how the analogous Tren–uranium(VI) nitride would react, since it lacks the requisite valence electron to engage in disproportionation chemistry. Complex **54** was reacted with CS_2 and after six days a new product was observed *via* ^{1}H NMR spectroscopic studies of the reaction mixture. This long reaction time is again a clear example of the difference in rate of reactions **115** and **54**, which was explored computationally earlier (Chapter 5, Section 2.4.). Recrystallisation of the crude mixture from pentane afforded green crystals of a proposed uranium(IV)–isothiocyanate complex, [U(Tren^{TIPS})(NCS)],

142. The molecular structure is illustrated in figure **6.12.**, alongside selected bond lengths and angles.

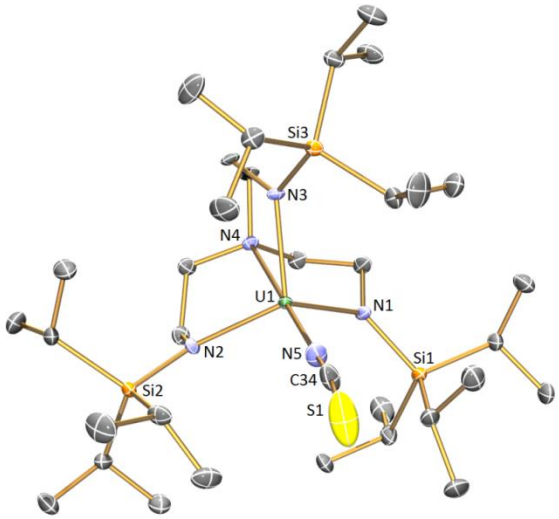


*Figure **6.12.** Molecular structure of [U(Tren^{TIPS})(NCS)], **142**. Thermal ellipsoids set at 40% probability. The disorder component of the isothiocyanate unit and hydrogen atoms are omitted for clarity. Selected distances (Å) and angles (°): U(1)-N(1) 2.238(3), U(1)-N(2) 2.240(3), U(1)-N(3) 2.237(3), U(1)-N(4) 2.626(4), U(1)-N(5) 2.377(4), N(5)-C(34)$_{av}$ 1.181(11), C(34)-S(1)$_{av}$ 1.590(10), N(4)-U(1)-N(5) 175.90(12), U(1)-N(5)-C(34)$_{av}$ 172(2), N(5)-C(34)-S(1)$_{av}$ 172(3).*

The molecular structure confirms the postulated uranium(IV)–isothiocyanate complex, which is reminiscent of the uranium(IV)–isocyanate complex (**135**) prepared by the reductive carbonylation of **54** by CO. The complex retains a trigonal bipyramidal geometry at uranium (τ = 1.06),[19,20] with the face-capping amine of Tren^{TIPS} and the thiocyanate ligand in the axial positions. Like **135**, the isothiocyanate unit is disordered over two positions and is essentially linear, with an average U(1)-N(5)-C(34) angle of 172(2)°. The U(1)-N$_{isothiocyanate}$ bond is 2.377(4) Å [*cf.* literature values for terminal isothiocyanate units ranging 2.32(3) – 2.526(17) Å],[8] which is ~0.03 Å longer than the corresponding distance in **135** [2.338(3) Å]. This could be attributed to the polarising power of oxygen in **135**, which draws electron density towards itself more strongly than sulfur in **142**. This results in a more δ^+ carbon and hence a more δ^- nitrogen atom within the cyanate, when compared to thiocyanate, and therefore a stronger (shorter) interaction with uranium.

The U(1)-N_{amide} and U(1)-N_{amine} distances [av: 2.238(3) and 2.626(4) Å] compare well to the analogous distances in **135**.

It is perhaps interesting here to note then that the divergent products of CS_2 chemistry with Tren–uranium nitrides, that is trithiocarbonates (**140** and **141**) and isothiocyanates (**142**), are both observed on the reaction of the bridged uranium nitride **58** prepared by Mazzanti *et al*., to prepare **103**.[3] As a result of the bridged nature of the thiocyanate unit in **103**, the uranium–nitrogen bonds are longer than in **142** [2.501(15) and 2.62(2) Å: the NCS fragment is disordered over two positions].

The ^{1}H NMR spectrum for **142** spans the range +9 to –37 ppm, which is in agreement with a uranium(IV) paramagnetic centre. The $^{29}Si\{^{1}H\}$ spectrum exhibits only one resonance at 2.4 ppm, which is consistent with a uranium(IV) complex[11] with approximate C_{3v} symmetry. The FTIR spectrum exhibits a strong absorbance at 2013 cm^{-1}, which is assigned as a thiocyanate stretch, which is typical of uranium(IV)–thiocyanate stretches (2000 – 2085 cm^{-1}).[29-31]

A solution of **142** in toluene was analysed by UV-vis-NIR electronic absorption spectroscopy, and this spectrum is illustrated in figure **6.13.**

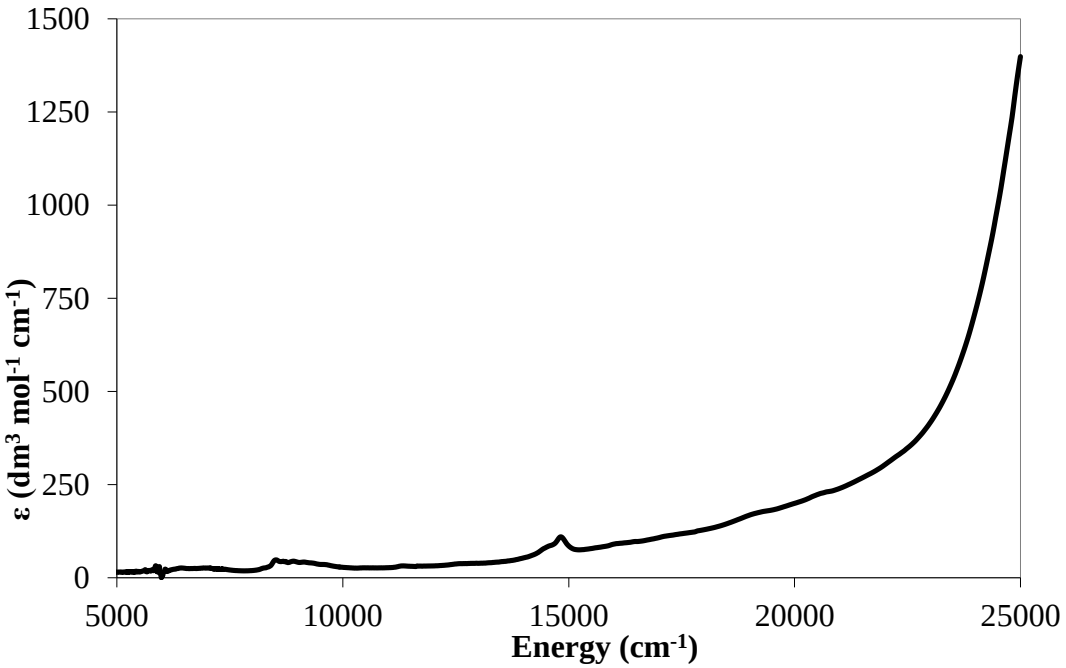


*Figure **6.13.** UV-vis-NIR electronic absorption spectrum of **142**.*

The spectrum of **142** is dominated by CT bands tailing in from the high energy region. There are some weak, Laporte forbidden *f-f* transitions visible, which arise from the U^{IV} $5f^2$ electronic configuration, but these are broad and poorly resolved, in-line with uranium(IV) electronic absorption spectra.

The Evans' method[12] room temperature solution magnetic moment in benzene was determined for **142**, and found to be 2.91 μ_B. Whilst this is lower than the theoretical value of 3.58 μ_B for a uranium(IV) $^3H_4$ ground state, it correlates well to experimentally observed values for μ_{eff} (1.8 – 3.6 μ_B).[13] Variable temperature SQUID magnetometry data for **142** reveals a magnetic moment of 2.52 μ_B at 298 K (which compares well to the solution phase magnetic moment) that decreases monotonously down to 0.24 μ_B at 2 K and tending to zero in-line with the magnetic singlet ground state of uranium(IV) at low temperature (figure **6.14.**).[13]

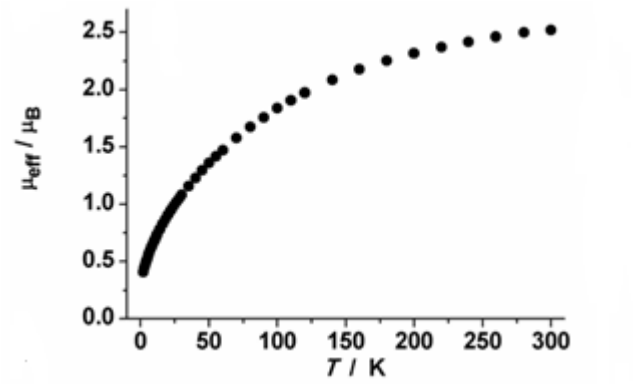
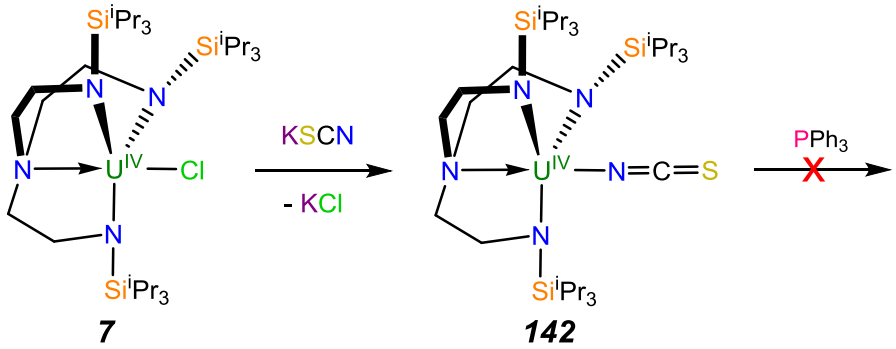
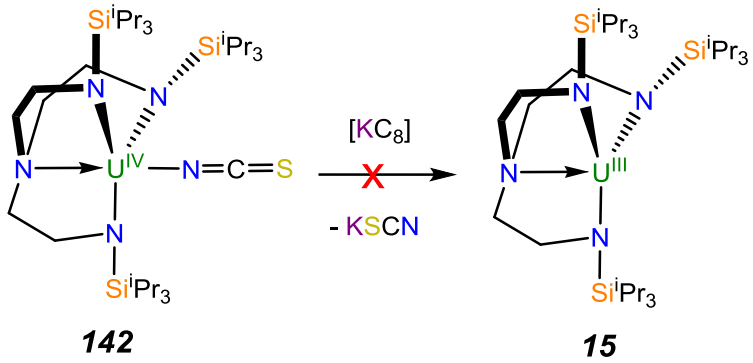


*Figure **6.14.** Magnetic susceptibility data [μ_{eff} (μ_B) vs T (K)] for **142**.*



*Scheme **6.10.** Alternative synthesis of **142** and control experiment for sulfur capture reactivity.*

Implicated in terms of mass balance upon the preparation of **142** from **54** and CS_2 is an "S" by-product. Sulfur would presumably be extruded from the putative complex "[U(Tren^{TIPS})(S)(NCS)]". To test this theory, we added Ph_3P as a sulfur scavenging reagent, either in one pot or after the six day reaction of **54** with CS_2, and observed the formation of Ph_3PS by ^{31}P NMR spectroscopy (^{31}P NMR: Ph_3P = –5.2, Ph_3PS = +42.8 ppm). An independent preparation of **142** *via* a salt elimination method, i.e. the reaction of **7** with KSCN, afforded **142** in good yield (53%), and all characterisation data were in agreement to that prepared *via* the reaction of **54** with CS_2. The most significant factor in this alternative synthetic method is the absence of a sulfur by-product ("S"). Control experiments were carried out to test against the abstraction of sulfur from **142** (prepared from **7**) by Ph_3P to afford the plausible cyanide complex "[U(Tren^{TIPS})(CN)]", or the direct reaction of Ph_3P with CS_2, and in neither case was the formation of Ph_3PS observed, even on extended reflux. This then verifies that sulfur is extruded from the reaction of **54** with CS_2 in the preparation of **142**.



142 ***15***

*Scheme **6.11.** Attempted preparation of **15** by the reduction of **142**.*

Finally, the reaction of **142** with KC_8 was investigated to see if complete nitrogen atom transfer could be enacted, as was the case for the reduction of **135** with KC_8 in the absence of crown to prepare **15** and KOCN. There was no observable reaction when KC_8 was added to **142**, as judged by inspection of the ^1H NMR spectrum, which contained no resonances attributable to **15**. This absence of reactivity is perhaps not unsurprising, as the most comparable chemistry, i.e. the reaction of **107** with CS_2, did not afford **15**, whereas the formation of **15** was observed for the reaction of **107** with CO. Instead, reaction of **107** with CS_2 was found to afford **54**

and **142** itself. Correspondingly, a cycle for the preparation of KSCN, similar to that demonstrated for the conversion of NaN_3 to NaOCN (demonstrated in Chapter 5), could not be realised.

6.2.3. Computational Analysis

Given the diversity of reaction products for the reaction of Tren–uranium nitrides **115** and **54** with heteroallenes, namely **138**, **122**, **140** or **142**, involving multiple bond metathesis steps, computational modelling using DFT calculations would allow an understanding of the reactivity observed. Furthermore, DFT would permit insight into the factors of oxidation state and chalcogenide, and how these govern this divergent reactivity. The reaction profiles were therefore modelled using DFT calculations at the B3PW91 level of theory. In all cases, the computed energy pathways were found to be kinetically and thermodynamically favourable and completely consistent with experimental outcomes.

6.2.3.1. [U(Tren^{TIPS})(N)][K(Bn-15C5)$_2$] (115) + CO_2

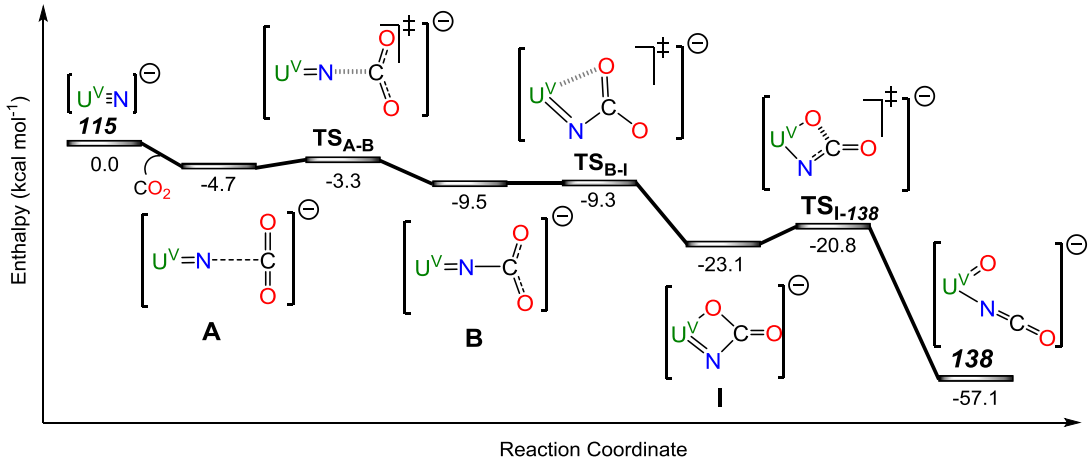


*Figure **6.15.** Energy profile (at 298 K) for the gas phase reaction of CO_2 with [U(Tren^{TIPS})(N)][K(Bn-15C5)$_2$] (**115**) computed at the B3PW91 level of theory.*

The computed energy pathway for the reaction of **115** with CO_2 (figure **6.15.**) is reminiscent of outer-sphere CO_2 addition, as reported by Cummins *et al.*[4,7] Indeed, a

very low-lying transition state (TS) was located (with an enthalpy barrier of 1.4 kcal mol^{-1}) where the CO_2 molecule bends to generate a free 2p-orbital at the carbon atom of CO_2, which overlaps with the σ-lone pair of the nitride. This then leads to an η^1-carbamate intermediate, which isomerises (with an energy barrier of 0.2 kcal mol^{-1}) to a stable, metal-based four-membered ring (–23.1 kcal mol^{-1}). A low-lying transition state involving bond metathesis (–20.8 kcal mol^{-1}) is followed by C-O bond cleavage to afford the oxo-isocyanate (**138**) that is 57.1 kcal mol^{-1} more stable than the start point (**115**).

6.2.3.2. [U(Tren^{TIPS})(N)] (54) + CO_2

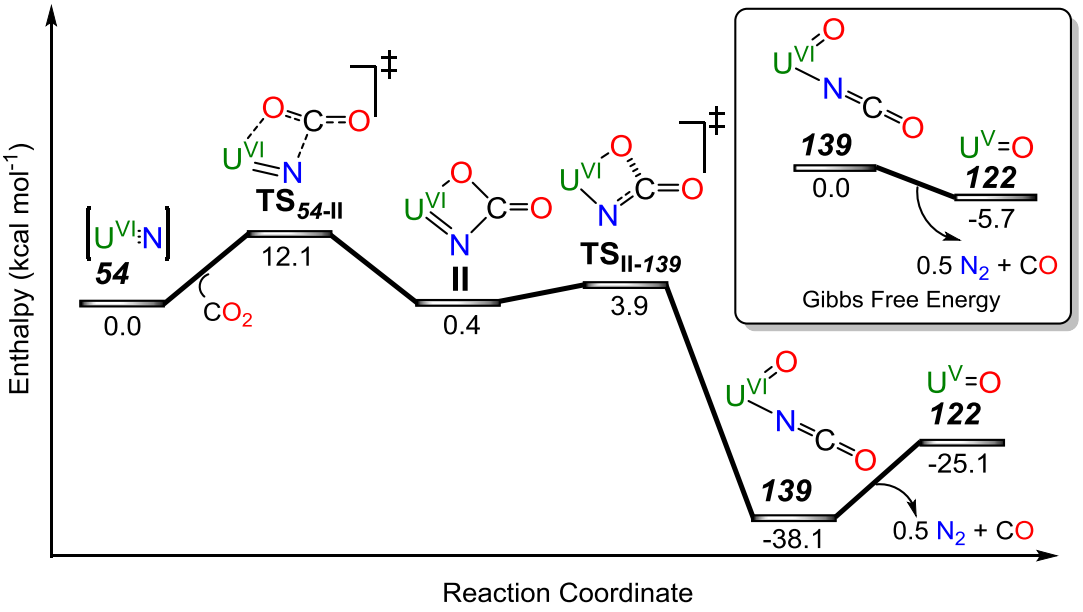


*Figure **6.16.** Energy profile (at 298 K) for the gas phase reaction of CO_2 with [U(Tren^{TIPS})(N)] (**54**) computed at the B3PW91 level of theory. Inset: Gibbs free energy of the conversion of **139** to **122** with concomitant elimination of N_2 and CO.*

In an analogous manner as reaction of **115** with CO_2, the energy profile was computed for the reaction of **54** with CO_2 (figure **6.16.**), at the same level of theory. Here, however, the mechanism is reminiscent of activated alkene metathesis.[32] Unlike **115**, for **54** an outer-sphere addition mechanism is not observed in the reaction profile, instead operating *via* a [2 + 2]-cycloaddition (0.4 kcal mol^{-1}, after a transition state at 12.1 kcal mol^{-1}). From this four-membered ring, the same steps are

observed as for **115**, namely a C-O bond breaking event which proceeds *via* a σ-bond metathesis transition state (3.9 kcal mol^{-1}) to afford the oxo–isocyanate, **139** (–38.1 kcal mol^{-1}). Whilst this is an enthalpic minimum with respect to **122** (–25.1 kcal mol^{-1}), when the Gibbs free energy term is considered the formation of **122** from **139** becomes more favourable by 5.7 kcal mol^{-1} (–43.8 kcal mol^{-1}), due to entropic gain from the elimination of N_2 and CO. This finding is in-line with the initial isolation of **139** but conversion to **122** upon attempted recrystallisation.

6.2.3.3. [U(Tren^{TIPS})(N)][K(Bn-15C5)$_2$] (115) + CS$_2$

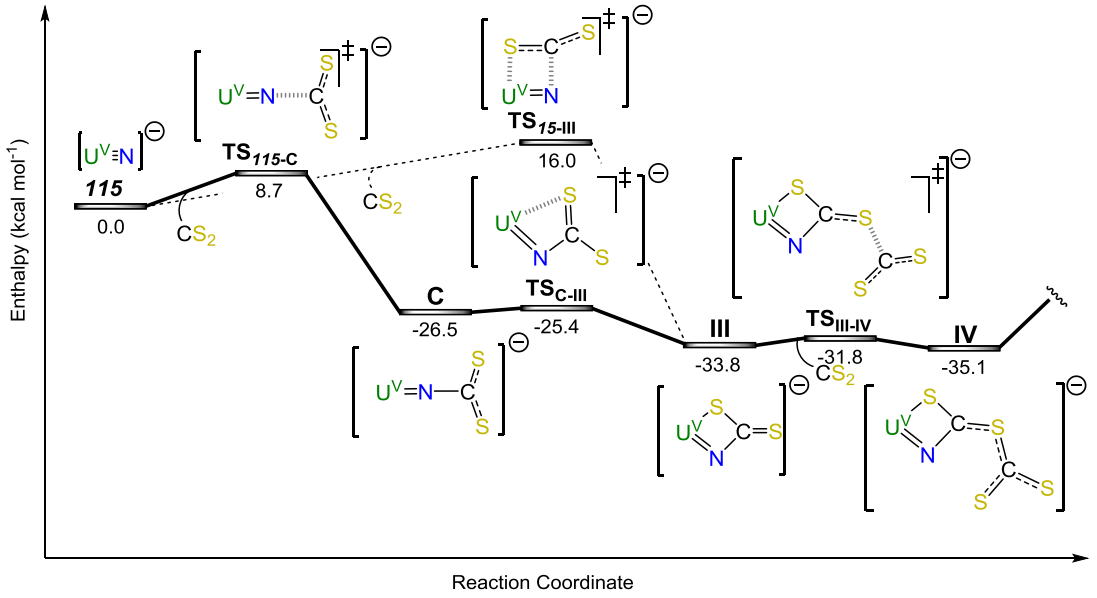


*Figure **6.17.** Energy profile (at 298 K) for the gas phase reaction of CS_2 with [U(Tren^{TIPS})(N)][K(Bn-15C5)$_2$] (**115**) computed at the B3PW91 level of theory (continued in figure **6.18.**).*

The reaction profile that was determined for the reaction of **115** with CS_2 accounts for the complexity of the experimental observations (figures **6.17.** and **6.18.**). The main features of the energy profile are initially similar to that computed for the reaction of **115** with CO_2, namely an outer-sphere addition step to afford an η^1-thiocarbamate (with an energy barrier of 8.7 $kcal^{-1}$), which like **115** readily isomerises to an η^2-thiocarbamate (a metal-based four-membered ring, –33.8 kcal

mol^{-1}). The barrier for [2 + 2]-cycloaddition of CS_2 to **115** was also calculated, and found to be higher in energy (16.0 kcal mol^{-1}) than the outer-sphere addition.

From here the reaction profiles for the reaction of **115** with CO_2 and CS_2 diverge. Instead of C-E bond cleavage (as observed for CO_2 following σ-bond metathesis) a second CS_2 electrophilically attacks the pendant sulfur atom of the thiocarbamate (*III*), with an enthalpy barrier of 2.0 kcal mol^{-1}. The corresponding outer-sphere addition of a CO_2 molecule to the pendant oxygen atom of the carbamate (*I*) does not result in coordination; every attempt to locate such a TS lead to the departure of the incoming CO_2 molecule.

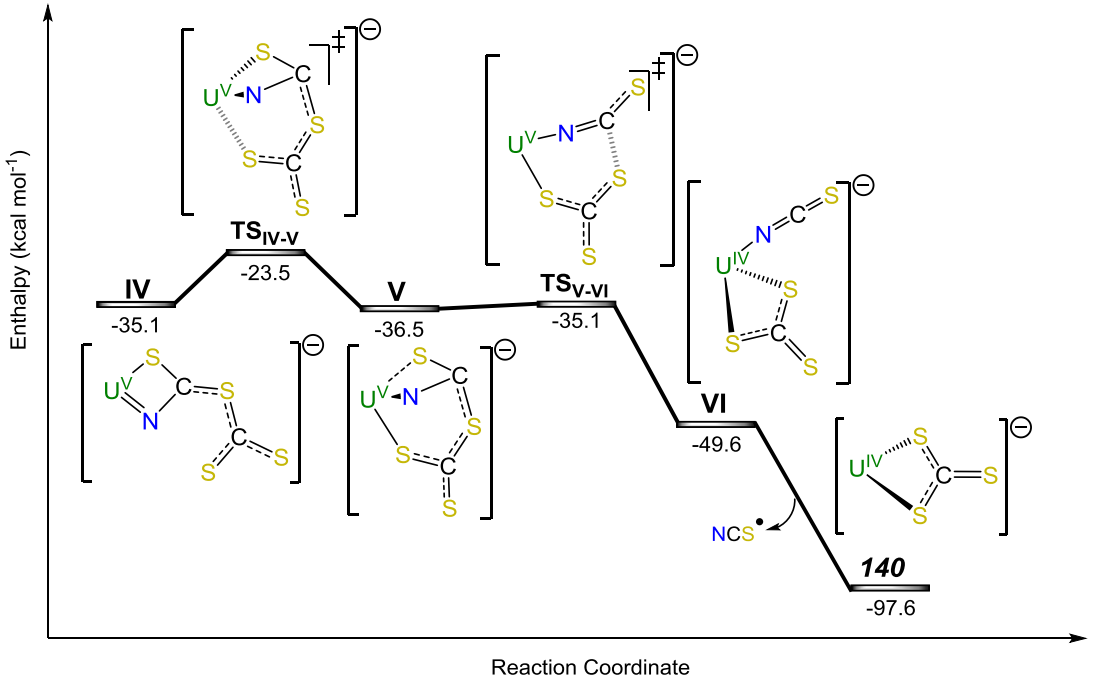


*Figure **6.18.** Continuation (from figure **6.17.**) of the energy profile (at 298 K) for the gas phase reaction of CS_2 with [U(Tren^{TIPS})(N)][K(Bn-15C5)$_2$] (**115**) computed at the B3PW91 level of theory.*

An isomerisation process (from *IV* to *V*, with an enthalpy barrier of 11.6 kcal mol^{-1}, figure **6.18.**) then affords a metal-based six-membered ring intermediate (–36.5 kcal mol^{-1}). In this species (*V*), a C-S bond is strongly activated and therefore easily broken (with an energy barrier of 1.4 kcal mol^{-1}) to afford an isocyanate–trithiocarbonate species (*VI*). Thiocyanate extrusion from *VI* to afford **140**, and the

subsequent oxidation of a second molecule of **115** to give **54** and $[K(Bn\text{-}15C5)_2][SCN]$ is highly favoured (–97.6 kcal mol^{-1}).

6.2.3.4. [U(Tren^{TIPS})(N)] (54) + CS_2

The reaction of **54** with CS_2 was computationally investigated (figure **6.19.**). The first steps were analogous to the previously described reaction profiles for the reaction of **54** with CO_2, i.e. a [2 + 2]-cycloaddition *via* a transition state (23.4 kcal mol^{-1}) yielding a thiocarbamate complex (–3.7 kcal mol^{-1}), which passes through a low-lying σ-bond metathesis transition state (1.4 kcal mol^{-1}), then C-S bond disruption affords the terminal sulfide-isothiocyanate complex (–19.6 kcal mol^{-1}). Extrusion of sulfur, which can be trapped as Ph_3PS, is highly favoured, yielding **142** (–57.9 kcal mol^{-1}).

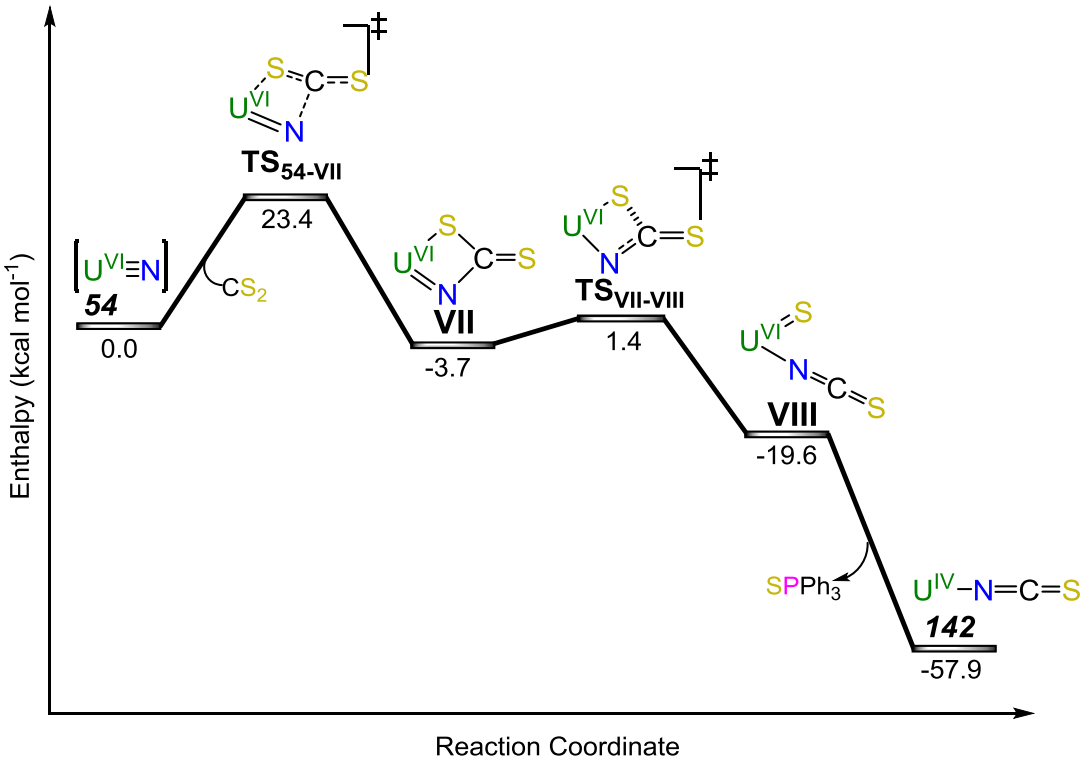


*Figure **6.19.** Energy profile (at 298 K) for the gas phase reaction of CS_2 with [U(Tren^{TIPS})(N)] (**54**) computed at the B3PW91 level of theory.*

6.2.4. Discussion of mechanistic insights

As discussed previously (Chapter 1), there are relatively few examples of reactivity of transition metal nitrides with the heteroallenes (CE_2; E = O, S).[4,7,33] Furthermore, there are even fewer reports of f-block reactivity (though concurrent studies to this work are beginning to emerge).[3,34,35]

The preparation of **138** by bond metathesis and C=O bond cleavage is notable as CO_2 is often considered a reasonably inert molecule, and this bond breaking is usually only accomplished in reductive cleavage reactions.[36-41] The reaction of group 5 nitrides $[M\{N(^tBu)(Ar)\}_3(N)Na]_2$ (M = V, Nb; Ar = 3,5-$Me_2C_6H_3$) to afford carbamates (see Chapter 1) is followed either by no further reaction (M = V) or for M = Nb, splitting of the carbamate $(NCO_2)^-$ to afford a cyanate carboxylate (masked oxo) species required the addition of external electrophiles (e.g. ^{t}BuCOCl).[4,7] Whilst *N*-carbamate intermediates are observed for the uranium(V) case (**115**), unlike these Group 5 examples, no external electrophile is required to cleave the C-O bond, and the *N*-carbamate species is only transiently formed. We believe this reflects the more polarised, more reactive U≡N triple bond, in comparison to d-block M≡N triple bonds, in addition to the formation of a highly favourable U=O bond. The four-membered ring rapidly converts to a more stable oxo-isocyanate, which has parallels in hafnium chemistry,[5] though in that instance, coordination to a second metal centre was required to permit the formation of the final complex. This is not the case in the Tren–uranium system, due to the oxophilicity of the uranium centre.

Within f-block chemistry, the reactivity of **115** towards CO_2 is reminiscent of the reaction of a uranium(V)–imide complex with CO_2 to give a uranium(V)–oxo and an organoisocyanate,[1] though here the important difference is that in our system, both functionalities remain bound to the uranium centre, and are not extruded.

When compared to the reaction of neutral **54** with CO_2, wherein NCO is extruded, the fact that the NCO moiety remains coordinated for the anionic analogue (**138**) may be superficially surprising, given that the steric demands of the $Tren^{TIPS}$ ligand framework might be expected not to accommodate these additional ligands due to steric crowding. However, our prior work (Chapter 5) examining the reductive carbonylation of terminal uranium nitrides identified $[U(Tren^{TIPS})(N)(CO)]$ as an

intermediate on the pathway towards **135**. The isolation of **138** and **139** provides experimental verification that there is room for an additional ligand in the coordination sphere of uranium in a [U(Tren^{TIPS})(X)(L)] type complex [X = anionic ligand, L = neutral or anionic ligand]. The one caveat to these complexes is that these additional ligands must be small and cylindrical. This is reminiscent of [M(η^5-C_5Me_5)$_3$] complexes (M = lanthanide or actinide), which were at first though unable to coordinate other ligands until it was discovered that they could accommodate small and/or cylindrical ligands such as NO, nitriles, N_2 or CO.[42-47]

The scission of the C-O bond of carbon dioxide to prepare **138** is a differing reactivity to that observed for group 5 nitrides. The reaction of **30** or **33** with CO_2 in both cases afforded the corresponding carbamates, **36-12C4** and **34-O**, i.e. no bond homolysis occurred.[4,7] External factors were required to induce bond scission, and in the case of **36**, thermolysis results in the isolation of the niobium–oxo species **37**, with the loss of NaOCN.

Whilst **138** is stable in the solid state, the uranium(VI) analogue (**139**) was only stable for 30 minutes in solution, and the cyanate group was rapidly lost, with **122** being the sole isolable product. The formation of **122** suggests that the cyanate group is ejected as a radical in a homolytic U-$N_{cyanate}$ bond cleavage step: this would provide the requisite electron for the reduction of the uranium(VI) centre.

Comparing the computed barriers for the first step of the reactions of Tren–uranium nitrides with CO_2 affords information with regard to the nucleophilicity of the nitrides in these complexes. The computed barrier for the uranium(VI) system is relatively low (12.1 kcal mol^{-1}), but this is still considerably greater than the equivalent point computed for the uranium(V) system (*cf*. *I* with *II*). This can be attributed to the bond length and the resultant bond strength of the U≡N triple bond, which is accordingly shorter and stronger in **54**. Despite this, the energy barrier for the C-O bond breaking in the carbamate intermediates is similar for both systems, which indicates that the oxophilicity of the uranium centres is little affected by the oxidation state.

The then subsequent reactivity observed for **139**, in contrast with the stable **138**, is attributed to steric hindrance around the metal centre. Shorter distances in the

uranium(VI) complex (resulting from the smaller size of the U^{VI} cation)[18] makes the geometry more compact around the metal centre and induces stronger interactions with the oxo ligand. This makes the uranium centre less available for interaction with the radical isocyanate, and therefore this undergoes entropically driven radical coupling to afford diisooxocyan (O=C=N–N=C=O), followed by decomposition to N_2 and 2CO, which has been computationally described previously.[15] This seems to be a credible fate for the cyanate radical, as indirect evidence suggests the formation of vanadocene carbonyl upon condensation of the gases upon vanadocene, a known CO-trap.[16,17] Though the elimination of cyanate is computed to be endothermic in terms of enthalpy, when entropic effects are considered this process becomes exothermic (i.e. the ejection of cyanate is entropically favoured).

Whilst **139** is more stable than its start point by 38.1 kcal mol^{-1}, **138** is more stable by a larger 57.1 kcal mol^{-1}. This must to an extent reflect the difference in size between the two cations,[18] where the larger uranium(V) is afforded greater stability by the coordination of an additional ligand by formation of a U-N bond, with minimal thermodynamic penalty from steric aspects. Furthermore, as uranium(VI) is more oxidising than uranium(V), it might be anticipated that it would be more prone to homolytic extrusion of cyanate. A parallel can be drawn to the reactivity of uranium–nitrides under photolytic conditions,[26,48] wherein uranium(V)–nitrides are stable, yet uranium(VI)–nitrides activate ancillary ligand C-H bonds to afford uranium(IV) centres, which can also be rationalised by the oxidising power of uranium(VI).

The fact that the cyanate linkage is lost from **139**, in preference to the oxo group, is testament both to the highly favourable nature of the U=O bond and that one electron redox events are far more common than two electron events in f-element chemistry. If the uranium centre were reduced by two units to generate [U($Tren^{TIPS}$)(NCO)] (**135**), this would require the elimination of oxidised "O" which would be expected to be thermodynamically unfavourable given the hard nature of electronegative oxide and its ability to stabilise high oxidation states at metals (i.e. resist oxidation).

The most striking feature of the CS_2 reactivities are the drastically different final outcomes of the reactions when compared to the reactions of Tren–uranium nitrides with CO_2. For **115**, the barrier for [2 + 2]-cycloaddition is 16.0 kcal mol^{-1}, which is higher than both the outer-sphere addition of CS_2 (computed at 8.7 kcal mol^{-1}) or the analogous outer-sphere addition of CO_2 (–3.3 kcal mol^{-1}). This cannot be ascribed to a difference in the nucleophilicity of the nitride, and must result from a difference in the bond polarisation of the heteroallene. Indeed, for CO_2, the carbon atom carries a formal δ^+ charge, whereas for CS_2 it is δ^-, which makes the formation of an empty 2p-orbital at the carbon more complicated and thus increases the energy barrier. This step produces a stable thiocarbamate complex (*III*, –33.8 kcal mol^{-1}), which is as stable as the carbamate analogue (*I*, –23.1 kcal mol^{-1}).

Interestingly, a second CS_2 molecule can attack *III*, which accounts for the formation of the thiocyanate adduct of **140** (*VI*). However, the thiocyanate ligand cannot react in an analogous manner to **139** (i.e. the coupling of cyanate ligands) as the radical coupling of two NCS· radicals would lead to the formation of two CS molecules, which are highly kinetically unstable.[49,50] Instead, NCS· extrusion occurs *via* a redox process. The radical reacts with a second equivalent of **115**, which acts as a single electron donor to the thiocyanate radial, to afford the neutral hexavalent uranium(VI)–nitride. This is therefore a new, albeit esoteric, method to prepare **54**. This releases a potassium cation that coordinates the thiocyanate anion to yield $[K(Bn\text{-}15C5)_2][SCN]$. This reaction is highly thermodynamically favourable (by 97.6 kcal mol^{-1}), and represents an alternative to the coupling of the thiocyanate radicals. The concomitant formation of a closed shell thiocyanate anion accounts for experimental observations.

The calculated reaction profile for the reaction of **54** with CS_2 supports the idea that the nitride nucleophilically attacks the CS_2 and undergoes bond metathesis to afford $[U(Tren^{TIPS})(S)(NCS)]$, by analogy to the previously described mechanism for the reaction of **54** with CO_2. Here the pathways diverge for the two heteroallenes studied and their reactions with **54**. Whilst for CO_2, **139** extruded cyanate, for the sulfur analogue this intermediate (*VIII*) instead eliminates sulfur. This represents the much rarer example of a two electron oxidation event, which as stated before is unusual in f-element chemistry.

We propose that these differing outcomes are attributable to the hard nature of oxide in comparison to the softer sulfide. Despite the oxidising nature of uranium(VI), it is unable to oxidise an oxide dianion (and therefore sacrifices cyanate), However, a sulfide dianion can be oxidised to elemental sulfur, which affords the uranium(IV)–isothiocyanate **142**.

The energy barrier for the [2 + 2]-cycloaddition of CS_2 to **54** is the highest of the four discussed here (23.4 kcal mol^{-1}). It is 14.7 kcal mol^{-1} higher than for the outer-sphere addition of CS_2 to **115**, which is attributed to the smaller size of the uranium(VI) anion,[18] the nucleophilicity of the nitride and bond polarisation of CS_2, as discussed above.

The barrier for C-S bond disruption in the uranium(VI)–thiocarbamate species is low (5.1 kcal mol^{-1}), and is similar to that in the uranium(V) analogue. The thiocyanate ligand is strongly bound in the uranium(VI) intermediate [U($Tren^{TIPS}$)(S)(NCS)] (25.6 kcal mol^{-1}) due to a relatively long U=S bond which renders the uranium centre more available for coordination with an extra ligand. This intermediate is less stable (–19.6 kcal mol^{-1}) than the products of the reactions of Tren–uranium nitrides with CO_2 [**138** –57.1 kcal mol^{-1}, **139** –38.1 kcal mol^{-1}] which reflects the more congested nature of smaller uranium(VI) centres (which is energetically unfavourable) and the weaker bonding of sulfides against oxides (U=S *vs* U=O).

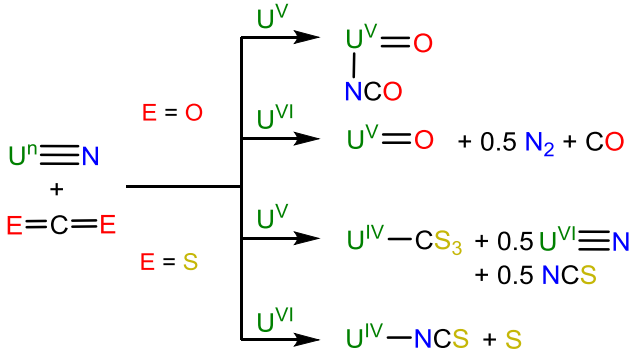
6.3. Summary and Conclusions

A reactivity study of Tren–uranium(V) and Tren–uranium(VI) nitrides towards the heteroallenes (CE_2; E = O, S) was carried out. Redox-free cleavage of these small molecules afforded common {U^n(E)(NCE)} intermediates for addition of CO_2 to both uranium(V) and uranium(VI)–nitrides and CS_2 to uranium(VI)–nitride. Subsequent zero, one and two electron redox events occur to give divergent products (Scheme **6.12.**).

For CO_2, [U($Tren^{TIPS}$)(N)][K(Bn-15C5)$_2$] (**115**) reacts to give a uranium oxo-isocyanate (**138**) by bond metathesis and cleavage of a C=O bond. [U($Tren^{TIPS}$)(N)] (**54**) reacts similarly to afford [U($Tren^{TIPS}$)(O)(NCO)] (**139**), then

subsequently decomposes to a uranium(V)–oxo (**122**) by elimination of a cyanate radical.

For CS_2, Tren–uranium(V) nitrides (**115** and **111**) afford uranium(IV)–trithiocarbonates (**140** and **141**) alongside uranium(VI)–nitride (**54**) and [K(Bn-15C5)$_2$][SCN], with overall disproportionation. [U(Tren^{TIPS})(N)] (**54**), which cannot disproportionate, instead prepares a uranium(IV)–isothiocyanate (**142**) with the extrusion of sulfur, which can be trapped by a Ph_3P scavenger.



Scheme ***6.12.*** *Summary of the reactivities of Tren–uranium(V) and Tren–uranium(VI) nitrides with heteroallenes (CO_2 and CS_2).*

Calculated reaction profiles consistently reproduce experimental outcomes, and together experimental and theoretical data verify the initial activation of CE_2 proceeds *via* outer-sphere attack of the heteroallene by uranium(V)–nitride, or direct [2 + 2]-cycloaddition for uranium(VI)–nitride. Dependent on the oxidation state of the metal and the heteroallene employed, these systems then undergo divergent reactivity. For CO_2, the uranium(V) system is stable, whereas for uranium(VI) a cyanate radical is eliminated. For CS_2 with uranium(V), a second molecule of CS_2 attacks this carbamate, which is followed by the elimination of a thiocyanate radical, which permits disproportionation chemistry. For uranium(VI), instead sulfur is eliminated, which is an example of an unusual (for f-block chemistry) two-electron reduction event.

This work highlights therefore the care that should be taken when using one of these heteroallenes as a reactivity surrogate of the other, as the subsequent reactivity can be dependent on the nature of the heteroallene.

6.4. References

(1) Schmidt, A.-C.; Heinemann, F. W.; Maron, L.; Meyer, K. *Inorg. Chem.* **2014**, *53*, 13142.
(2) Bart, S. C.; Anthon, C.; Heinemann, F. W.; Bill, E.; Edelstein, N. M.; Meyer, K. *J. Am. Chem. Soc.* **2008**, *130*, 12536.
(3) Falcone, M.; Chatelain, L.; Mazzanti, M. *Angew. Chem. Int. Ed.* **2016**, *55*, 4074.
(4) Silvia, J. S.; Cummins, C. C. *J. Am. Chem. Soc.* **2010**, *132*, 2169.
(5) Bernskoetter, W. H.; Lobkovsky, E.; Chirik, P. J. *Angew. Chem. Int. Ed.* **2007**, *46*, 2858.
(6) Kilgore, U. J.; Basuli, F.; Huffman, J. C.; Mindiola, D. J. *Inorg. Chem.* **2006**, *45*, 487.
(7) Brask, J. K.; Dura-Vila, V.; Diaconescu, P. L.; Cummins, C. C. *Chem. Commun. (Cambridge, U. K.)* **2002**, 902.
(8) *As evidenced by a search of the Cambridge Structural Database (CSD)*.
(9) King, D. M.; Tuna, F.; McMaster, J.; Lewis, W.; Blake, A. J.; McInnes, E. J. L.; Liddle, S. T. *Angew. Chem., Int. Ed.* **2013**, *52*, 4921.
(10) Camp, C.; Chatelain, L.; Kefalidis, C. E.; Pecaut, J.; Maron, L.; Mazzanti, M. *Chem. Commun.* **2015**, *51*, 15454.
(11) Windorff, C. J.; Evans, W. J. *Organomet.* **2014**, *33*, 3786.
(12) Evans, D. F. *J. Chem. Soc. (Res.)* **1959**, 2003.
(13) Kindra, D. R.; Evans, W. J. *Chem. Rev.* **2014**, *114*, 8865.
(14) Patel, D.; Tuna, F.; McInnes, E. J. L.; McMaster, J.; Lewis, W.; Blake, A. J.; Liddle, S. T. *Dalton Trans.* **2013**, *42*, 5224.
(15) Schulz, A.; Klapötke, T. M. *Inorg. Chem.* **1996**, *35*, 4791.
(16) Calderazzo, F.; Fachinetti, G.; Floriani, C. *J. Am. Chem. Soc.* **1974**, *96*, 3695.
(17) Mougel, V.; Camp, C.; Pécaut, J.; Copéret, C.; Maron, L.; Kefalidis, C. E.; Mazzanti, M. *Angew. Chem., Int. Ed.* **2012**, *51*, 12280.
(18) Shannon, R. *Acta Crystallographica Section A* **1976**, *32*, 751.
(19) Addison, A. W.; Rao, T. N.; Reedijk, J.; van Rijn, J.; Verschoor, G. C. *J. Chem. Soc., Dalton Trans.* **1984**, 1349.
(20) *τ is a measure of how trigonal bipyramidal the complex is:*

τ = (β – α)/60, where β is the largest angle, and α is the second largest angle; a perfect square based pyramid has a value of 0, whilst a perfect trigonal bipyramid has a value of 1; values larger than 1 arise due to distortion from the ideal angles of 180 and 120°, due to steric constraints of the ligand.
(21) Lam, O. P.; Castro, L.; Kosog, B.; Heinemann, F. W.; Maron, L.; Meyer, K. *Inorg. Chem.* **2012**, *51*, 781.
(22) Camp, C.; Cooper, O.; Andrez, J.; Pecaut, J.; Mazzanti, M. *Dalton Trans.* **2015**, *44*, 2650.
(23) Lescop, C.; Arliguie, T.; Lance, M.; Nierlich, M.; Ephritikhine, M. *J. Organomet. Chem.* **1999**, *580*, 137.
(24) Matson, E. M.; Breshears, A. T.; Kiernicki, J. J.; Newell, B. S.; Fanwick, P. E.; Shores, M. P.; Walensky, J. R.; Bart, S. C. *Inorg. Chem.* **2014**, *53*, 12977.
(25) King, D. M.; Tuna, F.; McInnes, E. J. L.; McMaster, J.; Lewis, W.; Blake, A. J.; Liddle, S. T. *Science* **2012**, *337*, 717.

(26) King, D. M.; Tuna, F.; McInnes, E. J. L.; McMaster, J.; Lewis, W.; Blake, A. J.; Liddle, S. T. *Nat. Chem.* **2013**, *5*, 482.
(27) Rao, C. N. R.; Venkataraghavan, R. *Spectrochimica Acta* **1962**, *18*, 541.
(28) Stueber, D.; Patterson, D.; Mayne, C. L.; Orendt, A. M.; Grant, D. M.; Parry, R. W. *Inorg. Chem.* **2001**, *40*, 1902.
(29) Camp, C.; Settineri, N.; Lefevre, J.; Jupp, A. R.; Goicoechea, J. M.; Maron, L.; Arnold, J. *Chem. Sci.* **2015**, *6*, 6379.
(30) Hashem, E.; Platts, J. A.; Hartl, F.; Lorusso, G.; Evangelisti, M.; Schulzke, C.; Baker, R. J. *Inorg. Chem.* **2014**, *53*, 8624.
(31) Lewis, A. J.; Nakamaru-Ogiso, E.; Kikkawa, J. M.; Carroll, P. J.; Schelter, E. J. *Chem. Commun.* **2012**, *48*, 4977.
(32) Liu, P.; Taylor, B. L. H.; Garcia-Lopez, J.; Houk, K. N. In *Handbook of Metathesis*; Wiley-VCH Verlag GmbH & Co. KGaA: 2015, p 199.
(33) Smith, J. M. In *Progress in Inorganic Chemistry Volume 58*; John Wiley & Sons, Inc.: 2014, p 417.
(34) La Pierre, H. S.; Meyer, K. In *Progress in Inorganic Chemistry Volume 58*; John Wiley & Sons, Inc.: 2014, p 303.
(35) Chatelain, L.; Scopelliti, R.; Mazzanti, M. *J. Am. Chem. Soc.* **2016**, *138*, 1784.
(36) Krogman, J. P.; Foxman, B. M.; Thomas, C. M. *J. Am. Chem. Soc.* **2011**, *133*, 14582.
(37) Sadique, A. R.; Brennessel, W. W.; Holland, P. L. *Inorg. Chem.* **2008**, *47*, 784.
(38) Lee, C. H.; Laitar, D. S.; Mueller, P.; Sadighi, J. P. *J. Am. Chem. Soc.* **2007**, *129*, 13802.
(39) Lu, C. C.; Saouma, C. T.; Day, M. W.; Peters, J. C. *J. Am. Chem. Soc.* **2007**, *129*, 4.
(40) Laitar, D. S.; Müller, P.; Sadighi, J. P. *J. Am. Chem. Soc.* **2005**, *127*, 17196.
(41) Fachinetti, G.; Floriani, C.; Chiesi-Villa, A.; Guastini, C. *J. Am. Chem. Soc.* **1979**, *101*, 1767.
(42) Siladke, N. A.; Meihaus, K. R.; Ziller, J. W.; Fang, M.; Furche, F.; Long, J. R.; Evans, W. J. *J. Am. Chem. Soc.* **2012**, *134*, 1243.
(43) Evans, W. J.; Mueller, T. J.; Ziller, J. W. *J. Am. Chem. Soc.* **2009**, *131*, 2678.
(44) Evans, W. J.; Kozimor, S. A.; Ziller, J. W. *J. Am. Chem. Soc.* **2003**, *125*, 14264.
(45) Evans, W. J.; Kozimor, S. A.; Nyce, G. W.; Ziller, J. W. *J. Am. Chem. Soc.* **2003**, *125*, 13831.
(46) Evans, W. J.; Davis, B. L. *Chem. Rev.* **2002**, *102*, 2119.
(47) Evans, W. J.; Nyce, G. W.; Johnston, M. A.; Ziller, J. W. *J. Am. Chem. Soc.* **2000**, *122*, 12019.
(48) Thomson, R. K.; Cantat, T.; Scott, B. L.; Morris, D. E.; Batista, E. R.; Kiplinger, J. L. *Nat. Chem.* **2010**, *2*, 723.
(49) Castro, L.; Labouille, S.; Kindra, D. R.; Ziller, J. W.; Nief, F.; Evans, W. J.; Maron, L. *Chem. -Eur. J.* **2012**, *18*, 7886.
(50) Castro, L.; Maron, L. *Chem. -Eur. J.* **2012**, *18*, 6610.

Chapter Seven

Supporting Information

Table of Contents

7.1. General Experimental Details.....264

7.1.1. General 264

7.1.2. Solvent Purification 264

7.1.3. Purchased and Synthesised Reagents.....264

7.1.4. Instrumentation.....266

7.2. Experimental Details 269

7.2.1. Chapter 2 269

7.2.1.1. Preparation of [{U(Tren^{TIPS})(μ-N)(μ-Li)}$_2$], **106**.....269

7.2.1.2. Preparation of [{U(Tren^{TIPS})(μ-N)(μ-Na)}$_2$], **51**.....269

7.2.1.3. Preparation of [{U(Tren^{TIPS})(μ-N)(μ-K)}$_2$], **107**.....270

7.2.1.4. Attempted preparation of [{U(Tren^{TIPS})(μ-N)(μ-K)}$_2$], **107**.....271

7.2.1.5. Preparation of [{U(Tren^{TIPS})(μ-N)(μ-Rb)}$_2$], **108**.....271

7.2.1.6. Preparation of [{U(Tren^{TIPS})(μ-N)(μ-Cs)}$_2$], **109** 272

7.2.1.7. Preparation of [U(Tren^{TIPS}){(μ-N)(μ-K)(Bn$_2$-18C6)}], **111** 272

7.2.1.8. Preparation of [U(Tren^{TIPS}){(μ-N)(μ-Rb)(18C6)}], **112**.....273

7.2.1.9. Preparation of [U(Tren^{TIPS}){(μ-N)(μ-Cs)(18C6)}], **113** 273

7.2.1.10. Preparation of [U(Tren^{TIPS})(N)][K(15C5)$_2$], **114** 274

7.2.1.11. Preparation of [U(Tren^{TIPS})(N)][K(Bn-15C5)$_2$], **115** 275

7.2.1.12. Preparation of [U(Tren^{TIPS})(N)][Rb(Bn-15C5)$_2$], **116**.....275

7.2.1.13. Preparation of [U(Tren^{TIPS})(N)][Cs(Bn-15C5)$_2$], **117**.....276

7.2.1.14. Preparation of [U(Tren^{TIPS}){(μ-N)(μ-Li)(12C4)}], **118**.....276

7.2.1.15. Preparation of [U(Tren^{TIPS}){(μ-N)(μ-Li)(Bn-9C3)$_3$}], **119**.....277

7.2.1.16. Preparation of [U(Tren^{TIPS}){(μ-N)Li(py)$_3$}], **121** 277

7.2.1.17. Preparation of [U(Tren^{TIPS}){(μ-N)(μ-Li)(η^3-tetraglyme)$_3$}], **120**.....278

7.2.1.18. Attempted preparations of [U(Tren^{TIPS})(N)][Li(co-ligand)$_n$].....279

7.2.1.19. Preparation of [U(Tren^{TIPS})(N)], **54** 279

7.2.2. Chapter 3 280

7.2.2.1. Preparation of [U{*C*H_2CH(Me)Si(^{i}Pr)$_2$*N*CH_2CH_2*N*(CH_2CH_2*N*Si^{i}Pr$_3$)$_2$}], **110** 280

7.2.2.2. Preparation of [Th(Tren^{TIPS})(CH_2Ph)], **124** 281

7.2.2.3. Preparation of [Th{*C*H_2CH(Me)Si(^{i}Pr)$_2$*N*CH_2CH_2*N*(CH_2CH_2*N*Si^{i}Pr$_3$)$_2$}], **125** 282

7.2.3. Chapter 5 283

7.2.3.1. Preparation of [U(Tren^{TIPS})(NCO)], **135** 283

7.2.3.2. Preparation of [U(Tren^{TIPS})(NCO)][K(Bn-15C5)$_2$], **136** 284

7.2.3.3. Preparation of [U(Tren^{TIPS}){(μ-NCO)(μ-K)(18C6)}], **137** 285

7.2.3.4. Preparation of [U(Tren^{TIPS})], **15** 286

7.2.3.5. Attempted synthetic cycle towards the conversion of NaN_3 to NaOCN .. 286

7.2.3.6. Attempted Reactivity Studies of [U(Tren^{TIPS})(N)] (**54**) with phosphines 287

7.2.3.7. Attempted Reactivity Studies of [U(Tren^{TIPS})(N)][K(Bn-15C5)$_2$] (**115**) with phosphines 287

7.2.4. Chapter 6 288

7.2.4.1. Preparation of [U(Tren^{TIPS})(O)(NCO)][K(Bn-15C5)$_2$], **138** 288

7.2.4.2. Reactivity study of [U(Tren^{TIPS}){μ-N)(μ-K)(Bn_2-18C6)}] (**111**) with CO_2 288

7.2.4.3. Reactivity study of [{U(Tren^{TIPS})(μ-N)(μ-K)}$_2$] (**107**) with CO_2 289

7.2.4.4. Attempted Preparations of [U(Tren^{TIPS})(O)(NCO)], **139** and decomposition to [U(Tren^{TIPS})(O)], **122** 289

7.2.4.5. Preparation of [U(Tren^{TIPS})(κ^2-CS_3)][K(Bn-15C5)$_2$], **140** 290

7.2.4.6. Preparation of [K(Bn-15C5)$_2$][SCN] 291

7.2.4.7. Synthesis of [{U(Tren^{TIPS})(μ-κ^2-CS_3)[K(Bn_2-18C6)]}$_2$(μ-C_6H_6)]•4(C_6H_6), **141** 292

7.2.4.8. Preparation of [K(Bn_2-18C6)][SCN] 292

7.2.4.9. Reactivity study of [{U(Tren^{TIPS})(μ-N)(μ-K)}$_2$] (**111**) with CS_2 292

7.2.4.10. Preparation of [U(Tren^{TIPS})(NCS)], **142** 293

7.2.4.11. Demonstration of the liberation of elemental sulfur from the reaction of [U(Tren^{TIPS})(N)] (**54**) and CS_2 294

7.2.4.12. Attempted preparation of [U(Tren^{TIPS})] (**15**) 295

7.3. X-ray Crystallographic Data 295

7.4. Magnetometric Measurements 304

7.4.1. Chapter 4 304

7.4.2. Chapter 5 314

7.4.3. Chapter 6 315

7.5. DFT and *ab initio* Calculations 316

7.5.1. Chapter 3 316

7.5.2. Chapter 4 319

7.5.3. Chapter 5 326

7.5.4. Chapter 6 327

7.6. References 328

7.1. General Experimental Details

7.1.1. General

All manipulations were carried out under an inert atmosphere of dry nitrogen using standard Schlenk techniques, or an MBraun UniLab glovebox operating under an atmosphere of dry nitrogen with H_2O and O_2 < 0.1 ppm. All glassware was dried either by overnight storage in an oven at 150 °C or by flame-drying with subsequent cooling under 10^{-3} mm Hg vacuum followed by repeated alternate evacuation and purging with nitrogen. Oxygen-free nitrogen gas cylinders were supplied by BOC Gases UK. Manipulations with CO and CO_2 were performed on two Schlenk lines, one remaining under inert atmospheric conditions, and a second, in a fumehood, purged of inert atmosphere by four x ten minute evacuation/refill with the desired reagent gas. Manipulations with lithium powder were conducted under an argon atmosphere.

7.1.2. Solvent Purification

The solvents THF, diethyl ether, toluene, hexanes and pentane were dried by passage through activated alumina towers and degassed before use. 1,2-dimethoxyethane (DME) and benzene were distilled from potassium. Dichloromethane (DCM) and pyridine were distilled from calcium hydride. All solvents were stored over potassium mirrors except for DCM, which was stored over activated 3 Å sieves, and ethers and pyridine which were stored over activated 4 Å sieves. Deuterated NMR solvents (d^6-benzene, d^8-toluene, d^8-tetrahydrofuran) were purchased from Goss Scientific Ltd and were distilled from potassium, degassed by three freeze-pump-thaw cycles and stored under nitrogen prior to use. Nujol was purchased from Sigma-Aldrich and used as received.

7.1.3. Purchased and Synthesised Reagents

Lithium powder, rubidium and caesium metals, iodine, hexamethylphosphoramide [HMPA, $OP(NMe_2)_3$], tetramethyl ethylene diamine [TMEDA,

$Me_2NCH_2CH_2NMe_2$], pentamethylene diethylene triamine [PMDETA, $MeN(CH_2CH_2NMe_2)_2$], 9-ane-S_3 ($C_6H_{12}S_3$), potassium azide (KN_3), trimethylphosphine (PMe_3), tributylphosphine, (P^nBu_3), 4-methylmorpholine N-oxide [$OC_4H_8N^+–O^{\bullet-}$], pyridine N-oxide [$C_5H_5N^+–O^{\bullet-}$], trimethylamine N-oxide, [$Me_3N^+–O^{\bullet-}$] and TEMPO [(2,2,6,6-Tetramethylpiperidin-1-yl)oxyl] were used as purchased. Potassium *tert*-butoxide (KO^tBu), benzo-15-crown-5 ether (Bn-15C5), 18-crown-6 (18C6), dibenzo-18-crown-6 (Bn_2-18C6), sodium cyanate (NaOCN), sodium azide (NaN_3), potassium thiocyanate (KSCN), triphenylphosphine (Ph_3P) and triphenylphosphine sulphide (Ph_3PS) were dried under vacuum for four hours prior to use. 12-crown-4 and 15-crown-5 ether were dissolved in diethyl ether, dried over activated 4 Å molecular sieves for 24 hours, decanted and the ether removed prior to use. Tren [$N(CH_2CH_2NH_2)_3$] was distilled prior to use. Carbon disulphide (CS_2) was prepared as a stock solution (0.5 M in toluene). Sodium flakes in paraffin wax were washed with hexanes prior to use. Tetraglyme [$Me(OCH_2CH_2)_4OMe$] was stirred over potassium at 80 °C for 16 hrs, then stored over molecular sieves in ether for 3 days, then dried over potassium again at 130 °C for 2 days. The tetraglyme was collected by distillation at 110 °C under dynamic vacuum. All reagents were purchased from Sigma-Aldrich and Alfa-Aesar. [$U(O)_3$] (>99.9 U^{238}) was supplied by the National Nuclear Laboratory. The following compounds were prepared using literature methods: [$U(Tren^{TIPS})(Cl)$] (**7**),[1] [$Tren^{TIPS}$ = $\{N(CH_2CH_2NSi^iPr_3)_3\}^{3-}$, ^iPr = $CH(CH_3)_2$], [$U(Tren^{TIPS})(I)$] (**10**),[1] [$U(Tren^{TIPS})(N_3)$] (**13**),[2] [$U(Tren^{TIPS})$] (**15**),[1] [$Th(Tren^{TIPS})(I)$] (**123**),[3] KC_8,[4] KCH_2Ph,[5] and benzo-9-crown-3 ether (Bn-9C3).[6] [$U(Tren^{TIPS})(N)$] (**54**)[2] was prepared *via* a modified literature procedure (*see below*).

*Note: Due to the light sensitive nature of Tren–uranium(VI) nitride, all manipulations using or affording [$U(Tren^{TIPS})(N)$] (**54**) should be conducted in the absence of light.*

7.1.4. Instrumentation

NMR Spectroscopy

^{1}H, ^{13}C, ^{29}Si, ^{31}P NMR spectra were recorded on a Bruker AV400 or AV(III)400 spectrometer [operating at 400.2 (^{1}H), 100.6 (^{13}C), 79.5 (^{29}Si), 162.0 (^{31}P) MHz, respectively] by PAC or by Dr Adrienne Davis, Kevin Butler or Shazad Aslam (University of Nottingham). Chemical shifts (δ) are quoted in ppm and are relative to external $SiMe_4$ (^{1}H, ^{13}C, ^{29}Si) and 85% H_3PO_4 (^{31}P). Samples were prepared in the glovebox and placed in J. Young PTFE 5mm screw-topped borosilicate NMR tubes. Crystals were examined by PAC, DMK, AJW, BMG, MJG or Dr W. Lewis (University of Nottingham) on a Bruker APEX CCD area detector diffractometer or an Oxford Diffraction Ltd. SuperNova Atlas CCD diffractometer.

Vibrational Spectra

FTIR spectra were recorded on a Bruker Tensor^{TM} 27 spectrometer and samples were prepared in the glovebox as Nujol mulls between KBr discs, or on a Bruker Alpha spectrometer with a Platinum-ATR module in the glovebox.

UV-Vis-NIR Absorption Spectroscopy

UV-Vis-NIR spectra were recorded on a Perkin Elmer LMD^{TM} 750 spectrometer. Data were collected in 1 mm path length cuvettes loaded in an MBraun UniLab glovebox and were run versus the appropriate reference solvent.

SQUID Magnetic Measurements

Variable-temperature magnetic moment data were recorded in an applied dc field of 0.1 T on a Quantum Design MPMS XL5 or Quantum Design MPMS XL7 a superconducting quantum interference device (SQUID) magnetometer using doubly recrystallised powdered samples performed by Dr F. Tuna or Prof. E. J. L. McInnes.

Samples were carefully checked for purity and data reproducibility between several independently prepared batches for each compound examined. Care was taken to ensure complete thermalisation of the sample before each data point was measured and samples were immobilised in an eicosane matrix to prevent sample reorientation during measurements. Diamagnetic corrections were applied using tabulated Pascal constants and measurements were corrected for the effect of the blank sample holders (flame sealed Wilmad NMR tube and straw) and eicosane matrix. AC susceptibility measurements were performed with an AC field of 1.55 G oscillating at frequencies ranging from 1 to 1200 Hz. Solution magnetic moments were recorded at room temperature using the Evans method.[7]

EPR Spectroscopy

Variable temperature (300-5 K) EPR spectra were measured at S-band (ca. 3.8 GHz) and Q-band (ca. 34.0 GHz) on a Bruker Elexsys E500 spectrometer with an ER4118SMS5 or ER5106QT resonator, respectively, by Dr F. Tuna and Prof E. J. L. McInnes at the University of Manchester. Polycrystalline samples were sealed under vacuum in 1 mm i.d. silica tubing and double-contained for EPR by insertion into an X-band silica tube or PTFE sleeve. Spectra were background corrected against blank sample holders measured under identical conditions.

Elemental Analysis

CHN microanalyses were carried out by Tong Liu (University of Nottingham).

X-Ray Crystallography

Crystals were examined variously on a Bruker APEX CCD area detector diffractometer using graphite-monochromated Mo Kα radiation (λ = 0.71073 Å), or on an Oxford Diffraction SuperNova Atlas CCD diffractometer using mirror-monochromated Cu Kα radiation (λ = 1.5418 Å). Intensities were integrated from

data recorded on 0.3° (APEX) or 1° (SuperNova) frames by ω rotation. Cell parameters were refined from the observed positions of all strong reflections in each data set. Semi-empirical absorption correction based on symmetry equivalent and repeat reflections (APEX) or Gaussian grid face-indexed absorption correction with a beam profile correction (Supernova) were applied. The structures were solved variously by direct and heavy atom methods and were refined by full-matrix least-squares on all unique F^2 values, with anisotropic displacement parameters for all non-hydrogen atoms, and with constrained riding hydrogen geometries; U^{iso}(H) was set at 1.2 (1.5 for methyl groups) times U_{eq} of the parent atom. The largest features in final difference syntheses were close to heavy atoms and were of no chemical significance. Programs were Bruker AXS SMART[8] and CrysAlisPro[9] (control), Bruker AXS SAINT[8] and CrysAlisPro[9] (integration), and SHELXTL[10] and Olex2[11] were employed for structure solution and refinement and for molecular graphics.

NB. for all data:

$$R = \frac{\sum\left||F_o| - F_c\right|}{\sum|F_o|}; R_w = \sqrt{\frac{\sum w(F_o^2 - F_c^2)^2}{\sum w(F_o^2)^2}}; S = \sqrt{\frac{\sum w(F_o^2 - F_c^2)^2}{no.data - no.parameters}}$$

Complete crystallographic data (list of bond lengths, bond angles, atomic coordinates and displacement parameters) for each structure are available on the attached CD as Crystallographic Information Files. A summary of the general crystallographic data can be found in the tables presented in section 3.

7.2. Experimental Details

7.2.1. Chapter 2

7.2.1.1. Preparation of [{U(Tren^{TIPS})(μ-N)(μ-Li)}$_2$], **106**

A solution of [U(Tren^{TIPS})(N$_3$)] (**13**, 3.57 g, 4.00 mmol) in toluene (10 ml) was added to a cold (−78 °C) slurry of Li metal (0.08 g, 11.60 mmol) in toluene (20 ml). The mixture was allowed to slowly warm to room temperature and then stirred for 5 days. Each day the mixture was sonicated for 1 hr. After this time a red precipitate had formed which was extracted and filtered through a frit using boiling toluene (60 ml). The residue was washed with boiling toluene (2 x 10 ml). The filtrate was concentrated to ~30 ml and stored at -30 °C to yield **106** as a red crystalline solid. The product was isolated by filtration, washed with pentane (2 x 10 ml) and dried *in vacuo*. Yield 1.22 g, 35%. Anal. calcd for $C_{66}H_{150}N_{10}Li_2Si_6U_2$: C, 45.49; H, 8.68; N, 8.04. Found: C, 45.46; H, 8.62; N, 7.99. ^{1}H NMR (C_6D_6, 298 K): δ 33.65 (s, 6H, CH_2), 7.84 (s, 6H, CH_2), −1.33 (s, 9H, CH(CH$_3$)$_2$), −2.74 ppm (s, 54H, CH(CH_3)$_2$). FTIR ν/cm^{-1} (Nujol): 1591 (w), 1302 (w), 1137 (w), 1052 (s), 965 (w), 932 (s), 882 (s), 737 (s), 672 (m), 633 (m), 567 (w), 545 (w), 516 (w). ^{29}Si{^{1}H} NMR and solution magnetic moment (Evans method) could not be conducted due to the insolubility of **106** in aromatic solvent once isolated. Manipulations of lithium metal were performed under an argon atmosphere, rather than a nitrogen atmosphere.

7.2.1.2. Preparation of [{U(Tren^{TIPS})(μ-N)(μ-Na)}$_2$], **51**

A solution of **13** (2.68 g, 3.00 mmol) in toluene (10 ml) was added to a cold (−78 °C) slurry of Na metal (0.07 g, 3.00 mmol) in toluene (20 ml). The mixture was allowed to slowly warm to room temperature and then stirred for 5 days. Each day the mixture was sonicated for 1 hr. After this time a red precipitate had formed which was extracted and filtered through a frit using boiling toluene (30 ml). The residue was washed with boiling toluene (2 x 10 ml). The filtrate was concentrated to ~10 ml and stored at –30 °C to yield [{U(Tren^{TIPS})(μ-N)(μ-Na)}$_2$] as a red crystalline solid. The product was isolated by filtration, washed with pentane (2 x 10 ml) and dried *in vacuo*. Yield 1.32 g, 50%. The identity of **51** was confirmed by comparison to

previously reported data,[1] however, reappraisal of the ^{1}H NMR spectrum, following recollection with more scans, allows for a reassignment of the spectrum, in corroboration with the spectra for **106** (*vide supra*) and [{U(Tren^{TIPS})(μ-N)(μ-Cs)}$_2$] (**117**, *vide infra*). ^{1}H NMR (C_6D_6, 298 K): δ 38.33 (s, 6H, C*H*$_2$), 7.70 (s, 6H, C*H*$_2$), −6.55 (s, 9H, C*H*(CH$_3$)$_2$), −6.82 ppm (s, 54H, CH(C*H*$_3$)$_2$).

7.2.1.3. Preparation of [{U(Tren^{TIPS})(μ-N)(μ-K)}$_2$], **107**

Method A: Toluene (15 ml) was added to a cold (−78 °C) stirring mixture of **13** (2.96 g, 3.30 mmol) and KC_8 (0.44 g, 3.30 mmol). The resulting mixture was allowed to warm to ambient temperature and stirred for a further 6 days to afford a dark brown suspension. After this time the mixture was allowed to thoroughly settle (1 hr) and carefully filtered to afford a dark brown solid that was washed with toluene (5 × 5 ml) until the washings obtained were colourless, at which point these were discarded. The solid was then extracted into hot benzene and quickly filtered through a frit to remove the graphite precipitate. The filtrate was stored at 7 °C for 16 hrs to yield dark red crystals of **107** which were isolated by filtration and dried *in vacuo.* Yield: 1.70 g, 57% (crystalline). ^{1}H, ^{29}Si{^{1}H} NMR and solution magnetic moment (Evans method) could not be obtained due to the insolubility of [{U(μ-N)(μ-K)(Tren^{TIPS})}$_2$] in aromatic solvent once isolated.

Method B: A solution of [U(Tren^{TIPS})(N)] (**54**, 0.12 g, 0.14 mmol) in toluene (15 ml) was added dropwise to KC_8 (0.02 g, 0.15 mmol) at –78 °C with stirring. The mixture was allowed to warm to room temperature with stirring over 16 hours. The mixture was allowed to settle (1 hour) and carefully filtered to afford a dark brown solid that was washed with toluene (3 × 5 ml) until the washings obtained were colourless, at which point these were discarded. The solid was then extracted into hot benzene and quickly filtered through a frit to remove the graphite precipitate. The filtrate was stored at 7 °C for 16 hours to yield dark red crystals of **107** which were isolated by filtration and dried *in vacuo.* Yield: 0.20 g, 16%.

Method C: Benzene (5 ml) was added to a stirring mixture of **51** (0.32 g, 0.18 mmol) and KO^{t}Bu (0.04 g, 0.36 mmol). The mixture was heated to 80 °C for 2 hours and allowed to cool affording a red precipitate. The precipitate was isolated by filtration, extracted into boiling benzene and filtered through a frit. The filtrate was stored at 7 °C yield **106** as red/orange crystals. Crystalline yield: 0.10, 31%.

Anal. calcd for $C_{66}H_{150}N_{10}K_2Si_6U_2$: C 43.88; H 8.37; N 7.75. Found: C 44.18; H 8.38; N 7.62. FTIR ν/cm^{-1} (Nujol): 1344 (w), 1134 (w), 1069 (s), 1056 (s), 992 (w), 932 (s), 880 (m), 851 (w), 780 (m), 746 (s), 671 (m), 626 (w), 571 (w), 545 (w), 515 (w). ^{1}H, ^{29}Si{^{1}H} NMR and solution magnetic moment (Evans method) could not be obtained due to the insolubility of [{U(Tren^{TIPS})(μ-N)(μ-K)}$_2$] in aromatic solvent once isolated.

7.2.1.4. Attempted preparation of [{U(Tren^{TIPS})(μ-N)(μ-K)}$_2$], **107**

Pyridine (30 ml) was added to a cold (−78 °C) stirring mixture of [U(Tren^{TIPS})] (**15**, 0.64 g, 0.75 mmol) and KN_3 (0.06 g, 0.75 mmol). The resulting mixture was allowed to warm to ambient temperature and stirred for a further 3 days to afford a dark brown suspension. Volatiles were removed *in vacuo* to afford a brown solid, which was extracted into pentane. ^{1}H NMR spectroscopic analysis of the resultant solid was inconclusive.

7.2.1.5. Preparation of [{U(Tren^{TIPS})(μ-N)(μ-Rb)}$_2$], **108**

A solution of **13** (3.57 g, 4 mmol) in toluene (10 ml) was added at once to a cold (−78 °C) slurry of Rb metal (0.38 g, 4.4 mmol) in toluene (10 ml). The mixture was allowed to slowly warm to room temperature and then stirred for 72 h. The resulting mixture was filtered and the remaining solid extracted with toluene (2 x 5 ml). The toluene extracts were combined and volatiles were removed *in vacuo* to afford a red-brown solid. Recrystallisation from hot benzene (10 ml) afforded **108** as a red crystalline solid on cooling to 7 °C. Yield 1.90 g, 50% (crystalline). Anal. calcd for $C_{66}H_{150}N_{10}Rb_2Si_6U_2$: C, 41.73; H, 7.96; N, 7.37. Found: C, 39.35; H, 7.29; N, 7.61.

FTIR ν/cm^{-1} (Nujol): 1337 (w), 1270 (w), 1135 (m), 1064 (s), 989 (m), 931 (s), 881 (m), 846 (m), 777 (s), 734 (s), 670 (m), 628 (w), 564 (w), 543 (w), 509 (w). ^{1}H and ^{29}Si{^{1}H} NMR and solution magnetic moment (Evans method) could not be obtained due to the insolubility of **108** in aromatic solvent once isolated.

7.2.1.6. Preparation of [{U(Tren^{TIPS})(μ-N)(μ-Cs)}$_2$], **109**

A solution of [U(Tren^{TIPS})(N$_3$)] (3.43 g, 3.85 mmol) in benzene (10 ml) was added at once to a cold (−78 °C) slurry of Cs metal (0.51 g, 3.85 mmol) in benzene (10 ml). The mixture was allowed to slowly warm to room temperature and then stirred for 72 h. The resulting mixture was filtered and the remaining solid extracted with hot benzene (2 x 5 ml). The benzene extracts were combined and volatiles were removed *in vacuo* to afford a red-brown solid. Recrystallisation from hot benzene (10 ml) afforded [{U(Tren^{TIPS})(μ-N)(μ-Cs)}$_2$] as a red crystalline solid on cooling to 7 °C. Yield 1.39 g, 36%. Anal. calcd for $C_{66}H_{150}Cs_2N_{10}Si_6U_2$: C, 39.75; H, 7.58; N, 7.02. Found: C, 40.12; H, 7.37; N, 7.02. ^{1}H NMR (C_6D_6, 298 K): δ 37.54 (s, 6H, CH_2), 8.19 (s, 6H, CH_2), −5.14 (s, 9H, CH(CH$_3$)$_2$), −5.64 ppm (s, 54H, CH(CH_3)$_2$). FTIR ν/cm^{-1} (Nujol): 1340 (w), 1251 (w), 1135 (m), 1059 (s), 1056 (s), 990 (m), 932 (s), 880 (m), 843 (m), 772 (s), 739 (s), 670 (m), 626 (w), 597 (m), 566 (w), 542 (w), 511 (w). μ_{eff} (Evans method, C_6D_6, 298 K): 1.89 μ_B. A ^{29}Si{^{1}H} NMR spectrum could not be obtained as **109** is only partially soluble in aromatic solvents once isolated.

7.2.1.7. Preparation of [U(Tren^{TIPS}){(μ-N)(μ-K)(Bn$_2$-18C6)}], **111**

Toluene (20 ml) was added to a cold (−78 °C) mixture of **107** (0.61 g, 0.34 mmol) and dibenzo-18-crown-6 (0.24 g, 0.68 mmol). The resulting red/brown mixture was allowed to warm to ambient temperature and stirred at room temperature for a further 16 hours. The solvent was removed *in vacuo* to yield a pale brown solid that was washed with hexane (4 × 5 ml) and dried *in vacuo*. Crystalline material was obtained from concentration of the hexane washings and storage at 5 °C overnight, yielding **111** as pale brown tablets. Yield: 0.56 g, 66% (crystalline). Anal. calcd for

$C_{53}H_{99}KN_5O_6Si_3U$: C, 50.37; H, 7.90; N, 5.54. Found: C, 48.58; H, 7.72; N, 4.85. ^{1}H NMR (C_6D_6, 298 K): δ 40.20 (s, 6H, CH_2), 9.30 (s, 16H, OCH_2), 8.18 (s, 4H, ArH), 7.91 (s, 6H, CH_2), 7.07 (s, 4H, ArH), −5.88 (s, 9H, CH(CH_3)$_2$), −7.24 ppm (s, 54H, CH(CH_3)$_2$). ^{29}Si{^{1}H} NMR (C_6D_6, 298 K): δ −13.30ppm . FTIR ν/cm^{-1} (Nujol): 1304 (s), 1259 (s), 1233 (m), 1215 (m), 1130 (s), 1092 (m), 1071 (s), 1061 (s), 1024 (m), 959 (w), 949 (w), 934 (m), 882 (w), 857 (w), 740 (s), 723 (s), 670 (w), 627 (w), 588 (w), 566 (w), 514 (w). λ_{max}/nm (ε/M^{-1}cm^{-1}) 1118 (31.8), 1434 (18.7), 1459 (23.6), 1473 (21.5), 1649 (25.5). μ_{eff} (Evans method, C_6D_6, 298 K): 2.72 μ_B.

7.2.1.8. Preparation of [U(Tren^{TIPS}){(μ-N)(μ-Rb)(18C6)}], **112**

Toluene (20 ml) was added to a cold (−78 °C) mixture of **108** (0.66 g, 0.35 mmol) and 18-crown-6 (0.18 g, 0.70 mmol). The resulting mixture was allowed to warm to room temperature with stirring over 16 h. Volatiles were removed *in vacuo* to afford a sticky brown solid. The solid was washed with hexanes (5ml) and filtered to afford [U(Tren^{TIPS}){(μ-N)(μ-Rb-18C6)}] as a brown powder. Crystalline material was obtained from a concentrated solution of **112** in hexanes. Yield 0.37 g, 44% (crystalline). Anal. calcd for $C_{45}H_{99}N_5O_6RbSi_3U$: C, 44.52; H, 8.22; N, 5.77. Found: C, 38.36; H, 6.93; N, 7.86. ^{1}H NMR (C_6D_6, 298 K): δ 41.91 (s, 6H, CH_2), 9.86 (s, 24H, OCH_2), 8.27 (s, 6H, CH_2), –6.37 (s, 9H, CH(CH_3)$_2$), –7.36 ppm (s, 54H, CH(CH_3)$_2$). ^{29}Si{^{1}H} NMR (C_6D_6, 298 K): δ –11.88 ppm. FTIR ν/cm^{-1} (Nujol): 1352 (s), 1284 (w), 1116 (s), 1079 (m), 1013 (m), 987 (w), 962 (w), 935 (m), 882 (m), 866 (w), 840 (m), 740 (s), 671 (m), 627 (m), 564 (w), 542 (w), 509 (w). UV-vis-NIR (toluene): λ_{max}/nm (ε/M^{-1}cm^{-1}) 1113 (30.3), 1432 (16.4), 1457 (20.6), 1479 (18.9), 1647 (17.4). μ_{eff} (Evans method, C_6D_6, 298 K): 1.89 μ_B.

7.2.1.9. Preparation of [U(Tren^{TIPS}){(μ-N)(μ-Cs)(18C6)}], **113**

Toluene (20 ml) was added to a cold (–78 °C) mixture of **109** (0.643 g, 0.32 mmol) and 18-crown-6 (0.169 g, 0.64 mmol). The resulting mixture was allowed to warm to room temperature with stirring over 16 h. Volatiles were removed *in vacuo* and the resulting brown solid washed with hexanes (5 ml). The solid was extracted into

toluene (5 ml), concentrated (~2 ml) and stored at –28 °C for 7 days to afford orange crystals of **113**. Yield: 0.135 g, 34%. Anal. Calcd for $C_{45}H_{99}CsN_5O_6Si_3U$: C, 42.85; H, 7.91; N, 5.55. Found: C, 42.80; H, 7.84; N, 5.32. ^{1}H NMR (C_6D_6, 298 K): δ 40.10 (s, 6H, CH_2), 10.89 (s, 12H, OCH_2), 7.91 (s, 12H, OCH_2), 3.61 (s, 6H, CH_2), –5.88 (s, 9H, CH(CH_3)$_2$), –6.71 ppm (s, 54H, CH(CH_3)$_2$). ^{29}Si{^{1}H} NMR (C_6D_6, 298 K): δ –13.32 ppm. FTIR ν/cm^{-1} (Nujol): 1351 (m), 1282 (w), 1112 (s), 1082 (m), 1013 (m), 959 (w), 933 (m), 881 (w), 858 (w), 837 (s), 792 (s), 739 (m), 669 (m), 624 (w), 588 (w), 543 (w), 526 (w), 508 (w). UV-vis-NIR (toluene): λ_{max}/nm (ε/M^{-1}cm^{-1}) 1132 (33.5), 1435 (19.7), 1459 (24.0), 1474 (20.4), 1651 (26.3). μ_{eff} (Evans method, C_6D_6, 298 K): 2.20 μ_B.

7.2.1.10. Preparation of [U(Tren^{TIPS})(N)][K(15C5)$_2$], **114**

To a cold (–78 °C) solution of **107** (0.98 g, 0.54 mmol) in toluene (15 ml) was added a solution of 15-crown-5 (0.48 g, 2.16 mmol) in toluene (10 ml). The red/brown mixture was allowed to warm to room temperature with stirring over 16 hours. The solvent was removed *in vacuo* to yield a brown oil that crystallised within 1 hour at room temperature. On occasions storage at 5 °C was necessary to obtain crystalline material. Crystals of **114** were isolated by thorough washing with pentane (5 × 5 ml) and were dried *in vacuo* to afford a brown solid. Yield: 0.94 g, 64%. Anal. calcd for $C_{53}H_{115}N_5KO_{10}Si_3U$: C 47.36; H 8.63; N 5.21. Found: C 47.47; H 8.44; N 4.93. ^{1}H NMR (C_6D_6, 298 K): δ 39.10 (s, 6H, CH_2), 11.92 (s, 6H, CH_2), 8.45 (s, 20H, OCH_2), 4.82 (s, 20H, OCH_2), −5.58 (s, 9H, CH(CH_3)$_2$), −6.36 ppm (s, 54H, CH(CH_3)$_2$). ^{29}Si{^{1}H} NMR (C_6D_6, 298 K): δ −15.13 ppm. FTIR ν/cm^{-1} (Nujol): 1302 (m), 1260 (m), 1124 (s), 1042 (m), 935 (m), 882 (m), 856 (w), 741 (m), 723 (m), 670 (w), 625 (w), 565 (w), 506 (w). UV-vis-NIR (toluene): λ_{max}/nm (ε/M^{-1}cm^{-1}) 1125 (31.8), 1436 (17.4), 1461 (21.5), 1655 (25.4). μ_{eff} (Evans method, C_6D_6, 298 K): 1.58 μ_B.

7.2.1.11. Preparation of [U(Tren^{TIPS})(N)][K(Bn-15C5)$_2$], **115**

Toluene (25 ml) was added dropwise to a cold (–78 °C) stirring mixture of **107** (1.63 g, 0.90 mmol) and benzo-15-crown-5 (0.97 g, 3.60 mmol). The red/brown mixture was allowed to warm to room temperature with stirring over 16 hours. The mixture was heated to ~80 °C for 5 mins, and allowed to cool slowly to room temperature and then filtered. The solvent was removed *in vacuo* to yield a brown solid. The product was washed with hexanes (2 x 10 ml) and dried *vacuo* to yield **115** as a brown powder. Red crystals of **115** were isolated from a concentrated solution of **115** in toluene. Yield: 1.91 g, 72%. Anal. calcd for $C_{61}H_{115}KN_5O_{10}Si_3U$: C 50.88; H 8.05; N 4.86;. Found: C 50.93; H 7.85; N 4.49. ^{1}H NMR (C_6D_6, 298 K): δ 38.58 (s, 6H, CH_2), 16.98 (s, 6H, CH_2), 10.03-6.80 (br m, 20H, CH_2, OCH_2, Ar-*H*), 3.85 (s, 20H, OCH_2), −5.61 (s, 9H, CH(CH$_3$)$_2$), −6.30 ppm (s, 54H, CH(CH_3)$_2$). ^{29}Si{^{1}H} NMR (C_6D_6, 298 K): δ −16.10 ppm. FTIR ν/cm^{-1} (Nujol): 1596 (m), 1348 (w), 1333 (w), 1296 (m), 1215 (m), 1127 (s), 1081 (s), 1048 (m), 935 (m), 882 (m), 869 (m), 854 (w), 739 (s), 670 (m), 627 (m), 542 (w), 507 (w). UV-vis-NIR (toluene): λ_{max}/nm (ε/M^{-1}cm^{-1}) 1125 (27.1), 1436 (14.6), 1461 (16.7), 1656 (19.4). μ_{eff} (Evans method, C_6D_6, 298 K): 1.93 μ_B.

7.2.1.12. Preparation of [U(Tren^{TIPS})(N)][Rb(Bn-15C5)$_2$], **116**

Toluene (20 ml) was added to a cold (−78 °C) mixture of **108** (0.76 g, 0.4 mmol) and benzo-15-crown-5 (0.43 g, 1.6 mmol). The resulting mixture was allowed to warm to room temperature with stirring over 16 h. Volatiles were removed *in vacuo* to afford a brown powder. Recrystallisation of the powder from warm toluene (10 ml) afforded **116** as a brown crystalline solid on cooling to ambient temperature. Yield 0.25 g, 21% (crystalline). Anal. calcd for $C_{61}H_{115}N_5O_{10}RbSi_3U$: C, 49.29; H, 7.80; N, 4.71. Found: C, 48.03; H, 7.48; N, 4.64. ^{1}H NMR (C_6D_6, 298 K): δ 38.62 (s, 6H, CH_2), 11.00 – 5.00 (br m, 46H, CH_2, OCH_2, Ar-*H*), −5.45 (s, 9H, CH(CH$_3$)$_2$), −6.18 ppm (s, 54H, CH(CH_3)$_2$). ^{29}Si{^{1}H} NMR (C_6D_6, 298 K): δ −15.80 ppm. FTIR ν/cm^{-1} (Nujol): 1595 (m), 1296 (m), 1217 (m), 1127 (s), 1077 (s), 1042 (m), 934 (m), 882 (m), 851 (w), 739 (s), 670 (m), 627 (m), 542 (w), 507 (w). UV-vis-NIR (toluene):

λ_{max}/nm (ε/$M^{-1}cm^{-1}$) 1131 (22.8), 1437 (12.06), 1463 (14.4), 1656 (18.8). μ_{eff} (Evans method, C_6D_6, 298 K): 2.46 μ_B.

7.2.1.13. Preparation of [U(Tren^{TIPS})(N)][Cs(Bn-15C5)$_2$], **117**

Toluene (30 ml) was added to a cold (–78 °C) mixture of **109** (0.50 g, 0.25 mmol) and benzo-15-crown-5 (0.266 g, 0.99 mmol). The resulting mixture was allowed to warm to room temperature with stirring over 16 h. Volatiles were removed *in vacuo*, and the product extracted into hot hexanes (10 ml). The mixture was filtered and concentrated to ~2 ml yielding a sticky solid. The solid was isolated by filtration, suspended in pentane (5 ml) and stored at –80 °C for 16 h. The pentane was filtered away to afford **117** as a brown-black solid. A concentrated solution of **117** in hexanes afforded brown-black crystals suitable for single crystal X-ray diffraction studies over 48 h. Yield 0.197 g, 50%. Anal. Calcd for $C_{61}H_{115}CsN_5O_{10}Si_3U$: C, 47.77; H, 7.56; N, 4.57. Found: C, 47.54; H, 7.55; N, 4.56. ^{1}H NMR (C_6D_6, 298 K): δ 38.30 (s, 6H, CH_2), 8.66 (s, 6H CH_2), 7.80 (s, 4H, Ar-C*H*), 7.43 (s, 4H, Ar-C*H*), 6.50 – 5.10 (br m, 32H, OCH_2), –5.38 (s, 9H, C*H*$(CH_3)_2$, –6.25 ppm (s, 54H, CH(CH_3)$_2$). ^{29}Si{^{1}H} NMR (C_6D_6, 298 K): δ –15.48 ppm. FTIR ν/cm^{-1} (Nujol): 1504 (m), 1409 (w), 1363 (m), 1234 (m), 1221 (m), 1075 (s), 1044 (s), 934 (s), 869 (w), 850 (m), 739 (s) 670 (m), 627 (w), 563 (w), 539 (w), 508 (w). UV-vis-NIR (toluene): λ_{max}/nm (ε/$M^{-1}cm^{-1}$) 1132 (22.7), 1437 (10.8), 1460 (12.4), 1661 (16.0). μ_{eff} (Evans method, C_6D_6, 298 K): 2.09 μ_B.

7.2.1.14. Preparation of [U(Tren^{TIPS}){(μ-N)(μ-Li)(12C4)}], **118**

Toluene (20 ml) was added to a cold (−78 °C) mixture of **106** (0.87 g, 0.5 mmol) and 12-crown-4 (0.35 g, 2.00 mmol). The resulting mixture was allowed to warm to room temperature with stirring over 16 h. Volatiles were removed *in vacuo* to afford a sticky brown solid. This solid was then washed with hexanes (5 ml) and filtered to afford **118** as a brown powder. Deep red crystals were grown from a concentrated solution of **118** in toluene at room temperature. Yield 0.43 g, 41% (crystalline). Anal. calcd for $C_{41}H_{91}N_5LiO_4Si_3U$: C 47.01; H 8.76; N 6.69. Found: C 45.70; H

8.67; N 6.54. ^{1}H NMR (C_6D_6, 298 K): δ 38.61 (s, 6H, CH_2), 14.04 (s, 8H, OCH_2), 11.28 (s, 8H, OCH_2), 7.62 (s, 6H, CH_2), −5.55 (s, 9H, CH(CH_3)$_2$), −6.74 ppm (s, 54H, CH(CH_3)$_2$). ^{29}Si{^{1}H} NMR (C_6D_6, 298 K): δ −17.67 ppm. FTIR ν/cm^{-1} (Nujol): 1363 (w), 1260 (s), 1135 (s), 1076 (s), 1026 (s), 934 (m), 883 (m), 861 (w), 736 (s), 670 (w), 629 (w), 589 (w), 565 (w), 544 (w), 508 (w). UV-vis-NIR (toluene): λ_{max}/nm (ε/M^{-1}cm^{-1}) 1125 (24.3), 1460 (17.6), 1652 (22.7). μ_{eff} (Evans method, C_6D_6, 298 K): 2.04 μ_B.

7.2.1.15. Preparation of [U(Tren^{TIPS}){(μ-N)(μ-Li)(Bn-9C3)$_3$}], **119**

Toluene (20 ml) was added to a cold (–78 °C) mixture of **106** (0.44 g, 0.25 mmol) and benzo-9-crown-3 (Bn-9C3) (0.18 g, 1.0 mmol). This mixture was heated at 60 °C for 5 min, and then stirred for one hour at room temperature. The mixture was filtered and volatiles were removed *in vacuo*. The resulting solid was extracted into pentane (5 ml) and concentrated to 2 ml. Storage of this solution at –30 °C afforded red crystals of **119**. Yield: 50 mg, 18% (crystalline). Co-crystallisation of contaminants including **54** and [U(Tren^{TIPS})(O)] (**122**), which could not be separated, prevented collection of meaningful elemental analysis and Evan's method solution magnetic data for **119**. ^{1}H NMR (C_6D_6, 298 K): δ 33.59 (s, 6H, CH_2), 7.91 (br, 4H, ArH), 7.84 (br, 6H, CH_2), 3.59 (br, 8H, crown-CH_2), −4.59 (s, 9H, CH(CH_3)$_2$), −5.14 ppm (s, 54H, CH(CH_3)$_2$). ^{29}Si{^{1}H} NMR (C_6D_6, 298 K): no resonance observed. FTIR ν/cm^{-1} (Nujol): 1462 (m), 1377 (m), 1260 (w), 1075 (w), 1014 (w), 931 (w), 883 (w), 798 (w), 739 (m). UV-vis-NIR (toluene): λ_{max}/nm (ε/M^{-1}cm^{-1}) 1111 (30.5), 1440 (16.6), 1661 (20.7).

7.2.1.16. Preparation of [U(Tren^{TIPS}){(μ-N)Li(py)$_3$}], **121**

To a cold slurry (−78 °C) of **106** (0.34 g, 0.20 mmol) in toluene (10 ml) was added pyridine (44 μl, 0.60 mmol) dropwise *via* syringe. The resulting mixture was allowed to warm to room temperature with stirring over 3 hrs. Volatiles were removed *in vacuo* to afford a red powder. The product was recrystallised from hexanes (2 ml, −30 °C, 16 hrs), isolated *via* filtration and dried to afford **121** as red crystalline

blocks. Yield 0.20 g, 90% (crystalline). Anal. calcd for $C_{48}H_{90}N_8LiSi_3U$: C, 52.01 ; H, 8.18; N, 10.11. Found: C, 50.11; H, 8.21; N, 9.35. ^{1}H NMR (C_6D_6, 298 K): δ 35.53 (s, 6H, CH_2), 17.03 (s, 6H, Py-*H*), 8.93 (s, 6H, Py-*H*), 8.69 (s, 3H, Py-*H*), 7.69 (s, 6H, CH_2), −5.32 (s, 9H, CH(CH_3)$_2$), −5.72 ppm (s, 54H, CH(CH_3)$_2$). ^{29}Si{^{1}H} NMR (C_6D_6, 298 K): δ −22.68 ppm. FTIR ν/cm^{-1} (Nujol): 1578 (m), 1545 (w), 1443 (m), 1412 (w), 1218 (w), 1072 (s), 933 (m), 914 (w), 882 (m), 768 (w), 740 (s), 702 (m), 671 (m), 627 (w), 597 (w), 590 (w), 565 (w), 549 (w), 509 (w). UV-vis-NIR (toluene): λ_{max}/nm (ε/M^{-1}cm^{-1}) 1132 (30.2), 1460 (17.7), 1661 (32.1). μ_{eff} (Evans method, C_6D_6, 298 K): 2.52 μ_B.

7.2.1.17. Preparation of [U(Tren^{TIPS}){(μ-N)(μ-Li)(η^3-tetraglyme)$_3$}], **120**

To a cold slurry (0 °C) of **106** (0.87 g, 0.50 mmol) in toluene (10 ml) was added a mixture of tetraglyme [Me(OCH$_2$CH$_2$)$_4$OMe] (0.22 g, 1.0 mmol) in toluene (5 ml). The resultant mixture was stirred for three hours before being concentrated to 5 ml. The mixture was filtered and upon storage at –28 °C for 16 hours afforded red-brown crystals. Unfortunately these were unsuitable for single crystal XRD study, and once isolated the compound was oily in nature. Yield: 0.84 g, 77%. Repeated attempts to recrystallise from other solvents were unsuccessful. ^{1}H NMR (C_6D_6, 298 K): δ 38.17 (s, 6H, CH_2), 32.03 (s, 2H, OCH_2), 9.10 (s, 6H, CH_2), 7.93 (s, 2H, OCH_2), 7.53 (s, 2H, OCH_2), 0.97 (t, 2H, OCH_2), 0.86 (t, 2H, OCH_2), –5.36 (s, 3H, OCH_3), –5.88 (s, 9H, CH), –6.56 (s, 54H, CH_3), –7.46 (s, 2H, CH_2), –11.04 (s, 2H, OCH_2), –15.04 (s, 2H, CH_2), –24.20 ppm (s, 3H, OCH_3). ^{29}Si{^{1}H} NMR (C_6D_6, 298 K): –19.34 ppm. FTIR ν/cm^{-1} (Nujol): 1462 (s), 1401 (w), 1378 (m), 1259 (m), 1200 (w), 1108 (s), 1071 (s), 1013 (s), 990 (s), 932 (s), 883 (s), 794 (m), 738 (s), 671 (m), 629 (m), 564 (w), 543 (w). UV-vis-NIR (toluene): λ_{max}/nm (ε/M^{-1}cm^{-1}) 1155 (26.7), 1458 (17.8), 1655 (21.0). μ_{eff} (Evans method, C_6D_6, 298 K): 2.39 μ_B. Elemental analysis could not be successfully performed due to the oily nature of this compound once isolated.

7.2.1.18. Attempted preparations of [U(Tren^{TIPS})(N)][Li(co-ligand)$_n$]

Method A: Under an inert atmosphere inside a glove box, scintillation vials were charged with **106** (0.02 g, 0.012 mmol). To these were added various solvent and co-ligand combinations, as detailed in the table below. None of these combinations afforded isolable products.

Solvent	Co-ligand
Toluene	HMPA [OP(NMe$_2$)$_3$]
Hexanes	HMPA
Toluene	TMEDA [Me$_2$NCH$_2$CH$_2$NMe$_2$]
Hexanes	TMEDA
Toluene	PMDETA [MeN(CH$_2$CH$_2$NMe$_2$)$_2$]
Hexanes	PMDETA
Toluene	DME

Method B: To a cold (–78 °C) stirring mixture of [{U(Tren^{TIPS})(μ-N)(μ-Li)}$_2$] (0.87 g, 0.50 mmol) and 9-ane-S$_3$ (0.36 g, 2.0 mmol) was added toluene (10 ml). The mixture was warmed to room temperature with stirring over 3 days. No reaction was observed. The mixture was refluxed at 80 °C for 6 hours, which resulted in decomposition of the starting material to afford an intractable mixture of unidentified products.

7.2.1.19. Preparation of [U(Tren^{TIPS})(N)], **54**

Method A: A solution of I_2 (0.06 g, 0.24 mmol) in toluene (5 ml) was added dropwise over 1 hr to a stirring solution of **114** (0.64 g, 0.48 mmol) in toluene (10 ml) at –78 °C. The brown mixture was allowed to warm to room temperature with stirring over 16 h. The mixture was filtered, and volatiles were removed *in vacuo* and the product was washed with cold pentane at –78 °C (2 x 5 ml). The solid was dried *in vacuo* to yield **54** as a red/brown powder. Yield: 0.24 g, 59%.

Method B: A solution of I_2 (0.19 g, 0.75 mmol) in toluene (30 ml) was added dropwise over 1 hr to a stirring solution of **115** (2.16 g, 1.50 mmol) in toluene (10 ml) at –78 °C. The brown mixture was allowed to warm to room temperature with stirring over 16 h. The mixture was filtered, and volatiles were removed *in vacuo* and the product was washed with cold pentane at 0 °C (2 x 5 ml). The solid was dried *in vacuo* to yield **54** as a red/brown powder. Yield: 1.05 g, 70%.

The identity of **54** was confirmed by comparison to previously reported methods.[9]

7.2.2. Chapter 3

7.2.2.1. Preparation of [U{*C*H_2CH(Me)Si(^{i}Pr)$_2$*N*CH_2CH_2*N*(CH_2CH_2*N*Si^{i}Pr$_3$)$_2$}], **110**

Method A: Toluene (40 ml) was added to cold (–78 °C) stirring mixture of **13** (0.89 g, 1.0 mmol) and benzyl potassium (0.13 g, 1.0 mmol). The mixture was allowed to warm to room temperature with stirring over 16 h. Volatiles were removed *in vacuo*, and the product extracted into hexanes, concentrated and stored at 4 °C to yield **110** as orange crystals. Yield: 40%, 0.34 g (crystalline).

Method B: Toluene (40 ml) was added to a cold (–78 °C) stirring mixture of [U(Tren^{TIPS})(Cl)] (**7**, 1.32 g, 1.5 mmol) and benzyl potassium (0.20 g, 1.5 mmol). The mixture was allowed to warm to room temperature with stirring over 72 h. Volatiles were removed *in vacuo*, and the product extracted into hexanes, concentrated and stored at 4 °C to yield **110** as orange crystals. Yield: 60%, 0.76 g (crystalline).

Method C: Toluene (30 ml) was added to a cold (–78 °C) stirring mixture of [U(Tren^{TIPS})(I)] (**10**, 0.98 g, 1.0 mmol) and benzyl potassium (0.13 g, 1.0 mmol). The mixture was allowed to warm to room temperature with stirring over 16 h. Volatiles were removed *in vacuo* and the product extracted into hexanes, concentrated to 2 ml and stored at 4 °C for 72 hours to yield **110** as orange crystals. Yield: 0.55 g, 65%.

Anal. calcd for $C_{33}H_{74}N_4Si_3U$: C, 46.67; H, 8.78; N, 6.60%. Found: C, 46.67; H, 8.81; N, 6.37%. ^{1}H NMR (C_6D_6, 298 K): δ 46.70 (1H, s, UCH_2), 32.63 (1H, s, CH_2),

28.87 (1H, s, CH_2), 23.19 (1H, s, CH_2), 15.94 (1H, s, UCH$_2$CH), 15.74 (3H, s, UCH$_2$CHCH_3), 11.35 (1H, s, CH_2), 11.25 (1H, m, CH), 9.53 (1H, m, CH), 8.39 (3H, d, $^3J_{HH}$ = 7.3 Hz, CH_3), 6.83 (1H, s, CH_2), 6.00 (3H, d, $^3J_{HH}$ = 7.3 Hz, CH_3), 5.66 (3H, d, $^3J_{HH}$ = 6.4 Hz, CH_3), 4.00 (9H, s, 3×CH_3), 3.70 (3H, d, $^3J_{HH}$ = 6.4 Hz, CH_3), 2.79 (1H, s, CH_2), 2.09 (1H, s, CH$_2$), 1.52 (3H, s, 3×CH), –0.52 (1H, s, CH_2), –1.27 (1H, s, CH_2), –2.61 (9H, s, 3×CH_3), –2.89 (9H, s, 3×CH_3), –4.70 (9H, s, 3×CH_3), –20.81 (3H, s, 3×CH), –23.06 (1H, s, CH_2), –24.11 (1H, s, CH_2), –31.59 (1H, s, CH_2), –35.16 ppm (1H, s, br, UCH_2). ^{29}Si{^{1}H} NMR (C$_6$D$_6$, 298 K): δ −112.25 (s, *Si*^{i}Pr$_3$), −118.04 (s, *Si*^{i}Pr$_3$), −125.66 ppm (s, *Si*^{i}Pr$_2$C[H]MeCH$_2$U). FTIR ν/cm^{-1} (Nujol): 1281 (w), 1135 (w), 1103 (s), 1064 (m), 1040 (m), 1011 (m), 990 (m), 922 (s), 904 (m), 881 (s) cm^{-1}. UV-vis-NIR (toluene): λ_{max}/nm (ε/M^{-1}cm^{-1}) 690 (19.9), 707 (17.8), 813 (7.1), 943 (7.4), 1048 (8.3), 1139 (13.2). μ_{eff} (Evans method, C$_6$D$_6$, 298 K): 2.90 μ_B.

7.2.2.2. Preparation of [Th(Tren^{TIPS})(CH$_2$Ph)], **124**

Toluene (15 ml) was added to a cold (−78 °C) mixture of [Th(Tren^{TIPS})(I)] (**123**, 2.00 g, 2.1 mmol) and benzyl potassium (0.27 g, 2.1 mmol). The resulting mixture was allowed to warm to ambient temperature with stirring for 16 hours to afford a yellow suspension, which was filtered. Volatiles were removed *in vacuo* to afford **124** as a yellow solid. Yield: 1.48 g, 77%. Crystalline material was obtained *via* extraction into warm (50 °C) methylcyclohexane (5 ml), filtration and reduction in volume to 2 ml. Storage at −30 °C for 18 hours afforded colourless crystals of **124** that were isolated by filtration at −10 °C, washed with pentane (2 × 2 ml) and dried *in vacuo* for 30 minutes. Yield: 0.58 g, 30% (crystalline).

Anal. calcd for C$_{40}$H$_{80}$N$_4$Si$_3$Th: C 51.36%; H 8.84%; N 5.99%. Found: C 50.18%; H 8.96%; N 5.94%. ^{1}H NMR (C$_6$D$_6$, 298 K): δ 1.23 (d, $^3J_{HH}$ = 5.3 Hz, 54H, 3×Si^i*Pr$_3$*), 1.26 (sept, $^3J_{HH}$ = 4.7 Hz, 9H, CH), 1.62 (s, 2H, CH_2Ph), 2.51 (t, $^2J_{HH}$ = 4.6 Hz, 6H, CH_2), 3.55 (t, $^2J_{HH}$ = 4.5 Hz, 6H, CH_2), 6.83 (t, $^2J_{HH}$ = 7.3 Hz, 1H, *p*-ArH), 7.06 (d, $^2J_{HH}$ = 7.2 Hz, 2H, *m*-ArH), 7.39 ppm (t, $^2J_{HH}$ = 7.9 Hz, 2H, *o*-ArH). ^{13}C{^{1}H} NMR (C$_6$D$_6$, 298 K): δ 14.13 (s, *C*H), 20.63 (s, *C*H$_3$), 46.69 (s, *C*H$_2$), 65.22 (s, *C*H$_2$), 114.46 (s, *C*H$_2$Ph), 120.01 (s, *p*-Ar*C*), 125.24 (s, *m*-Ar*C*), 128.51 (s, *o*-Ar*C*), 154.93

ppm (s, *i*-Ar*C*). ^{29}Si{^{1}H} NMR (C_6D_6, 298 K): δ 4.36 ppm. FTIR *v*/cm^{-1} (Nujol): 1303 (w), 1261 (s), 1202 (w), 1096 (s), 1047 (s), 1020 (s), 9256 (w), 882 (m), 800 (s), 723 (m), 678 (w), 653 (w), 634 (w), 609 (w) cm^{-1}.

7.2.2.3. Preparation of [Th{*C*H$_2$CH(Me)Si(^{i}Pr)$_2$*N*CH$_2$CH$_2$*N*(CH$_2$CH$_2$*N*Si^{i}Pr$_3$)$_2$}], **125**

A solution of **124** (1.48 g, 1.6 mmol) in toluene (15 ml) was heated at 80 °C for 2 hours. Volatiles were removed *in vacuo* to afford an off-white solid that was dissolved in warm (50 °C) hexane (10 ml), filtered and the volume of the solution reduced to 1.5 ml to afford **125** as a white solid. Yield: 1.31g, 90%. Crystalline material could be obtained by dissolution of **125** in hexanes (1.5 ml) and storage at 5 °C for 24 hours to afford colourless crystals of **125** that were isolated by filtration at 0 °C, washed with cold hexane (3 × 2 ml) and dried *in vacuo* for 30 minutes. A second crop of crystals was obtained by the reduction of the supernatant solution to 0.5 ml and storage at −30 °C for 24 hours. Yield: 0.65 g, 45% (crystalline).

Anal. calcd for $C_{33}H_{74}N_4Si_3Th$: C 47.00%; H 8.85%; N 6.65%. Found: C 46.36%; H 8.86%; N 6.41%. ^{1}H NMR (C_6D_6, 298 K): δ 0.68 (s, 1H, ThC*H*$_2$), 0.70 (d, $^{3}J_{HH}$ = 3.2 Hz, 1H, ThC*H*$_2$), 1.30 (s, 1H, C*H*), 1.31 (d, $^{3}J_{HH}$ = 6.0 Hz, 1H, C*H*), 1.32 (d, $^{3}J_{HH}$ = 4.0 Hz, 18H, 6×C*H*$_3$), 1.33 (d, $^{3}J_{HH}$ = 4.2 Hz, 18H, 6× C*H*$_3$), 1.35 (d, $^{3}J_{HH}$ = 7.5 Hz, 3H, 3×C*H*), 1.39 (m, 12H, 4× C*H*$_3$), 1.53 (d, $^{3}J_{HH}$ = 7.5 Hz, 3H, 3×C*H*), 1.69 (d, $^{3}J_{HH}$ = 7.0 Hz, 3H, ThCH$_2$CHC*H*$_3$), 1.89 (m, 1H, ThCH$_2$C*H* C*H*$_3$), 2.54 (m, 3H, C*H*$_2$), 2.71 (m, 3H, C*H*$_2$), 3.52 (m, 2H, C*H*$_2$), 3.67 (m, 3H, C*H*$_2$), 3.92 ppm (m, 1H, C*H*$_2$). ^{13}C{^{1}H} NMR (C_6D_6, 298 K): δ 11.73 (s, *C*H), 11.92 (s, *C*H), 12.30 (s, *C*H), 18.64 (s, *C*H$_3$), 18.82 (s, ThCH$_2$*C*HCH$_3$), 18.91 (s, *C*H$_3$), 19.06 (s, *C*H$_3$), 19.20 (s, *C*H$_3$), 19.48 (s, *C*H$_3$), 19.55 (s, *C*H$_3$), 19.72 (s, *C*H$_3$), 19.80 (s, *C*H$_3$), 26.69 (s, ThCH$_2$CH*C*H$_3$), 46.56 (s, *C*H$_2$), 46.92 (s, *C*H$_2$), 49.03 (s, *C*H$_2$), 58.69 (s, *C*H$_2$), 58.98 (s, *C*H$_2$), 59.24 (s, *C*H$_2$), 105.65 ppm (s, Th*C*H$_2$). Assignment of the ^{1}H and ^{13}C resonances for the ThCH$_2$CHCH$_3$ group observed in the ^{1}H and ^{13}C{^{1}H} NMR spectra were confirmed using additional DEPT45, DEPT90, DEPT135 and ^{1}H,^{13}C-HMBC NMR spectra. ^{29}Si{^{1}H} NMR (C_6D_6, 298 K): δ 1.84 (s, *Si*^{i}Pr$_3$), 2.33 (s, *Si*^{i}Pr$_3$), 4.31 ppm (s, *Si*^{i}Pr$_2$C[H]MeCH$_2$Th). FTIR *v*/cm^{-1} (Nujol): 1262 (s), 1179

(w), 1092 (s), 1075 (s), 1023 (s), 920 (m), 882 (m), 847 (w), 800 (m), 770 (s), 748 (m), 724 (m), 672 (m), 633 (w), 589 (w), 571 (w), 551 (w), 514 (w) cm^{-1}.

7.2.3. Chapter 5

7.2.3.1. Preparation of [U($Tren^{TIPS}$)(NCO)], **135**

Method A: A solution of **54** (0.50 g, 0.56 mmol) in toluene (10 ml) was degassed, cooled to –78 °C and exposed to an atmosphere of CO. The solution was allowed to warm to room temperature with stirring over 16 hours and slowly turned from red to light brown. Volatiles were removed *in vacuo* to yield **135** as an oily brown solid. Yield: 0.38 g, 76%.

Method B: THF (30 ml) was added dropwise to a cold (–78 °C) stirring mixture of [U($Tren^{TIPS}$)(Cl)] (**7**, 1.55 g, 1.75 mmol) and NaOCN (0.14 g, 2.15 mmol). The mixture was allowed to warm to room temperature with stirring over 16 hours. The mixture was heated to ~60 °C for 5 mins, and allowed to cool slowly to room temperature. Volatiles were removed *in vacuo*, and the product extracted into hot hexanes (20 ml) to remove the NaCl precipitate. Volatiles were removed *in vacuo* to afford **135** as a brown solid. The product was recrystallized from hot hexanes (5 ml, 60 °C) and stood at room temperature for 24 hours to afford **135** as green crystals. Yield: 1.16 g, 74%.

Method C: A solution of iodine (0.05 g, 0.20 mmol) in toluene (10 ml) was added dropwise to a cold (–78 °C) stirring solution of [U($Tren^{TIPS}$)(NCO)][K(Bn-15C5)$_2$] (**136**, 0.561 g, 0.38 mmol) in toluene (10 ml). The mixture was allowed to warm to room temperature with stirring over 5 hours. The mixture was and volatiles were removed *in vacuo* to yield **135** as an oily brown solid. Yield 0.25 g, 73%.

Anal. Calcd for $C_{34}H_{75}N_5OSi_3U$: C 45.77; H 8.47; N 7.85%. Found: C 45.48; H 8.53; N 7.46%. ^{1}H NMR (C_6D_6, 298 K): δ 7.35 (60H, br, CH_2 + CH(CH_3)$_2$), 6.51 (s, 9H, CH(CH_3)$_2$), –30.13 ppm (s, 6H, CH_2). ^{29}Si{^{1}H} NMR (C_6D_6, 298 K): δ −4.65 ppm. FTIR ν/cm^{-1} (Nujol): 2361 (w), 2187 (s), 2125 (m), 1343 (m), 1134 (m), 1060 (m), 1052 (m), 990 (m), 736 (s), 675 (m), 633 (m), 552 (m), 517 (m). UV-vis-NIR (toluene): λ_{max}/nm (ε/$M^{-1}cm^{-1}$): 448 (36.5), 462 (31.9), 486 (32.0), 524 (28.4), 582

(16.9), 608 (13.1), 625 (15.0), 674 (42.9), 687 (40.9), 802 (7.2), 884 (7.9), 1100 (20.9), 1131 (23.3), 1177 (28.9), 1211 (8.9). μ_{eff} (Evans method, C_6D_6, 298 K): 2.50 μ_B.

7.2.3.2. Preparation of [U(Tren^{TIPS})(NCO)][K(Bn-15C5)$_2$], **136**

Method A: Toluene (30 ml) was added dropwise to a cold (–78 °C) stirring mixture of **135** (1.03 g, 1.15 mmol) and KC_8 (0.16 g, 1.15 mmol). The mixture was allowed to warm to room temperature with stirring over 72 hours. Benzo-15-crown-5 (0.62 g, 2.30 mmol) was added and an immediate colour change to dark green was observed. The mixture was filtered and volatiles removed *in vacuo* to afford **136** as a dark green oily solid. Yield: 1.58 g, 93%.

Method B: Toluene (20 ml) was added to a stirring mixture of benzo-15-crown-5 (1.60 g, 5.95 mmol) and KNCO (0.241 g, 2.97 mmol). The mixture was added dropwise to a cold (–78 °C) stirring solution of [U(Tren^{TIPS})] (**15**, 2.53 g, 2.97 mmol) in toluene (20 ml). The mixture was allowed to warm to room temperature with stirring over 16 hours. The solution was filtered and volatiles were removed *in vacuo* to afford **136** as a dark green oil. Storage of this oil at room temperature for 72 hours yielded a small crop of dark green crystals of **136.** Alternatively, suspension of the oil in hexanes (10 ml), followed by storage at –80 °C for 3 hours yielded **136** as a dark green solid. Yield 1.95 g, 45%.

Method C: A solution of **115** (0.79 g, 0.55 mmol) in toluene (10 ml) was degassed, cooled to –78 °C and exposed to an atmosphere of CO. The solution immediately turned dark green and was allowed to warm slowly to room temperature with stirring over 16 hours. Volatiles were removed *in vacuo* to yield a dark green oil. Hexanes (10 ml) were added and the suspension stored at –80 °C for 3 hours to yield **136** as a dark green solid. Yield: 0.76 g, 94%.

Anal. Calcd for $C_{62}H_{115}KN_5O_{11}Si_3U$: C 50.73; H 7.90; N 4.77%. Found: C 50.62; H 7.96; N 4.20%. ^{1}H NMR (C_6D_6, 298 K): δ 8.85 (4H, s, CH_2), 6.95 (4H, s, crown-C*H*), 6.70 (4H, s, crown-C*H*), 3.45-4.05 (36H, m, crown-CH_2 + CH_2), 3.07 (3H, br, C*H*(CH$_3$)$_2$), 2.99 (18H, s, CH(CH_3)$_2$), 2.32 (6H, s, C*H*(CH$_3$)$_2$), 2.11 (4H, s, CH_2),

0.73 ppm (36H, s, CH(CH_3)$_2$). ^{29}Si{^{1}H} NMR (C_6D_6, 298 K): δ –16.45 ppm. FTIR ν/cm^{-1} (Nujol): 2195 (s), 2172 (s), 1639 (m), 1504 (s) 1220 (s), 1124 (s), 936 (m), 881 (m), 853 (m), 740 (s). UV-vis-NIR (toluene): λ_{max}/nm (ε/M^{-1}cm^{-1}) 573 (361.2), 679 (347.9), 902 (40.9), 927 (48.6), 943 (49.8), 979 (39.6), 1005 (44.0), 1038 (55.0), 1051 (57.0), 1087 (36.2), 1123 (40.9), 1206 (26.9), 1264 (25.7). μ_{eff} (Evans method, C_6D_6, 298 K): 2.76 μ_B.

7.2.3.3. Preparation of [U(Tren^{TIPS}){(μ-NCO)(μ-K)(18C6)}], **137**

Method A: Toluene (20 ml) was added to a cold (–78 °C) stirring mixture of [U(Tren^{TIPS})(μ-N)(μ-K)}$_2$] (0.46 g, 0.26 mmol) and 18-crown-6 (0.14 g, 0.54 mmol). The mixture was allowed to warm to room temperature with stirring over two hours. The resultant solution was degassed, cooled to –78 °C and exposed to an atmosphere of CO. The solution immediately turned dark green and was allowed to warm to room temperature over 30 mins. Volatiles were removed *in vacuo* to afford a dark green oil. Recrystallisation from a mixture of toluene (2 ml) and pentane (3ml) at room temperature afforded [U(Tren^{TIPS}){(μ-NCO)(μ-K)(18C6)}] as dark green crystals. Crystalline Yield: 96 mg, 16%.

Method B: Toluene (30 ml) was added to a cold (–78 °C) stirring mixture of [U(Tren^{TIPS})] (0.85 g, 1 mmol), 18-crown-6 (0.26 g, 1 mmol) and KOCN (0.081g, 1 mmol). The mixture was allowed to warm to room temperature with stirring over 16 hours. Volatiles were removed in vacuo to afford [U(Tren^{TIPS}){(μ-NCO)(μ-K)(18C6)}] as a dark green solid. Yield: 0.813 g, 68 %.

Elemental analysis could not be collected for **137** due to its oily nature. ^{1}H NMR (C_6D_6, 298 K): δ 8.33 (6H, s, CH_2), 3.18 (24H, s, crown-CH_2), 2.85 (9H, s, CH(CH$_3$)$_2$), 1.34 (54H, s, CH(CH_3)$_2$), –1.04 ppm (6H, s, CH_2). ^{29}Si{^{1}H} NMR (C_6D_6, 298 K): δ –12.69 ppm. FTIR ν/cm^{-1} (Nujol): 2361 (w), 2180 (s), 2150 (s), 1959 (w), 1540 (w), 1400 (m), 1352 (m), 1203 (w), 991 (m), 963 (m), 994 (m), 926 (m), 838 (m), 756 (m), 677 (m), 630 (m). UV-vis-NIR (toluene): λ_{max}/nm (ε/M^{-1}cm^{-1}) 593 (624.6), 604 (620.4), 681 (651.1), 690 (644.2), 860 (93.4), 927 (89.0), 941

(88.6), 959 (69.6), 1005 (72.5), 1039 (82.7), 1053 (87.3), 1088 (45.0), 1123 (57.9), 1205 (41.4), 1269 (44.6). μ_{eff} (Evans method, C_6D_6, 298 K): 2.85 μ_B.

7.2.3.4. Preparation of [U(Tren^{TIPS})], **15**

Method A: Toluene (30 ml) was added dropwise to a cold (–78 °C) stirring mixture of **135** (1.11 g, 1.24 mmol) and KC_8 (0.17 g, 1.25 mmol). The mixture was allowed to warm to room temperature with stirring over 72 hours. The suspension was allowed to settle for 1 hour, and filtered to afford a deep purple filtrate. The filtrand was washed thoroughly with toluene (3 x 5 ml) until the washings obtained were colourless. Volatiles were removed from the combined toluene extracts *in vacuo* to afford **15** as a dark blue-purple solid. Yield: 0.98 g, 93%. The filtrand was extracted into water (3 x 20 ml) and filtered under gravity to afford a pale yellow solution. Volatiles were removed *in vacuo* to afford KOCN as an off-white powder. Yield: 0.100 g, 100%.

Method B: C_6D_6 (0.5 ml) was added to a Young's Tap NMR tube charged with [{U(Tren^{TIPS})(μ-N)(μ-K)}$_2$] (15.3 mg, 8.5 μmol). The solution was freeze-thaw degassed, then exposed to an atmosphere of CO at –78 °C. As the suspension thawed, a dark blue-purple solution formed. ^{1}H NMR spectroscopic studies indicated 87% conversion to **15**.

Control experiment: C_6D_6 (0.5 ml) was added to a Young's Tap NMR Tube charged with [U(Tren^{TIPS})] (21.0 mg, 24.7 μmol) and KNCO (3.0 mg, 37.0 μmol). The sample was heated at 60 °C for 16 hours. ^{1}H NMR spectroscopic studies and no observable colour change indicated that no reaction had taken place.

The identity of **15** was confirmed by comparison to previously reported data.[8]

7.2.3.5. Attempted synthetic cycle towards the conversion of NaN_3 to NaOCN

Pyridine (10 ml) was added to a cold (–40 °C) stirring mixture of **15** (0.51 g, 0.60 mmol) and NaN_3 (0.39 g, 6.00 mmol). The suspension was freeze-thaw degassed and

returned to –40 °C and exposed to an atmosphere of CO. The solution was warmed slowly to room temperature with stirring for 16 hours, to yield a red solution. Volatiles were removed *in vacuo*. The ^{1}H NMR spectrum of the resultant mixture revealed resonances assigned to [U(Tren^{TIPS})(N$_3$)] (**13**) and [U(Tren^{TIPS})(NCO)] (**135**), with the absence of **15**. The FTIR spectrum (Nujol) exhibited absorbances assigned to NaOCN (2224 cm^{-1}), **135** (2187 cm^{-1}), NaN$_3$ (2121 cm^{-1}) and **13** (2087 cm^{-1}).

7.2.3.6. Attempted Reactivity Studies of [U(Tren^{TIPS})(N)] (**54**) with phosphines

To a solution of **54** (0.020 g, 0.02 μmol) in C_6D_6 (1 ml) was added P^{n}Bu$_3$ (4 mg, 0.02 μmol). The mixture was heated a 50 °C for 16 h, and no change was observed by ^{1}H or ^{31}P{^{1}H} NMR spectroscopic analysis.

To a solution of **54** (0.020 g, 0.02 μmol) in C_7D_8 (1 ml) was added PMe$_3$ (11% in toluene, 13 mg, 0.02 μmol). The mixture was heated a 50 °C for 16 h, and no change was observed by ^{1}H or ^{31}P{^{1}H} NMR spectroscopic analysis.

7.2.3.7. Attempted Reactivity Studies of [U(Tren^{TIPS})(N)][K(Bn-15C5)$_2$] (**115**) with phosphines

To a solution of **115** (0.020 g, 0.02 μmol) in C_6D_6 (1 ml) was added P^{n}Bu$_3$ (4 mg, 0.02 μmol). The mixture was heated a 50 °C for 16 h, and no change was observed by ^{1}H or ^{31}P{^{1}H} NMR spectroscopic analysis.

To a solution of **115** (0.020 g, 0.02 μmol) in C_7D_8 (1 ml) was added PMe$_3$ (11% in toluene, 13 mg, 0.02 μmol). The mixture was heated a 50 °C for 16 h, and no change was observed by ^{1}H or ^{31}P{^{1}H} NMR spectroscopic analysis.

7.2.4. Chapter 6

7.2.4.1. Preparation of [U(Tren^{TIPS})(O)(NCO)][K(Bn-15C5)$_2$], **138**

A solution of **115** (0.91 g, 0.63 mmol) in toluene (20 ml) was degassed, cooled to –78 °C and exposed to an atmosphere of CO_2. The solution was stirred for three minutes, after which a colour change from yellow-brown to red-brown was observed. Volatiles were removed *in vacuo* to yield a red-brown solid. The resulting solid was washed with hexanes (10 ml) and recrystallised from benzene (5 ml) to afford **138** as orange crystals on storage at 6 °C for 24 hrs. Yield: 0.36 g, 36%. Anal. calcd for $C_{62}H_{115}KN_5O_{12}Si_3U.C_6H_6$: C 50.78; H 8.06; N 4.63%;. Found: C 51.02; H 7.64; N 4.50%. ^{1}H NMR (C_6D_6, 298 K): δ 15.63 (br, 6H, CH_2), 12.96 (br, 6H, CH_2), 7.06 – 6.90 (m, 8H, Ar-*H*), 3.98 – 3.76 (m, 32H, crown-CH_2), 1.95 (br, 18H, CH(CH_3)$_3$), 1.43 (br, 3H, C*H*(CH$_3$)$_3$), –1.36 (br, 36H, CH(CH_3)$_3$) –2.19 ppm (br, 6H, C*H*(CH$_3$)$_3$). ^{29}Si{^{1}H} NMR (C_6D_6, 298 K): δ –27.11 (SiCH(CH$_3$)$_3$), –27.77 ppm (SiCH(CH$_3$)$_3$). FTIR ν/cm^{-1} (Nujol): 2194 (s), 1597 (w), 1506 (m), 1347 (m), 1293 (m), 1223 (w), 1126 (m), 1079 (m), 1064 (m), 1046 (m), 937 (m), 882 (m), 855 (w), 800 (s), 769 (m), 742 (m), 722 (s). UV-vis-NIR (toluene): λ_{max}/nm (ε/M^{-1}cm^{-1}): 962 (43), 1153 (7), 1374 (13), 1494 (43), 1637 (9), 1648 (13), 1683 (21), 1697 (23), 1716 (54), 1777 (9). μ_{eff} (Evans method, C_6D_6, 298 K): 1.69 μ_B.

7.2.4.2. Reactivity study of [U(Tren^{TIPS}){μ-N)(μ-K)(Bn$_2$-18C6)}] (**111**) with CO_2

A solution of **111** (0.81 g, 0.64 mmol) in toluene (20 ml) was degassed, cooled to –78 °C and exposed to an atmosphere of CO_2. The solution was stirred for three minutes, after which a colour change from yellow-brown to red-brown was observed. Volatiles were removed *in vacuo* to yield a red-brown solid. FTIR ν/cm^{-1} (Nujol): 2181 (m), 1596 (m), 1509 (s), 1454 (s), 1291 (w), 1255 (s), 1230(s), 1128 (s).

7.2.4.3. Reactivity study of [{U(Tren^{TIPS})(μ-N)(μ-K)}$_2$] (**107**) with CO_2

A suspension of **107** (0.90 g, 0.50 mmol) in toluene (20 ml) was degassed, cooled to –78 °C and exposed to an atmosphere of CO_2. The suspension was stirred for three minutes, after which a colour change from yellow-brown to red-brown was observed. Volatiles were removed *in vacuo* to yield a red-brown solid. ^{1}H NMR spectroscopic analysis revealed resonances attributable to **54**, [U(Tren^{TIPS})(O)] (**122**) and [U(Tren^{TIPS})(NCO)] (**135**). A hexanes extraction of the resultant solid afforded crystals of **122**. Yield 0.75 g, 87%. A small crop of crystals grown from a benzene extraction were revealed to be **54**.

7.2.4.4. Attempted Preparations of [U(Tren^{TIPS})(O)(NCO)], **139** and decomposition to [U(Tren^{TIPS})(O)], **122**

Method A: A solution of **54** (1.00 g, 1.16 mmol) in toluene (20 ml) was degassed, cooled to –78 °C and exposed to an atmosphere of CO_2. The solution was stirred for three minutes, raised to room temperature and stirred for a further 20 mins, upon which a colour change from brown to wine red was observed. Volatiles were removed *in vacuo* to yield **139** as a red solid. Samples of **139** decomposed in benzene or toluene or stored as solids decompose in 30 mins which precluded full analysis. ^{1}H NMR (C_6D_6, 298 K): δ 9.30 (br, 6H, CH_2), 3.98 (br, 6H, CH_2), 1.92 (sep, $^3J_{HH}$ = 7.13 Hz, 9H, CH(CH_3)$_2$), 1.38 ppm (d, $^3J_{HH}$ = 9.72 Hz, 54H, CH(CH_3)$_2$). ^{29}Si{^{1}H} NMR (C_6D_6, 298 K): no resonances could be observed before decomposition occurred. FTIR ν/cm^{-1} (ATR): 2940 (m), 2862 (m), 2176 (s), 1460 (m), 910 (m), 880 (s), 827 (m), 784 (w), 713 (s), 686 (s). UV-vis-NIR (toluene): λ_{max}/nm (ε/M^{-1}cm^{-1}): 765 (215).

Method B: To a cold (–78 °C) solution of **138** (0.34 g, 0.22 mmol) in toluene (20 ml) was added I_2 (0.03 g, 0.11 mmol) directly. The mixture was allowed to warm to room temperature with stirring over 16 hours. The resultant mixture was filtered and volatiles were removed *in vacuo* to afford a brown oil. No resonances observed in the ^{1}H NMR spectrum of the oil or absorptions in its FTIR spectrum correspond **139**.

Method C: C_6D_6 (1 ml) was added to a mixture of [U(Tren^{TIPS})(NCO)] (**135**, 0.03 g, 0.03 mmol) and trimethylamine N-oxide (0.003 g, 0.03 mmol). The solution turned a dark red colour immediately. Analysis of the ^{1}H NMR spectrum of this sample revealed absorptions attributable to **139**, **135** and **122** in a 6:1:1 ratio.

Method D: C_6D_6 (1 ml) was added to a mixture of **135** (0.02 g, 0.02 mmol) and 4-methylmorpholine N-oxide (0.002 g, 0.02 mmol). The solution turned a wine red colour immediately. Analysis of the ^{1}H NMR spectrum of this sample revealed absorptions attributable to **139**, **135** and **122** in a 3:2:2 ratio.

Method E: C_6D_6 (1 ml) was added to a mixture of **135** (0.02 g, 0.02 mmol) and pyridine N-oxide (0.002 g, 0.02 mmol). The solution turned a wine red colour immediately. Resonances observed in the ^{1}H NMR spectrum of this sample spanned +37 to –69 ppm, and the major uranium containing compound identifiable was **135**.

Method F: C_6D_6 (1 ml) was added to a mixture of **135** (0.03 g, 0.03 mmol) and TEMPO (0.003 g, 0.03 mmol). No immediate colour change was observed, and analysis of the ^{1}H NMR spectrum of this sample after 60 minutes revealed absorptions attributable to **135** only. The mixture was heated at 60 °C for 16 h, and no change was observed in the ^{1}H NMR spectrum after this time.

7.2.4.5. Preparation of [U(Tren^{TIPS})(κ^2-CS_3)][K(Bn-15C5)$_2$], **140**

A solution of CS_2 in toluene (0.5 M, 2.0 ml, 1.00 mmol) was added dropwise to a cold (–78 °C) stirring solution of **115** (1.41 g, 1.00 mmol) in toluene (20 ml). The mixture was allowed to warm to room temperature with stirring over 16 hours. Volatiles were removed *in vacuo* from the resulting brown mixture to afford an oily brown solid. The solid was washed with hexanes (10 ml), and dried *in vacuo* to afford a pale brown powder. The hexanes extract and pale brown powder were worked up independently. ^{1}H NMR spectroscopic analysis of the hexanes extract identified **54** as a by-product. Yield 0.12 g, 14%. The pale brown powder was worked up by two methods.

Method A: The resultant solid was extracted with toluene (10 ml) and these washings stored at –28 °C for 3 days to afford **140** as orange crystals. Yield: 20 mg, 1%. *Method B*: The resultant solid was extracted into hot benzene (2 x 10 ml). Upon cooling to room temperature, this solution afforded **140** as orange crystals. Yield: 62 mg, 4%.

All materials persistently insoluble in toluene or benzene were dried *in vacuo* to afford a pale brown solid. The FTIR spectrum (Nujol) of this solid exhibited an absorbance consistent with $[K(Bn\text{-}15C5)_2][SCN]$ (2052 cm^{-1}). Yield: 0.41g, 65%.

Anal. calcd for $C_{62}H_{115}KN_4O_{10}S_3Si_3U.0.5C_6H_6$: C 49.62; H 7.56; N 3.56%. Found: C 49.31; H 7.78; N 3.70%. ^{1}H NMR (C_6D_6, 298 K): δ 9.00 (s, 6H, CH_2), 7.99 (s, 9H, CH(CH_3)$_2$), 6.70 (s, 4H, Ar-*H*), 6.16 (s, 4H, Ar-*H*), 4.94 (s, 54H, CH(CH_3)$_2$), 2.88 (br, 8H, crown-CH_2), 2.48 – 2.36 (m, 24H, crown-CH_2), –25.53 ppm (s, 6H, CH_2); ^{29}Si{^{1}H} NMR: No resonances observed. FTIR ν/cm^{-1} (ATR): 2939 (m), 2861 (m), 2049 (w), 1595 (w), 1503 (m), 1453 (m), 1403 (w), 1381 (w), 1361 (w), 1336 (w), 1293 (w), 1256 (s), 1219 (m), 1121 (s), 1093 (s), 1076 (s), 1042 (s), 1012 (s), 959 (m), 934 (s), 881 (m), 853 (m), 798 (s), 729 (s). The low solubility of **140**, once crystallised, precluded the acquisition of meaningful solution magnetic data. UV-vis-NIR data was collected for a weak sample (THF, 10 mM), and is best interpreted in a qualitative manner: λ_{max}/nm (ε/$M^{-1}cm^{-1}$): 469 (243), 1081 (41).

7.2.4.6. Preparation of $[K(Bn\text{-}15C5)_2][SCN]$

THF (10 ml) was added to a mixture of KSCN (0.05 g, 0.50 mmol) and benzo-15-crown-5 (0.27 g, 1.00 mmol). The resulting suspension was heated at reflux for one hour. Volatiles were removed *in vacuo* to afford a colourless solid. FTIR ν/cm^{-1} (Nujol): 2052 (s).

7.2.4.7. Synthesis of [{U(Tren^{TIPS})(μ-κ^2-CS_3)[K(Bn_2-18C6)]}$_2$(μ-C_6H_6)]•4(C_6H_6), **141**

A solution of CS_2 in toluene (0.5 M, 0.9 ml, 0.45 mmol) was added dropwise to a cold (–78 °C) stirring solution of [U(Tren^{TIPS}){(μ-N)(μ-K)(Bn_2-18C6)}] (0.57 g, 0.45 mmol) in toluene (10 ml). The mixture was allowed to warm to room temperature with stirring over one hour. Volatiles were removed *in vacuo* to afford a red solid. The solid was washed with hexanes (5 ml). Storage of these washings at –28 °C for 42 days afforded orange crystals identified as [U(Tren^{TIPS})(N)]. Yield 50 mg, 13%. The hexane insoluble solid was dried *in vacuo*, then washed with benzene (5 ml). Storage of these washings at 6 °C for 5 days afforded orange crystals of **141**. Yield: 16 mg, 1%. The benzene insoluble solid was dried *in vacuo* to afford a brown solid. The FTIR spectrum of this solid (Nujol) exhibited absorbances consistent with [K(Bn_2-18C6)][SCN] (2064, 2056 cm^{-1}). Yield: 0.14 g, 86%. Elemental analysis could not be successfully collected for **141** due to salt contaminant. ^{1}H NMR (C_6D_6, 298 K): δ 8.87 (br, 9H, C*H*(CH_3)$_2$), 8.01 (br, 10H, Ar*H*), 6.50 (br, 6H, CH_2), 5.12 (br, 54H + 16H, CH(CH_3)$_2$ + crown-CH_2), –26.85 ppm (s, 6H, CH_2). FTIR ν/cm^{-1} (Nujol): 2064 (m), 2056 (m), 1596 (w), 1507 (m), 1457 (s), 1377 (m), 1258 (s), 1214 (m), 1126 (s), 1094 (m), 1067 (m), 1021 (m), 957 (w), 942 (w), 800 (s).

7.2.4.8. Preparation of [K(Bn_2-18C6)][SCN]

THF (10 ml) was added to a mixture of KSCN (0.10 g, 1.00 mmol) and dibenzo-18-crown-6 (0.36 g, 1.00 mmol). The resulting suspension was heated at reflux for one hour. Volatiles were removed *in vacuo* to afford a colourless solid. FTIR ν/cm^{-1} (Nujol): 2064 (s), 2056 (s).

7.2.4.9. Reactivity study of [{U(Tren^{TIPS})(μ-N)(μ-K)}$_2$] (**111**) with CS_2

A solution of CS_2 in toluene (0.5 M, 1.0 ml, 0.5 mmol) was added dropwise to a cold (–78 °C) stirring suspension of [{U(Tren^{TIPS})(μ-N)(μ-K)}$_2$] (0.46 g, 0.25 mmol) in toluene (20 ml). The solution was allowed to warm to room temperature with stirring

over 16 hours. Volatiles were removed *in vacuo* to afford a brown solid. ^{1}H NMR spectroscopic analysis of the resultant solid revealed resonances attributable to [U(Tren^{TIPS})(N)] and [U(Tren^{TIPS})(NCS)]. FTIR ν/cm^{-1} (Nujol): 2170 (w), 2013 (w), 1994 (w), 1959 (w), 1631 (w), 1462 (s), 1377 (s), 1261 (s), 1092 (s), 1019 (s), 915 (m), 883 (m), 800 (s), 768 (m), 733 (m). A small crop of crystals isolated from a hexanes extraction of the resultant solid were revealed to be [U(Tren^{TIPS})(N)].

7.2.4.10. Preparation of [U(Tren^{TIPS})(NCS)], **142**

Method A: A solution of CS_2 in toluene (0.5 M, 2.0 ml, 1.0 mmol) was added dropwise to a cold (–78 °C) stirring solution of **54** (0.84 g, 0.97 mmol) in toluene (10 ml). The solution was allowed to warm to room temperature with stirring over 6 days. Volatiles were removed *in vacuo*, and the product was extracted into pentane (10 ml). Storage of the pentane solution at room temperature yielded **142** as pale green crystals. Yield: 0.45 g, 51%.

Method B: THF (20 ml) was added dropwise to a cold (–78 °C) stirring mixture of [U(Tren^{TIPS})(Cl)] (**7**, 2.66 g, 3.00 mmol) and KSCN (0.32 g, 3.30 mmol). The mixture was allowed to warm to room temperature with stirring over 16 hours. The mixture was heated to ~60 °C for 5 mins, and allowed to cool slowly to room temperature. Volatiles were removed *in vacuo*, and the product extracted into hot hexanes (20 ml) which afforded green crystals of **142** on cooling to room temperature. Yield: 1.44 g, 53%.

Anal. calcd for $C_{34}H_{75}N_5SSi_3U$: C 44.96; H 8.32; N 7.71%. Found: C 44.59; H 8.17; N 7.52%. ^{1}H NMR (C_6D_6, 298 K): δ 8.88 (s, 54H, CH(CH_3)$_2$), 8.53 (s, 6H, CH_2), 7.31 (br, 9H, CH(CH$_3$)$_2$), –36.97 ppm (s, 6H, CH$_2$). ^{29}Si{^{1}H} NMR (C_6D_6, 298 K): δ 2.43 ppm. FTIR ν/cm^{-1} (Nujol): 2013 (s), 1631 (w), 1343 (w), 1135 (m), 1060 (m), 988 (m), 816 (m). UV-vis-NIR (toluene): λ_{max}/nm (ε/M^{-1}cm^{-1}): 675 (110), 882 (32), 1094 (43), 1122 (45), 1173 (48). μ_{eff} (Evans method, C_6D_6, 298 K): 2.91 μ_B.

7.2.4.11. Demonstration of the liberation of elemental sulfur from the reaction of [U(Tren^{TIPS})(N)] (**54**) and CS_2

Control experiment: Toluene (20 ml) was added to a stirring mixture of **142** (0.39 g, 0.4 mmol) and Ph_3P (0.11 g, 0.4 mmol). The resultant mixture was stirred for 16 hours. The mixture was heated to ~60 °C for 5 mins, and allowed to cool slowly to room temperature. Volatiles were removed *in vacuo*. Analysis of the resultant brown oil by ^1H and $^{31}P\{^1H\}$ NMR spectroscopy revealed no reaction had occurred. $^{31}P\{^1H\}$ NMR (C_6D_6, 298 K): δ –5.22 ppm (Ph_3P).

Control experiment: A solution of CS_2 in toluene (0.5 M, 1.0 ml, 0.5 mmol) was added dropwise to a stirring solution of Ph_3P (0.13 g, 0.5 mmol) in toluene (20 ml). The solution was stirred for 16 hours. Volatiles were removed *in vacuo*. Analysis of the resultant brown oil by ^1H and $^{31}P\{^1H\}$ NMR spectroscopy revealed no reaction had occurred. $^{31}P\{^1H\}$ NMR (C_6D_6, 298 K): δ –5.22 ppm (Ph_3P).

*Stepwise synthesis of [U(Tren^{TIPS})(NCS)] (**142**) and Ph_3P=S:* A solution of CS_2 in toluene (0.5 M, 1.2 ml, 0.60 mmol) was added dropwise to a cold (–78 °C) stirring solution of **54** (0.50 g, 0.58 mmol) in toluene (20 ml). The solution was allowed to warm to room temperature with stirring over 6 days. Volatiles were removed *in vacuo*, and Ph_3P (0.15 g, 0.58 mmol) was added to the resultant brown oil. Toluene (20 ml) was added to this mixture, and the mixture stirred for 16 hours. Volatiles were removed *in vacuo* to afford a brown oil. $^{31}P\{^1H\}$ NMR (C_6D_6, 298 K): δ 42.80 (Ph_3P=S), –5.22 ppm (Ph_3P).

*One pot synthesis of [U(Tren^{TIPS})(NCS)] (**142**) and Ph_3P=S:* A solution of CS_2 in toluene (0.5 M, 0.6 ml, 0.30 mmol) was added dropwise to a cold (–78 °C) stirring solution of **54** (0.26 g, 0.30 mmol) and Ph_3P (0.080 g, 0.30 mmol) in toluene (20 ml). The solution was allowed to warm to room temperature with stirring over 6 days. Volatiles were removed *in vacuo* to afford a brown oil. $^{31}P\{^1H\}$ NMR (C_6D_6, 298 K): δ 42.80 (Ph_3P=S, 66%), –5.22 ppm (Ph_3P, 34%). The ^{31}P data match those of authentic commercial samples.

7.2.4.12. Attempted preparation of [U(Tren^{TIPS})] (**15**)

Toluene (30 ml) was added to a cold (–78 °C) stirring mixture of **142** (0.38 g, 0.4 mmol) and KC_8 (0.05 g, 0.8 mmol). The solution was allowed to warm to room temperature with stirring over 5 days. Volatiles were removed *in vacuo*. Analysis of the resultant brown oil by ^{1}H NMR spectroscopy revealed no reaction had occurred.

7.3. X-ray Crystallographic Data

Compound	[{U(Tren^{TIPS})(μ-N)(μ-Li)}$_2$] (co-planar)	[{U(Tren^{TIPS})(μ-N)(μ-Li)}$_2$] (*trans*-bent)	[{U(Tren^{TIPS})(μ-N)(μ-K)}$_2$] (co-planar)
Number	**106**	**106**	**107**
Formula	$C_{66}H_{150}Li_2N_{10}Si_6U_2$	$C_{66}H_{150}Li_2N_{10}Si_6U_2$	$C_{66}H_{150}K_2N_{10}Si_6U_2$
RMM	1742.43	1742.43	1806.75
Crystal size, mm	0.12 x 0.09 x 0.08	0.14 x 0.08 x 0.05	0.22 x 0.14 x 0.12
Crystal system	Monoclinic	Monoclinic	Orthorhombic
Space group	*C*2/*c*	*P*2$_1$/*n*	*Pbca*
a, Å	37.092(2)	12.8078(3)	13.8074(7)
b, Å	15.8045(2)	27.2910(3)	23.2204(19)
c, Å	22.2156(12)	13.1188(2)	26.3621(15)
α, °	90.00	90.00	90.00
β, °	140.685(11)	117.063(3)	90.00
γ, °	90.00	90.00	90.00
V, Å^3	8251.2(14)	4083.43(15)	8452.0(9)
Z	4	2	4
ρ_{calcd}, g cm^{-3}	1.403	1.417	1.420
μ, mm^{-1}	12.10	12.225	12.70
no of reflns measd	27178	82799	20113
no of unique reflns, R_{int}	8290, 0.041	8193	8259, 0.056
no of reflns with $F^2 > 2\sigma(F^2)$	7775	7822	6749
transm coeff range	0.402-0.552	0.769-0.903	0.157-0.396
R, R_w ($F^2 > 2\sigma(F^2)$)	0.024, 0.059	0.043, 0.113	0.051, 0.129
R, Rw (all data)	0.026, 0.060	0.045, 0.114	0.064, 0.137
S[a]	1.04	1.207	1.06
Parameters	406	449	406
max, min diff map, e Å^{-3}	1.21, –1.09	3.434, –1.921	2.86, –1.40

Compound	[{U(Tren^{TIPS})(μ-N)(μ-K)}$_2$] (*trans*-bent)	[{U(Tren^{TIPS})(μ-N)(μ-Rb)}$_2$]	[{U(Tren^{TIPS})(μ-N)(μ-Cs)}$_2$]
Number	**107**	**108**	**109**
Formula	$C_{66}H_{150}K_2N_{10}Si_6U_2$	$C_{66}H_{150}N_{10}Rb_2Si_6U_2$	$C_{66}H_{150}Cs_2N_{10}Si_6U_2$
RMM	1806.75	1899.49	1994.37
Crystal size, mm	0.21 x 0.14 x 0.07	0.22 x 0.11 x 0.07	0.29 x 0.23 x 0.10
Crystal system	Monoclinic	Orthorhombic	Monoclinic
Space group	*I*2/*a*	*Pbca*	*I*2/*a*
a, Å	23.4469(5)	13.7527(3)	22.76348(12)
b, Å	15.8042(4)	23.1023(5)	17.09580(9)
c, Å	22.9843(2)	26.7606(4)	22.50605(12)
α, °	90.00	90.00	90.00
β, °	102.255(2)	90.00	100.7821(5)
γ, °	90.00	90.00	90.00
V, Å^3	8323.0(4)	8502.3(3)	8603.83(8)
Z	4	4	4
ρ_{calcd}, g cm^{-3}	1.442	1.484	1.540
μ, mm^{-1}	12.90	13.134	18.112
no of reflns measd	22897	40725	60370
no of unique reflns, R_{int}	8271, 0.045	8544, 0.064	8740, 0.043
no of reflns with $F^2 > 2\sigma(F^2)$	7779	7300	8719
transm coeff range	0.598-0.830	0.165-0.531	0.141-0.533
R, R_w ($F^2 > 2\sigma(F^2)$)	0.034, 0.091	0.031, 0.081	0.040, 0.103
R, Rw (all data)	0.036, 0.093	0.036, 0.082	0.040, 0.103
S[a]	1.05	0.980	1.074
Parameters	406	401	470
max, min diff map, e Å^{-3}	2.59, –1.55	2.65, –2.38	2.10, –1.93

Compound	[U(Tren^{TIPS}){(μ-N)(μ-K)(Bn_2-18C6)}]	[U(Tren^{TIPS}){(μ-N)(μ-Rb)(18C6)}] •C_6H_{14}	[U(Tren^{TIPS}){(μ-N)(μ-Cs)(18C6)}]
Number	**111**	**112**	**113**
Formula	$C_{53}H_{99}KN_5O_6Si_3U$	$C_{45}H_{99}N_5O_6RbSi_3U$ •C_6H_{14}	$C_{45}H_{99}CsN_5O_6Si_3U$
RMM	1263.77	1300.22	1261.50
Crystal size, mm	0.23 x 0.14 x 0.05	0.41 x 0.17 x 0.14	0.21 x 0.11 x 0.10
Crystal system	Orthorhombic	Cubic	Monoclinic
Space group	$P2_12_12_1$	Pb-3	$P2_1/c$
a, Å	11.83314(10)	23.7586(3)	14.5874(4)
b, Å	22.09845(18)	23.7586(3)	13.7318(3)
c, Å	22.89030(19)	23.7586(3)	28.4495(8)
α, °	90.00	90.00	90.00
β, °	90.00	90.00	91.520(3)
γ, °	90.00	90.00	90.00
V, $Å^3$	5985.68(9)	13411.0(4)	5696.7(3)
Z	4	8	4
ρ_{calcd}, g cm^{-3}	1.402	1.288	1.471
μ, mm^{-1}	9.211	8.542	13.882
no of reflns measd	32540	13287	20388
no of unique reflns, R_{int}	11257, 0.0243	4474, 0.028	11162, 0.056
no of reflns with $F^2 > 2\sigma(F^2)$	11201	3530	9585
transm coeff range	0.320-0.793	0.299-0.570	0.185-0.443
R, R_w ($F^2 > 2\sigma(F^2)$)	0.016, 0.037	0.070, 0.199	0.046, 0.120
R, Rw (all data)	0.016, 0.037	0.082, 0.212	0.054, 0.129
S[a]	1.062	1.061	1.03
Parameters	641	275	569
max, min diff map, e $Å^{-3}$	0.996, –0.6825	1.666, –1.538	2.89, –4.56

Compound	[U(Tren^{TIPS})(N)] [K(15C5)$_2$]	[U(Tren^{TIPS})(N)] [K(Bn-15C5)$_2$]	[U(Tren^{TIPS})(N)] [Rb(Bn-15C5)$_2$]
Number	**114**	**115**	**116**
Formula	$C_{33}H_{75}N_5Si_3U$ •$C_{20}H_{40}KO_{10}$	$C_{33}H_{75}N_5Si_3U$ •$C_{28}H_{40}KO_{10}$	$C_{33}H_{75}N_5Si_3U$ •$C_{28}H_{40}O_{10}Rb$
RMM	1343.89	1439.97	1486.34
Crystal size, mm	0.25 x 0.08 x 0.04	0.14 x 0.06 x 0.05	0.17 x 0.12 x 0.08
Crystal system	Triclinic	Monoclinic	Monoclinic
Space group	*P*-1	$P2_1/c$	$P2_1/c$
a, Å	11.3428(3)	15.8636(3)	15.8741(3)
b, Å	16.5053(5)	18.5210(4)	18.5622(3)
c, Å	18.3155(5)	24.6424(5)	24.7397(4)
α, °	79.554(3)	90.00	90.00
β, °	85.928(3)	104.413(2)	104.2695(16)
γ, °	81.641(2)	90.00	90.00
V, Å^3	3332.79(17)	7012.3(3)	7064.8(2)
Z	2	4	4
ρ_{calcd}, g cm^{-3}	1.339	1.364	1.397
μ, mm^{-1}	8.345	7.97	8.220
no of reflns measd	25566	59760	33199
no of unique reflns, R_{int}	13234, 0.038	14044, 0.067	14071, 0.028
no of reflns with $F^2 > 2\sigma(F^2)$	12396	11828	13145
transm coeff range	0.630-1.021	0.473-0.735	0.408-0.624
R, R_w ($F^2 > 2\sigma(F^2)$)	0.032, 0.080	0.030, 0.065	0.022, 0.053
R, Rw (all data)	0.035, 0.082	0.039, 0.069	0.025, 0.054
S[a]	1.044	1.02	1.02
Parameters	687	767	767
max, min diff map, e Å^{-3}	1.485, –2.565	0.99, –1.06	0.86, –0.82

Compound	[U(Tren^{TIPS})(N)][Cs(Bn-15C5)$_2$]	[U(Tren^{TIPS}}(μ-N)(μ-Li)(12C4)}]	[U(Tren^{TIPS}){μ-N)(μ-Li)(Bn-9C3)}]•0.75(C_5H_{12})
Number	**117**	**118**	**119**
Formula	$C_{33}H_{75}N_5Si_3U$ •$C_{28}H_{40}CsO_{10}$	$C_{41}H_{91}LiN_5O_4Si_3U$	$C_{43}H_{87}LiN_5Si_3U$ •0.75(C_5H_{12})
RMM	1533.78	1047.42	1105.52
Crystal size, mm	0.23 x 0.07 x 0.06	0.16 x 0.12 x 0.09	0.33 x 0.16 x 0.07
Crystal system	Monoclinic	Orthorhombic	Orthorhombic
Space group	$P2_1/c$	$Pn2_1a$	*Pbna*
a, Å	16.09798(19)	25.55190(20)	18.0538(6)
b, Å	18.4937(2)	13.37345(9)	18.9567(7)
c, Å	24.5732(3)	14.81292(10)	31.5799(11)
α, °	90.00	90.00	90.00
β, °	103.2246(12)	90.00	90.00
γ, °	90.00	90.00	90.00
V, Å^3	7121.73(15)	5061.83(6)	10807.9(7)
Z	4	4	8
ρ_{calcd}, g cm^{-3}	1.430	1.374	1.359
μ, mm^{-1}	11.25	10.02	9.397
no of reflns measd	52126	20152	30093
no of unique reflns, R_{int}	13224, 0.041	8470	10826, 0.0734
no of reflns with $F^2 > 2\sigma(F^2)$	11481	8007	8654
transm coeff range	0.717-1.001	0.335-0.628	0.203-0.619
R, R_w ($F^2 > 2\sigma(F^2)$)	0.059, 0.142	0.029, 0.071	0.093, 0.246
R, Rw (all data)	0.067, 0.149	0.030, 0.073	0.106, 0.252
S[a]	1.03	1.02	1.035
Parameters	885	697	523
max, min diff map, e Å^{-3}	8.17, –4.03	1.68, –1.20	4.287, –5.106

Compound	[U(Tren^{TIPS}){(μ-N)(μ-Li)(py)$_3$}]	[U{CH$_2$CH(Me)Si(^{i}Pr)$_2$*N*CH$_2$CH$_2$*N*(CH$_2$CH$_2$NSi^{i}Pr$_3$)$_2$}]	[Th(Tren^{TIPS})(CH$_2$Ph)]
Number	**121**	**110**	**124**
Formula	$C_{48}H_{90}LiN_8Si_3U$	$C_{33}H_{74}N_4Si_3U$	$C_{40}H_{82}N_4Si_3Th$
RMM	1108.52	849.26	935.40
Crystal size, mm	0.14 x 0.10 x 0.08	0.22 x 0.09 x 0.05	0.13 x 0.07 x 0.01
Crystal system	Monoclinic	Monoclinic	Triclinic
Space group	*P*2$_1$/*n*	*P*2$_1$/*n*	*P*-1
a, Å	16.05107(17)	9.347(2)	18.7387(6)
b, Å	17.67656(18)	22.333(6)	24.4559(7)
c, Å	19.9679(2)	18.920(5)	24.9335(8)
α, °	90.00	90.00	60.713(3)
β, °	91.497(1)	92.508(4)	89.936(3)
γ, °	90.00	90.00	69.909(3)
V, Å^3	5663.51	3945.8(17)	9163.0(6)
Z	4	4	8
ρ_{calcd}, g cm^{-3}	1.301	1.430	1.356
μ, mm^{-1}	8.95	4.231	11.46
no of reflns measd	24359	28004	81199
no of unique reflns, R_{int}	11249, 0.041	6939, 0.0861	36576, 0.054
no of reflns with $F^2 > 2\sigma(F^2)$	10216	6173	30222
transm coeff range	0.514-0.693	0.29-0.43	0.381-0.874
R, R_w ($F^2 > 2\sigma(F^2)$)	0.038, 0.099	0.132, 0.264	0.055, 0.132
R, Rw (all data)	0.041, 0.103	0.144, 0.269	0.068, 0.140
S[a]	1.02	1.381	1.08
Parameters	568	387	1860
max, min diff map, e Å^{-3}	1.93, –3.81	4.003, –6.174	2.88, –2.53

Compound	[Th{$CH_2CH(Me)Si(^iPr)_2NCH_2CH_2N(CH_2CH_2NSi^iPr_3)_2$}]	[U($Tren^{TIPS}$)(NCO)]	[U($Tren^{TIPS}$)(NCO)][K(Bn-15C5)$_2$]
Number	**125**	**135**	**136**
Formula	$C_{34}H_{75}N_5OSi_3Th$	$C_{34}H_{75}N_5OSi_3U$	$C_{34}H_{75}N_5OSi_3U \cdot C_{28}H_{40}KO_{10}$
RMM	843.27	892.29	1467.98
Crystal size, mm	0.30 x 0.23 x 0.20	0.12 x 0.09 x 0.06	0.14 x 0.10 x 0.050
Crystal system	Monoclinic	Monoclinic	Monoclinic
Space group	$P2_1/n$	$P2_1/n$	$P2_1/c$
a, Å	9.44392(19)	11.15129(17)	16.6175(5)
b, Å	22.3863(4)	21.0112(3)	19.7287(4)
c, Å	18.8042(5)	18.2822(3)	23.2630(7)
α, °	90.00	90.00	90.00
β, °	92.5386(19)	93.5548(13)	107.291(3)
γ, °	90.00	90.00	90.00
V, Å^3	3971.57	4275.30(11)	7281.9(3)
Z	4	4	4
ρ_{calcd}, g cm^{-3}	1.410	1.386	1.339
μ, mm^{-1}	13.16	11.712	7.699
no of reflns measd	18085	17352	51836
no of unique reflns, R_{int}	7883, 0.027	8393, 0.0318	13505, 0.0688
no of reflns with $F^2 > 2\sigma(F^2)$	7559	7361	10458
transm coeff range	0.090-0.325	0.425-0.622	0.531-0.804
R, R_w ($F^2 > 2\sigma(F^2)$)	0.028, 0.068	0.023, 0.053	0.054, 0.130
R, Rw (all data)	0.029, 0.069	0.030, 0.056	0.071, 0.143
S[a]	1.18	1.014	1.030
Parameters	387	437	786
max, min diff map, e Å^{-3}	1.45, –1.30	0.838, –0.763	1.114, –1.864

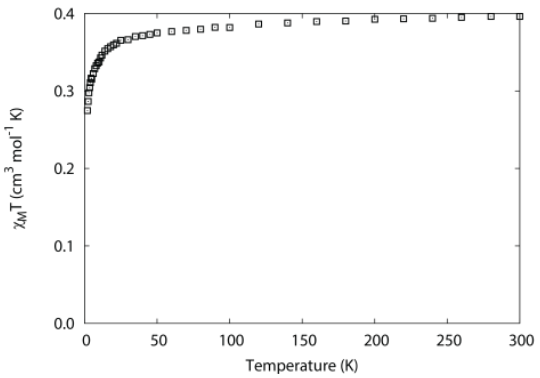
Compound	[U(Tren^{TIPS}){μ-NCO)(μ-K)(18C6)}]	[U(Tren^{TIPS})(O)(NCO)][K(Bn-15C5)$_2$]•C_6H_6	[U(Tren^{TIPS})(κ^2-CS_3)][K(Bn-15C5)$_2$] •C_6H_6
Number	**137**	**138**	**140**
Formula	$C_{46}H_{99}KN_5O_7Si_3U$	$C_{34}H_{75}N_5O_2Si_3U$ •$C_{28}H_{40}KO_{10}$•C_6H_6	$C_{34}H_{75}N_4S_3Si_3U$ •$C_{28}H_{40}KO_{10}$•C_6H_6
RMM	1194.69	1562.09	1612.26
Crystal size, mm	0.46 x 0.34 x 0.24	0.33 x 0.24 x 0.12	0.42 x 0.35 x 0.15
Crystal system	Monoclinic	Triclinic	Triclinic
Space group	$P2_1$	P-1	P-1
a, Å	14.0197(3)	16.4258(3)	13.3459(3)
b, Å	13.0612(3)	17.5135(3)	14.0966(3)
c, Å	16.2740(4)	26.5673(5)	21.1973(3)
α, °	90.00	83.7908(15)	79.8903(14)
β, °	104.161(3)	89.1603(14)	85.7060(14)
γ, °	90.00	89.8628(14)	83.3069(16)
V, Å^3	2889.45(13)	7597.0(2)	3893.17(12)
Z	2	4	2
ρ_{calcd}, g cm^{-3}	1.373	1.366	1.375
μ, mm^{-1}	9.518	7.43	7.97
no of reflns measd	55725	60097	169889
no of unique reflns, R_{int}	11448, 0.0339	30169, 0.049	15847, 0.061
no of reflns with $F^2 > 2\sigma(F^2)$	11382	27770	15698
transm coeff range	0.081-0.302	0.222-0.517	0.274-0.613
R, R_w ($F^2 > 2\sigma(F^2)$)	0.025, 0.063	0.071, 0.190	0.037, 0.096
R, Rw (all data)	0.025, 0.064	0.075, 0.192	0.038, 0.097
S[a]	1.052	1.13	1.02
Parameters	1127	1771	817
max, min diff map, e Å^{-3}	0.676, –2.410	7.77, –3.39	2.95, –1.86

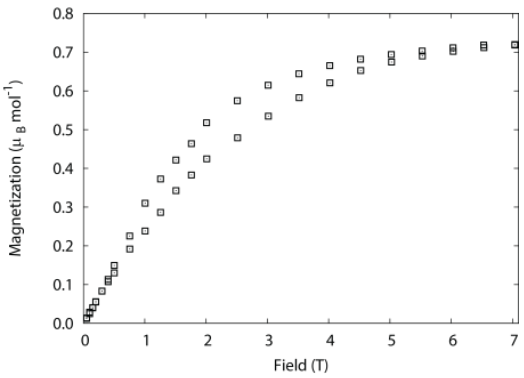
Compound	[{U(Tren^{TIPS})(μ-κ^2:κ^1-CS_3)[μ-K(Bn_2-18C6)]}$_2$(μ-C_6H_6)]•$4C_6H_6$	[U(Tren^{TIPS})(NCS)]
Number	**141**	**142**
Formula	$C_{114}H_{204}K_2N_8O_{12}S_6Si_6U$ •$4C_6H_6$	$C_{34}H_{75}N_5SSi_3U$
RMM	3106.43	908.35
Crystal size, mm	0.27 x 0.14 x 0.09	0.48 x 0.25 x 0.21
Crystal system	Triclinic	Monoclinic
Space group	*P*-1	$P2_1/n$
a, Å	13.8863(2)	11.7596(2)
b, Å	14.1559(3)	20.5649(4)
c, Å	22.4129(3)	18.0898(4)
α, °	93.2214(14)	90.00
β, °	100.8497(12)	92.1081(18)
γ, °	118.0568(17)	90.00
V, $Å^3$	3764.90(12)	4371.78(15)
Z	1	4
ρ_{calcd}, g cm^{-3}	1.370	1.380
μ, mm^{-1}	8.18	11.88
no of reflns measd	55791	39789
no of unique reflns, R_{int}	14960, 0.047	8830, 0.069
no of reflns with $F^2 > 2\sigma(F^2)$	14083	8420
transm coeff range	0.296-0.600	0.064-0.268
R, R_w ($F^2 > 2\sigma(F^2)$)	0.034, 0.088	0.041, 0.110
R, Rw (all data)	0.036, 0.090	0.042, 0.112
S[a]	1.08	1.07
Parameters	802	437
max, min diff map, e $Å^{-3}$	3.17, –1.29	3.13, –2.17

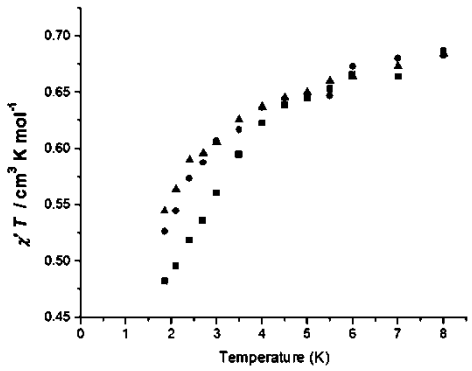
7.4. Magnetometric Measurements

7.4.1. Chapter 4

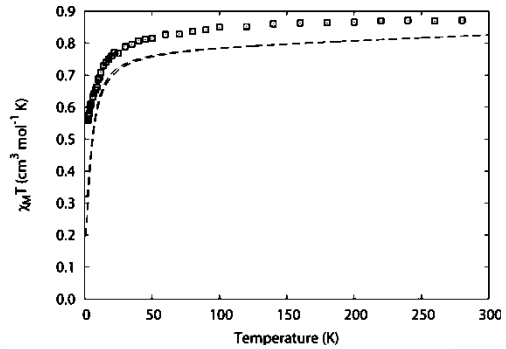
[{U(Tren^{TIPS})(μ-N)(μ-Li)}$_2$], **106**.

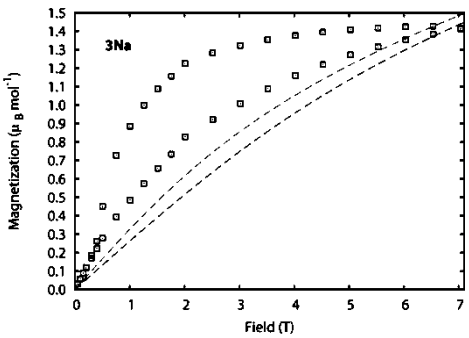


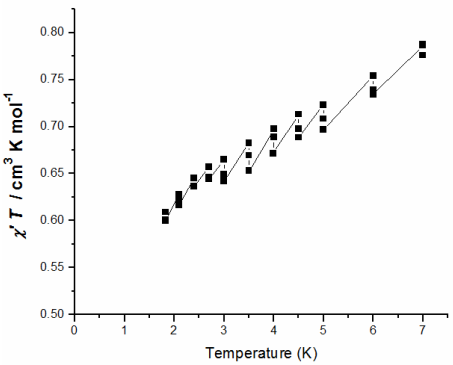




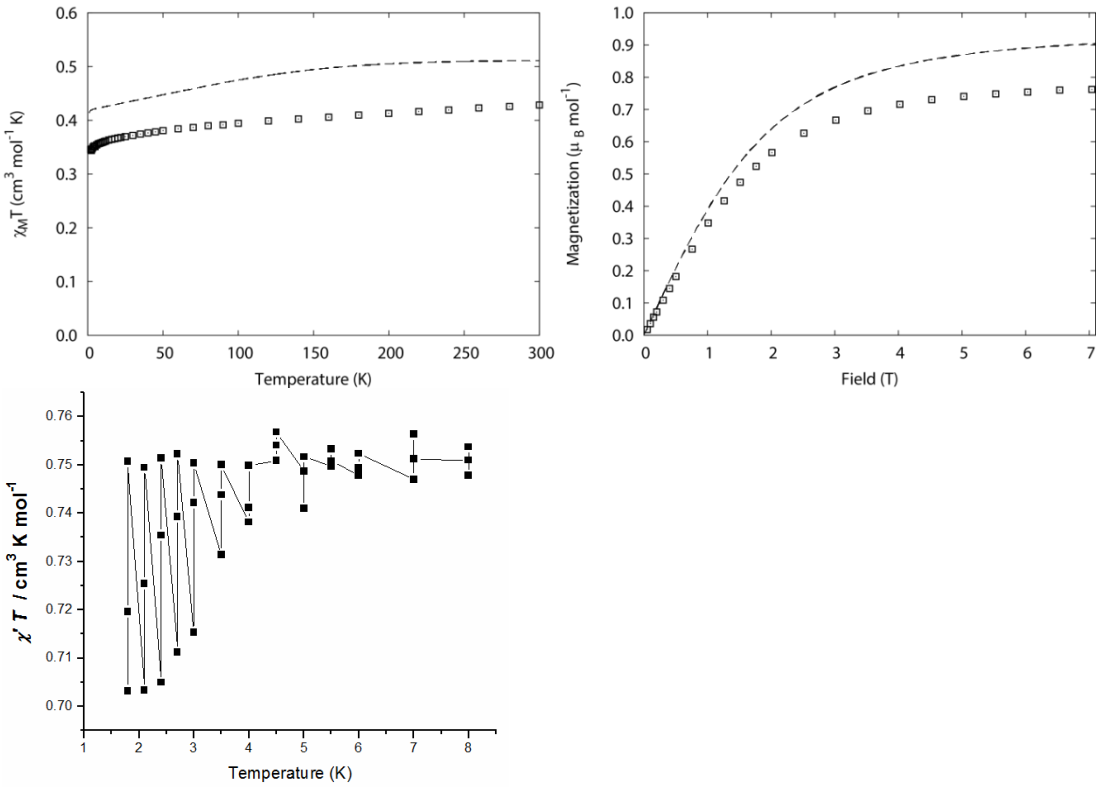
[{U(Tren^{TIPS})(μ-N)(μ-Na)}$_2$], **51**.

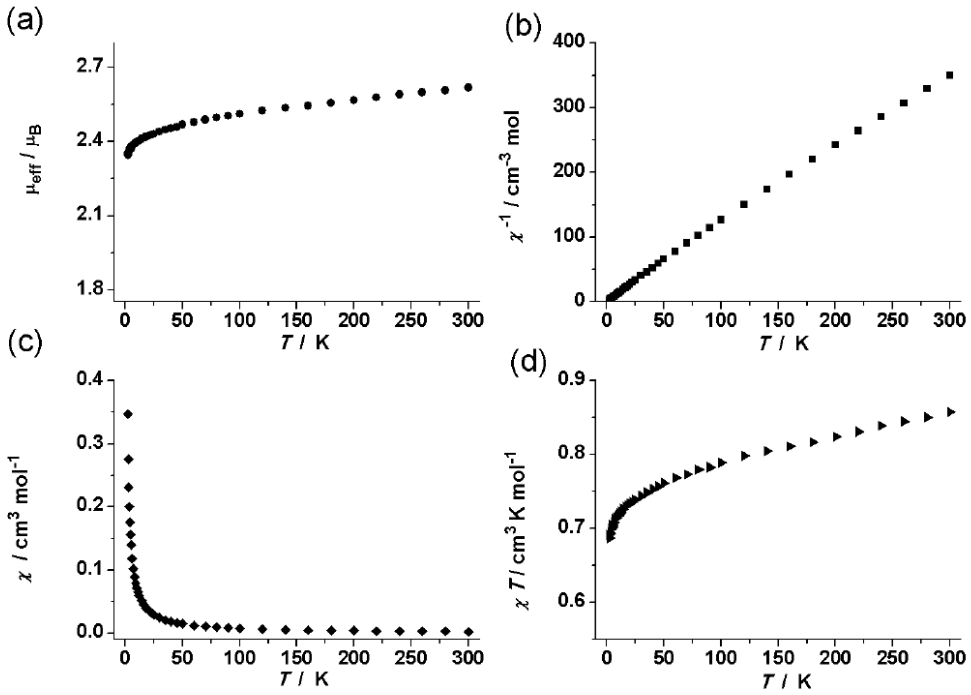




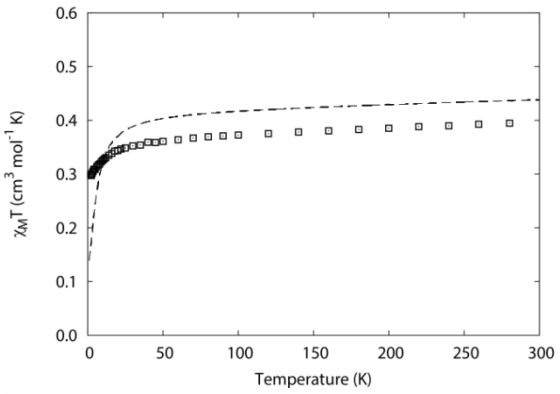


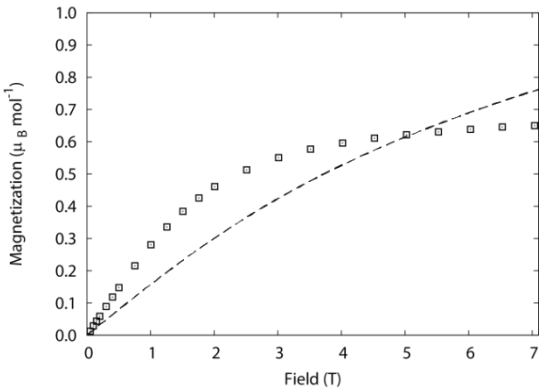
[{U(Tren^{TIPS})(μ-N)(μ-K)}$_2$], **107**.

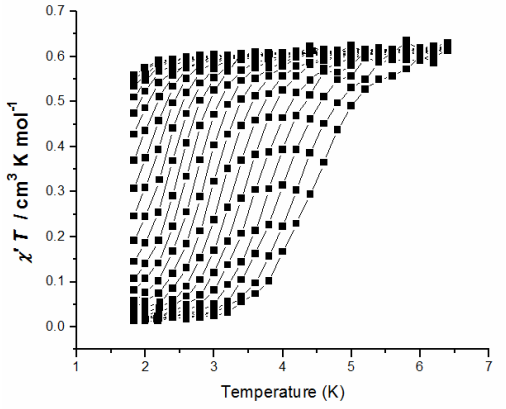




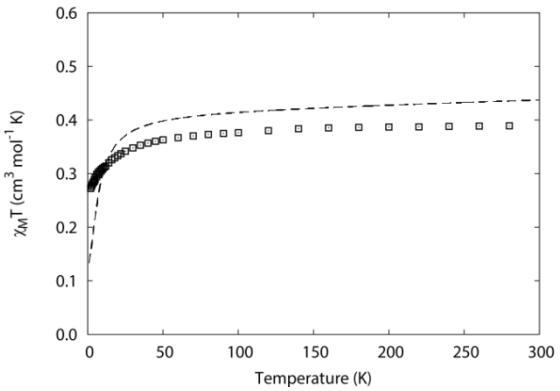
[{U(Tren^{TIPS})(μ-N)(μ-Rb)}$_2$], **108**.

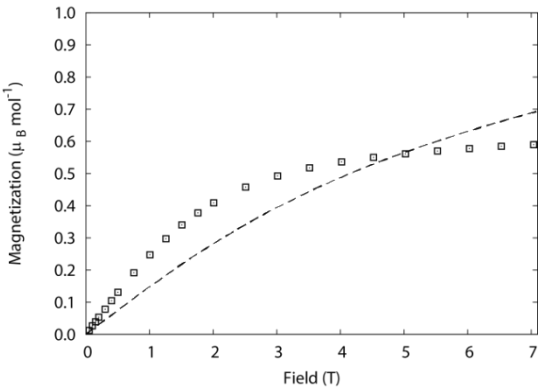


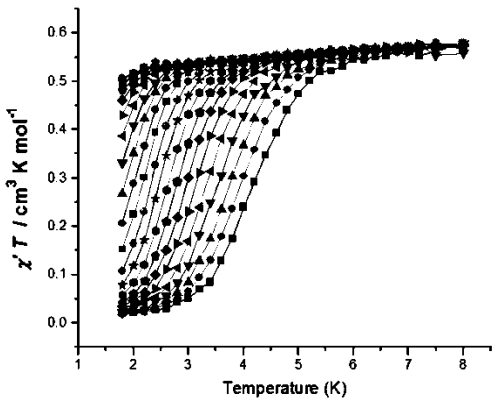




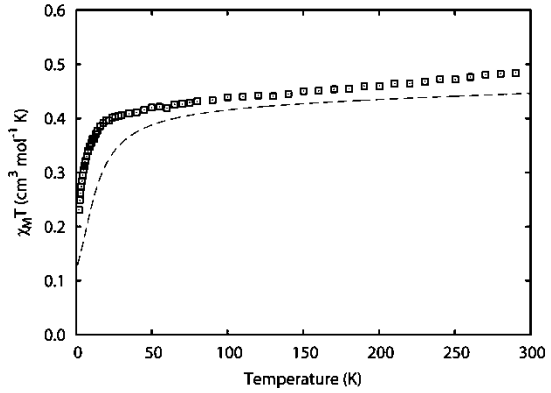
[{U(Tren^{TIPS})(μ-N)(μ-Cs)}$_2$], **109**.

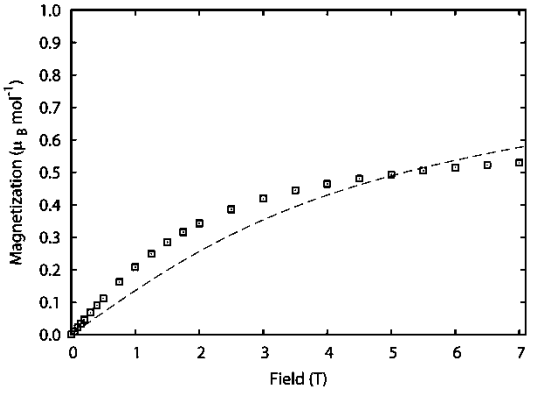


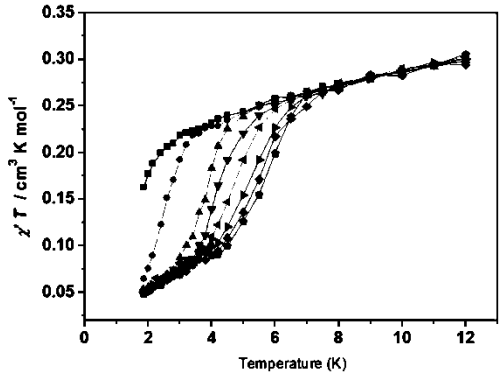




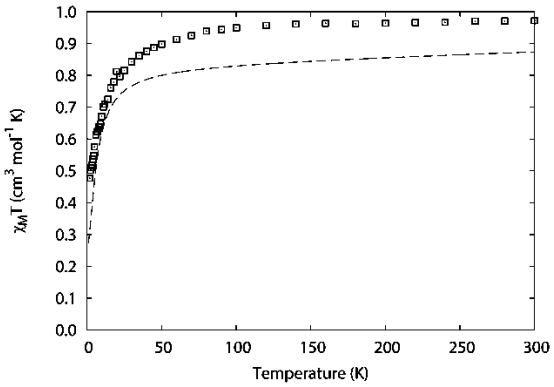
[U(Tren^{TIPS})(N)][Na(12C4)$_2$], **52**.

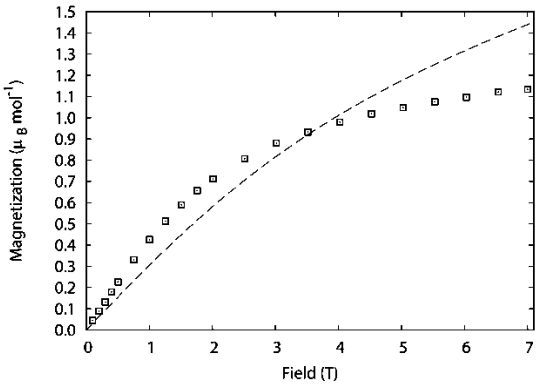


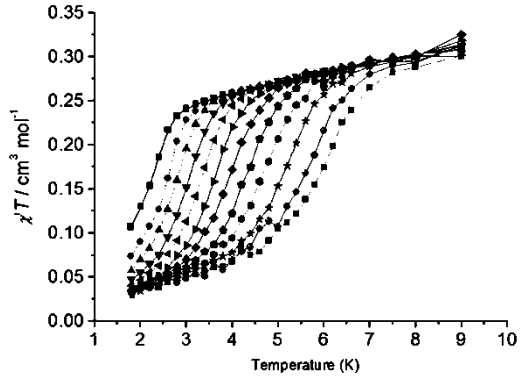




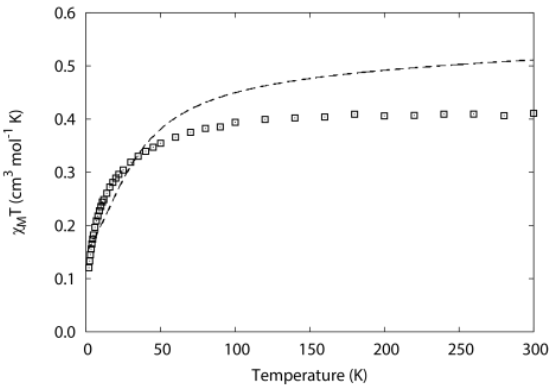
[U(Tren^{TIPS})(N)][K(15C5)$_2$], **114**.

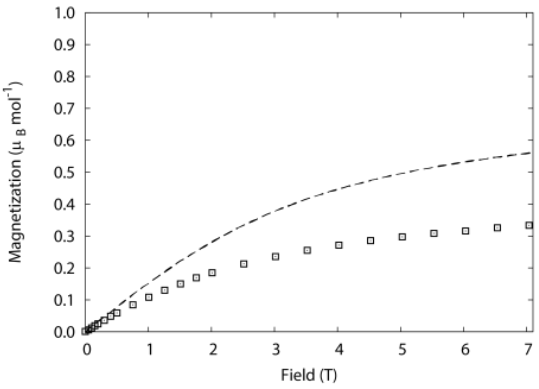


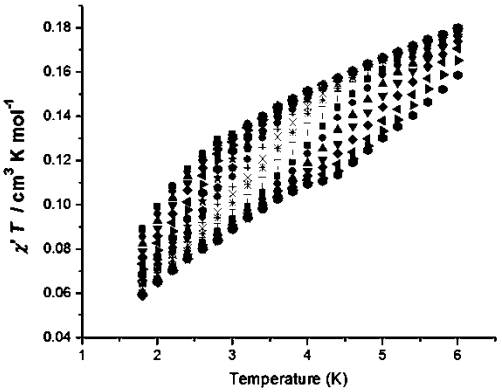




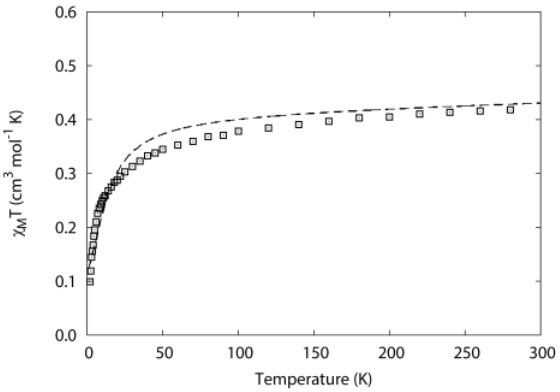
[U(Tren^{TIPS})(N)][Rb(Bn-15C5)$_2$], **116**.

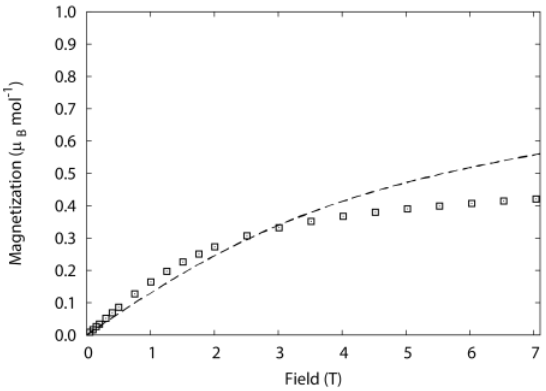


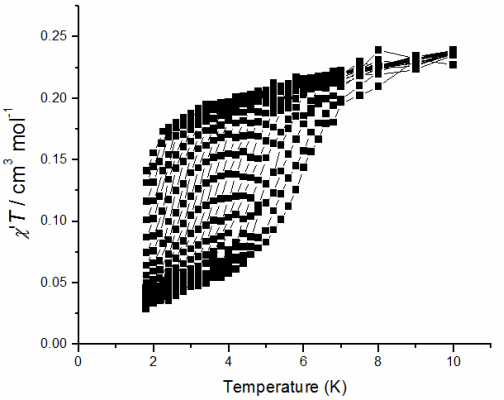




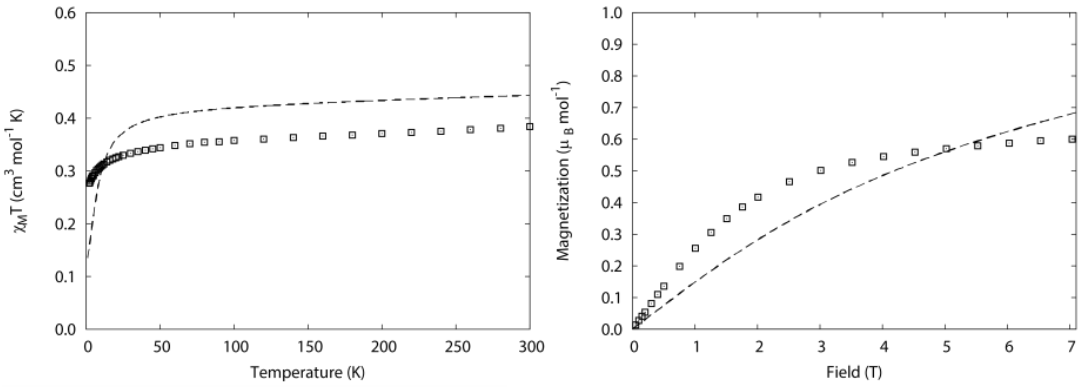
[U(Tren^{TIPS})(N)][Cs(Bn-15C5)$_2$], **117**.

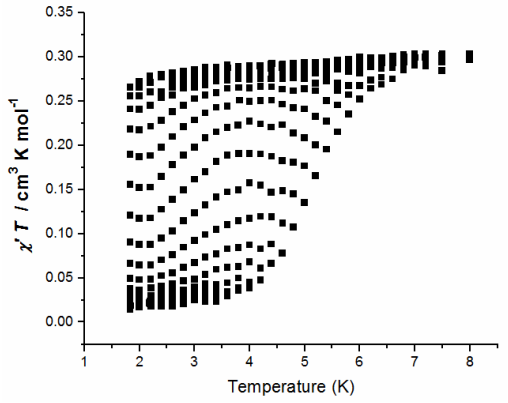




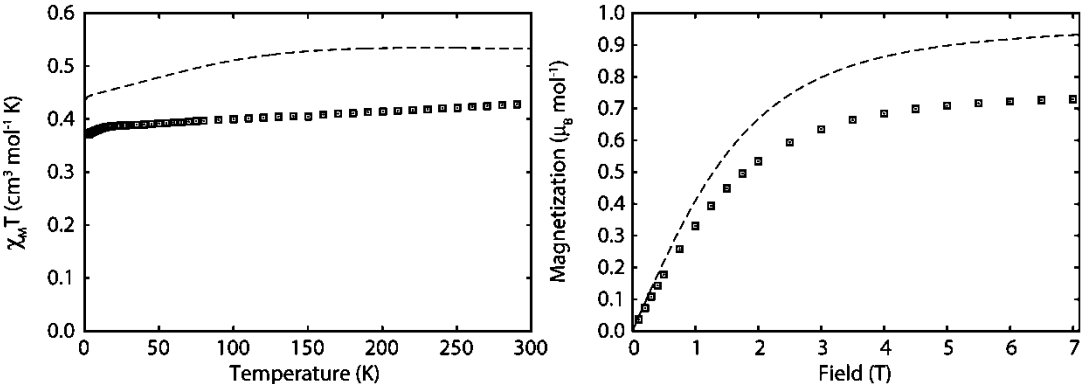


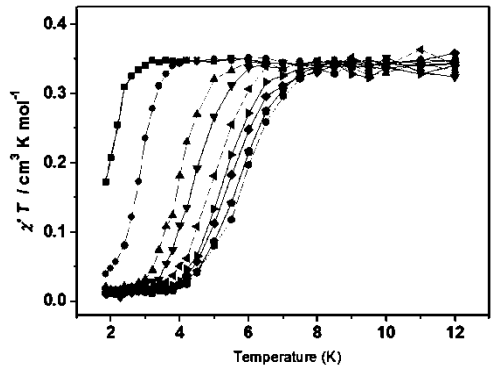
[U(Tren^{TIPS}){(μ-N)(μ-Li)(12C4)}], **118**.



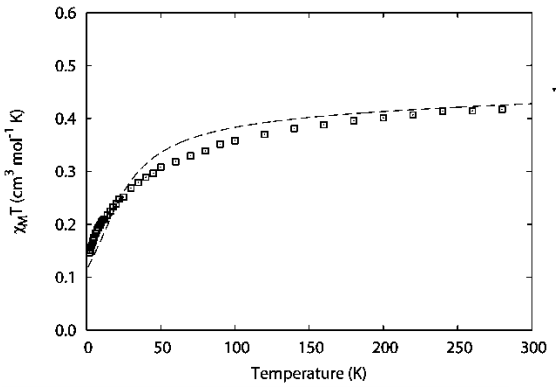


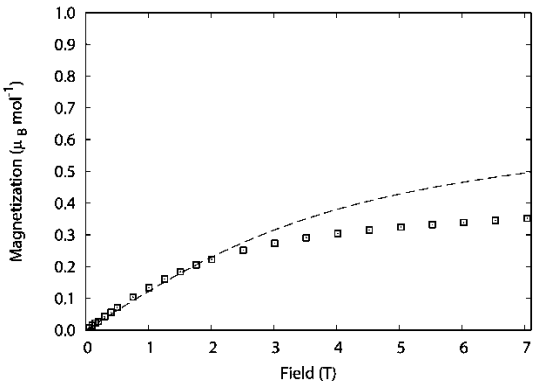
[U(Tren^{TIPS}){(μ-N)(μ-Na)(15C5)}], **53**.

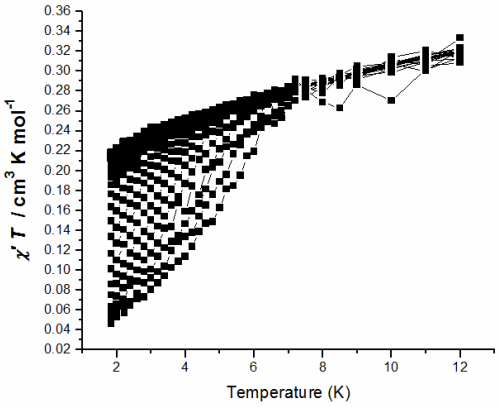




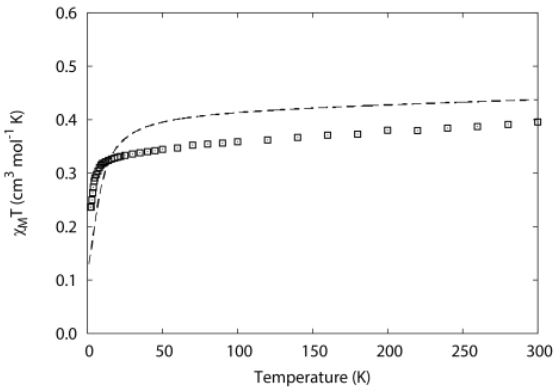
[U(Tren^{TIPS}){(μ-N)(μ-K)(Bn$_2$-18C6)}], **111**.

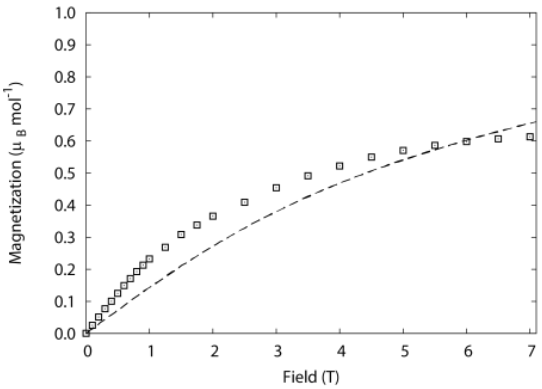


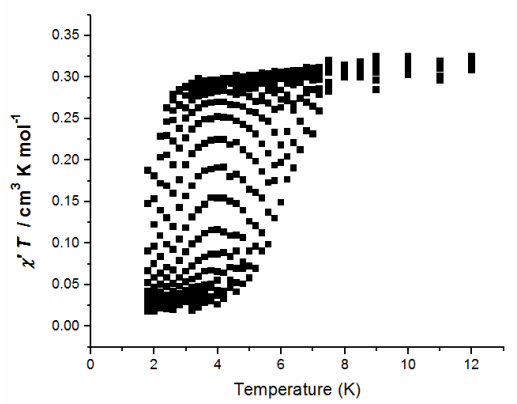




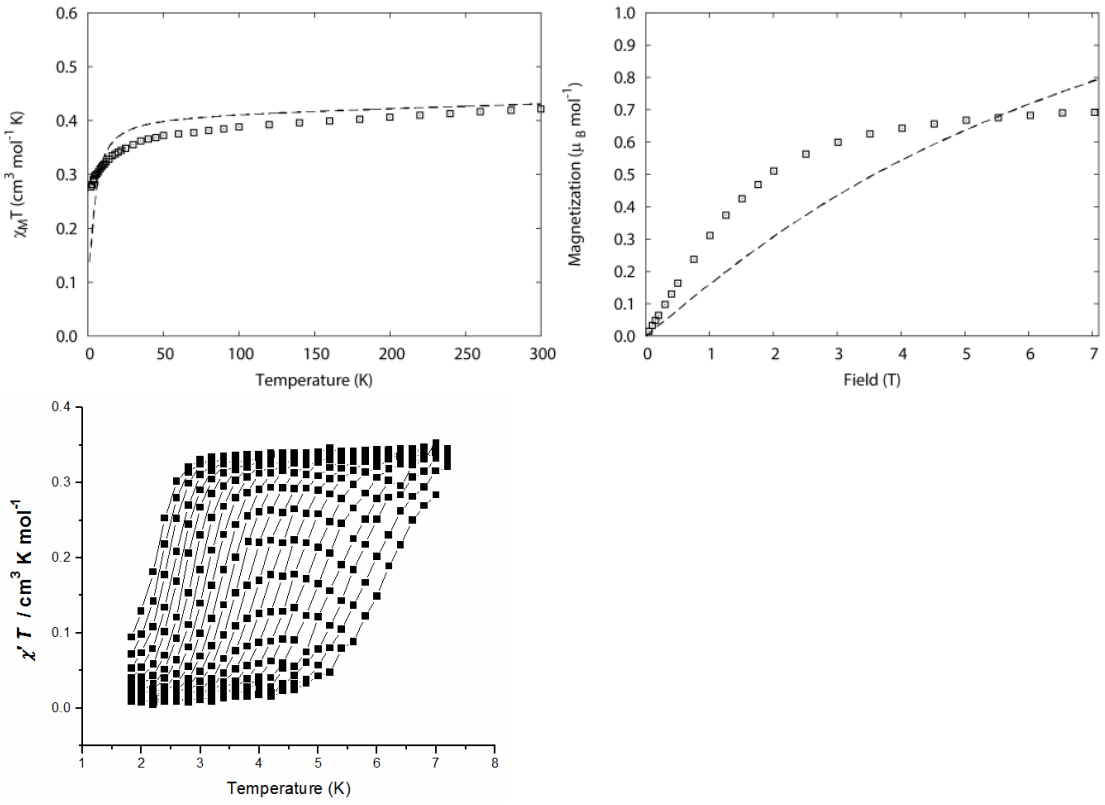
[U(Tren^{TIPS}){(μ-N)(μ-Rb)(18C6)}], **112**.



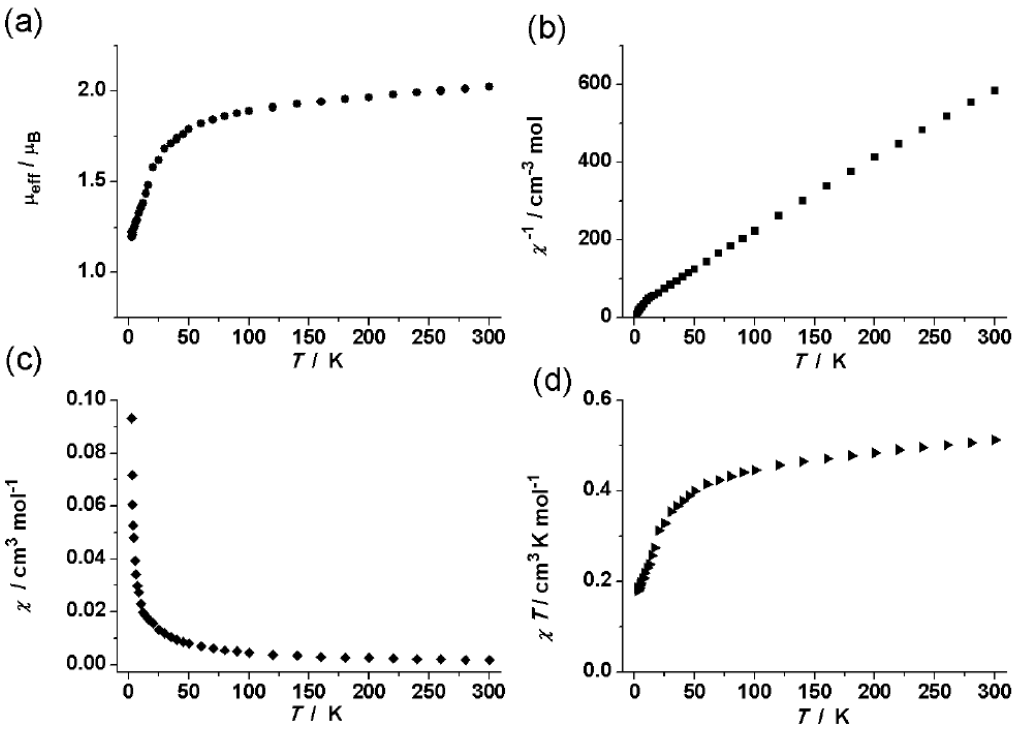




[U(Tren^{TIPS}){(μ-N)(μ-Cs)(18C6)}], **113**.

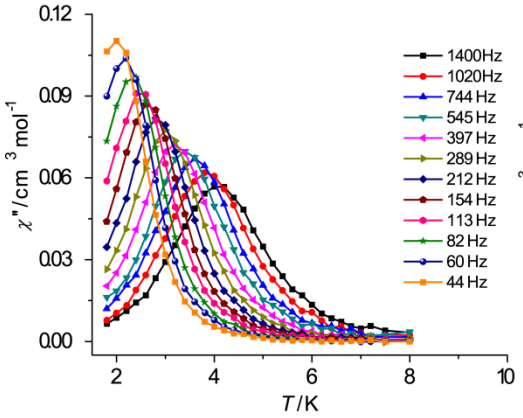


[U(Tren^{TIPS})(N)][K(Bn-15C5)$_2$], **115**.

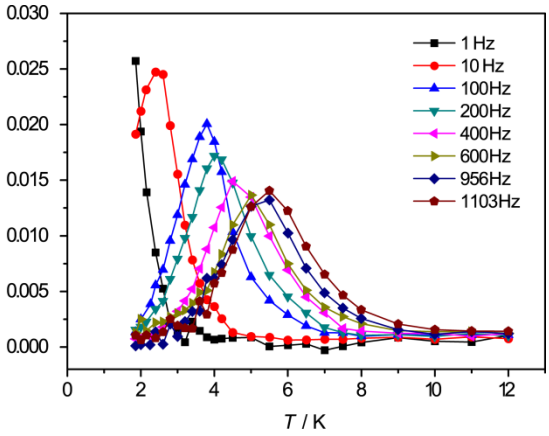


Out-of-phase susceptibilities.

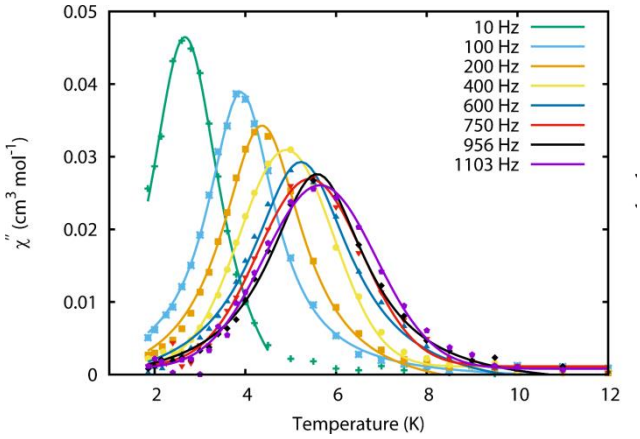
[{U(Tren^{TIPS})(μ-N)(μ-Cs)}$_2$], **109**.



[U(Tren^{TIPS})(N)][Na(12C4)$_2$], **52**.

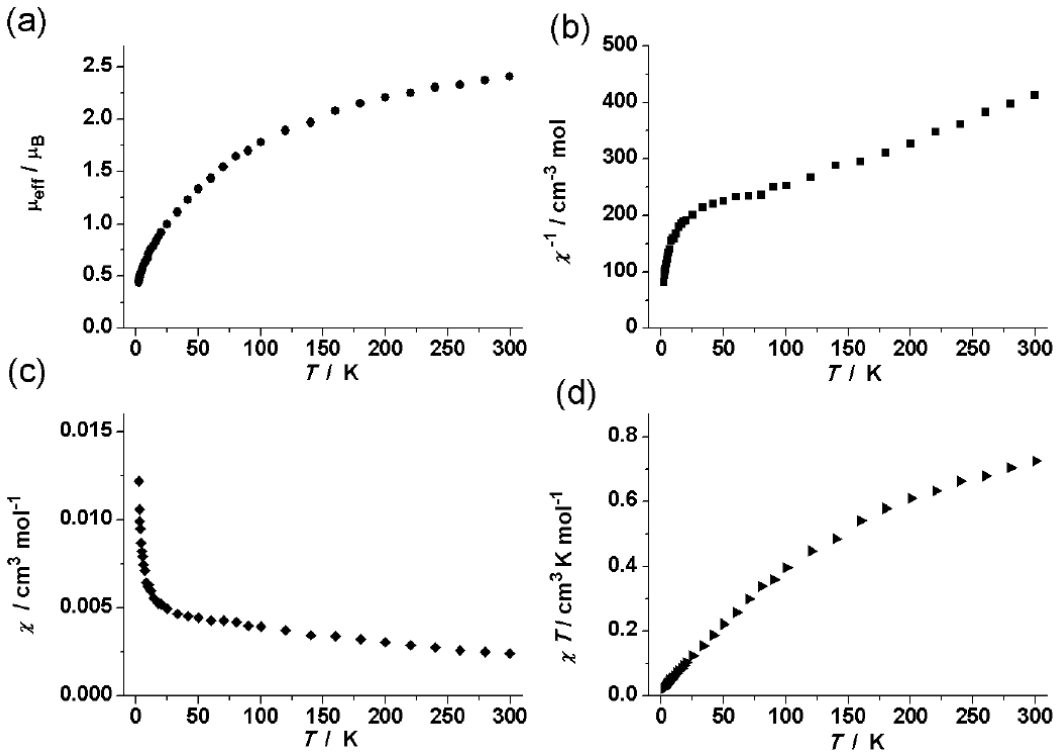


[U(Tren^{TIPS}){(μ-N)(μ-Na)(15C5)}], **53**.

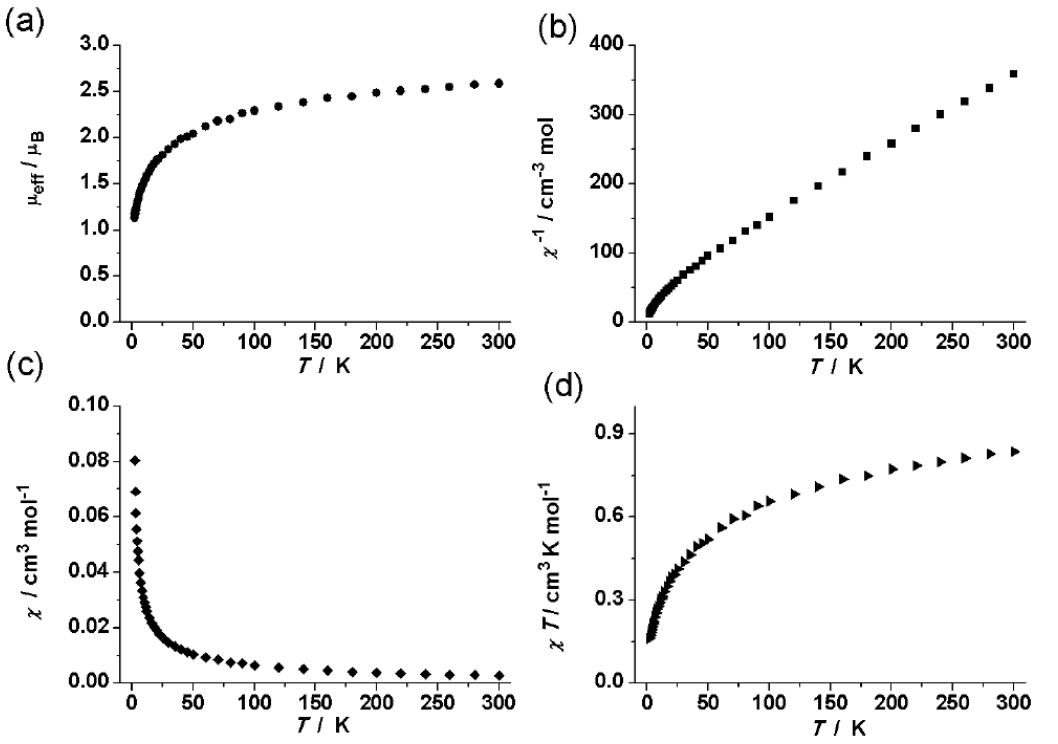


7.4.2. Chapter 5

[U(Tren^{TIPS})(NCO)], **135**.

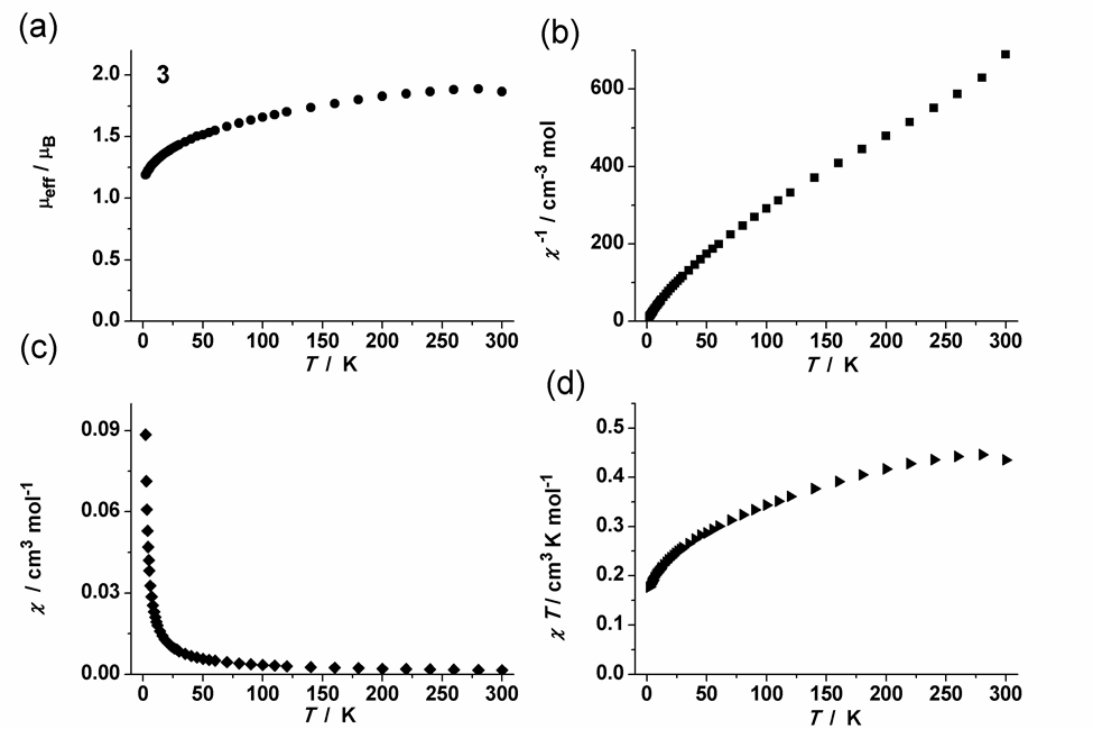


[U(Tren^{TIPS})(NCO)][K(Bn-15C5)$_2$], **136**.

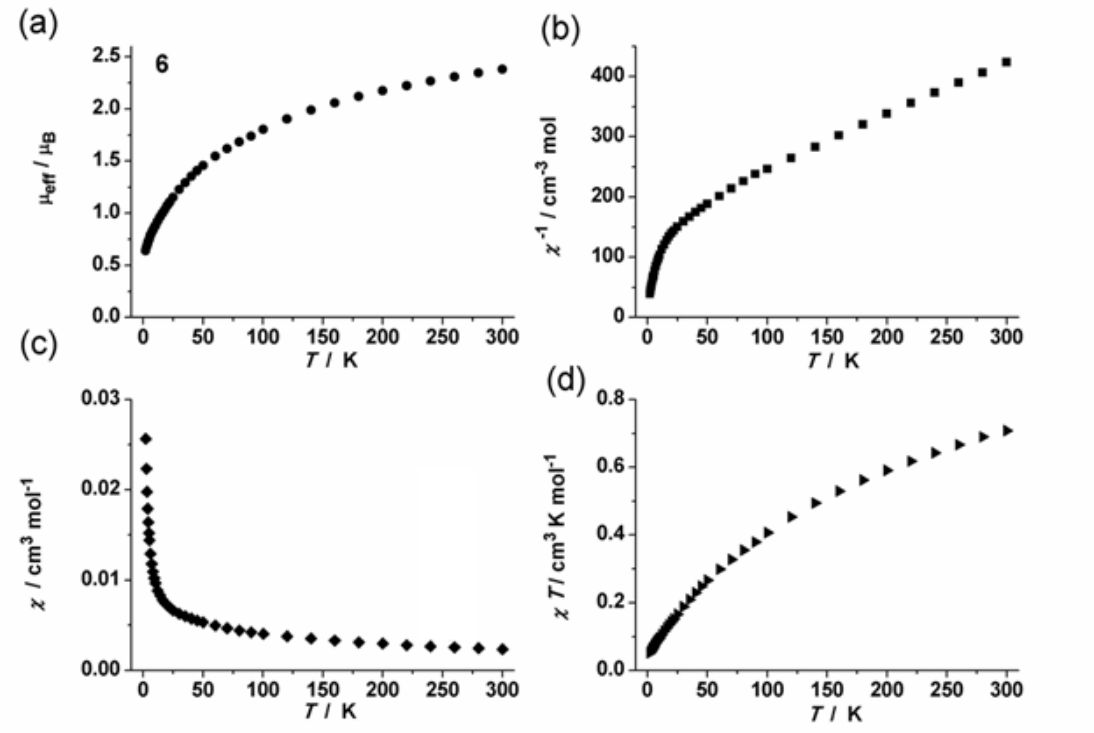


7.4.3. Chapter 6

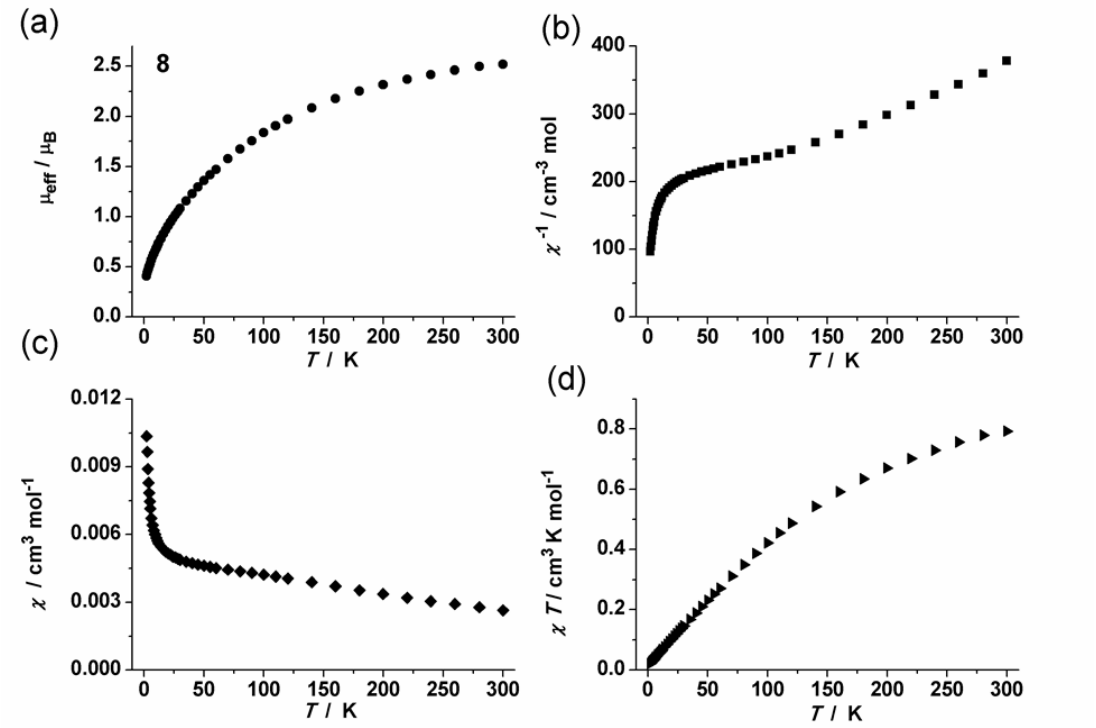
[U(Tren^{TIPS})(O)(NCO)][K(Bn-15C5)$_2$], **138**.



[U(Tren^{TIPS})(CS$_3$)][K(Bn-15C5)$_2$], **140**.



[U(Tren^{TIPS})(NCS)], **142**.



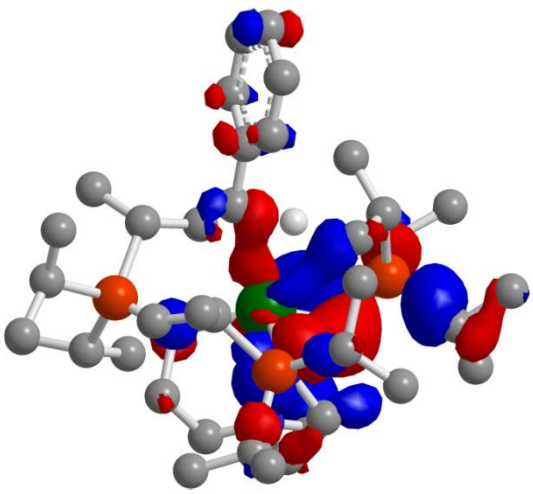
7.5. DFT and *ab initio* Calculations

7.5.1. Chapter 3

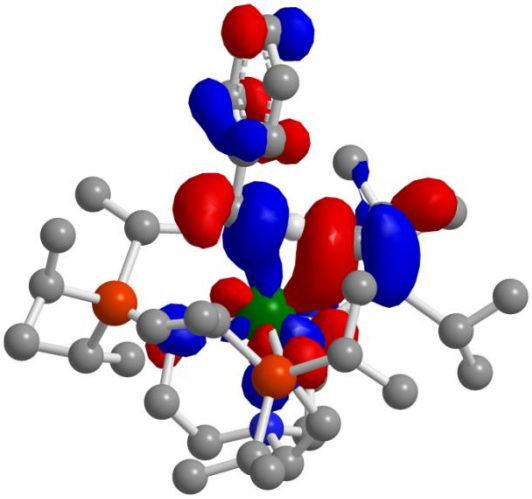
All structures were fully optimised with the Becke's 3-parameter hybrid functional combined with the non-local correlation functional provided by Perdew/Wang (denoted as B3PW91).[12,13] The basis set used for uranium and thorium atoms is the Stuttgart-Dresden small core RECP (relativistic effective core potential) in combination with its adapted basis set.[14-16] However, in order to study the effect of the f orbitals involvement on the cyclometallation step, the 5f-in-large-core ECPs (augmented by an f polarization function, α = 1.0) were used for fixed oxidation states IV.[17] In addition for the calculations involving the hypothetical Hf and Zr complexes the corresponding small core RECP SDD basis sets were used for describing these metals.[18,19] Also, Si and I atoms were treated as well with the corresponding Stuttgart-Dresden RECP in combination with their adapted basis sets,[20] each one augmented by an extra set of polarisation functions.[21] For the rest of the atoms the 6-31G(d,p) basis set was used.[22-24] In all computations no constrains

were imposed on the geometry. All stationary points have been identified for minimum (number of imaginary frequencies Nimag = 0) or transition states (Nimag = 1). Intrinsic Reaction Paths (IRPs) were traced from the various transition structures to verify the reactant to product linkage.[25,26] Enthalpy energies were obtained at T = 298.15 K within the harmonic approximation. The natural population analysis (NPA) was performed using Weinhold's methodology.[27] The GAUSSIAN09 program suite was used in all calculations.[28]

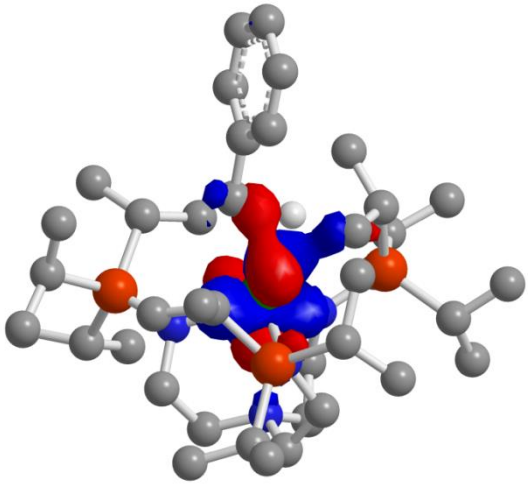
Molecular Orbitals, uranium



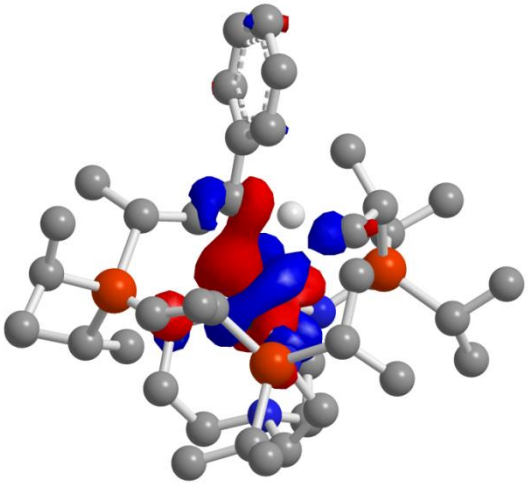
HOMO-3 (195a, -5.65 eV)



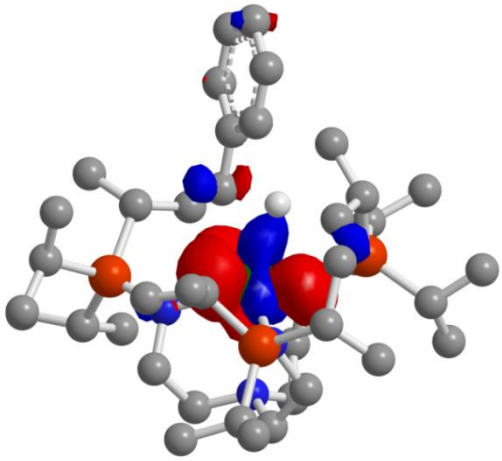
HOMO-2 (196a, -5.05 eV)



HOMO-1 (197a, -4.95 eV)

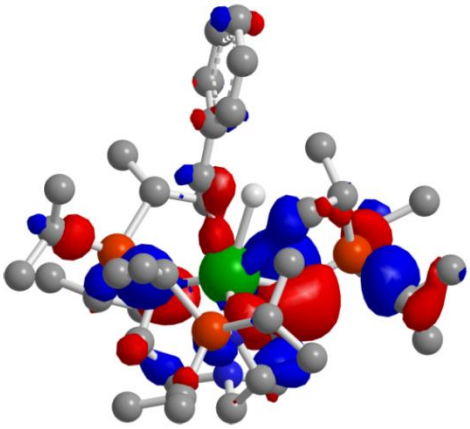


HOMO (198a, -4.83 eV)

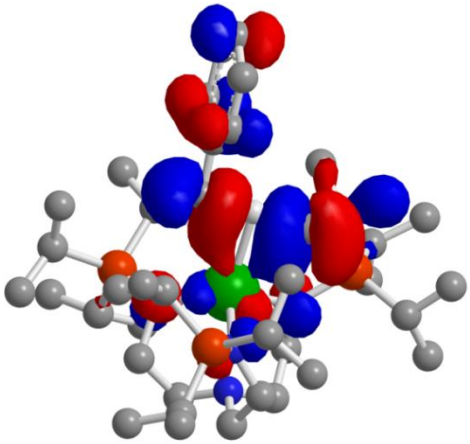


LUMO (199a, -1.45 eV)

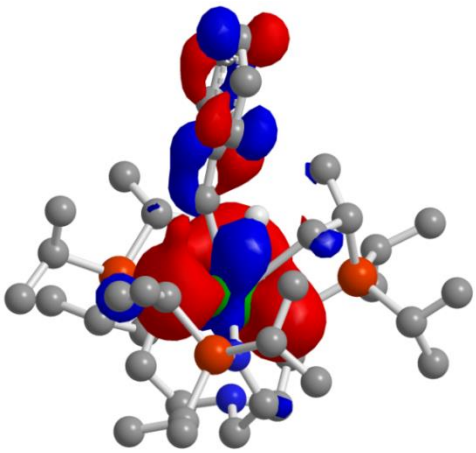
Molecular Orbitals, thorium



HOMO-1 (195, -5.58 eV)



HOMO (196, -4.88 eV)



LUMO (197, -0.24 eV)

7.5.2. Chapter 4

Table 7.1. Relative SO energies, and effective g-values, for **106** (U1) from *ab initio* calculations.

Doublet	**Relative energy (cm^{-1})**	**g_1**	**g_2**	**g_3**
1	0	3.74	0.45	0.56
2	637	2.78	0.66	0.30
3	4281	0.30	1.85	1.67
4	6743	0.80	1.68	5.27
5	7696	0.93	1.58	6.10
6	9421	3.94	0.03	0.22
7	14613	1.80	3.75	3.61

Table 7.2. Relative SO energies, and effective g-values, for **106** (U2) from *ab initio* calculations.

Doublet	**Relative energy (cm^{-1})**	**g_1**	**g_2**	**g_3**
1	0	3.60	0.52	0.71
2	580	3.07	0.36	0.77
3	4224	0.26	1.66	1.75
4	6670	0.88	1.48	5.31
5	7758	0.85	1.40	6.38
6	9267	3.95	0.04	0.17
7	14776	1.82	3.67	3.59

Table 7.3. Relative SO energies, and effective g-values, for **51** from *ab initio* calculations.

Doublet	**Relative energy (cm^{-1})**	**g_1**	**g_2**	**g_3**
1	0	3.76	0.37	0.45
2	554	2.87	0.50	0.34
3	4299	0.28	1.71	1.62
4	6682	0.98	1.66	5.07
5	7629	1.00	1.60	6.19
6	9254	3.88	0.04	0.20
7	15243	1.83	3.56	3.60

Table 7.4. Relative SO energies, and effective g-values, for **107** from *ab initio* calculations.

Doublet	**Relative energy (cm^{-1})**	**g_1**	**g_2**	**g_3**
1	0	3.84	0.35	0.25
2	521	2.35	0.34	0.12
3	4107	0.27	1.67	1.75
4	6772	1.44	2.24	3.98
5	7489	1.71	2.25	5.05
6	9119	3.71	0.05	0.17
7	14743	1.81	3.65	3.61

Table 7.5. Relative SO energies, and effective g-values, for **108** from *ab initio* calculations.

Doublet	Relative energy (cm^{-1})	g_1	g_2	g_3
1	0	3.84	0.43	0.34
2	527	2.60	0.49	0.27
3	4445	0.23	1.50	1.72
4	6644	1.13	1.85	4.74
5	7527	1.21	1.82	5.79
6	9309	3.82	0.09	0.25
7	15844	1.84	3.56	3.45

Table 7.6. Relative SO energies, and effective g-values, for **109** from *ab initio* calculations.

Doublet	Relative energy (cm^{-1})	g_1	g_2	g_3
1	0	3.87	0.27	0.22
2	523	2.59	0.31	0.36
3	4351	0.21	1.48	1.72
4	6664	4.61	1.19	1.91
5	7526	5.71	1.48	1.68
6	9220	3.77	0.13	0.32
7	15786	1.84	3.46	3.57

Table 7.7. Relative SO energies, and effective g-values, for **52** from *ab initio* calculations.

Doublet	Relative energy (cm^{-1})	g_1	g_2	g_3
1	0	3.86	0.11	0.20
2	824	2.13	0.21	0.12
3	4568	0.28	1.56	1.73
4	6839	0.02	2.85	3.05
5	7455	1.70	2.57	2.93
6	9424	3.59	0.13	0.04
7	16030	1.85	3.43	3.52

Table 7.8. Relative SO energies, and effective g-values, for **114** from *ab initio* calculations.

Doublet	Relative energy (cm^{-1})	g_1	g_2	g_3
1	0	3.88	0.27	0.22
2	794	2.28	0.35	0.13
3	4617	0.21	1.47	1.65
4	6750	0.24	2.40	4.29
5	7488	1.15	2.09	4.57
6	9403	3.73	0.03	0.21
7	16628	1.87	3.36	3.46

Table 7.9. Relative SO energies, and effective g-values, for **116** from *ab initio* calculations.

Doublet	Relative energy (cm^{-1})	g_1	g_2	g_3
1	0	3.90	0.05	0.01
2	696	2.17	0.09	0.04
3	4510	0.20	1.63	1.48
4	6765	1.01	2.90	2.79
5	7412	3.23	2.37	2.64
6	9248	3.60	0.05	0.00
7	16561	1.87	3.39	3.44

Table 7.10. Relative SO energies, and effective g-values, for **117** from *ab initio* calculations.

Doublet	Relative energy (cm^{-1})	g_1	g_2	g_3
1	0	3.90	0.02	0.08
2	677	2.15	0.02	0.08
3	4529	0.19	1.61	1.49
4	6743	1.24	2.76	2.77
5	7408	3.13	2.65	2.53
6	9262	3.60	0.02	0.06
7	16594	1.87	3.43	3.38

Table 7.11. Relative SO energies, and effective g-values, for **118** from *ab initio* calculations.

Doublet	Relative energy (cm^{-1})	g_1	g_2	g_3
1	0	3.83	0.34	0.24
2	639	2.73	0.43	0.24
3	4490	0.22	1.62	1.63
4	6669	0.79	1.81	5.08
5	7611	1.12	1.55	6.02
6	9373	3.82	0.11	0.28
7	15861	1.84	3.52	3.51

Table 7.12. Relative SO energies, and effective g-values, for **53** from *ab initio* calculations.

Doublet	Relative energy (cm^{-1})	g_1	g_2	g_3
1	0	3.88	0.08	0.03
2	656	2.12	0.04	0.02
3	4634	0.31	1.70	1.76
4	6765	1.79	2.65	2.68
5	7461	3.56	2.40	2.45
6	9601	3.60	0.01	0.02
7	15685	1.83	3.53	3.56

Table 7.13. Relative SO energies, and effective g-values, for **111** from *ab initio* calculations.

Doublet	Relative energy (cm^{-1})	g_1	g_2	g_3
1	0	3.87	0.41	0.31
2	715	2.22	0.05	0.44
3	4636	0.33	1.62	1.77
4	6792	0.92	2.25	4.21
5	7476	1.55	2.10	4.70
6	9585	3.76	0.12	0.00
7	15732	1.83	3.60	3.49

Table 7.14. Relative SO energies, and effective g-values, for **112** from *ab initio* calculations.

Doublet	Relative energy (cm^{-1})	g_1	g_2	g_3
1	0	3.90	0.04	0.04
2	613	2.13	0.00	0.00
3	4666	0.27	1.65	1.65
4	6731	1.99	2.60	2.60
5	7432	3.81	2.40	2.40
6	9507	3.61	0.00	0.00
7	16242	1.85	3.47	3.47

Table 7.15. Relative SO energies, and effective g-values, for **113** from *ab initio* calculations.

Doublet	Relative energy (cm^{-1})	g_1	g_2	g_3
1	0	3.90	0.19	0.13
2	526	2.22	0.25	0.07
3	4570	0.19	1.62	1.50
4	6649	1.78	2.37	3.34
5	7418	1.83	2.39	4.75
6	9326	3.72	0.17	0.06
7	16598	1.86	3.46	3.39

Table 7.16. Positions of UV-vis-NIR f-f transitions, in cm^{-1}.

52	114	116	117
4600	4650	4650	4650
6063	6051	6045	6037
6923	6904	6904	6895
9031	8900	8850	8900
-	17544	17466	17650

118	53	111	112	113
4600	4750	4750	4750	4750
6055	6094	6072	6072	6059
6885	6891	6894	6894	6901
8900	9000	9019	9000	8900
18724	18181	17634	17303	17152

7.5.3. Chapter 5

The assignment of *N*-bound cyanates in **135** and **136** was supported by DFT calculations. Unrestricted geometry optimizations were performed for the full models of **135** and the anion component of **136**, using coordinates derived from the X-ray crystal structures of **135** and **136** either as the *N*- or *O*-bound cyanate isomers. No constraints were imposed on the structures during the geometry optimizations. The calculations were performed using the Amsterdam Density Functional (ADF) suite version 2012.01.[29,30] The DFT geometry optimizations employed Slater type orbital (STO) triple-ζ-plus polarization all-electron basis sets (from the ZORA/TZP database of the ADF suite). Scalar relativistic approaches were used within the ZORA Hamiltonian for the inclusion of relativistic effects and the local density approximation (LDA) with the correlation potential due to Vosko *et al*.[31] was used in all of the calculations. Gradient corrections were performed using the functionals of Becke[32] and Perdew.[33]

All the structures involved in the reductive carbonylation reaction profile were fully optimized with the Becke's 3-parameter hybrid functional combined with the non-local correlation functional provided by Perdew/Wang (denoted as B3PW91).[12,13] The basis set used for uranium is the Stuttgart-Dresden small core RECP (relativistic effective core potential) in combination with its adapted basis set.[14,15] Si atoms were treated with the corresponding Stuttgart-Dresden RECP in combination with their adapted basis sets,[16] each one augmented by an extra set of polarization functions.[20,21] For the rest of the atoms the 6-31G(d,p) basis set was used.[22-24] In all computations no constraints were imposed on the geometry. All stationary points have been identified for minimum (number of imaginary frequencies Nimag = 0) or transition states (Nimag = 1). Intrinsic Reaction Paths (IRPs) were traced from the various transition structures to verify the reactant to product linkage.[25,26] GAUSSIAN09 program suite was used in all the calculations of the structures involved in the reductive carbonylation reaction profile.[28]

7.5.4. Chapter 6

Unrestricted geometry optimisations were performed for the full anion of **138** and neutral **139** using coordinates derived from the X-ray crystal structure of **138** as a start-point in both cases. No constraints were imposed on the structures during the geometry optimisations. The calculations were performed using the Amsterdam Density Functional (ADF) suite version 2012.01.[29,30] The DFT geometry optimisations employed Slater type orbital (STO) triple-ζ-plus polarisation all-electron basis sets (from the ZORA/TZP database of the ADF suite). Scalar relativistic approaches were used within the ZORA Hamiltonian for the inclusion of relativistic effects and the local density approximation (LDA) with the correlation potential due to Vosko *et al.*[31] was used in all of the calculations. Gradient corrections were performed using the functionals of Becke[32] and Perdew.[33]

For the structures concerning the reaction pathways, the GAUSSIAN09 program suite was used.[28] In particular, all the structures involved in the CE_2 reaction profiles were fully optimised with the Becke's 3-parameter hybrid functional combined with the non-local correlation functional provided by Perdew/Wang (denoted as B3PW91).[12,13] The basis set used for uranium is the Stuttgart-Dresden small core RECP (relativistic effective core potential) in combination with its adapted basis set.[14,15] Si atoms were treated with the corresponding Stuttgart-Dresden RECP in combination with their adapted basis sets,[16] each one augmented by an extra set of polarisation functions.[20,21] For the rest of the atoms the 6-31G(d,p) basis set was used.[22-24] In all computations no constraints were imposed on the geometry. All stationary points have been identified for minimum (number of imaginary frequencies Nimag = 0) or transition states (Nimag = 1) also allowing determination of the thermodynamic data. Due to the well-known difficulties to accurately compute entropy, the energy profiles are given in terms of enthalpy. Since the effects of the temperature is indirect in the calculations, the effect of changing temperature induces a very small change in enthalpy (mainly a global shift for all computed complexes) as it only changes the Δ(PV) term. The profiles are therefore given at room temperature. Finally, recent reports show that the interplay between solvent, dispersion and entropy can be quite artefactual[34,35] and therefore if not clearly stated in the text, the calculations were mainly carried out in gas phase but some

calculations were done in solution to compare. Intrinsic Reaction Paths (IRPs) were traced from the various transition structures to verify the reactant to product linkage.[25,26] In addition, in order to better estimate the net reaction between the U(V) complex, **138**, with CS_2, we have considered implicitly solvent effects by performing SMD[36] single point calculations using toluene as solvent on the gas-phase optimised geometries.

7.6. References

(1) King, D. M.; Tuna, F.; McInnes, E. J. L.; McMaster, J.; Lewis, W.; Blake, A. J.; Liddle, S. T. *Science* **2012**, *337*, 717.
(2) King, D. M.; Tuna, F.; McInnes, E. J. L.; McMaster, J.; Lewis, W.; Blake, A. J.; Liddle, S. T. *Nat. Chem.* **2013**, *5*, 482.
(3) Gardner, B. M.; Cleaves, P. A.; Kefalidis, C. E.; Fang, J.; Maron, L.; Lewis, W.; Blake, A. J.; Liddle, S. T. *Chem. Sci.* **2014**, *5*, 2489.
(4) Bergbreiter, D. E.; Killough, J. M. *J. Am. Chem. Soc.* **1978**, *100*, 2126.
(5) Schlosse.M; Hartmann, J. *Angew. Chem., Int. Ed. Engl.* **1973**, *12*, 508.
(6) Buchanan, G. W.; Driega, A. B.; Moghimi, A.; Bensimon, C.; Bourque, K. *Canadian Journal of Chemistry* **1993**, *71*, 951.
(7) Evans, D. F. *J. Chem. Soc. (Res.)* **1959**, 2003.
(8) SAINT and SMART, Bruker AXS Inc.: Madison, WI, 2001.
(9) CrysAlis PRO, Agilent Technologies: Yarnton, England, 2010.
(10) Sheldrick, G. *Acta Crystallographica Section A* **2008**, *64*, 112.
(11) Dolomanov, O. V.; Bourhis, L. J.; Gildea, R. J.; Howard, J. A. K.; Puschmann, H. *J. Appl. Cryst.* **2009**, *42*, 339.
(12) Becke, A. D. *J. Chem. Phys.* **1993**, *98*, 5648.
(13) Perdew, J. P.; Wang, Y. *Phys. Rev. B* **1992**, *45*, 13244.
(14) Kuchle, W.; Dolg, M.; Stoll, H.; Preuss, H. *J. Chem. Phys.* **1994**, *100*, 7535.
(15) Cao, X. Y.; Dolg, M.; Stoll, H. *J. Chem. Phys.* **2003**, *118*, 487.
(16) Cao, X. Y.; Dolg, M. *Theochem-J. Mol. Struct.* **2004**, *673*, 203.
(17) Moritz, A.; Cao, X.; Dolg, M. *Theoretical Chemistry Accounts* **2007**, *118*, 845.
(18) Andrae, D.; Häußermann, U.; Dolg, M.; Stoll, H.; Preuß, H. *Theor. Chim. Acta* **1990**, *77*, 123.
(19) Martin, J. M. L.; Sundermann, A. *J. Chem. Phys.* **2001**, *114*, 3408.
(20) Bergner, A.; Dolg, M.; Kuchle, W.; Stoll, H.; Preuss, H. *Mol. Phys.* **1993**, *80*, 1431.
(21) Ehlers, A. W.; Bohme, M.; Dapprich, S.; Gobbi, A.; Hollwarth, A.; Jonas, V.; Kohler, K. F.; Stegmann, R.; Veldkamp, A.; Frenking, G. *Chem. Phys. Lett.* **1993**, *208*, 111.
(22) Ditchfie.R; Hehre, W. J.; Pople, J. A. *J. Chem. Phys.* **1971**, *54*, 724.
(23) Hehre, W. J.; Ditchfie.R; Pople, J. A. *J. Chem. Phys.* **1972**, *56*, 2257.
(24) Harihara.Pc; Pople, J. A. *Theor. Chim. Acta* **1973**, *28*, 213.
(25) Gonzalez, C.; Schlegel, H. B. *J. Chem. Phys.* **1989**, *90*, 2154.

(26) Gonzalez, C.; Schlegel, H. B. *J. Phys. Chem.* **1990**, *94*, 5523.
(27) Reed, A. E.; Curtiss, L. A.; Weinhold, F. *Chem. Rev.* **1988**, *88*, 899.
(28) Frisch, M. J. T., G. W.; Schlegel, H. B.; Scuseria, G. E.; Robb, M. A.; Cheeseman, J. R.; Scalmani, G.; Barone, V.; Mennucci, B.; Petersson, G. A.; Nakatsuji, H.; Caricato, M.; Li, X.; Hratchian, H. P.; Izmaylov, A. F.; Bloino, J.; Zheng, G.; Sonnenberg, J. L.; Hada, M.; Ehara, M.; Toyota, K.; Fukuda, R.; Hasegawa, J.; Ishida, M.; Nakajima, T.; Honda, Y.; Kitao, O.; Nakai, H.; Vreven, T.; Montgomery, J. A., Jr.; Peralta, J. E.; Ogliaro, F.; Bearpark, M.; Heyd, J. J.; Brothers, E.; Kudin, K. N.; Staroverov, V. N.; Kobayashi, R.; Normand, J.; Raghavachari, K.; Rendell, A.; Burant, J. C.; Iyengar, S. S.; Tomasi, J.; Cossi, M.; Rega, N.; Millam, N. J.; Klene, M.; Knox, J. E.; Cross, J. B.; Bakken, V.; Adamo, C.; Jaramillo, J.; Gomperts, R.; Stratmann, R. E.; Yazyev, O.; Austin, A. J.; Cammi, R.; Pomelli, C.; Ochterski, J. W.; Martin, R. L.; Morokuma, K.; Zakrzewski, V. G.; Voth, G. A.; Salvador, P.; Dannenberg, J. J.; Dapprich, S.; Daniels, A. D.; Farkas, Ö.; Foresman, J. B.; Ortiz, J. V.; Cioslowski, J.; Fox, D. J. *Gaussian 09, Revision D.01,* ; Gaussian, Inc.: Wallingford CT.
(29) Fonseca Guerra, C.; Snijders, G. J.; te Velde, G.; Baerends, J. E. *Theoretical Chemistry Accounts* **1998**, *99*, 391.
(30) te Velde, G.; Bickelhaupt, F. M.; Baerends, E. J.; Guerra, C. F.; Van Gisbergen, S. J. A.; Snijders, J. G.; Ziegler, T. *J. Comput. Chem.* **2001**, *22*, 931.
(31) Vosko, S. H.; Wilk, L.; Nusair, M. *Can. J. Phys.* **1980**, *58*, 1200.
(32) Becke, A. D. *Phys. Rev. A* **1988**, *38*, 3098.
(33) Perdew, J. P. *Phys. Rev. B* **1986**, *33*, 8822.
(34) Weymuth, T.; Couzijn, E. P. A.; Chen, P.; Reiher, M. *Journal of Chemical Theory and Computation* **2014**, *10*, 3092.
(35) Castro, L.; Kirillov, E.; Miserque, O.; Welle, A.; Haspeslagh, L.; Carpentier, J.-F.; Maron, L. *ACS Catalysis* **2015**, *5*, 416.
(36) Marenich, A. V.; Cramer, C. J.; Truhlar, D. G. *J. Phys Chem B* **2009**, *113*, 6378.